Studies on Antimicrobial Sesquiterpenes in the Leaves of Rugosa Rose (*Rosa rugosa* Thunb.)

ハマナス（Rosa rugosa Thunb.）葉中の抗菌性セスキテルペンに関する研究

Volume I

YASUYUKI HASHIDOKO
Doctor's Course, Division of
Agricultural Chemistry

March 1990

農芸化学専攻　博士課程

橋床　泰之

Contents

Acknowledgment

First of all, author is grateful to Professor Junya Mizutani, Laboratory of Agricultural Organic Chemistry, Faculty of Agriculture, Hokkaido University, for his considerable guidance and encouragement. He also became a chief judge of this thesis, and corrected the thesis. The author also extends a special acknowledgment to Professor Akitami Ichihara, Utilization of Agricultural Product Lab., Faculty of Agriculture, Hokkaido University, for his judgment on the thesis as well, and Dr. Jun Kawabata, for his very available advice especially in the area of theoretical chemical reactions, high performance NMR analyses and MM2 program utilization. Dr. Yukiharu Fukushi also gave several suggestion to the author, especially in chemical reactions. The author would like to express special acknowledgments to Dr. Satoshi Tahara, Associate Professor, who gave numerous numbers of useful suggestions and advice, and sometimes critical opinion, too. Without thousands of discussions with him and his very noticeable correction for English, this thesis would not have been completed. Here, the author thanks to him for his attitude that he has regarded his students as an independent and ambitious "egg of researcher".

The author is very grateful to Professor Shonosuke Sagisaka, in Physiology Section of Institute of Low Temperature Science, Hokkaido University, for his considerable suggestions especially from the side of plant physiology and enzymology. Dr. Tadashi Araki in the Section also gave the author several advice for OD determination and kindly lent the author his instrument. Professor Tatsuji Tujii, Director of The Botanic Garden of Hokkaido University kindly supplied leaves of several *Rosa* plants as a sample from their collections. Professor Toshihiko Iizuka, in Sericology Lab., kindly provided the author larva of silk worms to use the bioassay. Dr. Takane Fujimori and Dr. Shigeo Ishiguro in

Japan Tobacco Industry (Ltd) willingfully carried out the cytotoxic test. Mr. Satoshi Ichikawa, who is the author's friend, kindly supplied leaves of some wild roses from Yaku Island in Kagoshima. The author also thanks to Mrs. Sizuko Kawamura for her official care.

Mr. Kenji Watanabe, the technician in the Professor J. Mizutani's lab., is mostly indebted for so many spectroscopic analyses, especially in FI-MS, FD-MS and NMR including NOE and COSY analyses. Mr. Mitsuhiko Ikura, NMR lab. in Faculty of Science of Hokkaido University, and Mrs. Yumiko Misu, Spectroscopic Analysis Center of Pharmacology in Hokkaido University, measured NMR spectra. Especially Mrs. Y. Misu took most of COSY and INADEQUATE and so on. Mr. Fujinori Hanawa, a student in the master course is as well. Mrs. Yoshiko Sugiyama and Miss Eri Matsumiya, GC-MS-NMR Comity of Faculty of Agriculture are also grateful for EI-MS, EI-HR-MS and GC-MS operation. Mr. Hideyuki Kurihara and Mr. Takeshi Horio are as well. Mr. Atsushi Nagaki supplied callus of the material plant.

When the author had stayed in Alberta, Canada during 1987-1988, Professor Chuji Hiruki, Plant Pathology Lab. in Plant Science, The University of Alberta accepted him as an exchange graduate student to his lab. The author specially thanks for his guidance in identity for science and also direction for English writing. Mr. Juichi Takahashi, Chief of International Association Section of Hokkaido Government, and Dr. Larry Henderson, Alberta Government, who supported the author as the sponsors are grateful as well. Mrs. Delyse Forster, Chief Staff in ESL Program of The University of Lethbridge, Alberta, Canada gave the author useful English lessons. For the sake of their help, he was able to write this thesis in English. Dr. Emile B. Waggenaar is as well.

This work was partly supported by Miss Noriko Iwaya who have finished master course of Graduate School of Hokkaido University in 1989 under Professor J. Mizutani and Dr. S. Tahara, and Miss Sayaka

Watanabe who will finish bachelor degree of Hokkaido University until this thesis is printed and booked. The author wishes to introduce their accomplishments: Miss N. Iwaya elucidated the absolute configuration of the main compound and isolated two novel exoperoxy bisabolanoids. Furthermore, she carried out to a preliminary quantitation of the carotane peroxides in *Rosa rugosa* tissues through summer season in 1988, which work gave the author several suggestion in biochemical research, he did not afford to write this series of study. On the other hand, Miss S. Watanabe surveyed carotane glucosides in *Rosa rugosa*. Although her aimed compound was not found in the extract, her achievement in the chromatography of the high polar constituent gave some important suggestion to discuss carotane glucosides. They also helped the author a lot by sample collections and preparations. Here, the author is repeatedly acknowledged to them for their accomplishment.

During the work, the author also owed so many corporations from Mizutani Plant Ecochemical Project of ERATO Program by Education and Science, especially research staff in the Seiseikiko Group, Dr. Masatoshi Kanauchi, Dr. Satoru Kondo, Dr. Satoru Kawai, Dr. Takashi Seto, Dr. Yuko Yoshizawa, Dr. Hideo Kakuta, Miss Yoko Matsuzawa and Miss Manami Chida are acknowledged. Dr. Labunmi Lajide, Dr. Pierre Escoubas and Dr. Y. Yoshizawa kindly corrected th thesis. Some illustrations in the thesis were written by Miss Y. Matsuzawa.

This work was completed by several colaborations and supports by members of the laboratories in 1989, Mr. Akihiko Yamane, Dr. Hanny Wijjaya, Mr. H. Krihara, Mr. T. Horio, Mr. F. Hanawa, Miss Yomiko Matsukura, Mr. A. Nagaki, Mr. Junji Fujikura, Mr. Manabu Mishima, Mr. Masaaki Moriyama, Mr. Takato Nakayama and Miss S. Watanabe. Thank to each of them, especially for many helps with typing of the number and copying the manuscript. Last but not least, the author thanks to his families for their understanding.

Chapter 1 Introduction

Among organisms on the earth, vertebrates are the most advanced organism in their defense system. In addition to their mobility which has become an significant means for escape from predators or a physical danger, vartebrates have acquired and established another effective defense system, the immune system which functions against invisible and inescapable microbial or viral invasions. Plants however have adapted themselves to fixed conditions on the ground, they are unable to avoid any danger by their translocation. Plants having no immune system due to lack of the circulation system in the body, they have developed their own defense system in physical and chemical ways. In physical defense systems, thorns or hard cuticle layers on the leaf and stem are the most common example. Furthermore, very simple structure of plant bodies also contributes to protect themselves. It is, in many plant, commonly observed that they discard some parts of their body infected with a pathogen by the underlying healthy tissues. When tissues are spoiled by the infection, they push outward the infected parts to remove the pathogen and form scab on the parts [1]. Such a protective way is certainly reasonable for plants, because they can get over serious damage and regenerate any part of their body (Fig. 1-1). This type of plant defense is called "kamikaze suicide" among plant pathologists [2] (Fig. 1-2).

Plants have also developed chemical defense systems instead of the immune system evolved in the animal kingdom, especially among vertebrates. Chemical substances functioning as defense agent in plants and even their roles in the ecosystem have currently been unraveled. Among higher plants, the chemical defense system has much evolved and become complicated in several aspects, such as the variation of defense compounds and of their physiological activities, the synthetic process of those compounds, and their roles in the ecosystem. Some typical defense substances in plants

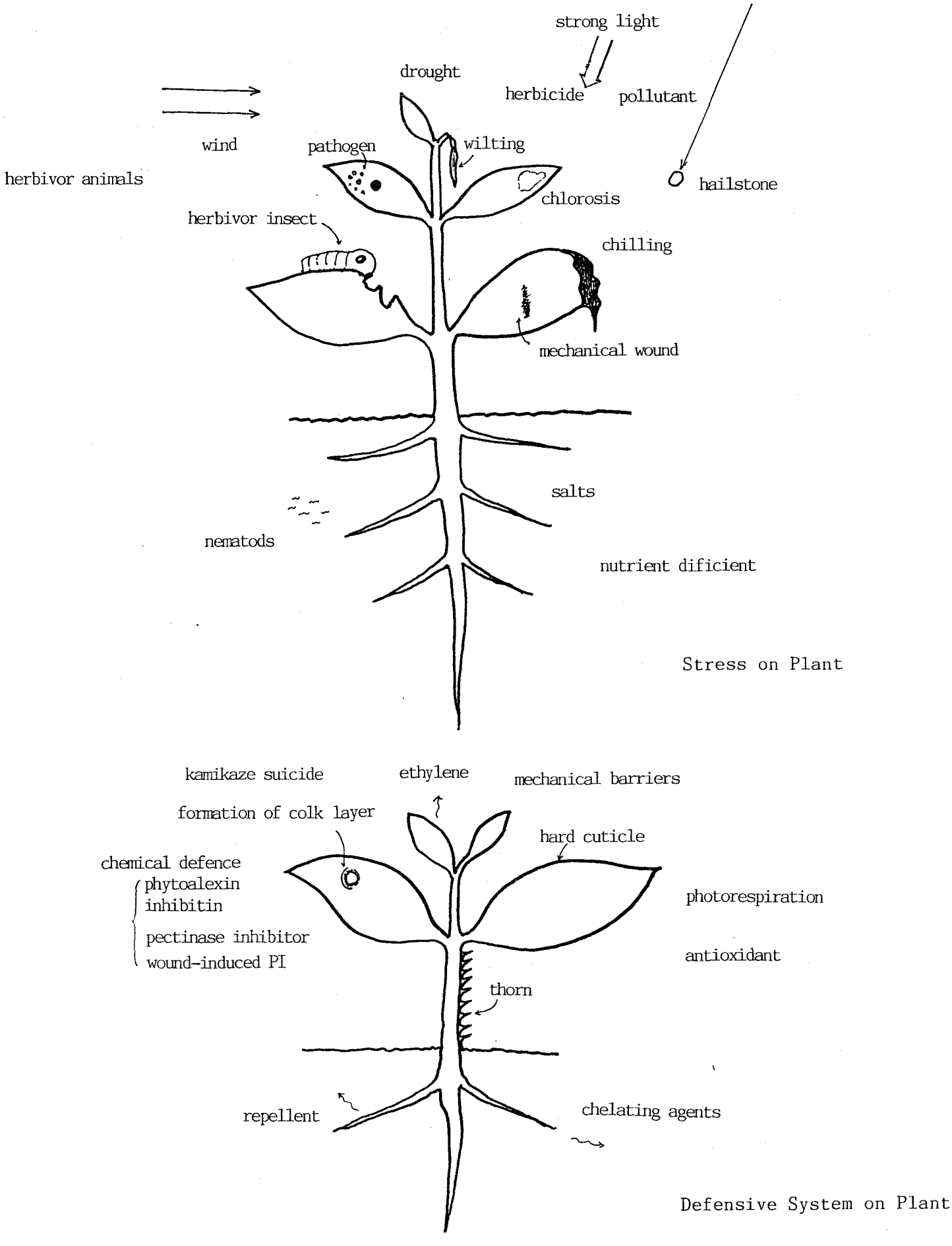

Fig. 1-1 Physical and Chemical Stress on Plants and Defense System of Plants against the Stress

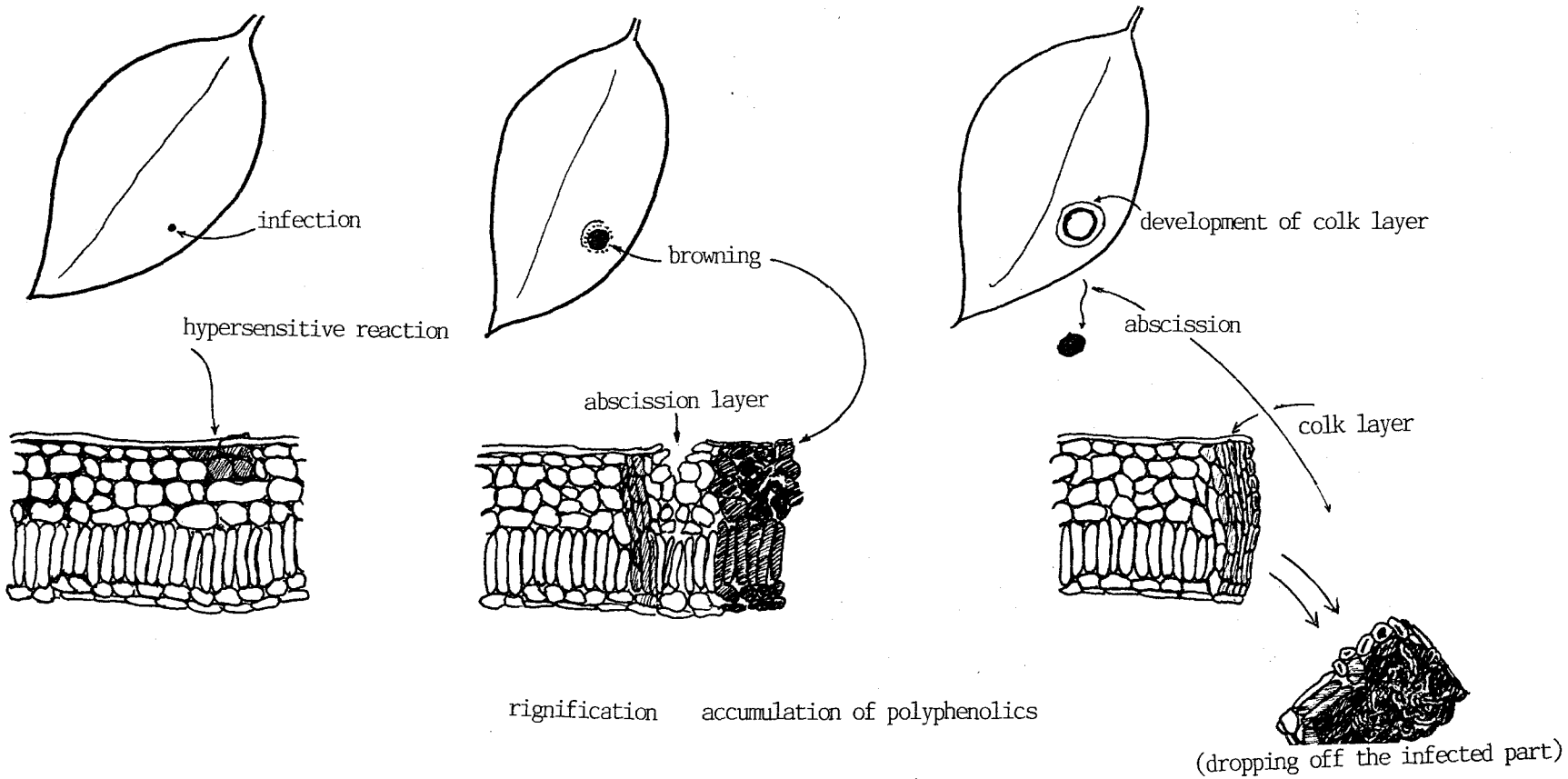

Fig. 1-2 "Kamikaze Suicide", a Physical and/or Chemical Defense System on Aerial Part of Plants: Positively making scab on the infected part results in removal of the pathogens.

are shown in Table 1-1 and Fig. 1-3 [3-10], and those defense compounds described are classified according to their structures, activities, and their mode of function.

In chemical defense of plants, several types of activity, effect and defensive form of chemical agents are known. Antimicrobial activities against pathogens and oral toxicities to herbivorous insects are the typical ones. On the other hand, antifeedants and repellents belong to a rather passive type of defense agents. In a special case, some plants contain an insect hormone-like substance, such as a phytoecdysone or a juvenile hormone analog which inhibits growth of an insect feeding on the plant [7,11,12].

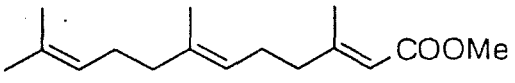

2-*E*-6-*E*-methyl farnesiate

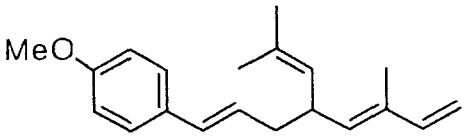

juvocimene I

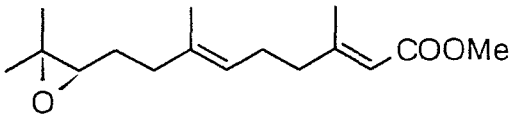

juvenyl hormone III

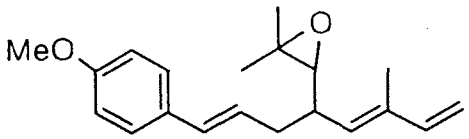

juvocimene II

Classification of the defense substances according to the biogenetic (or biosynthetic) feature is favored by natural product (or secondary plant product) chemists and plant chemotaxonomists. As a rare but quite significant defense compound, the presence of proteins [proteinase inhibitor (PI)] in some higher plant families is well known [8,13]. However, most of the defense substances are low molecular compounds. In many plants, terpenoids (mono-, sesqui-, di- and tri-terpenes including steroids) and their derivatives form one of the most common group of defense compounds

Table 1-1 Typical defense substances of plants

trivial name	No.	source (scientific name)	class	activity	other remarkes	reference
risitin	a	potato (*Solanum tuberosum*)	terpenoid	antimicrobial	phytoalexin	[3]
luteone	b	lupin (*Lupinus albus*)	flavonoid	antimicrobial	inhibitin	[4]
juglone	c	wall nut (*Juglas nigra*)	phenolics	antimicrobial antifeedant	post-inhibitin	[5]
DIMBOA	d	corn (*Zea mays*)	alkaloid	antimicrobial antifeedant	post-inhibitin	[6]
ponasterone A	e	fern (*Podocarpus nakaii*)	steroid	insect hormone	phytoecdysone	[7]
proteinase inhibitor	-	tomato (*Lycopersicon esculentum*)	protein	antifeedant	wound-inducing	[8]
-farnesen	f	potato(*Solanum berthaultii*)	terpenoid	repellent	aphid control	[9]
cis-dehydro-matricaria ester	g	golden rod weed (*Solidago altissima*)	polyacetylene	allelochemics		[10]

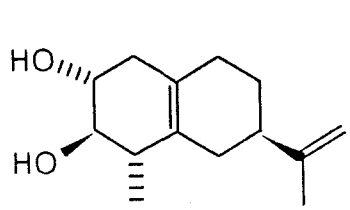

rishitin (**a**)

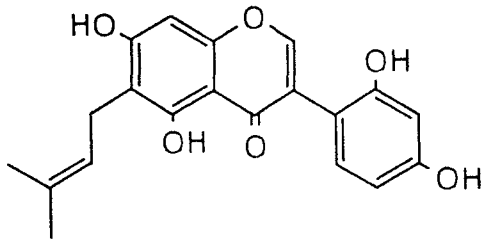

luteone (**b**)

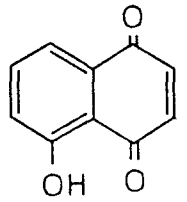

juglone (**c**)

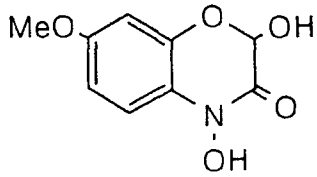

DIMBOA (**d**)

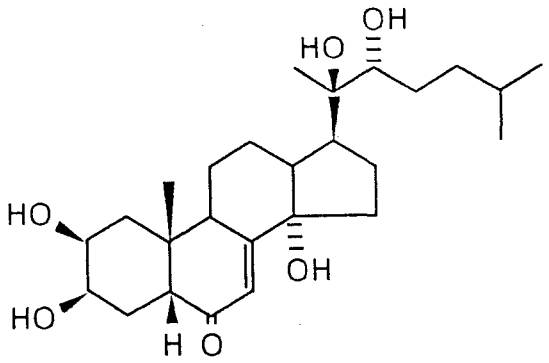

ponasterone A (**e**)

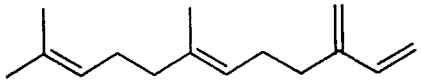

β-farnesene (**f**)

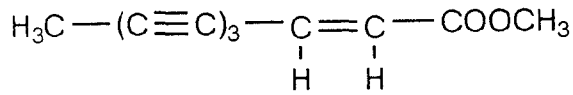

cis - dehydromatricaria ester (**g**)

Fig. 1-3 Chemical Structures of the Defense Agent

As other major examples, are known non-protein amino acids, alkaloids, polyphenols (simple phenols, flavonoids, phenylpropanoids), and so forth. These compounds are mostly secondary metabolites of plants.

The term "secondary metabolite" means a chemical compound which is not essential in cellular functioning, unlike glucose, lipids, nucleic acids or amino acids, for example, concerned in the basal cellular activity. Secondary metabolites had commonly been regarded as metabolic wastes stored in a cellular organ such as a vacuole, since plants lack excretory organs. However, the secondary metabolites are now considered to be under dynamic regulations in the tissue and taking certain important roles in the chemical communication and defense systems of plants. Many of the secondary metabolites therefore comply with the conceptions of "semiochemicals".

In 1973, Ingham and Harborne proposed a definition to classify plant antimicrobial substances into four divisions - prohibitin, inhibitin, post-inhibitin and phytoalexin - according to the properties of their development in plants (Table 1-2) [14,15]. Phytoalexin, of which conception was initially proposed by Muller and Borger in 1940 [16], is considered to be the most advanced chemical defense system of plants, because phytoalexins are inducibly produced in response to biotic or abiotic stress.

Unlike inherent antimicrobial substances, phytoalexin is produced through the biosynthetic pathways established *via* gene activation, only when the tissue got some stress, and this response is somehow similar to the immune system in mammals. The most different aspect of the phytoalexin production from the immune system is probably that a low molecular compound works as a defense agent, and more importantly, phytoalexin is a defense factor showing host-specificity. In other words, plant have not acquired any memorial function or recognition system against an individual pathogen in phytoalexin production, unlike the immune system of

Table 1-2 Classification of antifungal substance originated in plants

Class	Definition
Pre-infectional compound	
1. Prohibitin	A metabolite which reduces or completely halt the *in vivo* development of microorganisms
2. Inhibitin	A metabolite which undergos post-infectional increase in order to express full toxicity
Post-infectional compound	
1. Post-inhibitin	A metabolite formed by the hydrolysis or oxidation of pre-existing non-toxic substrate
2. Phytoalexin	A metabolite formed de novo after invasion by gene repression or activation of latent enzyme system

[14,15]

vertebrates which produce an antigen-specific immunoglobulin antibody. Even in change of the active level of some enzymes [for example, peroxidase (PO), phenylalanine ammonia lyase (PAL), polyphenol oxidase (PPO) and lypoxygenase (LOX), and so on], the response of a plant against several kinds of stress is utterly the same [17]. Furthermore, ability of plants to produce a phytoalexin is still restricted in a part of families among higher plant, even though some screenings have been carried out [18,19].

When a phytoalexin-producing plant is invaded by a pathogen, the plant can make a response to the invasion by accepting a stimulant called an elicitor, which is confirmed to be released from the infected part (from damaged plant tissues and/or the pathogen). One of elicitors is currently recognized as a cell wall fragment exogenously (originated in the invader) or endogenously released from the infected cell. This elicitor is believed to stimulate healthy cells around the disrupted cells. Then, the cells accept an elicitor from the infected cell start out to change their metabolic pathway. This metabolic change is due to both activation of specific gene(s) in the chromosome and cell disruption (Fig. 1-4) [20]. An elicitor was recently proved to be an oligosaccharide [21]; however, some researchers are still doubtful of its proposed structure.

In this current work, it is suggested that H_2O_2 or other active oxygens behave as elicitor-like messengers in the phytoalexin production [22]. Interestingly, it is known that $\cdot O_2^-$ behave as a stimulant in the immune system in mammals. This simple but active molecule can activate phagocytosis of phagocyte which is known to be predatory white blood corpuscles in the immune system, so that $\cdot O_2^-$ is regarded as a messenger concerned with the defense system of vertebrates (Fig. 1-5) [23]. More importantly, superoxide anion plays a role as a disinfectant in the white blood corpuscle.

On the contrary, any significant role of $\cdot O_2^-$ in defense

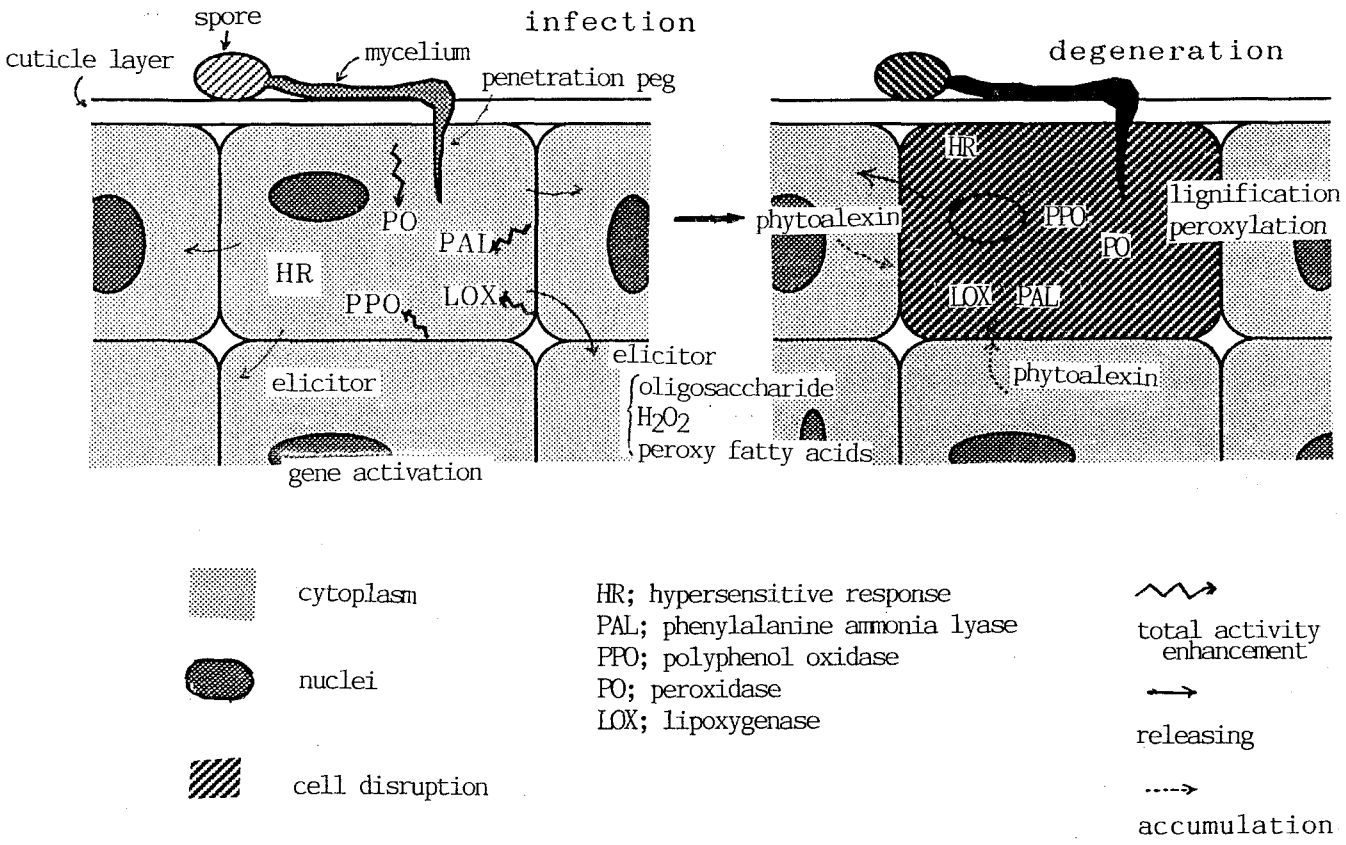

Fig. 1-4 Process for the Hypersensitive reaction and Phytoalexin Production

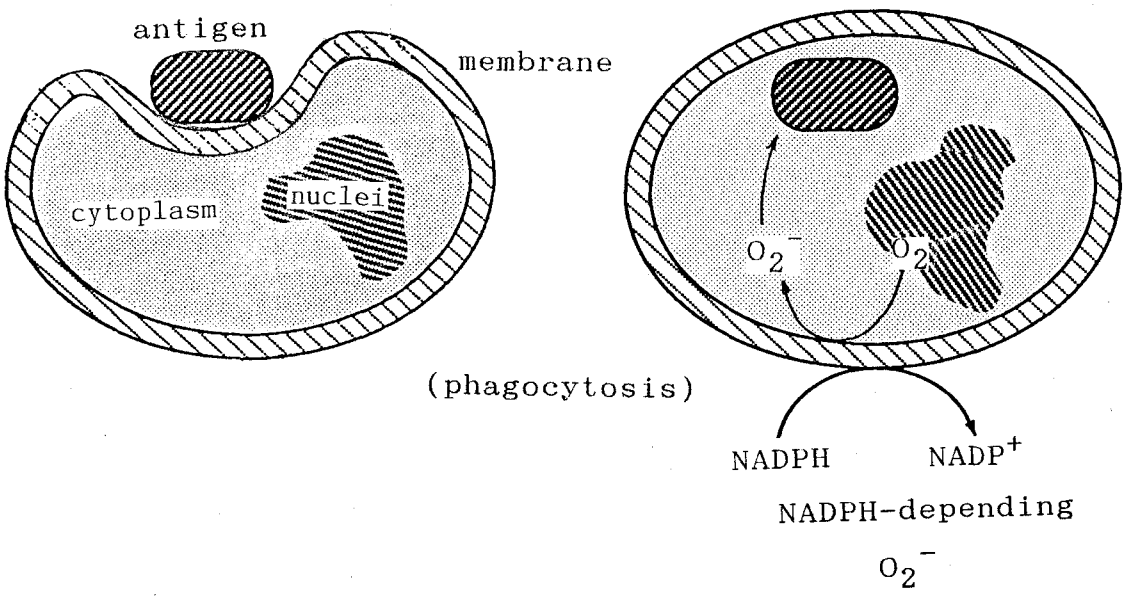

Fig. 1-5 Model of O_2^- Releasing during Phagocytosis in White Blood Corpuscles

system of a plant has not been proved, although releasing of $\cdot O_2^-$ during hypersensitive cellular disruption is observed. Superoxide anion being a strong oxidant agent, plants rather have to protect their tissues from the oxidant under a normal condition. For the scavenging of $\cdot O_2^-$, a plant cell has prepared several means, like superoxide dismutase (SOD) and catalase that are involved in the reactions shown below.

$$\cdot O_2^- + 2H_2O \rightarrow 2H_2O_2 \quad \text{(SOD)}$$
$$2H_2O_2 \rightarrow 2H_2O + O_2 \quad \text{(catalase)}$$

Some secondary metabolites cooperating with an enzyme also function as an antioxidant or a scavenger against superoxide anion and other oxide radicals. As the typical antioxidants are known ascorbic acid (**i**), α-tocopherol (**j**), glutathione (**k**), β-carotene (**l**) (Fig. 1-6). Those substances mainly protect unsaturated fatty acids such as linoleic acid (**l**), linolenic acid (**m**), arachidonic acid (**n**) and eicosapentaenoic acid (**o**) (Fig. 1-7) in cell membrane from peroxidation by active oxygens [24-26].

In plant tissues, active oxygens are detoxificated by the antioxidants and some secondary metabolites like phenolics and terpenoids. However, some plants such as soybean (*Glycine max*) rather positively enhance total activity of the lipoxygenase and result in accumulation of peroxy-linolenic acids in the leaves, when they are wounded [27]. This kind of response is also observed in rice plant (*Oryza sativa*), during its necrotic defense reaction [28]. In the latter case, the derivatives of hydroxylated fatty acids were isolated as phytoalexin-like substances (self defensive agent) of disease-resistant rice. This fact indicates that plants can disrupt the infected tissues by themselves through peroxylation of polyunsaturated fatty acids on the cell membrane. As the initial step, the infected or wounded cells enhance the level of

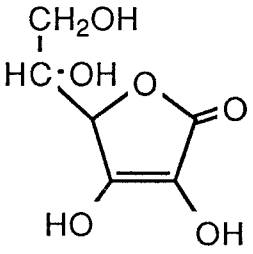

ascorbic acid (**i**)

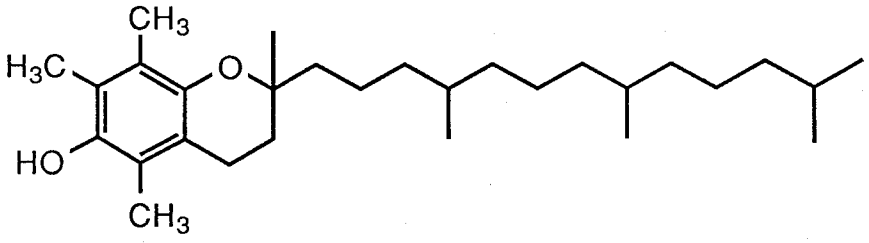

α-tocopherol (**j**)

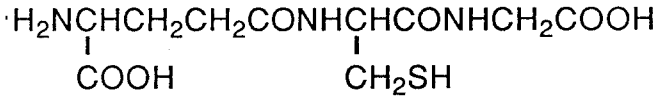

glutathione (**k**)

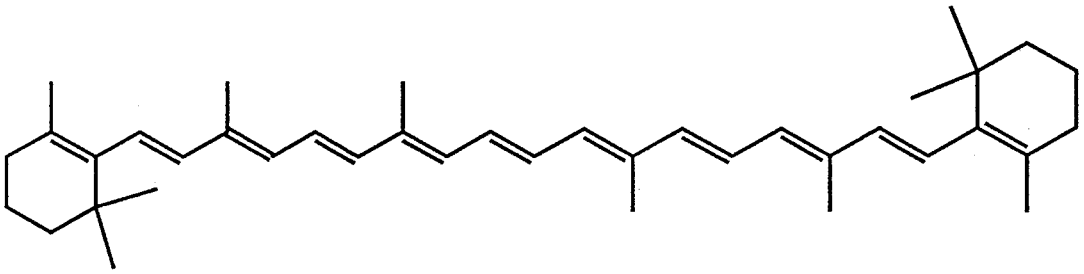

β-carotene (**l**)

Fig. 1-6 Common Antioxidants

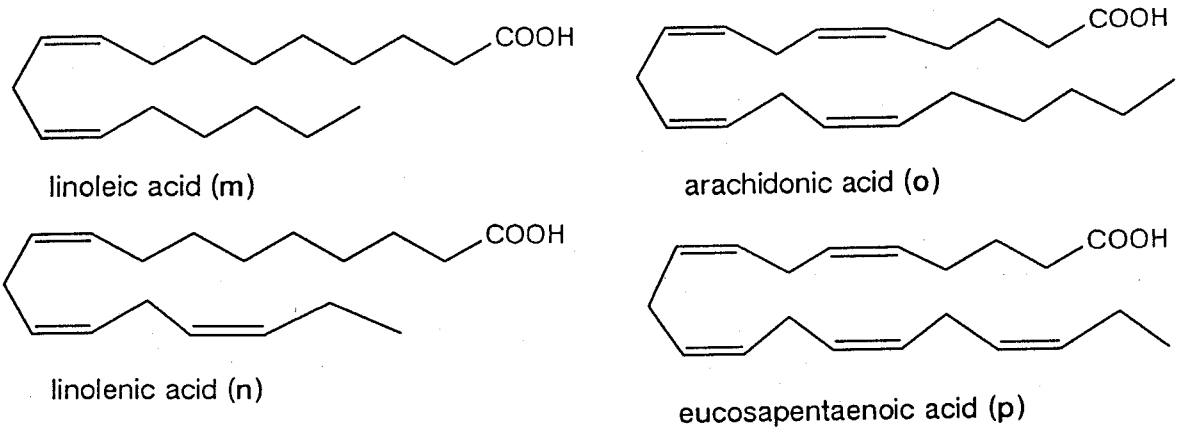

Fig. 1-7 Polyunsaturated Fatty Acid Originated in Plants

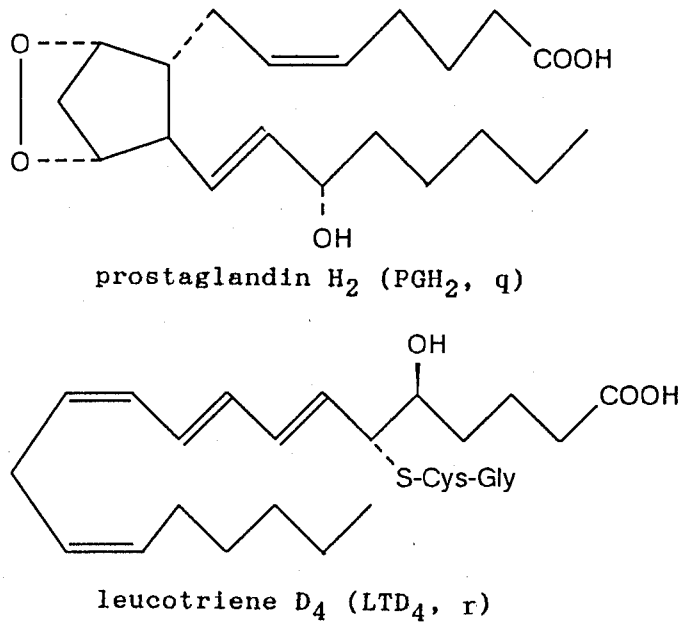

Fig. 1-8 Typical Physiologically Active Prostanoids, PGH_2 and LTD_4

endogenous lipoxygenase [29]. Even it is suggested that peroxylated fatty acids act as promoter for hypersensitive reaction [30].

In mammalian cells, the unsaturated fatty acids are also enzymatically oxygenated to yield their oxidation products. The group of the oxygenated fatty acids known as prostanoids exhibits several and dramatic physiological activities in the mammalian body. One of prostanoids well known is prostaglandin H_2 (PGH_2, **q**) which functions as a contraction factor for smooth muscle (Fig. 1-8) [31], and another one is leucotriene D_4 (LTD_4, **r**) found as an inflammation mediator [32]. In the physiological meaning, the prostanoids resemble to the plant-originating oxidation products of polyunsaturated fatty acids.

In plants also, some of those functional oxygenated-fatty acids have gradually been isolated and elucidated their structures and roles [33-35] (Fig. 1-9). However, any typical secondary metabolites such as terpenoids have not been examined from the view point of biological peroxidation. Among naturally occurring compounds originated in plant, numerous numbers and several types of peroxides not related to fatty acids have been reported; however, systematic research on the peroxy compounds concerned with their functions and biosynthetic pathways has hardly been carried out.

In the present thesis, the author examined a sesquiterpene peroxide found in rugosa rose (*Rosa rugosa*) leaves, including its structure, chemical conversion, related compounds and biogenesis. On the basis of these results, the chemical defense system of this plant was further discussed from the physiological viewpoints. The peroxide, rugosal A (**1**) initially isolated as an antifungal substance from damaged leaves of *Rosa rugosa* was revealed to have a carotane skeleton oxygenated at C-14 and possess a unique 1,5-endoperoxide bridge. One of the peroxy oxygens was intramolecularly hydrogen-bonded with a hydroxyl group at allylic carbon, and

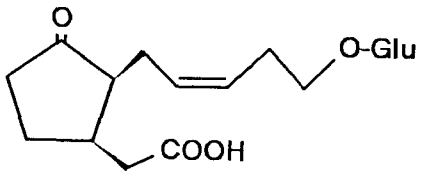

tuber-inducing stimulus [33]

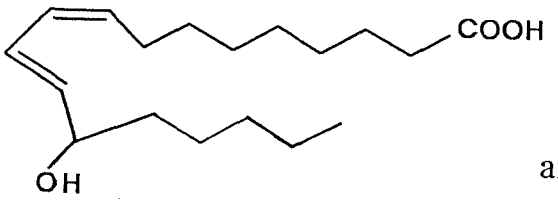

antifungal HR-promotor [34]

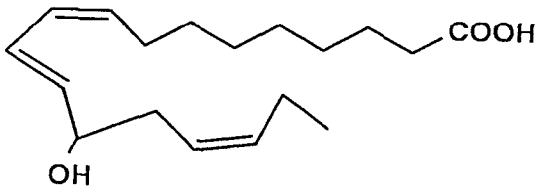

antifungal [35]

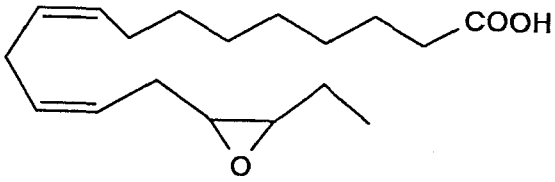

antifungal [35]

Fig. 1-9 Some Functional Oxygenated Fatty Acids in Plants

this novel sesquiterpene was the first example of a carotanoid from Rosaceae [36]. Furthermore, many novel carotanoids were isolated and identified from *Rosa rugosa* leaves together with some other sesquiterpenoids as shown in Fig. 1-10.

The presence of carotanoids have only been restricted among Umbelliferae (Apitaceae) [37-55] and Compositae (Asteraceae) [56-58] in higher plants until the survey of constituents in *Rosa rugosa* leaves. In comparatively primitive organisms, carotanoids have also been found in a green moss, *Barbilophozia lycopodioides* (Hepaticeae) [59] and a fungus, *Aspergillus terreus* [60]. Most of the carotanoids from plants are modified by esterification to give a benzoate, a *p*-anisate, an *iso*-vanillate, an angelate and so forth at a hydroxyl group on the skeleton. Structures of naturally occuring carotanoids reported so far are depicted in Fig. 1-11.

Recently, a communication describing the isolation and identification of rugosal A (1) from the dried roots of *Nardostachys chiensis* (Valerianaceae) was received and it was pointed out that Valerianaceae is the fourth family of carotanoid source among higher plants [61].

The biosynthetic pathway for carotanoids have been examined to reveal their precursor, *cis,trans*-farnesyl pyrophosphate, common to bisabolanoids [62,63]. In fact, Umbelliferae and Compositae both containing carotanoid producing plants commonly possess a biosynthetic pathway of bisabolanoids [64,65]. Those biosynthetic pathways are shown in Scheme 1-1. Interestingly, bisabolanoids are also biosynthesized in *Rosa rugosa* leaves as its major sesquiterpenoid. Like bisaborosaol A (19), all *Rosa* bisabolanoids found so far are oxygenated at C-7 which is biogenetically equivalent to C-14 in the carotanoid. The specific oxygenation may be explicable with the biosynthetic relation between these two types of sesquiterpenoids.

The fact that rugosal A exhibits a marked antifungal activity indicates that this substance presumably functions as a defense

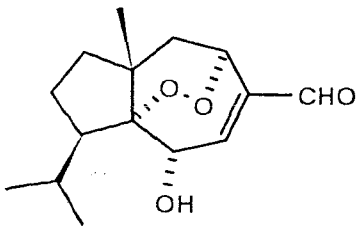

1; rugosal A

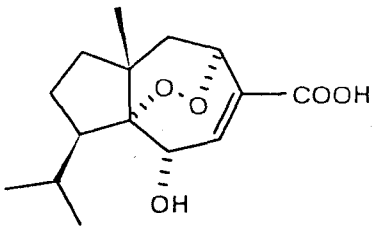

2; rugosic acid A

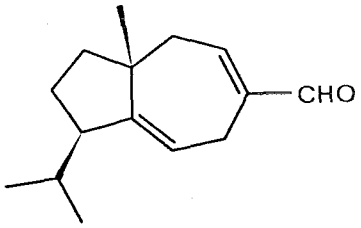

3; carota-1,4-dienaldehyde (RL-C)

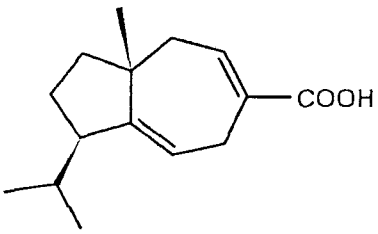

4; carota-1,4-dienoic acid (RL-115MA)

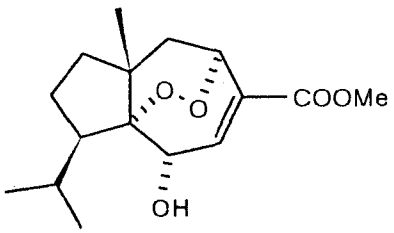

5; rugosic acid A methyl ester (RL-PERO-3)

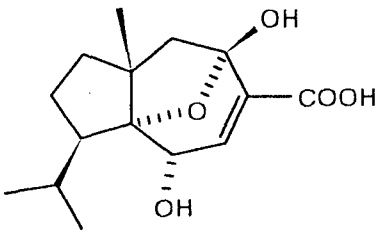

6; rugosic acid B

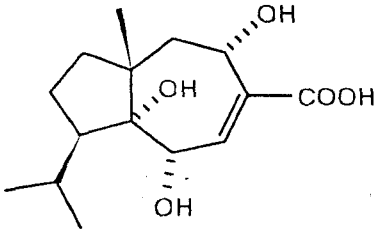

7; rugosic acid C

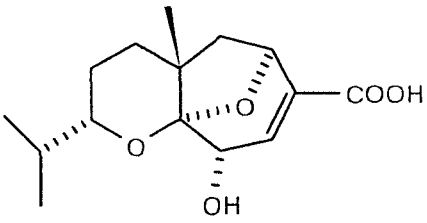

8; rugosic acid D

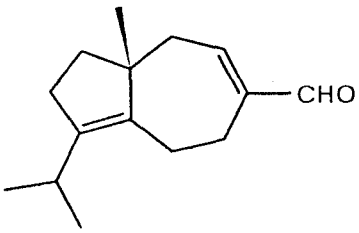

9; daucenaldehyde (RL-A)

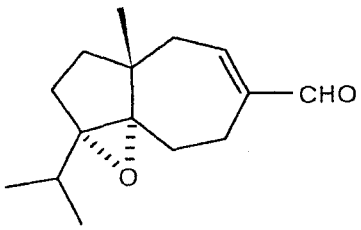

10; epoxydaucenaldehyde A (RL-109B)

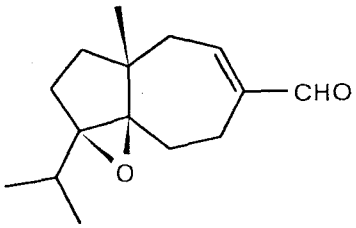

11; epoxydaucenaldehyde B (RL-109A)

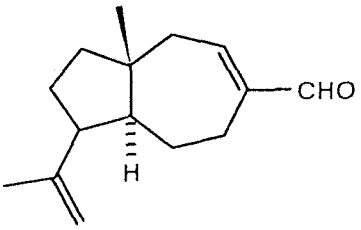

12; isodaucenaldehyde (RL-E)

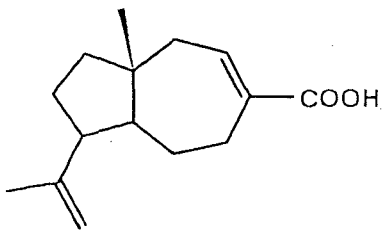

13; isodaucenoic acid (RL-115M-B)

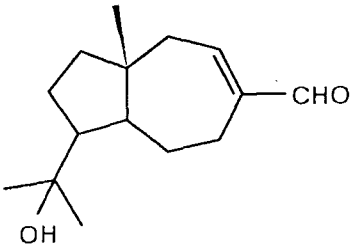

14; hydroxycarotanaldehyde (RL-117C)

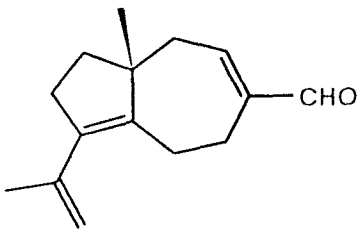

15; dehydrodaucenaldehyde (RL-D)

Fig. 1-10 Sesquiterpenes Isolated from *Rosa rugosa* Leaves

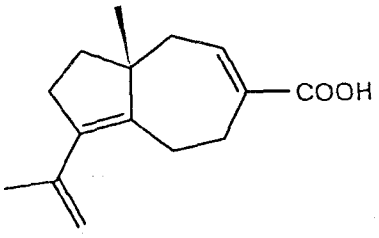

16; dehydrodaucenoic acid

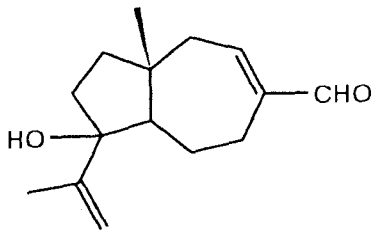

17; hydroxyisodaucenaldehyde (RL-119A)

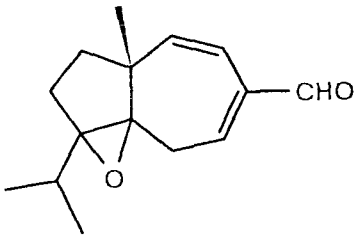

18; isotrienecarotanal epoxide (RL-PERO-4)

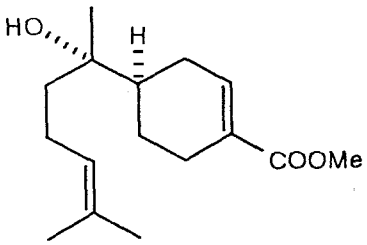

19; bisaborosaol A (RL-116)

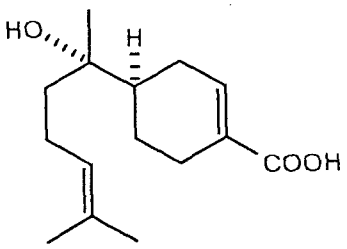

20; bisaborosaic acid A (RL-123A)

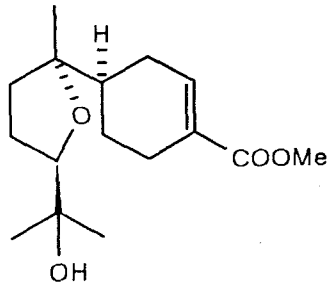

21; bisaborosaol B1 (RL-117B)

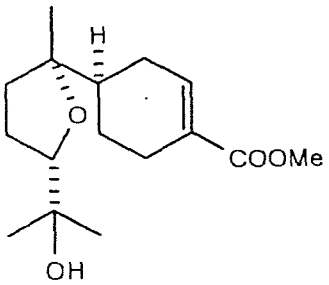

22; bisaborosaol B2 (RL-118B)

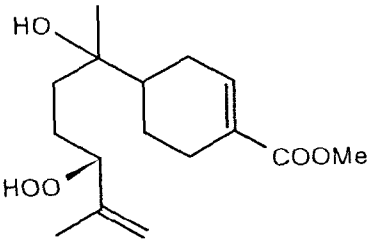

23; bisaborosaol C1 (RL-PERO-5)

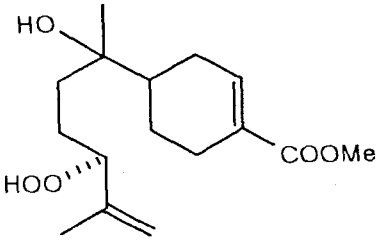

24; bisaborosaol C2 (RL-PERO-6)

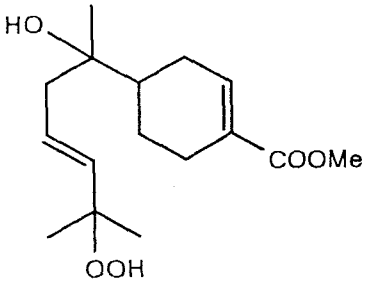

25; bisaborosaol D (RL-PERO-7)

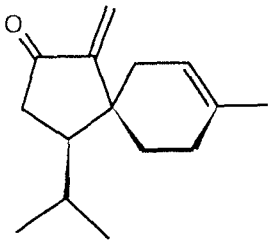

26; rosacoranone (RL-B)

Fig. 1-10b Continued

from Umberifellae

Daucus carota

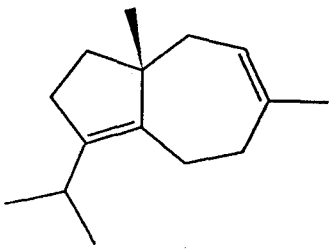

27; daucene [37]

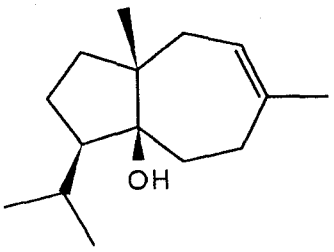

28; carotol [38,39]

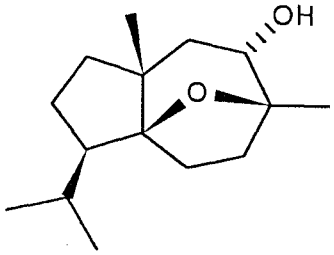

29; daucol [38,39]

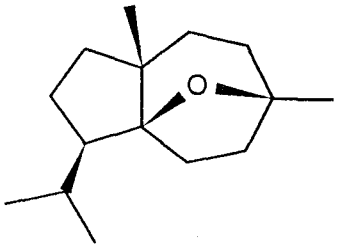

30; carota-1,4-β-oxide [54]

Laserpitium latifolium

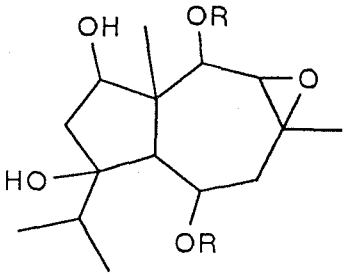

31; isolaserpitin [40]
R=angelate

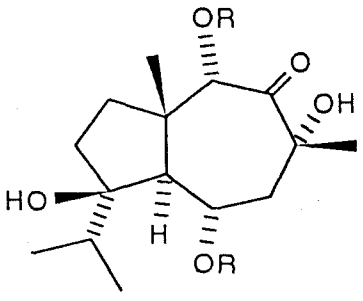

32 R=angelate [41]

Fig. 1-11a Some Naturally Occurring Carotane Sesquiterpenes

Ferula jaeschkeana

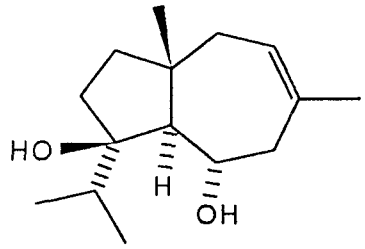

33; jaeschkeanadiol [42]

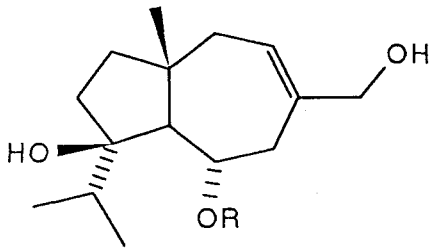

34; feruginidin [52]
R=*p*-hydroxybenzoate

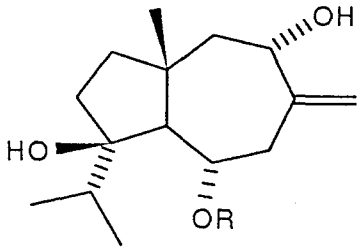

35 R=*p*-hydroxybenzoate [52]

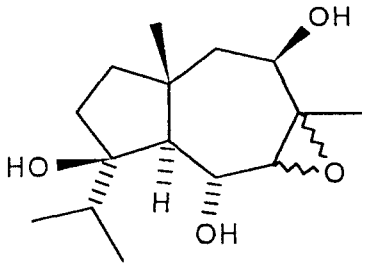

36 [53]

Ferula linkii

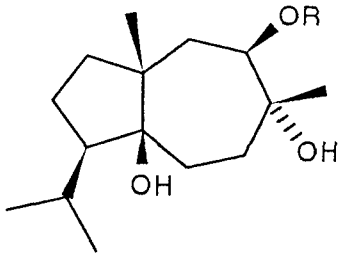

37; linkiol [43]
R=angelate

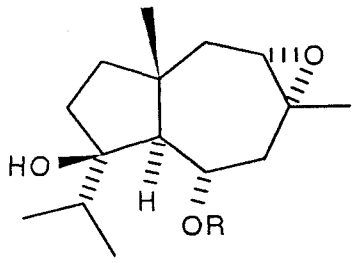

38 R=isovanillate [48]

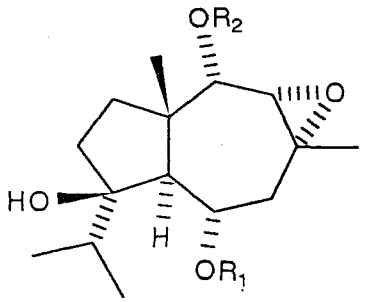

39 R1=angelate, R2=acetate [48]

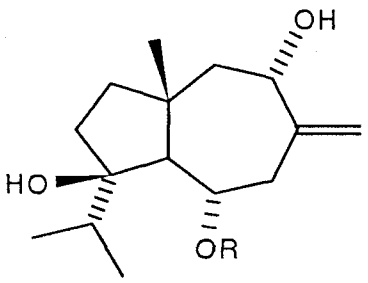

40 R=isovanillate [49]

Fig. 1-11b Continued

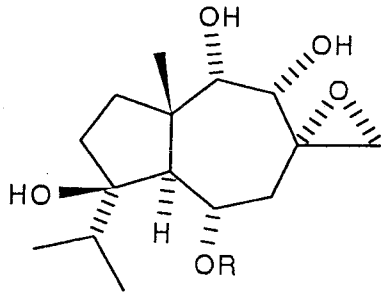

41 R=isovanillate [49]

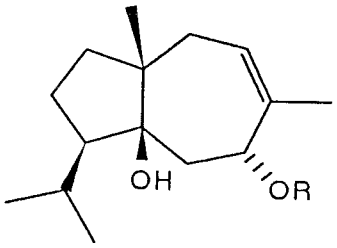

42 R=acetate [50]

Ferula elaeochytris

Ferula tingitana

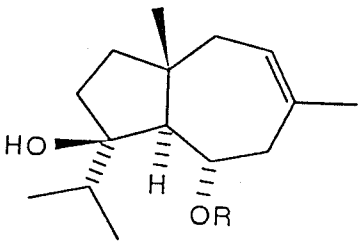

43 R=angelate [44]

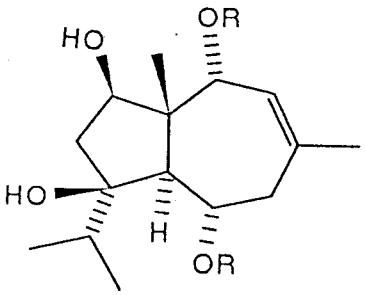

44; tingitanol [45]
R=angelate

Ferula communis (subsp. *communis*)

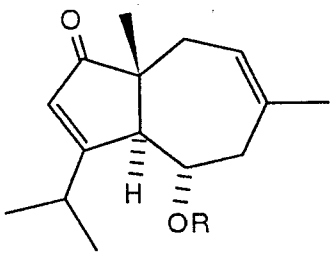

45 R=*p*-anisate [46]

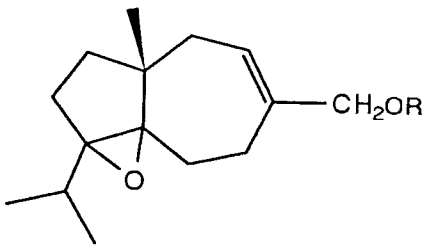

46 R=*p*-anisate [46]

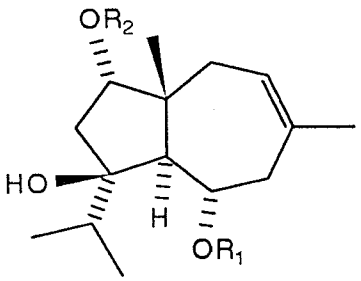

47 R1=benzoate, R2=acetate [46]

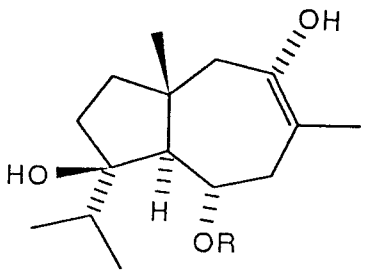

48 R=*p*-anisate [46]

Fig. 1-11c Continued

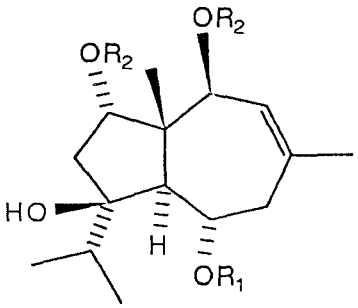

49 R1=*p*-anisate, R2=acetate [46]

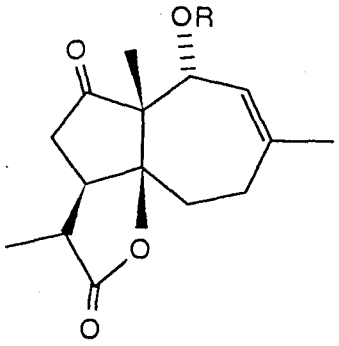

50; fercolide [47]
R=*p*-anisate

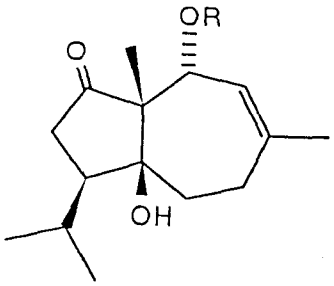

51; fercomin [47]
R=*p*-anisate

Ferula communis

Ferula communis (var. *brevifolia*)

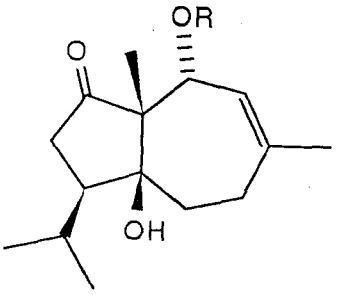

52 R=*p*-hydroxybenzoate [51]

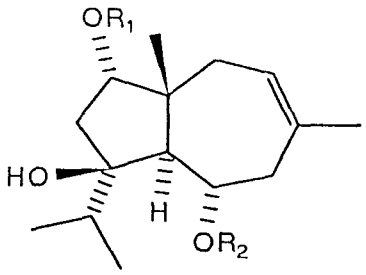

53 R1=*p*-hydroxybenzoate, R2=acetate [55]

Fig. 1-11d Continued

from Compositae

Inula crithmoides

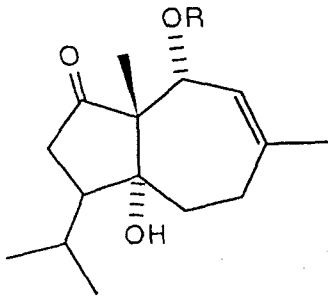

54 R=angelate [56]

Lasinantheae fruticosa

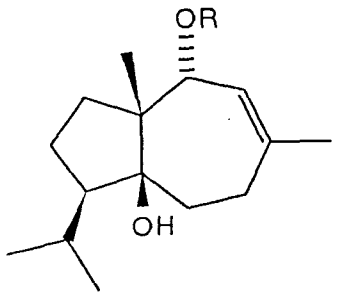

55; lasidiol angelate [57]
R=angelate

Agrratum fastigiatum

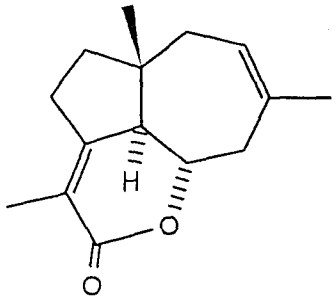

56 [58]

from green moss
(Hepataceae)

Baebilophozia lycopodioides

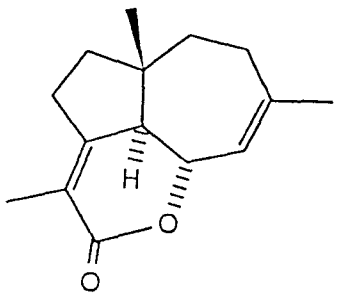

56 [59]

from fungus

Aspergillus terreus

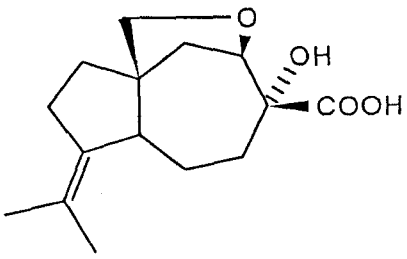

57; aspeterric acid [60]

Fig. 1-11e Continued

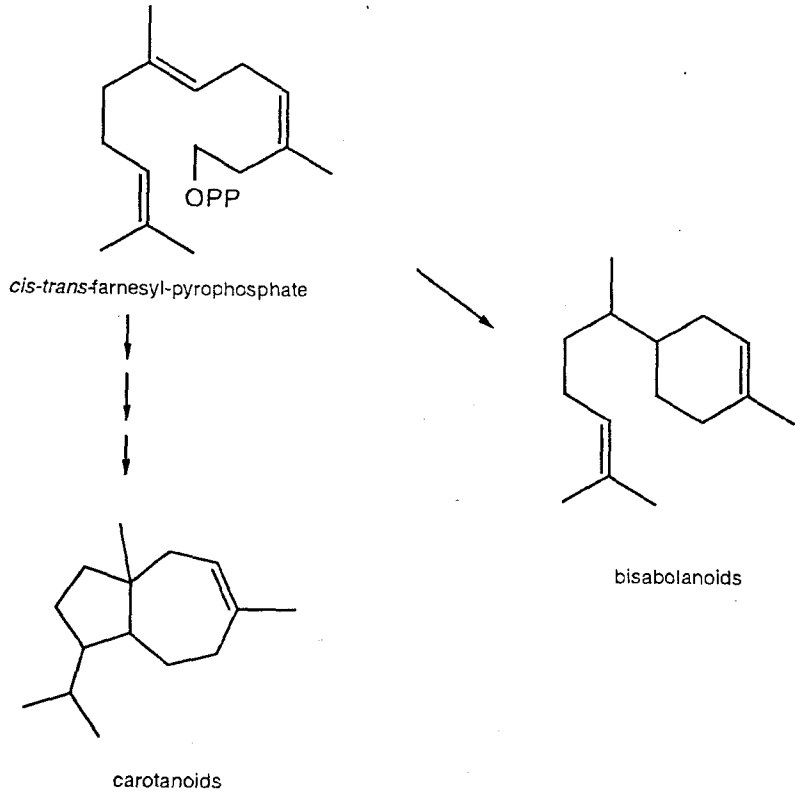

Scheme 1-1 Biosynthetic pathways of carotanoids and bisabolanoids

substance. Successive isolation of the precursor, carota-1,4-dienaldehyde (3) gave further consideration that rugosal A (1) is converted from the precursor through oxidation at the 1,4-diene moiety [66]. In short, carota-1,4-dienaldehyde (3) was found to be comparatively unstable and easily oxygenated by autoxidation to yield some peroxides, one of which is a major and comparatively stable rugosal A that functions in the defense system against microorganisms. Thus, it was suggested that *Rosa rugosa* possessed an effective self-defense system, in which carotanoid plays two roles as an antioxidant during being carota-1,4-dienaldehyde (3), and as an antimicrobial after being oxygenated. This aspect gave a speculation that the defense system in *Rosa rugosa* is a post-inhibitin type of defense system probably depending on singlet oxygen or a lipoxygenase.

The biosynthetic pathway for 1 was, on a basis of the constituents, revealed as shown in Scheme 1-3. On the synthetic pathway of the carotanoids in the tissues, carota-1,4-dienaldehyde (3), rugosal A (1) and rugosic acid A (2) are considered to occupy an main part. The defense substance produced through oxidation of a substrate might be classified into post-inhibitin according to the definition in Table 1-2.

Rosa rugosa and its hybrid cultivars only contain carotanoids. On the contrary, not only carotanoids but also other sesquiterpenoids are rather rare in other *Rosa* plants, and only farnesol (**58**) [67], damascenone (**59**) [68] and bisabolane aldehyde (**60**) [69] are reported (Fig. 3-12). From the view point of phytoalexin, the Rosaceae is also recognized as family commonly lacks the ability for phytoalexin production. Only few phytoalexins are reported in Rosaceae, and are mostly simple phenolics [18,70-73], suggesting family Rosaceae as terpenoid-poor plants (Fig. 1-13).

In *Rosa rugosa*, any sesquiterpenoids in the leaves had not ever been examined, even though some tannins, flavonoids, carotenoids and steroids have well been investigated as major

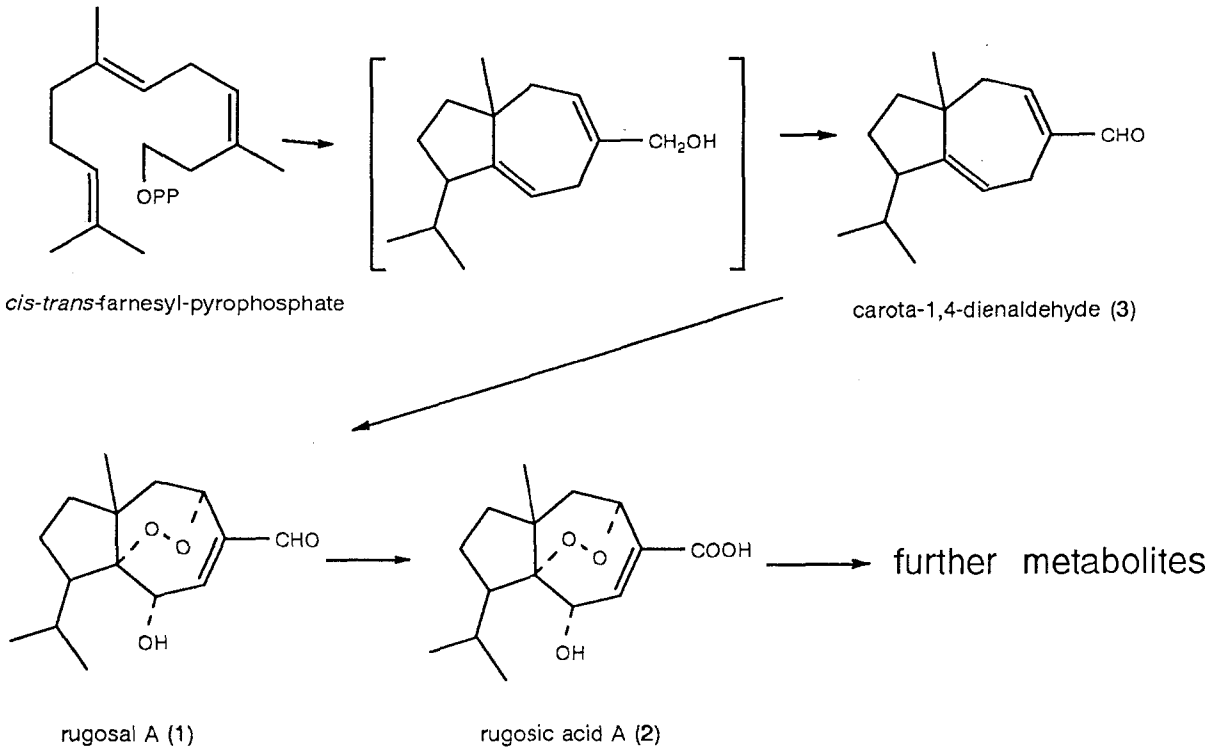

Scheme 1-2 Biosynthetic pathway for rugosal A

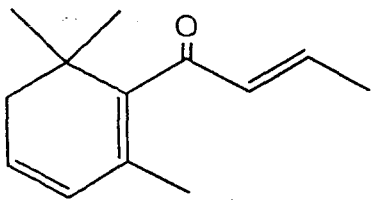

59; damascenone [68]

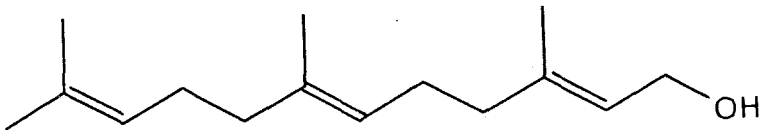

58; farnesol [67]

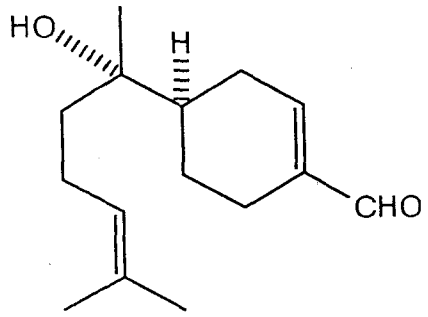

60; a bisabolane aldehyde [69]

Fig. 1-12 Sesquiterpenes from *Rosa* plants

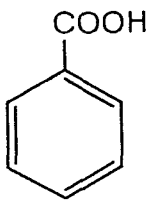

benzoic acid (**61**) [70]

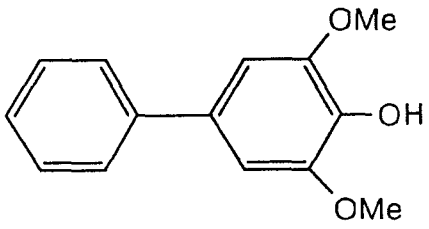

acuparin (**62**) [71]

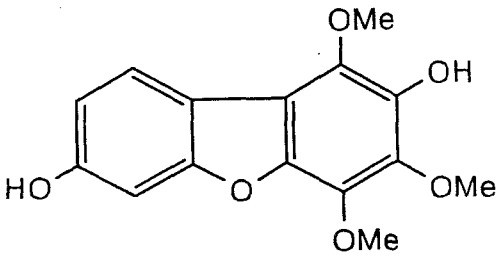

cotonefuran (**63**) [72]

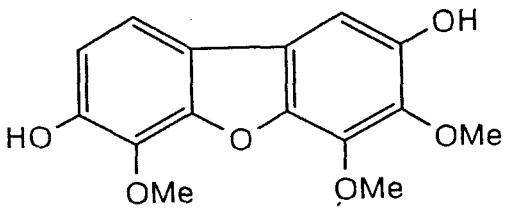

γ-pyrufuran (**64**) [72]

Fig. 1-13 Phytoalexins of Rosaceae Plants

constituents in the aerial parts or the roots [74-81] (Fig. 1-14). Related to the resistance of roses against some pathogen-caused diseases, an interesting research has been carried out by Mashchenko *et al.* [81]. They surveyed the content of sterols in the leaves of several roses including disease-sensitive garden roses, and suggested disease-resistant factor of some wild roses was cholesterol in the leaves; whose contents were four-times higher in the resistant roses involving *Rosa rugosa* than those of the sensitive ones. This result attracted the author's interest, since they tried to explain the resiatant factor of roses against pathogenic infection, only with a chemical substance. As rugosal A (1) was only found in *Rosa rugosa* and its hybrids, their remarkable disease-free nature may be caused by the defence agent.

Rugosa rose (*Rosa rugosa* Thunberg in Fig. 1-15) distributing in the wilderness throughout coastal area of northeast Asia is known as a rare rose resistant to black spot disease which is caused by a fungus *Diplocarpon rosae* and most widely spread among garden roses. For the nature, this wild rose had been introduced into North America to crossbreed with several ornamental roses (Fig. 1-16). As the result, rugosa rose has widely been transplanted and naturalized in northern Europe and eastern North America, especially in coastal area of New England [82].

Rosa rugosa is naturally well adapted to the coastal area. Firstly, this plant has a surprisingly long and deep root system, which may help it to absorb water and nutrients in the coastal sandy soil. Secondly, *Rosa rugosa* propagates itself by rhizome running under the soil of 10-20 cm depth, which may bring advantage for the propagation and colonization on the semi-dried soil. Thirdly, the plant molds a low bush to avoid a strong wind from the sea.

Such a progressive adaptation of a plant, on the other hand, sometimes causes it to lose its flexibility for a new circumstance. Accordingly, most of such plants are died from malnutrition or

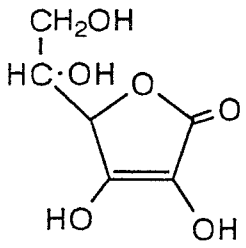

ascorbic acid (65)
[79]

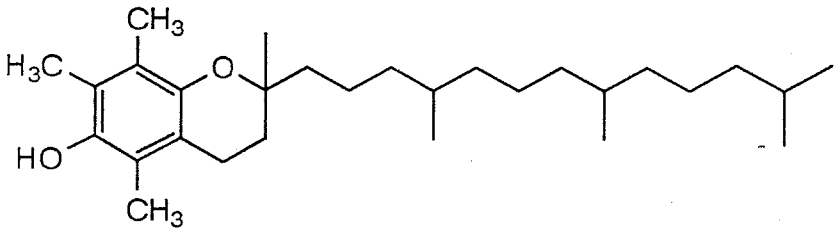

a-tochopherol (66)
[79]

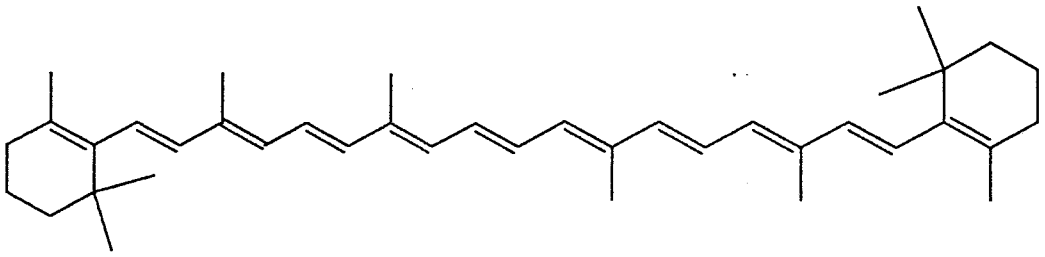

β-carotene (67)
[79]

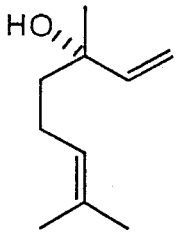

linalool (68)
[74]

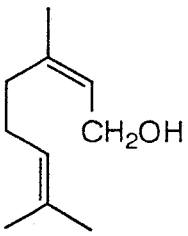

geraniol (69)
[74]

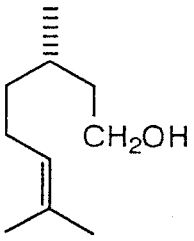

citronellol (70)
[74]

Fig. 1-14a Constituents of *Rosa rugosa*

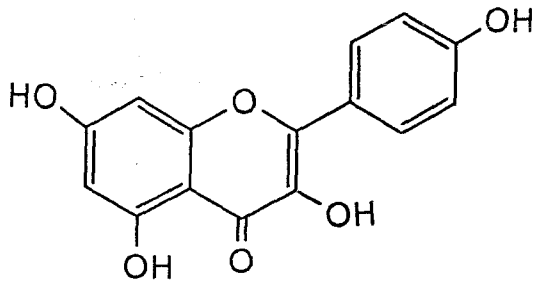

kaempferol (71)
[75]

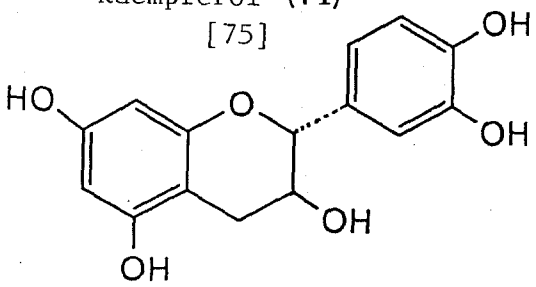

(+)-catechin (72)

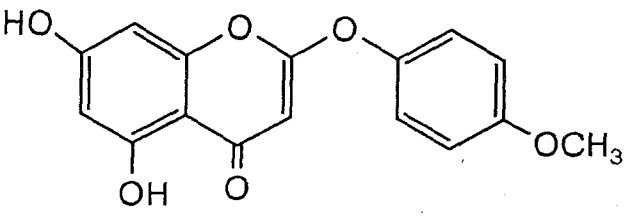

6-demethoxy-4'-methylcapirallisin (73)
[78]

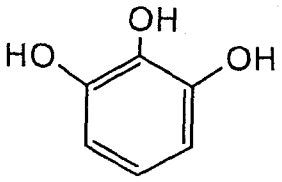

pyrogallol (74)
[78]

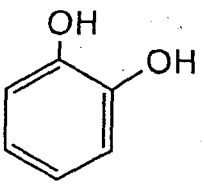

pyrocatechol (75)
[78]

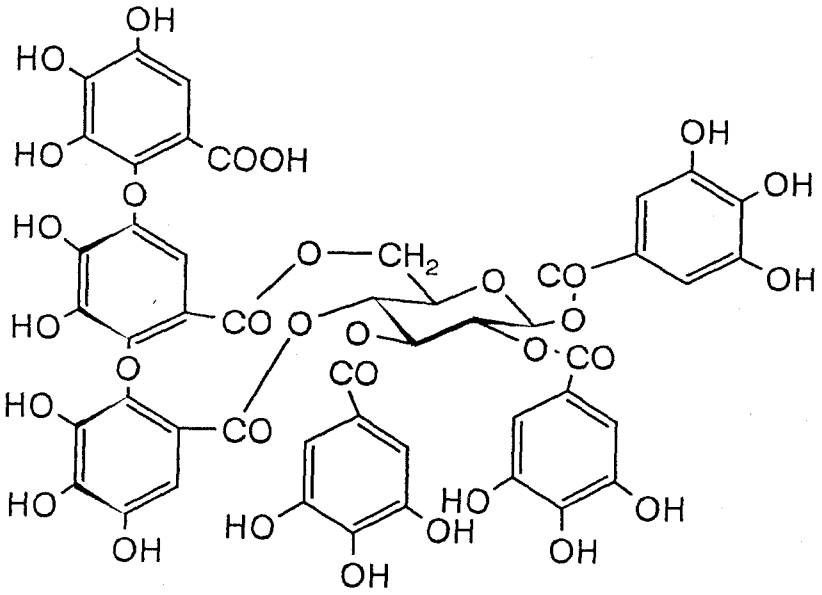

rugosin A (77) [77]

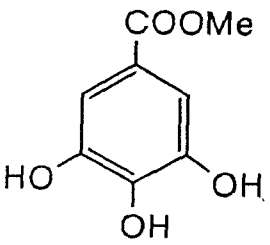

methyl gallate (76)
[78]

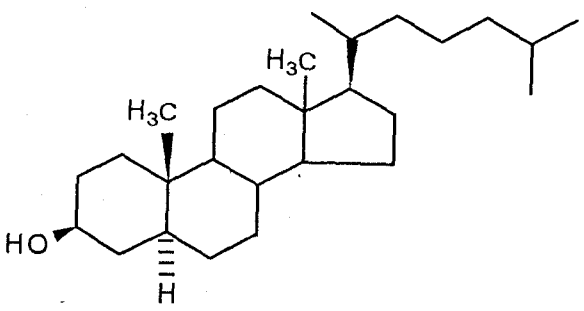

cholesterol (78) [76]

Fig. 1-14b Continued

Fig. 1-9 Rugosa rose (*Rosa rugosa* Thunberg) Aerial and Floral Parts

Fig. 1-10 Distribution of *Rosa rugosa*

• native

/// transplanted

disease by a pathogenic attack. However, *Rosa rugosa* is still tough in a garden where its adaptations to a coastal condition seem not to be so meaningful. In a personal view, the author considers as follows: this rose possesses a quite adaptable nature, and also has an effective manner to control pathogens. Then, what is the other factor? Presumably, the disease-free nature of this wild rose is partly due to the presence of the carotane sesquiterpenoids. In fact, so far as the author's investigation, other Rosaceae are rather poor in sesquiterpenes in their leaves, except rugosa rose hybrids. After a study on *Rosa rugosa* antifungal sesquiterpene has reported in an academic journal, some researchers have pointed out that *Rosa rugosa* is a rare rose which is free from black spot disease of garden roses [83].

Chapter 2 describes general methods and materials, while in Chapter 3, chemical and structural aspects of carotane sesquiterpenes and other sesquiterpenes isolated from *Rosa rugosa* are described in detail. In succession to the introduction (Section 1), isolation, structural elucidation, chemical conversion of rugosal A (1) are described in Section 2. Section 3 is allotted to rugosic acid A (2), an acid corresponding to rugosal A, since this compound provided important information for eventual solution of the planar structure of rugosal A. Chemical properties of the unique endoperoxide bridge on rugosal A and rugosic acid A are mentioned in Section 4, in comparison with those of other peroxides.

In Section 5, carota-1,4-dienaldehyde (3) and its related compounds are described. Firstly, isolation and structural elucidation of rugosal A precursor, carota-1,4-dienaldehyde and a related compound, carota-1,4-dienoic acid (4) are mentioned. Successively, the chemical conversion of carota-1,4-dienaldehyde, including its air oxidation to give rugosal A, rugosic acid A, some byproducts and intermediary peroxide are described. In the last part of this section, the oxidation process is discussed.

Section 6 is allotted to minor carotanoids. In the first part, some carotanoids which were isolated as a metabolites of rugosal A are described, together with short discussion on main biosynthetic and metabolic pathway of *Rosa rugosa* carotanoids. Other minor carotanoids branchig out from the main pathway of carotanoid and being further modified to a oxygenated form are all described in Section 7. Section 8 is for bisabolanoids of *Rosa rugosa*. Not only their chemical aspects but also biochemical relationships with carotanoids and physiological significance are described there. In Section 9, an acoranoid is described. Results of bioassays using the sesquiterpenoids are described in Section 10.

Chapters 4 is assigned to summary and discussion, in which summary of this thesis and further discussion through the thesis, including physiological aspects, are described. Successively, abstract in Japanese and references cited therein are alloted to the end of the thesis.

The novel sesquiterpenes were all given a trivial name with reference to scientific name of the plant, *Rosa rugosa*. Alphabetical order of those trivial names, such as rugosic acid A, was based on the proposed biogenetic scheme. Isolated in the present study were given a compound number, and chemically derivatized products were given a number of their starting natural products with an alphabetical suffix. In the case that two derivatives from different natural compounds exhibit the same structure, those were given the number of original compound which possess younger one. Derivatives having the same structure but different conversion pathway were given same compound number but given different notation.

Chapter 2 Materials and Methods

In this chapter, materials and experimental methods generally used and applied throughout the research are described. Each concrete method is mentioned in the following chapters.

2-1 Plant Materials

The rugosa rose (*Rosa rugosa*) leaves used for preparation of the organic substances were collected at the campus of Hokkaido University in Sapporo or at Ishikari coastal area in Hokkaido, during summer seasons in 1986-1989. Usually, the compound leaves were wrested from the stems, leaves in budding stage which were separated from the shoots cut with a sharp cutter. As mentioned in Chapter 3, sesquiterpenes in *Rosa rugosa* leaves show a dynamic change through development and maturation of the leaves. The date of collecting leaves materials is therefore recorded here (Table 2-1).

Table 2-1 Rosa rugosa *leaves collected in Ishikari beach*

Sample	Date	Fresh weight	Main use
I	5th June 1986	4.6 kg	$CuCl_2$ treatment
II	25th June 1986	1.3 kg	rugosal A isolation
III	5th August 1986	3.4 kg	rugosic acid A isolation
IV	25th June 1987	7.1 kg	constituent survey
V	22th May 1987 - 24th July	9.6 kg	constituent survey
VI	31st August 1987	1.0 kg	constituent survey
VII	6th July 1988	6.0 kg	precursor isolation
VIII	24th September 1988	0.6 kg	metabolite survey

2-2 Spectrometry and Chromatography

Here, analytical instruments including measuring conditions are described. Chromatographic materials and detecting reagents are also mentioned here.

2-2-1 Instrumantation

1) Gas Liquid Chromatography (GLC)

A Shimazu GC-4CM (FID) equipped with a glass column (4 mm i.d. x 1.0 m) packed with 5 % PEG 20 M on 80/100 mesh Celite AW. Carrier gas: N_2, 40 ml/min. Initial temp. at 120 °C, programmed at a rate of 5 °C/min. The gas chromatograph was mainly used for the detection of carotane aldehyde dienes.

2) High Performance Liquid Chromatography (HPLC)

A Jasco (Japan Spectroscopic Co., LTD) 10G 115H equipped with a 20 mm i.d. x 20 cm column of Unisil Q 100-5 (5 μm) (with pressure meter PG-350D and UV detector UVIDEC-100-II) was used, mainly for the purification and isolation of the *Rosa rugosa* constituents. Samples for HPLC were injected as *n*-hexane solutions. A flow rate and chart speed were usually set at 2 ml/min and 5 mm/min, respectively.

3) Mass Spectrometry (MS)

A JEOL JMS-DX-300 computerized with JEOL JMA-5000 for EI-MS, EI-HR-MS and GC-MS analyses (ionization potential 70 eV) and JEOL JMS-OISG-2 computerized with a JEOL JMA-2000 for FI-MS and FD-MS analyses were effectively used in the present study.

4) Nuclear Magnetic Resonance Spectrometry (NMR)

Three kinds of the spectrometer were used for various NMR

analyses. A JOEL JNM GX-500 for ^{1}H- (NON, DEC) NMR analyses. JEOL JNM GX-270 for ^{1}H- (NON, COSY, DEC, NOE, NOESY) NMR and ^{13}C- (COM, OFF RESONANCE, INEPT, INADEQUATE, *J* RESOLVED, CH-COSY) NMR analyses. A Brucker AM-500 for ^{1}H- (NON, DEC, COSY, NOE, NOESY) and ^{13}C- (COM, DEPT, CH-COSY, COLOC) analyses. Analytical conditions (solvent and MHz) are given to each figure or table. As an internal standard, TMS was used in all NMR.

5) Infrared Spectrometry (IR)

On a Hitachi Model 285, samples were usually measured as a KBr disc, a CCl_4 solution, or a thin film between KBr discs. An absorbance of polyethylene film at 1601.5 cm-1 was recorded for correction of wave numbers.

6) Ultra Violet Spectrometry (UV)

A Hitach Model EPS-3T Spectrometer, and a Hitach U-3210 Spectrometer were used. Solvent used is shown in each table. A methanolic HCl solution was used as a shift reagent.

7) Optical Rotatory Dispersion (ORD) and Circular Dichroism (CD)

JASCO Model J-20. Cell length, solvent and sample concentration are added to each table.

8) Melting Point (mp)

Melting points were determined by the micro hot-plate method. The melting points were uncorrected.

2-2-2 Chromatography

1) Column Chromatography (CC)

Wako-gel C-200 (Wako Pure Chemical Industries, Ltd.) was used

for column chromatography of low molecular plant constituents. Organic solvent used in the present study was abbreviated as follows:

n-hexane: H
acetone: AT
benzene: B
chloroform ($CHCl_3$): C
dichloromethane (CH_2Cl_2): DCM
methanol (MeOH): M
ethyl acetate (EtOAc): EA
formic acid (HCOOH): FA

mixed solvent:
n-hexane:EtOAc = *x*:*y* ⟶ abbreviated to H-EA *x*:*y*
a mixture containing *x* % of EtOAc in *n*-hexane, v/v ⟶ *x* % EA/H

2) Thin Layer Chromatography (TLC)

Art 5715 DC-Fertigplatten Kieselgel $60F_{254}$ (Schichtdicke 0.25 mm), Merck Ltd, mainly for preparative TLC (PTLC) and TLC bioautography. Art 5744 DC-Fertigplatten Kieselgel $60F_{254}$ (Schichtdicke 0.5 mm), Merck Ltd, for PTLC. Art 5554 DC-Alufolien Kieselgel $60F_{254}$ (Schichtdicke 0.2 mm, aluminum sheets), Merck Ltd, for compound detection and colorization test with a spray reagent.

Compounds on TLC were detected under UV light, or by spraying colorization reagents as followes:.

a; UV light (short wave, 2536 A): UV can detect a compound possessing a conjugation system in the molecule as a quenching spot on a silica gel thin-layer impregnanted with a fluorescer.

b; Vanillin-H_2SO_4 reagent (vanillin-EtOH-conc. H_2SO_4 0.5 g: 20 ml:80 ml): The vanillin-H_2SO_4 reagent is applicable to most of terpenoids and fatty acids, but this reagent shows a negative response to most of aromatic compounds [84]. This reagent was sprayed onto TL plates which had previously been developed, at which point the plates were heated on an electric heater until a clear coloration appeared. The vanillin-H_2SO_4 test is useful in checking the purity of an interested compound, and sometimes used as a marker to detect compounds containing specific part structure (*e.g.* yellow colorlation to tetrahydrofurane derivatives).

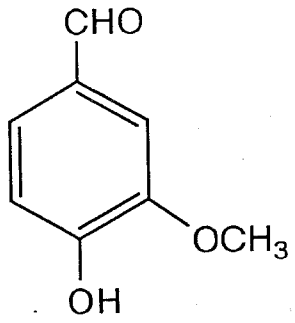

vanillin

c; *N,N*-dimethyl-*p*-phenylenediamine sulfate reagent (0.5 g in 50 ml AcOH): *N,N*-dimethyl-*p*-phenylenediamine sulfate reagent was used in the peroxide detection test [85]. On the peroxide test, a typical peroxide shows coloration of a pinkish red on TL plates, and some endoperoxides which possess an aldehyde group in the molecule indicate a weak and reddish yellow color. In this case, the response can be sensitized by heating. This reagent is sensitive enough to detect a trace amount of a peroxide, and an exoperoxide tends to give a wider coloring area than that of an endoperoxide.

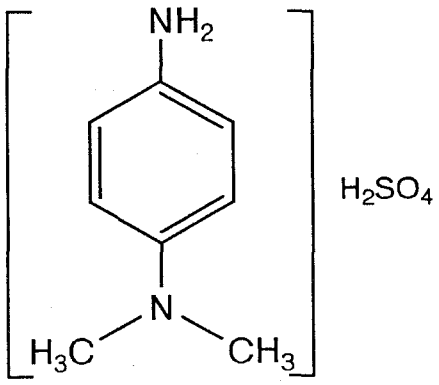

N,N-dimethyl-*p*-phenylenediamine

d; dinitrophenylhydrazine (DNPH) reagent (0.1 g in 100 ml of 1 % conc. HCl/EtOH): DNPH reagent known as a carbonyl reagent is also used in the present study. By spraying this reagent, carbonyl compounds (ketones and aldehydes) show a yellow/orange colorl [86].

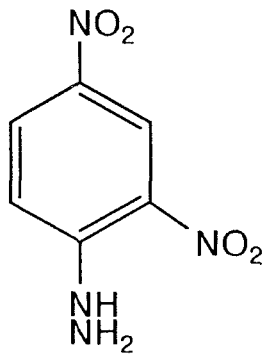

dinitrophenylhydrazine

2-3 Bioassay

2-3-1 Antimicrobial Assay

1) TLC Bioautography

Cladosporium herbarum (AHU 9262, from Laboratory of Applied Microbiology, Hokkaido University) was used as a test fungus. The fungus inoculated on an agar (PYG; 5 % glucose, 1 % peptone, 0.1 % yeast extract, and 2 % agar in distilled water) produces deep green spore after 1 week incubation. Onto this slant, 5-10 ml of a salt mixture (0.1 % NaCl, 0.7 % KH_2PO_4, 0.3 % $Na_2HPO_4.2H_2O$, 0.4 % KNO_3, and 0.1 % $MgSO_4 \cdot 7H_2O$ in deionized water containing 2 drops of Tween 20 per 100 ml) was poured and shaken enough to obtain a spore suspension. After filtration through gauze, 60 ml of the spore suspension was further mixed with 10 ml of 30 % glucose solution. This suspension was uniformly sprayed onto TLC plates previously developed or absorbed the test samples. The plate was then kept in an incubator for 2-3 days at 25 °C in the dark and moistured condition. An area absorbed an antifungal substance appears as a white zone [87].

2) Paper Disc Method as an Antimicrobial Assay

Agar plates were similarly prepared to that for the slant to grow *Cladosporium herbarum*. To each agar plate (10 ml, 2 % agar), 2 ml of a microbial/0.2 % agar suspension (kept at 40 °C) was poured and was spread on the plate. After the medium was cooled enough, paper discs (8 mm diameter x 2 mm thickness) charged an acetone solution (25 µl) of a test compound and removed the solvent in a desiccator, were put on. The plates were kept at 25 °C in the dark for 1~3 days [88].

3) Spore Germination Assay and Field Assay

An inhibitory activity against plant pathogens was examined by

spore germination assay. Using several plant pathogens, this assay was carried out by Hokko Kagaku Kogyo, K. K.

2-3-2 Other Bioassay

1) Antifeedant Assay

Antifeeding activity was also examined. The antifeedant assay was carried out by Hokko Kagaku Kogyo K.K., using larva of rice moss (rice worm, *Chilo suppressalis*) and armyworm (*Prodenia litura*) fed a artificial solid-feed.

2) Cytotoxic Assay

The *in vitro* cytotoxic assay was carried out by Japan Tobacco Industry Co. using mouse leukemia cell line, P-388.

2-4 Chemicals and Other Reagent

2-4-1 Abbreviation of Chemicals

Chemical reagents frequently used in the experiment were mostly described with abbreviation form. The abbreviation on the thesis was listed below, except organic solvents which were shown in Section 2 of this chapter and widely accepted one (for example HCl, or NaCl).

m-CPBA	*metha*-chloroperoxybenzoic acid
p-TSA	*para*-toluenesulfonic acid
PCC	pyridinium chlorochromate
TsCl	*para*-toluenesulfonyl chloride
Et_3N	triethylamine
THF	tetrahydrofuran

2-4-2 Authentic Compounds

1) 4*S*,8*S*-(-)-α-Bisabolol

This sesquiterpene was used as a material of chemical synthesis. The sample was purchased from Funakoshi Yakuhin K.K

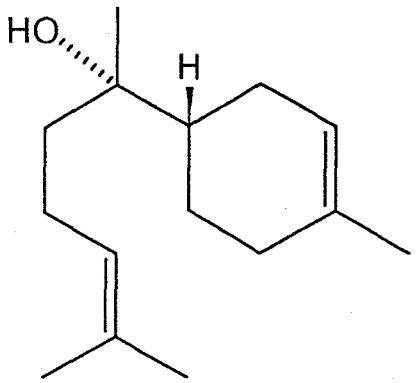

(-)-α-bisabolol

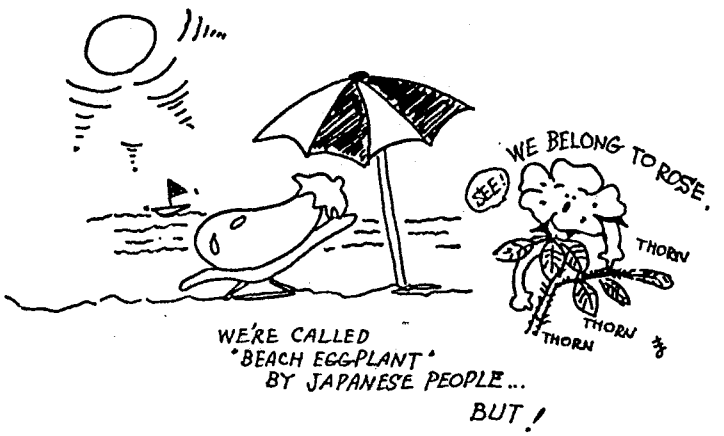

Chapter 3 Sesquiterpene in *Rosa rugosa*

3-1 Introduction

Carotanoids are, as being described in Chapter 1, a major sesquiterpenes found in *Rosa rugosa* leaves as a series of the secondary metabolites and the defense substances [36]. As 5,7-bicyclic sesquiterpenoids are known four kinds of skeletal variation, guaianoids, pseudoguaianoids, isocarotanoids, and carotanoids (Fig. 3-1). Unlike guaianoids widely distributed throughout higher plant families, the presence of carotanoids has been restricted to Umbelliferae (Apitaceae) [37-55], Compositae (Asteraceae) [56-58] and few primitive plants - a green moss *Barbilophozia lycopodioides* (Hepaticeae) [59] and a fungus *Aspergillus terreus* [60] (See Fig. 1-2).

Biochemically, carotanoids are synthesized from *cis-trans*-farnesyl-pyrophosphate via a branch of bisabolanoid biosynthesis pathway, as shown in Scheme 3-1 [63]. In fact, Umbelliferae and

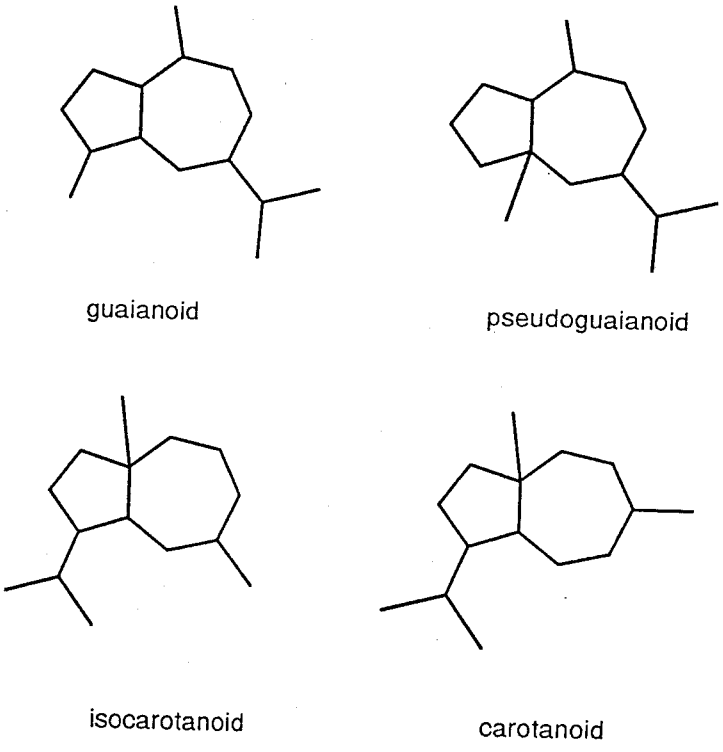

Fig. 3-1 5,7-Bicyclic Sesquiterpene Skeletons

Compositae are an abundant source of bisabolanoids [64,65], and from *Rosa rugosa* (Rosaceae) having been known as the third family of carotanoid source, some bisabolanoids have also been found [89] as described in Chapter 1. A remarkable skeletal feature of carotanoids in *Rosa rugosa* is regio-specific oxygenation at the C-14 carbon to yield an aldehyde or a carboxyl group, which is mostly conjugated with an olefinic bond to form an α,β-unsaturated carbonyl compound.

Research or survey of sesquiterpenes in Rosaceae seems to be rarely carried out, probably because researchers had only paid their attention into the monoterpenes of this family which occupies an important area in flavor chemistry. In *Rosa rugosa*, flavonoids [75,78], carotenoids [79] and polyphenolics [77,80] have well been studied in addition to monoterpenes [74] and steroids [76] (See Fig. 1-3); however, survey of sesquiterpenes had been abandoned as with other Rosaceae plants.

In this chapter, the author describes sesquiterpenes in *Rosa rugosa* mainly from view points of organic chemistry and of biogenesis.

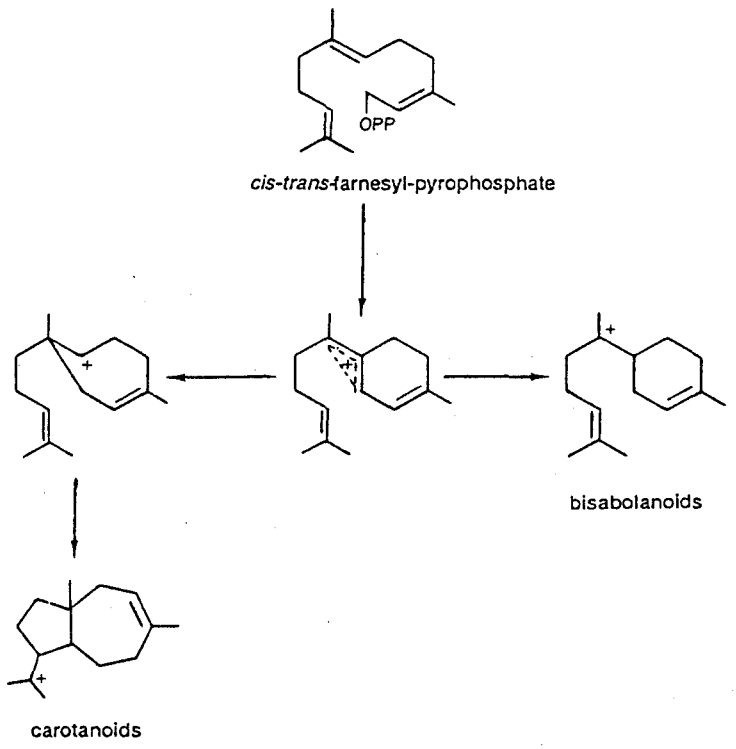

Scheme 3-1 Biosynthetic Pathway for Carotanoids and Bisabolanoids

3-2 Antifungal Sesquiterpene, Rugosal A

3-2-1 Survey and Isolation of Antifungal Substance

Initial attention to an antimicrobial agent in *Rosa rugosa* was drawn by an observation that aqueous diffusates of wounded *Rosa rugosa* leaves inhibited the growth of microorganisms, contrary to water steeped with uninjured one (Fig. 3-2). For the purpose of confirming the presumable antimicrobial substance(s) diffused into the water from the damaged leaves, 1.3 kg of fresh leaves (Sample II) were mechanically and slightly injured with a wooden hammer, and then soaked in *ca* 7 liters of tap water to cover 4/5 leaves and kept at 25 °C in darkness for 12 hr. At which point the leaves were once turned over and successively soaked for another 12 hr. Then, all the water layer slightly browned and presumably containing the diffusates from the damaged leaves was collected, and was once extracted with 2000 ml of EtOAc.

The EtOAc layer was dried over Na_2SO_4, and then concentrated *in vacuo* to give *ca* 3 g of solubles. The extract tentatively named CR fraction was partly subjected to a silica gel thine-layer (TLC) (developed in H-EA 4:1) for testing its antifungal activity by TLC bioautography using *Cladosporium herbarum* [87,90]. Under a diluted condition (5 µl/ diffusate from *ca* 25 mg of the leaf tissues), CR fraction gave only one antifungal area around *Rf* 0.3 where a quenching spot was observed under UV 256 nm light on F_{256} plates (Fig. 3-3).

Being focused the antifungal substance, the extractives were fractionated by silica gel column chromatography. As shown in Table 3-1, CR fraction was eluted with a mixture of *n*-hexane-EtOAc, and the focused substance was contained in Fr-3, 4 and 5 as shown in Fig. 3-4. Fr-4 mainly involving the substance yielded crystallines when the concentrated eluate was chilled in the refrigerator overnight. The crude crystallines were subsequently

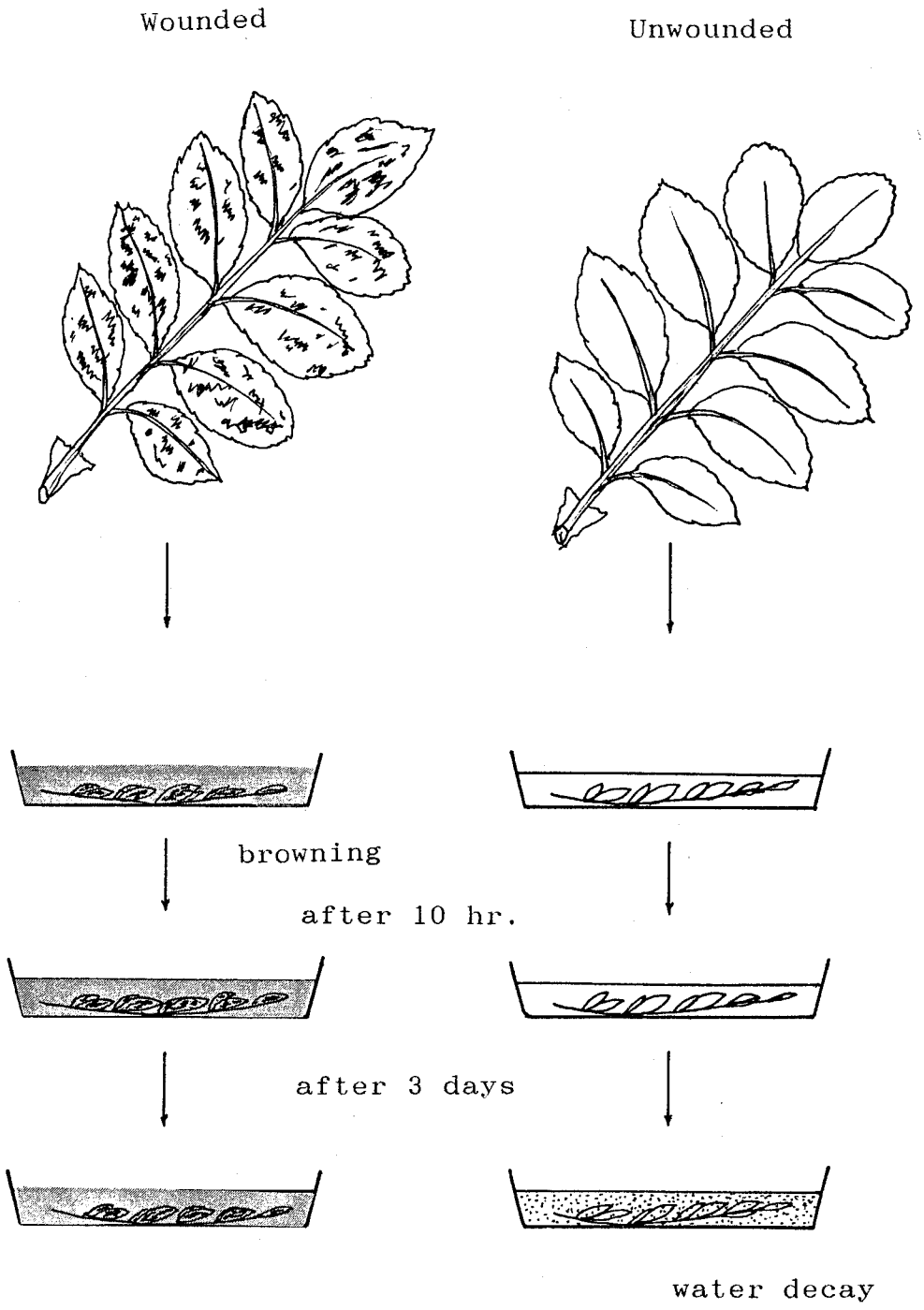

Fig. 3-2 Initial Observation of an Antifungal Factor in Injured Leaves of *Rosa rugosa*: The leaves used in this treatment were collected in early June

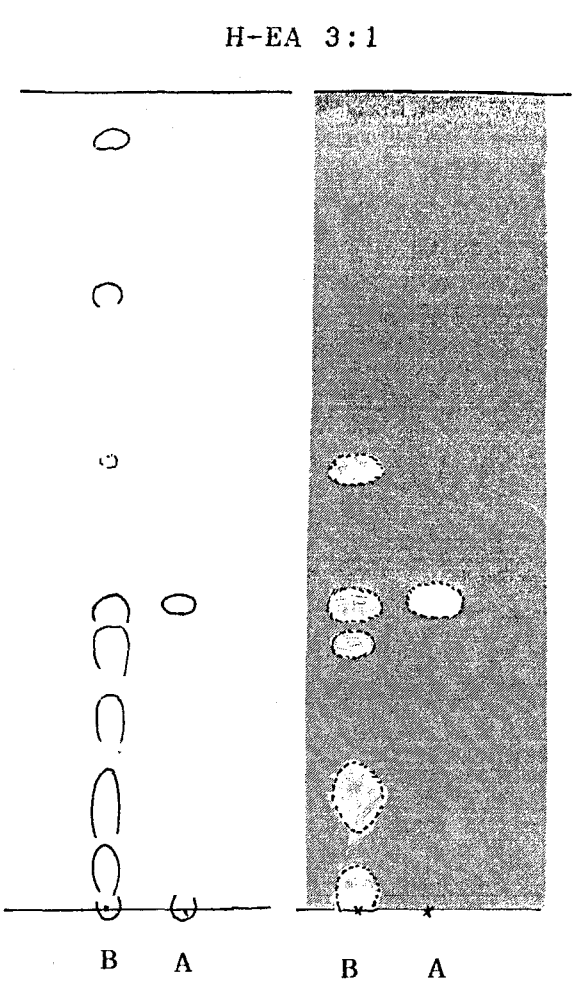

Fig. 3-3 Direction of an Antifungal Substance in the Diffusates from Damaged and healthy *Rosa rugosa* leaves: (A) 25 g of pinnates of *Rosa rugosa* leaves mechanically damaged were soaked in distilled water (250 ml) and then the aqueous layer was extracted with 100 ml of EtOAc. The organic layer was concentrated to 5 ml, whose 5 µl (corresponding to the diffusates from 25 mg fresh leaves) was charged on TLC. (B) 10 g of uninjured leaves were extracted with EtOAc (250 ml), and the concentrated (5 ml) whose 5 µl (corresponding to the diffusates from 10 mg fresh leaves) was also charged on TLC.

Table 3-1 Eluants of silica gel column chromatography for CR fraction (from Sample II)

Fraction	Eluting solvent	Volume (ml)
Fr-II-1	50 % EtOAc/*n*-hexane	100
Fr-II-2	50 % EtOAc/*n*-hexane	40
Fr-II-3	50 % EtOAc/*n*-hexane	40
Fr-II-4	50 % EtOAc/*n*-hexane	40
Fr-II-5	50 % EtOAc/*n*-hexane	40
Fr-II-6	50 % EtOAc/*n*-hexane	40
Fr-II-7	50 % EtOAc/*n*-hexane	40
Fr-II-8	50 % EtOAc/*n*-hexane	40
Fr-II-9	50 % EtOAc/*n*-hexane	40
Fr-II-10	50 % EtOAc/*n*-hexane	40
Fr-II-11	50 % EtOAc/*n*-hexane	40
Fr-II-12	50 % EtOAc/*n*-hexane	40
Fr-II-13	50 % EtOAc/*n*-hexane	40

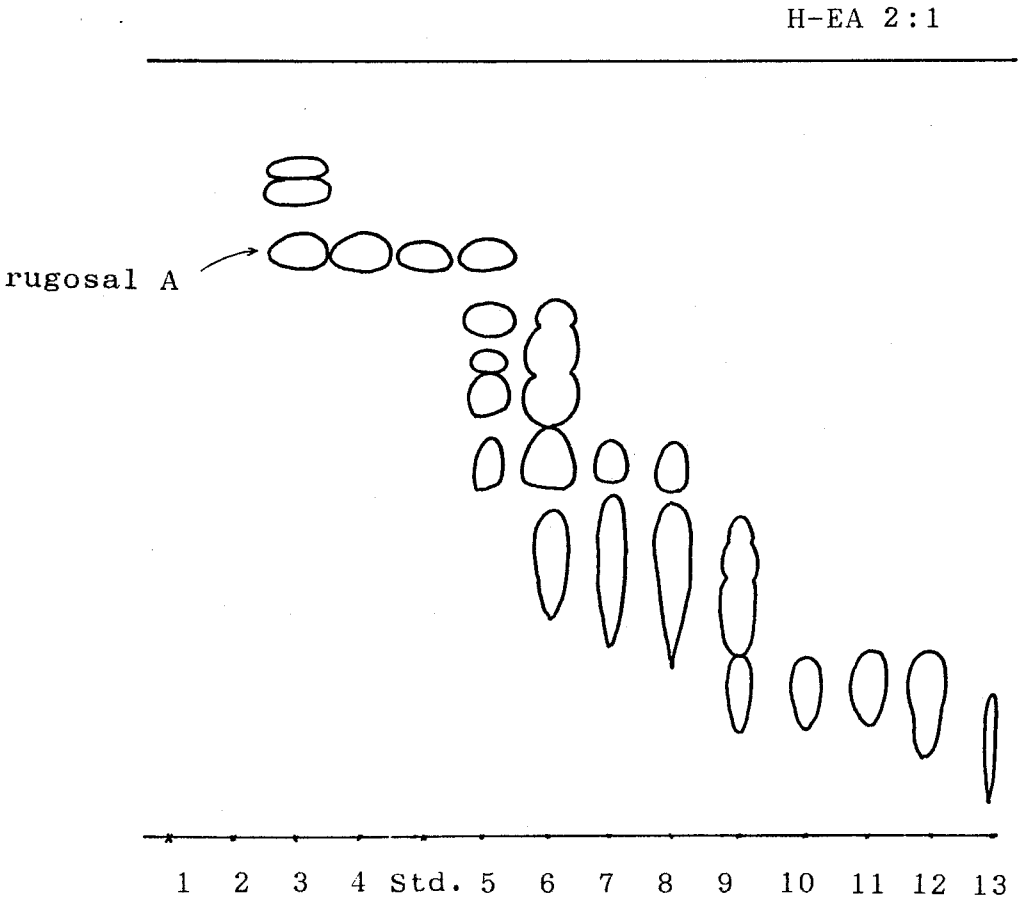

Fig. 3-4 TL Chromatogram of CR Fraction Eluted from Silica gel Column: Std.= "rugosal A" (see pp. 48)

washed with *n*-hexane and recrystallized from *n*-hexane containing *ca* 15 % EtOAc to give 74 mg of pure colorless needles. Furthermore, another 45 mg of the substance was isolated from Fr-II-3, Fr-II-5 and the mother liquor and washings of Fr-II-4 by PTLC (H-EA 3:1). Those isolates were used for determination of the structure by spectroscopic and chemical methods. The compound was consequently found to be a novel sesquiterpene and named "rugosal A".

On the other hand, rugosal A as a constituent of uninjured *Rosa rugosa* leaves were carefully surveyed. Subsequently, rugosal A was undetectable in the diffusates from the uninjured leaves soaked aqueous solution of 3 mM of $CuCl_2$ or tap water. However, as the result of survey in MeOH extracts of the uninjured leaves, a marked amount of rugosal A was detected during a partial purification by PTLC (B-EA 5:1). Through a rough quantitative determination of rugosal A in the MeOH extract (using UV method), it was revealed that 2-3 times of inherent rugosal A was contained in the fresh leaves, compared with that in the diffusates. Consequently, rugosal A was considered to be a defense agent not inducibly produced in the wounded tissues but involved inherently accumulated in the tissues.

3-2-2 Elucidation of the Structure (by Spectroscopic Analyses)

1) UV, EI-MS, FI-MS and IR Analyses

FI-MS analysis revealed M^+ 266 (100 %) for rugosal A (Fig. 3-5), and EI-HR-MS indicated its molecular formula $C_{15}H_{22}O_4$ (found, 266.156; calcd., 266.152). EI-MS fragmentation was indicative of the presence of an -OH group (*m/z* 248; M^+-18, 3.1 %), a -CHO group (*m/z* 237; M^+-29, 4.5 %) and a $-CH(CH_3)_2$ group (*m/z* 205; M^+-H_2O-43, 4.0 %). A fragment at *m/z* 233 (M^+-33, 1.6 %) was also observed, although its fragmentation was uncharacterized at that point. Other major fragments at *m/z* 109 (28 %), 69 (100 %) and 55 (62 %) were also detected (Fig. 3-6), suggesting a sesquiterpenoid property of this compound, together with its molecular formula.

A methanolic UV maximum was observed at 228 nm (ε 7400) as a simple absorption peak, which can be deduced to a conjugation

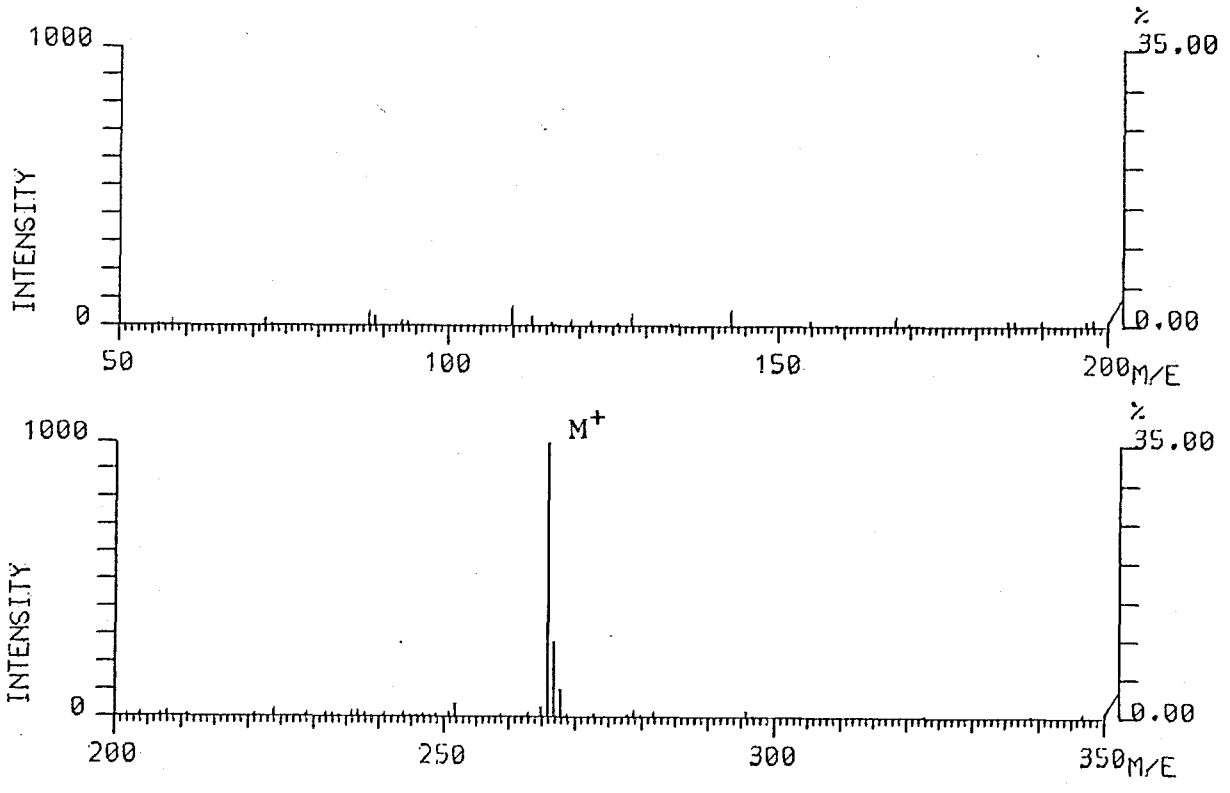

Fig. 3-5 FI-Mass Spectrum of Rugosal A

system *e.g.* an α,β-unsaturated carbonyl group. As another notable property in UV spectrum, rugosal A showed a complete disappearance of the absorption when some drops of 1N HCl was added to the MeOH solution (Fig. 3-7). A collapse of the conjugation system was speculated on this observation. The mechanism for this phenomenon was elucidated later; however, at that moment it was only presumable that the conjugation system, probably attributable to an α,β-unsaturated aldehyde group, is somehow unusually labile under acidic conditions.

IR spectrum of rugosal A (KBr disc) was indicative of the presence of an α,β-unsaturated aldehyde group (λ_{max} 2820 and 2730 cm^{-1}; O=C-H, 1690 cm^{-1}; =C-C=O) and a hydroxyl group (λ_{max} 3450 cm^{-1}, sharp). Especially, the sharp absorption band in the hydroxyl area was indicative of an intra- or inter-molecularly hydrogen-bonding OH group (Fig. 3-8) [91]. To examine the exact property of this hydroxyl group, the IR spectrum was measured in a highly diluted non-polar solution (0.3 mM in CCl_4), and consequently its intramolecular hydrogen-bonding property (λ_{max} 3563 cm^{-1}, sharp) was proved [91].

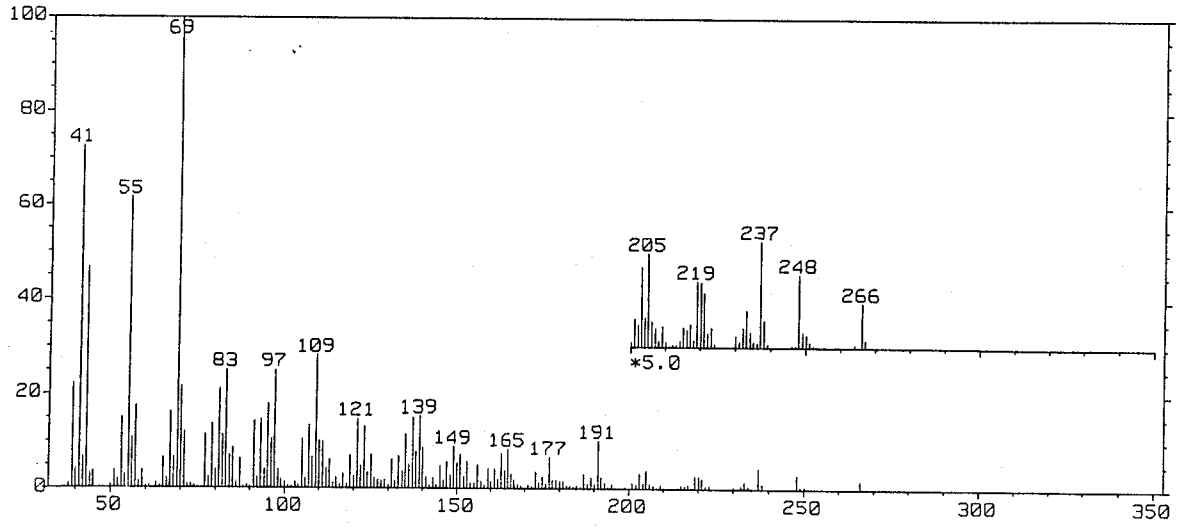

Fig. 3-6 EI-Mass Spectrum of Rugosal A

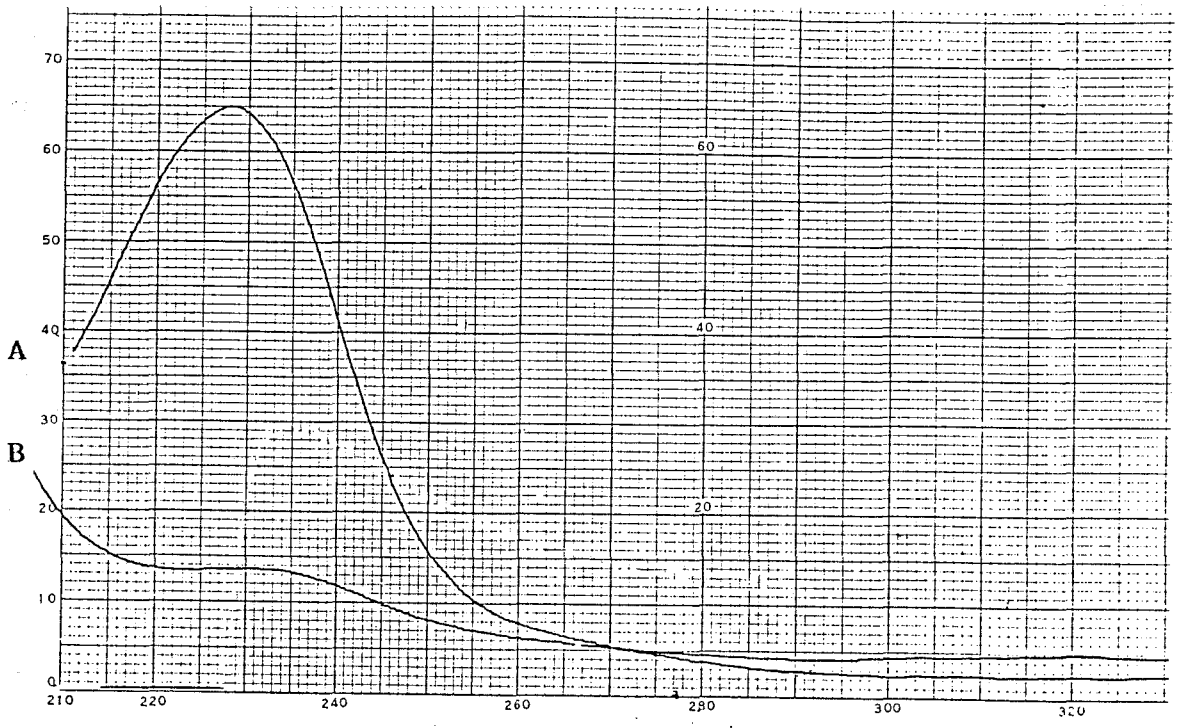

Fig. 3-7 UV Spectra of Rugosal A (in MeOH)

A: in MeOH

B: in MeOH with minute HCl

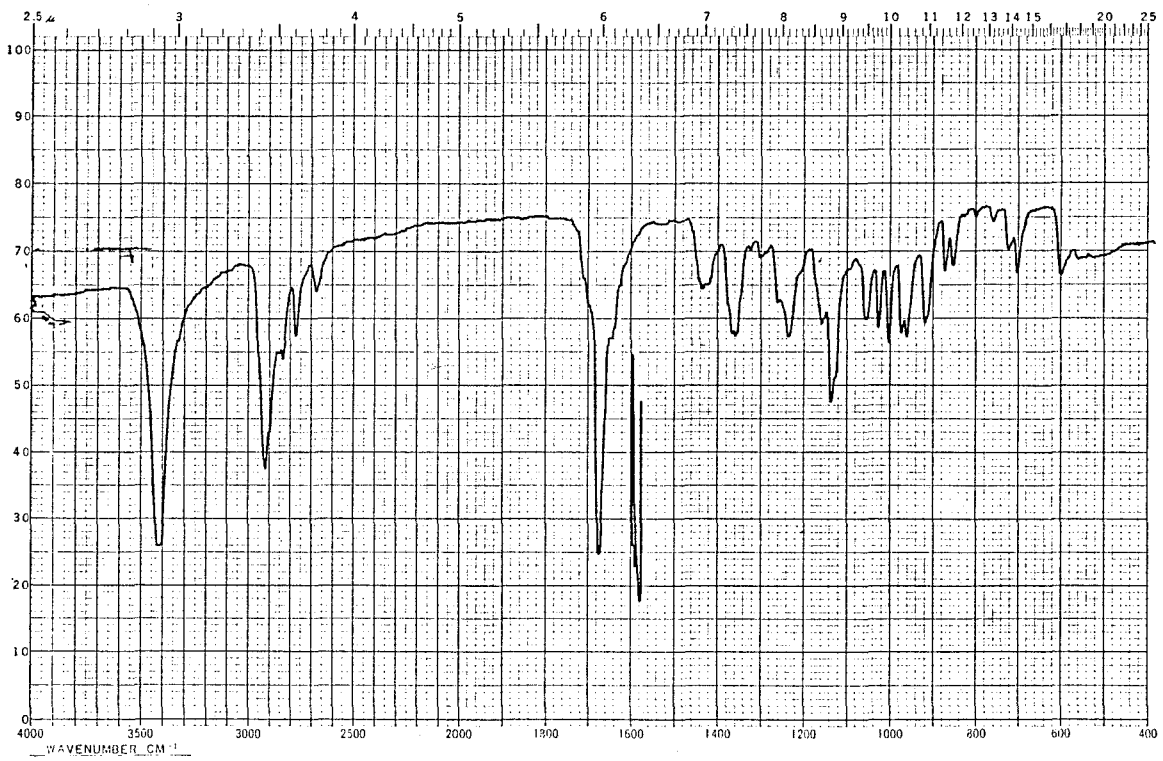

Fig. 3-8 IR Spectrum of Rugosal A (KBr disc)

2) Elucidation of the Substructure by NMR Analyses

^{1}H-NMR analyses (NON, 270 MHz in $CDCl_3$) proved the presence of an aldehyde group (δ_H 9.539, 1H, s), an olefinic proton (δ_H 6.850, 1H, dd, J= 6.0 and 1.1 Hz), an isopropyl group (δ_H 0.980 and 0.946, each 3H, d, J= 6.6 Hz, and δ_H 2.630, 1H, double sept., J= 6.9 and 2.2 Hz) and a methyl group probaply as a resident on a quarternary carbon (δ_H 0.883, 3H, s) (Fig. 3-9 and Table 3-2). However, some signals detected in the field ranging from 1.6 ppm to 2.0 ppm were too much crowded to read the signal patterns correctly. To solve this problem, benzene-d_6 (C_6D_6) was chosen as a solvent for the NMR anlyses, in which the ^{1}H-NMR spectrum showed a good resolution especially in the higher magnetic field. Following NMR spectra of rugosal A were accordingly taken in C_6D_6, including COSY (HH-COSY and CH-COSY) and ^{13}C-NMR (COM and INEPT) spectra (Fig. 3-10, 11, 12, 13 and Tables 3-3, 4, 5). Since the ^{1}H-NMR taken at 500 MHz gave slightly different chemical shifts from those at 270 MHz (See Table 3-3), the data described in the text were all uniformed to the measure by 270 MHz. Afterwords it was found that the ^{1}H-NMR spectrum at 500 MHz showed a complete separation of the proton signals even in $CDCl_3$.

As shown in Fig. 3-14, the NMR analyses deduced three sub-structures of rugosal A. By the ^{13}C-NMR spectrum, an α,β-unsaturated aldehyde group firstly appeared to consist of the C,C-double bond (CH=C) present just one in the molecule. Three sp^2 carbons detected at δ_C 190.7 (CHO), 149.4 (=CH-) and 146.5 (=C<) were all attributable to the conjugation system. An olefinic proton detected at δ_H 5.998 (1H, dd, J= 6.2 and 1.1 Hz) was allocated to the β-olefinic carbon. Two methine protons resonated at δ_H 4.185 (1H, dd, J= 11.7 and 6.2 Hz) and 5.280 (1H, ddd, J= 5.1, 2.6 and 1.1 Hz) both showing a cross peak with an oxygenated methine carbon (δ_C 69.1 and 70.1, respectively) were each coupled with the olefinic proton (J= 6.2 Hz; vicinal coupling, and 1.1 Hz; allyl coupling, respectively).

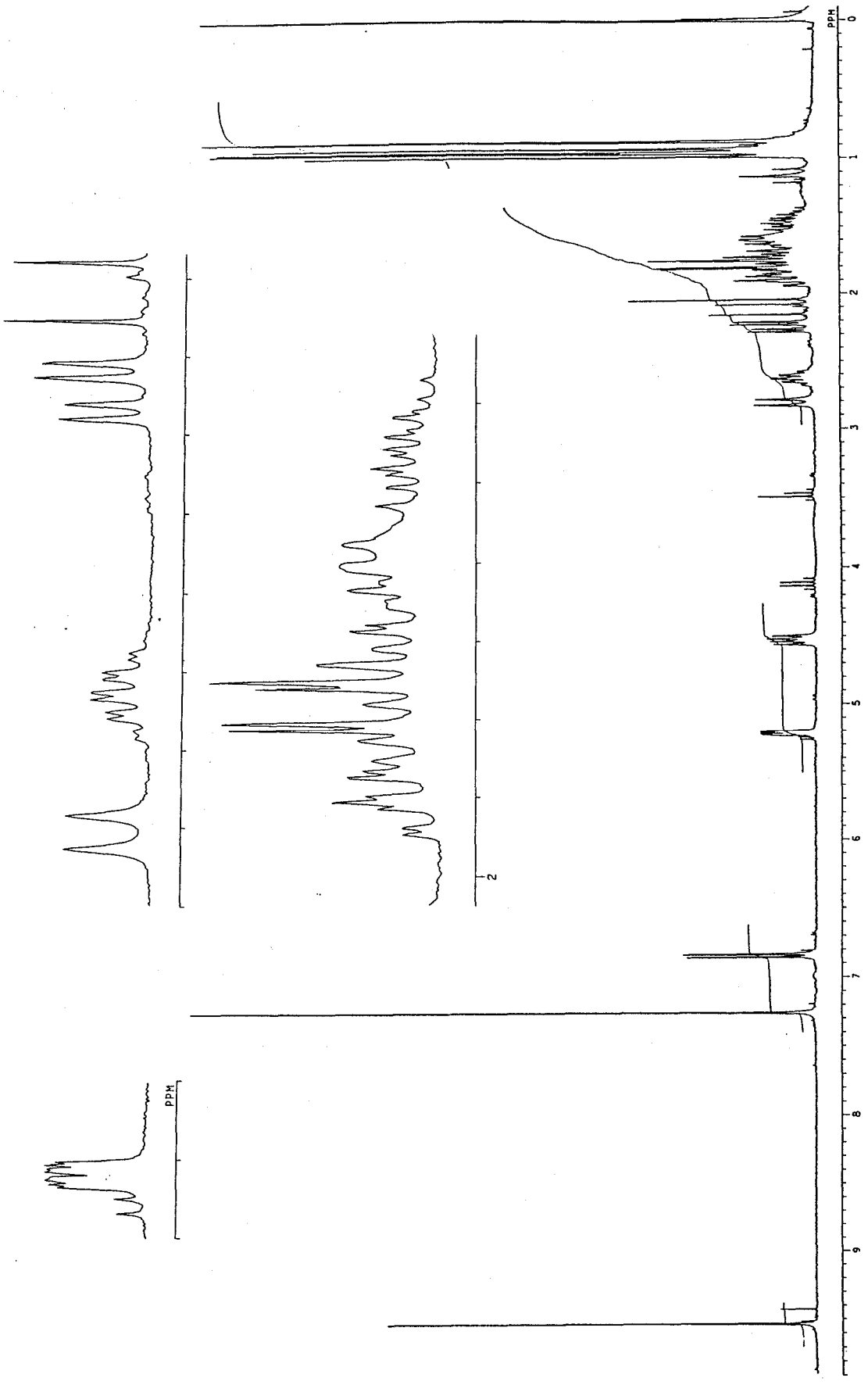

Fig. 3-9 ^{1}H-NMR Spectrum of Rugosal A (at 270 MHz. in $CDCl_3$)

Table 3-2 ^{1}H-NMR chemical shift values for rugosal A

(270 MHz, in $CDCl_3$, TMS as an int. std.)

δ_H		J(Hz)
9.539	s	
6.850	dd	6.0 and 1.1
5.200	ddd	5.0, 2.2 and 1.1
4.532	dd	11.5 and 6.0
2.870	d	11.5
2.630	double sept	6.6 and 2.2
2.246	dd	14.3 and 5.0
1.907	ddd	11.0, 8.8 and 2.2
1.785	dd	14.3 and 2.2
1.841	ddd	12.6, 12.1 and 7.4
1.720	dd	12.1 and 6.6
1.63 (approx.)	m	
1.450	dddd	13.2, 12.5, 11.0 and 6.6
0.980	d (3H)	6.6
0.946	d (3H)	6.6
0.883	s (3H)	

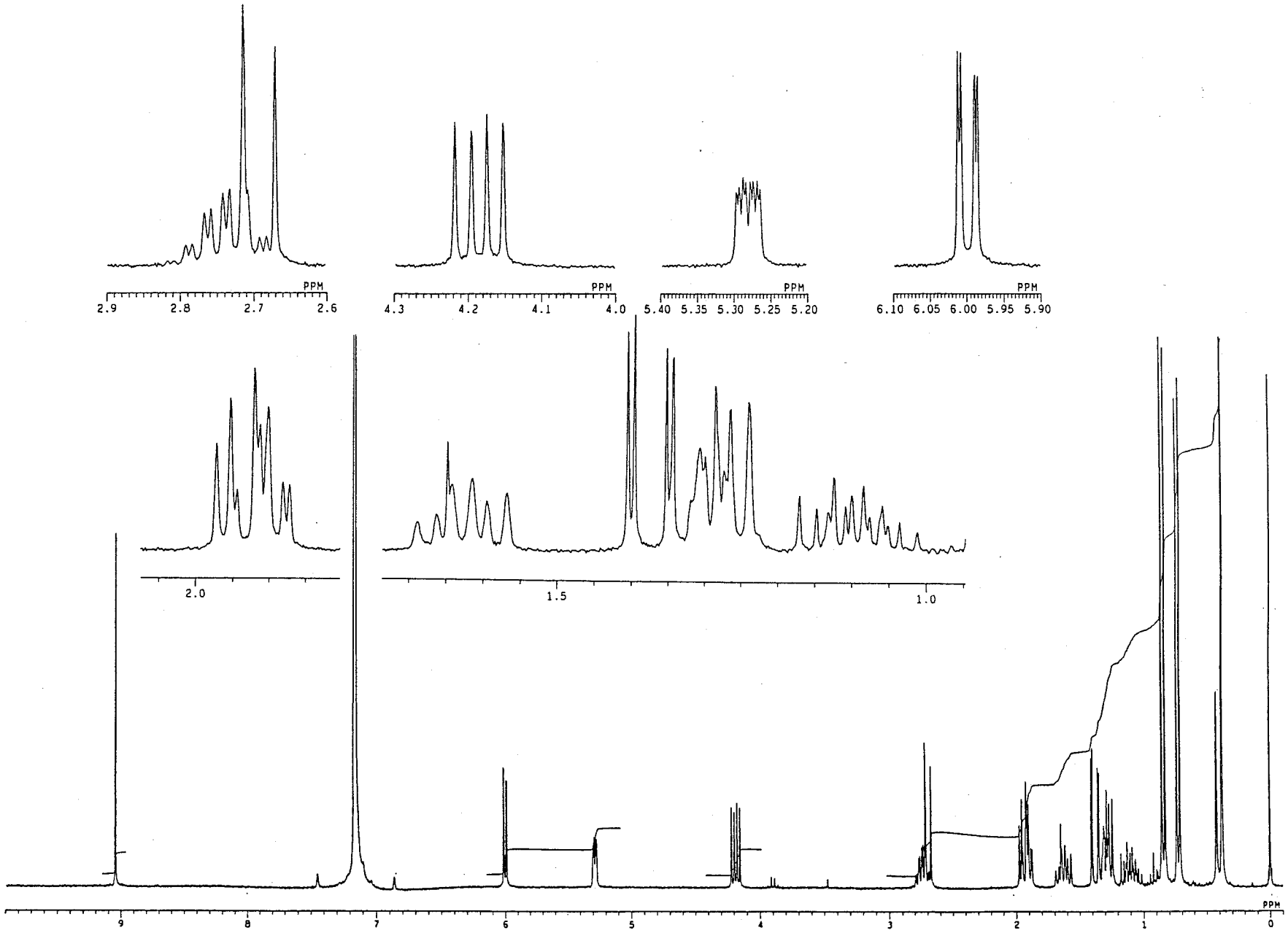

Fig. 3-10 ^{1}H-NMR Spectrum of Rugosal A (270 MHz, in C_6D_6)

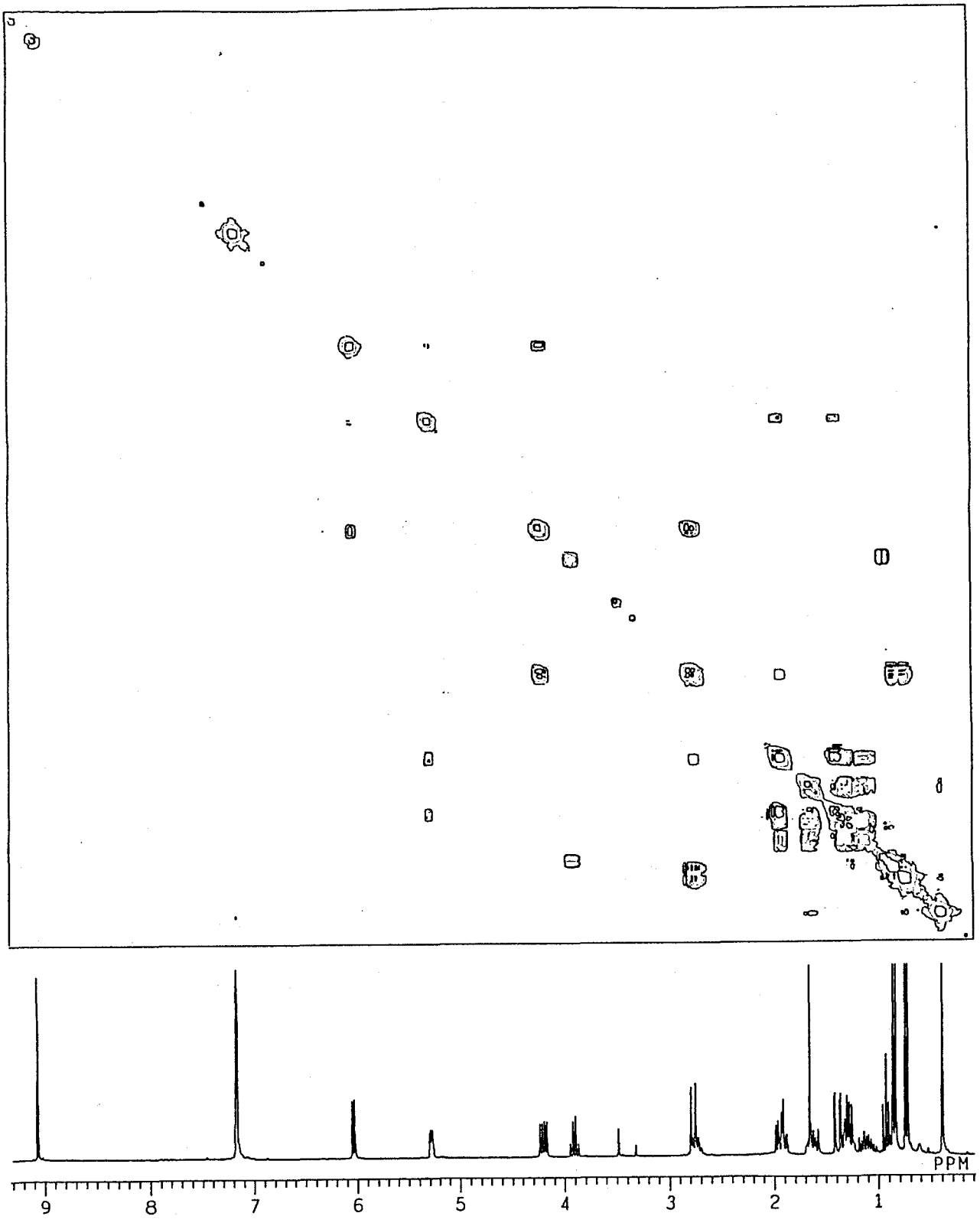

Fig. 3-11a HH-COSY Spectrum of Rugosal A (270 MHz, in C_6D_6)

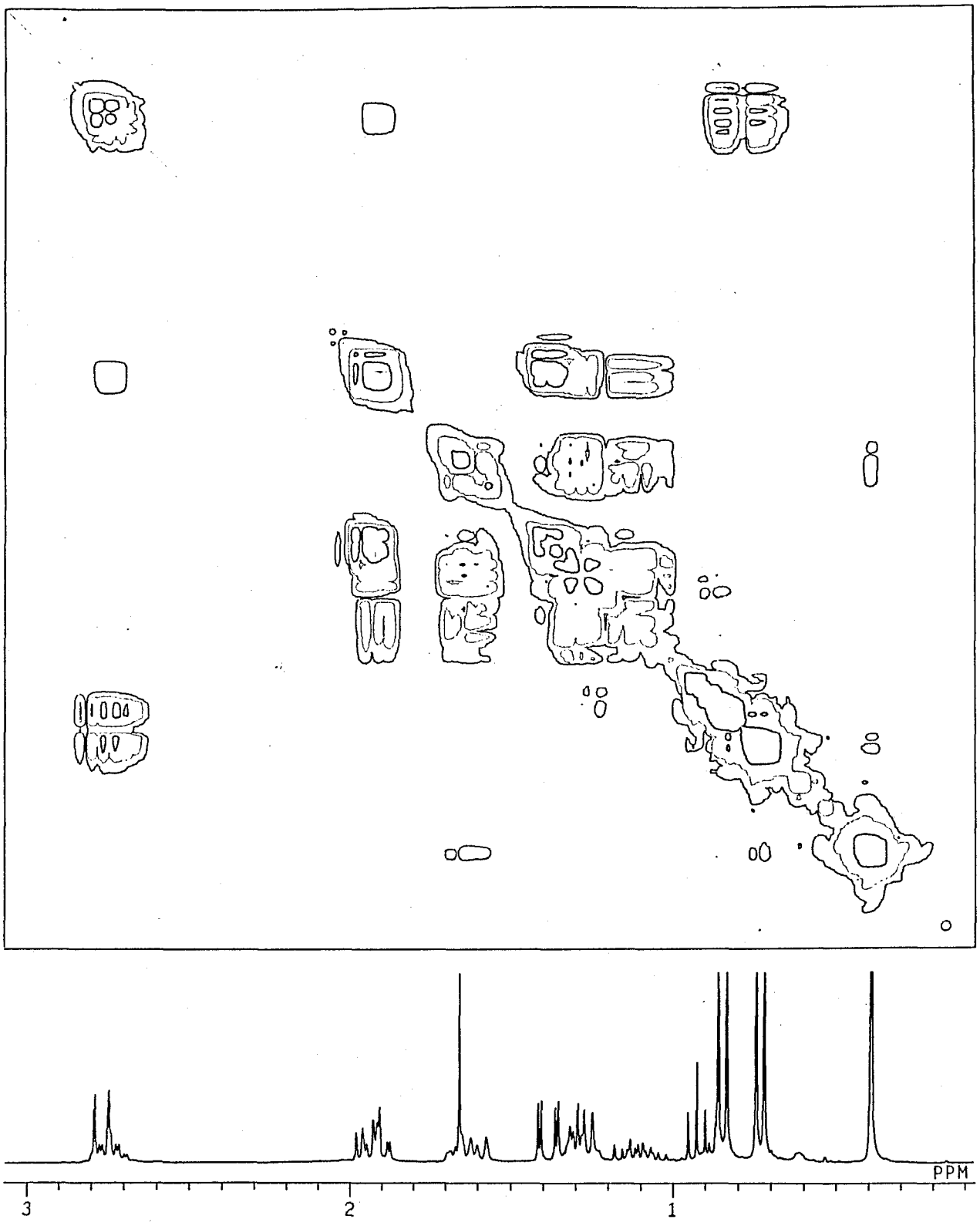

Fig. 3-11b Continued (Magnified in High Magnetic Field)

Table 3-3 ^{1}*H-NMR chemical shift values of rugosal A*

(270 MHz, in C_6D_6, TMS as an int. std.)

δ_H	*J*(Hz)	*cf* 500 MHz, in C_6D_6
9.045 s		9.048 s
5.998 dd	(6.2, 1.1)	6.031 (6.4)*
5.280 ddd	(5.1, 2.6, 1.1)	5.277 (4.9, 2.0)
4.185 dd	(11.7, 6.2)	4.198 (11.7, 6.4)
2.737 d. sept	(7.0, 2.6)	2.739 (6.8, 2.6)
2.711 d (11.7)	exchangeable with D_2O	2.758 (11.7)**
1.938 dd	(14.2, 5.1)	1.942 (14.2, 4.9)
1.912 ddd	(10.6, 8.8, 2.6)	1.912 (10.8, 9.5, 2.6)
1.628 ddd	(12.8, 12.5, 7.3)	1.630 (12.7, 12.2, 7.3)
1.374 dd	(14.2, 2.6)	1.384 (14.2, 2.6)
1.295 (approx.) m		1.299 m
1.275 br. dd	(12.5, 6.6)	1.282 (12.2, 6.8)
1.092 dddd	(12.8, 12.5, 10.6, 6.2)	1.105 (12.7, 12.2, 10.8, 6.8)
0.840 d (3H)	(7.0)	0.845 (6.8)
0.725 d (3H)	(7.0)	0.732 (6.8)
0.378 s (3H)		0.393 s

* Depending on a condition of the instrument, the allyl coupling becomes visible.

** This proton may shift according to the water content of the solvent.

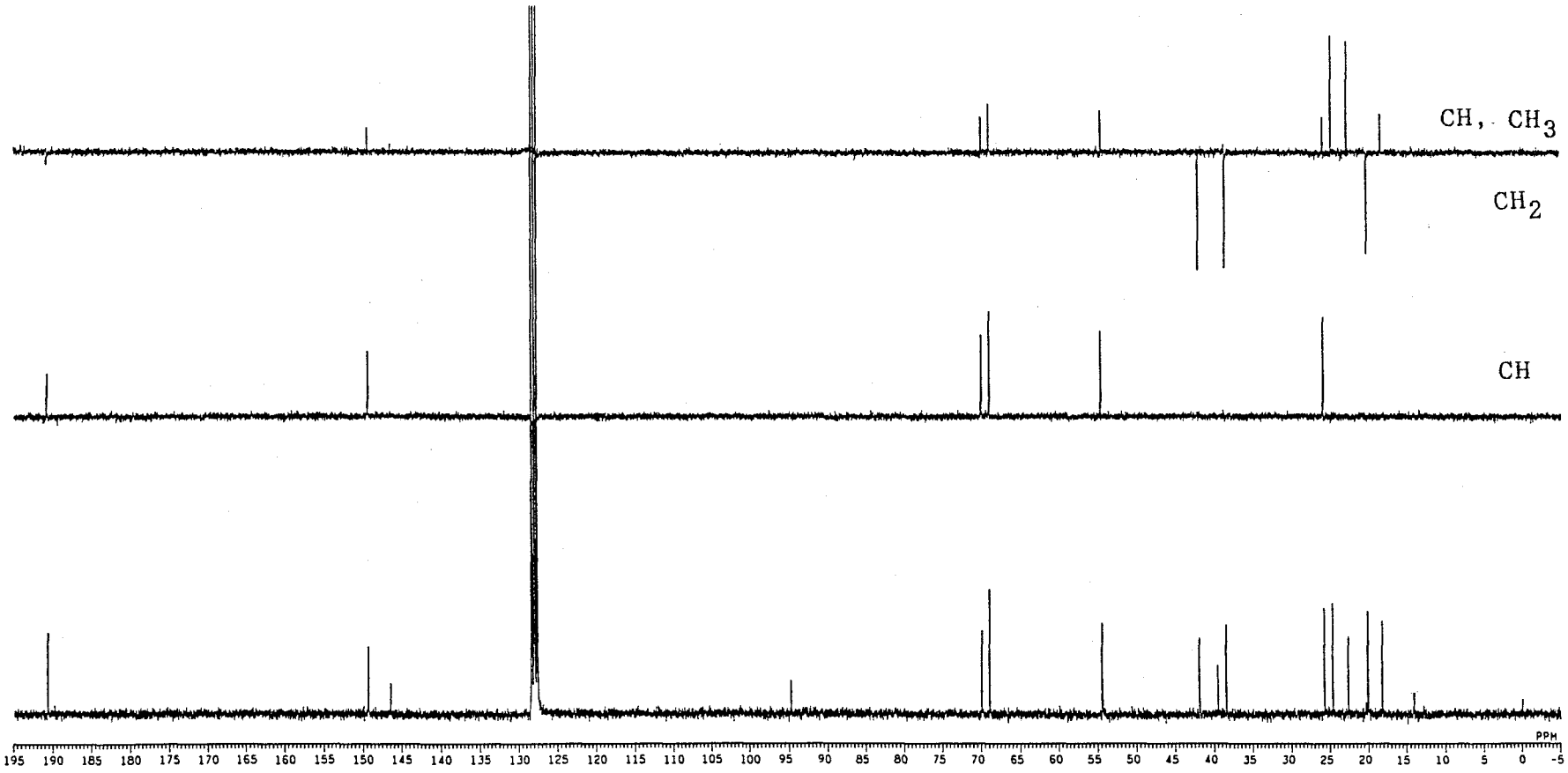

Fig. 3-12 ^{13}C-NMR Spectra of Rugosal A (68 MHz, in C_6D_6, COM and INEPT)

Table 3-4 Carbon chemical shift values of rugosal A

(68 MHz, in C_6D_6, TMS as an int. std.)

δ_C	H	Properties	Final Assignment
190.75	CH	-CHO	C-14
149.41	CH	-C=CH-	C-3
146.55	C	-C=CH-	C-4
94.80	C	-COx-	C-1
70.06	CH	-CH-O	C-5
69.05	CH	-CH-O	C-2
54.57	CH		C-10
42.00	CH_2		C-6
39.60	C		C-7
38.54	CH_2		C-8
25.87	CH_3		C-15
24.79	CH		C-11
22.76	CH_3		C-12
20.23	CH_2		C-9
18.36	CH_3		C-13

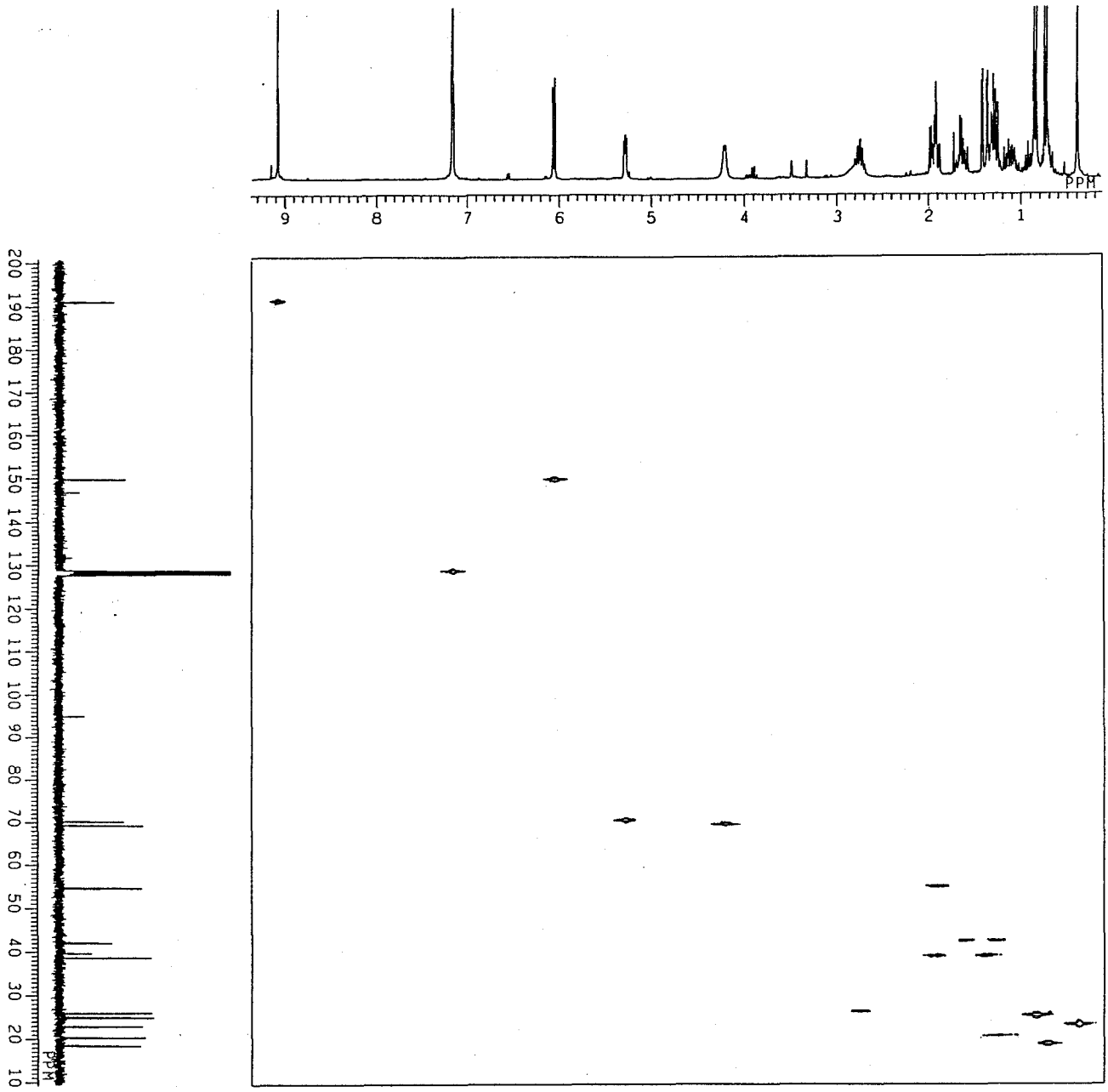

Fig. 3-13a CH-COSY Spectrum of Rugosal A (270 and 68 MHz, in C_6D_6)

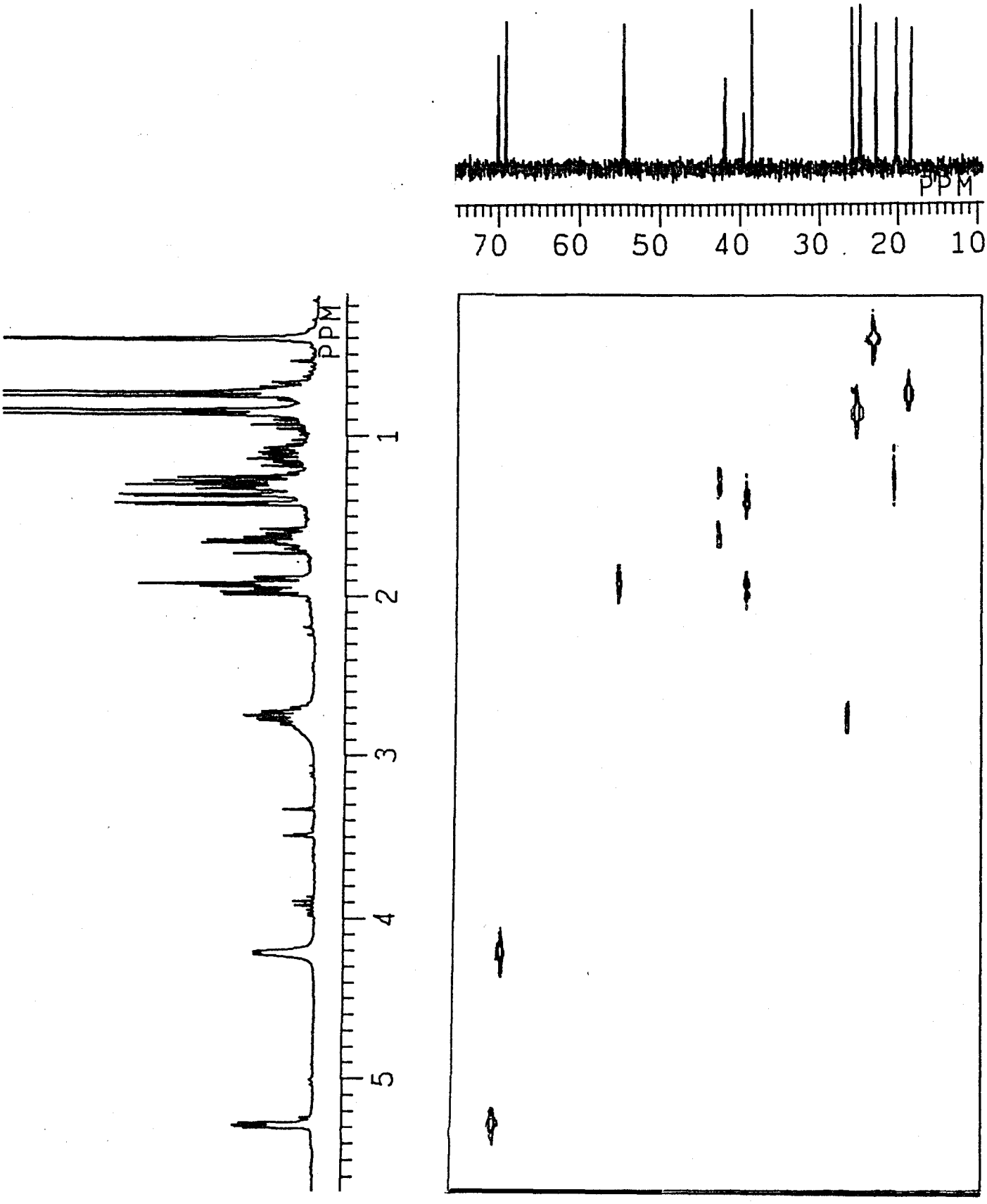

Fig. 3-13b Continued (Magnified in High Magnetic Field)

Table 3-5 Corelation between protons and carbons in rugosal A

(68 MHz and 270 MHz, in C_6D_6, TMS as an int. std.)

δ_C	δ_H	Final Assignment
190.7	9.045	C-14
149.4	5.998	C-3
146.5	-	C-4
94.8	-	C-1
70.1	5.280	C-5
69.1	4.185	C-2
54.6	1.912	C-10
42.0	1.938 and 1.374	C-6
39.6	-	C-7
38.5	1.628 and 1.275	C-8
25.9	0.378	C-15
24.8	2.737	C-11
22.8	0.840	C-12
20.2	*ca* 1.295 and 1.092	C-9
18.4	0.725	C-13

When D_2O was added, a signal observed at δ_H 2.758 as a doublet (1H, *J*= 11.7 Hz) disappeared completely. Furtheremore, the δ_H 4.185 methine proton was collapsed into a doublet (*J*= 6.2 Hz). This result indicated that the exchangable prtoton is assignable to a hydroxyl proton vicinal to the collapsed methine proton, and that the proton sequence in this side is closed (Fig. 3-15). The OH proton showed an abnormally large coupling constant value between the vicinal methine proton, although they may comply with Jackman-Sternhell function [92] under a free condition of the hydroxyl proton. It was therefore suggested that the dihedral angle of these two protons, regarding the C-O bond as the axis, took almost 0 ° or 180 ° possibly due to a fixation of the OH proton by the intramolecular hydrogen-bond and a steric effect around the methine proton (Fig. 3-16).

The other allylic methine proton at δ_H 5.280 locating on an oxygen-binding carbon (δ_C 70.1) was further coupled with a pair of vicinal methylene protons (δ_H 1.938, dd, *J*= 14.2 and 5.1 Hz, and 1.374, dd, *J*= 14.2 and 2.6 Hz) showing cross peaks with a methylene carbon at δ_C 42.0 in the CH-COSY spectrum. This proton coupling sequence also indicated that the methylene carbon is adjacent to a non-hydrogen-bearing carbon, too (Fig. 3-17). Location of the aldehyde group was proved by the deshielding effect on the methine proton at δ_H 5.280 allocated to the β-position [93]. The geometry at the C,C-double bond was presumed to be *cis* form regarding the olefinic proton (δ_H 5.998) and aldehyde group, since a deshielding effect of the formyl group on the olefinic proton (δ_H 6.850 in $CDCl_3$) was only compatible with the *cis* configuration (Table 3-6) [93,94]. In addition, the fact that the compound must take a tricyclic structure elucidated by total of five unsaturation number including two double bonds also supported the *cis* configuration. The presence of *trans* olefinic bond seemed unreasonable in a tricyclic compound.

The HH-COSY and CH-COSY spectra showed another coupling

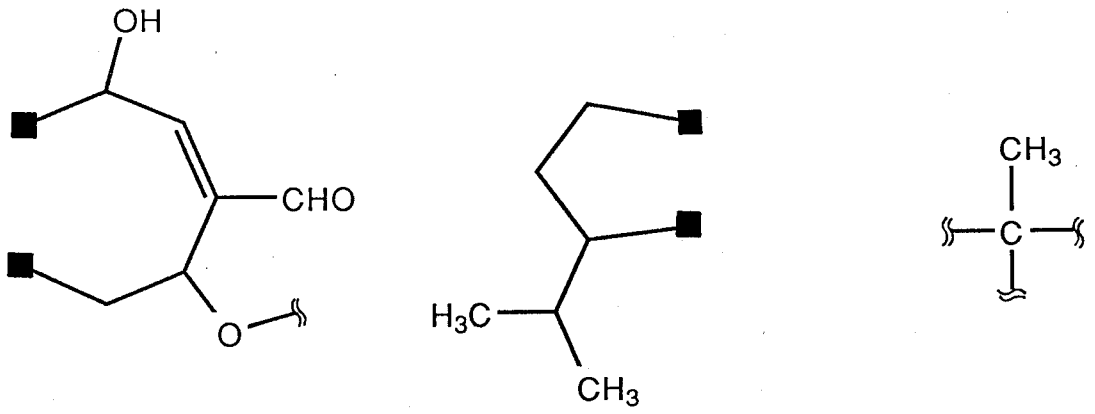

Fig. 3-14 Three Partial Structures of Rugosal A: Symbol ■ indicates a non-hydrogen-bearing carbon, and ≀ means a single bond where CH and HH coupling sequence is discountinued.

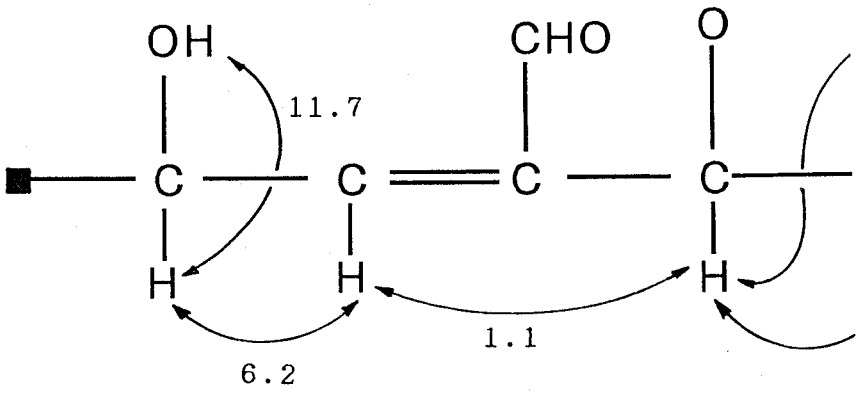

Fig. 3-15 Proton Coupling Sequence around the Olefinic Proton

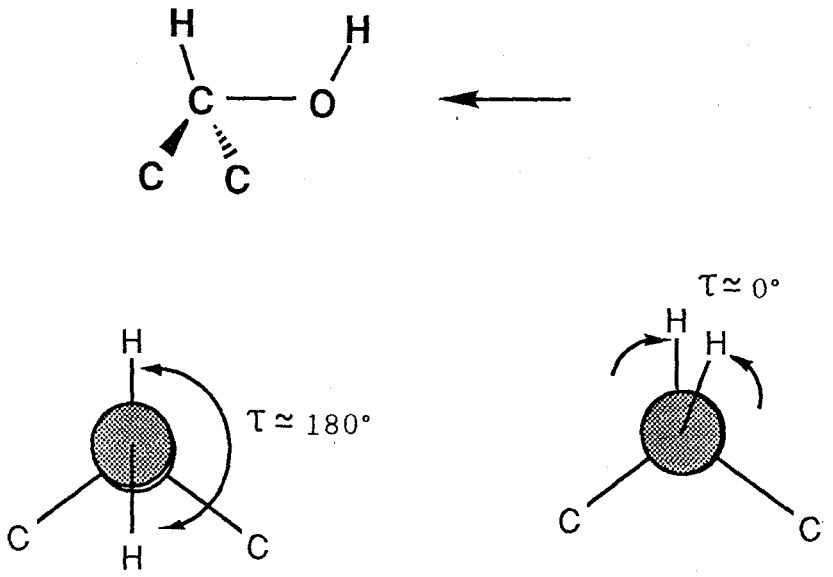

Fig. 3-16 Presumable Dihedral Angle between H-C-O and C-O-H Planes

Table 3-6 Deshielding Effect of Carbony Group on α- or β-Proton: δ_H Values in $CDCl_3$

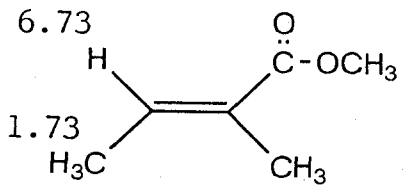

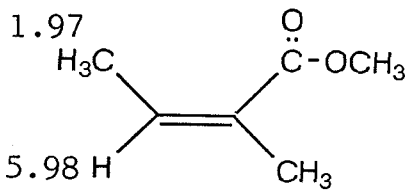

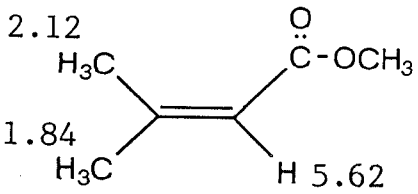

[88]

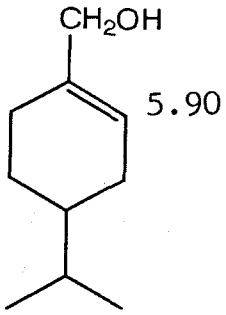

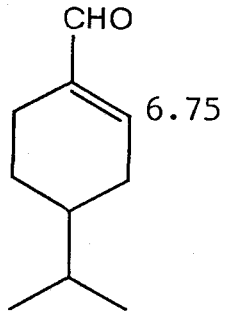

[89]

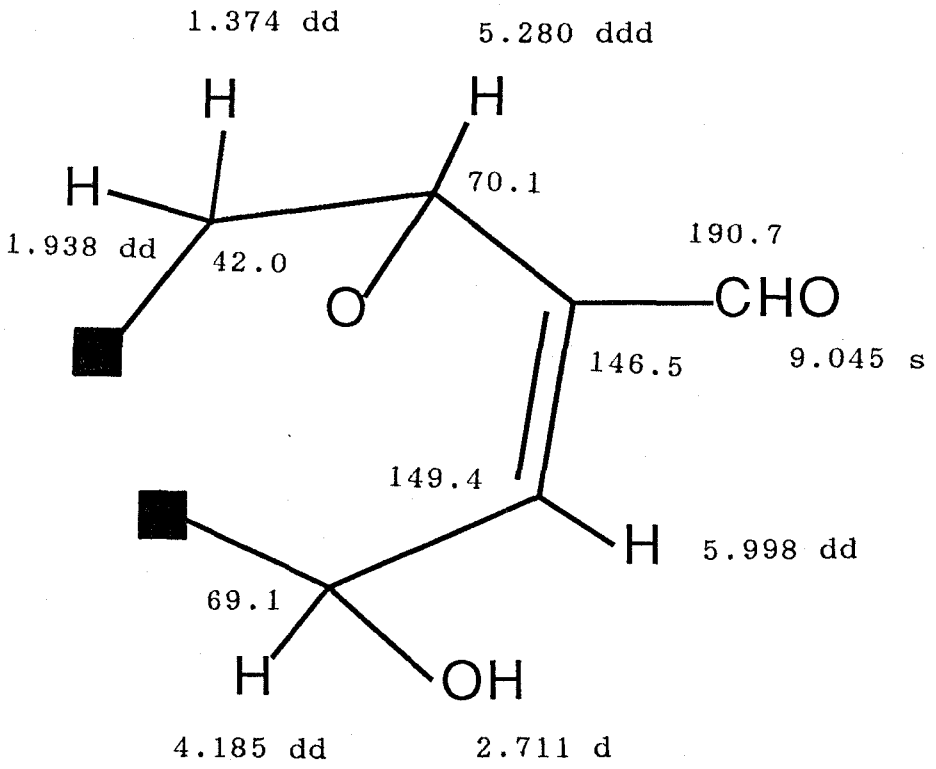

Fig. 3-15 Crobon and Proton Assignments for Substructure A

sequence for substructure B. Two isopropyl methyl signals resonated at δ_H 0.840 (3H, d, *J*= 7.0 Hz) and 0.725 (3H, d, *J*= 7.0 Hz) were both coupled with a methine proton (double-septet, *J*= 7.0 and 2.6 Hz) resonating at δ_H 2.737. The coupling sequence was further extended to another methine proton observed at δ_H 1.912 (ddd, *J*= 10.6, 8.8 and 2.6 Hz) which showed a cross peak with δ_C 54.6 carbon in the CH-COSY spectrum. On the other hand, with a pair of methylene protons detected at *ca* δ_H 1.31 (m) and 1.092 (dddd, *J*= 12.8, 12.5, 10.6 and 6.2 Hz) the 1.912 methine proton also showed cross peaks in the HH-COSY spectrum, and the coupling sequence was further extended to another pair of methylene protons (δ_H 1.628, ddd, *J*= 12.8, 12.5 and 7.3 Hz, and 1.275, dd, *J*= 12.5 and 6.6 Hz, respectively). By the CH-COSY spectrum, the carbon signals at δ_C 20.2 and 38.5 were assigned to these methylene carbons, respective-ly. The coupling sequence was closed there with revealing all the carbon in the sub-structure. This proton-proton coupling sequence was, as mentioned above, more clearly observed by the analysis with 500 MHz (in $CDCl_3$) as shown in Fig. 3-18. Accordingly, the partial stucture [■-CH_2-CH_2-CH-$(CH_3)_2$] was deduced for substructure B (Fig. 3-19).

Including substructure C, an isolated methyl group observed in a markedly higher magnetic field (singlet, δ_H 0.378 in C_6D_6, or 0.883 in $CDCl_3$) presumably locating on a δ_C 39.6 quaternary carbon [94], the 13 carbons out of 15 in rugosal A were thus assigned.

3) Elucidation of Planar and Stereochemical Structure

To contract a planar structure for rugosal A, these sub-structures were connected each other through two non-hydrogen-bearing carbons detected at δ_C 94.8 (I) and 39.6 (II). The former carbon (I) resonating at a lower magnetic field is indicative of two possibilities in its substituted state; one is a dioxygenated carbon (*e.g.* ketal) and the other is a monoxygenated one. The first possibility was eventually rejected. In case of the ketal

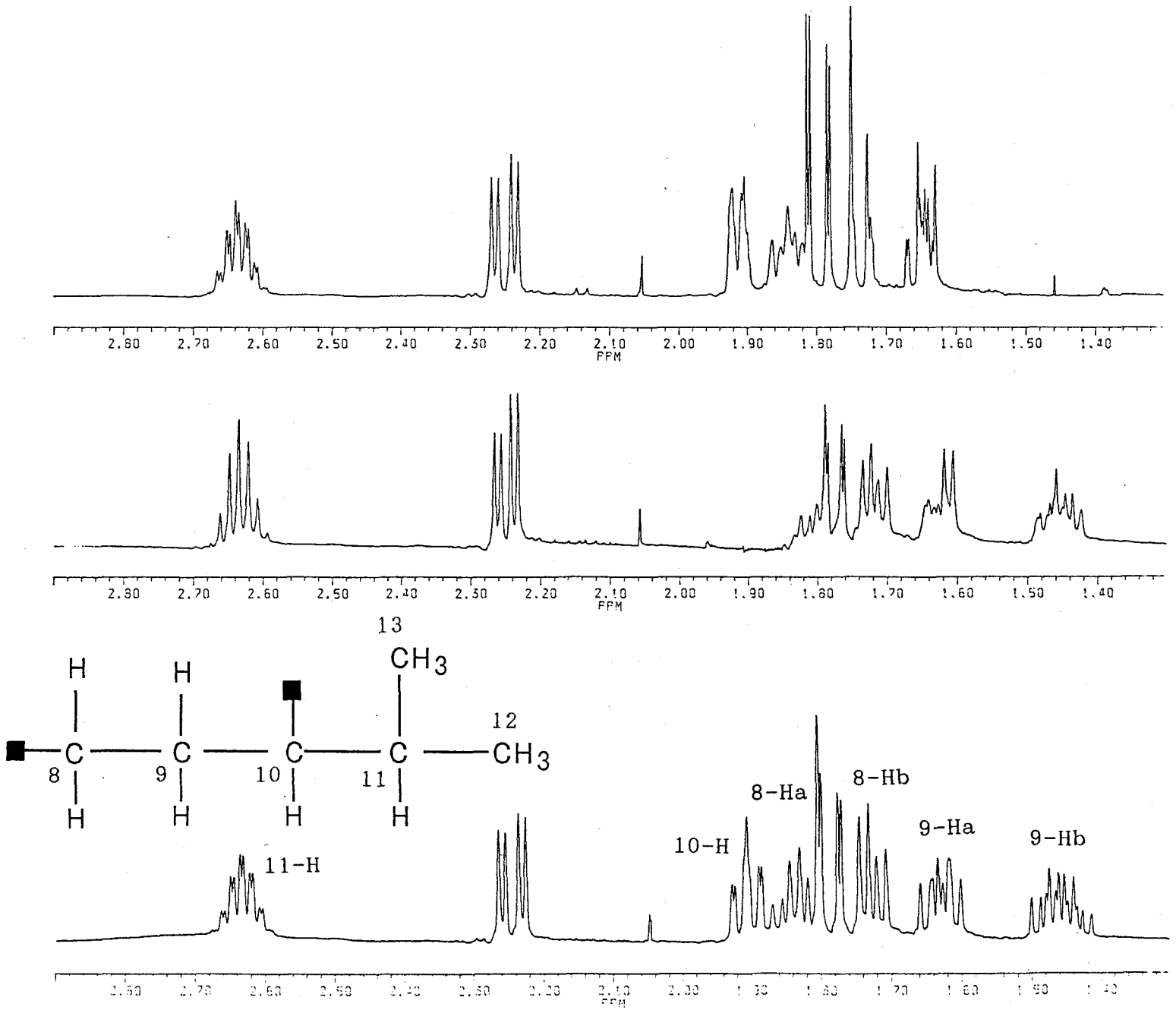

Fig. 3-18 Proton Signals Assignable to Substructure B (500 MHz, in $CDCl_3$)

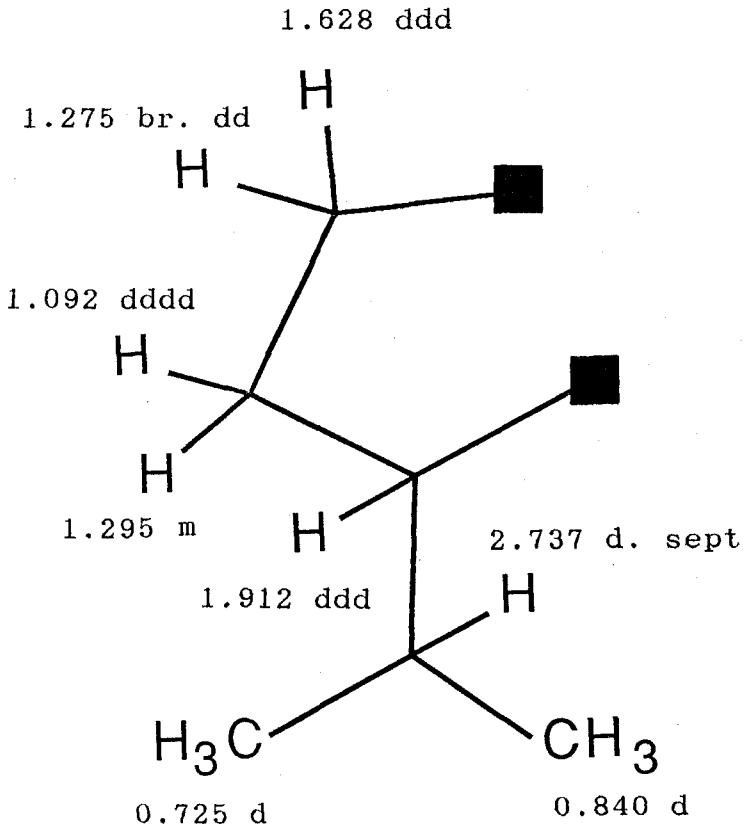

Fig. 3-19 Proton and Carbon Assgnments for Substructure B

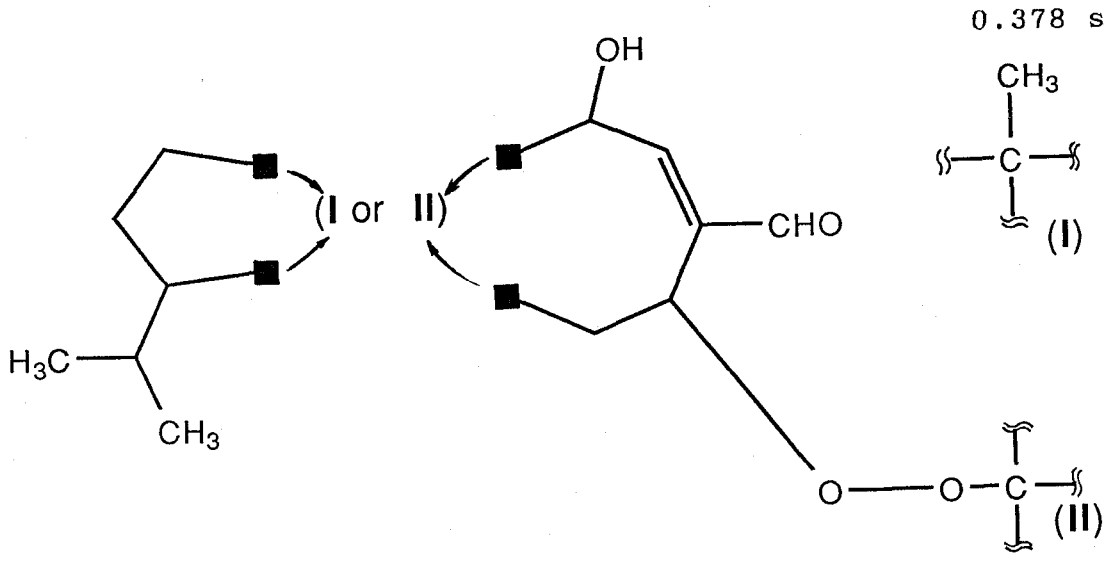

Fig. 3-20 Partial Structures for Rugosal A: Three substructures can be combined via two non-hydrogen-bearing carbons (I and II)

carbon, one of the oxygens contributing to this substitution cannot find any partnar to connect with, since all hydrogens have already been assigned to three of the substructures by ^{1}H- and ^{13}C-NMR. Consequently, the monoxyganated carbon was preferred. On the other hand, δ_C 39.6 carbon (II) was reasonably assigned to the quarternary carbon on which the bridgehead methyl group is located (accordingly substructure C).

Two oxygen atoms out of the total of four in the molecule has been assigned to the carbonyl and the hydroxyl groups in the substructure A, respectively. The remaining two, one linked to the allyl methine carbon at δ_C 70.1 and the other to the non-hydrogen-bearing carbon (I in Fig. 3-20), were therefore presumed to form a peroxy bridge between these two carbons, as neither hydrogen nor oxygenated carbon remains (See Fig. 3-20). The presence of an endoperoxy bridge was confirmed by the potassium iodide starch test [95] and *N,N*-dimethyl-*p*-phenylenediamine sulfate test [85] for detecting a peroxy group. Both tests showed a positive response, coloring into a dark blue and a reddish pink, respectively. In addition, the presence of an endoperoxy linkage was also revealed in EI-HR-MS analyses. The M^+-33 fragment showing 233.151 ($C_{15}H_{21}O_2$ = M^+-OOH, *cf.* M^+-48, 218.130 $C_{14}H_{20}O_2$= M^+-CO-H_2O) was proved to be risen by the fission of the endoperoxy linkage.

The possibility that substructure B forms a cyclobutane ring was excluded by $^{1}J_{CH}$ values of the methylene carbons locating to the substructure B. The values (129.1 and 130.1 Hz for δ_C 38.5 and 20.2 carbons, respectively) measured by *J* resolution experiment were indicative of a cyclopentane nature ($^{1}J_{CH}$ for cyclobutane: 136$\pm$ 1 Hz, and for cyclopentane: 131$\pm$ 2 Hz [96,97]) for substructure B (Fig. 3-21 and Table 3-7). Therefore, it was proved that substructure B should take a five-membered ring forming 5,7-bicyclic skeleton by the connection with substructure A.

After consideration of the above requirements, possible structures for rugosal A were accordingly restricted to following

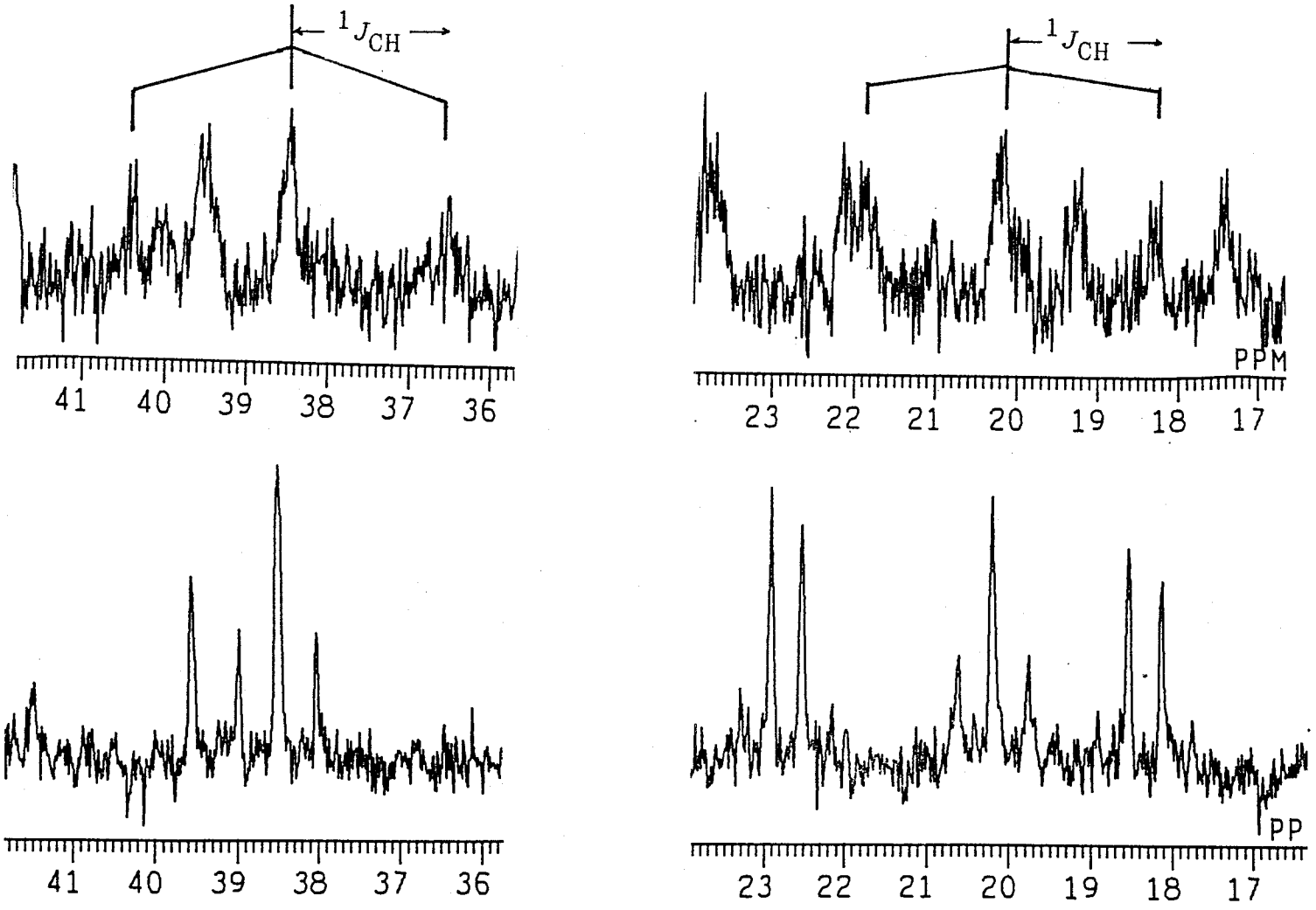

Fig. 3-21 $^1J_{CH}$ Resolved NMR Experiment on B-1 and B-2 Carbons of Substructure B (68 MHz, in C_6D_6)

Table 3-7 $^{1}J_{CH}$ *Values for the Several Alicyclic and Heterocyclic Compounds* [92,93*]

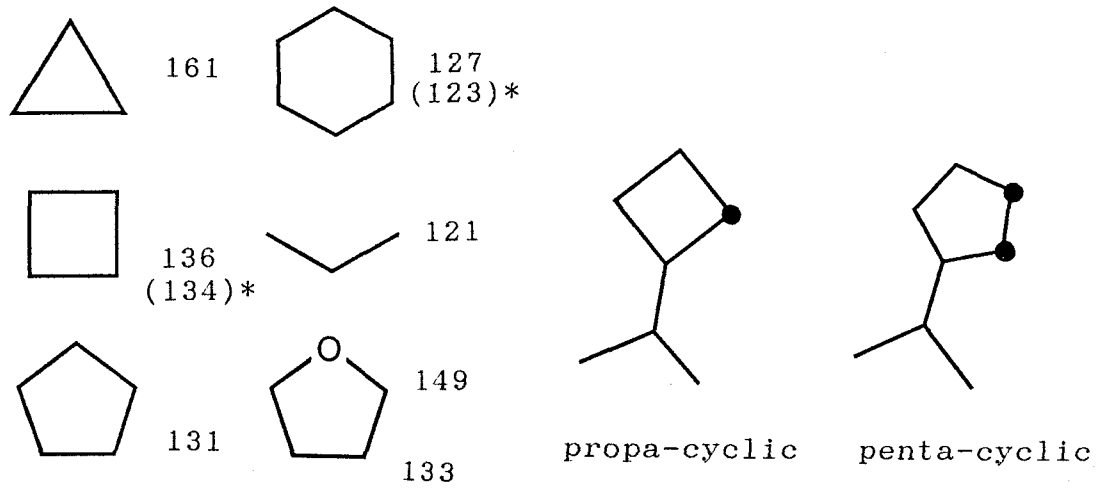

four D, E, F and G depicted in Fig. 3-22. The structure D and E were tentatively discounted for three reasons; firstly, the C-10 methine carbon resonating at a low field (δ_C 54.6) is presumably located adjacent to the oxygenated carbon (II). Secondly, both structures do not comply with the isoprene rule, contrary to F and G forming carotane skeleton known as one of groups of naturally occurring sesquiterpenoids. Thirdly, a long range coupling among the bridgehead methyl proton at δ_H 0.378 and a methylene proton at δ_H 1.630 was observed in the HH-COSY spectrum (See Fig. 3-11b). The structure D and E cannot afford the long range coupling. A characteristic deshielding of a methine carbon which bears an isopropyl group and an oxygenated carbon was pointed out by Wiemer *et al.* in structure elucidation of a carotanoid, lasidiol angelate (**55**) [57,98]. When the five-membered ring carbons of rugosal A was compared in the chemical shift values with those of **55**, daucol (**29**) and carotol (**28**), all showed a good correspondence (Table 3-8).

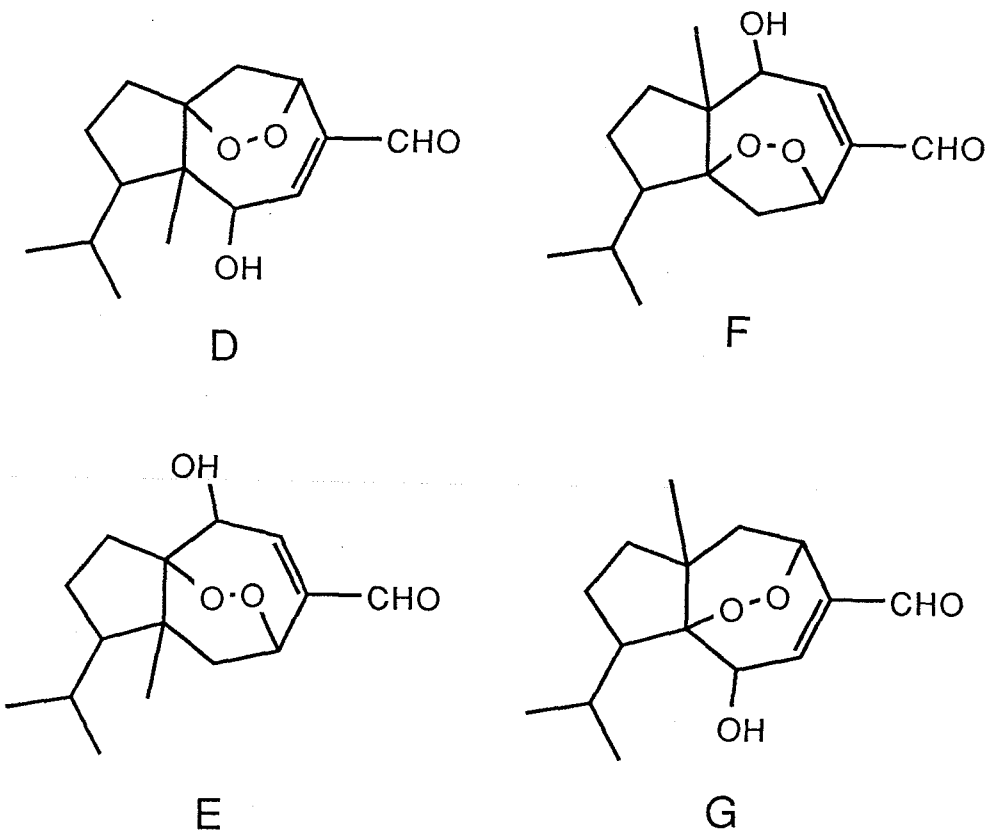

Fig. 3-22 Four Possible Structures for Rugosal A

Table 3-8 Comparison of rugosal A with lasidiol angelate (55) daucol (29) and carotol (28) in ^{13}C-NMR chemical shift values (in $CDCl_3$)

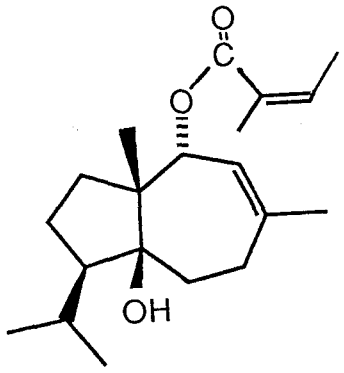

lasidiol angelate (55)

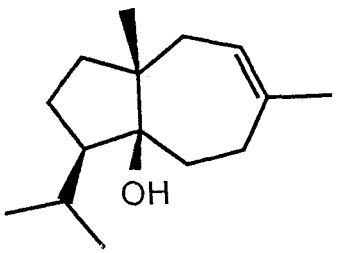

carotol (28)

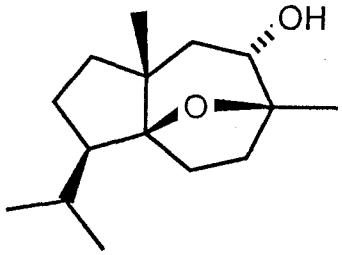

daucol (29)

	rugosal A	55	29	28
Carbon				
1	94.8	83.2	91.8	83.8
(2)*	69.1**	35.3	29.6	33.9
7	39.6	53.5	45.9	48.5
8*	38.5	35.8	41.2	38.2
9*	20.2	24.8	26.5	24.0
10	54.6	56.2	52.8	52.0

* In the known carotanoids, chemical shifts of C-2, C-8 and C-9 listed here have been assigned as C-9, C-2 and C-8, respectively, in the original paper [57]; however, these assignments based on empirical data are probably incorrect.

** Oxygenated carbon

For further elucidation of the planar structure of rugosal A, NOESY experiment was carried out after the dead space of the NMR tube containing a C_6D_6 solution of rugosal A was filled with N_2 gas. Taking into consideration of the NOESY spectrum as shown in Fig. 3-23, planar structure and relative configuration for rugosal A was further discussed (Table 3-9). While the NOESY analysis gave nice information for the structural elucidation, the result must be compatible with another important character of rugosal A, the presence of the intramolecular hydrogen bond in the molecule. The NOE **e** (Fig. 3-24) gave reliable evidence for a *cis* configuration at the C,C-double bond, as initially postulated. Then, a possibility of the hydrogen-bond between the allylic OH and the carbonyl oxygen of the aldehyde group was discounted, and accordingly, the hydrogen-bond between the OH and one of the endoperoxy oxygen atoms was approved. To make a compose the hydrogen bond between these two groups, the allylic OH and the endoperoxy bridge are on the same side of the seven-membered ring (Fig. 3-25).

Table 3-9 NOEs on rugosal A by NOESY experiment

NOE	Proton (δ_H)	Proton (δ_H)
a	0.840	0.378
b	0.725	0.378
c	0.725	4.185
d	1.374	0.378
e	9.045	5.998
f	1.912	0.840
g	1.938	1.628
h	5.998	2.711
i	1.938	1.628

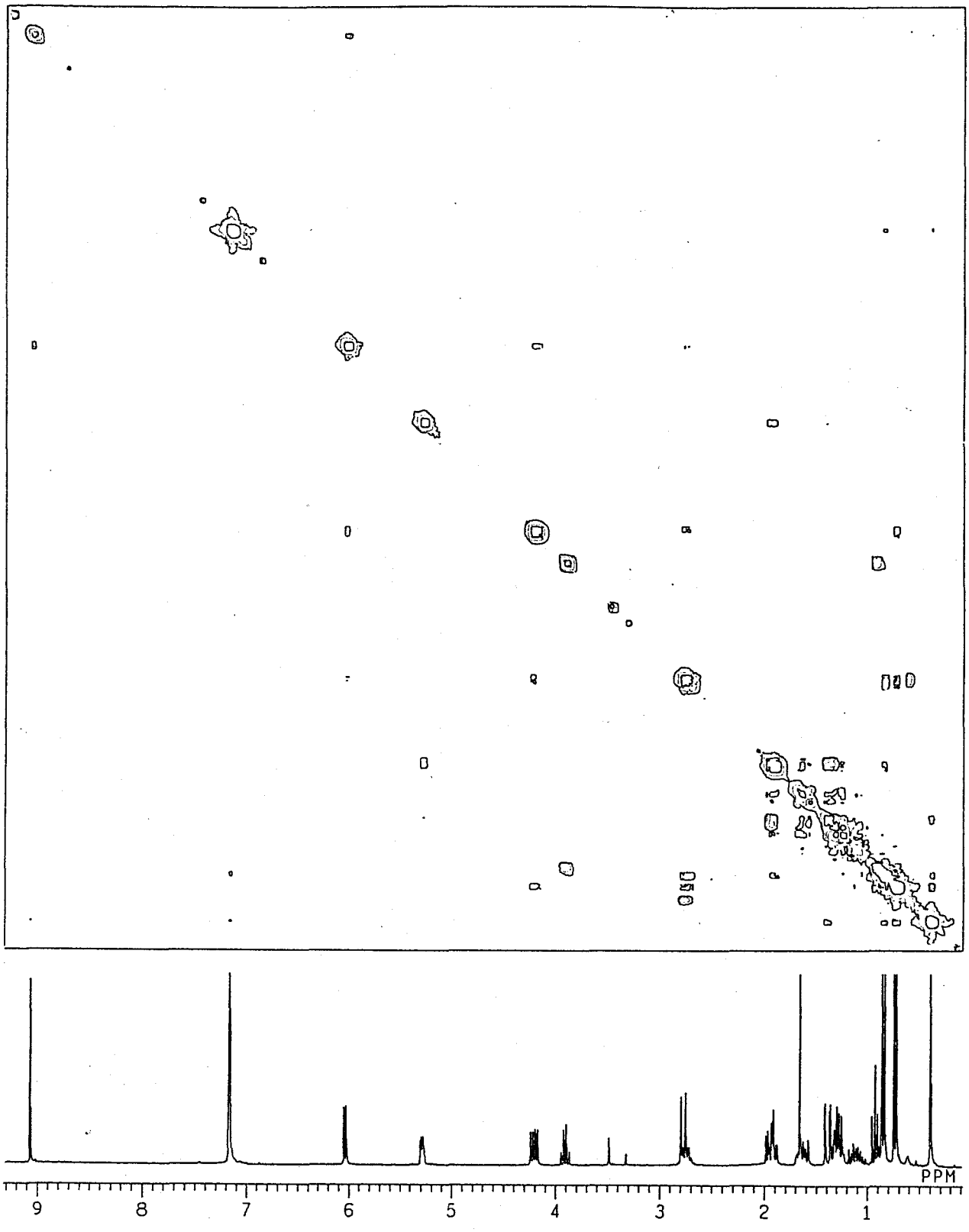

Fig. 3-23 NOESY Spectrum of Rugosal A (270 MHz, in C_6D_6)

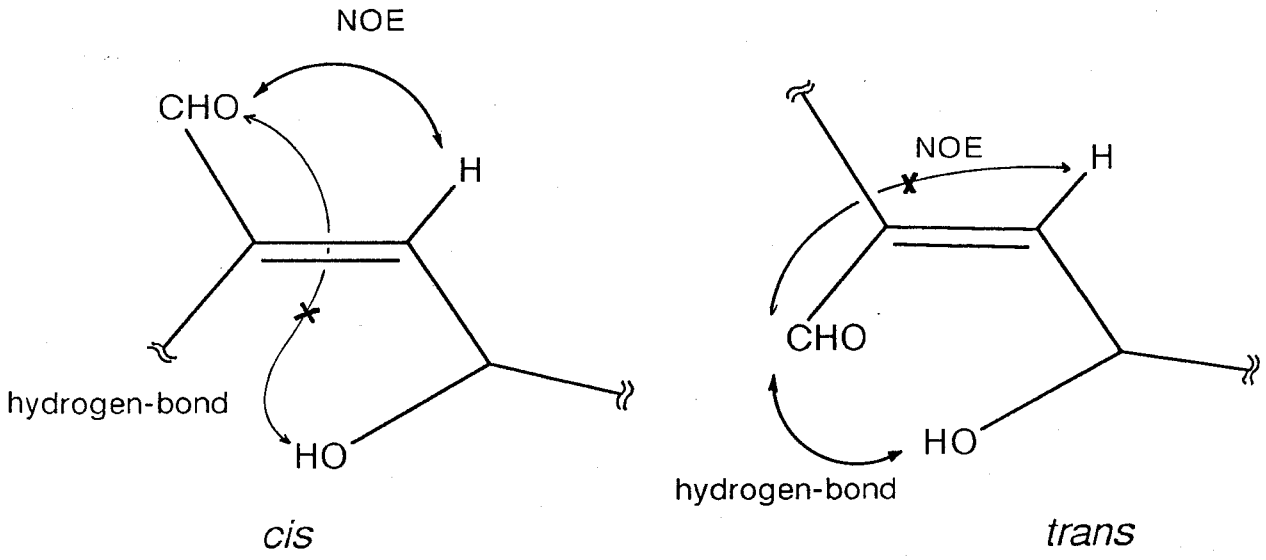

Fig. 3-23 Possible Intramolecular Hydrogen Bond: Since an NOE is observed between formyl proton and olefinic proton (*cis* form), allylic -OH cannot afford hydrogen bond with the carbonyl group.

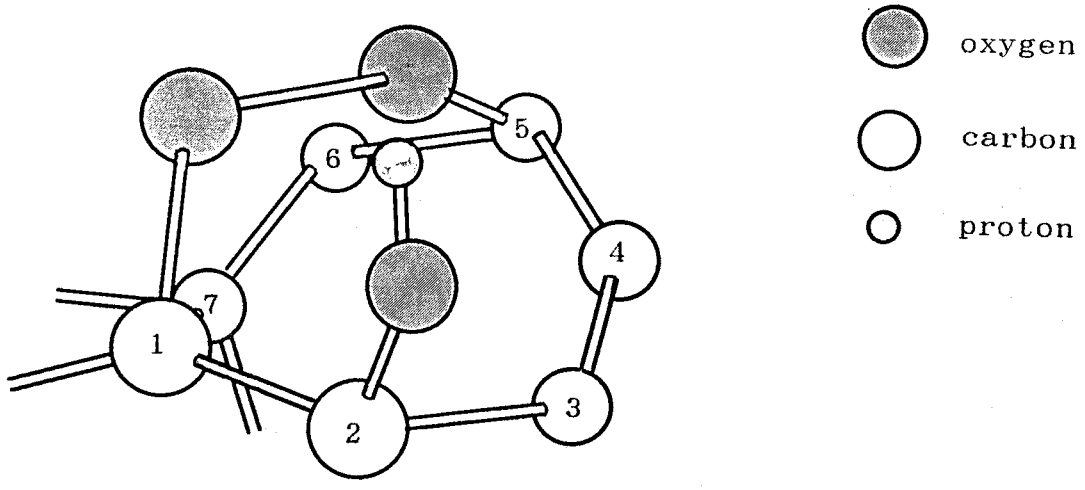

Fig. 3-24 Stereostructure around the Endoperoxide Bridge and the Hydrogen-Bonding Allylic OH Group

The structure F for rugosal A was discounted for the clear reason that the NOE **c** observed between the hydroxylated allylic methine proton resonated at δ_H 4.198 and one of the isopropyl methyl group at δ_H 0.732 was hardly explicable for the structure despite the configuration of two groups. Namely, distance of these two groups is too far to cause an NOE in structure F (Fig. 3-25). In addition, structures D and E were also contradictry to the result of NOE experiment. In D, the NOE **c** and **d** cannot be valid simultaneously, while E is contradictory to fulfill the NOE **a**, **b** and **c** at the same time. Thus, only structure G hereby persisted. Numbering for the carbons in the proposed planar structure G was tentatively fixed as depicted in Fig. 3-26.

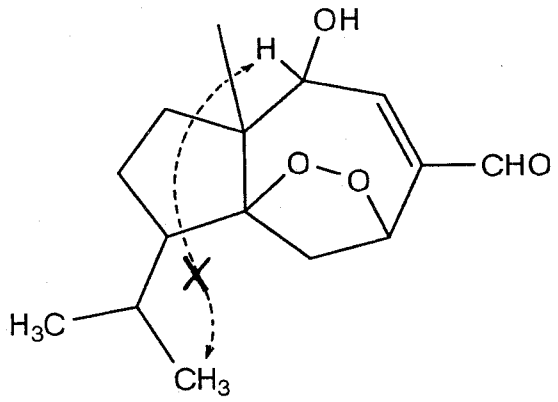

Fig. 3-25 Structure F Incompatible with the Results of NOE **c** (See Fig. 3-27)

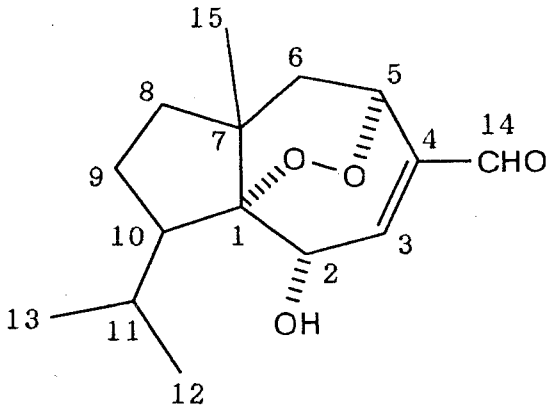

Fig. 3-26 Proposed Structure for Rugosal A with Carbon Numbering

In consideration of all NOEs observed by the NOESY experiment, a relative configuration for rugosal A was successively given (Fig. 3-27). When C-7 carbon is temporarily fixed as ***S*** configuration, C-10 carbon necessarily appears to ***R***, for NOE **a** and **b**. Furthermore, C-2 must be ***R*** to cover NOE **c**, and then, according to the stereochemical requirement for the hydrogen-bonding endoperoxy linkage and the hydroxyl group, the configuration at C-1 and C-5 become feasible to be ***S*** and ***R***, respectively. Thus, elucidated relative configuration for rugosal A (**1**) made other NOEs (**e**, **f**, **g**, **h**, and **i**) reasonable.

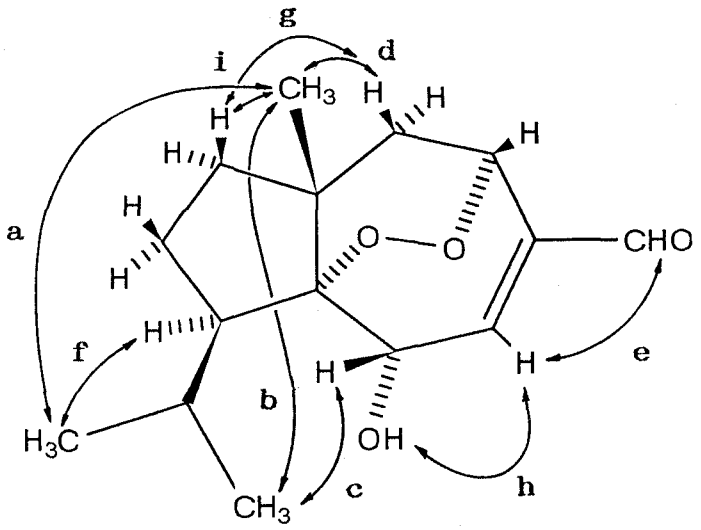

Fig. 3-27 Relative Configuration of Rugosal A and Observed NOEs in the NOESY Expriment

The hydrogen-bond formation between an endoperoxy group and a hydroxyl group found in rugosal A is a unique property; however, some similar compounds possible to make intra-molecular hydrogen-bond between -OH and -OO- have been reported (Fig. 3-28). An endoperoxy guaianoid (**79**) isolated from *Liabum floribundum* (Compositae) by Jakupovic *et al.* may have this type of hydrogen-bond [99]. However, the authors did not refere to any property indicative of the hydrogen bond between its allylic hydroxyl group and endoperoxy bridge. As a basic difference from **1**, **79** possesses a 1,4-endoperoxy bridge which is formed via a Diels-Alder reaction between a singlet oxygen and the corresponding 1,3-diene precursor, unlike **1** having a 1,5-linkage in the molecle. Indeed, they proposed a scheme for the endoperoxide formation via this type of a Diels-Alder reaction (Scheme 3-2) [99].

On the other hand, another guaiane endoperoxide, hanalpinol (**80**), gave evidence for structure **1**. Hanalpinol (**80**) isolated from *Alpinia japonica* (Zingiberaceae) by Itokawa *et al.* has relatively the same *endo*-peroxide system as that of **1**, including an allylic hydroxyl group and an olefinic bond [100]. This guaianoid exhibited quite similar physicochemical properties to those of **1** (M^+-33 in EI-MS, 3400 cm^{-1} of hydrogen-bonded-OH absorption in IR spectrum and δ_H 2.29 of OH proton showing vicinal coupling J= 12 Hz in ^{1}H-NMR) raised from the hydrogen-bonding endoperoxide system [100]. Thus, some of spectroscopic properties initially observed on **1** has now revealed due to its unique intramolecular hydrogen-bonding endoperoxide structure. To establish the proposed structure **1** for rugosal A, some chemical conversions were further carried out as described in the next subsection.

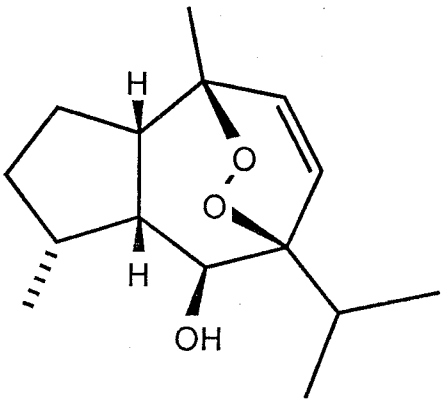

endoperoxy guaianoid 79
from *Liabum floribundum*

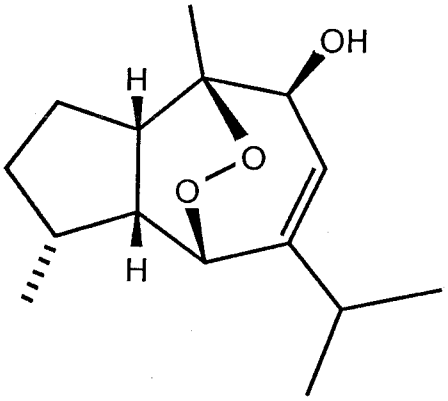

hanalpinol 80
from *Alpinia japonica*

Fig. 3-28 Sesquiterpene Peroxides Possibly Having a Hydrogen Bond between the Peroxide Group and the Hydroxyl Group

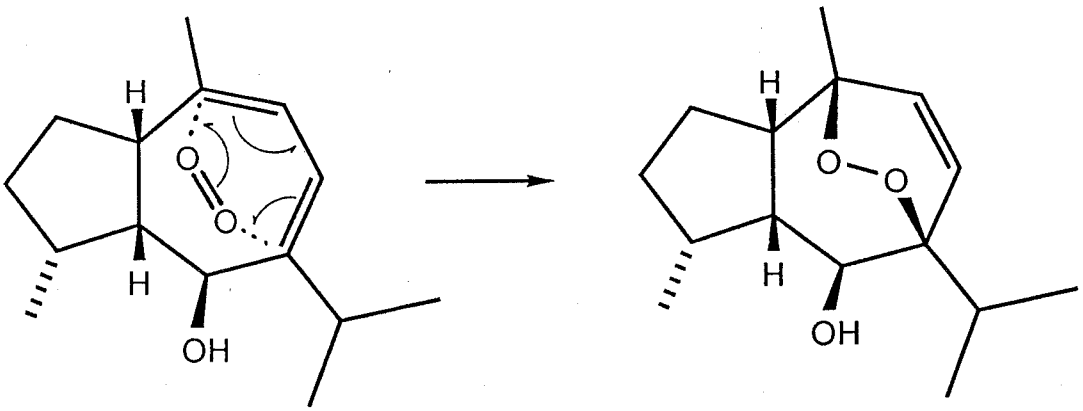

Scheme 3-2 Proposed Synthetic Pathway for a 1,4-Peroxyguaiane

Table 3-10 Physicochemical properties of rugosal A (1)

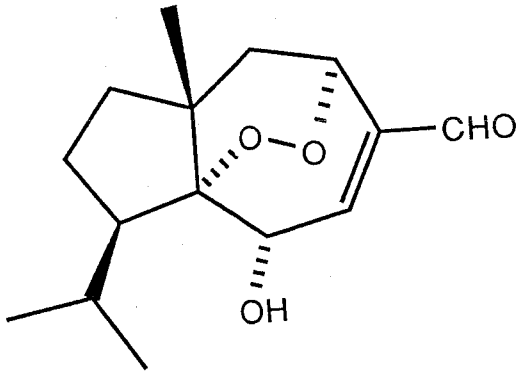

1

Colorless needles, mp 145-147 °C

Rf: 0.42 (H-EA 3:1)

Vanillin-H_2SO_4 color: grayish blue/brown

N,N-dimethyl-*p*-phenylenediamine sulfate test: positive (pink/orange when heated)

$[\alpha]_D$: + 183 ° (*c* 0.1 in MeOH)

CD [θ] (nm): 360 (sh), 345 (+), 263 (-), 230 (+)

UVλ_{max}^{MeOH}: 228 nm (ε 7400) (disappeared with minute HCl)

FI-MS *m/z* (%): 266 (M^+, 100)

EI-HR-MS: M^+ 266.156 ($C_{15}H_{22}O_4$, requires 266.152)

EI-MS *m/z* (%): 266 (M^+, 1.9), 248 (M^+-H_2O, 3.1), 238 (M^+-CO, 1.2), 237 (M^+-CHO, 4.5), 233 (M^+-HO_2, 1.6), 221 (2.4), 220 (2.8), 219 (M^+-H_2O-CHO, 2.8), 205 ($M^+-C_3H_7-HO_2$, 4.0), 203 (3.4), 191 (10), 139 (16), 137 (15), 123 (13), 121 (15), 109 (28), 107 (14), 97 (25), 95 (18), 93 (15), 91 (14), 83 (25), 81 (21), 79 (14), 71 (12), 70 (22), 69 (100), 67 (16), 57 (18), 55 (62), 53 (15), 43 (47), 41 (73).

IRν_{max}^{KBr} (cm^{-1}): 3450 (OH), 2950 (CH), 2820 and 2730 (CHO), 1690 (C=O), 1450, 1380, 1260, 1160, 1080, 1050, 1020, 990, 940.

IR$\nu_{max}^{CCl_4}$ (cm^{-1}) (0.31 mM): 3563 (intramolecularly hydrogen-bonding OH).

^{1}H-NMR data are shown in Tables 3-2 and 3-3.

^{13}C-NMR data are shown in Tables 3-4 and 3-5.

3-2-3 Structure Elucidation of Rugosal A (by Chemical Conversion)

1) Acetylation

Since rugosal A (1) has a secondary allylic OH group at C-2, 1 is convertible to the corresponding monoacetate with a standard acetylation reaction. Crystallines of 1 (12.0 mg) dissolved in 1.6 ml of an acetic anhydride/pyridine mixture (1:1) were heated to 80 °C in an ampoule for 3 hr, at which point the reaction mixture was diluted with excess amount of toluene and then removed the solvent *in vacuo*. The residue was dissolved in small volume of EtOAc and then checked on TLC (H-EA 3:1) as shown in Fig. 3-29. Practically two products were detected under UV 254 nm light and Vanillin-H_2SO_4 test. To purify these products, the whole mixture was subjected to PTLC (H-EA 3:1) to give RSA-AC-1 (*Rf* 0.44) and RSA-AC-2 (*Rf* 0.37), respectively.

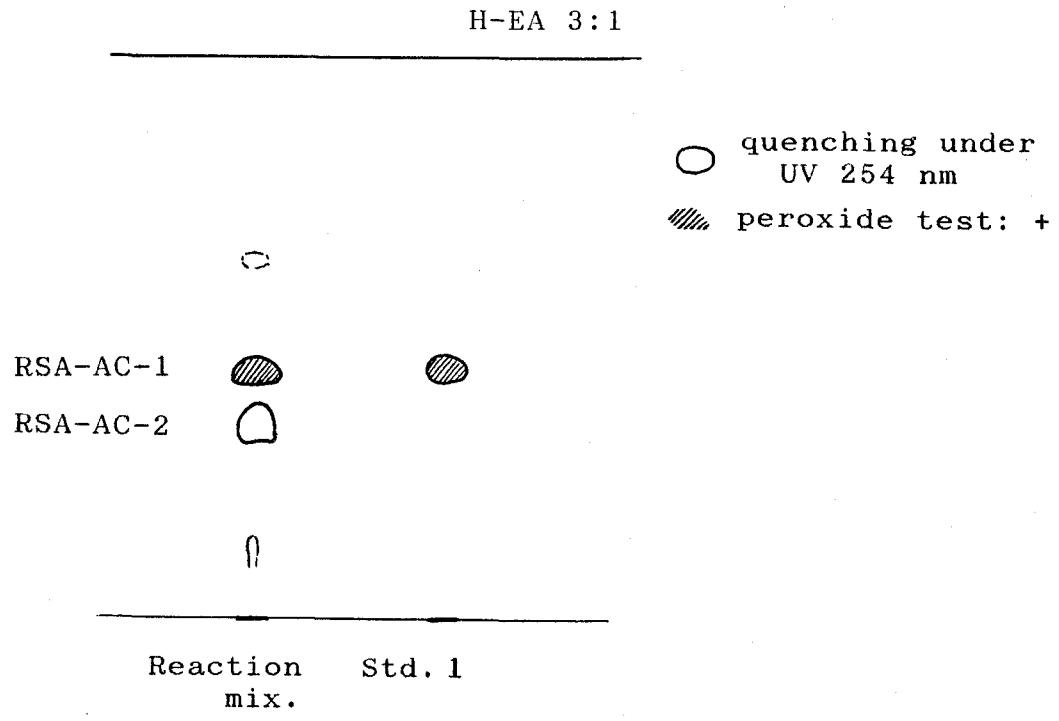

Fig. 3-29 TL Chromatogram of Acetylation Products of Rugosal A (1)

The main product, RSA-AC-1 obtained as 7.5 mg of colorless needles (yield 54 %) showed in EI-MS M^+ 308 (1.1 %) corresponding to that of rugosal A monoacetate. The other characteristic fragments were *m/z* 266 (M^+-CH_2CO, 3.1 %) and 248 ($M^+-CH_2CO+H_2O$, 2.2 %) due to fragmentation at -OAc, and *m/z* 234 (M^+-CH_2CO-32, 1.5 %) and 216 ($M^+-CH_3COOH-32$, 2.1 %) presumably both partly due to a cleavage of the endoperoxy bridge (Fig. 3-30).

Together with disappearance of C-2-OH proton in ^{1}H-NMR spectrum, RSA-AC-1 showed an acetoxy methyl singlet at δ_H 1.722 (3H, -O-CO-C$\underline{H}_3$) not detected in **1**. A remarkable downfield shift (by approx. 1.5 ppm) of C-2 methine proton at δ_H 5.685 was indicative of successful acethylation on the C-2-OH group. Furthermore, the fact that the other protons showed a good correspondence with those of **1** indicated the preservation of the basal structure of the starting material including its endoperoxy linkage (Fig. 3-31 and Table 3-11). Thus, structure of RSA-AC-1 was confirmed to be **1a**. The acetylation afforded a shilding effect on C-11 proton and a slight deshielding effect on C-10 proton. These shifting effects were indicative of the relative orientation of each protons to the C-2-OH, and this fact gave further evidence for the proposed stereostructure of rugosal A (Fig. 3-32).

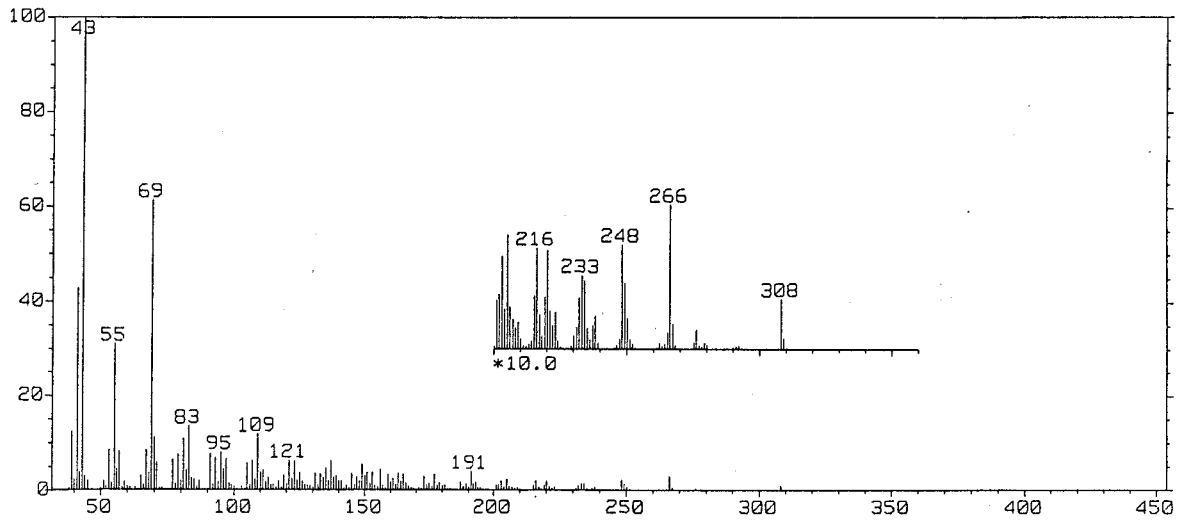

Fig. 3-30 EI-Mass Spectrum of RSA-AC-1

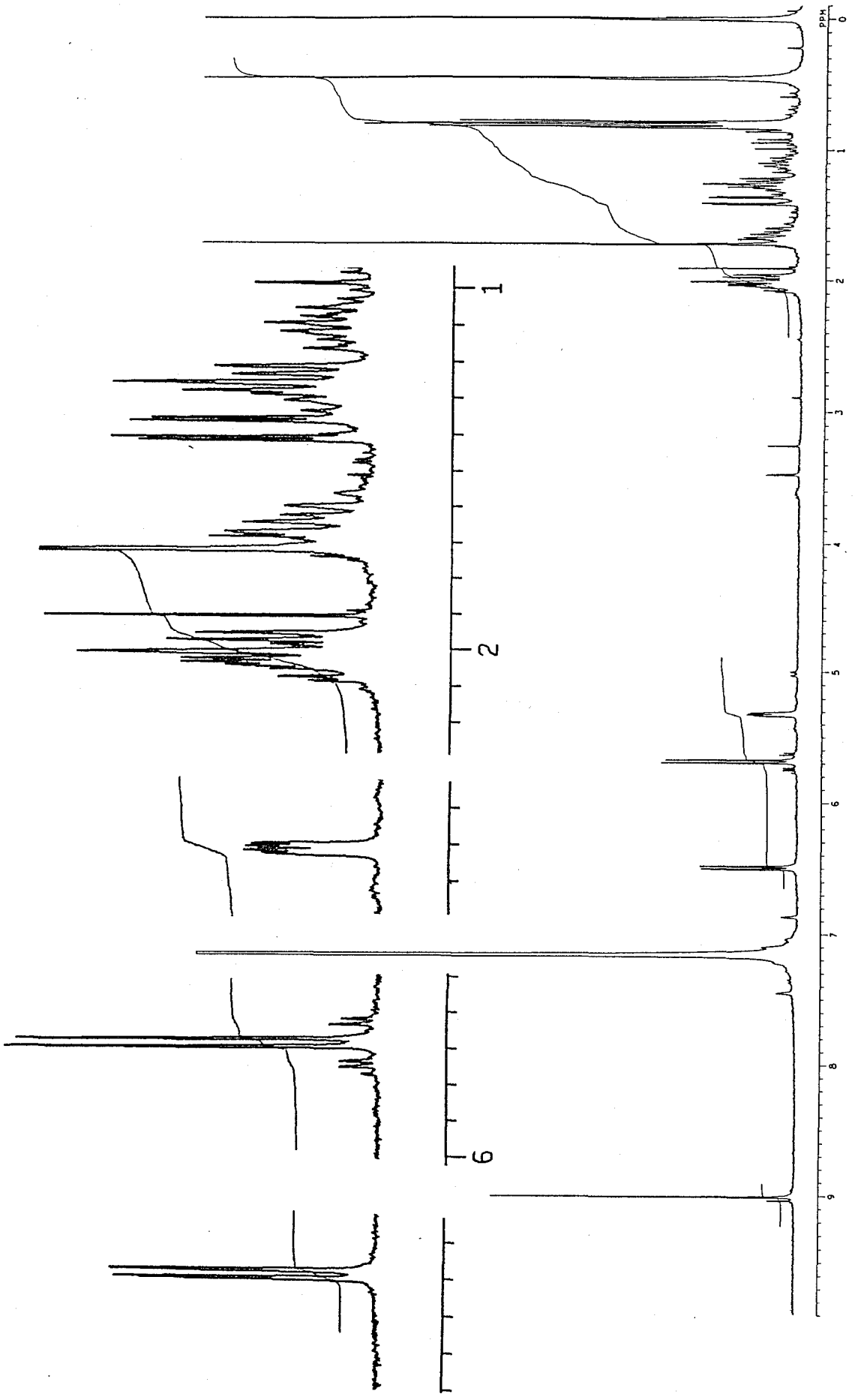

Fig. 3-31 ^{1}H-NMR Spectrum of RSA-AC-1 (270 MHz, in C_6D_6)

Table 3-11 ^{1}*H-NMR chemical shift values for RSA-AC-1 compared with rugosal A*

(270 MHz, in C_6D_6, TMS as an int. std.)

δ_H	*J*(Hz)	Assignment	rugosal A (1)	δ_H
5.685	d (5.9)	C-2-H	4.185	+1.50
6.491	dd (5.9, 0.7)	C-3-H	5.998	+0.49
5.327	ddd (5.5, 2.6, 0.7)	C-5-H	5.280	+0.05
2.010	dd (14.3, 5.5)	C-6-Ha	1.938	+0.07
1.389	dd (14.3, 2.6)	C-6-Hb	1.374	+0.02
1.659	ddd (12.3, *ca* 12, 6.2)	C-8-Ha	1.628	+0.03
1.248	dd (12.3,6.2)	C-8-Hb	*ca* 1.31	-0.06
1.271	m	C-9-Ha	1.275	±0
1.107	dddd (unread)	C-9-Hb	1.092	-0.02
2.011	m (overlapped)	C-10-H	1.912	+0.10
2.023	double-sept (6.6, 2.6)	C-11-H	2.737	-0.71
0.814	d (6.6)	C-12-H_3	0.840	-0.03
0.795	d (6.6)	C-13-H_3	0.725	+0.07
9.003	s	C-14-H	9.045	-0.04
0.454	s	C-15-H_3	0.378	+0.08
1.722	s	C-3-$OCOCH_3$	-	

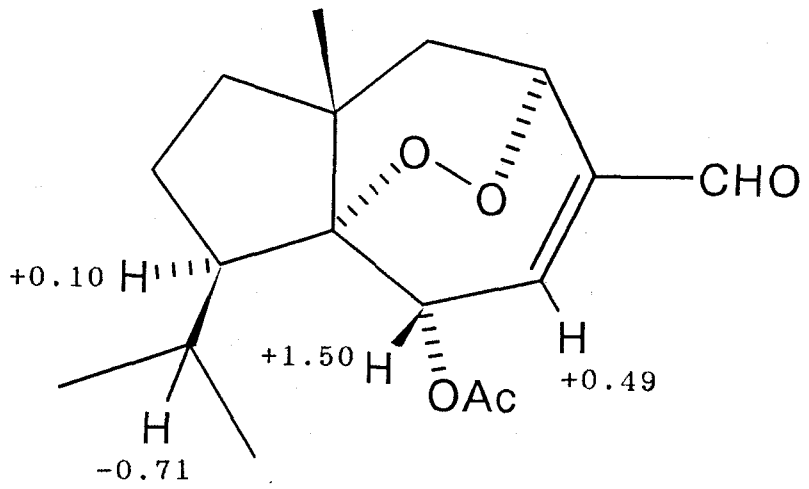

Fig. 3-32 Deshielding Effect of -OAc Group on Some Other Protons

Table 3-12 Physicochemical properties of RSA-AC-1 (1a)

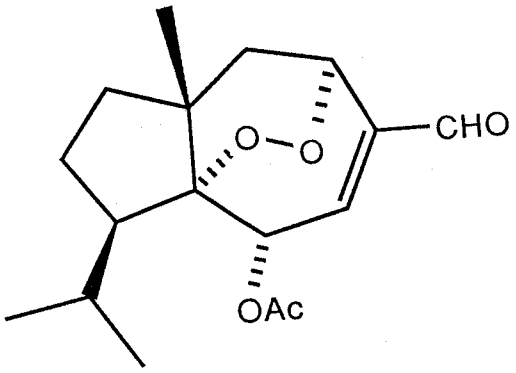

1a

Colorless fine plates, mp 108-109 °C

Rf: 0.44 (H-EA 3:1)

Vanillin-H_2SO_4 test: brown

N,*N*-dimethyl-*p*-phenylenediamine sulfate test: positive (brownish red)

UVλ_{max}^{MeOH}: 226 nm

EI-MS *m/z* (%): 308 (M^+, 1.1), 266 (M^+-$OCOCH_2$, 3.1), 248 (2.2), 234 (M^+-42-32, 1.5), 233 (1.6), 220 (2.1), 216 (2.1), 205 (2.4), 203 (2.0), 193 (1.8), 191 (4.1), 187 (1.8), 179 (1.7), 177 (3.4), 175 (1.5), 173 (3.0), 165 (3.5), 163 (3.7), 161 (2.6), 109 (12), 83 (14), 81 (11), 70 (11), 69 (62), 55 (31), 43 (100), 41 (43).

^{1}H-NMR data are shown in Table 3-11.

The second product, RSA-AC-2 isolated as a colorless syrup (2.4 mg, in a yield of 15 %) showed in EI-MS *m/z* 350 (M^+, 2.7 %) indicative of the corresponding diacetate (Fig. 3-32). Since **1** has only one hydroxyl group at C-2, additional acetylation might occur unexpectedly on the starting molecule or on a rearranged one. Two acetoxy methyl groups were detected at δ_H 1.714 and 1.627 in ^{1}H-NMR spectrum of RSA-AC-2. Furthermore, a pair of doublets was observed at δ_H 2.215 and 1.967 (each 1H, *J*= 12.1 Hz, presumably due to a geminal coupling) as the characteristic signals of RSA-AC-2, and the methine proton signal also disappeared (Fig. 3-34). In addition, this compound showed a negative response to the peroxide test. On the basis of these aspects, it was cosidered that some rearrangement might occur around the C-5 methine proton and/or the peroxy bridge during the acylation. Finally, two possible structures for RSA-AC-2 (structure H and I) were proposed as shown in Fig. 3-35. ^{13}C-NMR spectrometry seemed to be promising to differenciate which was the exact product.

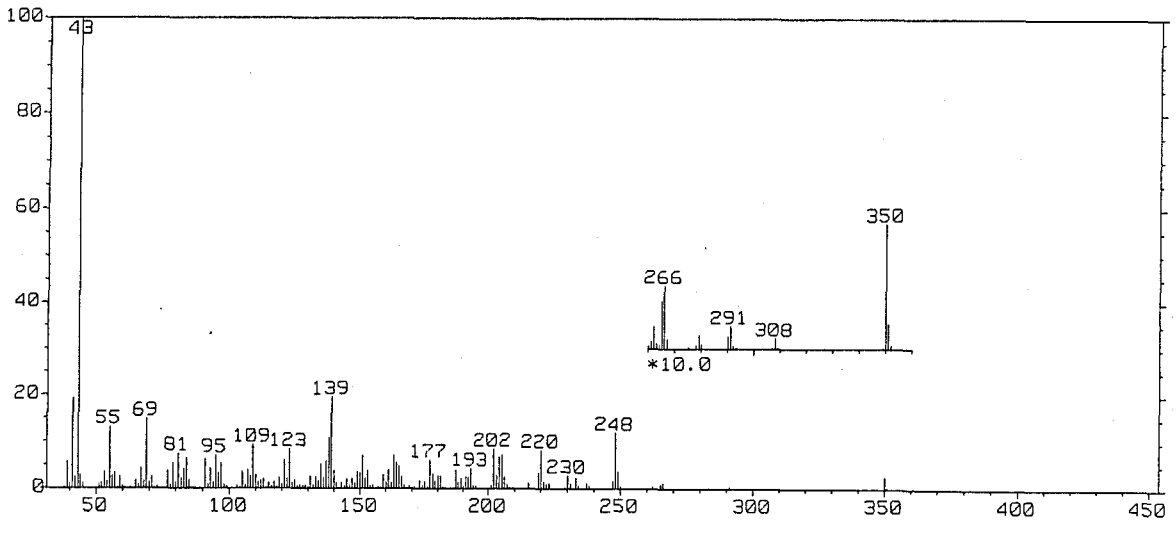

Fig. 3-33 EI-Mass Spectrum of RSA-AC-2

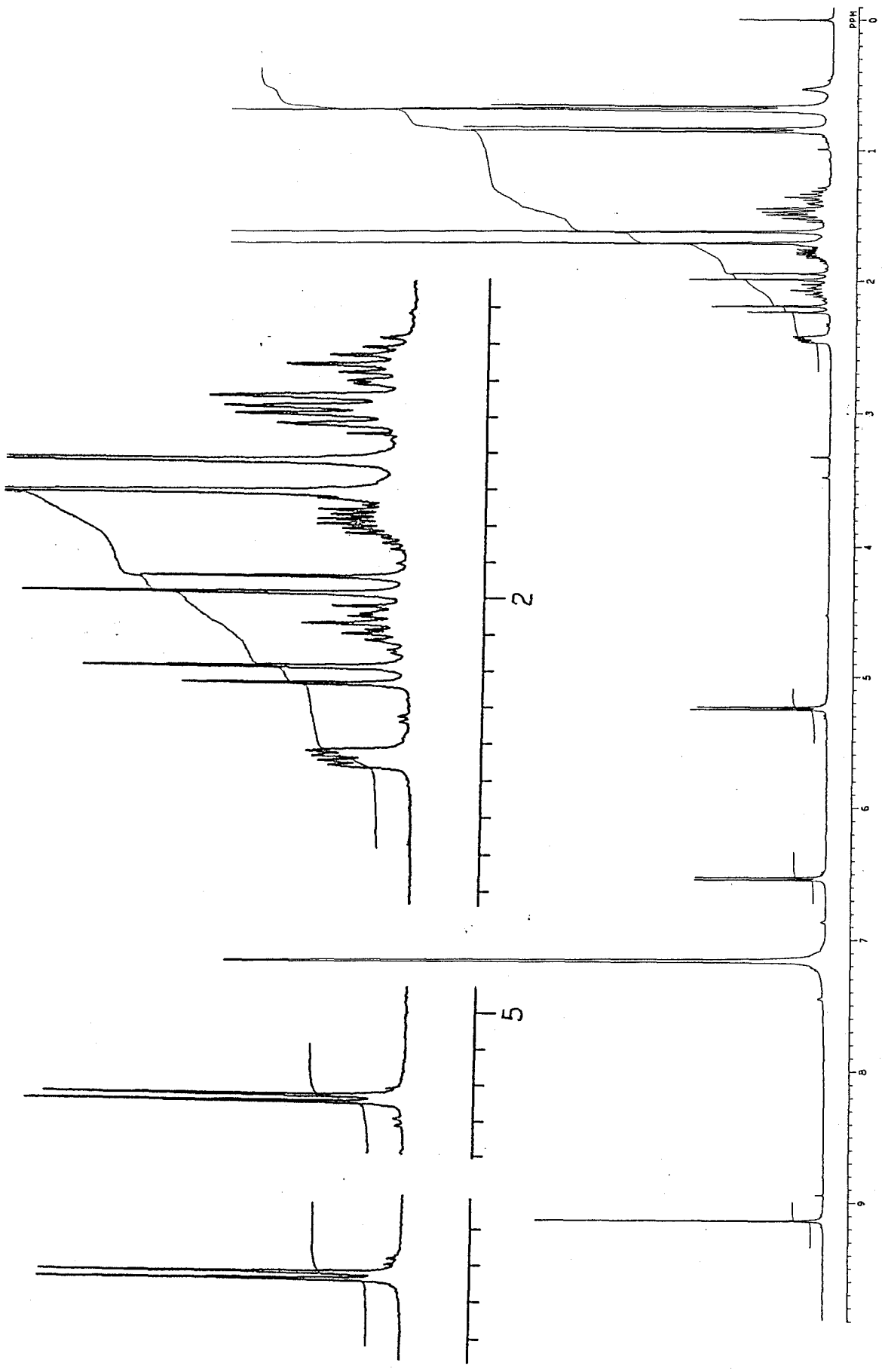

Fig. 3-34 ^{1}H-NMR Spectrum of RSA-AC-2 (270 MHz, in C_6D_6)

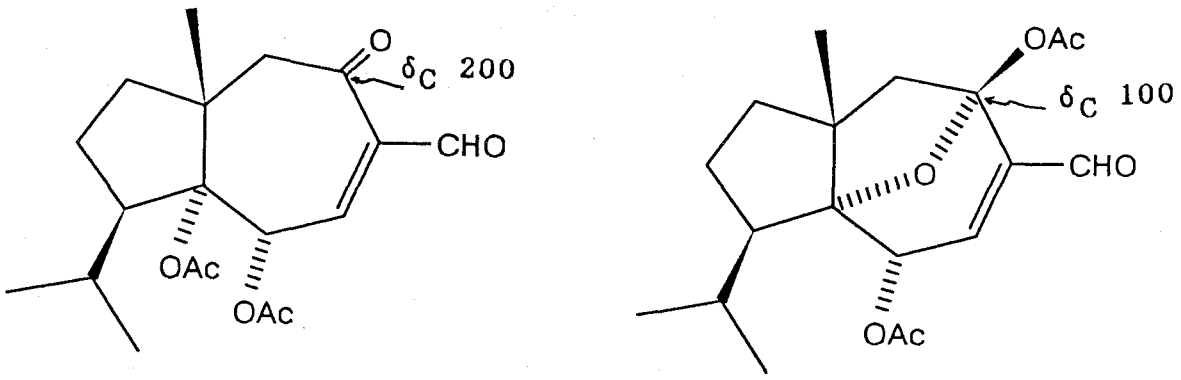

Fig. 3-35 Two Possible Structures for RSA-AC-2: In ^{13}C-NMR spectrum, H should show a ketone carbon signal around δ_C 200, while I should have a ketal carbon around δ_C 100.

The ^{13}C-NMR (COM) spectrum of RSA-AC-2 was therefore measured (Fig. 3-36 and Table 3-13), and as the result, a new signal in place of C-5 in 1 (δ_C 70.1) was detected at δ_C 101.1 assignable to a ketal or hemiacetal carbon. Consequently, the structure 1 was favored to RSA-AC-2, and it was concluded that a base catalyzed rearrangement of 1 resulted in the corresponding hemiacetal derivative. Thus, RSA-AC-2 was deduced to be **1b**.

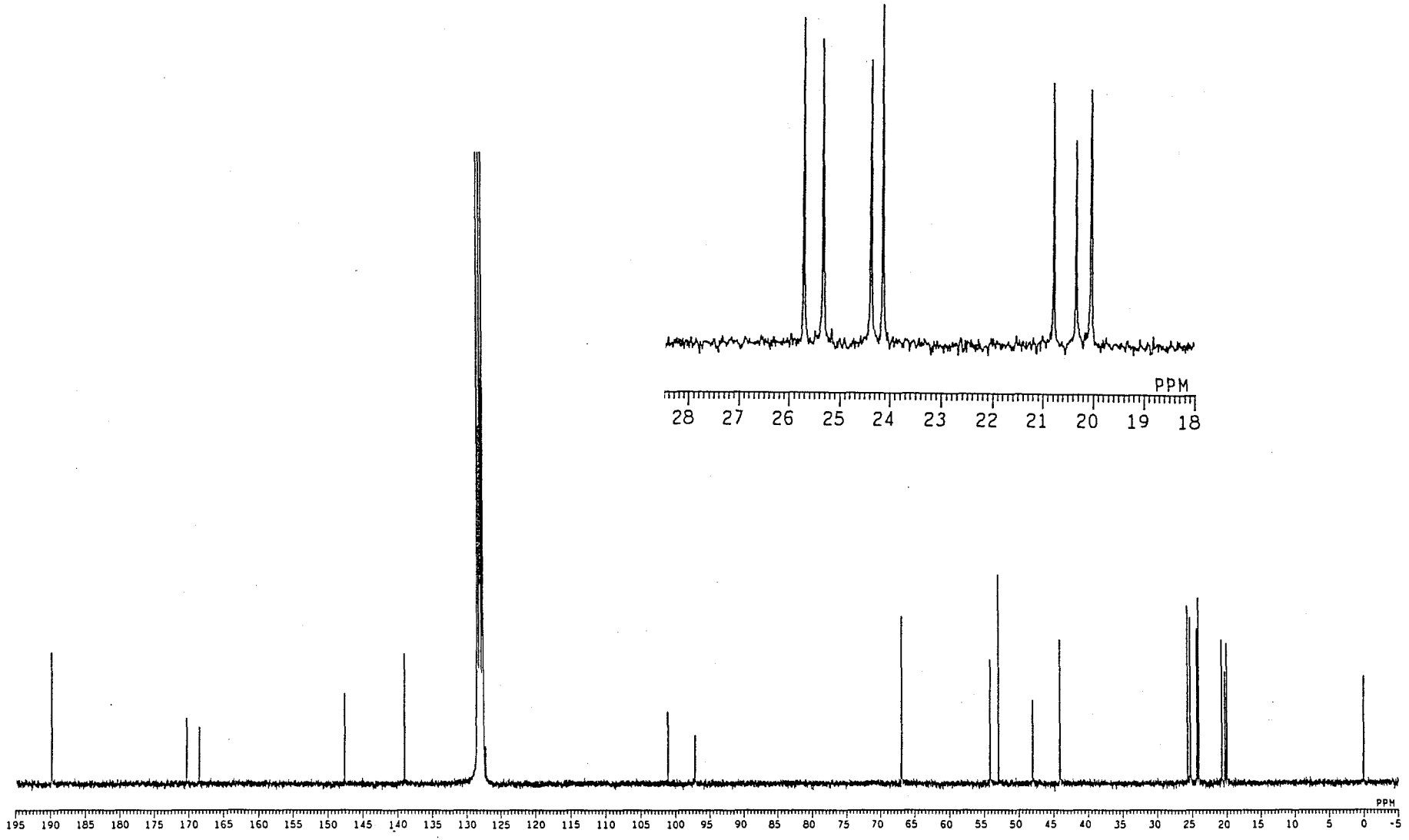

Fig. 3-36 ^{13}C-NMR Spectrum of RSA-AC-2 (68 MHz, in C_6D_6, COM)

Table 3-13 Carbon chemical shift values of RSA-AC-2 compared with rugosal A (1)

(68 MHz, in C_6D_6, TMS as an int. std.)

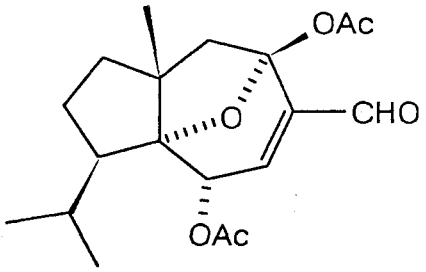

RSA-AC-2 (1b)

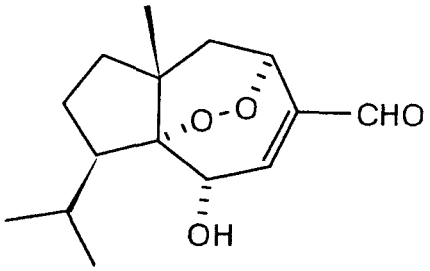

Rugosal A (1)

1b	1	$\Delta\delta_C$	C-No
189.9	190.7	- 0.8	14
170.3	-	-	Ac
168.5	-	-	Ac
147.7	146.5	+ 1.2	3
139.0	149.0	-10.4	4
101.1	70.1	+31.0	5
97.1	94.8	+ 2.3	1
67.0	69.1	- 2.1	2
54.2	42.0	+12.2	6
53.0	54.6	- 1.6	10
48.1	39.6	+ 8.5	7
44.1	38.5	+ 5.6	8
25.7	25.9	- 0.3	15
25.4	22.8	+ 2.6	12
24.4	24.8	- 0.4	11
24.2	20.2	+ 4.0	9
20.8	-	-	Ac
20.4	-	-	Ac
20.1	18.4	+ 1.7	13

Table 3-14 Physicochemical properties of RSA-AC-2 (1b)

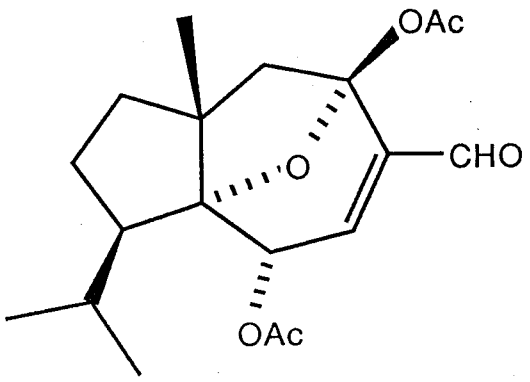

1b

A colorless syrup

Rf: 0.37 (H-EA 3:1)

Vanillin-H_2SO_4 color: yellowish brown

N,N-dimethyl-*p*-phenylenediamine sulfate test: negative

EI-MS *m/z* (%): 350 (M^+, 2.7), 308 (M^+-$COCH_2$, 0.3), 291 (M^+-59, 0.5), 279 (0.3), 266 (M^+-$2COCH_2$, 1.4), 265 (1.1), 248 (12), 233 (2.3), 230 (2.7), 220 (8.3), 205 (7.3), 204 (6.8), 202 (8.6), 193 (4.4), 187 (4.2), 177 (6.2), 164 (5.6), 163 (7.2), 151 (7.1), 139 (20), 138 (11), 123 (8.5) 109 (9.4), 95 (7.2), 81 (7.6), 69 (15), 55 (13), 43 (100), 41 (19).

^{1}H-NMR $\delta^{C_6D_6}_{TMS}$ (270 MHz): 5.243 (1H, d, *J*= 5.1 Hz, C-2-H), 6.535 (1H, d, *J*= 5.1 Hz, C-3-H), 2.215 (1H, d, *J*= 12.1 Hz, C-6-Ha), 1.967 (1H, d, *J*= 12.1 Hz, C-6-Hb), 1.488 (2H, dd, *J*= Hz, C-8-H_2), 2.073 (1H, m, C-9-Ha), 1.351 (1H, ddd, *J*= Hz, C-9-Hb), 2.443 (1H, dd, *J*= 6.6 and 3.7 Hz, C-10-H), 1.792 (1H, double sept., *J*= 6.6, 3.7 Hz, C-11-H), 0.846 (3H, d, *J*= 6.6 Hz, C-12-H_3), 0.679 (3H, d, *J*= 6.6 Hz, C-13-H_3), 9.138 (1H, s, C-14-H), 0.698 (3H, s, C-15-H_3), 1.714* (3H, s, C-2-$OCOCH_3$), 1.627* (3H, s, C-5-$OCOCH_3$).

* Assignment of these protons may be exchanged.

^{13}C-NMR data are shown in Table 3-12.

2) Reduction with $NaBH_4$

Rugosal A (1) dissolved in 20 % $MeOH/EtO_2$ (7.5 mg/2 ml) was mixed with excess amount of $NaBH_4$ (8 mg), and stirred overnight, at which point the reaction mixture was concentrated *in vacuo* and then dissolved in a small volume of EtOAc. Being checked by TLC with vanillin-H_2SO_4 coloration, two products at *Rf* 0.30 and 0.07 (H-EA 1:1) were detected as a non-quenching but coloring a yellowish brown (RSA-NBH-1) or a yellowish orange (RSA-NBH-2) spot, respectively (Fig. 3-37). The whole mixture was accordingly subjected to PTLC (H-EA 1:1) to give 4.4 mg of RSA-NBH-1 (colorless needles, in a 58 % yield) and 2.6 mg of RSA-NBH-2 (semisolid, 26 % yield).

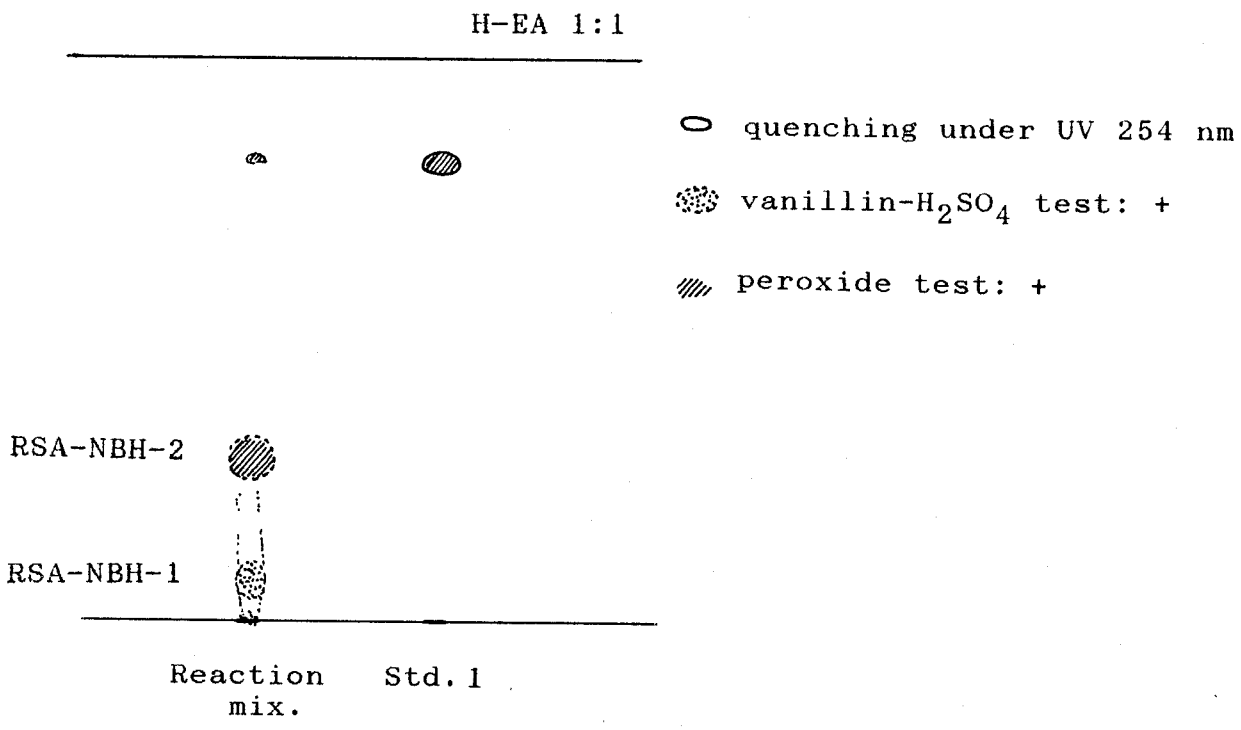

Fig. 3-37 TL Chromatogram of $NaBH_4$ Reduction Products of Rugosal A (1)

The major product, RSA-NBH-1 featureless above 210 nm in UV spectrum, showed M^+ 268 (1 + H_2) in FI-MS (Fig. 3-38). In addition, the EI-MS fragment at *m/z* 238 (M^+-CH_2O, 0.6 %) was indicative of its primary alcoholic property (Fig. 3-39). A positive response of the product to the peroxide test was suggestive that only C-14 aldehyde group of **1** was reduced to hydroxyl group. ^{1}H-NMR spectrum of RSA-NBH-1 showing the carbinol methylene protons at δ_H 4.392 as a broad singlet was further provided a proof of the expected reduction. Similar to this methylene signal, protons detected around 3-5 ppm all showed broad and complicated signals (Fig. 3-40). When D_2O was added, however, these signals became sharpened. Moreover, a doublet signal at δ_H 2.836 assignable to C-2-O<u>H</u> proton (*J*= 11.7 Hz) disappeared with collapse of δ_H 4.256 proton (dd) into a doublet (*J*= 6.2 Hz) (Fig. 3-41). All proton sequence attributable to the carotane-endoperoxied skeleton for RSA-NBH-1 (Fig. 3-42) became feasible. Together with some lines of evidence mentioned-above, a good correspondence in ^{1}H-NMR spectrum between **1** and RSA-NBH-1 except the carbinol methylene (Table 3-15) eventually gave **1c** as the reasonable structure to the $NaBH_4$ reduction product.

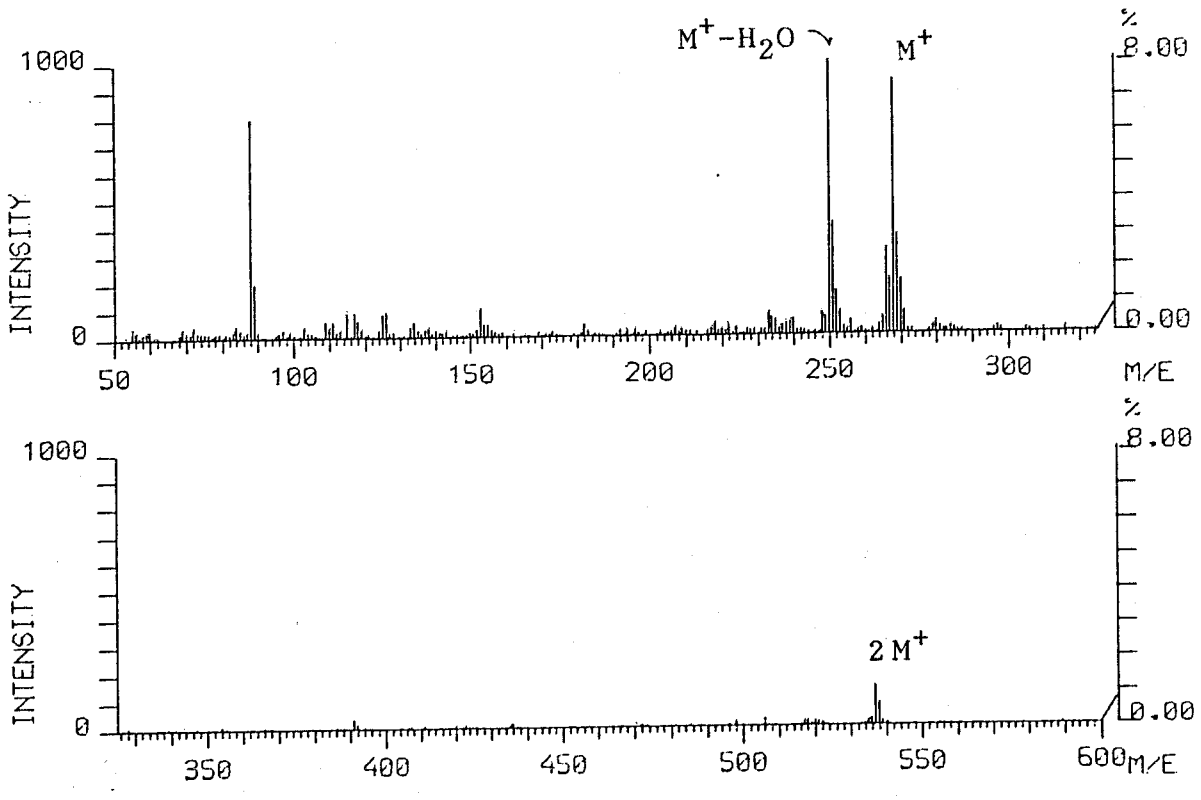

Fig. 3-38 FD-Mass Spectrum of RSA-NBH-1

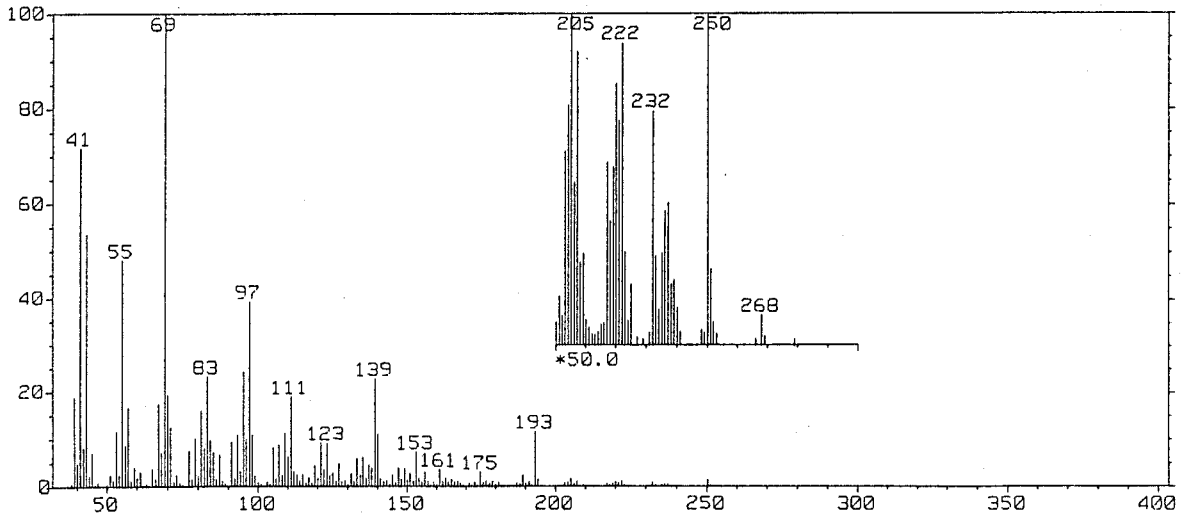

Fig. 3-39 EI-Mass Spectrum of RSA-NBH-1

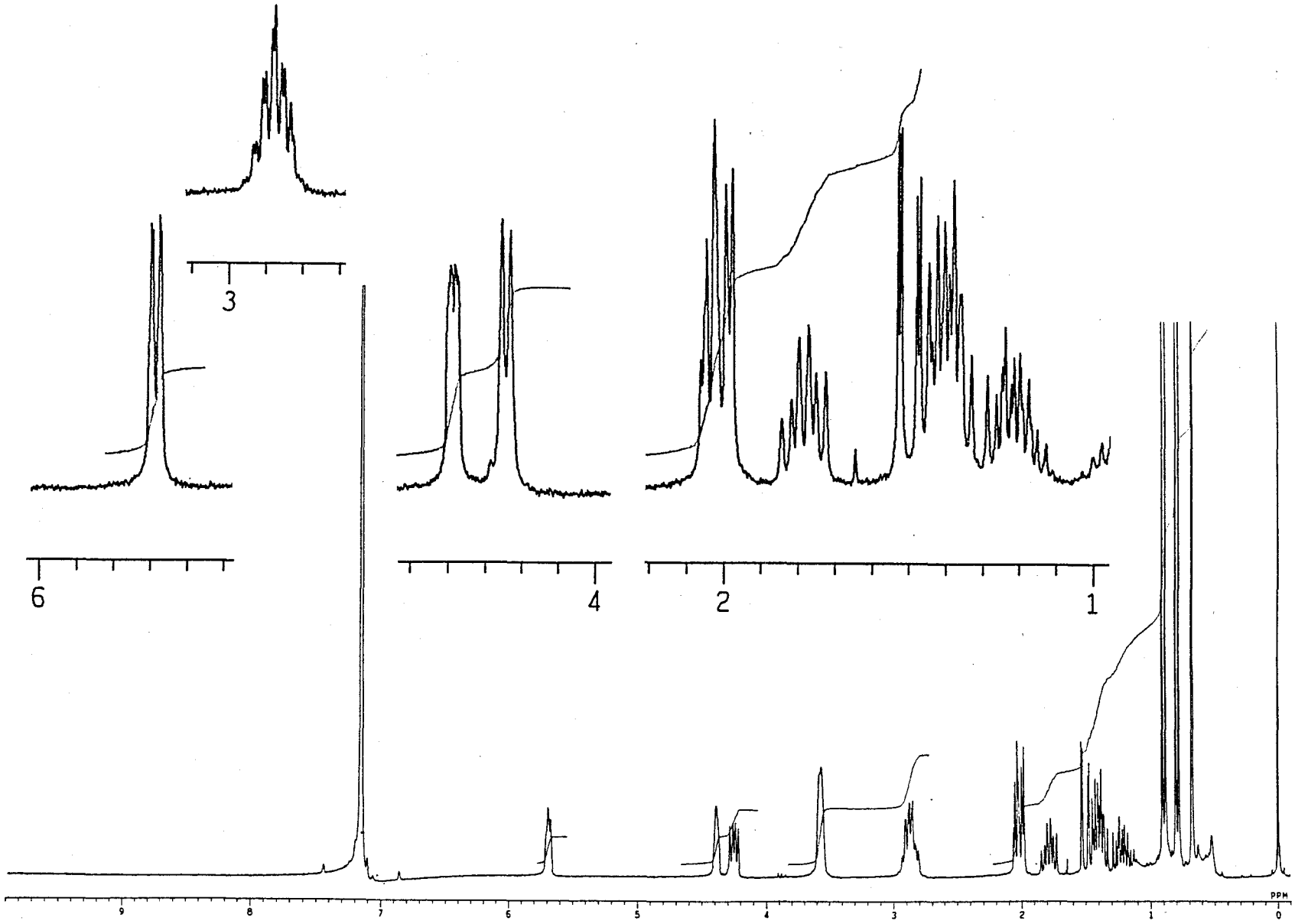

Fig. 3-40 ^{1}H-NMR Spectrum of RSA-NBH-1 (270 MHz, in C_6D_6)
The magnified signals were revealed after D_2O addition

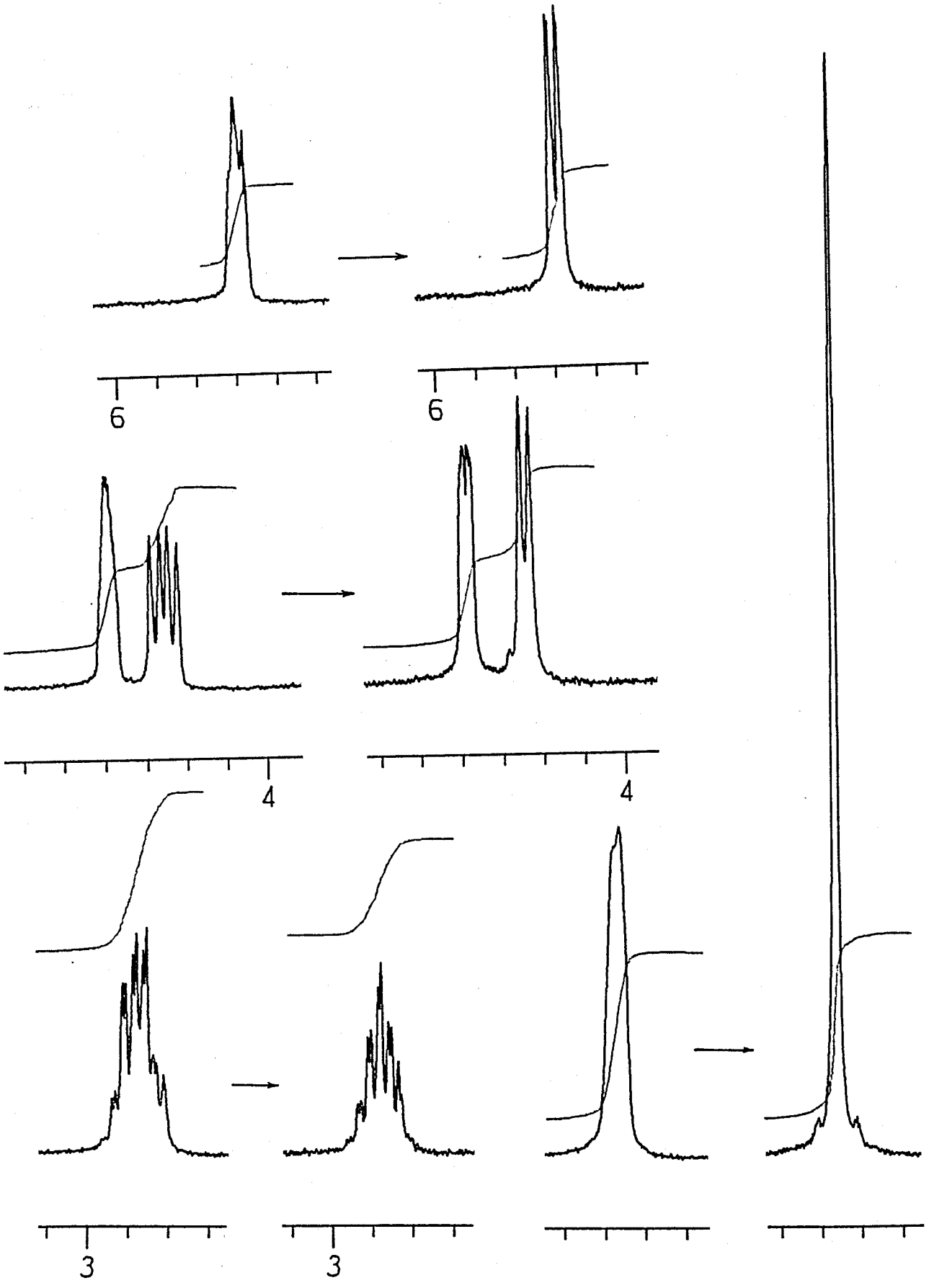

Fig. 3-41 Signal Change by D_2O Addition in RSA-NBH-1

Table 3-15 *^{1}H-NMR chemical shift values of RSA-NBH-1 compared with those of rugosal A (1)*

(270 MHz, in C_6D_6, TMS as an int. std.)

δ_H	*J*(Hz)*	Assignment	1	*J*(Hz)
4.256	dd (11.7, 6.2)	C-2-H	4.185	dd (11.7, 6.4)
5.697	dd (6.2, 1.1)	C-3-H	5.998	dd (6.4, 1.1)
4.392	ddd (5.1, 2.2, 1.1)	C-5-H	5.280	ddd (5.1, 2.6, 1.1)
2.018	dd (13.9, 5.1)	C-6-Ha	1.938	dd (13.9, 5.1)
1.389	dd (13.9, 2.2)	C-6-Hb	1.374	dd (13.9, 2.6)
1.789	ddd (12.5, 12.5, 7.3)	C-8-Ha	1.628	ddd (12.8, 12.5, 7.3)
1.416	dd (12.1, 6.6)	C-8-Hb	1.275	dd (12.5, 6.6)
1.387	m	C-9-Ha	*ca* 1.31	m
1.210	dddd (13.2, 13.2,11.0, 6.6)	C-9-Hb	1.092	dddd (12.8, 10.6, 10.3, 6.6)
2.060	ddd (8.8, 8.4, 2.2)	C-10-H	1.912	ddd (10.6, 9.7, 2.6)
2.886	double sept (6.8, 2.2)	C-11-H	2.737	double sept (6.8, 2.6)
0.896	d (6.8)	C-12-H_3	0.840	d (6.8)
0.793	d (6.8)	C-13-H_3	0.725	d (6.8)
3.569	br. s	C-14-H_2	9.045	s
0.678	s	C-15-H_3	0.378	s
2.836	d (11.7)	C-2-OH	2.711	d (11.7)

* Coupling constants were depicted upon addition of D_2O.

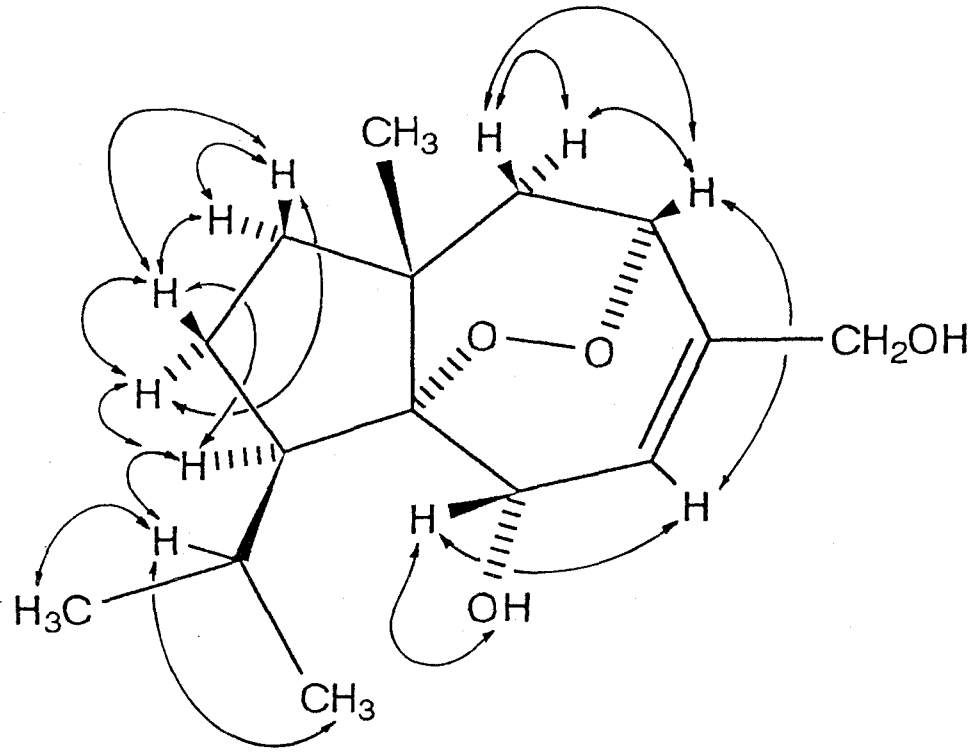

Fig. 3-42 Proton Coupling Sequences in RSA-NBH-1

Table 3-16 Physicochemical properties of RSA-NBH-1 (1c)

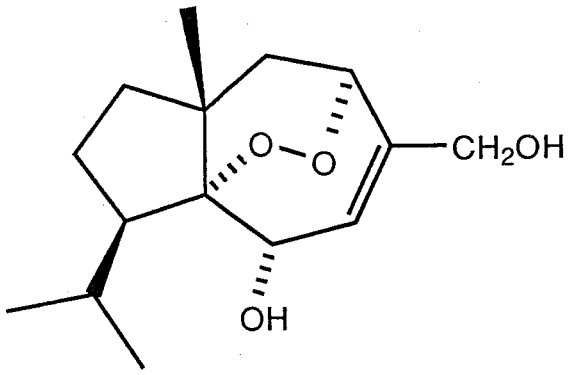

1c

Colorless needles, mp 117-118 °C

Rf: 0.30 (H-EA 1:1, *cf.* **1**; 0.82), 0.52 (C-M 50:4)

Vanillin-H_2SO_4 color: grayish yellow

N,*N*-dimethyl-*p*-phenylenediamine sulfate test: positive (pinkish red)

UV λ_{max}^{MeOH}: featureless above 210 nm

FD-MS *m/z* (%): 537 ($2M^+$+1, 15), 269 (M^++1, 37), 268 (M^+, 93), 251 (41), 250 (M^+-H_2O, 100), 88 (80).

EI-MS *m/z* (%): 268 (M^+, 0.1), 250 (M^+-H_2O, 1.4), 238 (M^+-CH_2O, 0.6), 205 (1.7), 193 (12), 153 (7.5), 140 (11), 139 (23), 123 (9.3), 121 (9.4), 111 (19), 97 (40), 95 (25), 83 (24), 69 (100), 55 (48), 43 (54), 41 (72).

^{1}H-NMR data are shown in Table 3-17.

The minor product, RSA-NBH-2 was indicated to be a rearranged product at the peroxide bridge due to a negative response to *N,N*-dimethyl-*p*-phenylenediamine sulfate test. In spite of the presence of some impurities, the product showed M^+ 268 (65 %) in FD-MS (Fig. 3-43), as with **1c**. In the EI-MS, *m/z* 139 appeared as the base peak (Fig. 3-44). ^{1}H-NMR spectrum of RSA-NBH-2 taken in $CDCl_3/CD_3OD$ (1:1) showed a pair of unequivalent two protons of C-14-H_2 at δ_H 4.278 and 4.080 (both d, *J*= 14.3 Hz). Furthermore, C-5 methine proton disappeared (Fig. 3-45). These features in ^{1}H-NMR spectrum were partly similar to RSA-AC-2 (**1b**), a peroxide-rearranged diacetate of rugosal A (**1**). Therefore, structure of RSA-NBH-2 was tentatively deduced to be **1d**, which was probably yielded by Na^+ as a catalytic base.

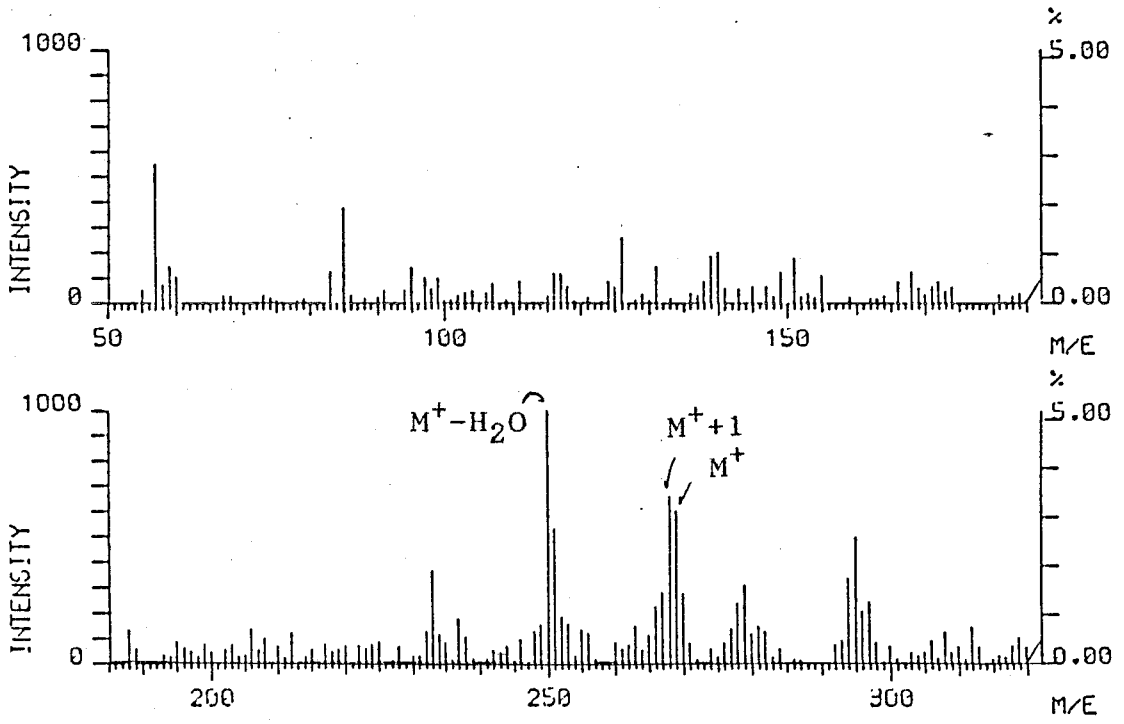

Fig. 3-43 FI-Mass Spectrum of RSA-NBH-2

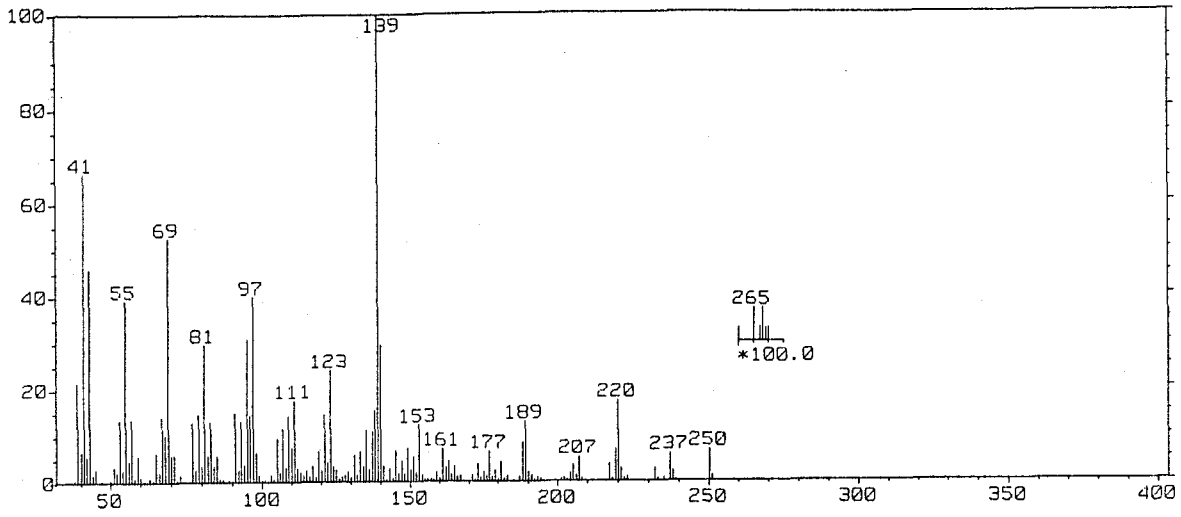

Fig. 3-44 EI-Mass Spectrum of RSA-NBH-2

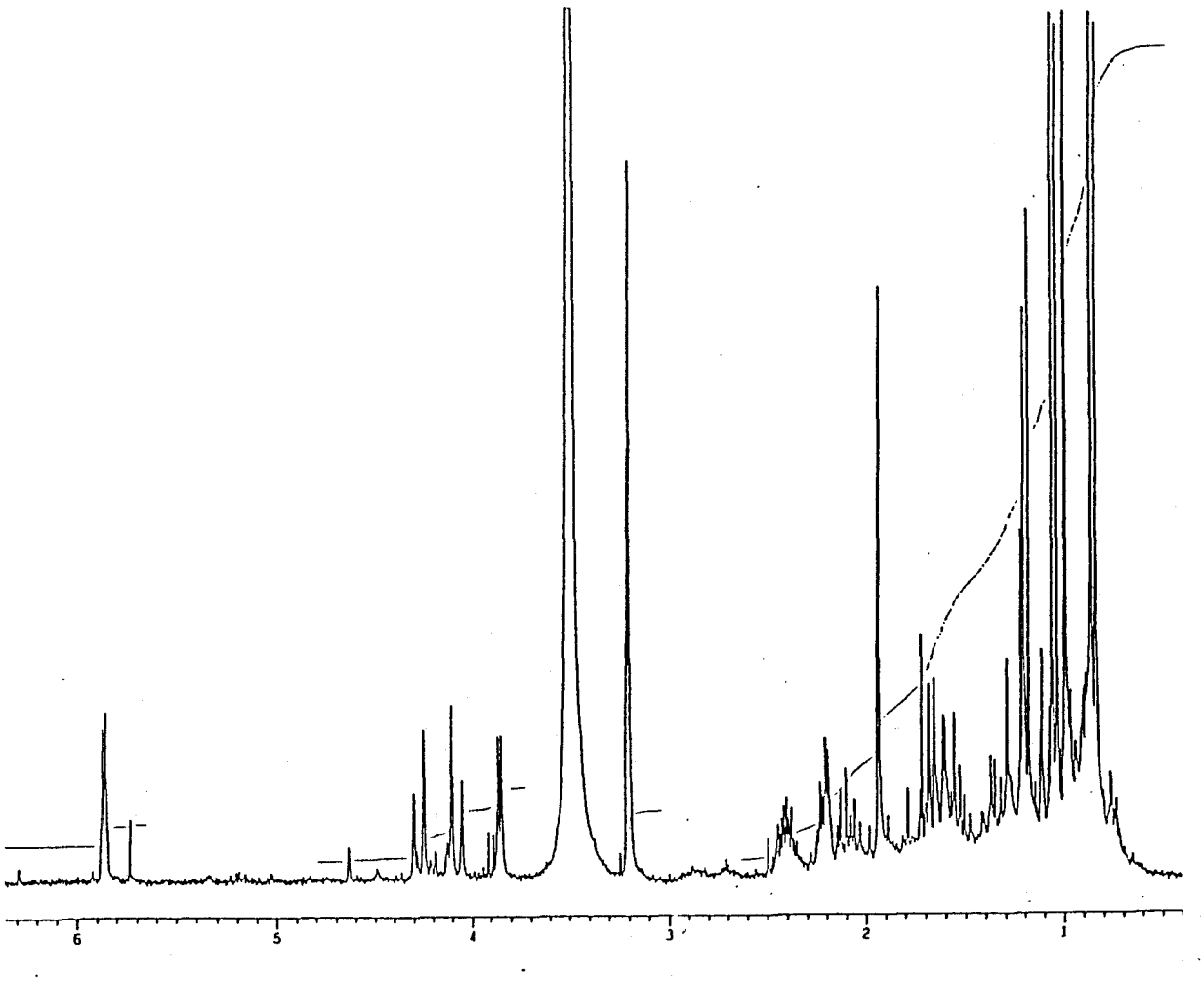

Fig. 3-45 ^{1}H-NMR Spectrum of RSA-NBH-2 (270 MHz, in $CDCl_3/CD_3OD$ mix.) Magnified the area from 7 ~ 1 ppm.

Table 3-17 Physicochemical properties of RSA-NBH-2 (1d)

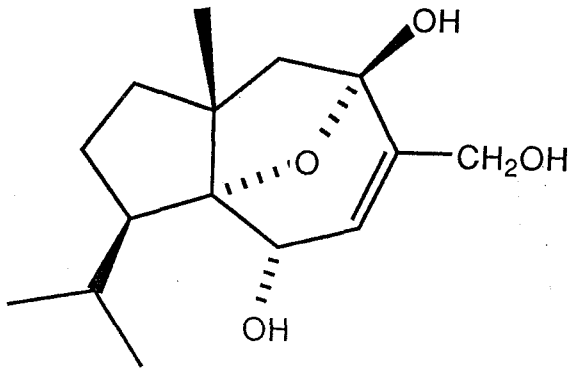

1d (tentative)

A colorless semisolid

Rf: 0.07 (H-EA 1:1)

Vanillin-H_2SO_4 color: yellowish orange

N,*N*-dimethyl-*p*-phenylenediamine sulfate test: negative

FD-MS *m/z* (%): 268 (M^+, 100)

EI-MS *m/z* (%): 268 (M^+, trace), 250 (M^+-H_2O, 6.6), 237 (M^+-OCH_3, 5.8), 220 (17), 207 (4.9), 189 (13), 153 (12), 140 (30), 139 (100), 123 (24), 111 (18), 97 (40), 95 (31), 81 (30), 69 (53), 55 (39), 43 (46), 41 (67).

^{1}H-NMR $\delta_{TMS}^{CDCl_3}$ /CD_3OD (270 MHz): 5.870 (1H, br. d, *J*= 4.8 Hz, C-3-H), 4.278 (1H, d, *J*= 14.3 Hz, C-14-Ha), 4.080 (1H, d, *J*= 14.3 Hz, C-14-Hb), 3.855 (1H, d, *J*= 4.8 Hz, C-2-H). Some signals were invisible because of overlapping with large solvent and water peaks.

3) Reduction with Thiourea

Thiourea is known as a reducing reagent which can selectively cleave an endoperoxide to yield a diol under a mild condition without any reduction of carbonyl groups [101]. This reagent was, therefore, applied to rugosal A (1) to obtain a trihydroxy carotanoid. Crystallines of 1 (6.3 mg) was dissolved in 3 ml of MeOH with 11.1 mg of thiourea, and stirred overnight at room temperature. The reaction mixture was then concentrated to a small volume and subjected to PTLC (C-M 50:4) to give 1.8 mg of a polar product (RSA-TU, yield 29 %) together with unchanged material(3.8 mg, 60 %) (Fig. 3-46).

The product obtained as a colorless syrup showed *m/z* 269 (M^++1, 100 %) and 250 (M^+-H_2O, 34 %) in FD-MS, which was indicative of two proton additions (Fig. 3-47). In EI-MS analysis, a dehydration fragment at *m/z* 250 (0.4 %) was detected as the largest mass fragment, and a fragment *m/z* 232 (2.0 %) caused by further dehydration was also observed (Fig. 3-48). As shown in Fig. 3-49,

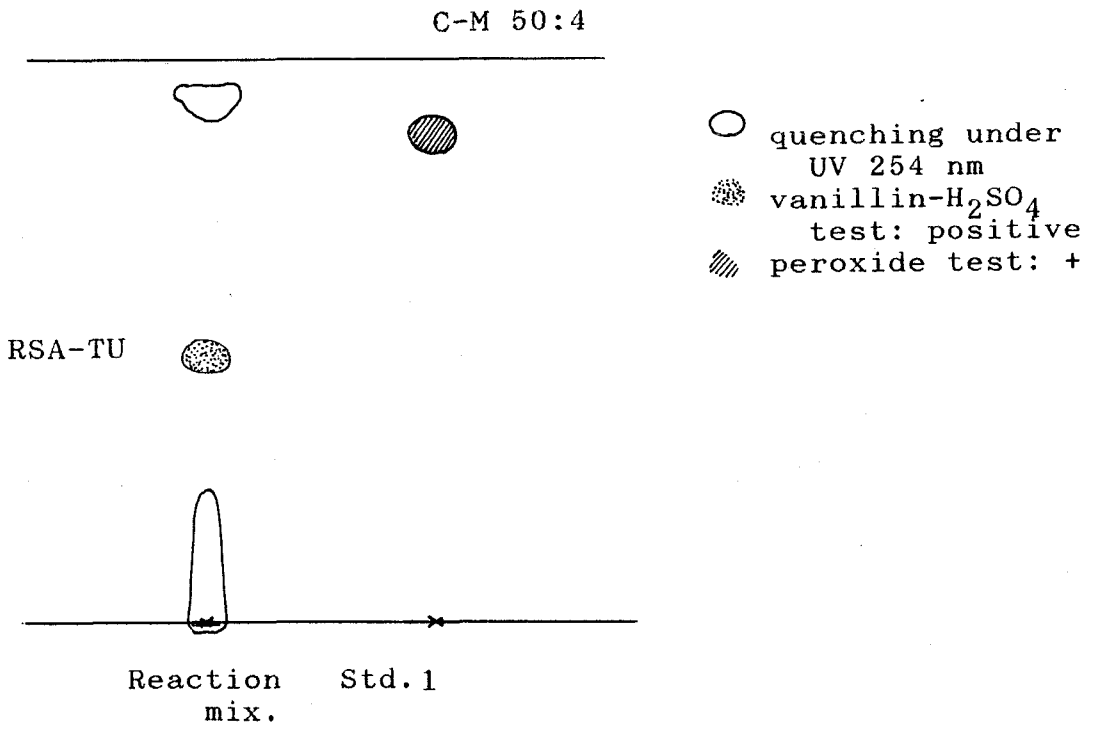

Fig. 3-46 TL Chromatogram of Reaction Product Obtained by Reduction of Rugosal A (1) with Thiourea

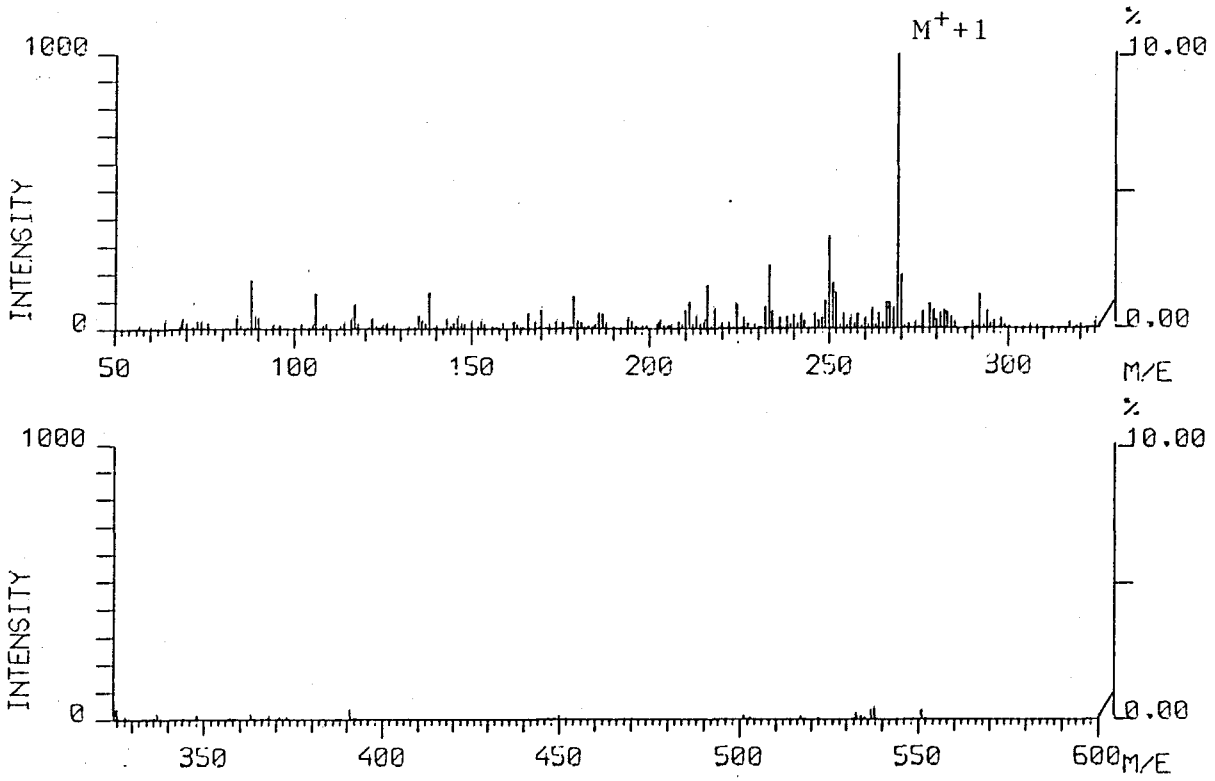

Fig. 3-47 FD-Mass Spectrum of RSA-TU

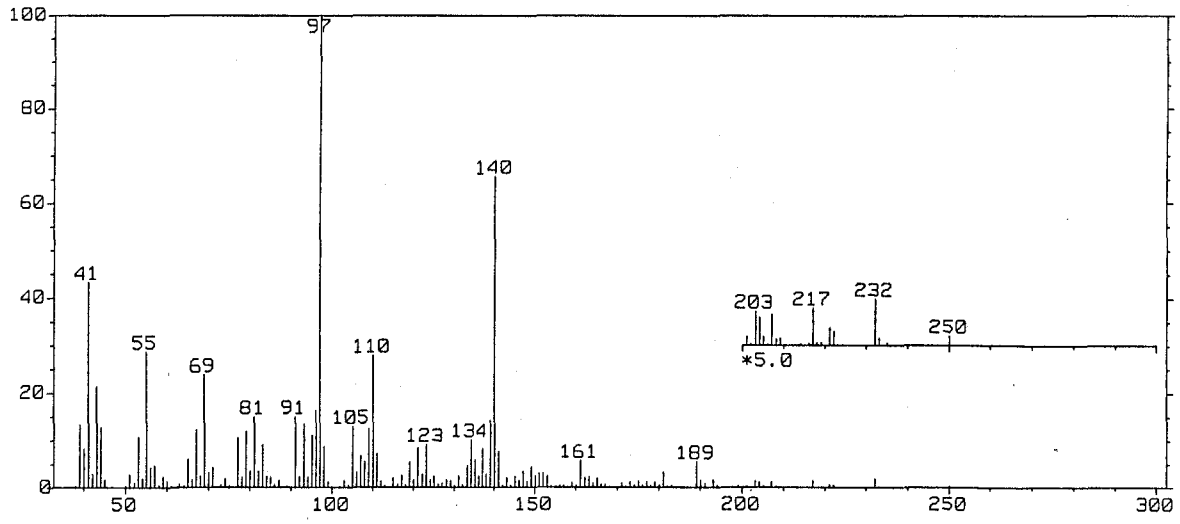

Fig. 3-48 EI-Mass Spectrum of RSA-TU

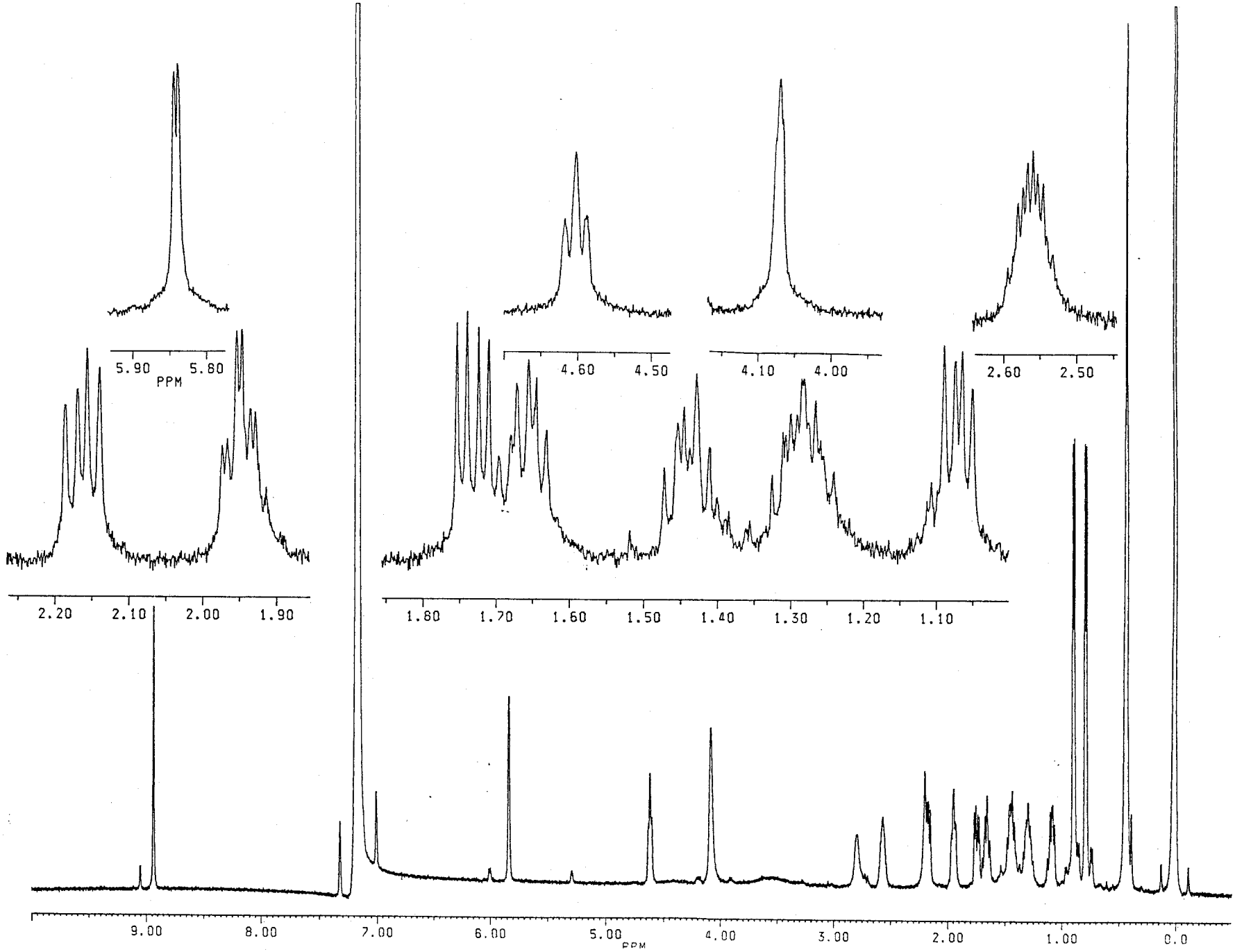

Fig. 3-49 ^{1}H-NMR Spectrum of RSA-TU (500 MHz, in C_6D_6)
The magnified signals were revealed after D_2O addition.

Table 3-18 ^1H-NMR chemical shift of RSA-TU (1e)

(500 MHz, in C_6D_6, TMS as an int. std.)

δ_H*	Coupling*	Assignment
8.927	s	C-14-H
5.841	d *J*= 2.7 Hz	C-3-H
4.603	br. dd *J*= 8.2, 6.8 Hz	C-5-H
4.074	incomplete d	C-2-H
2.78 (approx.)	br.**	C-5-OH
2.563	double sept *J*= 6.8, 3.0 Hz	C-11-H
2.184	s**	C-2-OH
2.163	dd *J*= 14.8, 8.2 Hz	C-6-Ha
1.952	ddd *J*= 9.0, 3.0 Hz	C-10-H
1.732	dd *J*= 14.8, 6.8 Hz	C-6-Hb
1.678	m	C-8-Ha
1.438	m	C-9-Ha
1.287	m	C-9-Hb
1.071	dd *J*= 12.2, 7.2 Hz	C-8-Hb
0.884	d *J*= 6.8 Hz	C-12-H_3
0.780	d *J*= 6.8 Hz	C-13-H_3
0.417	s	C-15-H_3

* Chemical shifts and coupling constants were picked up after D_2O was added.

** These protons were exchangeable with D_2O.

the ^{1}H-NMR spectrum showed a basal skeleton of 1, including a formyl proton observed at δ_H 8.927 (1H, s) and a C-5 methine proton at δ_H 4.603. From the proton chemical shifts and the coupling sequences (Table 3-18), the structure of RSA-TU was elucidated as 1e.

Table 3-19 Physicochemical properties of RSA-TU (1e)

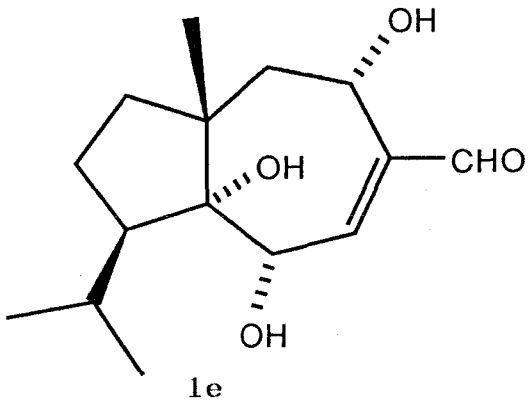

1e

A colorless syrup

Rf: 0.48 (C-M 50:4)

Vanillin-H_2SO_4 color: grayish yellow → light pinkish gray

N,*N*-dimethyl-*p*-phenylenediamine sulfate test: negative

FD-MS *m/z* (%): 269 (M^++1, 100), 250 (M^+-H_2O, 34)

EI-MS *m/z* (%): 250 (M^+-H_2O, 0.4), 232 (M^+-2H_2O, 2.0), 221 (0.8), 217 (1.6), 207 (1.4), 203 (1.5), 189 (5.7), 181 (3.2), 161 (5.9), 140 (66), 139 (14), 134 (10), 110 (28), 109 (13), 105 (13), 97 (100), 96 (17), 91 (15), 81 (15), 69 (24), 55 (29), 43 (22), 41 (43).

^{1}H-NMR are shown in Table 3-18.

4) Reduction with $LiAlH_4$

In reductions of rugosal A (1), $LiAlH_4$ gave a high polar and non-quenching product distinguishable from RSA-NBH-1 (1c), RSA-NBH-2 (1d) and RSA-TU (1e) in a small yield (Fig. 3-50). When 7.0 mg of 1 dissolved in THF was stirred with an excess amount of $LiAlH_4$ (5 mg, *ca* 20 equivalent) for 1 hr, the starting material disappeared on TLC. The reaction mixture was then diluted with 20 ml of a saturated NaCl solution, successively acidified with 4 N HCl to pH 4.0 and extracted with EtOAc (15 ml x 3). The combined extracts was concentrated and subjected to PTLC ($CHCl_3$-MeOH 50:4) to give less than 1 mg of a main product RSA-LAH (*Rf* 0.17). Since the product, RSA-LAH showed M^+ 270 in FD-MS (Fig. 3-51, *cf.* EI-MS in Fig. 3-52), the product was estimated to be the expected tetraol, 1f. Although the ^1H-NMR spectrum of RSA-LAH was partly invisible due to broadened signals and a large water peak, the proposed structure (1f) for RSA-LAH was partly supported by protons at δ_H *ca* 4.51, 4.374, and 4.252 and 4.212 assignable to C-5-H, C-2-H and C-14-H_2, respectively (Fig. 3-53).

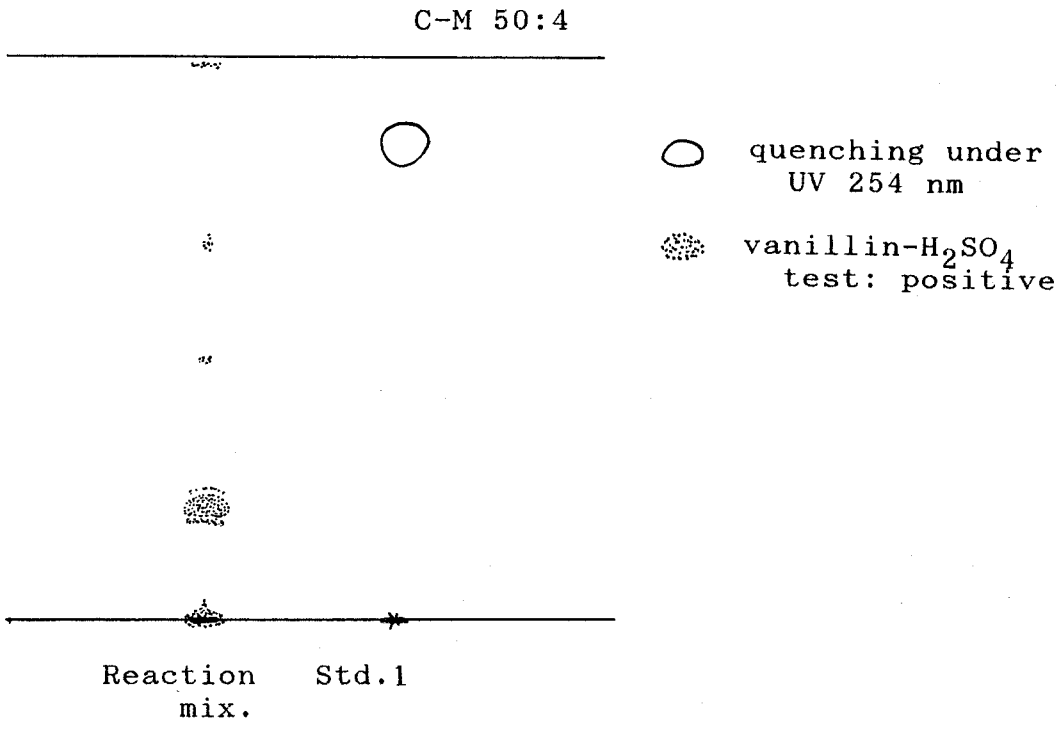

Fig. 3-50 TL-Chromatogram of Reaction Product Obtained by Reduction of Rugosal A (1) with $LiAlH_4$

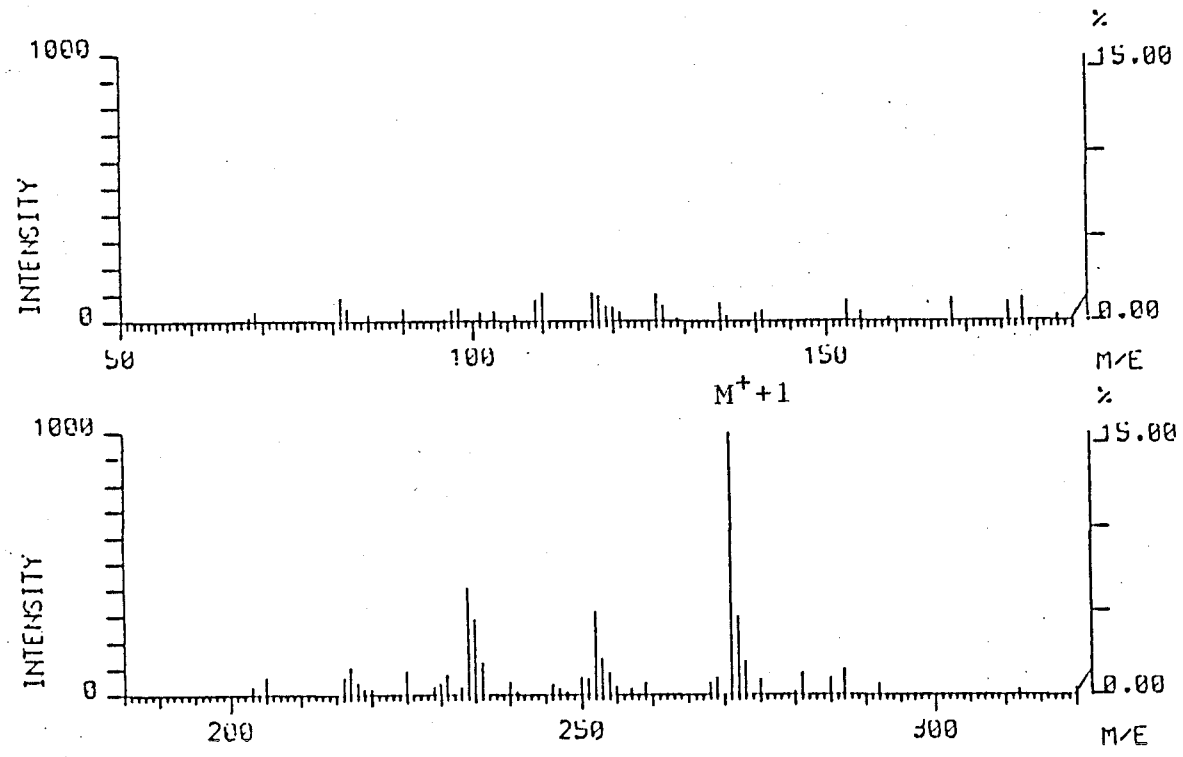

Fig. 3-51 FD-Mass Spectrum of RSA-LAH

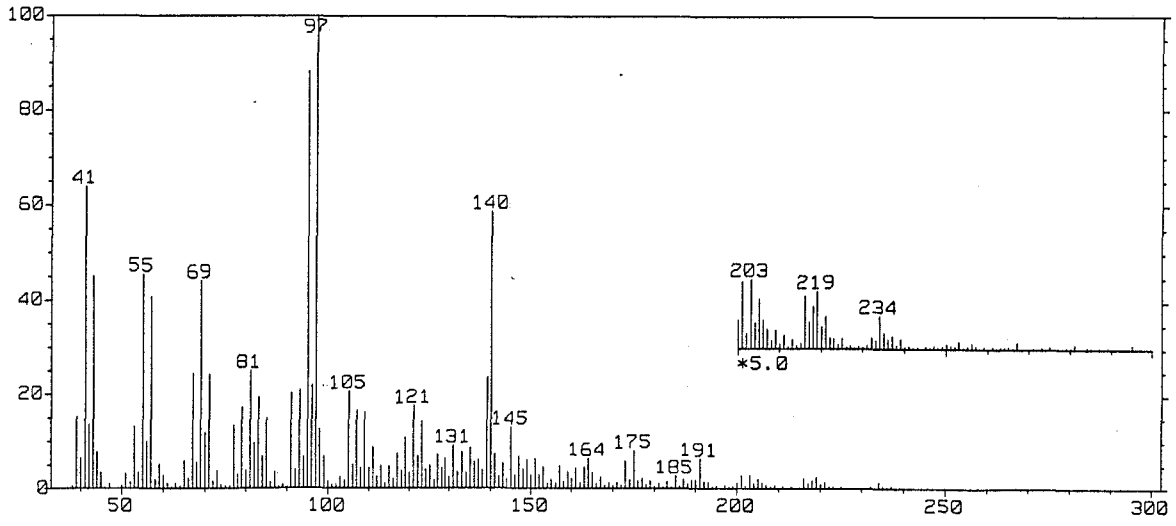

Fig. 3-52 EI-Mass Spectrum of RSA-LAH

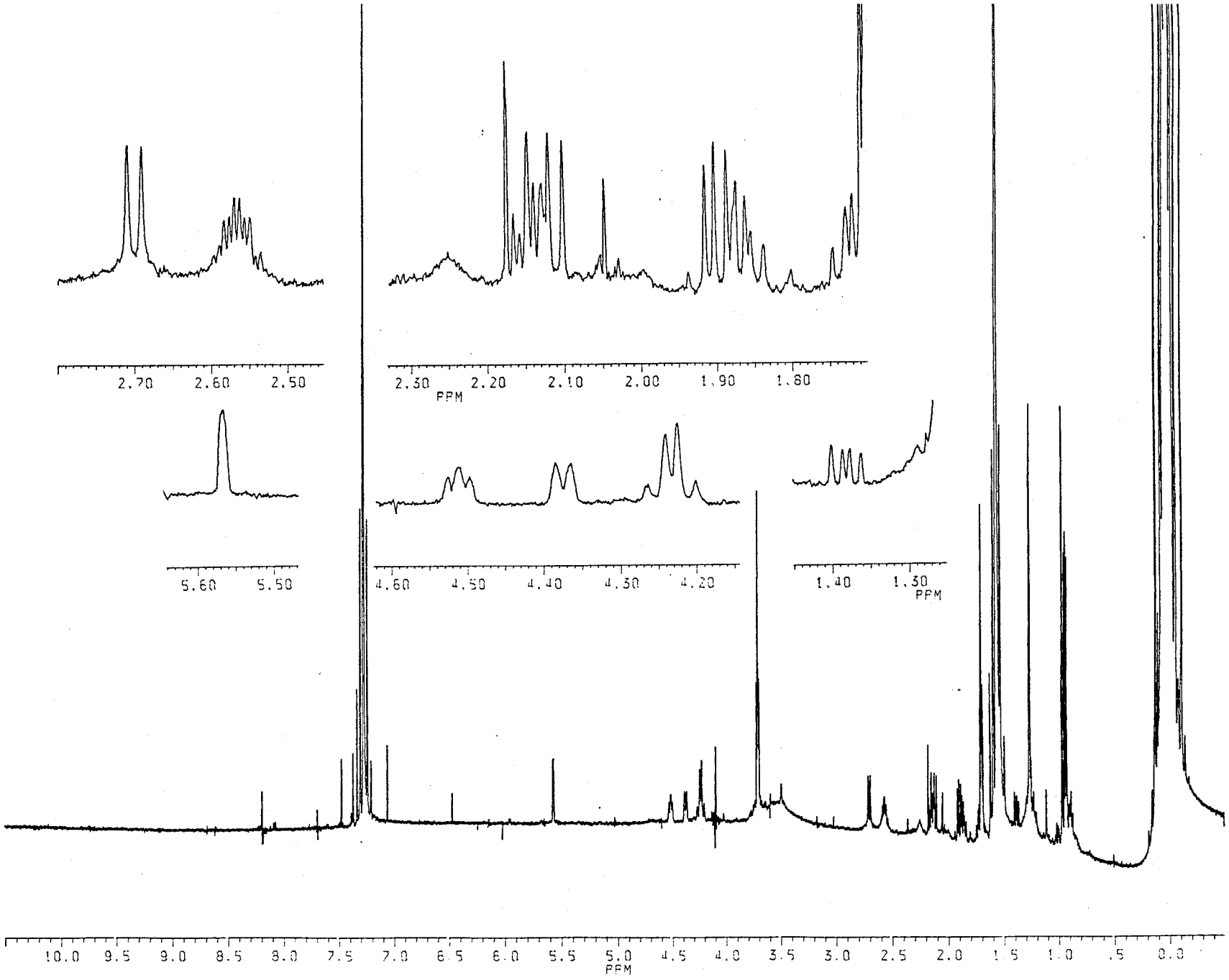

Fig. 3-53 ^{1}H-NMR Spectrum of RSA-LAH (500 MHz, in $CDCl_3$)

Table 3-20 Physicochemical properties of RSA-LAH

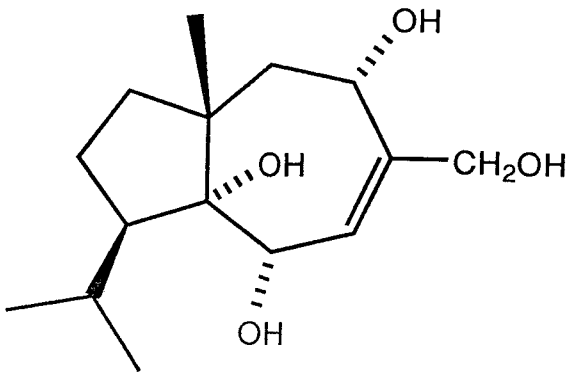

1f (tentative)

Colorless syrup

Rf: 0.17 (C-M 50:4)

Vanillin-H_2SO_4 color: moss green

N,*N*-dimethyl-*p*-phenylenediamine sulfate test: negative

FD-MS *m/z* (%): 270 (100)

EI-MS *m/z* (%): 234 (M^+-$2H_2O$, 1.4), 219 (2.5), 218 (1.8), 216 (2.3), 205 (2.1), 203 (3.0), 201 (2.9), 191 (6.5), 175 (8.2), 173 (6.0), 164 (6.5), 145 (13), 140 (59), 139 (24), 97 (100), 96 (22), 95 (88), 81 (25), 71 (24), 69 (44), 67 (24), 57 (41), 55 (46), 43 (45), 41 (64).

^{1}H-NMR $\delta_{TMS}^{CDCl_3}$(270 MHz): 4.374 (1H, br. d, *J*= 9.5 Hz, C-2-H), 2.698 (1H, d, *J*= 9.5 Hz, C-2-OH), *ca* 5.56 (1H, br., C-3-H), *ca* 4.51 (1H, br. t-like, C-5-H), 2.123 (1H, dd, *J*= 13.8 and 9.0 Hz, C-6-Ha), 1.994 (1H, dd, *J*= 13.8 and 6.1 Hz, C-6-Hb), 1.867 (1H, ddd, *J*= 12.0, 11.9 and 8.3 Hz, C-8-Ha), 1.380 (1H, dd, *J*= 12.0 and 7.4 Hz, C-8-Hb), 1.705 (12.8 and 11.9 and 8.8 Hz, C-9-Ha), 2.142 (1H, ddd, *J*= 9.3, 9.2 and 3.6 Hz, C-10-H), 2.565 (1H, double sept., *J*= 6.8 and 3.6 Hz, C-11-H), 0.934 (3H, d, *J*= 6.8 Hz, C-12-H_3), 0.926 (3H, d, *J*= 6.8 Hz, C-13-H_3), 4.252 (1H, d, *J*= 11.6 Hz, C-14-Ha), 4.212 (1H, d, *J*- 11.6 Hz, C-14-Hb), 0.961 (3H, s, C-15-H_3). C-9-Hb was invisible probably due to overlapping with H_2O peak.

To obtain enough amount of **1f** for ^{1}H-NMR analysis, the preparation route was improved as follows: As the tetraol derivative **1f** may be convertible from RSA-NBH-1 (**1c**) by reductive cleavage of the endoperoxide bridge, **1c** (11.2 mg) was treated with thiourea (16 mg) in MeOH (2 ml) overnight at room temperature. Consequently, 2.1 mg of a colorless syrup (RSA-NBH-TU, *Rf* 0.16 in C-M 50:4) was obtained in a yield of 19 % (*cf.* recovered **1c**, 9.0 mg, 80 %) (Fig. 3-54). Its *Rf* value and FD-MS showing the moleclar weight 270 (Fig. 3-55) agreed with those of **1f**. Moreover, RSA-NBH-TU and the former **1f** were also indistinguishable from each other in EI-MS (Fig. 3-56). ^{1}H-NMR spectrum of the product was in good accordance with that of **1f**, although C-2-OH was undetectable in RSA-NBH-TU (in $CDCl_3$, Fig. 3-57 and Table 3-21). Thus, the tetraol (**1f**) was prepared both by reduction of RSA-NBH-1 (**1c**) with thiourea (indirect but in a good yield) and by direct reduction of **1** with $LiAlH_4$.

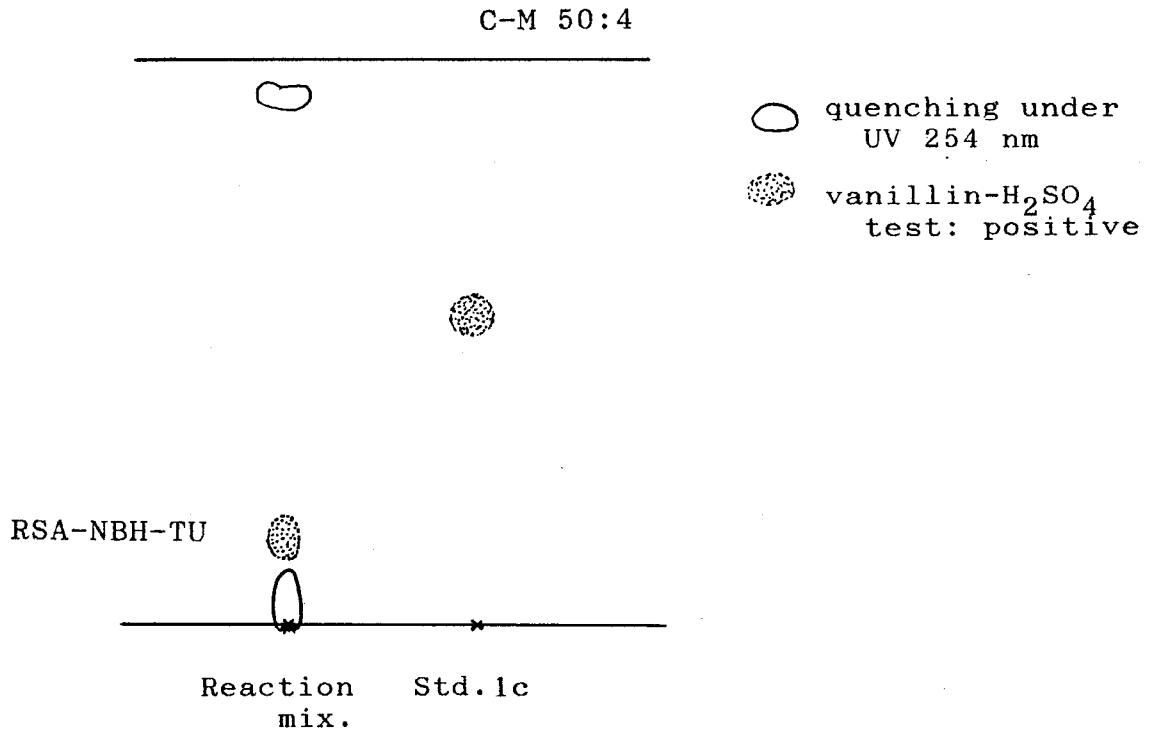

Fig. 3-54 TL Chromatigram of Reaction Product Obtained by Reduction of RSA-NBH-1 (**1c**) with Thiourea

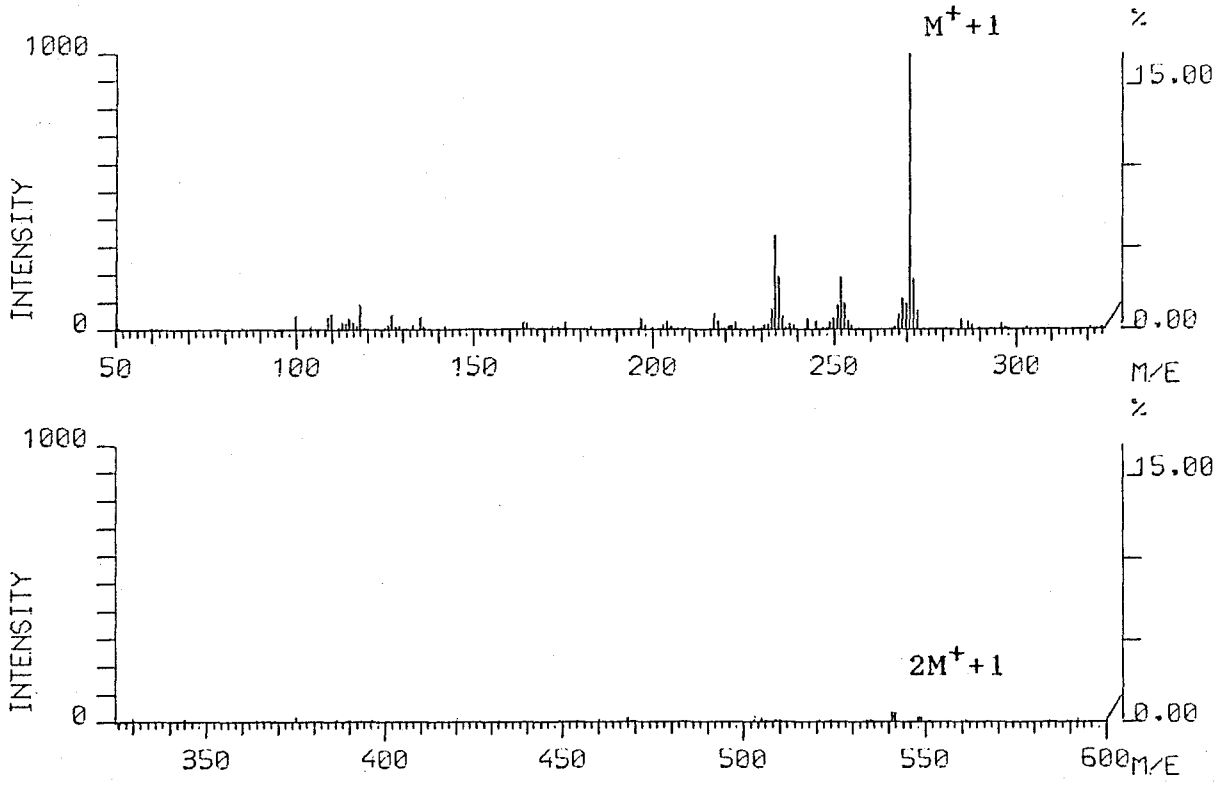

Fig. 3-55 FD-Mass Spectrum of RSA-NBH-TU

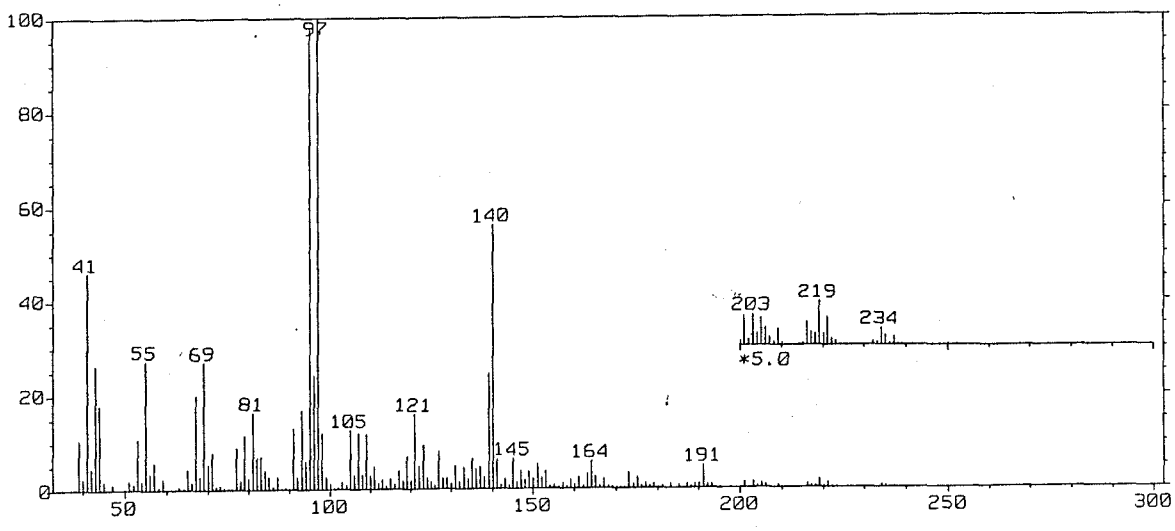

Fig. 3-56 EI-Mass Spectrum of RSA-NBH-TU

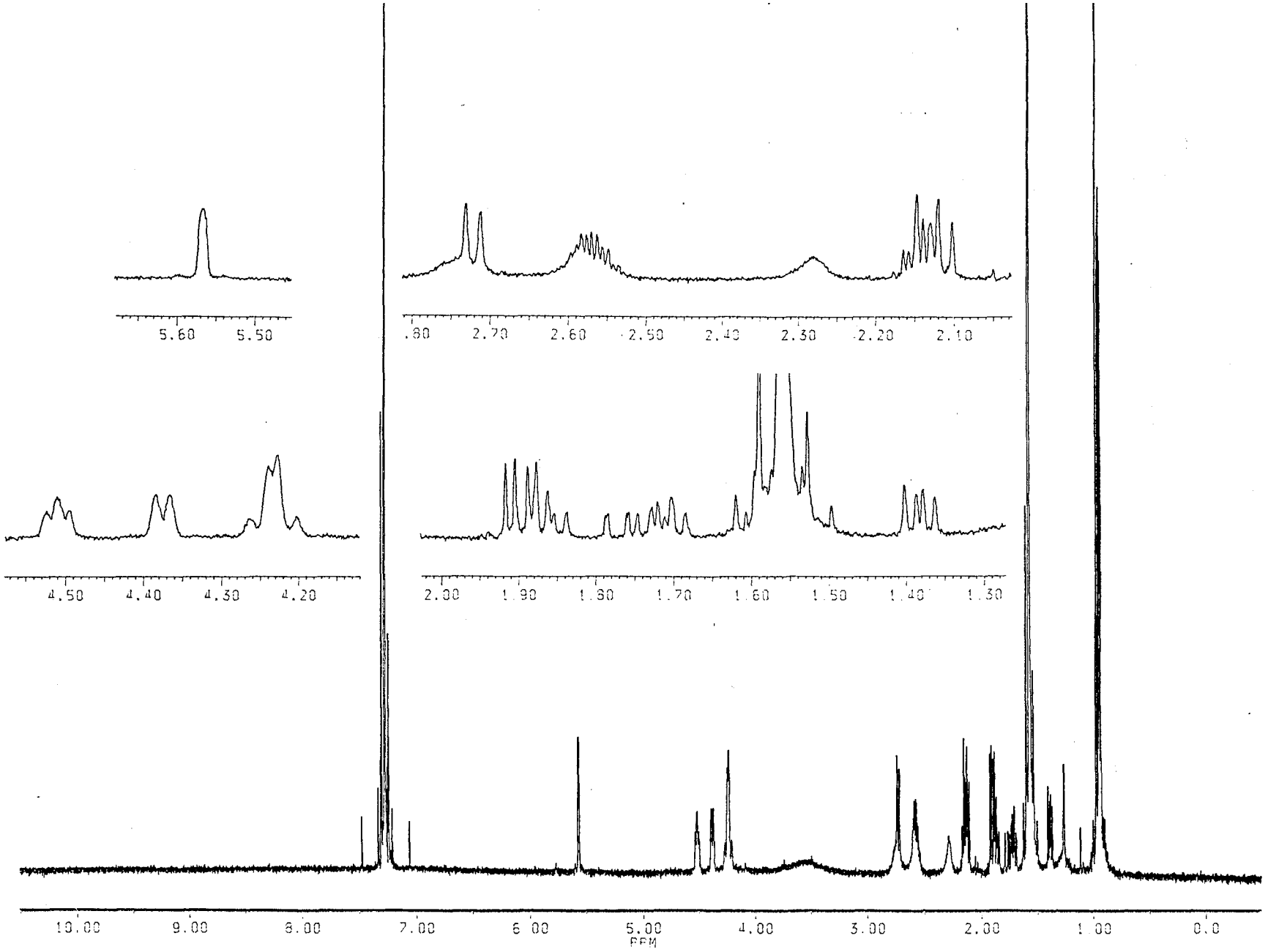

Fig. 3-57 ^{1}H-NMR Spectrum of RSA-NBH-TU (500 MHz, in $CDCl_3$)

Table 3-21 *^{1}H-NMR chemical shift values for RSA-NBH-TU (1f)*

(500 MHz, in $CDCl_3$, TMS as an int. std.)

Chemical shift*	Proton	Coupling (*J*=Hz)	Assignment
4.374	1H	br. d (9.0)	C-2-H
5.565	1H	br.	C-3-H
4.509	1H	br. t-like (*ca* 7)	C-5-H
2.123	1H	dd (13.6, 8.8)	C-6-Ha
1.895	1H	dd (13.6, 6.2)	C-6-Hb
1.868	1H	ddd (12.1, 12.0, 8.1)	C-8-Ha
1.381	1H	dd (12.0, 7.5)	C-8-Hb
1.714	1H	ddd (13.2, 9.0, 8.5)	C-9-Ha
1.57 (approx.)	1H	partly overlapped to H_2O	C-9-Hb
2.142	1H	ddd (9.4, *ca* 9, 3.5)	C-10-H
2.565	1H	d. sept (6.8, 3.5)	C-11-H
0.936	3H	d (6.8 Hz)	C-12-H_3
0.927	3H	d (6.8 Hz)	C-13-H_3
4.251	1H	br. d (11.7)	C-14-Ha
4.214	1H	br. d (11.7)	C-14-Hb
0.961	3H	s	C-15-H_3

* Two hydroxyl groups (C-1-OH and C-5-OH) were observed at δ_H 2.28 and 2.59, respectively.

Table 3-22 Physicochemical properties of RSA-NBH-TU (= RSA-LAH, 1f)

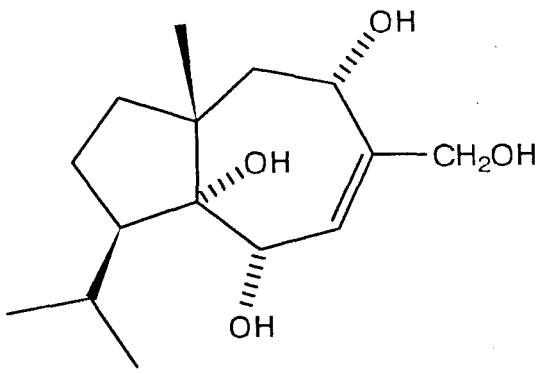

1f

A colorless syrup

Rf: 0.16 (C-M 50:4)

Vanillin-H_2SO_4 color: bluish moss green

FD-MS *m/z* (%): 541 ($2M^+$+1, 4.6), 271 (M^++1, 100), 252 (M^+-H_2O, 19), 234 (M^+-2H_2O, 34).

EI-MS *m/z* (%): 234 (M^+-2H_2O, 0.8), 221 (1.2), 219 (1.9), 205 (1.2), 203 (1.4), 201 (1.3), 191 (5.0), 164 (6.0), 140 (56), 139 (25), 121 (16), 109 (12), 107 (12), 105 (13), 98 (12), 97 (100), 96 (24), 95 (98), 93 (17), 81 (16), 69 (27), 67 (20), 55 (27), 44 (18), 43 (26), 41 (46).

^{1}H-NMR data are shown in Table 3-21.

5) Base-catalyzed Rearrangement

In pyridine solusion, rugosal A (1) seemed to be unstable and give gradually a quenching product. To obtain this more polar product, 1 was treated with hot pyridine. Crystallines of 1 (9.6 mg) in 1 ml of pyridine was heated at 80 °C for 1.5 hr, at which point, the reaction mixture was diluted with excess amount of toluene and the solvents were removed *in vacuo*. The major product, RSA-PY was isolated by PTLC successively in H-EA 1:1 (*Rf* 0.43), and in C-M 50:4 (*Rf* 0.50) to give 6.2 mg of colorless semisolid in a yield of 65 % (Fig. 3-58).

Its FI-MS indicated M^++1 267 (100 %) and M^+ 266 (53 %), while in EI-MS the molecular ion was undetectable and the dehydration fragment at *m/z* 248 (M^+-H_2O, 2.8 %) was observed (Fig. 3-59 and

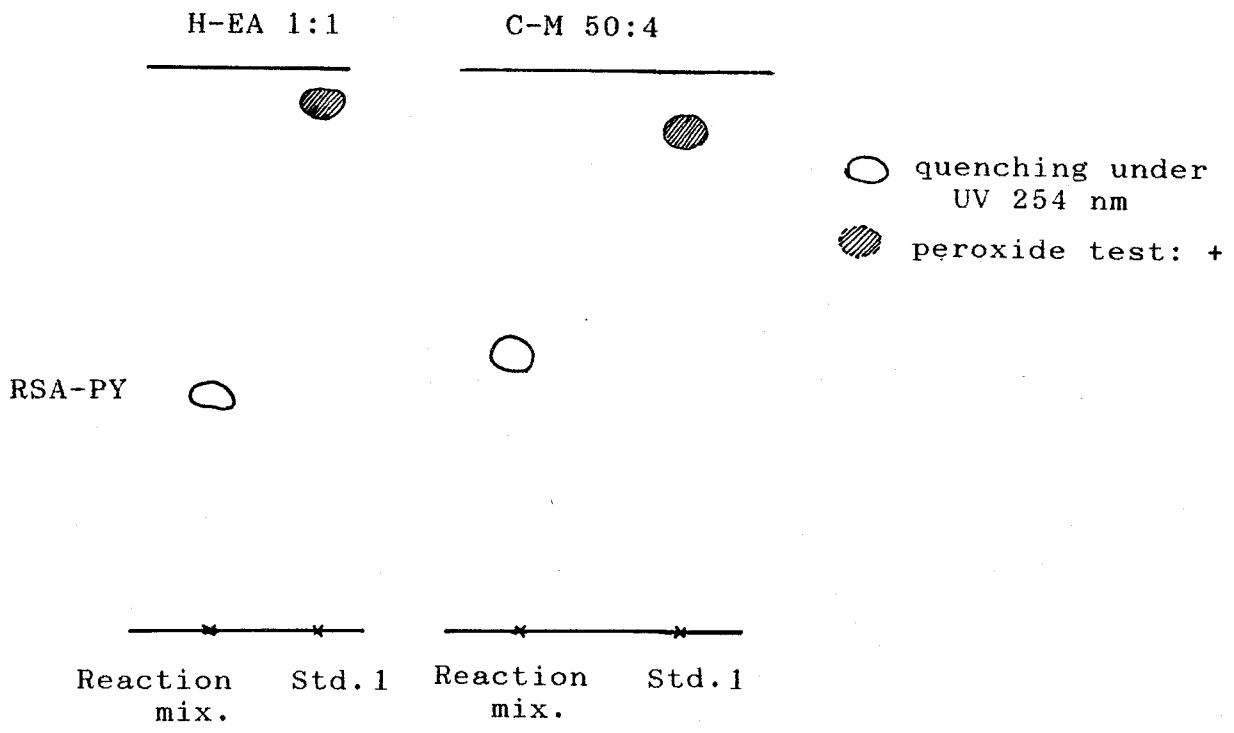

Fig. 3-58 TL Chromatograms of Reaction mixture Obtained by Heating of Rugosal A (1) in Ryridine

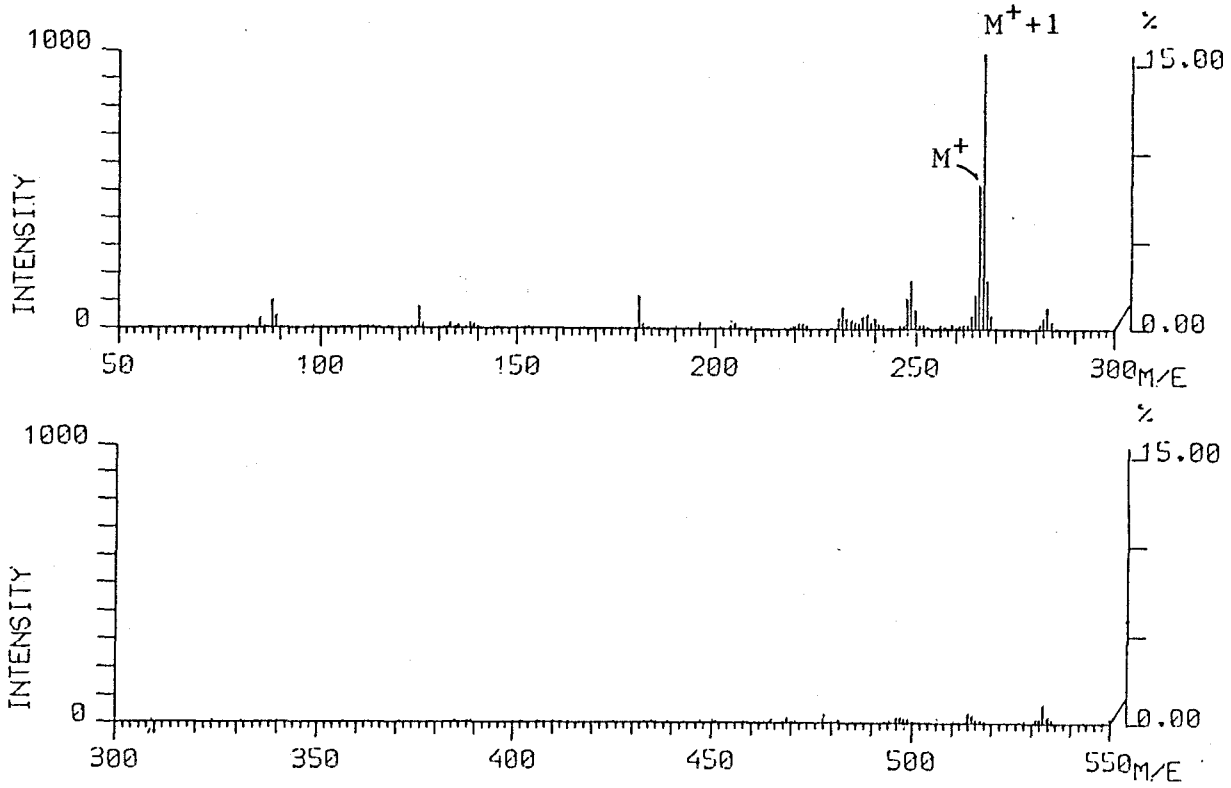

Fig. 3-59 FD-Mass Spectrum of RSA-PY

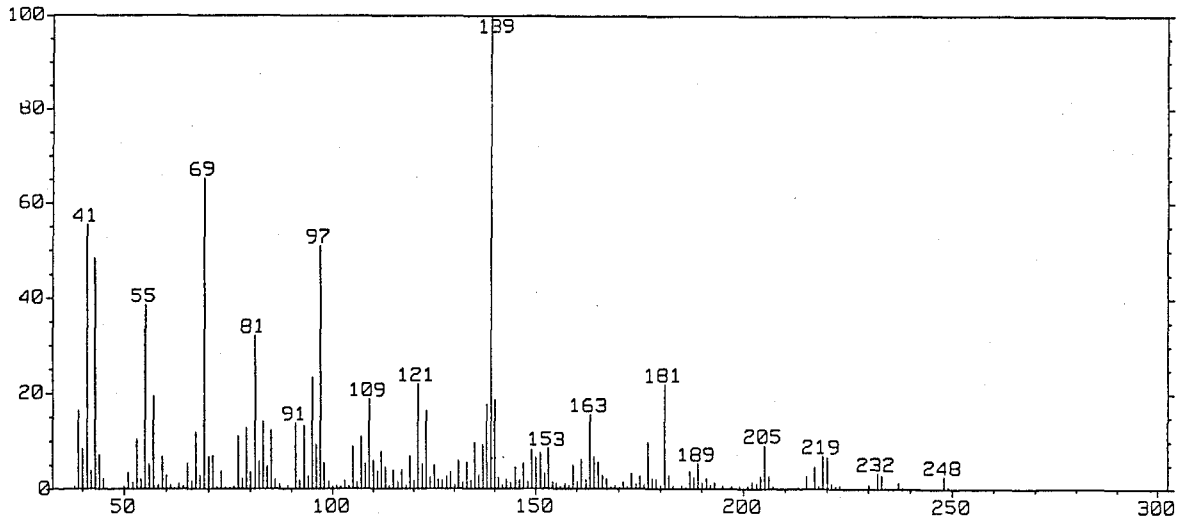

Fig. 3-60 EI-Mass Spectrum of RSA-PY

60). ^{1}H-NMR spectrum of RSA-PY revealed its structure as an endoperoxide rearrangement product which was postulated as an intermediate during acetylation reaction of 1 to yield RSA-AC-2 (**1b**). A pair of separated methylene protons showing a geminal coupling was observed at δ_H 1.916 and 1.696 (each 1H, d, *J*= 12.1 Hz), together with disappearance of the C-5 methine signal proton as shown in ^{1}H-NMR of **1b** (Fig. 3-61 and Table 3-23). Furthermore, instead of oxygenated methine carbon (C-5, δ_C 70.1 in 1), a new signal appeared at δ_C 101.8, which is assignable to the C-5 hemiacetal carbon (Fig. 3-62 and Table 3-24).

The hydroxyl proton at C-3-O<u>H</u> was observed at δ_H 2.178 as a doublet (*J*= 11.9 Hz), showing a vicinal coupling with C-2 methine proton (δ_H 3.683, 1H, dd, *J*= 11.9 and 4.7 Hz). When D_2O was added, together with the C-3-O<u>H</u>, a sharp singlet proton at δ_H 4.738 (1H) also disappeared (Fig. 3-63). The latter exchangeable proton was presumably assigned to C-5-OH proton, since C-5 position can afford hydrogen bonding with C-14-carbonyl group and the sharp signal was compatible with its hydrogen-bonding nature. In addition, its resonance in a lower magnetic field (δ_H 4.738) suggested a deshielding effect of the aldehyde group on C-5-O<u>H</u>.

Thus, structure of RSA-PY was deduced to be **1g**, corresponding to 2,5-O-deacyl **1b**. This reaction proved that the carotane endoperoxide rearrangement into hemiacetal easily occurs under an alkaline condition as previously discussed. Mechanism of the base-catalyzed reaction of **1** is described in Section 4.

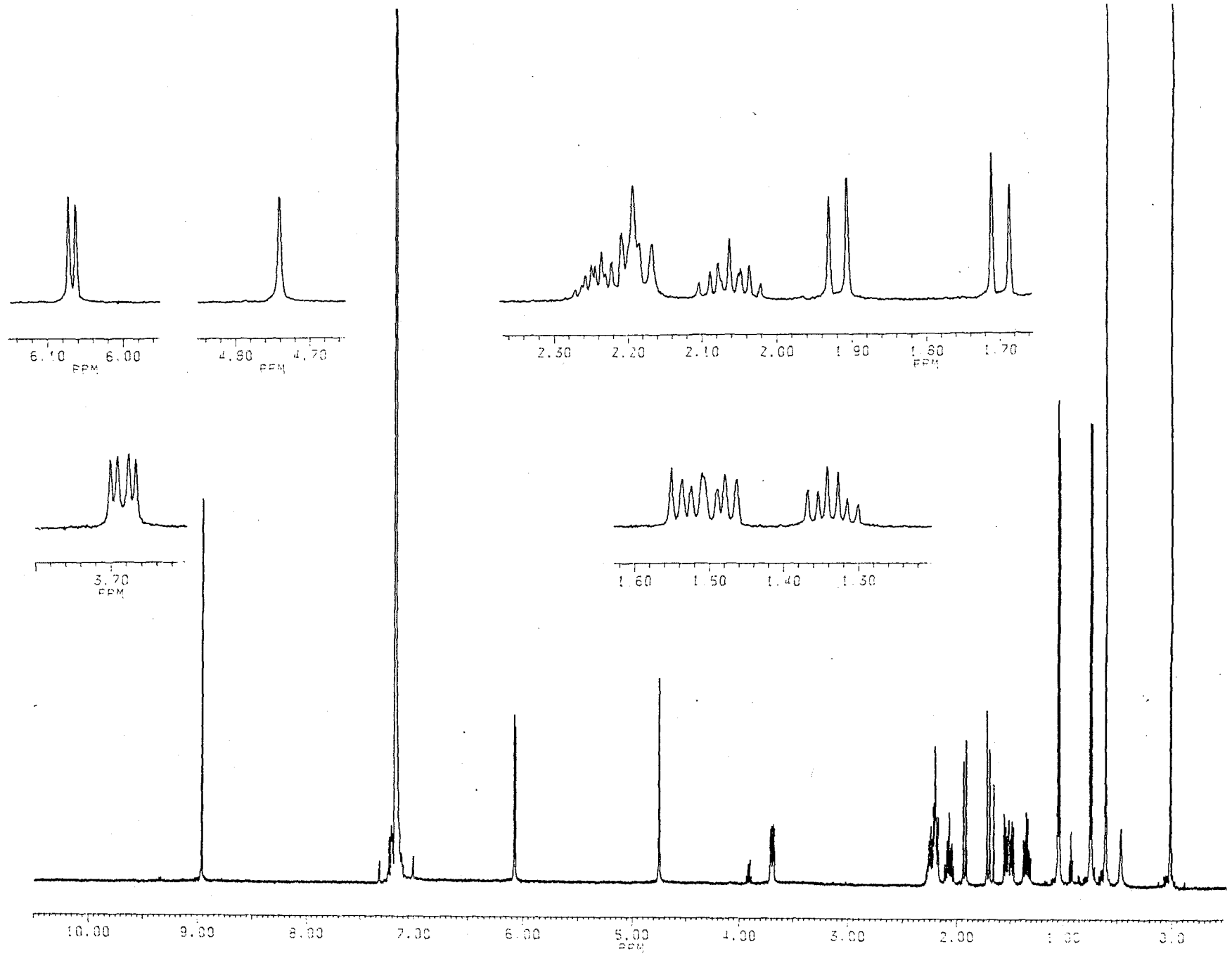

Fig. 3-61 ^{1}H-NMR Spectrum of RSA-PY (500 MHz, in C_6D_6)

Table 3-23 Proton chemical shift values of RSA-PY (1g)

(500 MHz, in C_6D_6, TMS as an int. std.)

δ_H	Proton	(*J*=Hz)	Assignment
3.683	1H	d (11.0, 4.8)	C-2-H
2.178	1H	d (11.0)	C-2-OH
6.065	1H	d (4.8)	C-3-H
4.738	1H	s	C-5-OH
1.916	1H	d (12.1)	C-6-Ha
1.696	1H	d (12.1)	C-6-Hb
1.529	1H	dd (13.2, 7.2)	C-8-Ha
1.483	1H	dd (13.2, 7.9)	C-8-Hb
2.061	1H	m	C-9-Ha
1.333	1H	ddd (13.2, 13.1, 7.2)	C-9-Hb
2.202	1H	m	C-10-H
2.245	1H	m	C-11-H
1.034	3H	d (6.6)	C-12-H_3
0.734	3H	d (6.6)	C-13-H_3
8.952	1H	s	C-14-H
0.595	3H	s	C-15-H_3

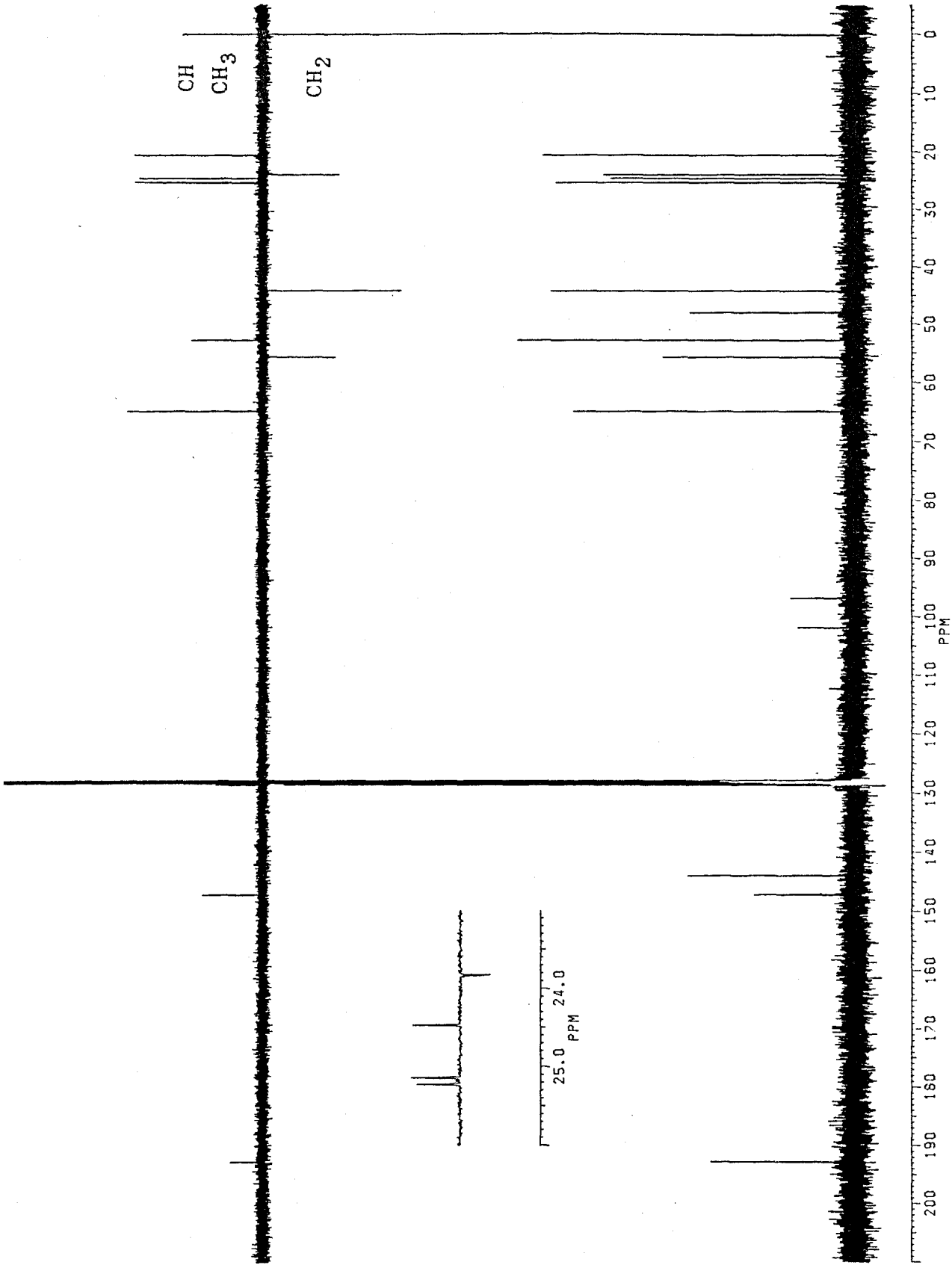

Fig. 3-62 ^{13}C-NMR Spectrum of RSA-PY (125 MHz, in C_6D_6)

Tabel ***3-24*** *Carbon shift values of RSA-PY (1g) and RSA-AC-2 (1b)*

(125 MHz, in C_6D_6, TMS as an int. std.)

δ_C	Assignment*	*cf.* RSA-AC-2 (1b)	δ_C** (1b-1g)
96.7	1-C	97.1	+ 0.4
64.9	2-CH	67.0	+ 2.1
147.1	3-CH	147.7	+ 0.6
143.8	4-C	139.0	- 4.8
101.8	5-C	101.1	- 0.7
55.6	6-CH_2	54.2	- 1.4
47.9	7-C	48.1	+ 0.2
44.1	8-CH_2	44.1	$\pm$ 0
23.8	9-CH_2	24.2	+ 0.4
52.7	10-CH	53.0	+ 0.3
24.5	11-CH	24.4	- o.1
25.1	12-CH_3	25.4	+ 0.3
20.5	13-CH_3	20.1	- 0.4
192.8	14-CH	189.9	- 2.9
25.2	15-CH_3	25.7	+ 0.5

* Hydrogenation was elucidated by DEPT experiment.

** The spectrum was measured at 68 Hz

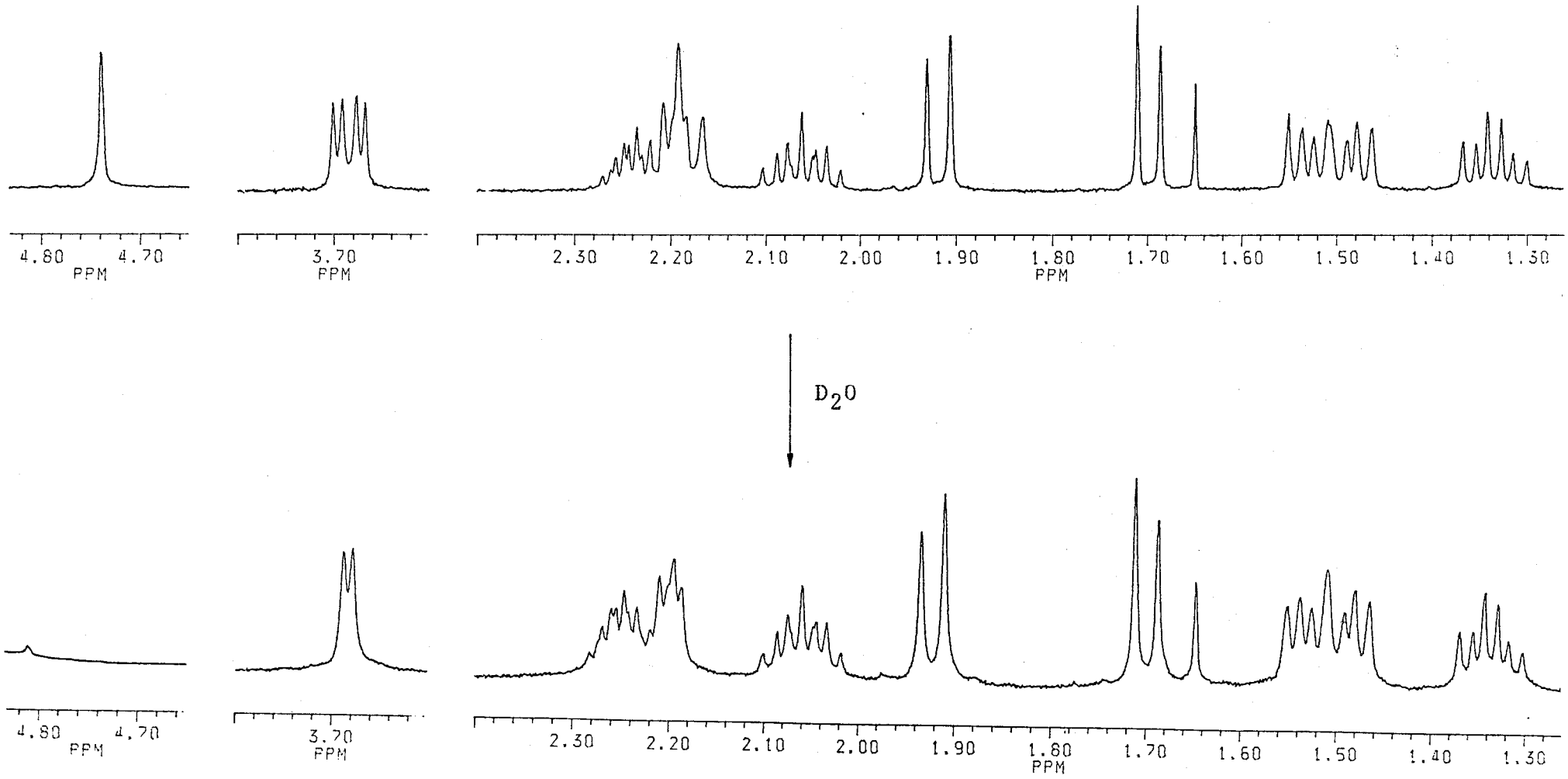

Fig. 3-63 Signal Changes upon D_2O Addition in RSA-PY

Table 3-25 Physicochemical properties of RSA-PY (1g)

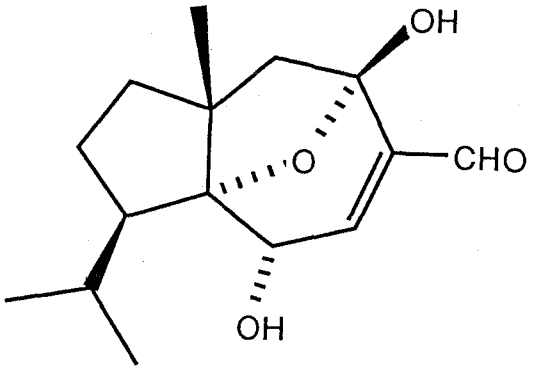

1g

A colorless semisolid

Rf: 0.43 (H-EA 1:1), 0.50 (C-M 50:4)

Vanillin-H_2SO_4 color: greish yellow

FD-MS *m/z* (%): 267 (M^++1, 100), 266 (M^+, 53)

EI-MS *m/z* (%): 248 (M^+-H_2O, 2.7), 232 (3.4), 220 (6.6), 219 (7.1), 205 (9.3), 181 (22), 163 (16), 139 (100), 121 (22), 109 (19), 97 (51), 81 (32), 69 (65), 55 (39).

^{1}H-NMR and ^{13}C-NMR data are shown in Tables 3-23 and 3-24, respectively.

6) Treatment with Dilute HCl/MeOH

When small amount of HCl is added to a MeOH solution of rugosal A (1), UV absorption maximum at 228 nm due to α,β-unsaturated aldehyde chromophore in 1 disappeared. To reveal the mechanism for collapse of the conjugation system, 1 was treated with dilute HCl/MeOH to isolate the UV transparent product. To 1 ml of MeOH dissolved pure 3.6 mg of 1, 4 drops of 0.5 N HCl was added and mixed well. After 30 minutes standing, the solution was diluted with water (*ca* 20 ml), and then extracted with an equal volume of EtOAc. The extracted dried over Na_2SO_4 was concentrated *in vacuo*, and the reaction mixture was analyzed by TLC (H-EA 3:1). Together with the starting material, a non-quenching spot was detected at *Rf* 0.34 with vanillin-H_2SO_4 reagent (reddish yellow) and phosphomolybudate reagent (dark blue) (Fig. 3-64). The reaction mixture was subjected to PTLC (H-AT 4:1, developed twice) to give 2.3 mg of colorless needles (RSA-HCL, yield 54 %) and 1.3 mg of unchanged 1 (36 %).

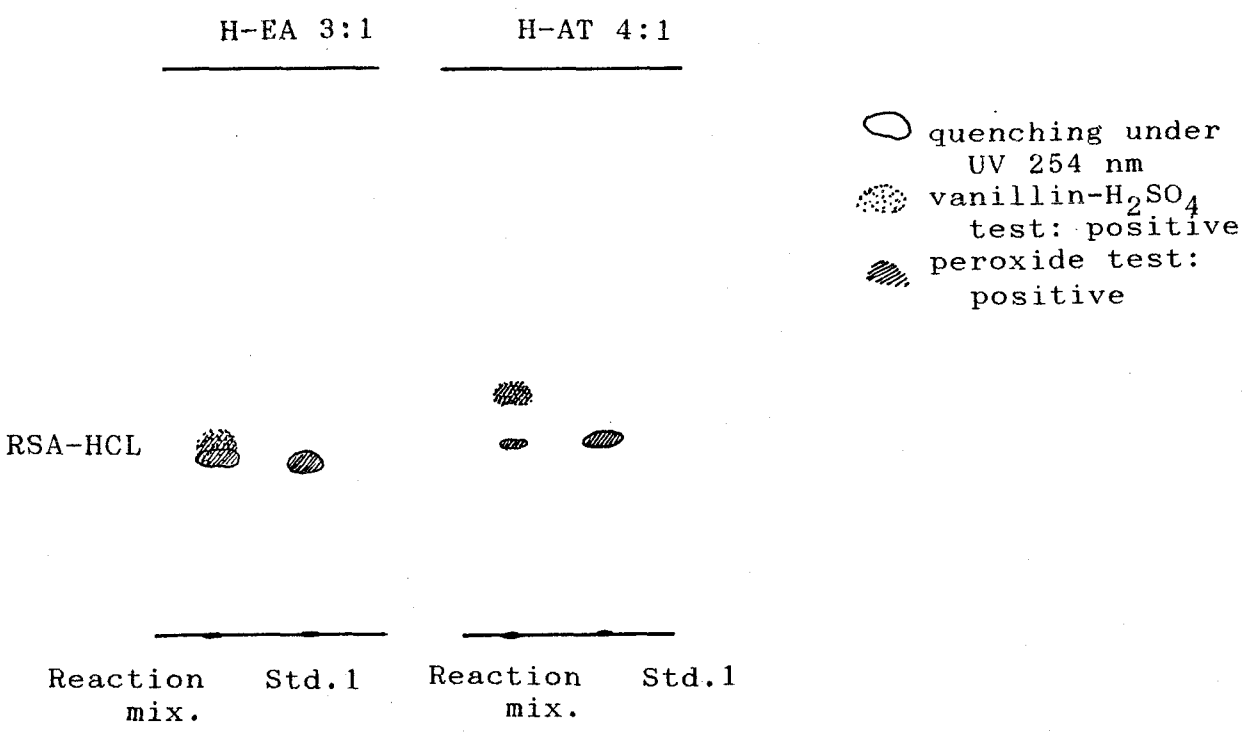

Fig. 3-64 TL Chromatograms of RSA-HCL Obtained by Treatment of Rugosal A (1) with HCl/MeOH

RSA-HCL, featureless above 210 nm in UV spectrum, gave M^+ 312 (100 %, 1 + 46 mass unit) in FI-MS (Fig. 3-65). With molecular ion peak at *m/z* 312 (M^+, 0.1 %), characteristic fragments at *m/z* 294 (M^+-H_2O, 0.3 %), 280 (M^+-32, 2.4 %), 263 (M^+-H_2O-31, 1.4 %), 248 (M^+-H_2O-46, 4.4 %) and 237 (M^+-75, 7.1 %) were detected in EI-MS (Fig. 3-66). Except C-14-proton, the other protons in RSA-HCL indicated an approximately good correspondence with those of 1 in ^{1}H-NMR (Fig. 3-67 and Table 3-26). Two methoxy signals ($-OCH_3$ x2) at δ_H 3.092 and 3.042 (each 3H, s) and an isolated methine proton (δ_H 4.308, 1H, s) were newly observed in ^{1}H-NMR spectrum of RSA-HCL, instead of formyl proton in 1. These protons were assignable to a dimethyl acetal group, which is presumably converted from an α,β-unsaturated aldehyde group in MeOH containing catalytic amounts of HCl.

The presence of the dimethyl acetal group in RSA-HCL was also supported by EI-MS fragments at *m/z* 237 [$M^+-CH(OCH_3)_2$, 7.1 %] and 75 [$CH(OCH_3)_2^+$, 100 %] (Fig. 3-68). Thus, structure of RSA-HCL was elucidated to be **1h**, with which the disintegration of the conjugation system in 1 was well explicable. Although several chemical reactions to yield acetals from carbonyl compounds are known, most of them must be carried out under strong conditions [98]. It is unusual that an α,β-unsaturated aldehyde group is so easily converted into an acetal group in dilute HCl/MeOH at room temperature.

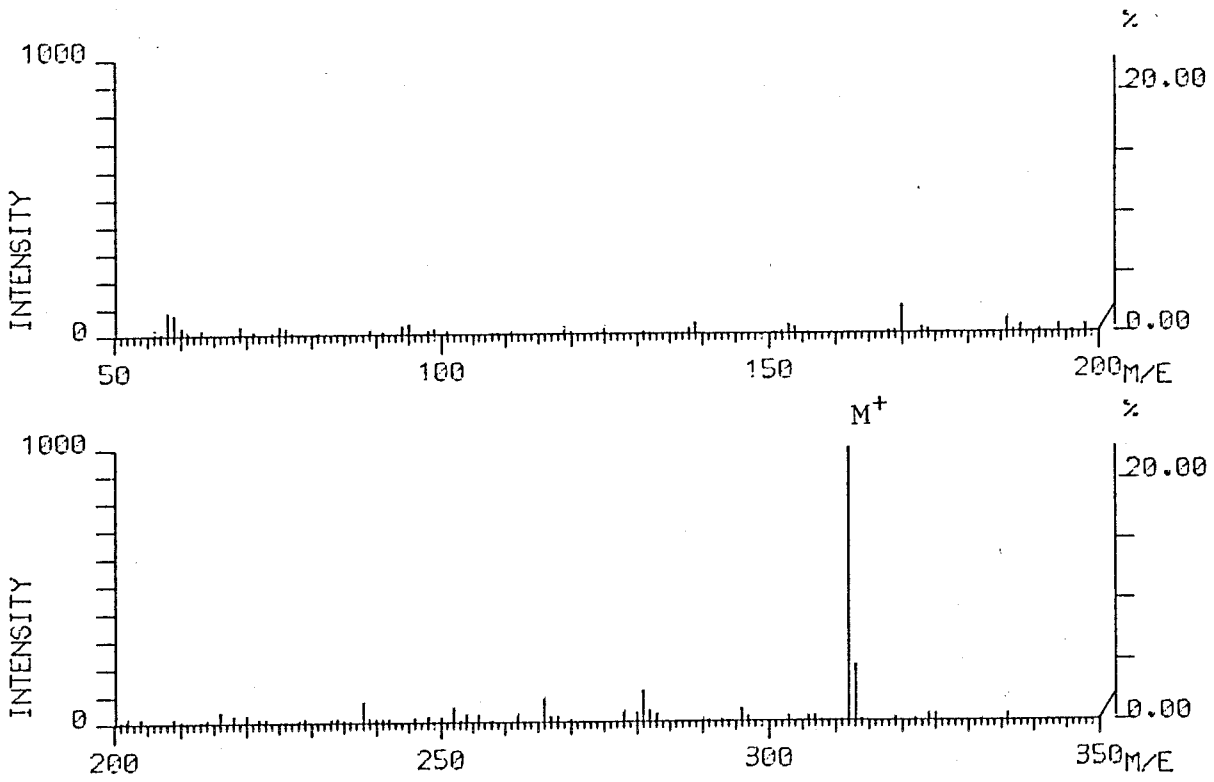

Fig. 3-65 FI-Mass Spectrum of RSA-HCL

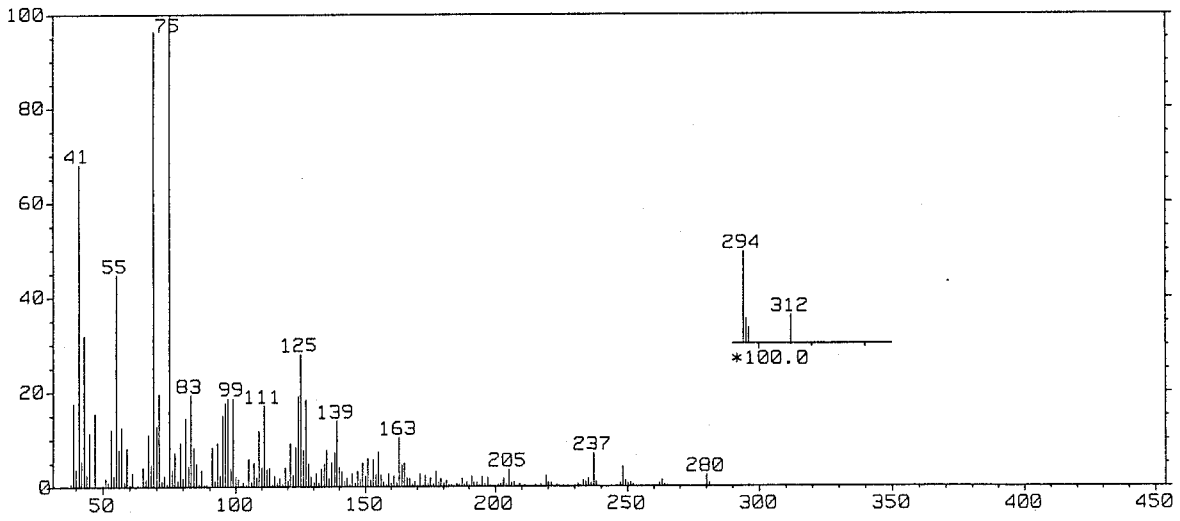

Fig. 3-66 EI-Mass Spectrum of RSA-HCL

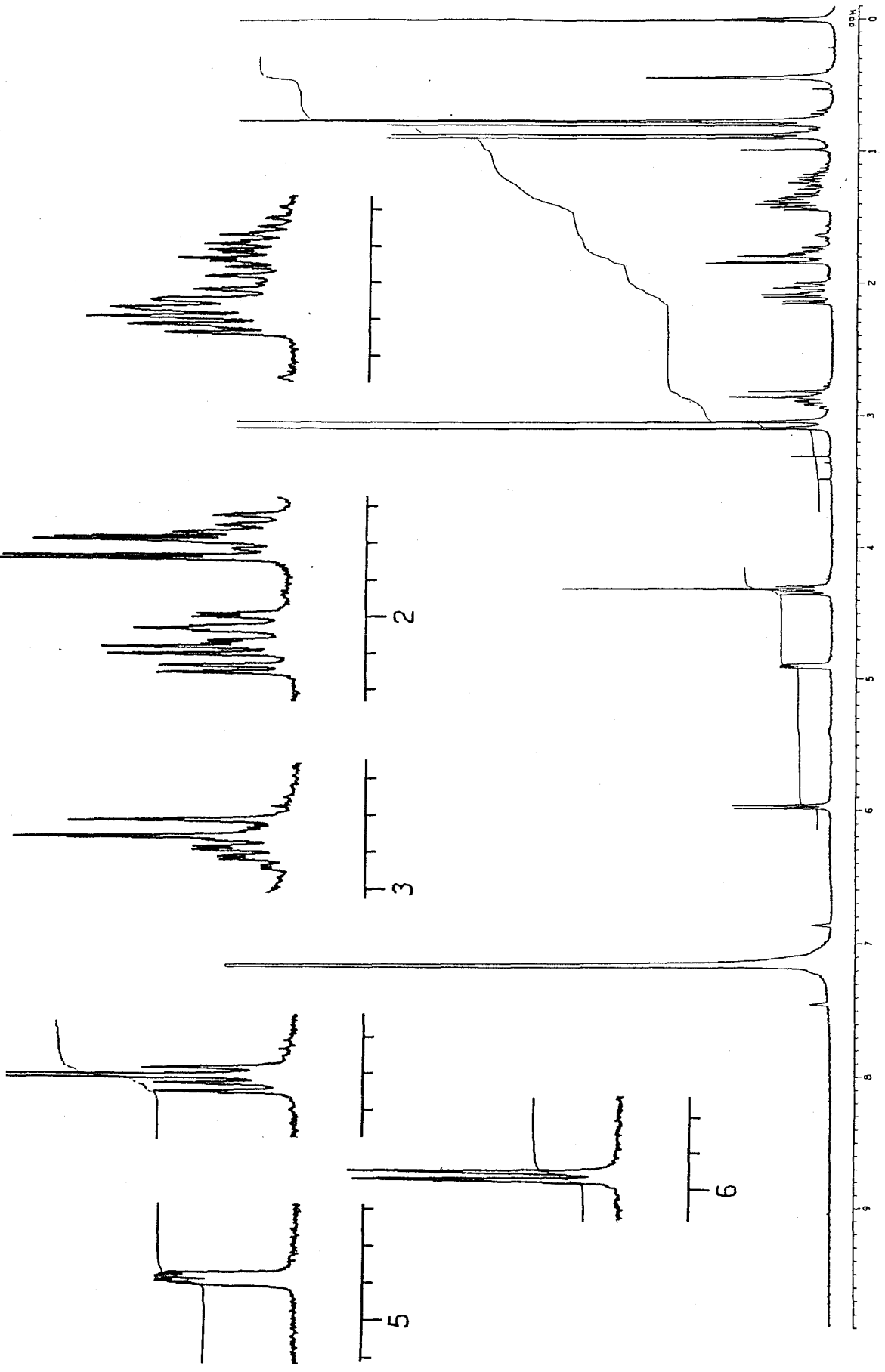

Fig. 3-67 ^{1}H-NMR Spectrum of RSA-HCL (270 MHz, in C_6D_6)

Table ***3-26*** *^{1}H-NMR chemical shift values for RSA-HCL (**1h**)*

(270 MHz, in C_6D_6, TMS as an int. std.)

δ_H	Proton (*J*=Hz)	Assignment
4.319	dd (11.7, 6.2)	C-2-H
2.836	d (11.7)	C-2-OH
5.967	dd (6.2, 1.1)	C-3-H
4.897	ddd (5.1, 2.2, 1.1)	C-5-H
2.121	dd (13.9, 5.1)	C-6-Ha
1.816	dd (13.9, 2.2)	C-6-Hb
1.785	ddd (12.8, 12.1, 7.0)	C-8-Ha
1.412	dd (12.1, 6.4)	C-8-Hb
1.366	m	C-9-Ha
1.208	dddd (13.2, 12.8, 11.0, 6.4)	C-9-Hb
2.036	ddd (11.0, 10.6, 2.2)	C-10-H
2.890	double sept. (6.8, 2.6)	C-11-H
0.883	d (6.8)	C-12-H_3
0.787	d (6.8)	C-13-H_3
4.308	s	C-14-H
0.762	s	C-15-H_3
3.092	s	C-14'a-H_3
3.042	s	C-14'b-H_3

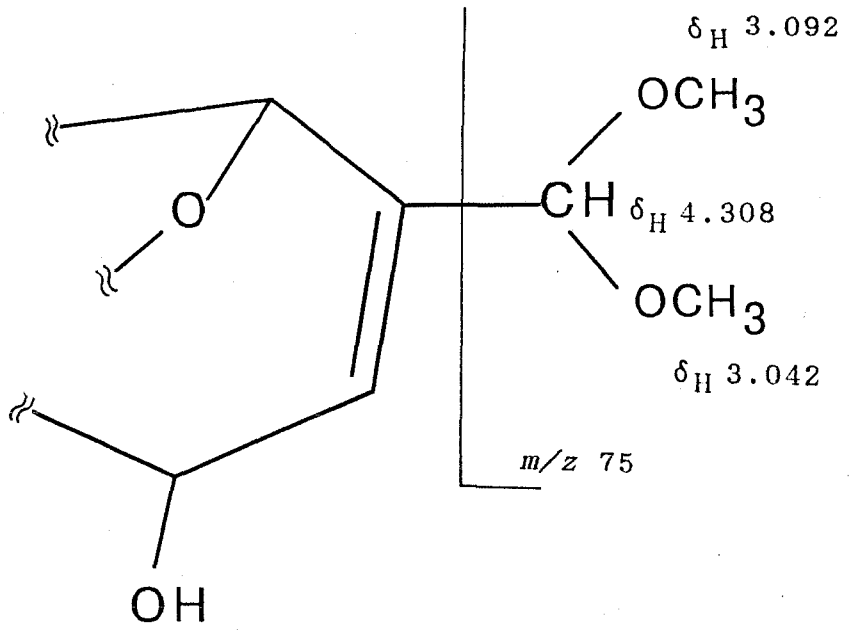

Fig. 3-68 Partial Structure of RSA-HCL with Some Physicochemical Data

*Table 3-27 Physicochemical properties of RSA-HCL (**1h**)*

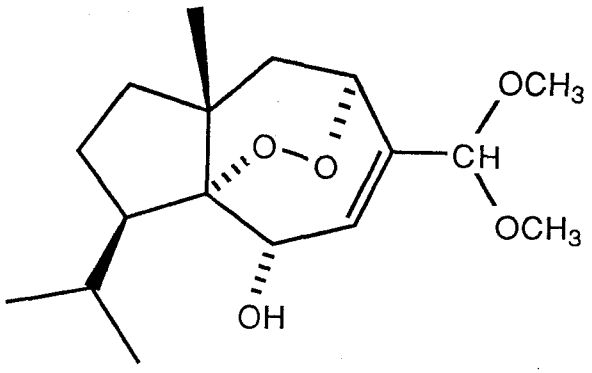

1h

Colorless needles, mp 119-120.5 °C

Rf: 0.34 (H-EA 3:1, *cf.* **1**; 0.33), 0.43 (H-AT 4:1, *cf.* **1**; 0.34)

Vanillin-H_2SO_4 color: grayish yellow

N,N-dimethyl-*p*-phenylenediamine sulfate test: positive
(pink when heated)

UVλ_{max}^{MeOH}: featureless above 210 nm

FI-MS *m/z* (%): 312 (M^+, 100)

EI-MS *m/z* (%): 312 (M^+, 0.1), 294 (M^+-H_2O, 0.3), 280 (2.4), 263 (1.4), 248 (4.4), 237 (7.1), 205 (3.3), 163 (11), 139 (14), 125 (28), 111 (17), 99 (19), 97 (19), 83 (19), 75 [$CH(COCH_3)_2$, 100], 69 (97), 55 (45), 41 (68).

^{1}H-NMR data are shown in Table 3-26.

7) Rearrangement with *p*-TSA

Regarding hanalpinol (**80**), acid-catalyzed cleavage was reported by Itokawa *et al.* [100]. In this reaction, as shown in Scheme 3-3, **80** was easily cleaved to furopelagone B (**81**). In their report, the reaction conditions are described as follows: excess amounts of *p*-TSA (257 mg) and 60 mg of substrate dissolved in 3 ml of benzene were stirred for 17 hr at room temperature to give **81** in *ca* 50 % yield [100]. According to the reaction scheme, rogosal A (1) was also expected to give a compound cleaved at the endoperoxide bridge (Scheme 3-4), since 1 possesses the same endoperoxide system as **80**. Contrary to this expectation, the acid-catalyzed C,C-bond cleavage through a protonation at the oxygen-oxygen bond hardly occurred in 1 under the same reaction conditions as mentioned above.

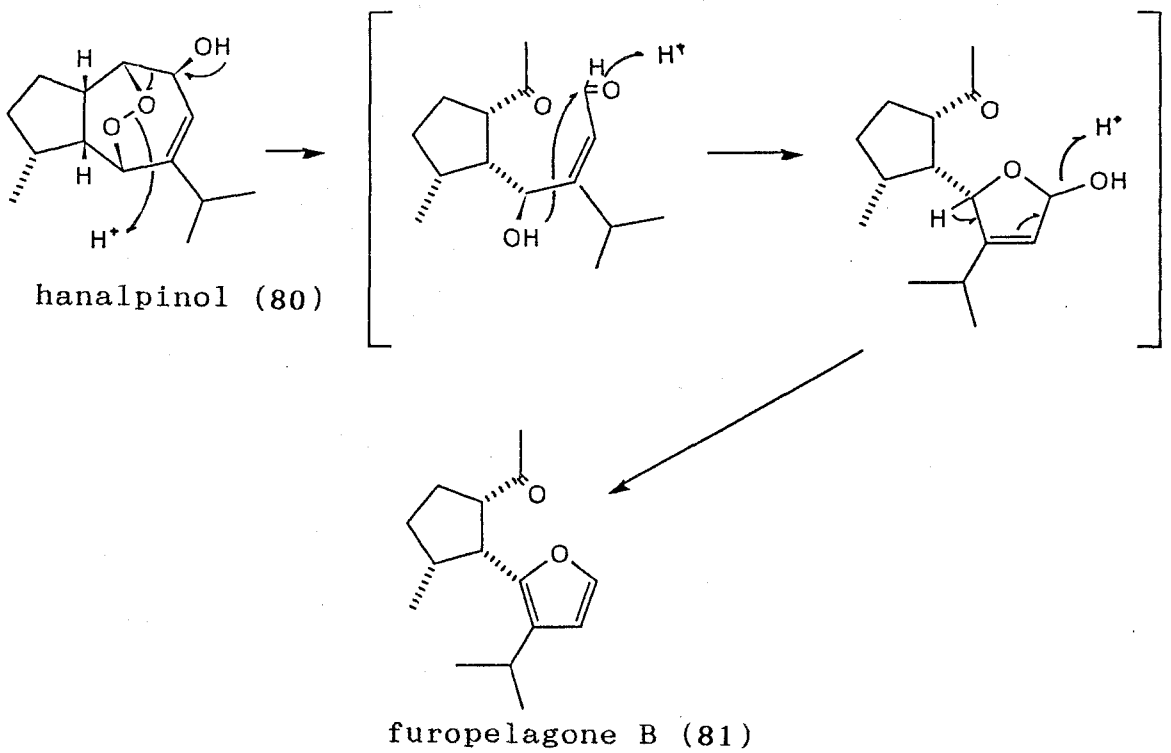

hanalpinol (80)

furopelagone B (81)

Scheme 3-3 Conversion of Hanalpinol into Furopelargone B in Benzene Containing *p*-TSA

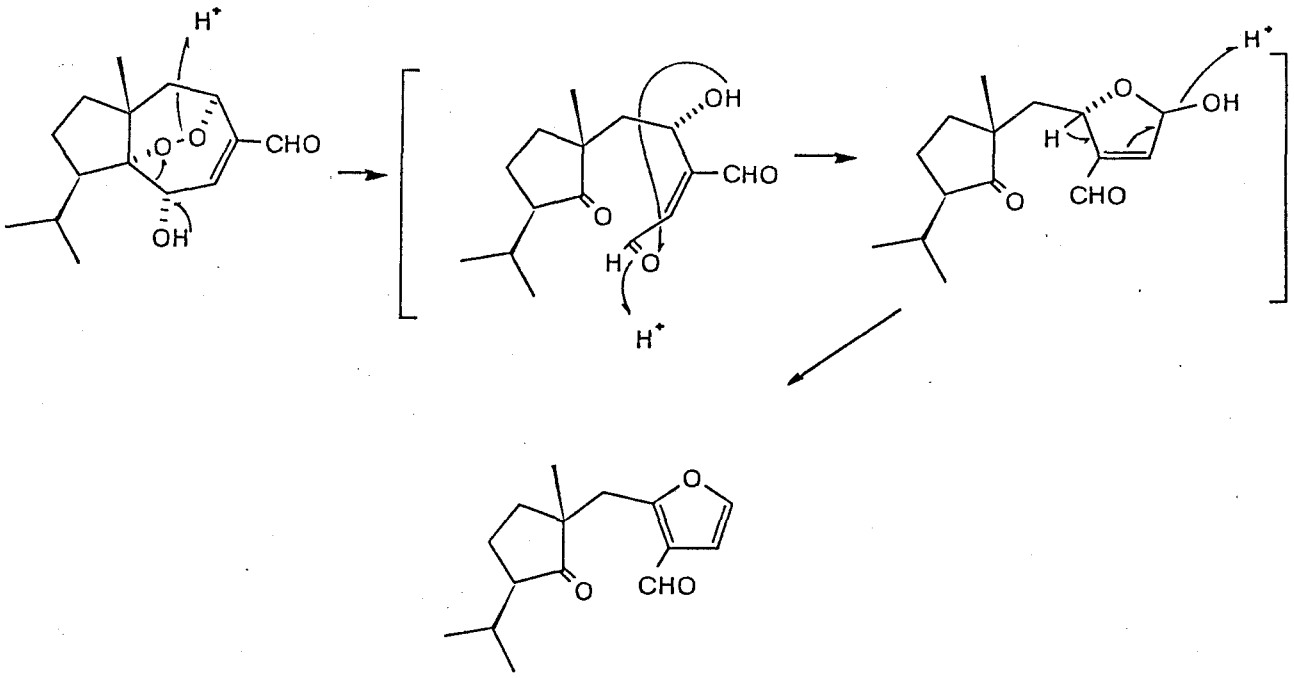

Scheme 3-4 Possible Pathway for Rugosal A under Unhydrous Acidic Condition Drown after Scheme 3-3

Therefore, the reaction mixture was heated in hopes to obtain the expected derivative. Rugosal A (16.9 mg) and 23.0 mg of *p*-TSA were mixed in 1.5 ml of benzene in ampoule, and kept at 80 °C for 6 hr. The reaction mixture was then concentrated and subjected to PTLC. A unique quenching product negative to peroxide test (H-EA 3:1, and C-M 50:2, *Rf* 0.23 and 0.44, respectively) was isolated to give a colorless syrup (RSA-TSA: 8.3 mg, yield 49 %) (Fig. 3-69). The molecular ion of RSA-TSA was detected at *m/z* 266 (86 %) in FI-MS (Fig. 3-70), which indicated that neither fission nor addition occurred in 1 during the reaction. On the other hand, EI-MS analysis gave no peak at *m/z* 266, and instead of M^+, the dehydration fragment at *m/z* 248 (M^+-H_2O, 0.4 %) was observed (Fig. 3-71).

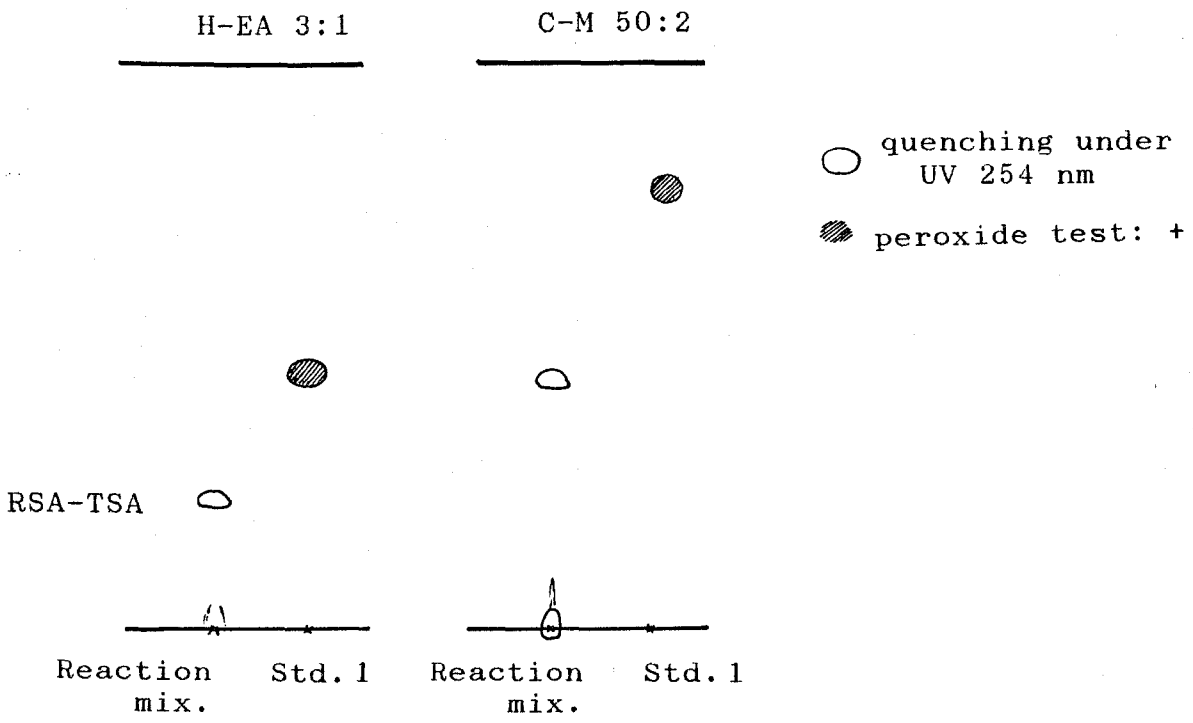

Fig. 3-69 TL Chromatograms of Reaction Product Obtained by Treatment of Rugosal A (1) with *p*-Toluenesulfonic Acid

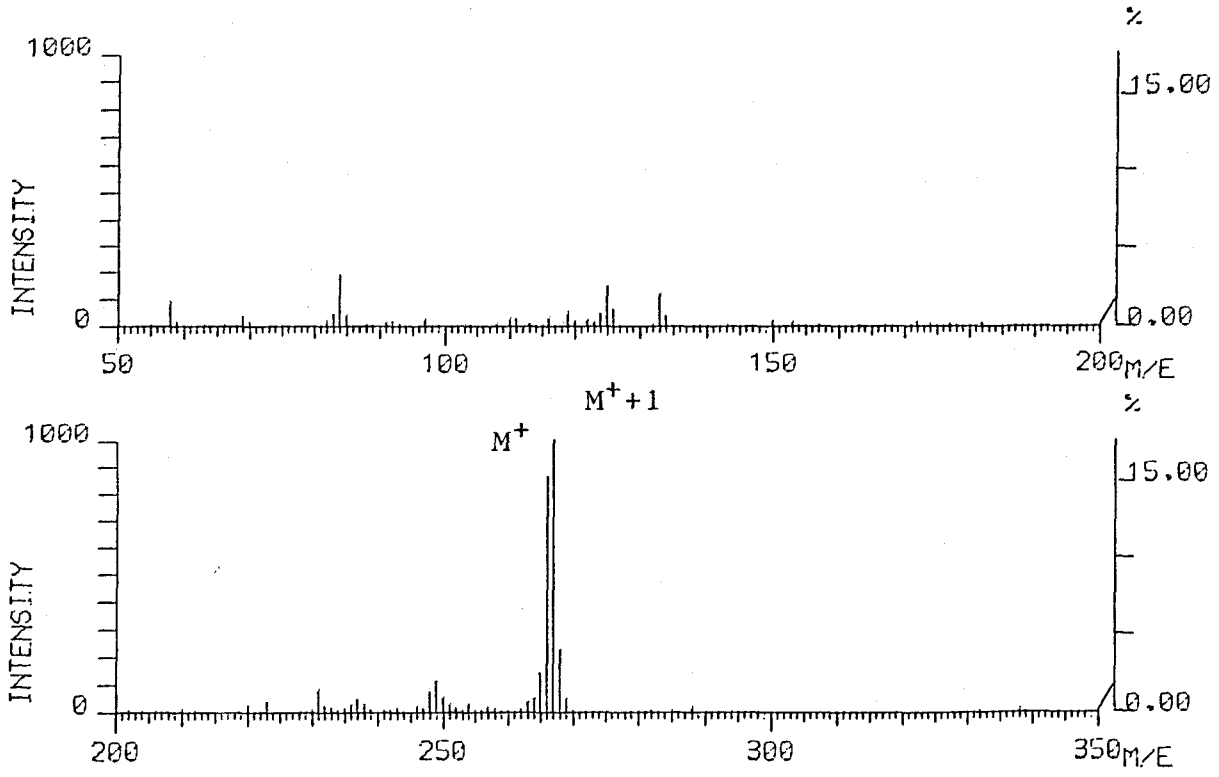

Fig. 3-70 FI-Mass Spectrum of RSA-TSA

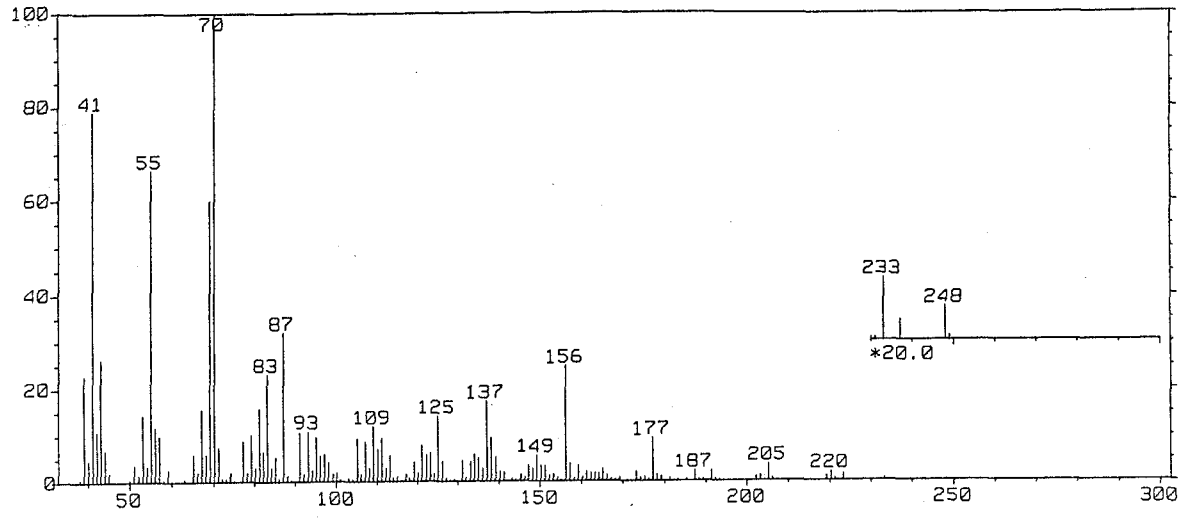

Fig. 3-71 EI-Mass Spectrum of RSA-TSA

Chemical structure of the derivative was eventually elucidated by ^{1}H- and ^{13}C-NMR analyses including spin-spin proton decoupling and CH-COSY experiments. The proton signals showed a good accordance with those of 1 except C-10 methine proton, which was unexpectedly detected in a lower magnetic field at δ_H 3.605 as a double-double-doublet (in 1, 1.912, ddd) (Fig. 3-72 and Table 3-28). When this proton was irradiated, an isopropyl methine signal at δ_H 1.516 previously divided into an octet-like signal became a clear septet (J= 6.8 Hz). The result was unambiguous evidence for the fact the methine proton at δ_H 3.605 was located vicinal to the isopropyl methine (broad octet-like, J= 6.5 Hz). However, the chemical shift for C-10-H, δ_H 3.605 was abnormally too low to assign it to a non-oxygenated methine proton.

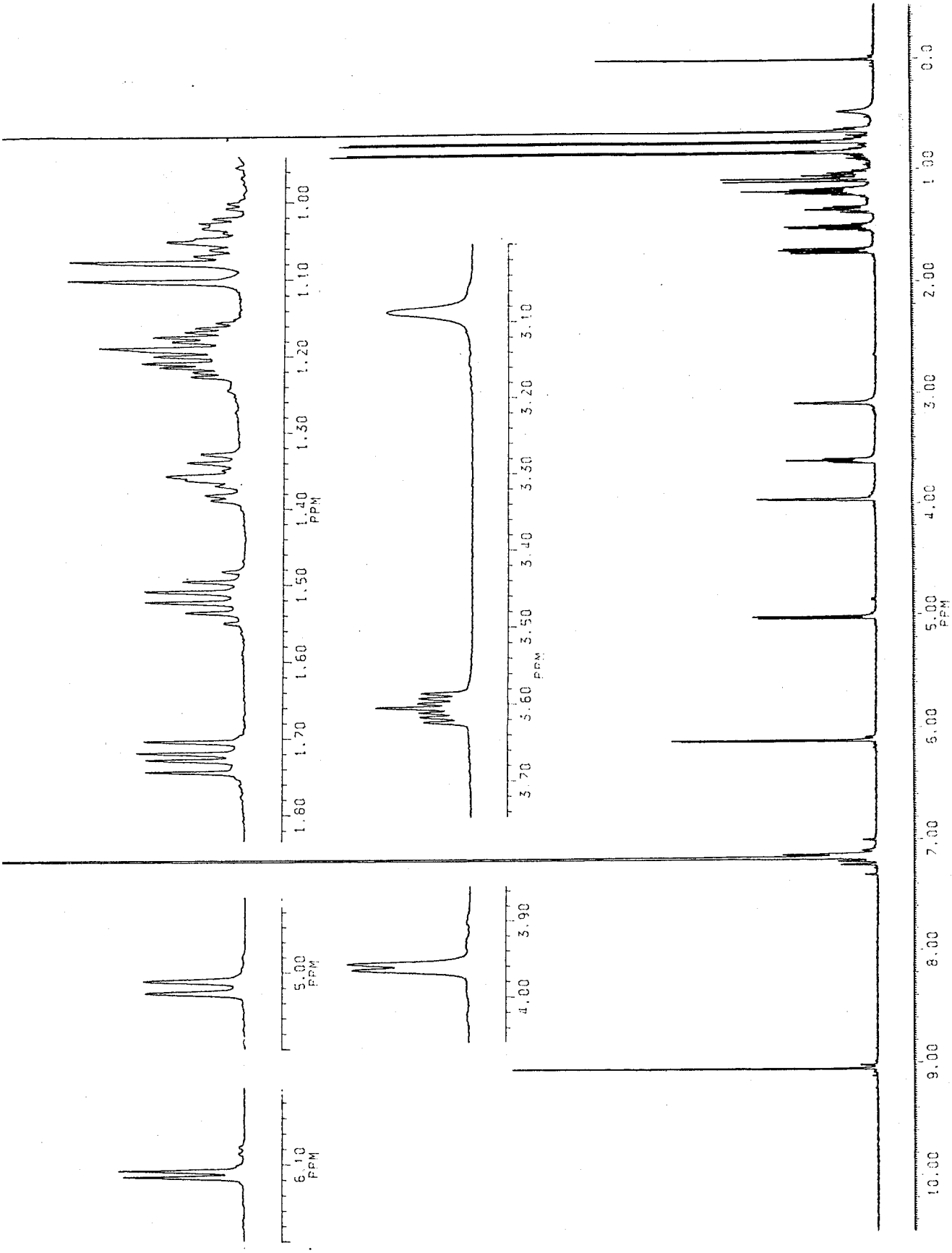

Fig. 3-72 ^{1}H-NMR Spectrum of RSA-TSA (500 MHz, in C_6D_6)

Table 3-28 *^{1}H-NMR chemical shift values of RSA-TSA (1i)*

(500 MHz, in C_6D_6, TMS as an int. std.)

δ_H	Proton (*J*=Hz)	Assignment
3.961	br. d (3.9)	C-2-H
3.088	br. s	C-2-OH
6.112	d (3.9)	C-3-H
5.018	br. d (7.7)	C-5-H
1.724	dd (12.3, 7.7)	C-6-Ha
1.090	br. d (12.3)	C-6-Hb
1.357	m	C-8-Ha
1.212	m	C-8-Hb
1.171	m	C-9-Ha
1.043	m	C-9-Hb
3.605	ddd (9.4, 6.5, 2.3)	C-10-H
1.516	double sept (6.8, 6.5)	C-11-H
0.838	d (6.8)	C-12-H_3
0.745	d (6.8)	C-13-H_3
9.048	s	C-14-H
0.652	s	C-15-H_3

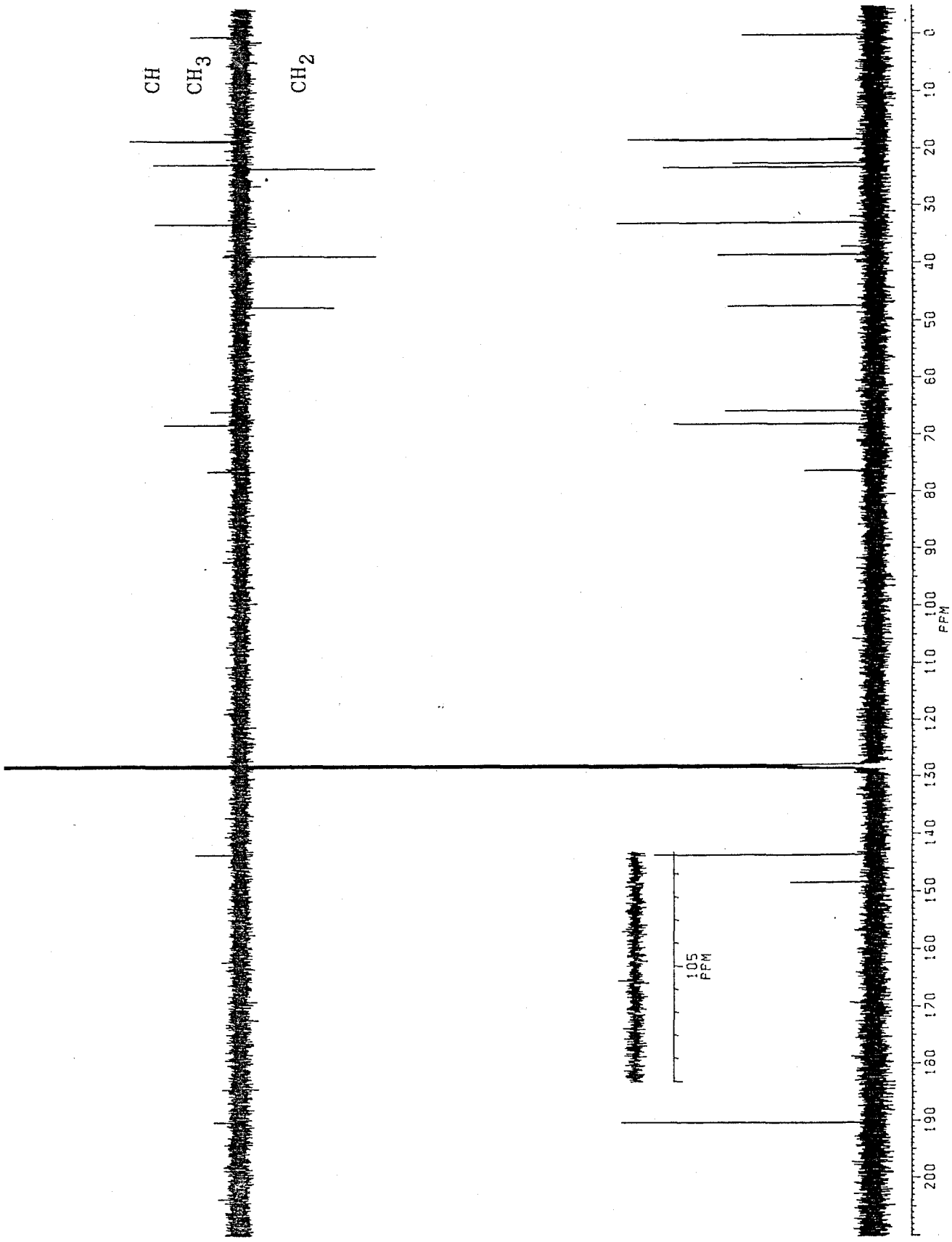

Fig. 3-73 ^{13}C-NMR Spectra of RSA-TSA (125 MHz, in C_6D_6, COM and DEPT)

The initially expected structure (Scheme 3-5) for the product was eliminated by ^{13}C-NMR analyses, because only one carbonyl carbon assignable to C-14 aldehyde group was observed in ^{13}C-NMR of RSA-TSA at δ_C 190.2 (Fig. 3-73 and Table 3-29). On the other hand, the ^{13}C-NMR spectrum showed the presence of four oxygenated sp^3 carbons, three of which were revealed to be a methine carbon (δ_C 76.3, 68.0 and 65.7). This fact was only explicable for illustrating the structure of RSA-TSA with oxygenated C-10 carbon. To confirm this speculation, CH-COSY spectrum of RSA-TSA was taken (Fig. 3-74) to reveal a cross peak between δ_H 3.605 and δ_C 76.3. Together with former spectroscopic data, the CH-COSY analysis permitted to assign all the carbon (See Table 3-29), and the C-10 carbon was inevitably oxygenated.

Moreover, a non-hydrogen bearing carbon detected at δ_C 105.7 was reasonably assigned to a ketal carbon. Since both proton sequences for the five-membered ring involving the isopropyl group and for the seven-membered ring were revealed and almost all of protons were observed around a similar magnetic field to those of **1**, this ketal carbon was only assignable to C-1. In conclusion, RSA-TSA should be a derivative of **1** rearranged its endoperoxide bridge into a ketal group at C-1. Accordingly, planar structure of RSA-TSA was proved to be **1i**.

The stereostructure of **1i** was successively examined. By the NOE experiments of the derivative, some NOEs were observed as shown in Fig. 3-75. NOEs between C-10-H $\longleftrightarrow$ C-8-Hb and C-10-H $\longleftrightarrow$ C-9-Hb gave a speculation that stereostructure of the isopropyl group was reversed, as C-8 methylene proton showed an NOE between C-15-H_3. To satisfy the requirement for these NOEs, C-10-H and C-8-Hb must take a 1,3-diaxal form, and C-8-Hb and C-15-H_3 also should be on

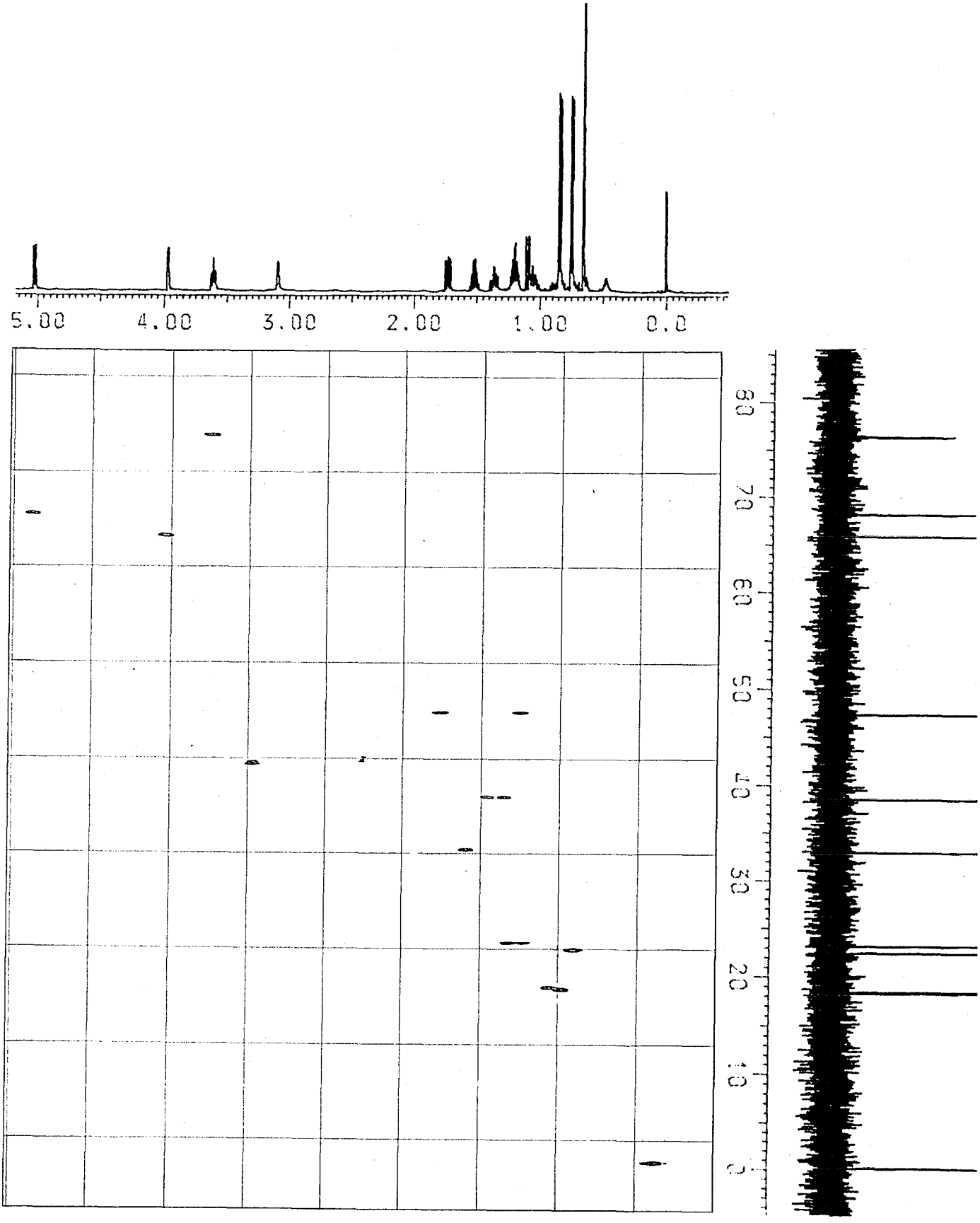

Fig. 3-74 CH-COSY Spectrum of RSA-TSA (500 and 125 MHz, in C_6D_6)

Table 3-29 *^{13}C-NMR chemical shft values of RSA-TSA*

(125 MHz, in C_6D_6, TMS as an int. std.)

δ_C	Proton*	Assignment
105.7	C	C-1
65.7	CH	C-2
143.4	CH	C-3
148.2	C	C-4
68.0	CH	C-5
47.2	CH_2	C-6
37.0	C	C-7
23.0	CH_2	C-8
38.4	CH_2	C-9
76.3	CH	C-10
32.8	CH	C-11
18.3	CH_3	C-12
18.2	CH_3	C-13
190.2	CH	C-14
22.3	CH_3	C-15

* Hydrogenation degrees on the carbons were revealed by the DEPT experiment, and the assignment of the carbons is due to the result of the CH-COSY experiment.

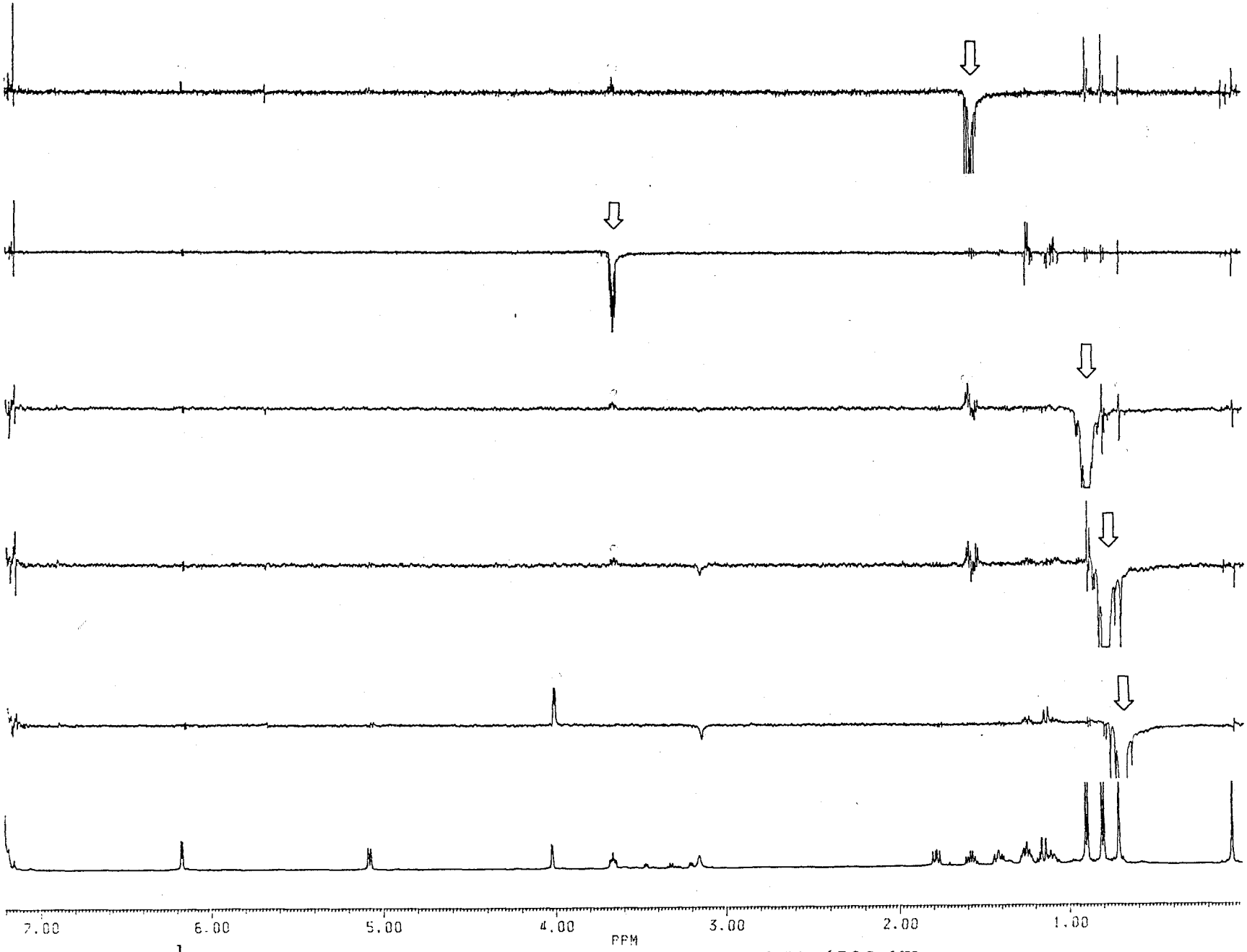

Fig. 3-75 ^{1}H-NMR Spectrum for NOE experiments on RSA-TSA (500 MHz, in C_6D_6): From the top, C-11, C-10, C-12, C-13 and C-5 protons were irradiated in turn.

the same side of the six-membered heteroring with a boat form (Fig 3-76). The isopropyl group is, therefore, to be *trans* to the bridgehead methyl group. Since these groups of the starting material are *cis*, this acidic conversion process is probably accompanied with a stereo-inversion at a C-10 chiral carbon.

As the conversion involves an unusual process in the C,C-single bond cleavage concerted with oxygen-migration, the reaction mechanism will be discussed in Section 4, including stereo-selectivity at C-10 during the reaction.

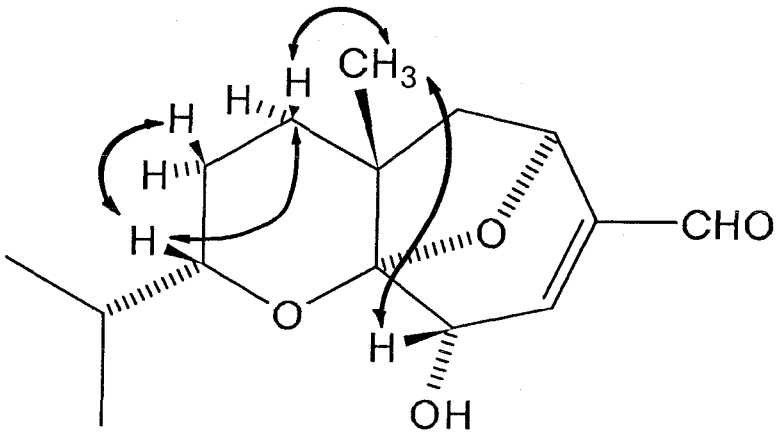

Fig. 3-76 Stereostructure of RSA-TSA to Satisfy the Observed NOEs between C-10-H and C-8-Hb, C-10-H and C-9-Hb, and C-15-H_3 and C-8-Hb

Table 3-30 Physicochemical properties of RSA-TSA (1i)

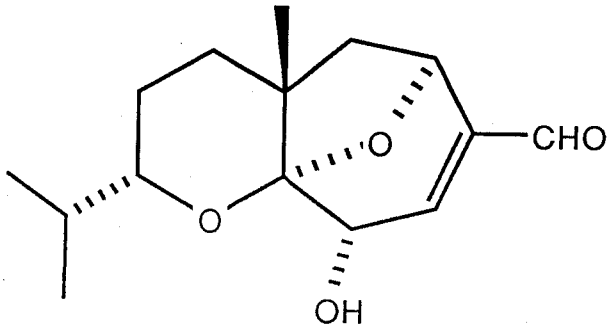

1i

A colorless syrup

Rf: 0.23 (H-EA 3:1), 0.44 (C-M 50:2)

Vanillin-H_2SO_4 color: grayish yellow → dark purple

N,*N*-dimethyl-*p*-phenylenediamine sulfate test: negative

FI-MS *m/z* (%): 267 (M^++1, 100), 266 (M^+, 86)

EI-MS *m/z* (%): 248 (M^+-H_2O, 0.4), 233 (0.7), 223 (M^+-C_3H_7, 0.8), 220 (2.1), 205 (M^+-H_2O-43, 3.8), 177 (9.6), 156 (25), 137 (17), 125 (14), 109 (12), 93 (11), 91 (11), 87 (32), 83 (23), 81 (16), 79 (10), 70 (100), 69 (60), 67 (16), 55 (67), 43 (26), 41 (79).

^{1}H-NMR data are shown in Table 3-28.

^{13}C-NMR data are shown in Tables 3-29.

8) Oxidation with PCC

Since rugosal A (1) has a secondary allyl OH group, it might be oxidized to the corresponding ketone. Crystallines of 1 (11.6 mg) and 30.7 mg of pyridinium chlorochromate (PCC) were dissolved in 2 ml of CH_2Cl_2 and mechanically stirred overnight at room temperature. The reaction mixture was then diluted with saturated NaCl solution (20 ml), and successively extracted with 20 ml of Et_2O (x 2). After dried over Na_2SO_4, the extract was concentrated *in vacuo* and subjected to PTLC (H-EA 3:1) to give a main quenching product, RSA-PCC (1.9 mg, *Rf* 0.67, yield 17 %) and unchanged 1 (3.7 mg, *Rf* 0.42, 32 %) (Fig. 3-77).

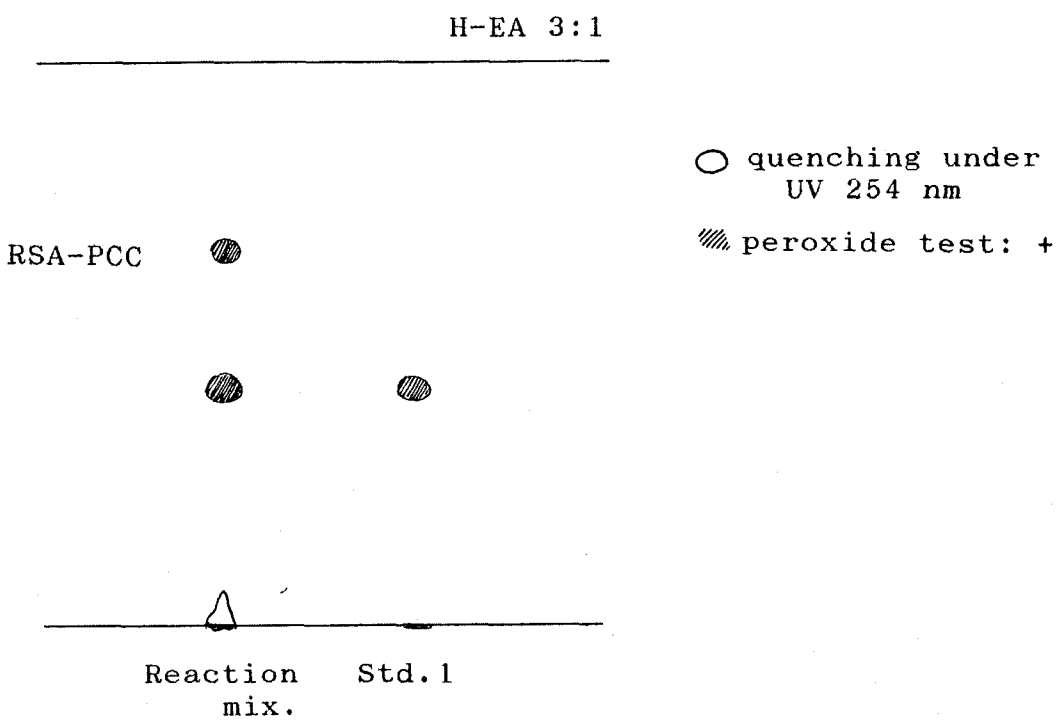

Fig. 3-77 TL Chromatogram of Reaction Product Obtained by PCC Oxidation of Rugosal A (1)

RSA-PCC positive to the peroxide reagent showed its molecular ion at *m/z* 264 (100 %) in FD-MS (Fig. 3-78). In EI-MS, the detection of a fragment at *m/z* 236 (M^+-CO, 2.0 %) was indicative of the presence of an aldehyde group in the product (Fig. 3-79). A dehydration fragment characteristic of the starting material (1) was not detected in RSA-PCC. UV absorption maximum at 232 nm of the product was characteristic of 1,4-diketo-2-ene moiety [103]. It was therefore apparent that oxidation at C-2 hydroxyl group yielded a keto derivative RSA-PCC (structure **1j**).

^{1}H-NMR spectrum of RSA-PCC proved the structure of the product (Fig. 3-80 and Table 3-31). The olefinic proton at C-3 (δ_H 6.072) was detected as a singlet peak, indicating that the vicinal C-2 methine proton (δ_H 4.185, dd, in 1) disappeared by the reaction: CH-OH → C=O. By some decoupling experiments (Fig. 3-81), all other protons were assigned. When C-5 methine proton showing a broad doublet was irradiated, two signals at δ_H 1.800 (dd, *J*= 14.2 and 6.9 Hz) and 0.817 (dd, *J*= 14.2 and 1.3 Hz) were both collapsed into two doublets geminally coupled (*J*= 14.2 Hz) each other. The poor sensitivity of C-2-OH to PCC may be due to its hydrogen bonding nature.

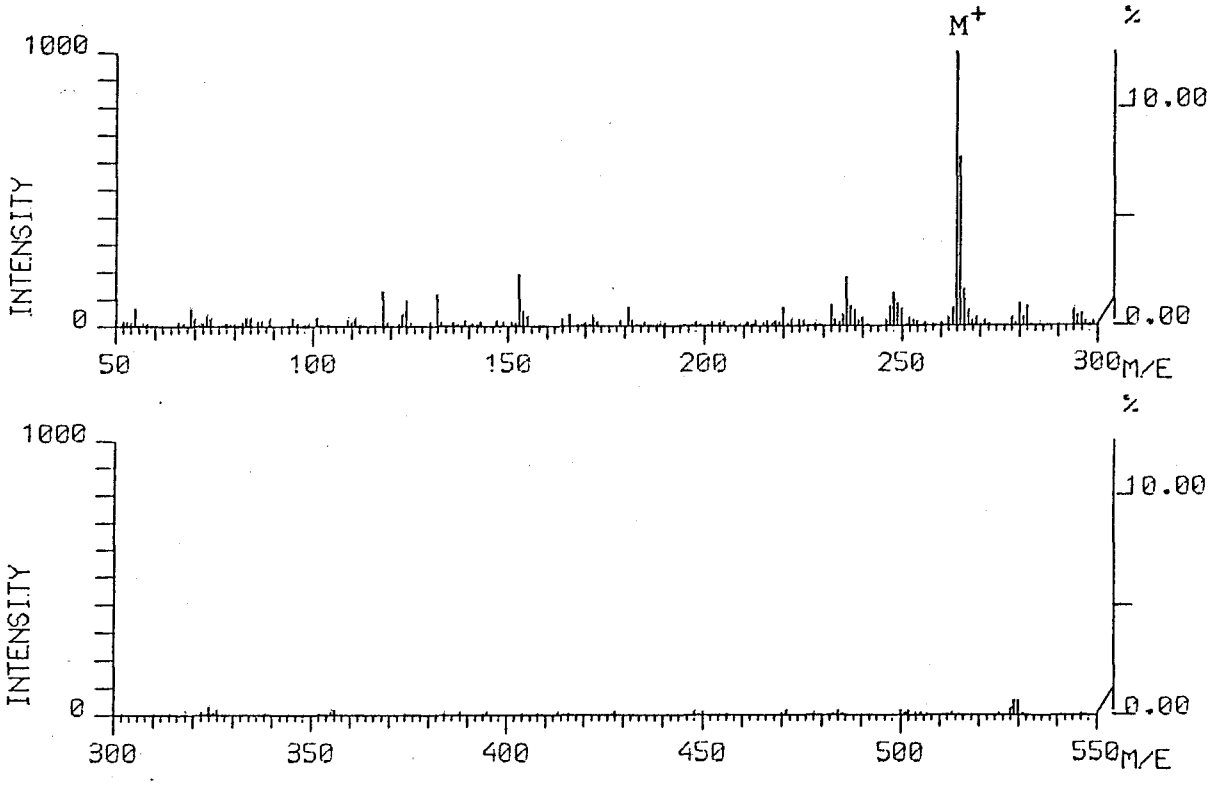

Fig. 3-79 FD-Mass Spectrum of RSA-PCC

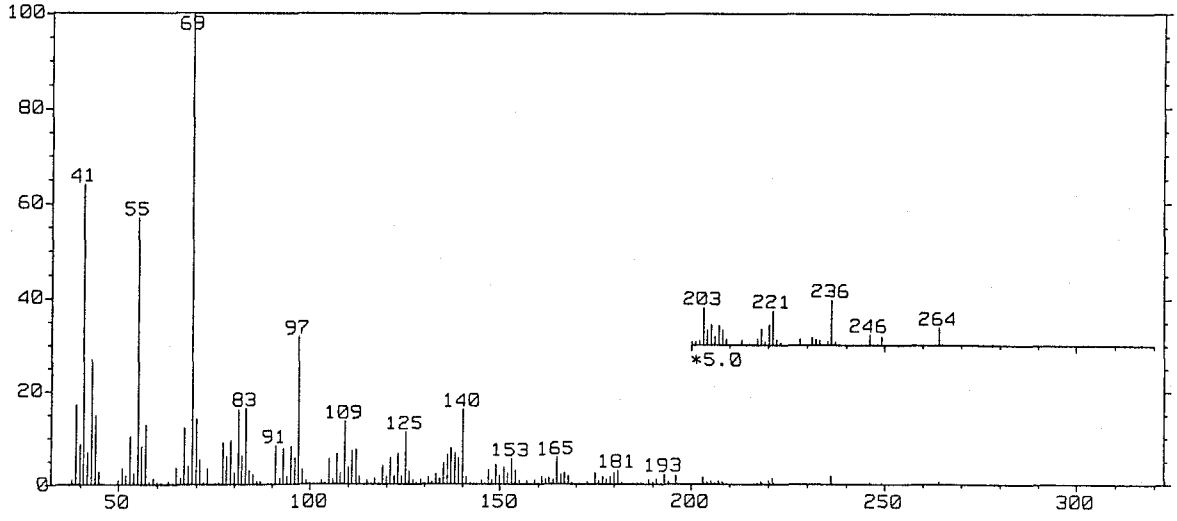

Fig. 3-80 EI-Mass Spectrum of RSA-PCC

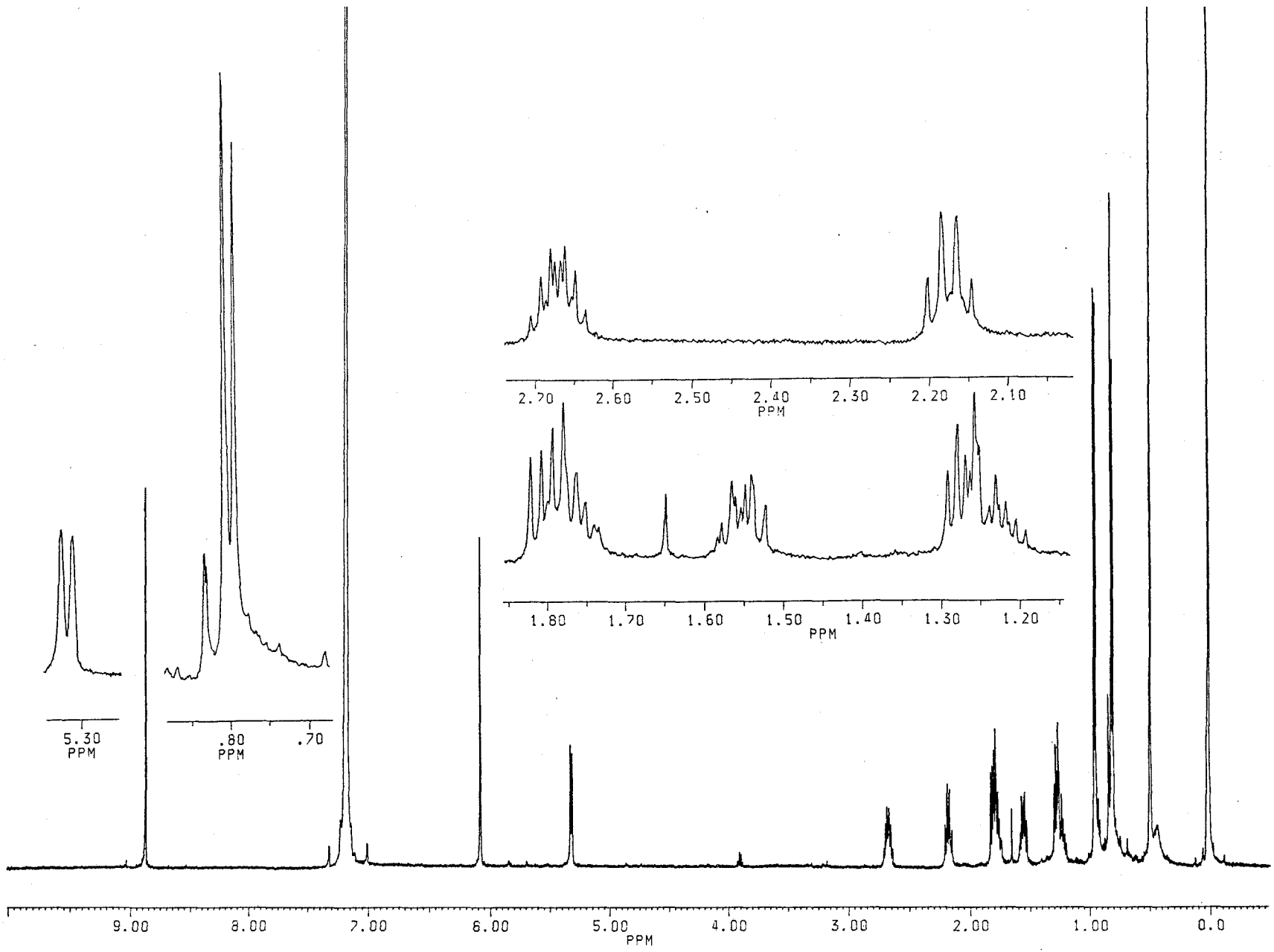

Fig. 3-81 ^{1}H-NMR Spectrum of RSA-PCC (500 MHz, in C_6D_6)

Table 3-31 ^{1}*H-NMR chemical shift values of RSA-PCC (1j)*

(500 MHz, in C_6D_6, TMS as an int. std.)

δ_H	Proton (*J*=Hz)	Assignment
6.072	s	C-3-H
5.317	br. d (6.8)	C-5-H
1.800	dd (14.2, 6.9)	C-6-Ha
0.817	dd (14.2, 1.3)	C-6-Hb
1.771	ddd (13.5, 11.5, 6.0)	C-8-Ha
1.274	dd (11.5, 6.2)	C-8-Hb
1.550	m	C-9-Ha
1.234	m	C-9-Hb
2.036	br. dd (18.7, 9.1)	C-10-H
2.890	double sept. (18.7, 6.5)	C-11-H
0.944	d (6.5)	C-12-H_3
0.798	d (6.5)	C-13-H_3
8.861	s	C-14-H
0.482	s	C-15-H_3

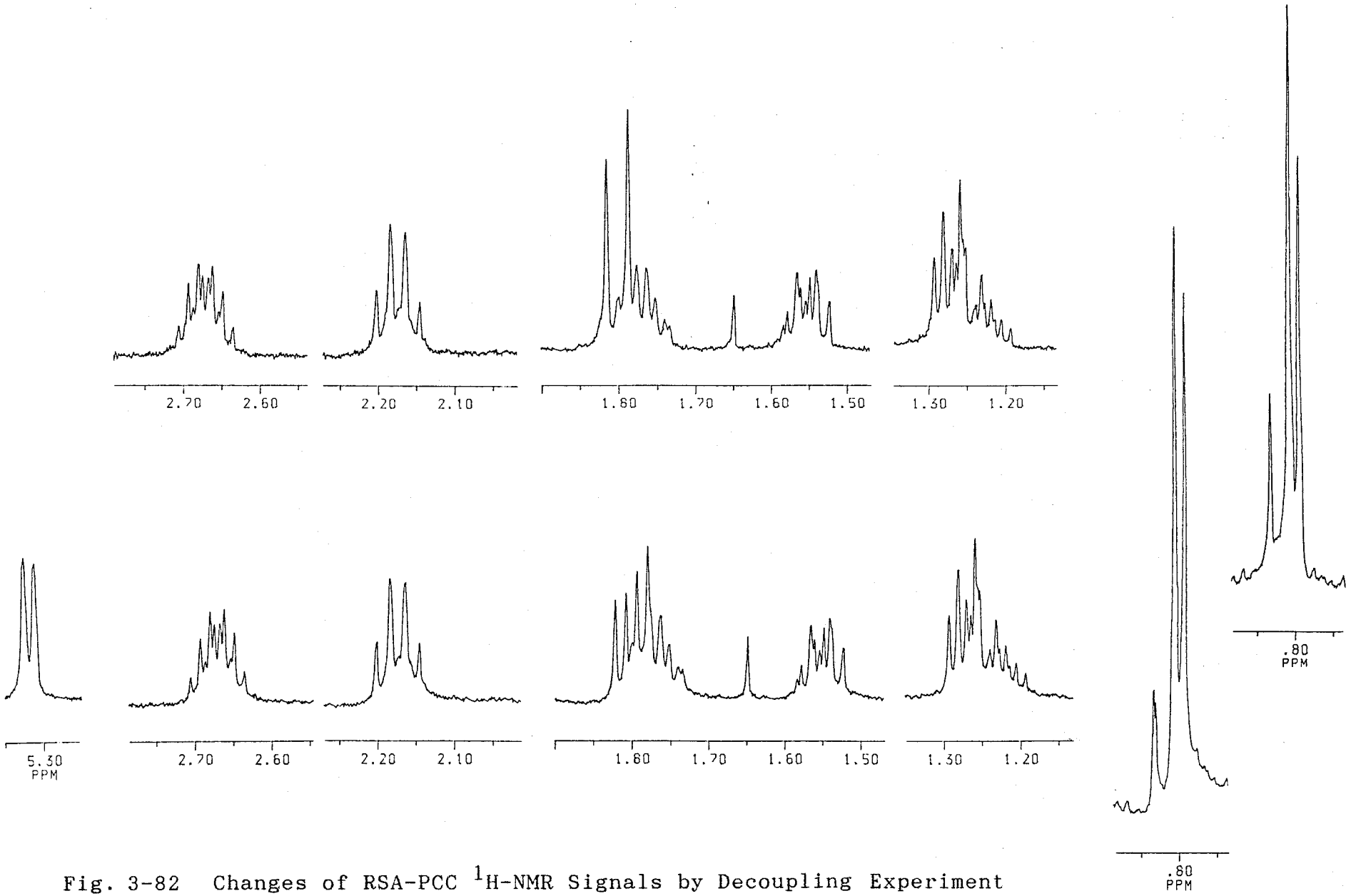

Fig. 3-82 Changes of RSA-PCC ^{1}H-NMR Signals by Decoupling Experiment

Table 3-32 Physicochemical properties of RSA-PCC (1j)

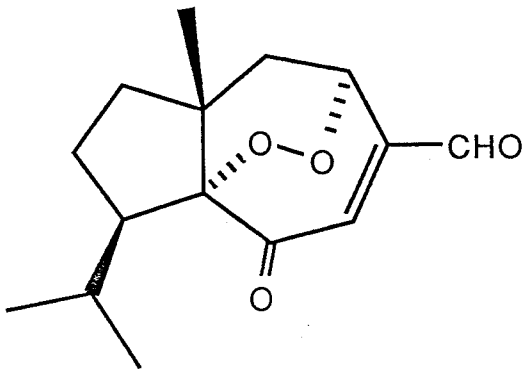

1j

Pale yellow needles, mp 54-55°C

Rf: 0.67 (H-EA 3:1)

Vanillin-H_2SO_4 color: graysh yellow

N,*N*-dimethyl-*p*-phenylenediamine sulfate test: positive (pinkish red)

UVλ_{max}^{MeOH}: 232 nm

FI-MS *m/z* (%): 265 (M^++1, 62), 264 (M^+, 100), 236 (18), 118 (14)

EI-MS *m/z* (%): 264 (M^+, 0.8), 246 (0.5), 236 (M^+-CO, 2.0), 221 ($M^+-C_3H_7$, 1.5), 203 (1.6), 196 (2.1), 193 (2.3), 181 (3.2), 175 (2.7), 165 (5.9), 153 (5.6), 140 (16), 137 (7.9), 125 (11), 109 (14), 97 (32), 83 (16), 81 (16), 70 (14), 69 (100), 67 (12), 57 (13), 55 (57), 53 (10), 44 (15), 43 (27), 41 (64).

^{1}H-NMR data are shown in Table 3-31.

9) Conversion to the Methoxycarbonyl Compound

Applied Corey's method [104], the aldehyde group of 1 was converted into a methoxycarbonyl group. The procedures for the reaction and the isolation of the product are shown in Scheme 3-5

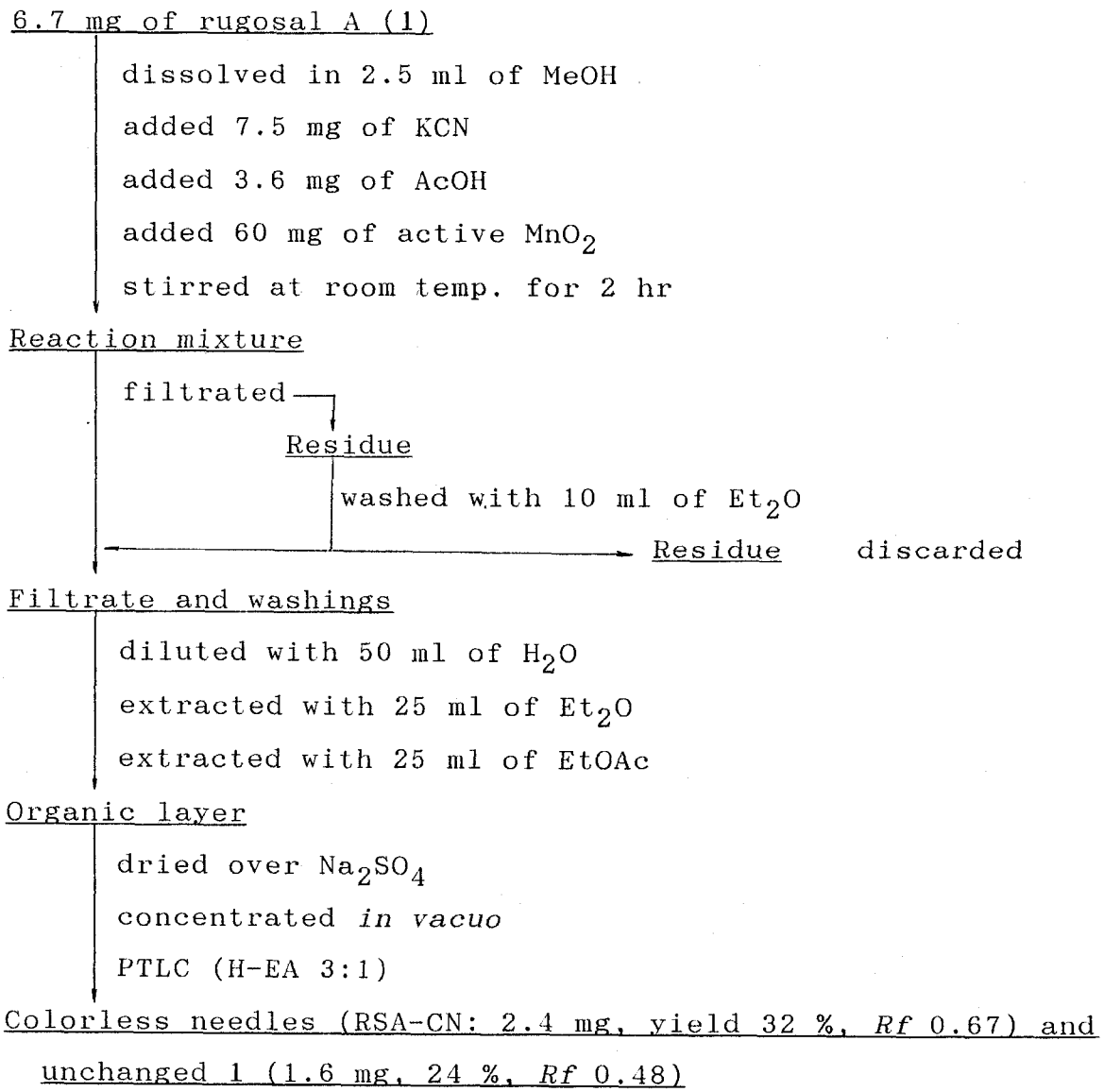

Scheme 3-5 Process to obtain RSA-CN (1k) from rugosal A (1)

The main product RSA-CN positive to the peroxide reagent (Fig. 3-82) indicated M^+ 296 (100 %) in FI-MS (Fig. 3-83). Its EI-MS fragmentation suggested the presence of a hydroxyl group and a methoxy carbonyl group [*m/z* 278 (M^+-H_2O, 1.8 %), 264 (M^+-$HOCH_3$, 4.1 %), and 219 (M^+-H_2O-$COOCH_3$, 7.1 %)] (Fig. 3-84). In the IR spectrum, a hydrogen-bonding hydroxyl group (ν_{max}^{KBr} 3460 cm^{-1}) and an α, β-unsaturated methoxycarbonyl group (1730 cm^{-1}) were visible (Fig. 3-85). The methoxy carbonyl proton became feasible in ^{1}H-NMR spectrum at δ_H 3.773 (3H, s). Other signals exhibited a good correspondence with those of **1**. These result suggested that **1** was successfully converted into the corresponding methoxy carbonyl derivative, without any peroxide rearrangement (Fig. 3-86 and Table 3-33). Accordingly, structure of RSA-CN was elucidated as **1k**. Moreover, the carbon chemical shifts of RSA-CN in the ^{13}C-NMR spectrum showed a good correspondence with those of **1**, except the C-14 and the olefinic carbons, confirming its proposed structure (Fig. 3-87 and Table 3-34).

This derivative became a key compound to establish unambiguously the planar structure of **1**. A free acid corresponding to **1** was obtained from the acidic constituents of the leaves of *Rosa rugosa*, and its methylation product being completely identical with **1k** was subjected to 2D-^{13}C-NMR (INADEQUATE) to reveal the carbon-carbon sequences. The results will be dercribed in details in the next section.

Furthermore, the compound identical with **1k** was also isolated from *Rosa rugosa* leaves as a naturally occuring carotanoid. This natural compound (rugosic acid A methyl ester) was comparatively rich in the old leaves, even though the content was rather lower than **1**. This isolation procedure is also separately described in Section 6.

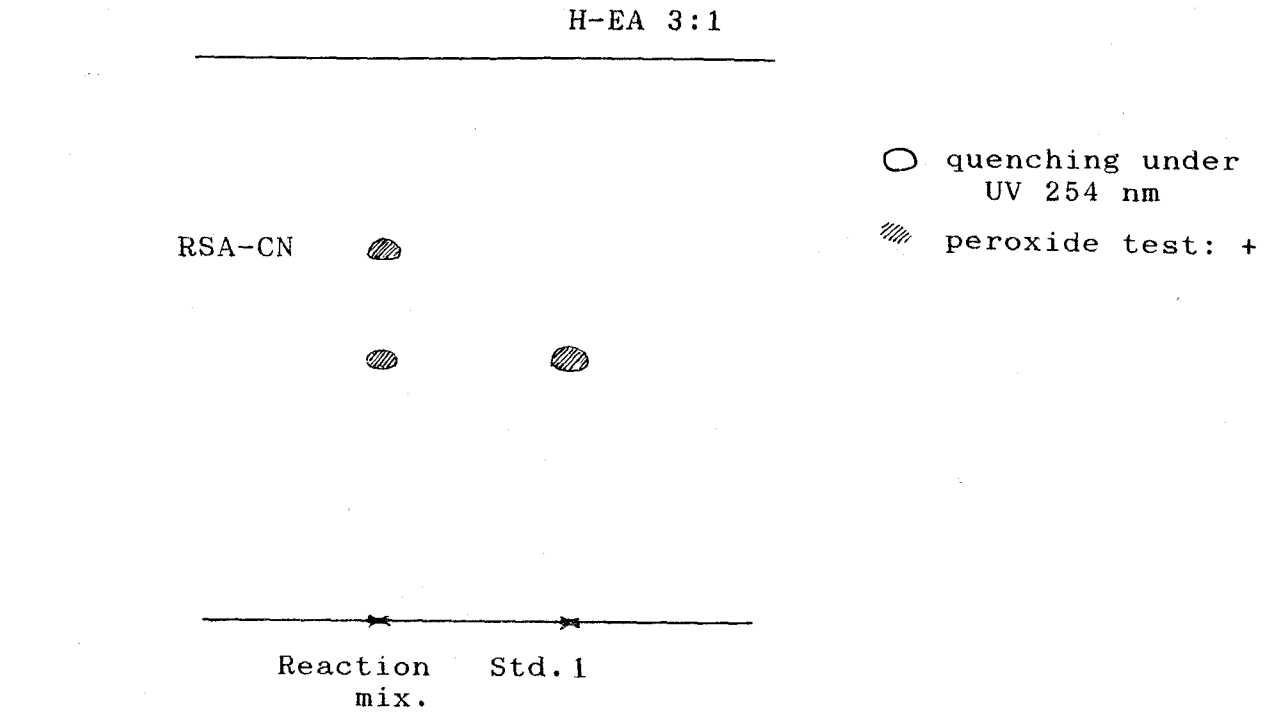

Fig. 3-82 TL Chromatograms of Reaction Product Obtained by Conversion of Rugosal A (1) into Methoxycarobonyl Derivative

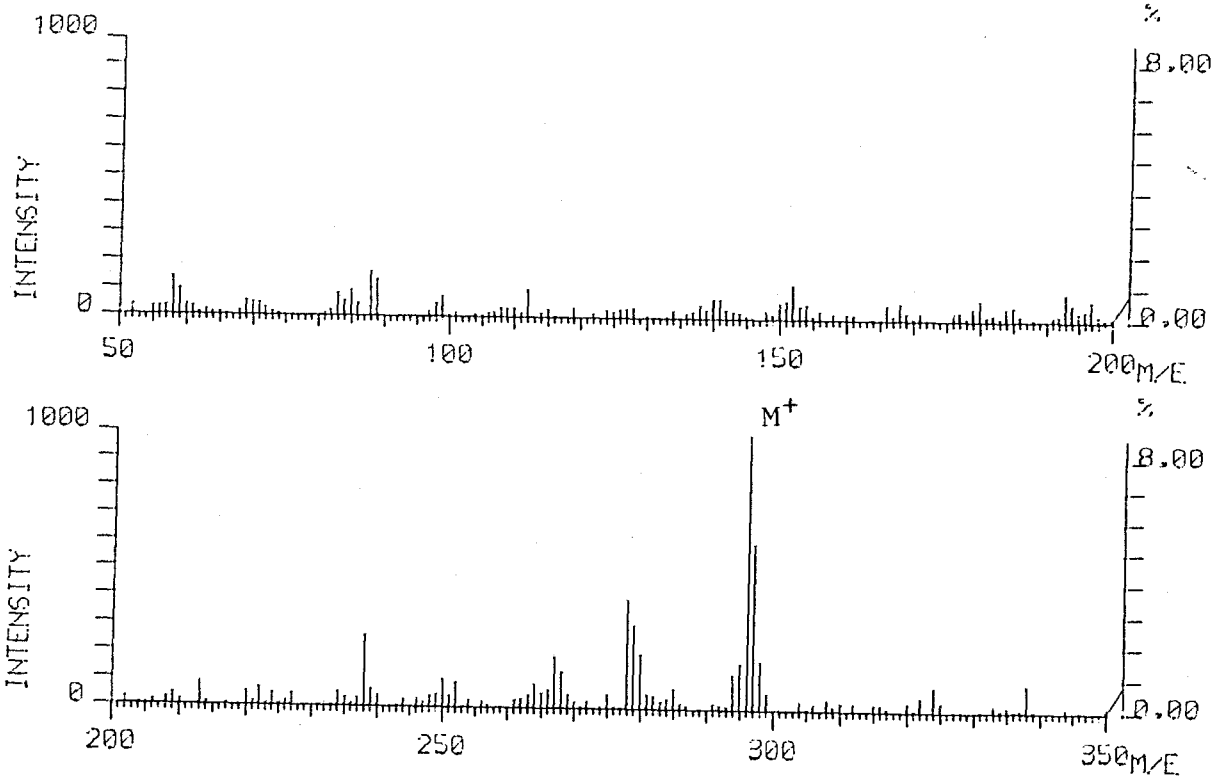

Fig. 3-83 FI-Mass Spectrum of RSA-CN

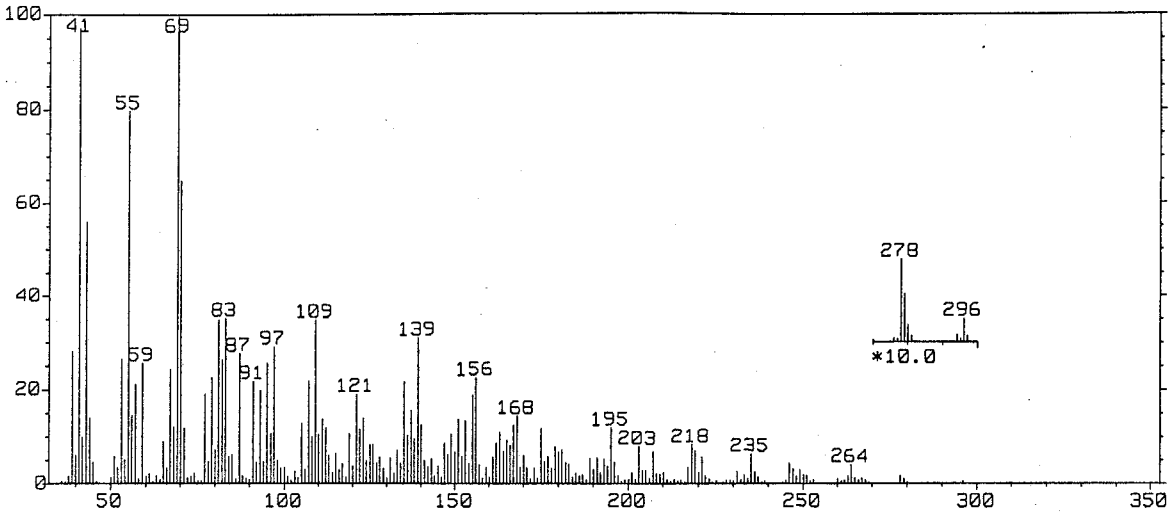

Fig. 3-84 EI-Mass Spectrum of RSA-CN

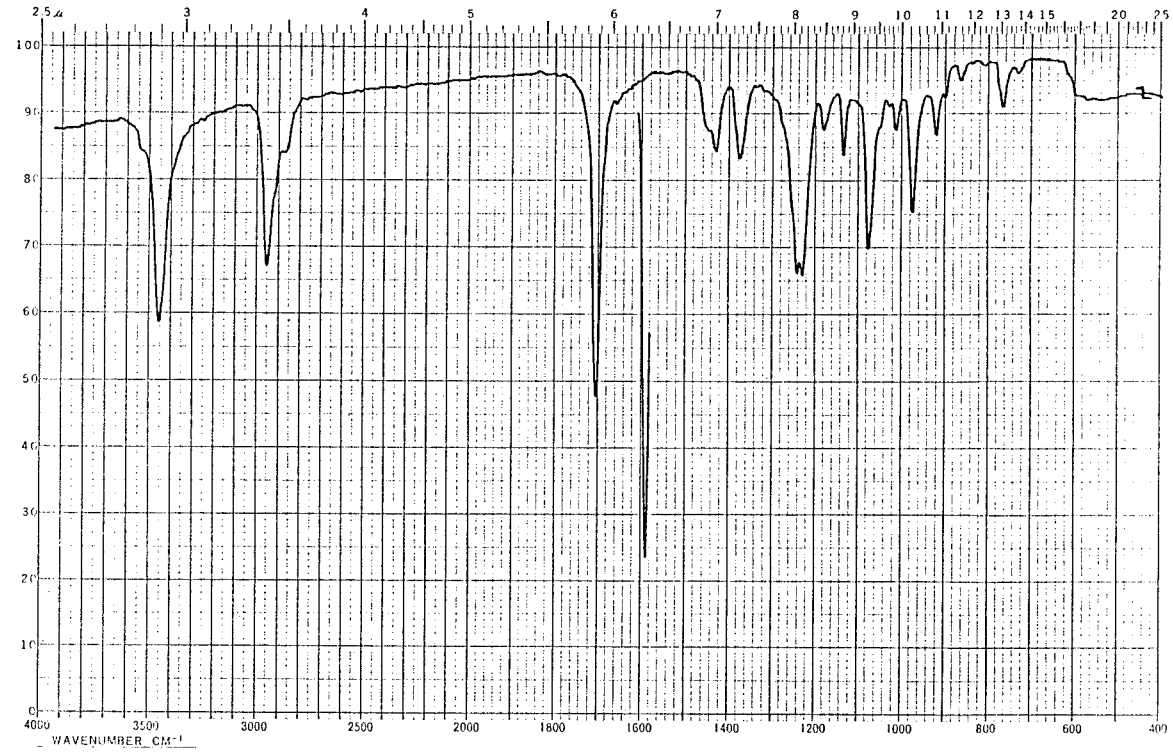

Fig. 3-85 IR Spectrum of RSA-CN (KBr disc)

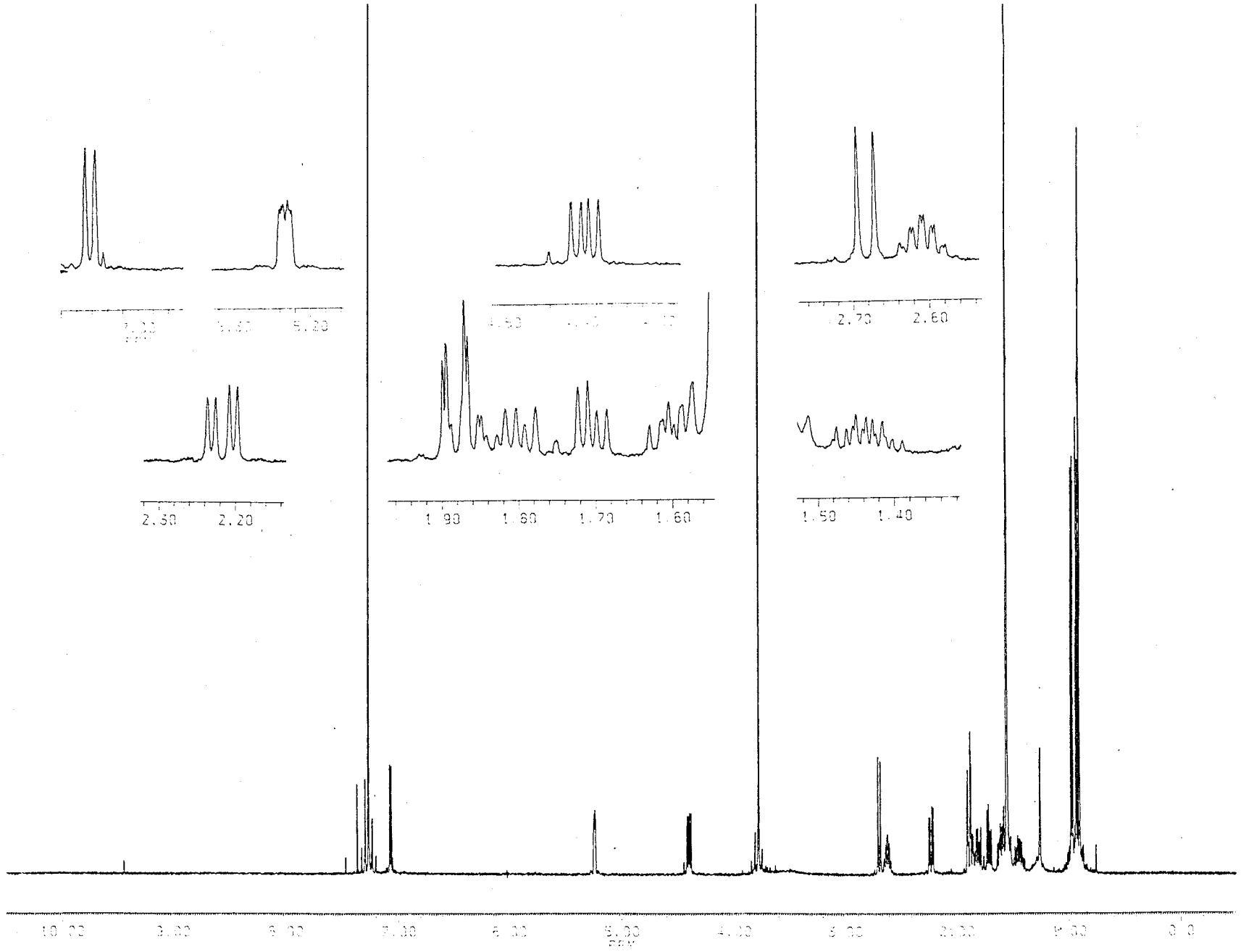

Fig. 3-86 ^{1}H-NMR Spectrum of RSA-CN (500 MHz, in $CDCl_3$)

Table 3-33 *^{1}H-NMR chemical shift values for RSA-CN (1k)*

(500 MHz, in $CDCl_3$, TMS as an int. std.)

δ_H	Proton (*J*=Hz)	Assignment
4.394	dd (11.5, 6.4)	C-2-H
2.681	d (11.5)	C-2-OH
7.060	d (6.4)	C-3-H
5.231	dd (5.2, 2.5)	C-5-H
2.216	dd (14.2, 5.2)	C-6-Ha
1.881	dd (14.2, 2.5)	C-6-Hb
1.810	ddd (13.0, 12.2, 7.1)	C-8-Ha
1.703	dd (12.2, 6.5)	C-8-Hb
1.600	ddd (15.7, 8.7, 7.1)	C-9-Ha
1.431	dddd (15.7, 13.0, 10.8, 6.5)	C-9-Hb
1.870	overlapped ddd (2.2)	C-10-H
2.607	double sept. (6.8, 2.2)	C-11-H
0.963	d (6.8)	C-12-H_3
0.918	d (6.8)	C-13-H_3
0.896	s	C-15-H_3
3.773	s	C-14'-H_3

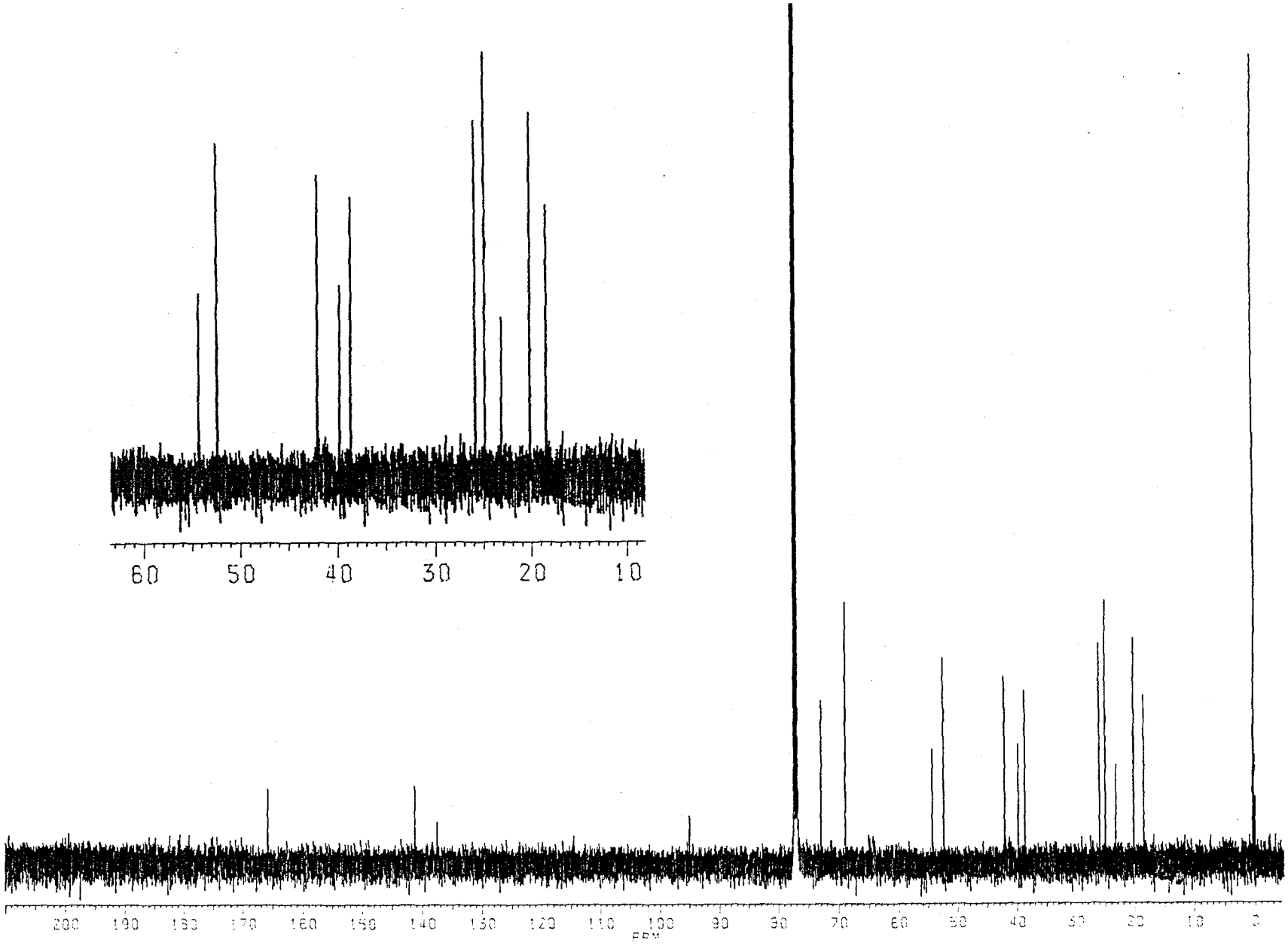

Fig. 3-87 ^{13}H-NMR Spectrua of RSA-CN (125 MHz, in $CDCl_3$, COM and DEPT)

Tabel 3-34 Carbon shift values of RSA-CN (1k) and rugosal A (1)

RSA-CN (1k) (125 MHz, in $CDCl_3$)		Rugosal A (1) (68 MHz, in C_6D_6)		
$\delta_{\underline{C}}$		$\delta_{\underline{H}}$	<u>CH*n*</u>	Assignment
165.73	-COO-	190.7	CH	14
141.08		149.4	CH	3
137.42		146.5	C	4
94.89		94.8	C	1
72.79		70.1	CH	5
68.75		69.1	CH	2
54.10		54.6	CH	10
52.19	$-COO\underline{C}H_3$	-		14'
41.88		42.0	CH_2	6
39.58		39.6	C	7
38.46		38.5	CH_2	8
25.72		25.9	CH_3	12
24.72		24.8	CH	11
23.00		22.8	CH_3	15
19.96		20.2	CH_2	9
18.30		18.4	CH_3	13

Table 3-35 Physicochemical properties of RSA-CN (1k)

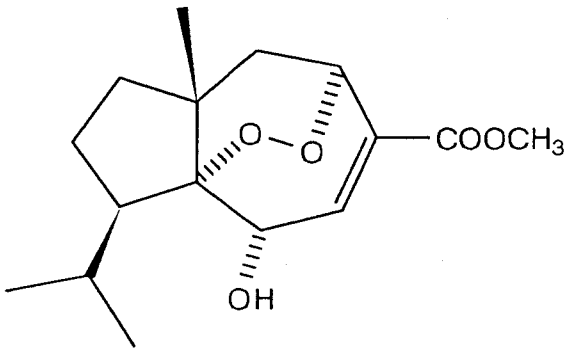

1k

Colorless needles, mp 150-151 °C

Rf: 0.67 (H-EA 3:1)

Vanillin-H_2SO_4 color: reddish pink

N,*N*-dimethyl-*p*-phenylenediamine sulfate test: positive (pinkish red)

$[\alpha]_D$: + 128 ° (*c* 0.02 in acetone)

IRν_{max}^{KBr} (cm^{-1}): 3460 (OH), 2960, 1730 (C=O), 1440, 1380, 1250, 1230, 1080, 980

FI-MS *m/z* (%): 297 (M^++1, 61), 296 (M^+, 100), 279 (31), 278 (M^+-H_2O, 56), 238 (26).

EI-MS *m/z* (%): 296 (M^+, 0.5), 279 (1.0), 278 (M^+-H_2O, 1.8), 264 (M^+-$HOCH_3$, 4.1), 249 (3.0), 247 (3.3), 246 (4.5), 235 (6.4), 221 (5.7), 219 (M^+-H_2O-$COOCH_3$, 7.1), 218 (8.4), 203 (8.0), 207 (6.9), 203 (8.0), 195 (12), 175 (12), 168 (14), 167 (12), 163 (11), 156 (23), 155 (19), 139 (31), 135 (22), 109 (35), 107 (22), 97 (29), 95 (26), 87 (28), 83 (35), 82 (27), 81 (35), 70 (65), 69 (100), 59 (26), 55 (80), 53 (27), 43 (56), 41 (97).

^{1}H-NMR and ^{13}C-NMR data are shown in Tables 3-33 and 3-34.

3-2-4 Elucidation of Rugosal A Absolute Configuration

1) Introduction of the Exciton Chirality Method

Since rugosal A has an allylic alcohol partial structure, the exciton chirality method [105,104] is applicable to the corresponding benzoate for determination of the absolute configuration of 1. The exciton chirality method, covering Mills' rule [105], Brewster's rule [106] and the benzoate sector rule [107] all of which are empirical rules ever used in determination of absolute configurations, has theoretically been established. From the sign of Cotton effect in CD spectrum recorded for the benzoate, the absolute configuration of a hydroxylated allyl carbon can be determined.

The benzoate chromophore exhibits $\pi \longrightarrow \pi^*$ intramolecular charge-transfer band at 230 nm. On the other hand, the olefinic bond possesses the $\pi \longrightarrow \pi^*$ transition at 195 nm. These two transitions are polarized along the long axes on the chromophores [103]. The first Cotton effect at 230 nm observed as positive one is due to a positive exciton chirality (right-handed screwness) between the two long axes of the benzoate and the olefine chromophore. On the contrary, negative exciton chirality between them (left-handed screwness) submits a negative Cotton effect at the wave length (Fig. 3-88).

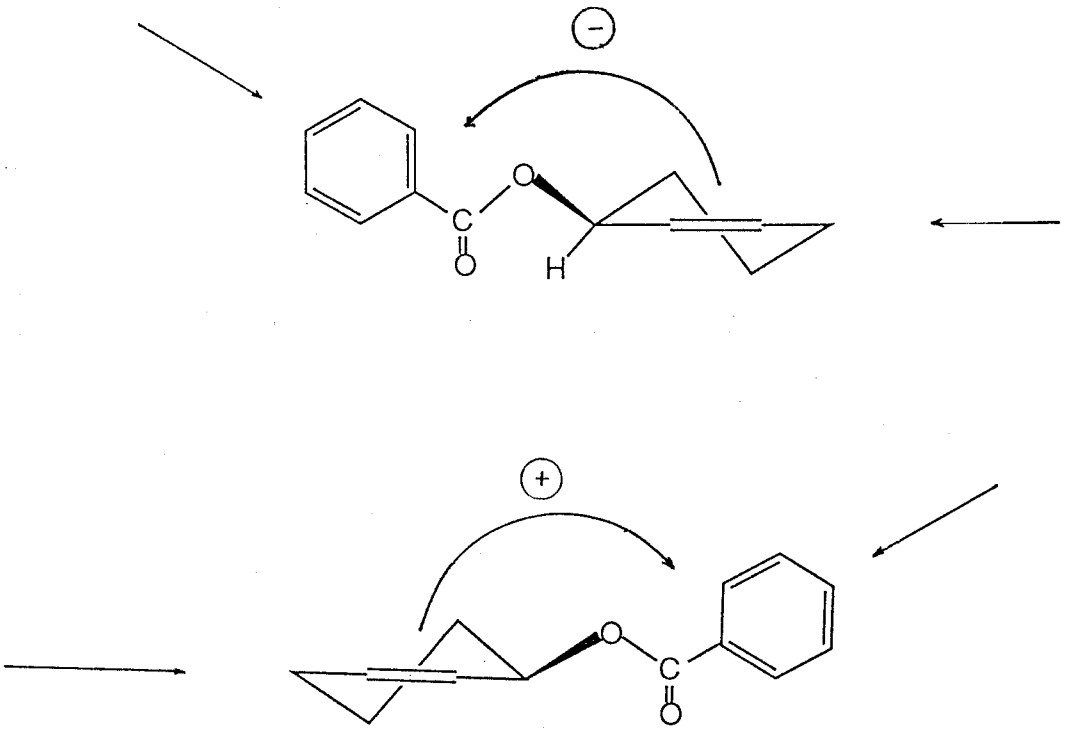

Fig. 3-88 Right- and Left-handed Screwness between Long Axes of the Benzoate and Olefine Chromophore on Allyl Benzoate, and Each Cotton Effect Observed at 230 nm

2) Preparation of the Benzoate from Rugosal A

Rugosal A (1, 40.2 mg) was treated with benzoic anhydride (56.6 mg) in 2 ml of Et_3N for 1 hr at 80 °C to obtain C-2-benzoate. The reaction mixture was diluted with EtOAc and successively washed twice with saturated NaCl solution and four times with 0.2 N HCl/saturated NaCl solution [108]. The organic layer was dried over Na_2SO_4 and passed through a small silica gel column. The resulting solution was concentrated and subjected to TLC. However, the expected product was not yielded at all, and small amounts of a by-product (RSA-BA) was obtained as the only one product coupled with benzoic acid. The major part of the starting material seemed to be dehydrated under the reaction conditions. The focused RSA-BA was purified by PTLC firstly in hexane-EtOAc 1:3 (*Rf* 0.87) and secondly in benzene-EtOAc 5:1 (*Rf* 0.51) to give 3.1 mg of a

colorless syrup in a yield of 6 % (Fig. 3-89).

The isolate negative to the peroxide reagent showed the molecular ion at *m/z* 370 (in FD-MS, M^+ 100 %) (Fig. 3-90). These results indicated that some rearrangements had occurred around the peroxy bridge during the esterification reaction. From some dehydration fragments [*e.g.* *m/z* 352 (M^+-H_2O, 0.3 %), *m/z* 230 ($M^+-C_6H_5COOH-H_2O$, 0.9 %)] in EI-MS (Fig. 3-91), RSA-BA was expected to possess a free OH group in the molecule. ^{1}H-NMR spectrum of RSA-BA showed a pair of geminally coupled methylene protons at δ_H 1.996 and 1.778 (each 1H, d, *J*= 12.5 Hz) assignable to C-6-H_2 (Fig. 3-92 and Table 3-36). The disappearance of C-5 methine proton gave an evidence that the endoperoxide was rearranged into a hemiacetal, like **1g**. A methine proton, vicinally coupled with C-3 olefinic proton and attributable to C-2-H, was observed in a markedly lower magnetic field at δ_H 5.506 (1H, d, *J*= 4.4 Hz). This deshielding of C-2-H (by 1.84 ppm from that of **1g**) was explicable with the presence of a benzoyloxy group on the C-2 carbon. Accordingly, the structure of RSA-BA was elucidated as **11**. However, its small yield from the starting material (6 %) remained a problem.

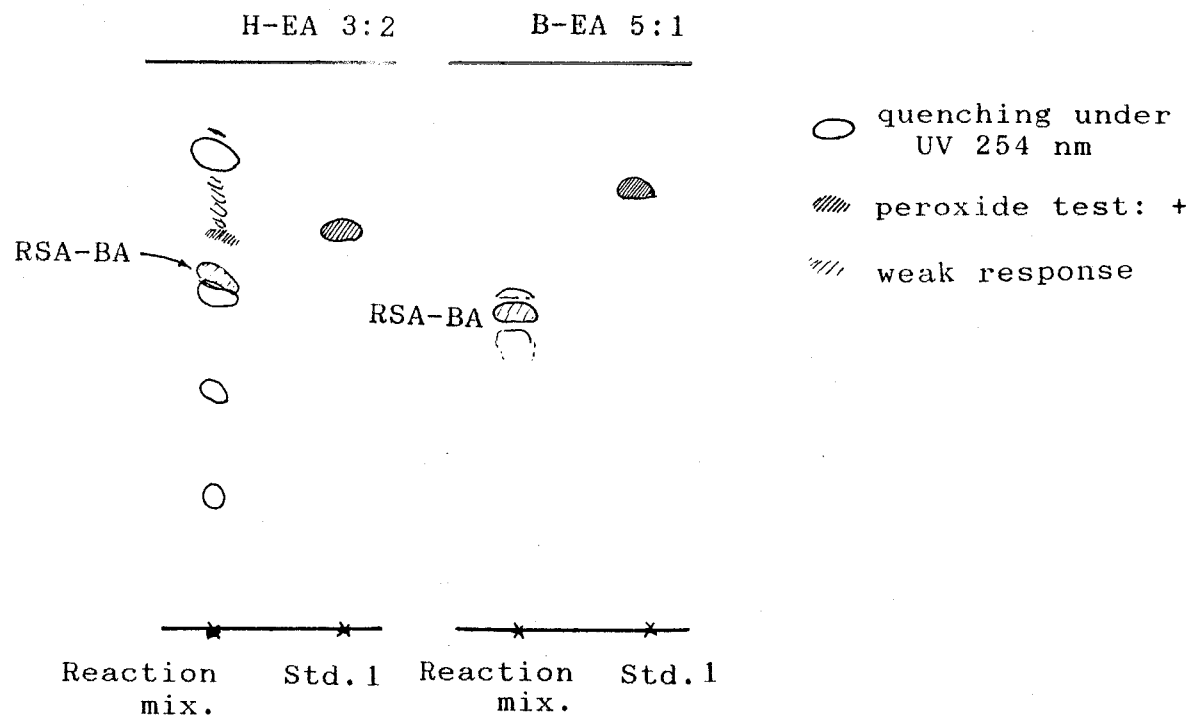

Fig. 3-89 TL Chromatograms of Reaction Products Obtained by Esterification Reaction of Rugosal A (1) with Benzoic Anhydride

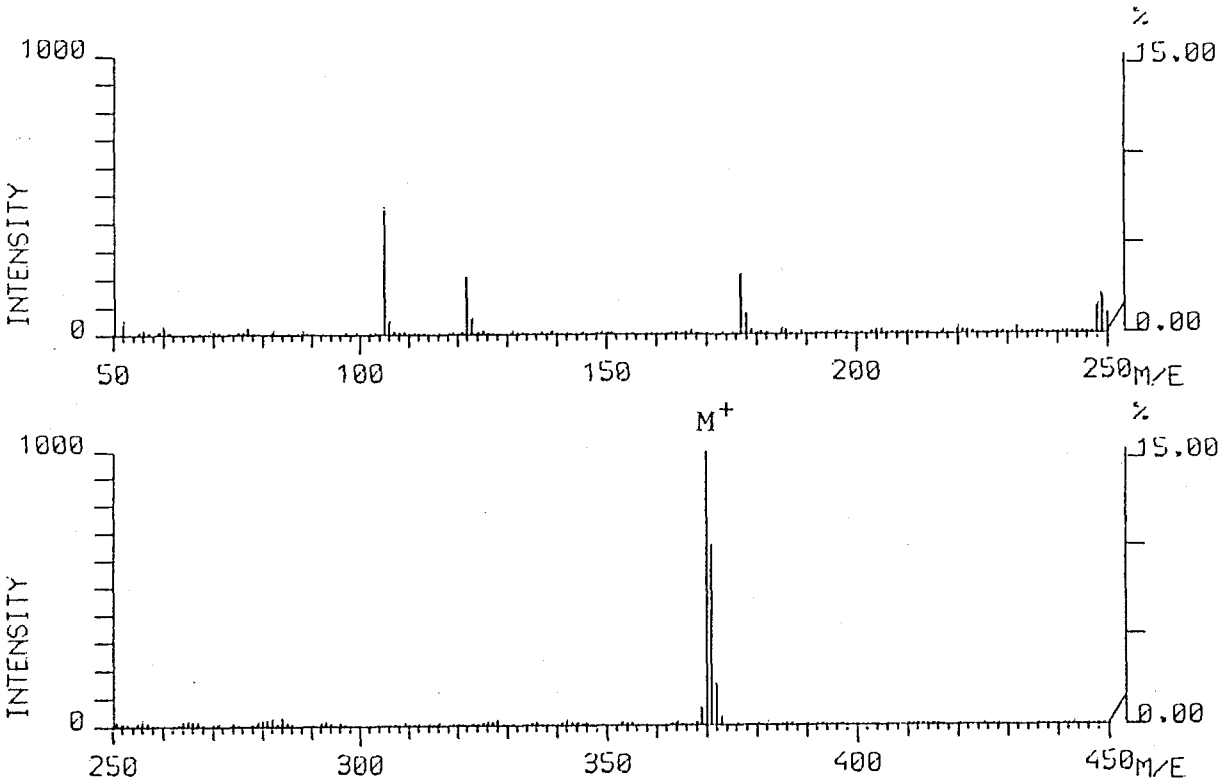

Fig. 3-90 FD-Mass Spectrum of RSA-BA

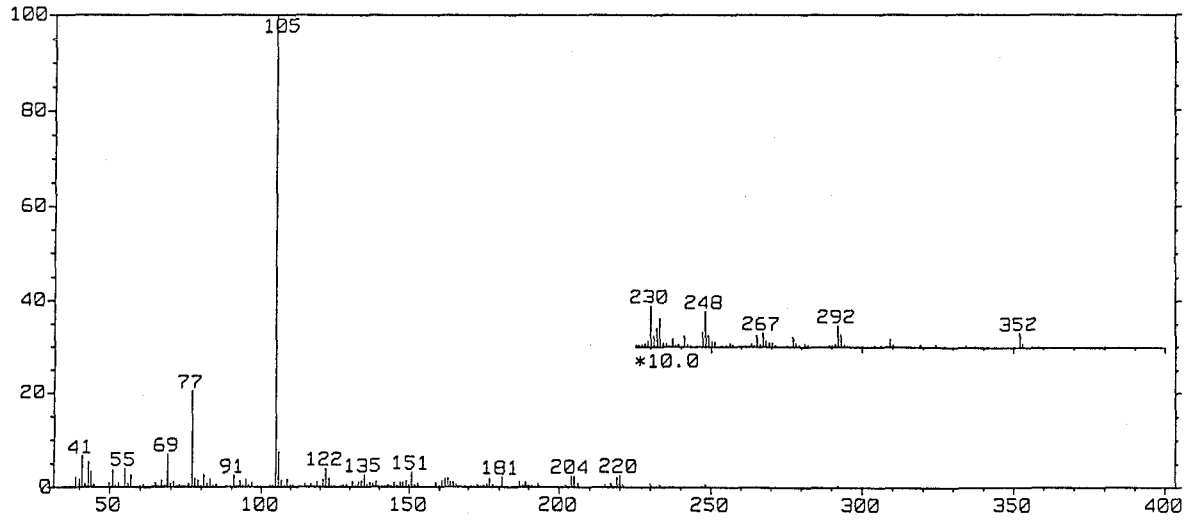

Fig. 3-91 EI-Mass Spectrum of RSA-BA

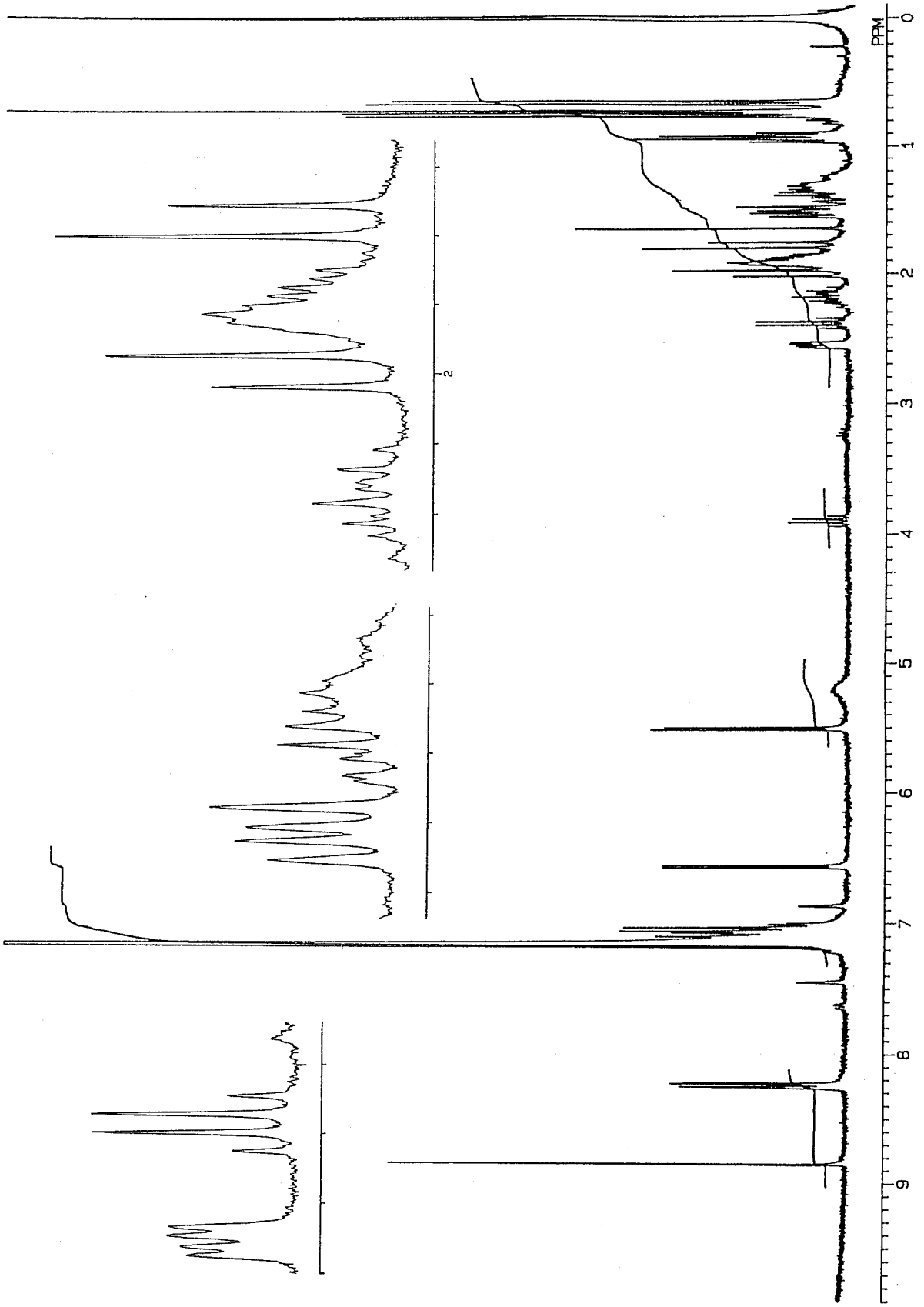

Fig. 3-92 ^{1}H-NMR Spectrum of RSA-BA (270 MHz, in C_6D_6)

Table 3-36 ^{1}*H-NMR chemical shift values for RSA-BA (11)*

(500 MHz, in C_6D_6, TMS as an int. std.)

δ_H	Coupling	Assignment
5.506	d *J*= 4.4 Hz	C-2-H
6.562	d *J*= 4.4 Hz	C-3-H
5.2 (approx.)	br. s	C-5-O<u>H</u>
1.996	d *J*= 12.5 Hz	C-6-Ha
1.778	d *J*= 12.5 Hz	C-6-Hb
1.517	br. dd *J*= 13.2 & 7.7 Hz	C-8-H_2
2.185	m	C-9-Ha
1.375	m	C-9-Hb
2.555	dd *J*= 7.7 & 3.3 Hz	C-10-H
1.882	double sept. *J*= 7.0 & 3.3 Hz	C-11-H
0.751	d *J*= 7.0 Hz	C-12-H_3
0.654	d *J*= 7.0 Hz	C-13-H_3
8.848	s	C-14-H
0.719	s	C-15-H_3
8.242	dd *J*= 8.1 & 1.5 Hz	C-2'&6'-H
7.06 (approx.)	m	C-3',4'&5'-H

Tabel 3-37 Physicochemical properties of RSA-BA (11)

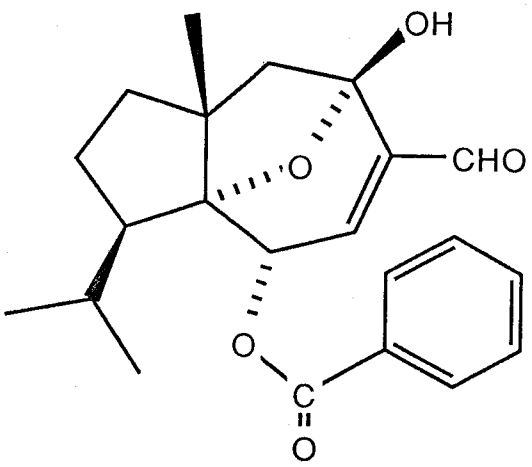

11

Colorless gum

Rf: 0.72 (C-M 50:4), 0.63 (H-EA 3:2, *cf.* 1; 0.69)

Vanillin-H_2SO_4 color: brown

N,*N*-dimethyl-*p*-phenylene diamine sulfate test: negative (yellow)

UVλ_{max}^{MeOH}: 229 nm

FD-MS *m/z* (%): 370 (M^+, 100)

EI-MS *m/z* (%): 352 (M^+-H_2O, 0.3), 292 (0.5), 267 ($M^+-C_6H_4CO$, 0.3), 248 ($M^+-C_6H_5COOH$, 0.8), 230 ($M^+-C_6H_5COOH-H_2O$, 0.9), 220 (2.7), 204 (2.6), 151 (3.3), 122 (4.1), 105 ($C_6H_5CO^+$, 100), 77 (20), 69 (7.1).

^{1}H-NMR data are shown in Table 3-36.

On the other hand, it has been found that transformation of 1 into RSA-PY (**1g**) easily occurs in a high yield (in hot pyridine at 80 °C, 65 % yield) as described above (pp. 125). If **1g** is convertible into the benzoate RSA-BA, clear evidence for the proposed structure (**11**) for RSA-BA will be absolutely confirmed. Accordingly, RSA-PY (**1g**) was directly treated with benzoic anhydride in Et_3N. Pure 2.9 mg of **1g** was dissolved in 0.5 ml of Et_3N, and then 60 mg of benzoic anhydride was added to the solution. The mixture was kept at 60 °C for 1 hr, at which point the reaction mixture was diluted with *ca* 20 ml of EtOAc and the resulting mixture was washed with 30 ml of 5 % $NaHCO_3$ solution. The organic layer was, after dried over Na_2SO_4 and concentrated, subjected to PTLC (in C-M 50:4, and successively in H-EA 3:2). A quenching product (RSA-PY-BA, *Rf* 0.72 in C-M and 0.63 in H-EA, respectively) was obtained as a colorless syrup (2.1 mg, yield 52 %, together with 1.1 mg of unchanged **1g** (38 %). The former was agreeable with **11** in TLC, EI-MS and ^{1}H-NMR spectrum (Fig. 3-93, 94 95 and Table 3-38). RSA-PY-BA derived from **1g** in a high yield was thus confirmed to be identical with RSA-BA, and the fact afforded the validity of structure **11** for RSA-BA (Scheme 3-6).

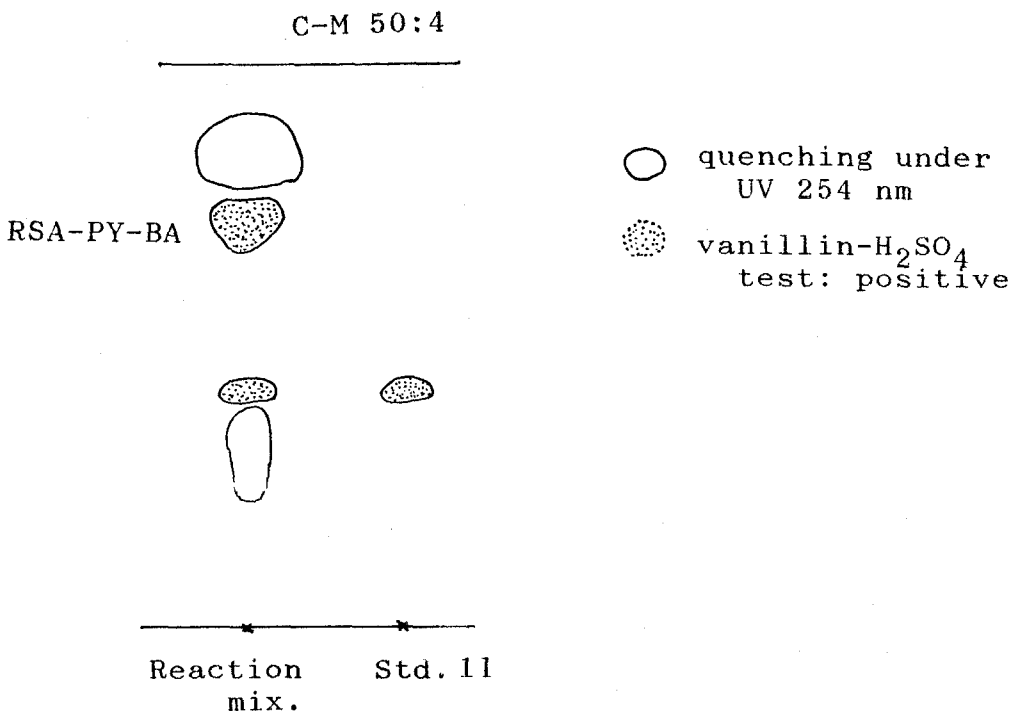

Fig. 3-93 TL Chromatograms of Reaction Product Obtained by Esterification of RSA-PY (1g) with Benzoic Anhydride

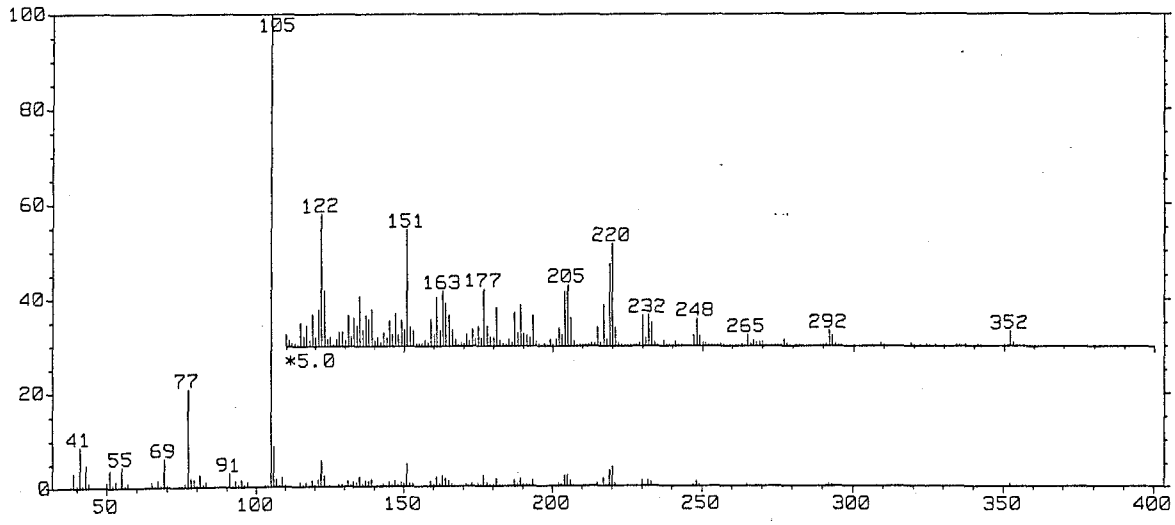

Fig. 3-94 EI-Mass Spectrum of RSA-PY-BA

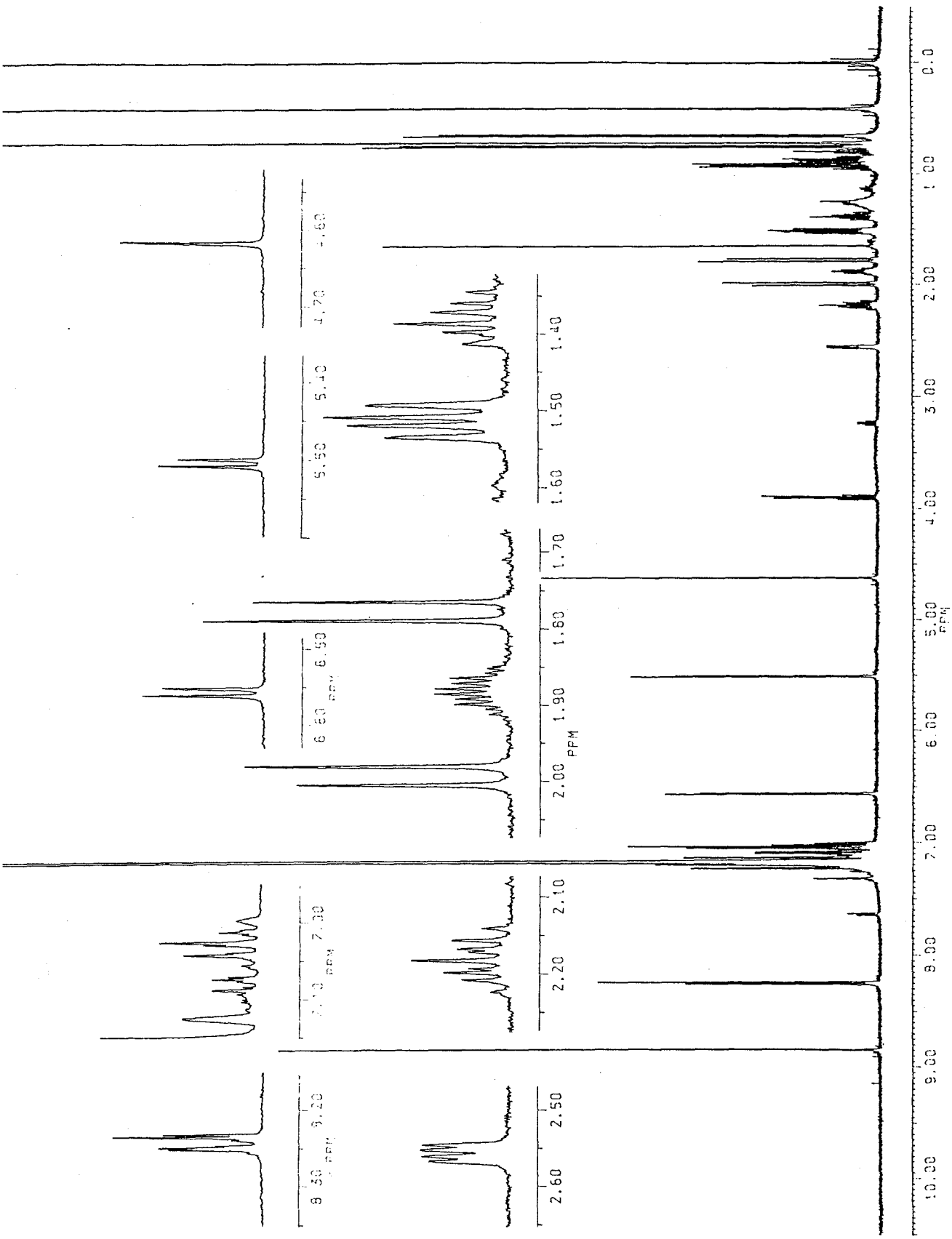

Fig. 3-95 ^{1}H-NMR Spectrum of RSA-PY-BA (500 MHz, in C_6D_6)

Table 3-38 ^{1}*H-NMR chemical shift values of RSA-PY-BA (=RSA-BA, 11)*

(500 MHz, in C_6D_6, TMS as an int. std.)

δ_H	Coupling (*J*=Hz)	Assignment	*cf.* RSA-BA
5.505	d (4.7)	C-2-H	5.506
6.557	d (4.7)	C-3-H	6.562
4.7 (approx.)		C-5-O<u>H</u>	5.2 (approx.)
1.992	d (12.2)	C-6-Ha	1.996
1.776	d (12.2)	C-6-Hb	1.778
1.512	br. dd (12.9, 7.4)	C-8-H_2	1.517
2.182	dddd (13.0, 13.0, 7.7, 7.7)	C-9-Ha	2.185
1.377	ddd (13.0, 12.9, 7.7)	C-9-Hb	1.375
2.556	dd (7.5, 3.4)	C-10-H	2.555
1.880	double sept. (6.8, 3.4)	C-11-H	1.882
0.749	d (6.8)	C-12-H_3	0.751
0.653	d (6.8)	C-13-H_3	0.654
8.838	s	C-14-H	8.848
0.716	s	C-15-H_3	0.719
8.224	dd (7.1, 1.5)	C-2'&6'-H	8.242
7.05 (approx.)	m	C-3',4'&5'-H	7.06 (approx.)

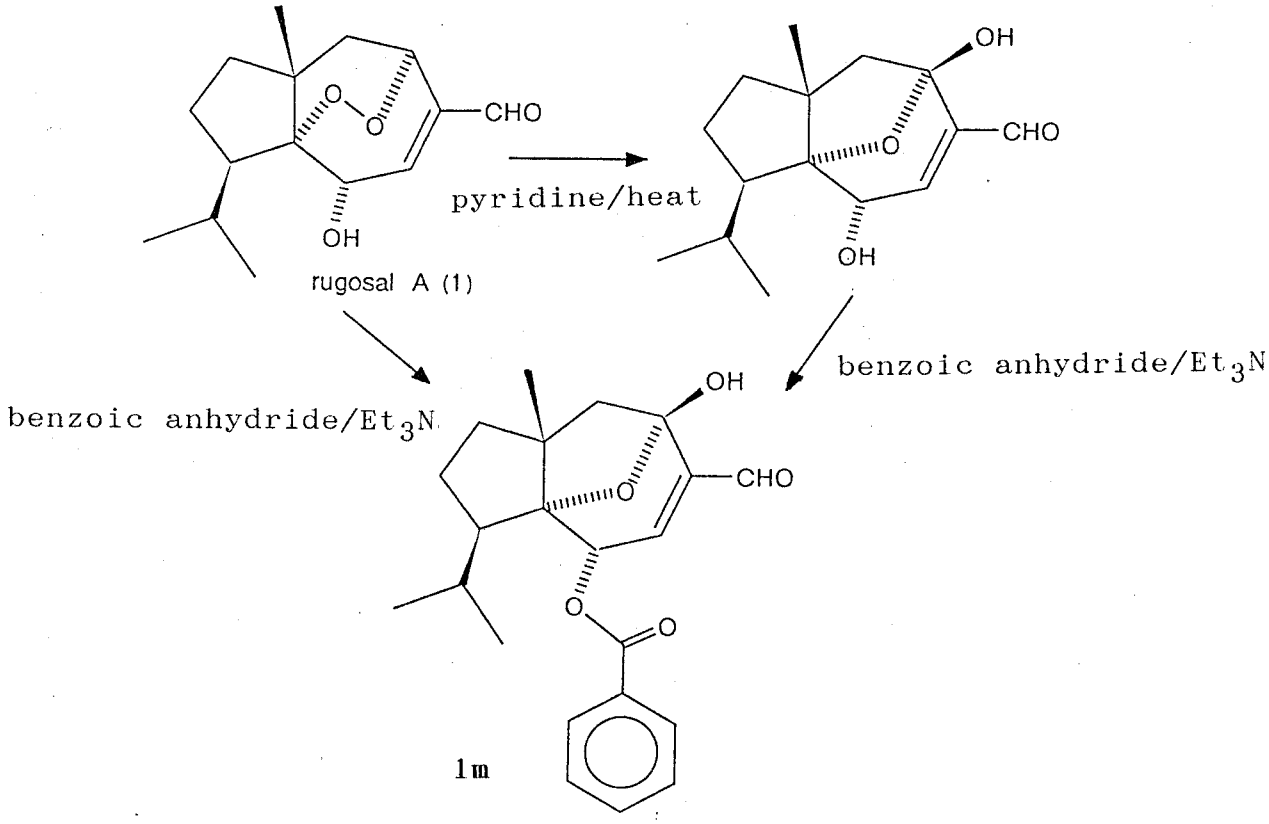

Scheme 3-6 Two Pathway for the Chemical Conversion of Rugosal A (1) into a Benzoate (11)

Tabel 3-39 Physicochemical properties of RSA-PY-BA (11)

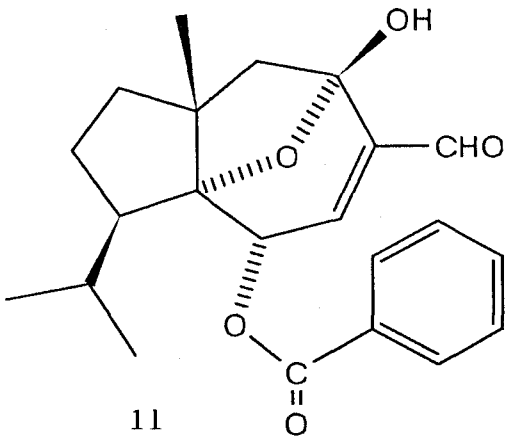

11

Colorless gum

Rf: 0.72 (C-M 50:4), 0.63 (H-EA 3:2, *cf.* 1; 0.69)

Vanillin-H_2SO_4 color: brown

N,N-dimethyl-*p*-phenylene diamine sulfate test: negative (yellow)

EI-MS *m/z* (%): 352 (M^+-H_2O, 0.6), 292 (0.7), 248 (M^+-C_6H_5COOH, 1.2), 232 (1.3), 220 (4.4), 219 (3.5), 205 (2.6), 151 (5.0), 122 (5.6), 105 ($C_6H_5CO^+$, 100), 77 (21), 69 (6.3), 41 (8.7).

^{1}H-NMR data are shown in Table 3-38.

Observation of NOE between C-2-H and C-15-H_3 in RSA-BA (11) proved that the relative configuration at C-2 was preserved during the rearrangement (Fig 3-96). Although the initially expected benzoate of 1 was unable to prepare, 11 is equivalent to the expected benzoate when the exciton chirality method is applied.

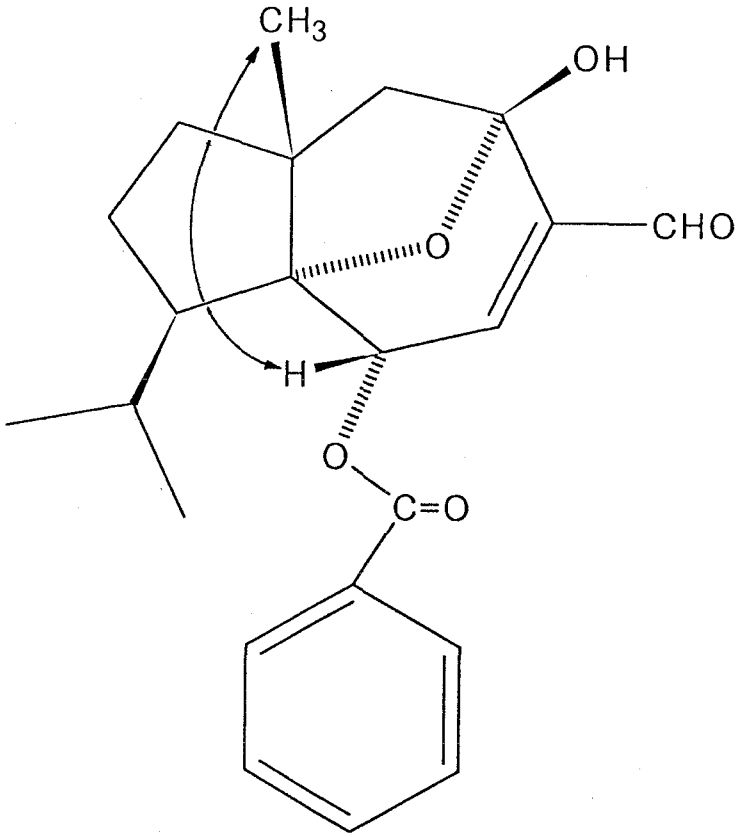

Fig. 3-96 NOE Observed by irradition at δ_H 5.506 (C-2-H) in ^1H-NMR of RSA-BA

3) Reduction of RSA-BA to the Corresponding Alcohol

To exclude a presumable effect of the aldehyde chromophore on the CD spectrum, it was requested to reduce the aldehyde group in **11** to a hydroxymethyl group. For the reaction, 1.0 mg of RSA-BA was dissolved in 1 ml of MeOH and stirred overnight with excess amount of $NaBH_4$ (1.0 mg) at room temperature. The reaction mixture was diluted with *ca* 20 ml of EtOAc and then washed with with an equal volume of a saturated NaCl solution containing 0.2 N HCl. The major product RSA-BA-RD (**1m**) in the organic layer, being dried over Na_2SO_4 and concentrated *in vacuo*, was isolated by PTLC (development x 2 in benzene-EtOAc 5:1, **1m**; *Rf* 0.18 and **11**; *Rf* 0.51) to give 0.4 mg of RSA-BA-RD (in a yield of 40 %) (Fig. 3-97). The strucute of **1m** was confirmed by FD- and EI-MS and ^1H-NMR analysis (Fig. 3-98, 99 and 100, and Table 3-40). Its molecular ion at *m/z* 372 in FD-MS and a pair of non-equevalent methylene protons at δ_H 3.939 and 3.693 (each 1H, d *J*= 13.7 Hz, 14-CH_2OH) in stead of a formyl proton were both indicative of the proposed structure **1m**.

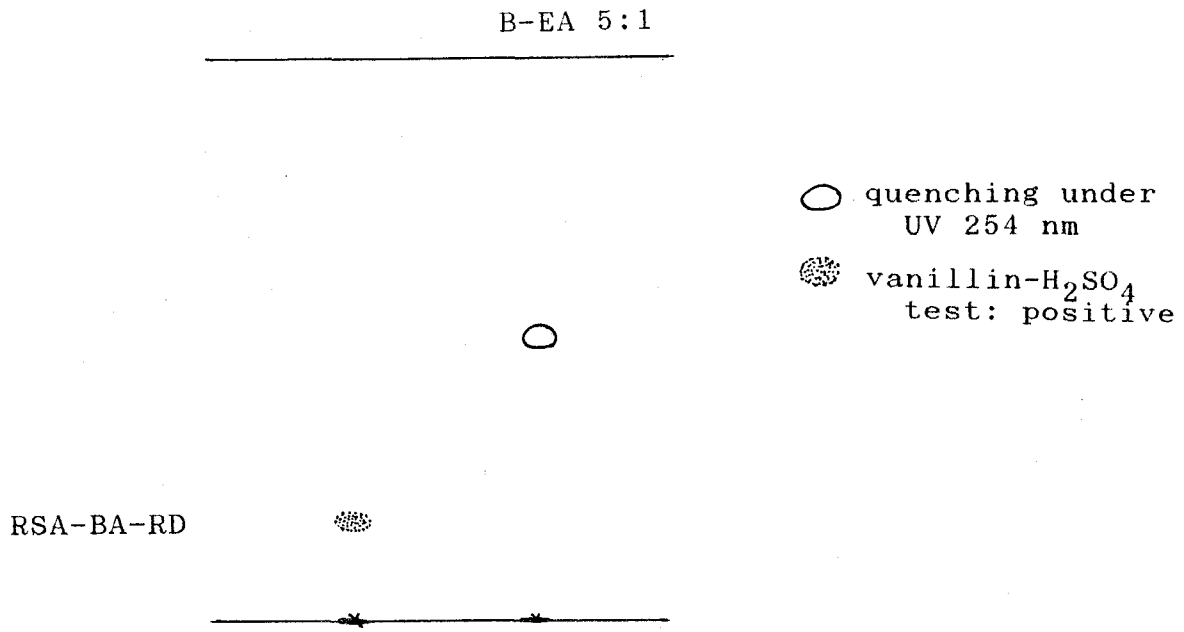

Fig. 3-97 TL Chromatogram of Reaction Product Obtained by $NaBH_4$ Reduction of Rugosal A (1)

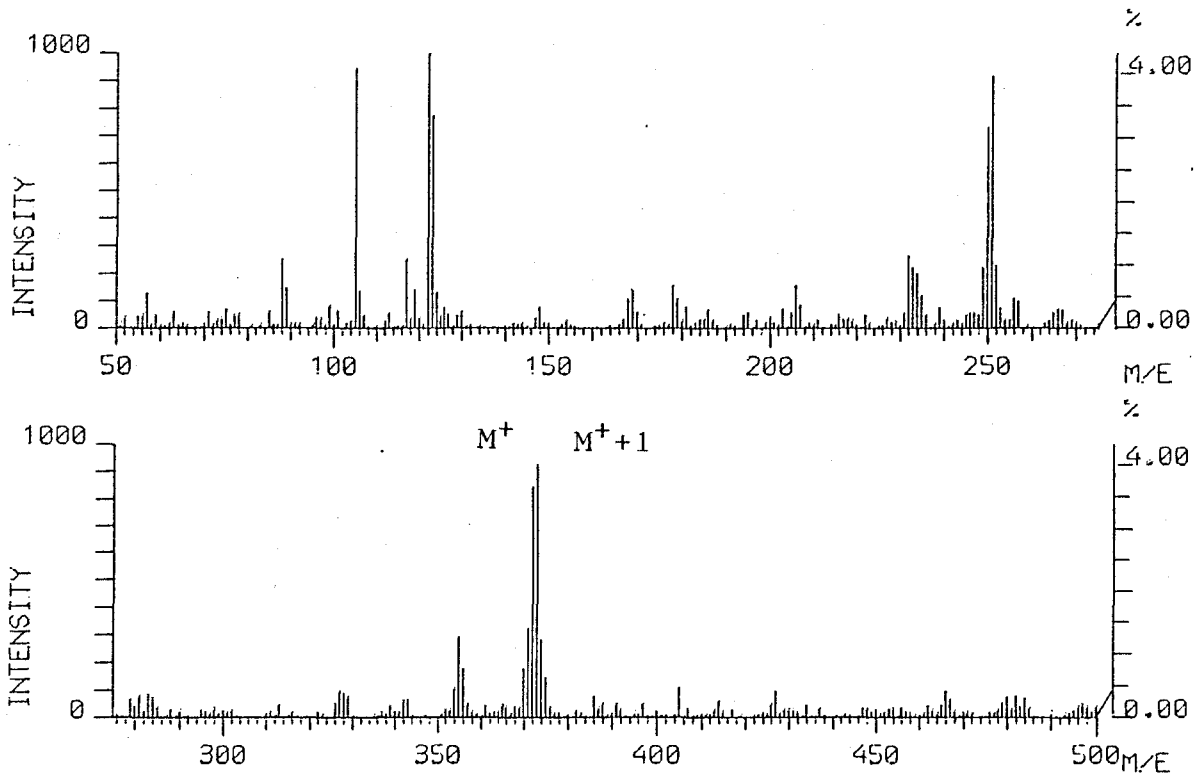

Fig. 3-98 FD-Mass Spectrum of RSA-BA-RD

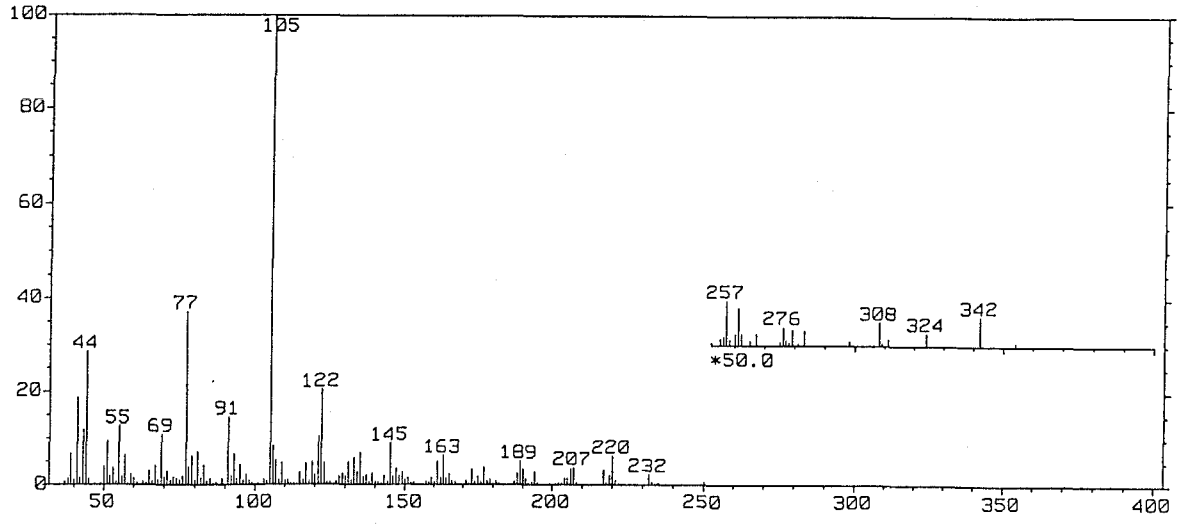

Fig. 3-99 EI-Mass Spectrum of RSA-BA-RD

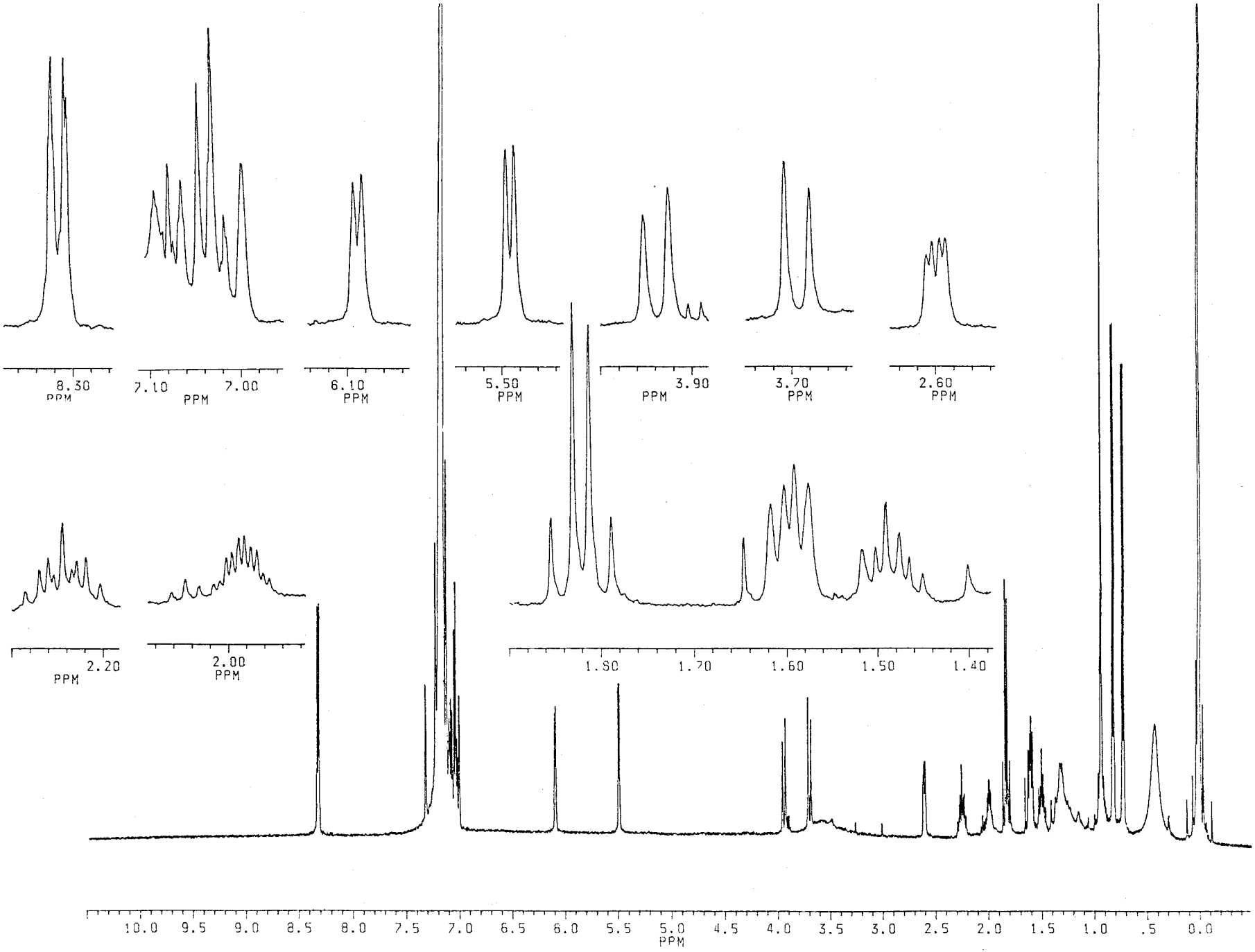

Fig. 3-100 ^{1}H-NMR Spectrum of RSA-BA-RD (500 MHz, in C_6D_6)

Table ***3-40*** *^{1}H-NMR chemical shift values of RSA-BA-RD (**1m**)*

(500 MHz, in C_6D_6, TMS as an int. std.)

δ_H	proton	coupling (*J*=Hz)	assignment
5.490	1H	d (4.5)	C-2-H
6.088	1H	d (4.5)	C-3-H
1.842	1H	d (12.0)	C-6-Ha
1.800	1H	d (12.0)	C-6-Hb
1.596	2H	br. dd (13.0, 7.6)	C-8-H_2
2.244	1H	m	C-9-Ha
1.483	1H	ddd (13.0, 12.9, 7.4)	C-9-Hb
2.599	1H	dd (7.4, 3.2)	C-10-H
1.985	1H	double sept (6.9, 3.2)	C-11-H
0.814	3H	d (6.9)	C-12-H_3
0.720	3H	d (6.9)	C-13-H_3
3.939	1H	d (13.7)	C-14-Ha
3.693	1H	d (13.7)	C-14-Hb
0.928	3H	s	C-15-H_3
8.316	2H	br. d (7.0)	C-2'& 6'-H
7.04 (approx.)	3H	m	C-3', 4' & 5'-H

Table 3-41 Physicochemical properties of RSA-BZ-RD (1m)

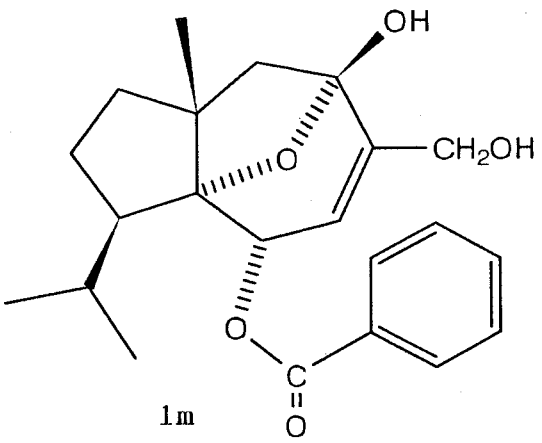

1m

Colorless syrup

Rf: 0.18 (B-EA 5:1)

Vanillin-H_2SO_4 color: orange

FD-MS *m/z* (%): 373 (M^++1, 93), 372 (M^+, 85), 122 (100)

EI-MS *m/z* (%): 354 (M^+-H_2O, trace), 342 (M^+-CH_2O, 0.1), 308 (0.1), 261 (0.2), 257 (0.2), 232 (2.8), 220 (6.3), 145 (9.1), 122 (20), 105 (100), 91 (15), 77 (37), 69 (11).

^{1}H-NMR data are shown in Table 3-40.

4) CD Determination and the Absolute Configuration of Rugosal A

The CD spectrum of **1m** in MeOH showed an apparent positive Cotton effect at 229 nm (Fig. 3-101). The positive Cotton effect, in the light of the exciton chirality method, indicated a positive chirality between the two axes of electric transition moments. The absolute configuration at C-2 is hence represented by **1m** in Table 3-38 (*S* at C-2). Accordingly, the absolute configuration of **1** was established to be C-1 *R*, C-2 *S*, C-5 *S*, C-7 *R* and C-10 *R* as shown in Fig. 3-102.

The elucidated stereochemistry of rugosal A (**1**) was agreed with other naturally occurring carotanoids defined its absolute configuration at C-7 and C-10, except a hydroxylated chiral center at C-10. This fact gave a hypothesis that carotanoid skeleton of *Rosa rugosa* is biochemically synthesized in the same stereo-selective process as other carotanoids originated in Umbelliferae and Compositae plants, as well as that of a fungus. Here, are listed some typical carotanoids defined each absolute configuration through X-ray crystaogeography or total synthesis (Fig. 3-103) [33,42,52,109,110].

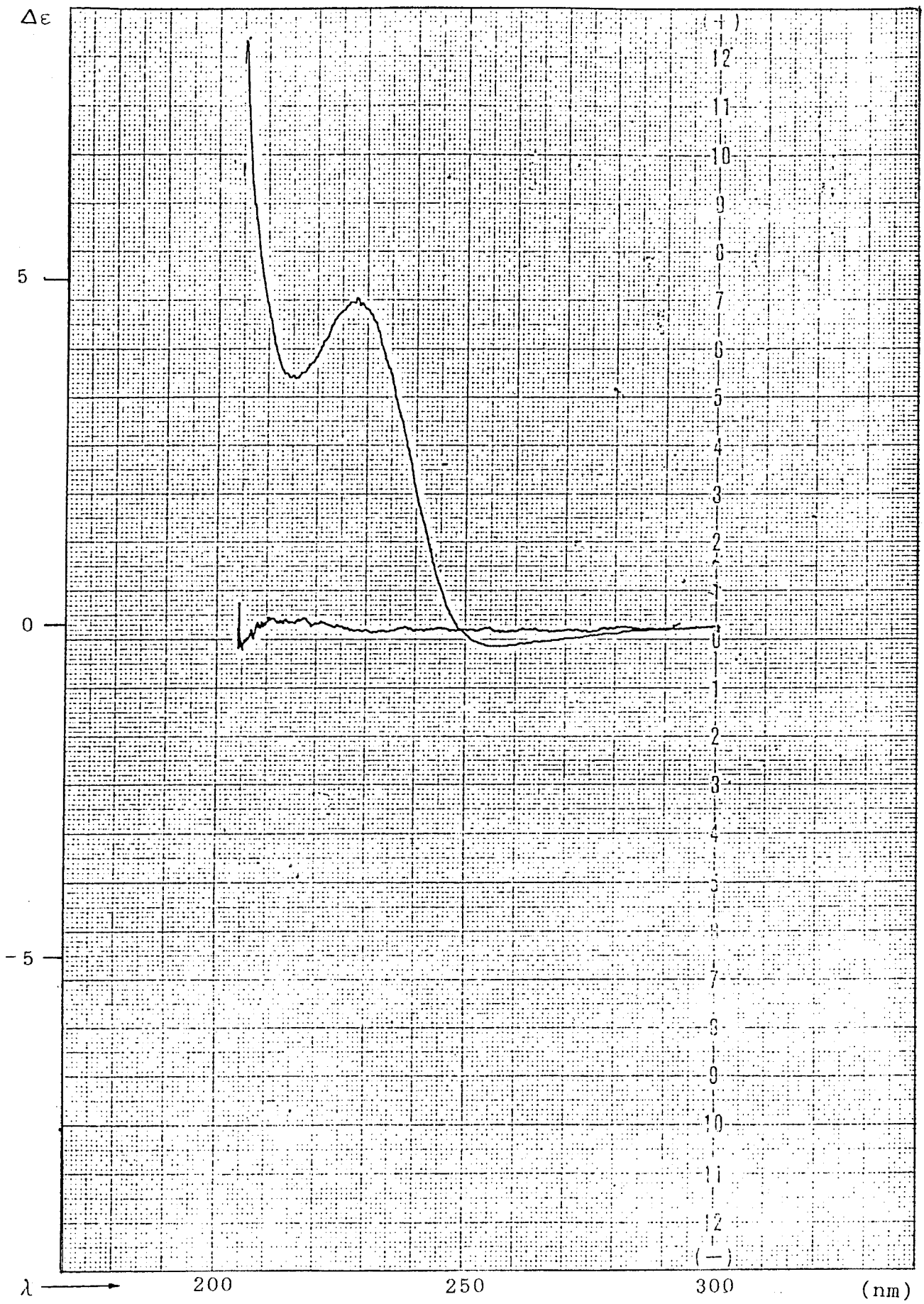

Fig. 3-101 Positive Cotton Effect of RSA-BA-RD: At 230 nm the first Cotton effct originated in $\pi \longrightarrow \pi^*$intramolecular charge transfer band benzoate chromophore are observed.

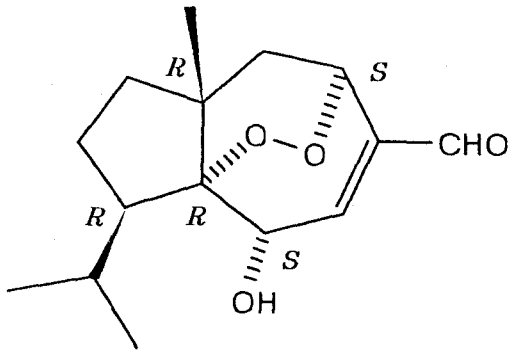

Fig. 3-102 Absolute Configuration of Rugosal A Elucidated by the Benzoate Exciton Chirality Method

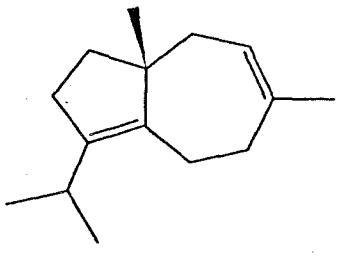

daucene (27) [111]

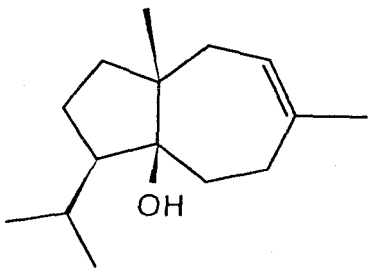

carotol (28) [112]

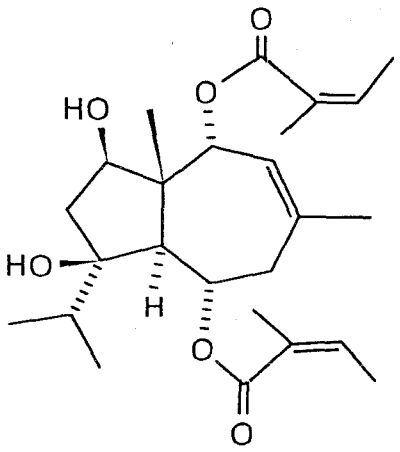

tingitanol (44) [45]

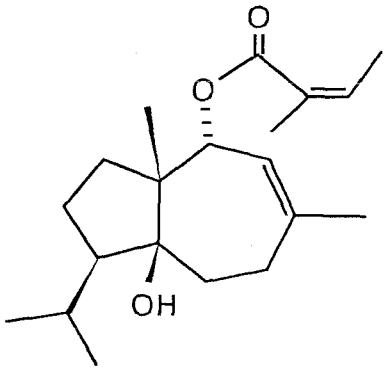

rasidiol angelate (55) [57]

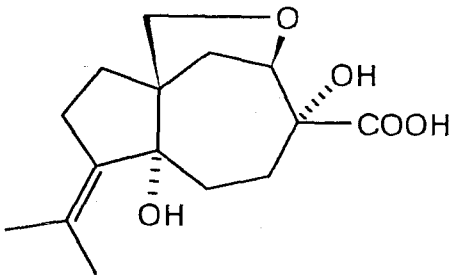

aspeterric acid (57) [60]

Fig. 3-103 Some Naturally Occurring Carotanoids Whose Absolute Configulations Were Determined by X-ray Crystaogeograpy or Total Synthesis

3-3 Related Compound Rugosic Acid A

3-3-1 Isolation of Rugosic Acid A

The diffusates from injured leaves of *Rosa rugosa* contained notable amounts of acidic substances. Indeed, 2.2 g of acidic substance was obtained from 3 g of CR fraction (See Section 3-1, pp. 48), as the result of partition between EtOAc and 5 % $NaHCO_3$ solution and followed by re-extraction of the acidified aqueous layer with EtOAc. As the acidic constituents indicated a similar pattern on TLC to another acidic extractives (*ca* 8 g) obtained from 4.5 kg of matured and injured leaves (Sample III), those acidic constituents were combined to chromatograph on silica gel column (gel volume, 800 ml). Elution with solvents shown in Table 3-42 resulted in 12 fractions (Fr-A-1~12). From Fr-A-3, remarkable amounts of colorless crystallines were precipitated during concentration. The collected colorless needles were washed with *n*-hexane containing 20 % of EtOAc under a chilled condition to affoed *ca* 650 mg of crude crystallines. Successively, the acidic compounds were recrystallized from $CHCl_3$ containing *n*-hexane to give 350 mg of fine needles. The crystallized compound soluble to MeOH and partly to $CHCl_3$ was detected on TLC as a quenching spot with a severe tailing (H-EA 2:1, *Rf* 0.28-0.05). However, the compound was detected as a circular spot when developed in *n*-hexane-EtOAc containing small amounts of formic acid (*Rf* 0.29 in H-EA-F 50:50:0.25). The isolate later named rugosic acid A was, as shown in Fig. 3-104, mainly contained in the fractions Fr-A-3 and 4.

This acidic constituent was involved in a MeOH extract of uninjured leaves (>100 mg/kg in Sample IV). The fact provides a proof that rugosic acid A is an inherent acid of *Rosa rugosa* leaves.

Table 3-42 Eluates from silica gel column charged with acidic constituents

Fraction	Solvent	Volume
Fr-I/II-A-1	40 % EtOAc/*n*-hexane	250 ml
Fr-I/II-A-2	40 % EtOAc/*n*-hexan	250 ml
Fr-I/II-A-3	40 % EtOAc/*n*-hexane	250 ml
Fr-I/II-A-4	40 % EtOAc/*n*-hexane	250 ml
Fr-I/II-A-5	60 % EtOAc/*n*-hexane	250 ml
Fr-I/II-A-6	60 % EtOAc/*n*-hexane	250 ml

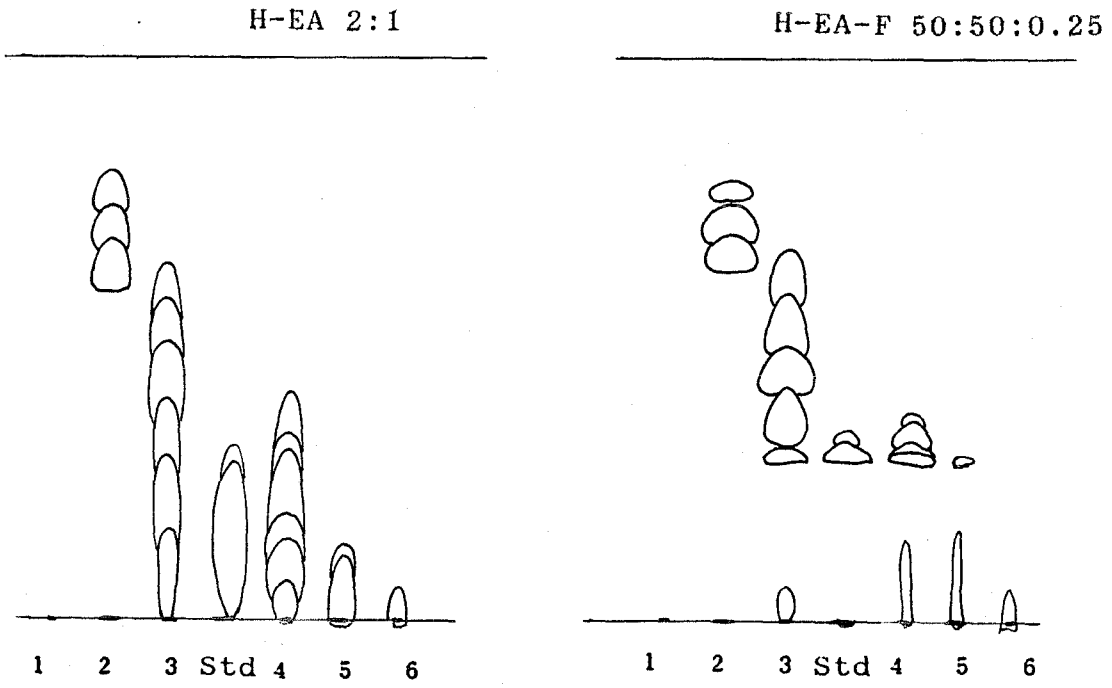

Fig. 3-104 TL Chromatograms of Column Fractions of Acidic Constituents (Std = crystallins)

3-3-2 Structure Elucidation of Rugosic Acid A

1) Spectroscopic Analyses

Rugosic acid A clearly showed a positive response to *N,N*-dimethyl-*p*-phenylenediamine sulfate reagent on TLC, revealing the presence of a peroxy group in the molecule. The FD-MS showed its molecular ion at *m/z* 282 (282.146 in EI-HR-MS; $C_{15}H_{22}O_5$, requires 282.147) (Fig. 3-105). IR spectrum showed the presence of a -COOH (3260 cm^{-1}, broad), an -OH (3560 cm^{-1}, hydrogen-bonding) and an α,β-unsaturated carboxyl (1710 cm^{-1}) groups (Fig. 3-106). Furthermore, the methanolic UV spectrum showed a simple absorption maximum at 218 nm, suggesting the presence of an α,β-unsaturated carboxyl group as a sole conjugation system in the molecule. EI-MS of rugosic acid A certainly indicated a dehydration fragment at *m/z* 264 (4.8 %) and a fragment at *m/z* 220 (12 %) originating in a successive loss of carboxyl group (- CO_2), and the fragmentation pattern was indicative of a sesquiterpene carboxylic acid property for rugosic acid A (Fig. 3-107).

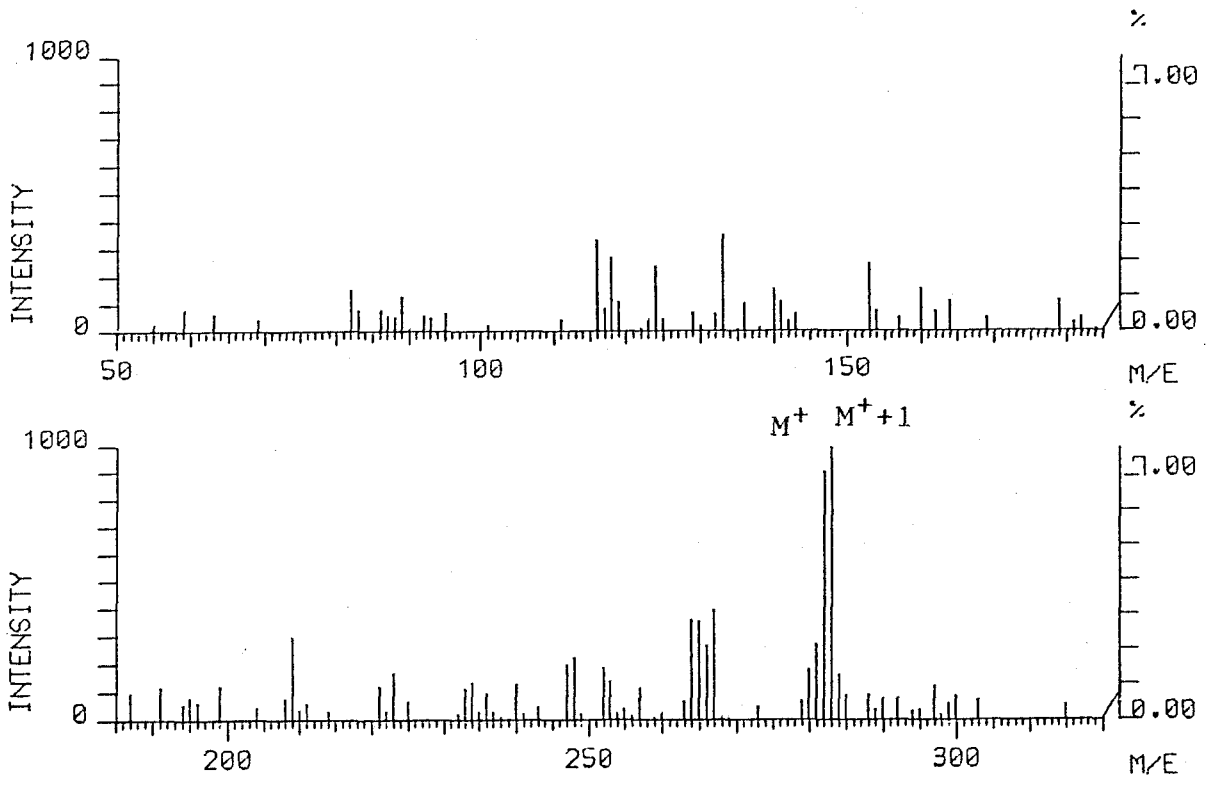

Fig. 3-105 FD-Mass Spectrum of Rugosic Acid A

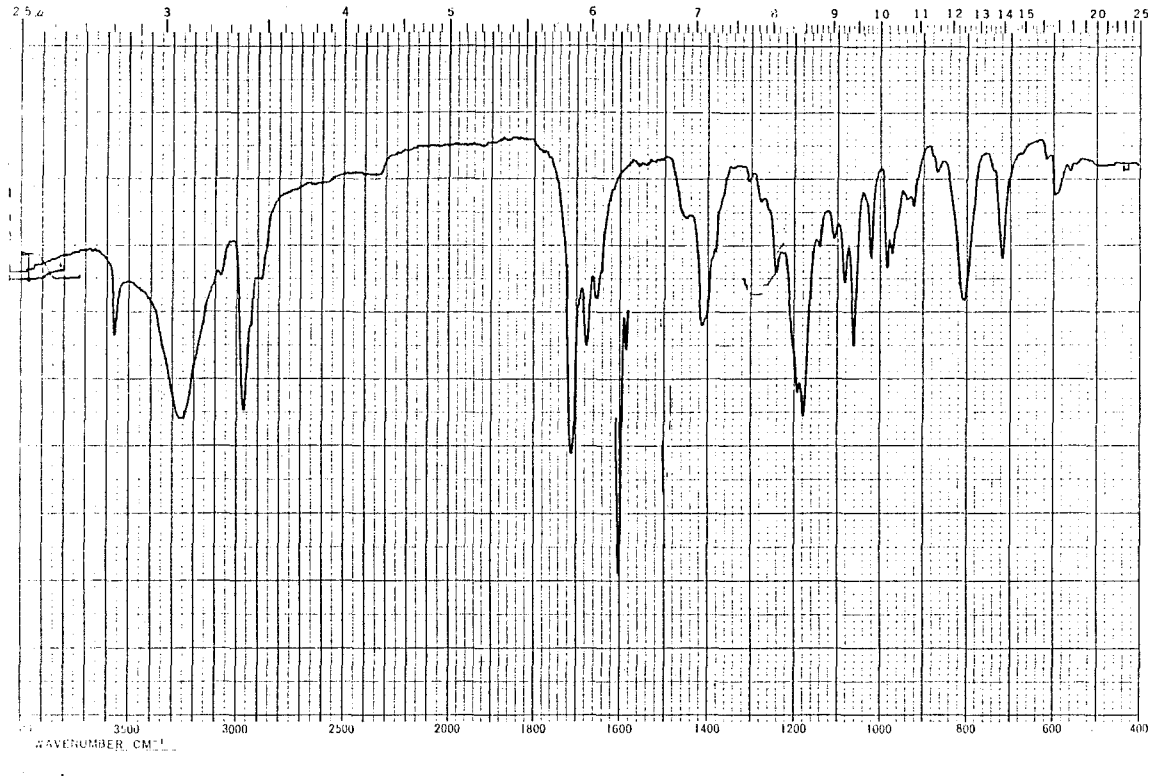

Fig. 3-106 IR Spectrum of Rugosic Acid A

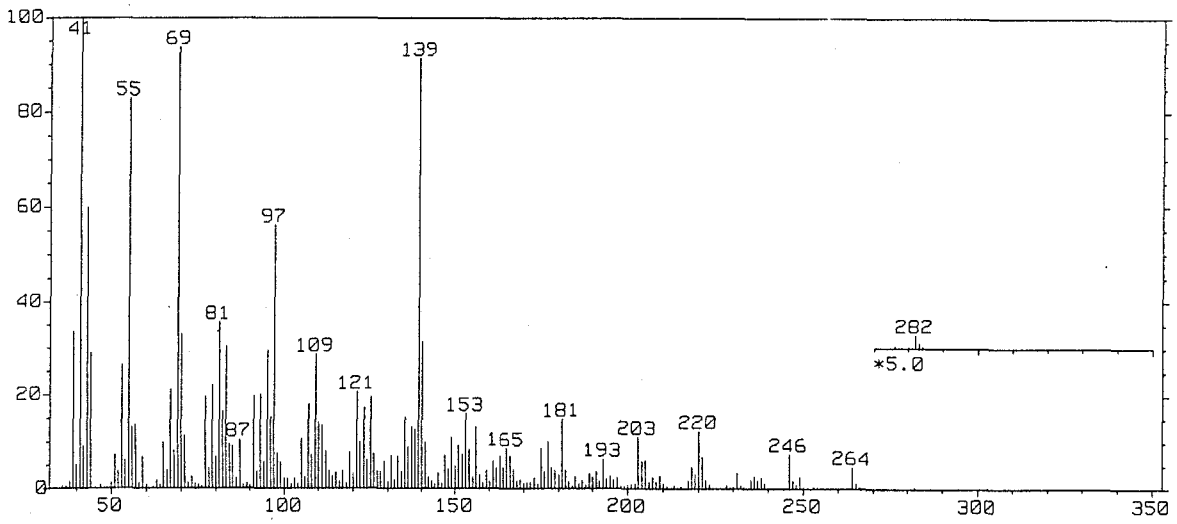

Fig. 3-107 EI-Mass Spectrum of Rugosic Acid A

^{1}H-NMR spectrum of rugosic acid A in $CDCl_3$ showed a clear correspondence with that of rugosal A (1), except the fromyl and OH protons of 1 (Fig. 3-108 and Table 3-43). This similarity in ^{1}H-NMR spectrum suggested that rugosic acid A has a sesquiterpene structure possessing an endoperoxy system like 1. Thus, structure 2 in which the C-14 α,β-unsaturated aldehyde group of 1 was further oxidized to a carboxyl group was proposed for rugosic acid A. Although not only the carboxyl proton but also the hydroxyl proton of C-2-OH was undetectable in the ^{1}H-NMR spectrum taken in $CDCl_3$, hydroxylation at C-2 was obvious because the C-2 methine proton was detected at such a lower field (δ_H 4.429).

^{13}C-NMR data for rugosic acid A was also supported well compatible with the proposed structure (Fig. 3-109 and Table 3-44). Except the carboxyl carbon (δ_C 169.7), all carbons showed a good correspondence with those of 1. Thus, structure of rugosic acid A was elucidated as 2.

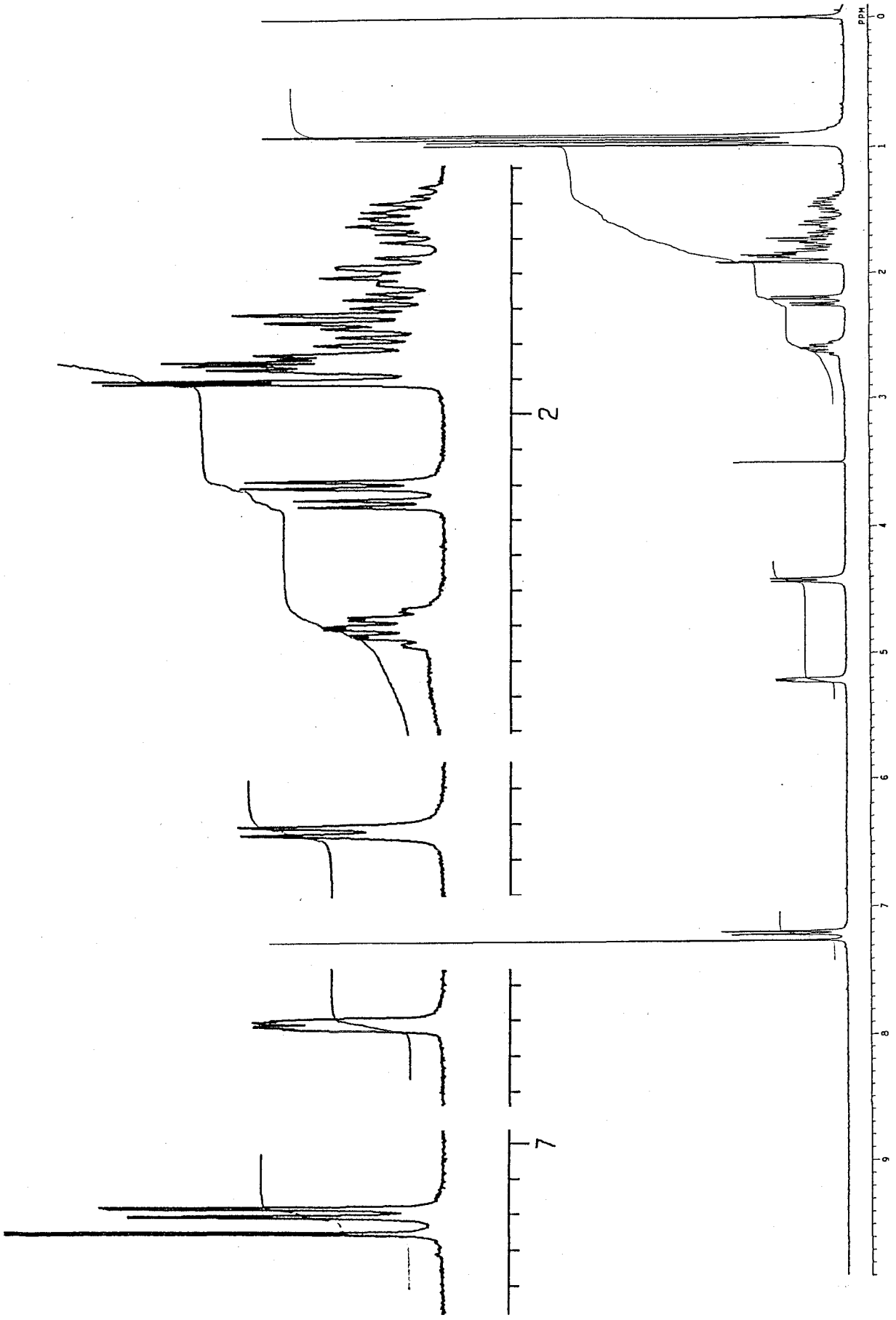

Fig. 3-108 ^{1}H-NMR Spectrum of Rugosic Acid A (270 MHz, in $CDCl_3$)

Table 3-43 ^{1}*H-NMR chemical shift values of rugosic acid A*

(270 MHz, in $CDCl_3$*, TMS as an int. std.)

δ_H		*J*(Hz)	Assignment	*cf.* rugosal A (1)
4.429	d	(6.6)	C-2-H	4.532
7.204	dd	(6.6, 0.9)	C-3-H	6.850
5.219	ddd	(5.1, 2.6, 0.9)	C-5-H	5.200
2.234	dd	(14.3, 5.1)	C-6-Ha	2.246
1.892	dd	(14.3, 2.6)	C-6-Hb	1.785
1.602	m		C-8-Ha	1.841
1.75 (approx.)	m		C-8-Hb	1.720
1.450	m		C-9-Ha	1.631
1.73 (approx.)	m		C-9-Hb	1.450
1.862	m		C-10-H	1.907
2.613	double sept	(6.8, 2.2)	C-11-H	2.630
0.972	d	(6.8)	C-12-H_3	0.980
0.928	d	(6.8)	C-13-H_3	0.946
0.909	s		C-15-H_3	0.883

* C-2-O<u>H</u> and C-14-COO<u>H</u> were undetectable.

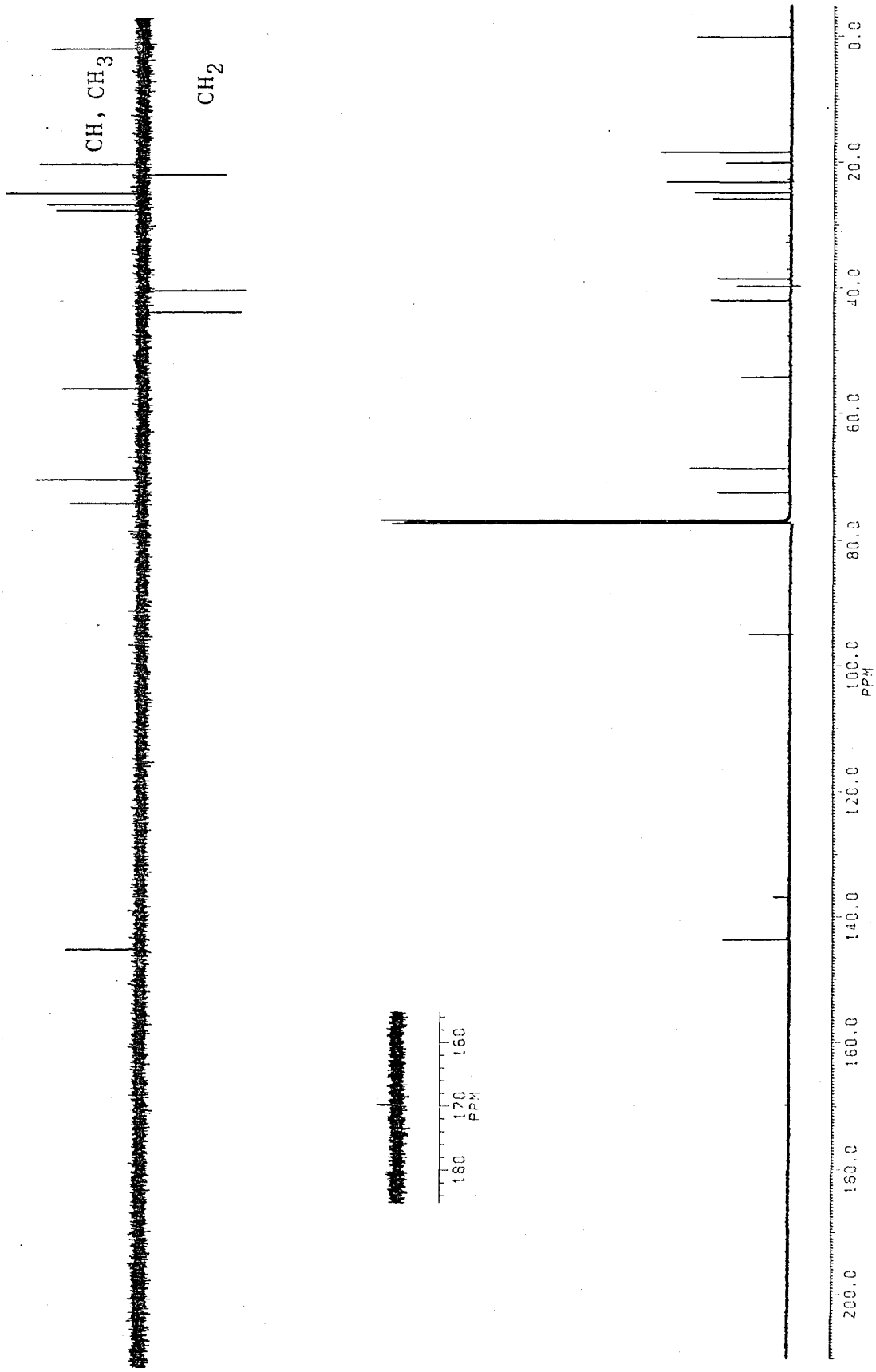

Fig. 3-109 ^{13}C-NMR Spectrum of Rugosic Acid A (125 MHz, in $CDCl_3$)

Table 3-44 Carbon chemical shift values for rugosic acid A with those of rugosal A (1) for the purpose of comparison

rugosic acid A (125 MHz, $CDCl_3$)		*cf.* rugosal A (1)*	
δ_C	Property	δ_C	Number
169.7	-COOH	190.7	14
143.5	=CH	149.4	3
136.8	=C	146.5	4
94.9	-CO*x*	94.8	1
72.4	-CH-O	70.1	5
68.6	-CH-O	69.1	2
54.1	CH	54.6	10
41.9	CH_2	42.0	6
39.6	C	39.6	7
38.4	CH_2	38.5	8
25.7	CH_3	25.9	15
24.7	CH	24.8	11
23.0	CH_3	22.8	12
20.0	CH_2	20.2	9
18.3	CH_3	18.4	13

* 68 MHz, in C_6D_6

Table 3-45 Physicochemical properties of rugosic acid A (2)

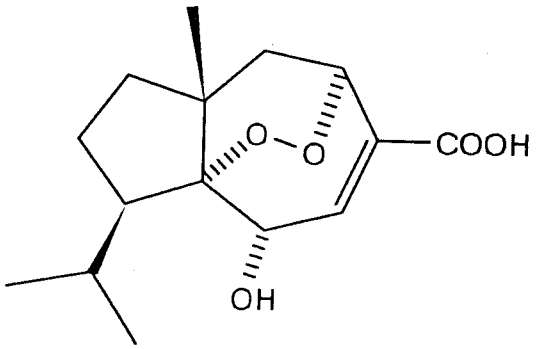

2

Colorless needles, mp 142-144 °C

Rf: 0.29 (H-EA-F 50:50:0.25), 0.58 (C-M-F 50:2:1)

Vanillin-H_2SO_4 color: grayish blue

N,*N*-dimethyl-*p*-phenylenediamine sulfate test: positive (clear red)

$[\alpha]_D$: + 159 ° (*c* 0.08 in MeOH)

UV λ_{max}^{MeOH}: 216 nm

IR ν_{max} : 3360 (OH), 3400-3100 (COOH), 2960, 1710 (C=O), 1675, 1410, 1180, 1060, 810, 720.

FD-MS *m/z* (%): 283 (M^++1, 100), 282 (M^+, 91)

EI-HR-MS: 282.146, $C_{15}H_{22}O_5$ (calucd. 282.147)

EI-MS *m/z* (%): 282 (M^+, 0.6), 264 (M^+-H_2O, 4.8), 246 (7.6), 220 (12), 203 (11), 181 (15), 152 (16), 140 (32), 139 (92), 125 (20), 121 (21), 109 (29), 97 (56), 83 (31), 81 (36), 70 (33), 69 (94), 55 (83), 43 (60), 41 (100).

^1H- and ^{13}C-NMR data are shown in Tables 3-43 and 3-44, respectively.

2) Methylation Product of Rugosic Acid A

To obtain further evidence for the proposed structure, rugosic acid A (**2**) was methylated by diazomethane (CH_2N_2), since the expected product (**2a**) can be directly compared with the methoxycarbonyl derivative (RSA-CN, **1k**) previously obtained by chemical conversion of rugosal A (**1**). To rugosic acid A (26.2 mg) dissolved in a small amount of EtOAc was added a large excess of CH_2N_2 in CH_2Cl_2. This mixture was left overnight at *room* temperature, and then the solvent was removed *in vacuo*. As the reaction mixture showed nearly a single spot on TLC (H-EA 3:1, *Rf* 0.66), the main product was easily isolated by PTLC developed in the former solvent to give colorless needles (RDA-ME, 19.9 mg, yield 72 %) (Fig. 3-109). On TLC, this derivative was agreeable with RSA-CN (**1k**) in *Rf* value and response to vanillin-H_2SO_4 reagent.

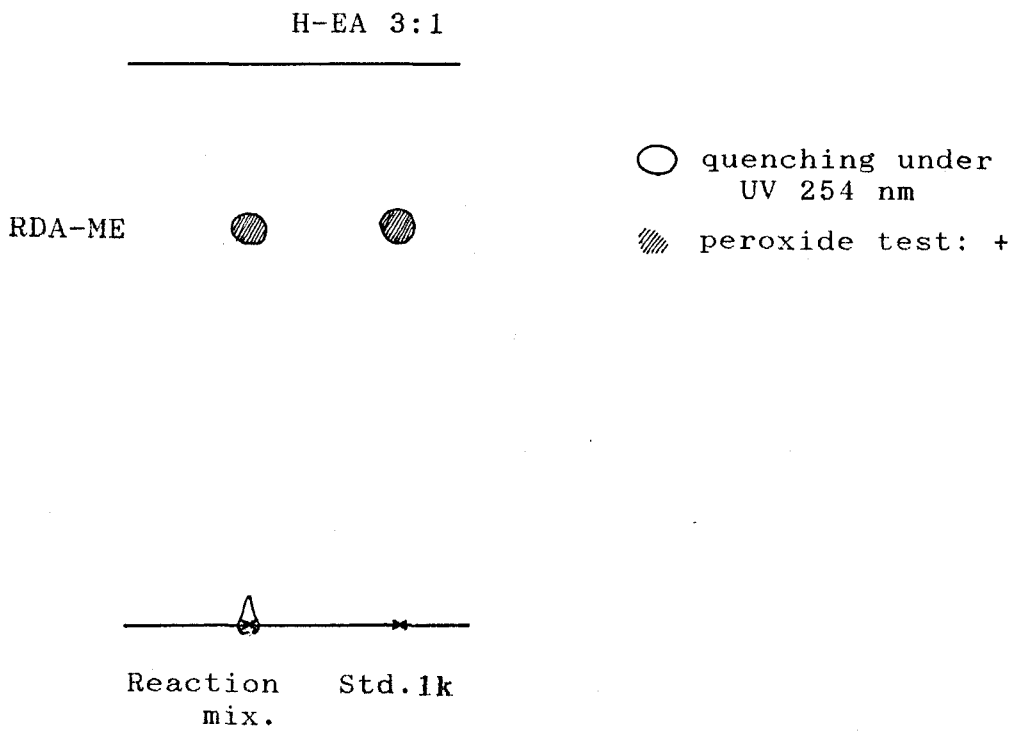

Fig. 3-110 TL Chromatogram of Methyl Ester of Rugosic Acid A

RDA-ME showed in EI-MS a dehydration fragment at *m/z* 278 (2.3 %), and a fragment of further methoxy fission at *m/z* 246 ($M^+-H_2O-OCH_3$, 3.1 %), together with the weak molecular ion (*m/z* 296, 0.8 %) (Fig. 3-111). Those fragments were also observed in EI-MS of **1k**. Futhermore, IR spectrum of RDA-ME showed a good correspondence with that of **1k** (Fig. 3-112). In the ^{1}H-NMR spectrum of RDA-ME (in $CDCl_3$, Fig. 3-113), methoxy proton signal was detected at δ_H 3.732 (3H, s). Furthermore, C-2-OH hydroxyl proton undetectable in the ^{1}H-NMR of **2** became feasible at δ_H 2.698 as a doublet signal (*J*= 9.5 Hz). The C-2 methine proton was reasonably observed as a double-doublet signal at δ_H 4.449 (*J*= 9.5, and 6.9 Hz) vicinally coupled with the C-2-OH and C-3 olefinic protons. All the proton signals were completely indistinguishable from **1k** (Table 3-45). The ^{13}C-NMR spectrum of the product was further agreeable with that of **1k**. In addition, optical rotaion of RDA-ME was approximately the same as that of **1k** (+ 154 ° in acetone, *c* 0.02, *cf.* **1k** + 128 °). Consequently, the chemical correlation between rugosic acid A (**2**) and rugosal A (**1**) was established, and the proposed structure **2** for rugosic acid A was thus established.

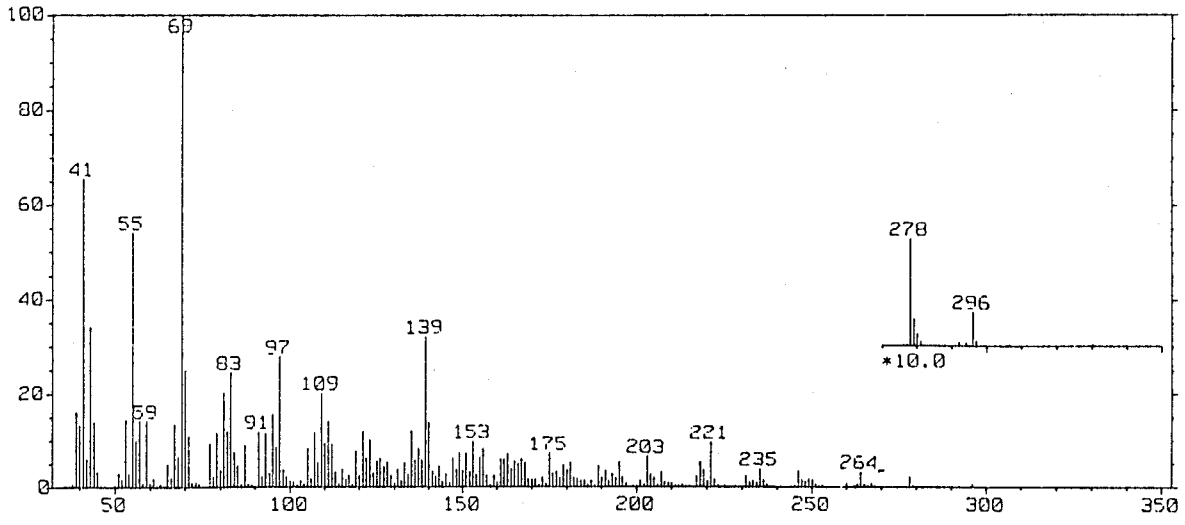

Fig. 3-111 EI-Mass Spectrum of RDA-ME

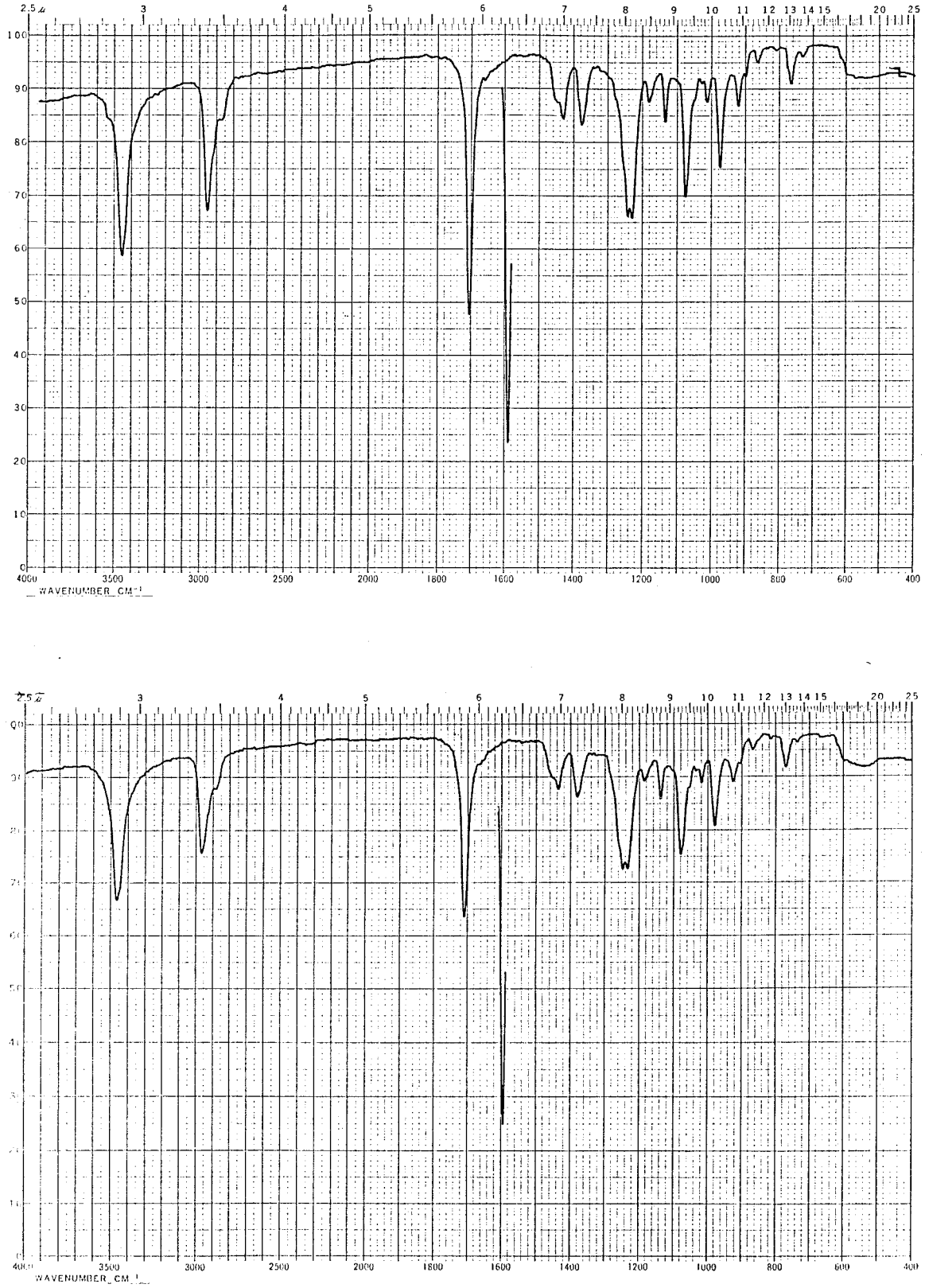

Fig. 3-112 IR Spectra of RSA-CN (top) and RDA-ME (bottom)
These spectra were completely superimposable.

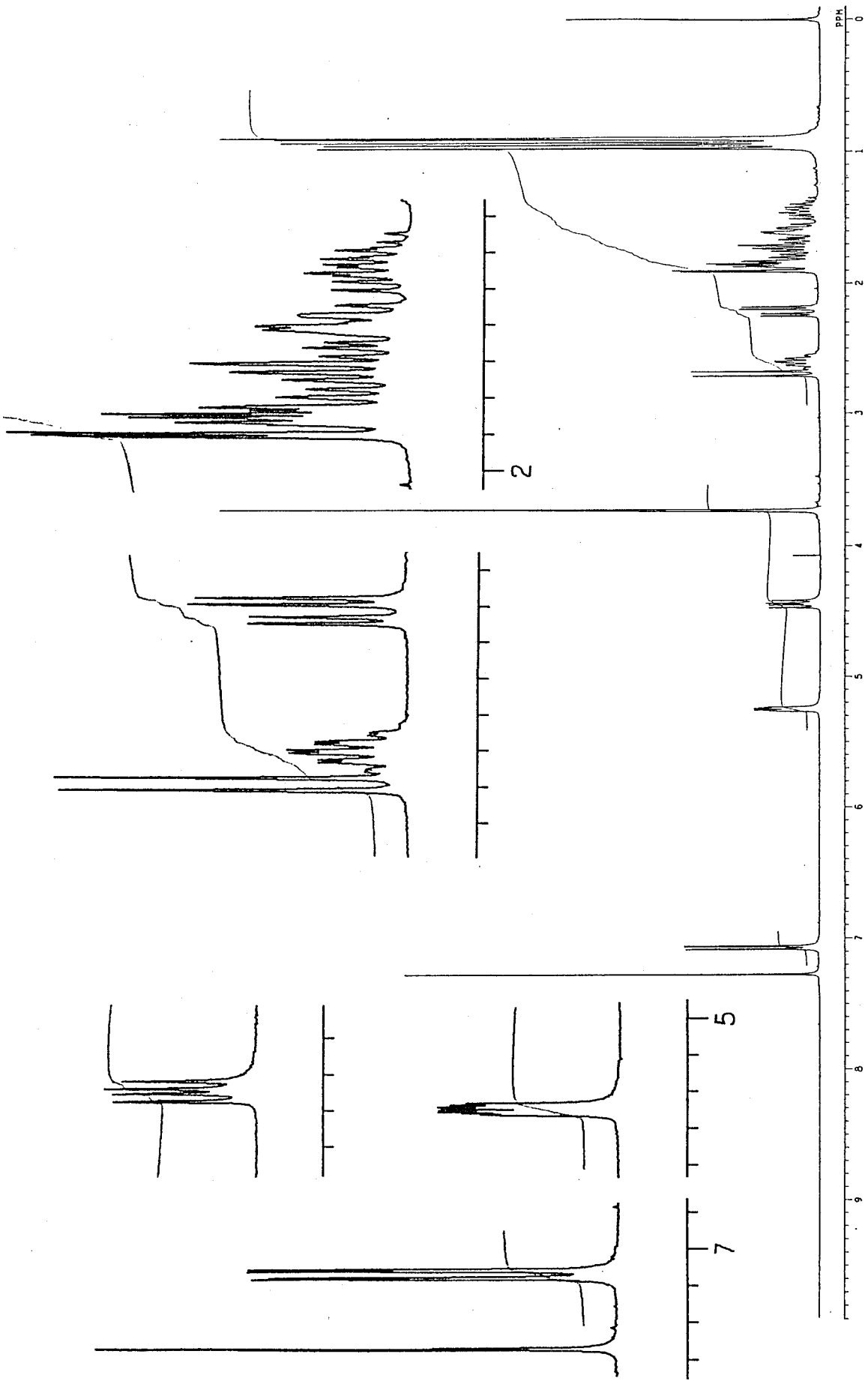

Fig. 3-113 ^{1}H-NMR Spectrum of RDA-ME (270 MHz, in $CDCl_3$)

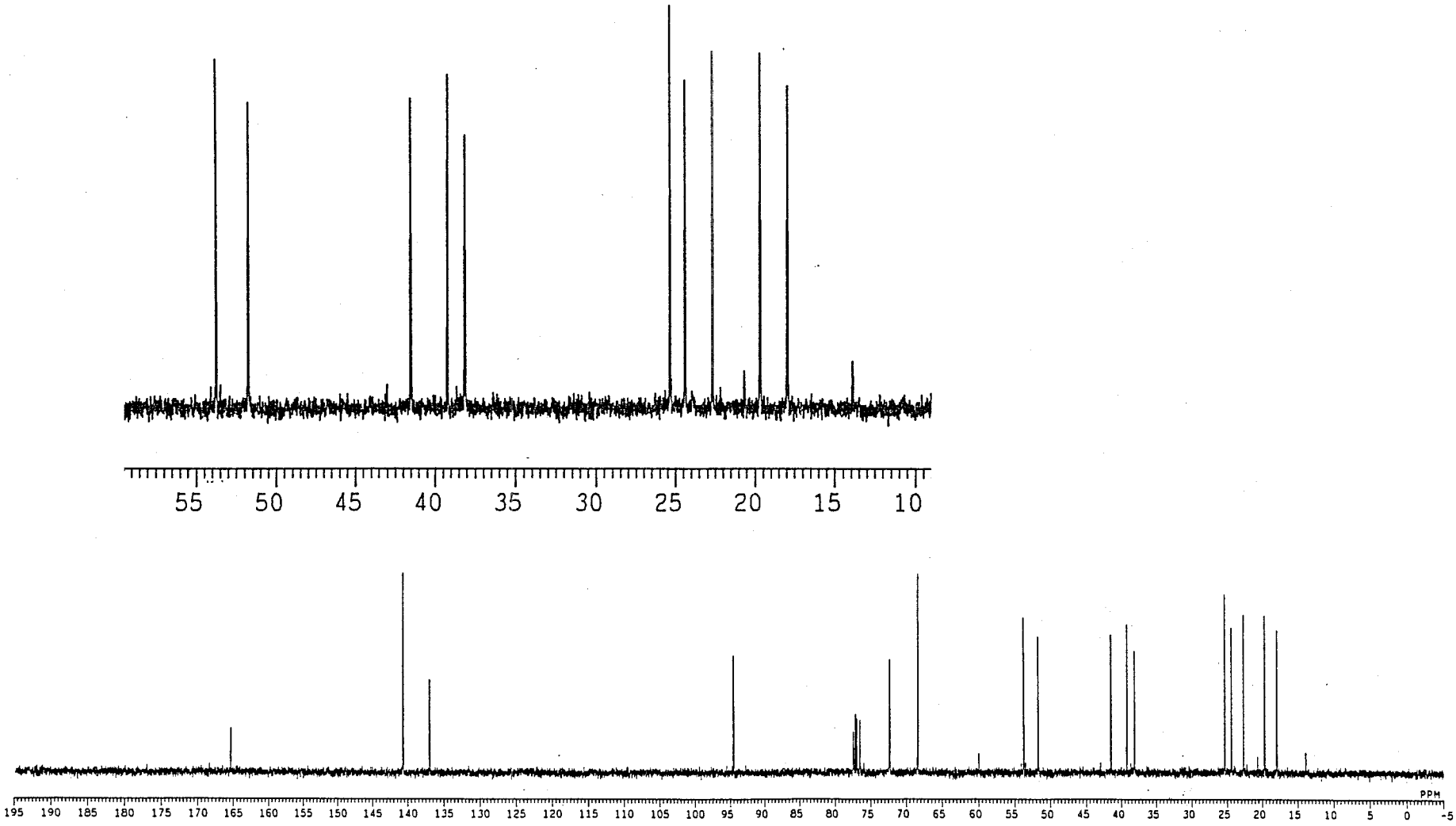

Fig. 3-114 ^{13}C-NMR Spectrum of RDA-ME (68 MHz, in $CDCl_3$): All the signals were completely agreeable with those of RSA-CN (1k) as shown in Table 3-47.

Table 3-45 Proton and carbon chemical shift values for RDA-ME and RSA-CN (1k)

(in $CDCl_3$, TMS as an int. std.)

RDA-ME (**2a**)*			RSA-CN (**1k**)**	
Proton	Carbon	Assignment	Proton	Carbon
-	94.8	1-C	-	94.9
4.449 dd (9.5, 5.9)	68.7	2-CH	4.394	68.8
7.075 dd (5.9, 1.1)	141.1	3-CH	7.060	141.1
-	137.3	4-C	-	137.4
5.253 ddd (4.8, 2.2, 1.1)	72.6	5-CH	5.231	72.8
2.218 dd (13.9, 4.8)	38.5	6-CH_2	2.216	38.5
1.882 dd (13.9, 2.2)			1.881	
-	39.5	7-C	-	39.6
1.819 m	41.9	8-CH_2	1.810	41.9
1.725 dd (12.1, 5.5)			1.703	
1.604 m	20.0	9-CH_2	1.600	20.0
1.443 ddd (12.8, 12.5, 10.6, 6.2)			1.431	
1.874 ddd	54.1	10-CH	1.870	54.1
2.608 double sept (6.8, 2.2)	24.7	11-CH	2.607	24.7
0.968 d (6.8)	25.7	12-CH_3	0.963	25.7
0.945 d (6.8)	18.3	13-CH_3	0.918	18.3
0.902 s	23.0	15-CH_3	0.896	23.0
3.732 s	52.1	14'-CH_3	3.773	52.2
2.698 d (9.5)	-	2-C-O<u>H</u>	2.681	-

* 270 and 68 MHz for ^1H- and ^{13}C-NMR, respectively.

** 500 and 125 MHz for ^1H- and ^{13}C-NMR, respectively.

Table 3-46 Physicochemical properties of RDA-ME (1k)

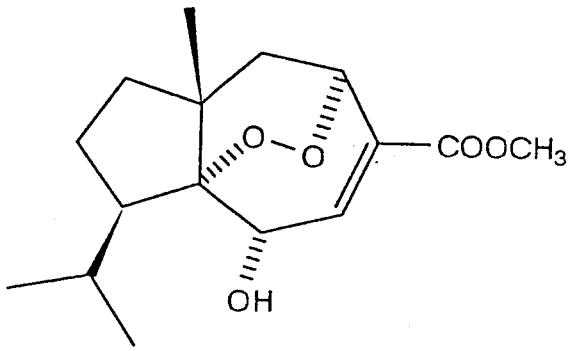

1k

Colorless needles, mp 150-151 °C

Rf: 0.66 (H-EA 3:1)

Vanillin-H_2SO_4 color: grayish pink

N,*N*-dimethyl-*p*-phenylenediamine sulfate test: positive (clear red)

$[\alpha]_D$: + 154 ° (in acetone; *c* 0.02)

UVλ_{max}^{MeOH}: 218 nm

IRν_{max} : 3460, 2960, 1730, 1440, 1380, 1250, 1230, 1080, 980.

EI-MS *m/z* (%): 296 (M^+, 0.8), 278 (M^+-H_2O, 2.3), 264 (M^+-CH_3OH, 2.7), 246 ($M^+-H_2O-OCH_3$, 3.1), 235 (3.5), 221 (8.9), 218 (4.9), 203 (5.8), 175 (7.0), 153 (10), 140 (13), 139 (31), 109 (20), 97 (27), 83 (24), 69 (100), 55 (54), 43 (34), 41 (66).

^1H- and ^{13}C-NMR data are shown in Tables 3-45.

Successively, 230 mg of RDA-ME (1k) was prepared by a large scale of the reaction, and then ^{13}C-2D-NMR (INADEQUATE, in $CDCl_3$, 68 MHz) experiment for RDA-ME was carried out to re-confirm the carotane skeleton for rugosal A (1) and rugosic acid A (2) by detecting carbon-carbon sequences.

At first, CH-correlation NMR spectrum (CH-COSY) of **1k** was measured in $CDCl_3$ to make sure the peak assignment of each hydrogenated carbon with the corresponding proton signals (Fig. 3-115), and as the result, all the hydrogen-bearing carbons were unambiguously assigned (See Table 3-45). Successively, INADEQUATE experiment for **1k** was carried out to reveal C-C correlation of all the carbon (Fig. 3-116). As shown in Fig. 3-117, most of the carbon sequences became feasible. Even though some C-C sequences gave an ambiguous or incomplete results, most of the important sequences between non-hydrogen-bearing carbons and protonated carbon were revealed to confirm the skeleton of **1k**. Accordingly, the sequence of C-1 and C-10, of which justification had only been given by some lines of spectroscopic evidence, such as the carbon sift value at C-10 or NOESY experiment, was completely established Thus, INADEQUATE of **1k** provided conclusive proof of the planar structures for rugosal A (1) and rugosic acid A (2).

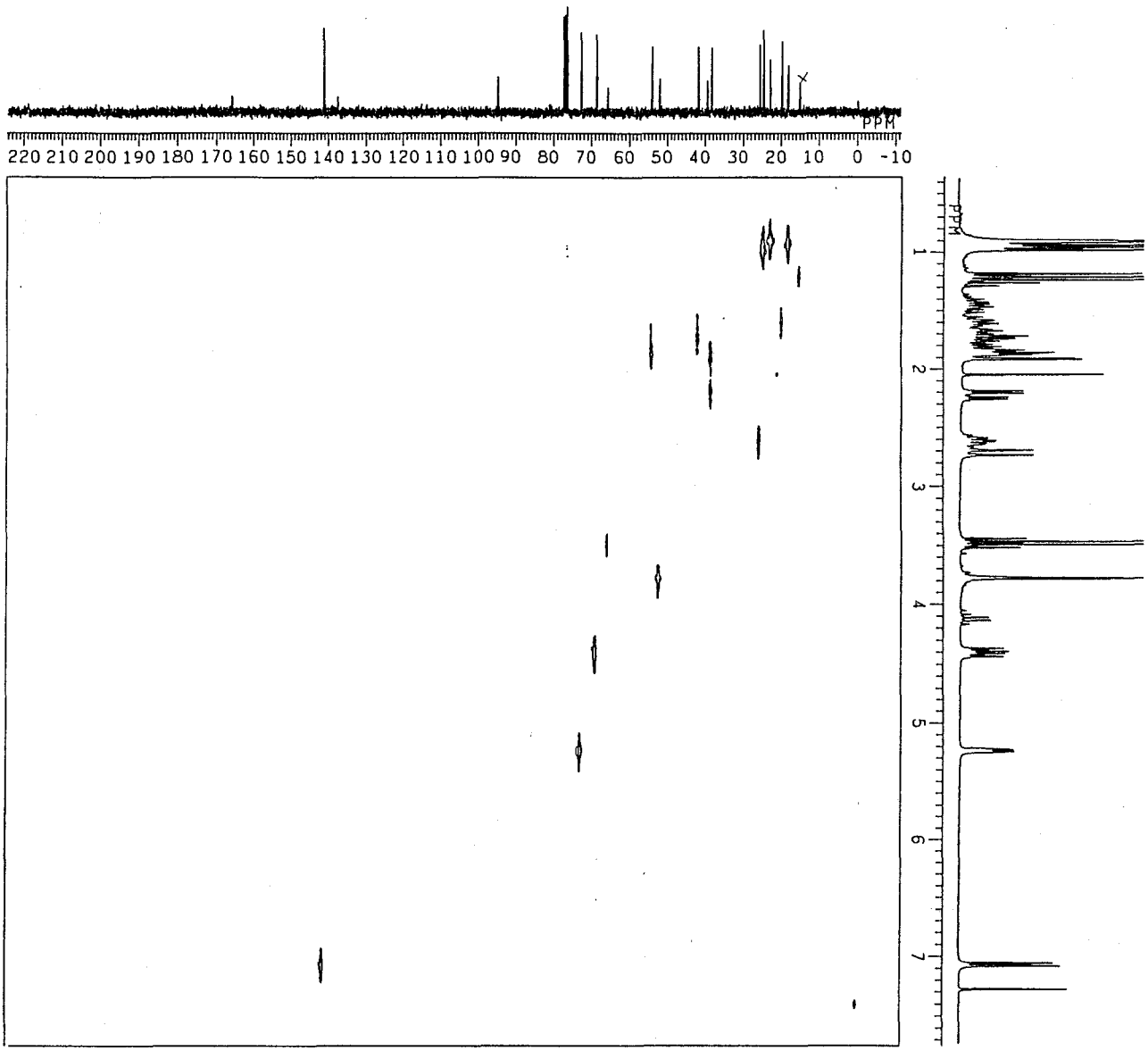

Fig. 3-115a CH-COSY Spectrum of RDA-ME (270 and 68 MHz, in $CDCl_3$)
The asignments of the carbons are shown in Table 3-47.

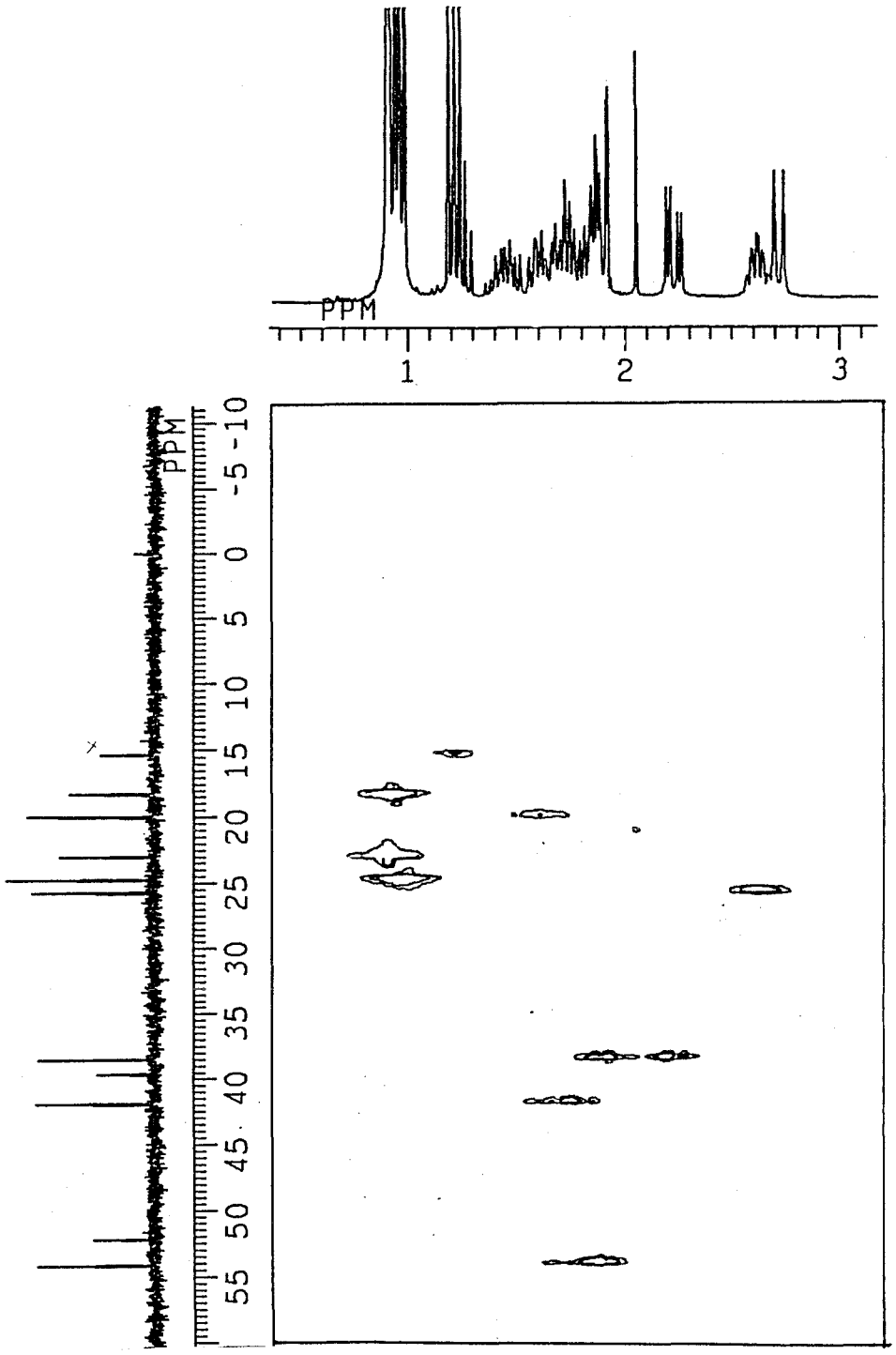

Fig. 3-115b Contined (Magnified in Higher Magnetic Field)

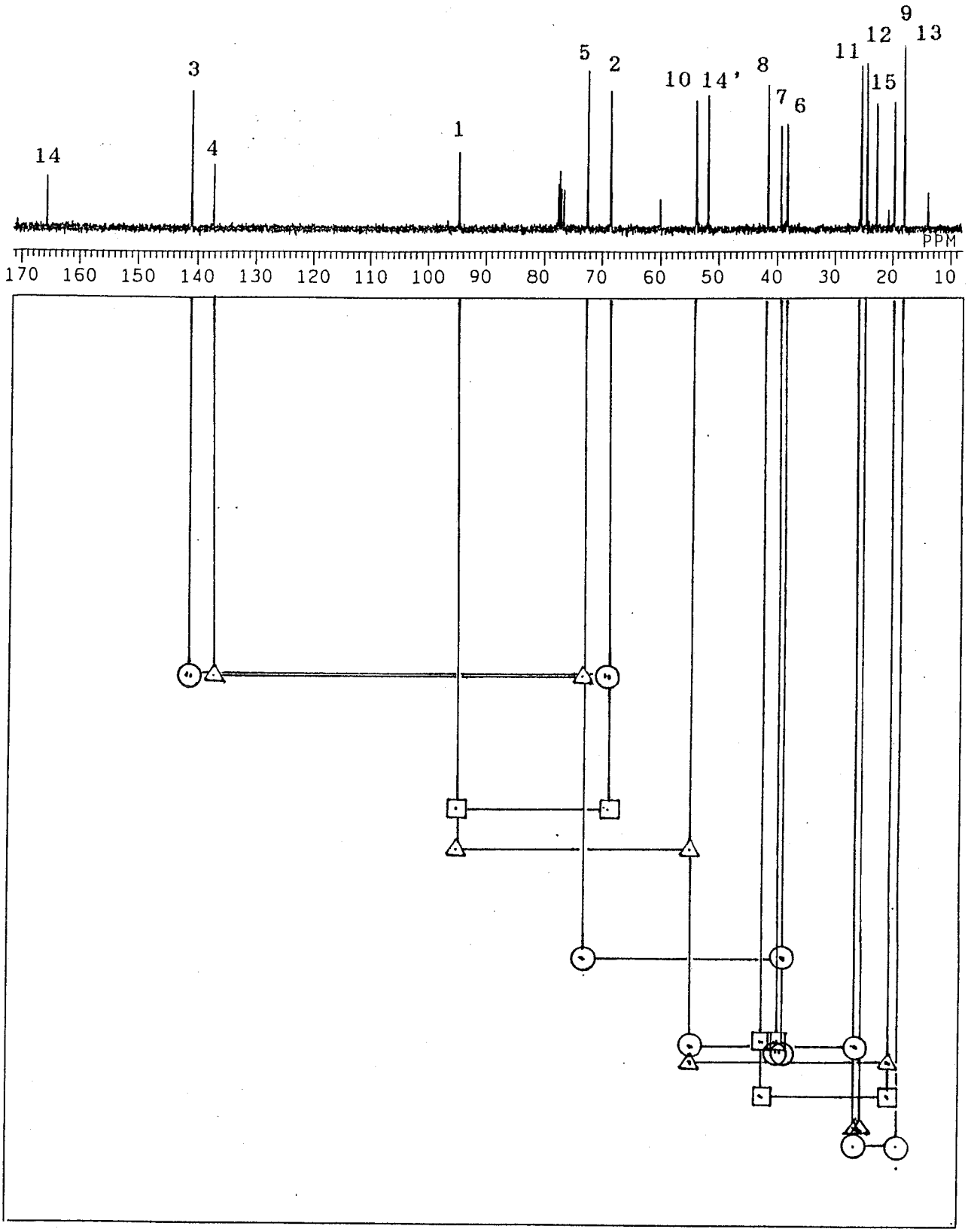

Fig. 3-116 INADEQUATE Spectrum of RDA-ME (68 MHz, in CDCl)

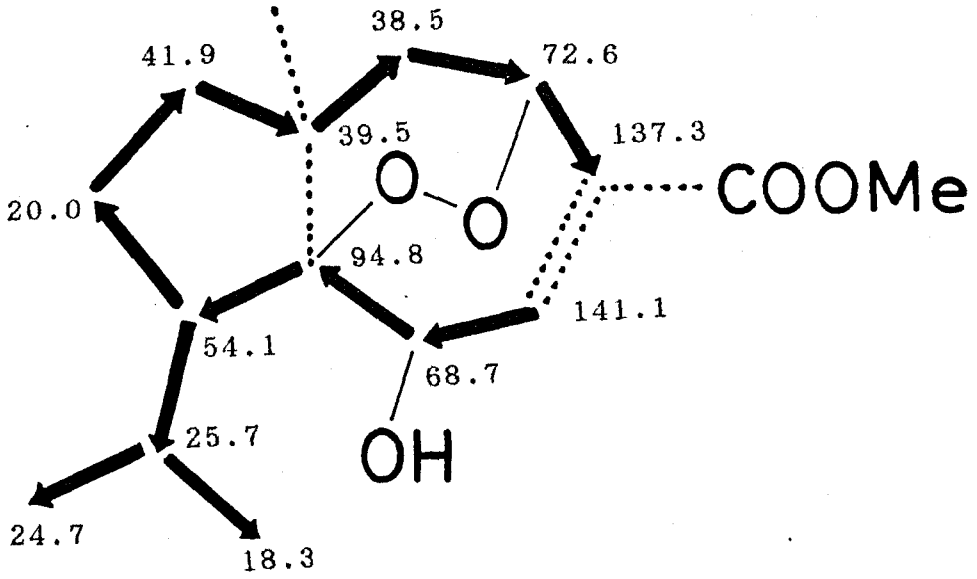

Fig. 3-117 Carbon Sequence of RDA-ME Confirmed by the INADEQUATE Experiment

Observed C-C bond

Incomplete result

C-O or O-O bond

3) Auto-oxidation of Rugosal A into Rugosic Acid A

When rugosal A (1) is left at room temperature, as crystalline under air or even solution in EtOAc, the compound was gradually decomposed to give a more polar substance positive to the peroxide test (Fig. 3-118). This product (RSA-DEC, *ca* 2 mg from 12 mg of 1) was, in comparison of TLC, EI-MS, ^{1}H-NMR and ^{13}C-NMR, identical with rugosic acid A (2) (Fig. 3-119, 120 and 121). Thus, RSA-DEC was certainly derived from 1 as the result of auto-oxidation at C-14 (Scheme 3-7). Although the air oxidation of 1 to 2 is not reasonable to consider that 2 contained in *Rosa rugosa* leaf-tissues is all autoxidation product, since 1 is comparatively stable in a crystalline form and its half-life is markedly long even in water (*e.g.* 0.5 mg of 2 was obtained from 15 mg of 1 by air oxidation for 4 weeks). Therefore, oxidation process from 1 to 2 is probably mediated by a specific enzyme in the plant tissues. Anyhow, above fact certainly indicated that 2 is more stable (consequently less harmful) than 1 to be pooled in *Rosa rugosa* leaves (See Scheme 3-7).

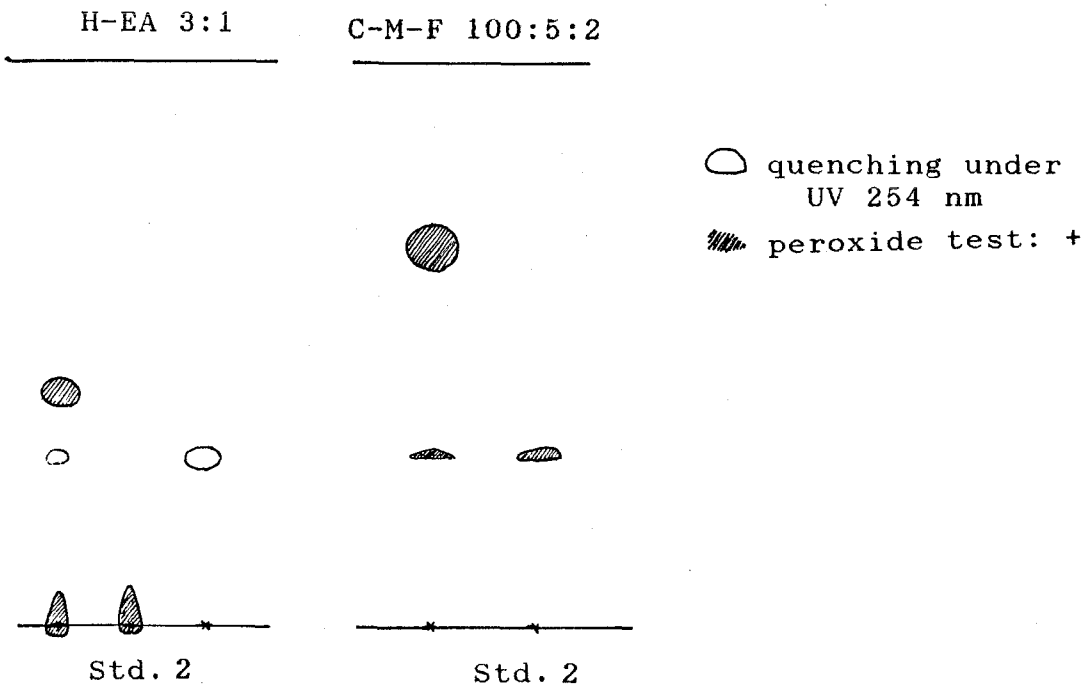

Fig. 3-118 TL Chromatograns of RSA-DEC
* The mixture also contained a trace amount of RSA-TSA (1i).

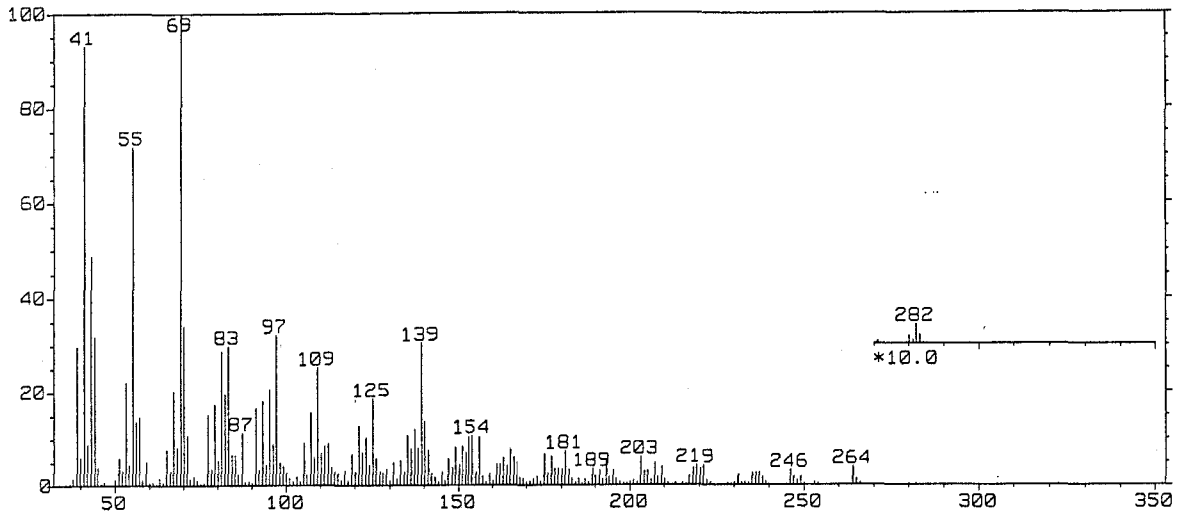

Fig. 3-119 EI-Mass Spectrum of RSA-DEC

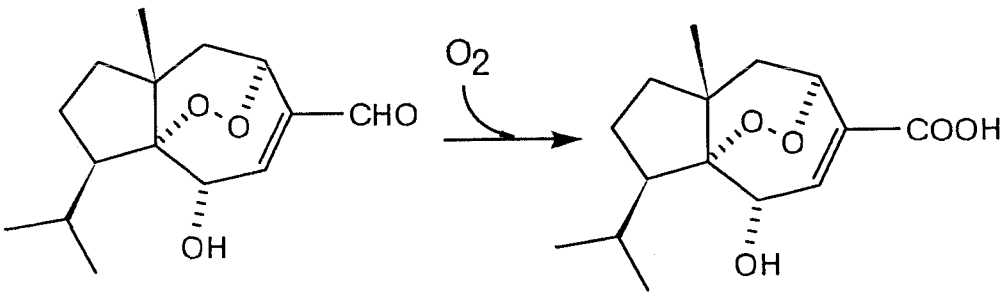

Scheme 3-7 Oxidation of rugosal A (1) to yield rugosic acid A (2)

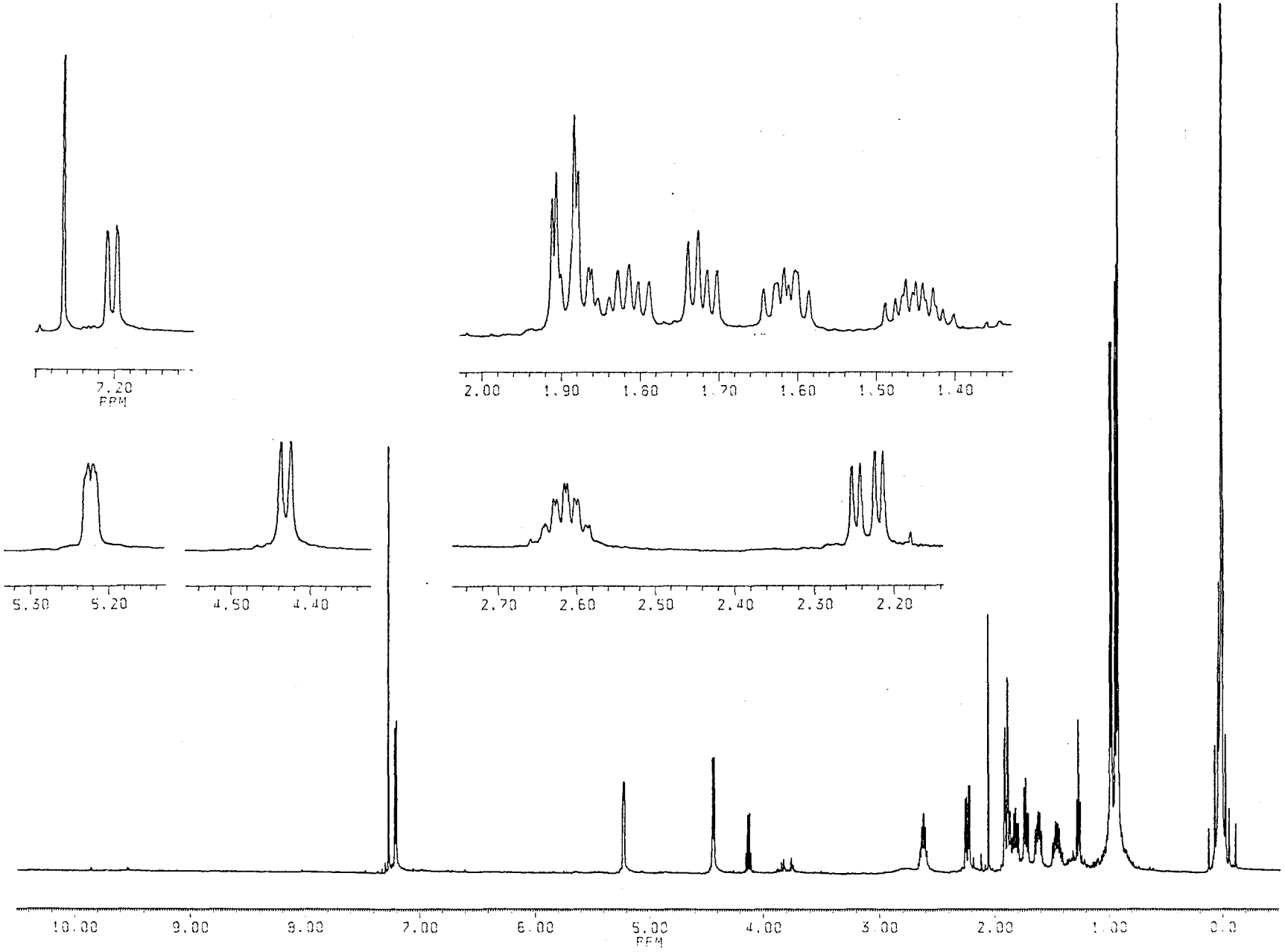

Fig. 3-120 ^{1}H-NMR Spectrum of RSA-DEC (500 MHz, in $CDCl_3$)

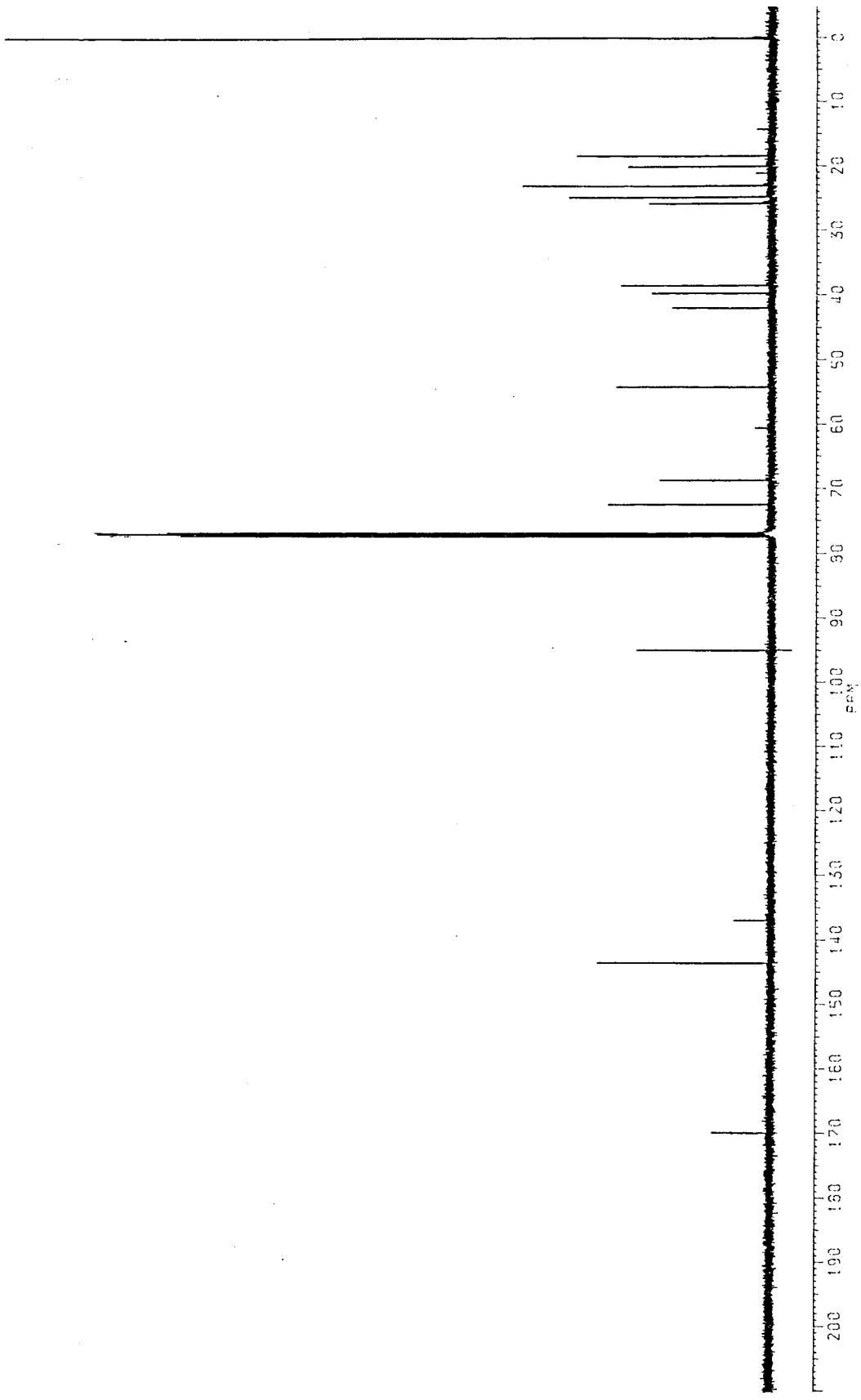

Fig. 3-121 ^{13}C-NMR Spectrum of RSA-DEC (125 MHz, in $CDCl_3$)

Table 3-47 Physicochemical properties of RSA-DEC (2)

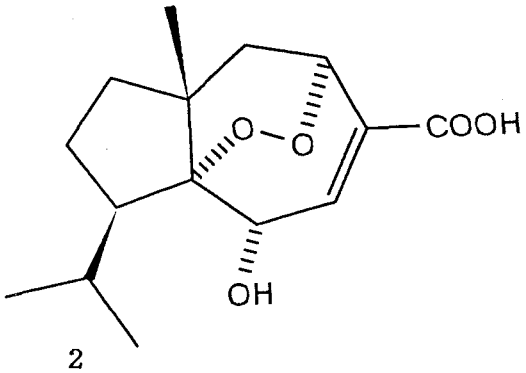

2

A colorless semisolid

Rf: 0.31 (C-M-F 100:5:2)

N,*N*-dimethyl-*p*-phenylenediamine sulfate test: positive (clear red)

EI-MS *m/z* (%): 282 (M^+, 0.4), 264 (M^+-H_2O, 4.0), 246 (3.4), 221 (4.3), 219 (4.4), 203 (6.2), 181 (7.4), 165 (7.7), 156 (10), 154 (11), 139 (30), 125 (19), 109 (25), 97 (32), 83 (30), 81 (29), 70 (34), 69 (100), 55 (72), 44 (32), 43 (49), 41 (93).

^{1}H-NMR $\delta_{TMS}^{CDCl_3}$(500 MHz): 4.431 (d, *J*= 6.3, C-2-H), 7.202 (d, *J*= 6.3, C-3-H), 5.222 (br. m, C-5-H), 2.232 (dd, *J*= 14.2, 5.1, C-6-Ha), 1.893 (dd, *J*= 14.2, 2.5, C-6-Hb), 1.820 (ddd, *J*= 13.0, 12.1, 7.1, C-8-Ha), 1.720 (br. dd, *J*= 12.1, 6.5, C-8-Hb), 1.613 (ddd, *J*= 12.8, 8.6, 7.1, C-9-Ha), 1.444 (dddd, *J*= 13.0, 12.8, 10.8, 6.5, C-9-Hb), 1.882 (ddd, *J*= 10.8, 8.6, 2.1, C-10-H), 2.613 (d. sept, *J*= 6.8, 2.1, C-11-H), 0.972 (d, *J*= 6.8, C-12-H_3), 0.929 (d, *J*= 6.8, C-13-H_3), 0.910 (s, C-15-H_3).

^{13}C-NMR $\delta_{TMS}^{CDCl_3}$(125 MHz): 169.9 (14-C), 143.4 (3-CH), 136.6 (4-C), 94.9 (1-C), 72.4 (5-CH), 68.7 (2-CH), 54.1 (10-CH), 41.9 (8-CH_2), 39.6 (7-C), 38.4 (6-CH_2), 25.7 (12-CH_3), 24.7 (11-CH), 23.0 (15-CH_3), 20.0 (9-CH_2), 18.3 (13-CH_3).

3-3-3 Chemical Conversion of Rugosic Acid A

1) Reduction with Thiourea

Rugosic acid A (2) also has an endoperoxy linkage. Compared with the aldehyde group of rugosal A (1), the carboxyl group of 2 Therefore, endoperoxide cleavage with the reducing reagent seemed to undergo more selectively. However, 2 was unexpectedly resistant against $LiAlH_4$ in THF or benzene. Only in MeOH, 2 gave a high polar product in a yield of 68 % (*cf.* unreacted 2, 24 %); however, it was not a desired derivative but an unknown product converted by the base-catalyzed reaction.

Since the endoperoxy bridge was not cleaved in the reaction with $LiAlH_4$, thiourea was used, which was an effective reagent as shown in the reaction of rugosal A (1). Accordingly, 19.7 mg of 2 in 2 ml of MeOH was stirred with 16.5 mg of thiourea overnight at room temperature. The reaction mixture concentrated under reduced pressure was dissolved in 25 ml of EtOAc, and then washed with 25 ml of distilled water. The organic layer containing reaction products was dried and evacuated, then subjected to PTLC (C-M-F 100:5:2). Main product appearing at *Rf* 0.13 was obtained as a colorless syrup (RDA-TU, 14.2 mg, 70 %) (Fig. 3-122).

The isolate, RDA-TU indicated M^++1 at *m/z* 285 (100 %), together with a dehydration fragment (*m/z* 266, 22 %) and a further dehydrated peak (M^++1 $-2H_2O$, *m/z* 249, 40 %) in FD-MS (Fig. 3-123, *cf.* EI-MS in Fig. 3-124). In the ^{1}H-NMR spectrum, proton signals found in that of the starting material were all detected (Fig. 3-125). Based on several properties of RDA-TU, such as a negative response to the endoperoxy reagent, or M^+ 284, the reaction product was deduced to be a trihyroxycarotanoic acid (**2a**).

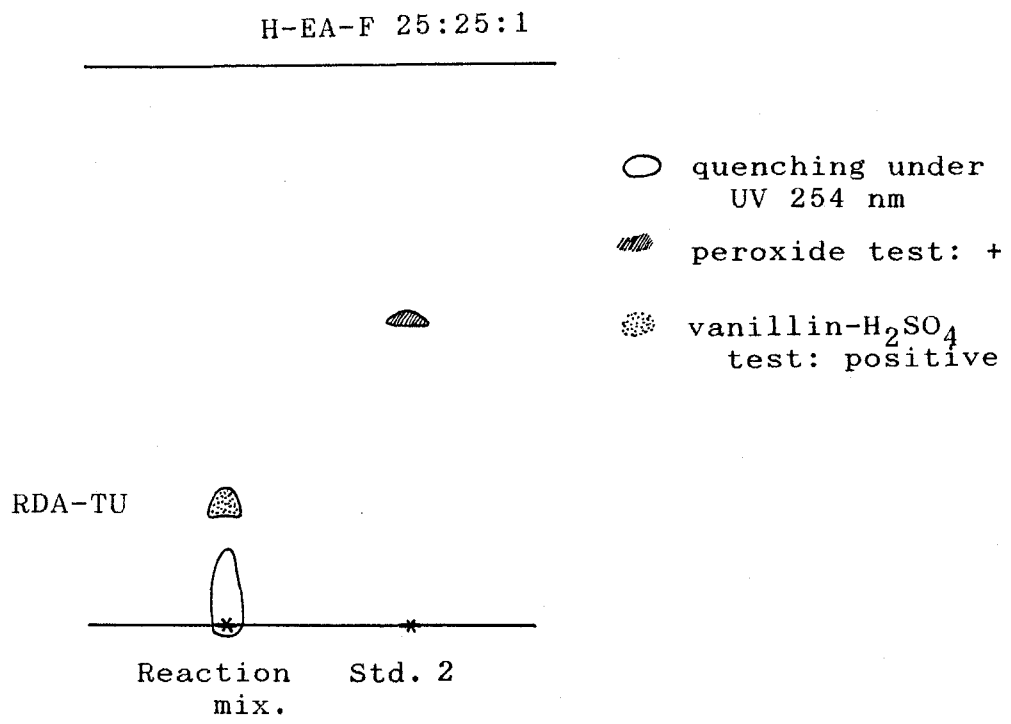

Fig. 3-122 TL Chromatogram of Reduction Product Obtained by Treatment of Rugosic Acid A with Thiourea

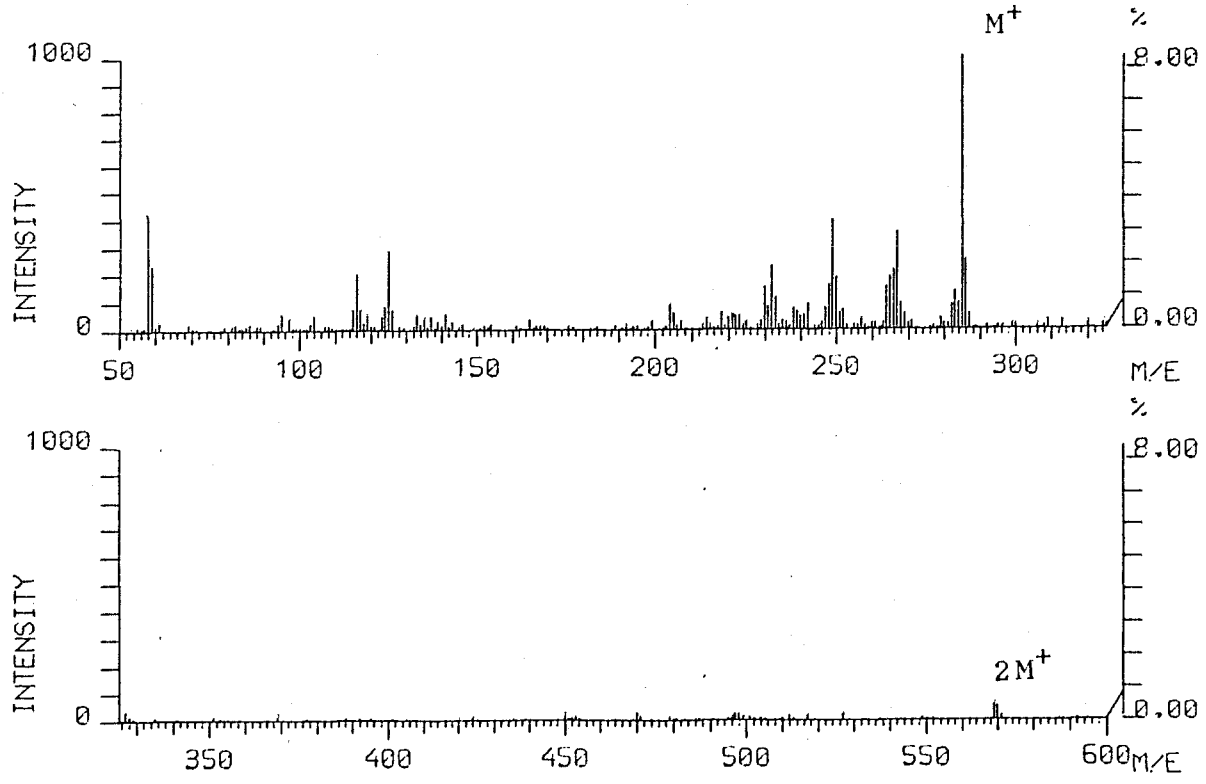

Fig. 3-123 FD-Mass Spectrum of RDA-TU

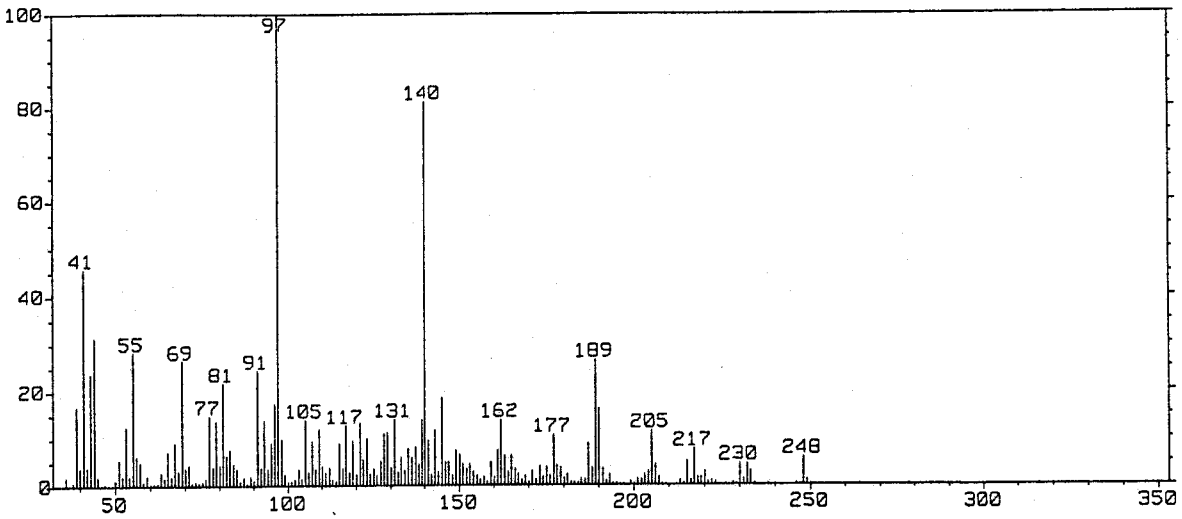

Fig. 3-124 EI-Mass Spectrum of RDA-TU

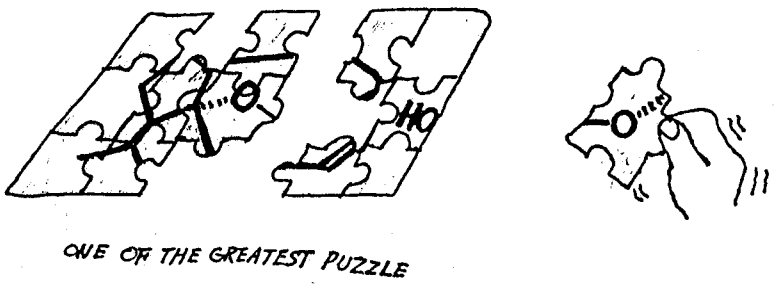

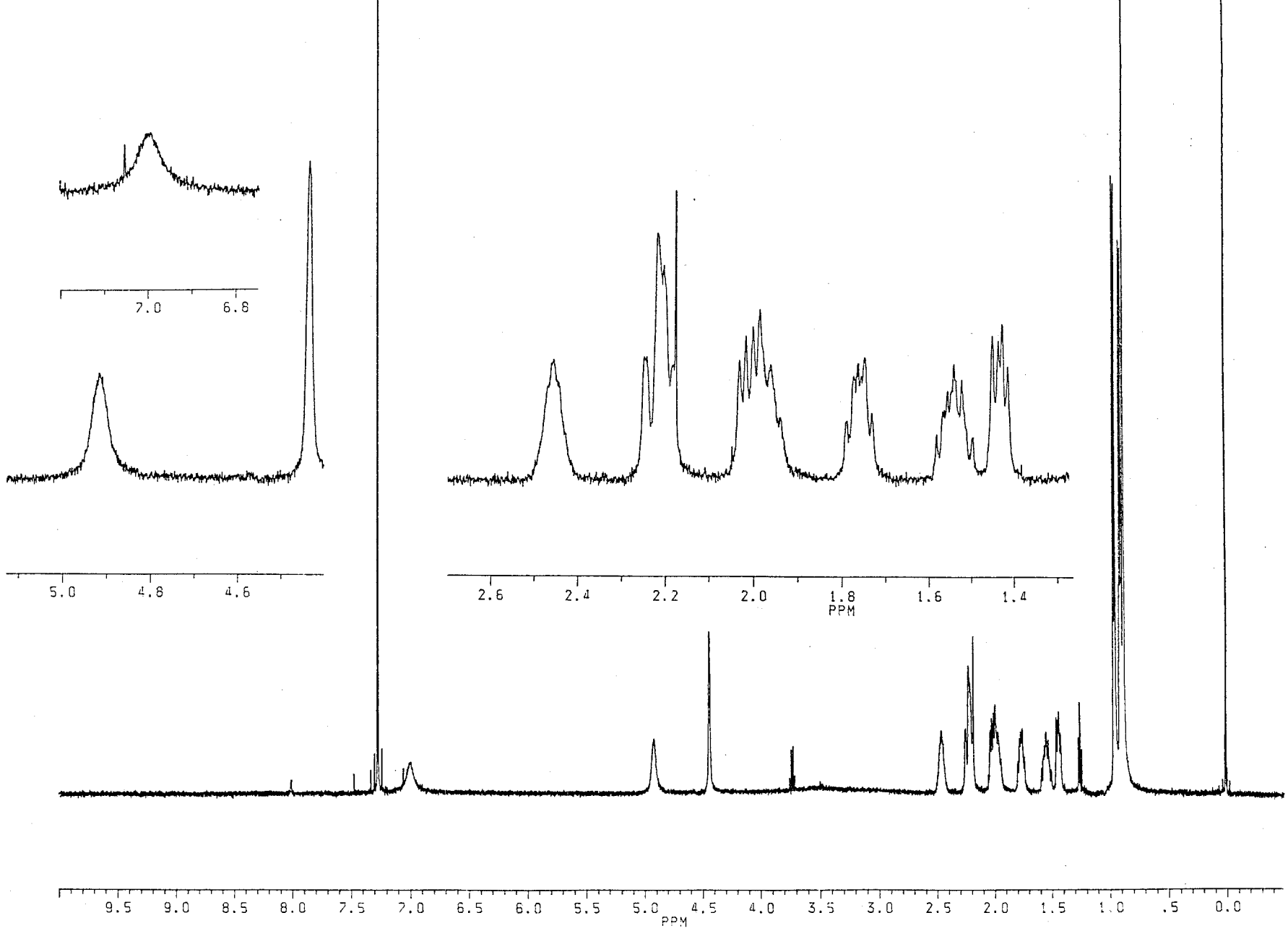

Fig. 3-125 ^{1}H-NMR Spectrum of RDA-TU (500 MHz, in $CDCl_3$)

Table 3-48 Physicochemical properties of RDA-TU (2a)

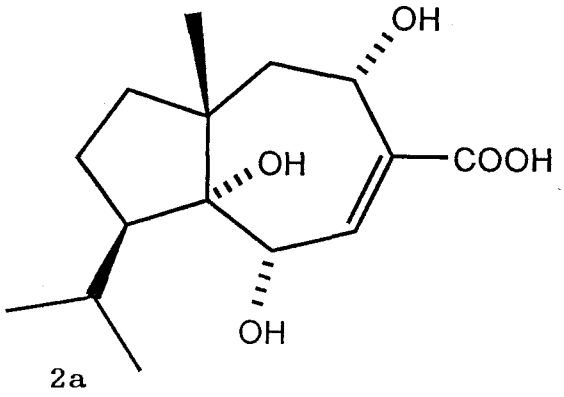

2a

A colorless solid

N,N-dimethyl-*p*-phenylenediamine sulfate test: negative

Rf: 0.13 (C-M-F 100:5:2), 0.23 (H-EA-F 25:25:1, *cf.* 2; 0.55)

Vanillin-H_2SO_4 color: graish yellow → graish pink

FD-MS *m/z* (%): 285 (M^+, 100), 267 (36), 266 (M^+-H_2O, 22), 249 (M^+-2H_2O, 40), 125 (29), 58 (43).

EI-MS *m/z* (%): 248 (M^+-2H_2O, 6.0), 232 (4.5), 230 (4.7), 217 (7.7), 215 (5.1), 205 (12), 190 (16), 189 (27), 177 (11), 162 (14), 145 (18), 140 (81), 139 (14), 121 (13), 117 (13), 105 (14), 97 (100), 96 (17), 93 (14), 91 (24), 81 (22), 79 (14), 77 (15), 69 (26), 55 (28), 44 (31), 43 (24), 41 (46).

^{1}H-NMR $\delta_{TMS}^{CDCl_3}$(500 MHz): 4.43 (1H, br., C-2-H), 7.00 (1H, br., C-3-H) 4.92 (1H, br., C-5-H), 2.21 (1H, m, C-6-Ha), 2.01 (1H, dd, *J*= 15.3 and 7.3 Hz, C-6-Hb), 1.98 (1H, m, C-8-Ha), 1.43 (1H, dd, *J*= 11.3 and 6.8 Hz, C-8-Hb), 1.76 (1H, m, C-9-Ha), 1.54 (1H, m, C-9-Hb), 2.20 (1H, m, C-10-H), 2.44 (1H, br., C-11-H), 0.95 (3H, d, *J*= 6.8 Hz, C-12-H_3), 0.89 (3H, d, *J*= 6.8 Hz, C-13-H_3), 0.87 (3H, s, C-15-H_3). The chemical shift values were calculated to the second decimal place because of the poor resolution.

Although it was possible to pick up approximate signals, the ^{1}H-NMR spectrum taken in $CDCl_3$ exhibited broad signals unable to read their coupling constants. This low resolution was possibly due to poor solubility of **2a** in $CDCl_3$. To solve this problem, **2a** was methylated with CH_2N_2. Consequently, 8.0 mg of mathylation product was obtained from 14.6 mg of **2b** (RDA-TU-ME, yield 54 %) (Fig. 3-126). In the EI-MS, the product indicated a typical fragmentation of methyl esters (Fig. 3-127 and Table 3-49). The structure of RDA-TU-ME was then analyzed on a basis of the ^{1}H-NMR spectrum in C_6D_6 (Fig. 3-128). Upon the methylation, the proton sequences became much clear, and by the decoupling examination, all proton signals were assigned including their coupling constants. Consequently, structure **2b** for RDA-TU-ME and **2a** for RDA-TU were established.

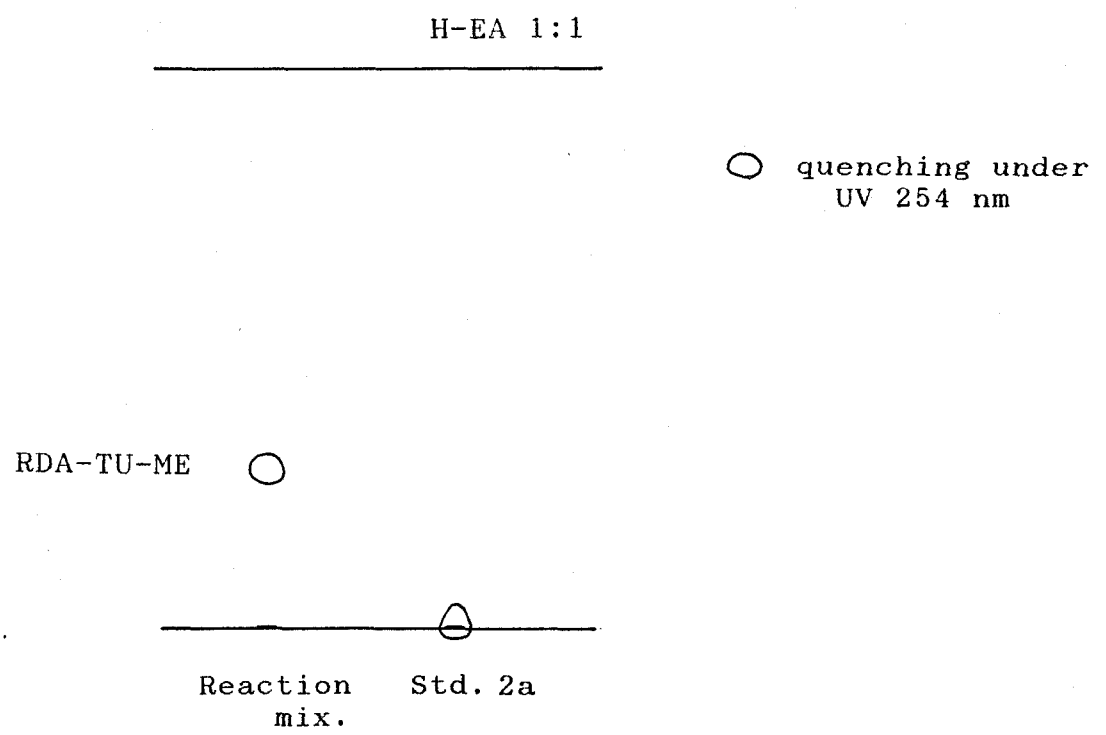

Fig. 3-126 TL Chromatogram of Methyl Ester of RSA-TU Obtained by CH_2N_2 Treatment

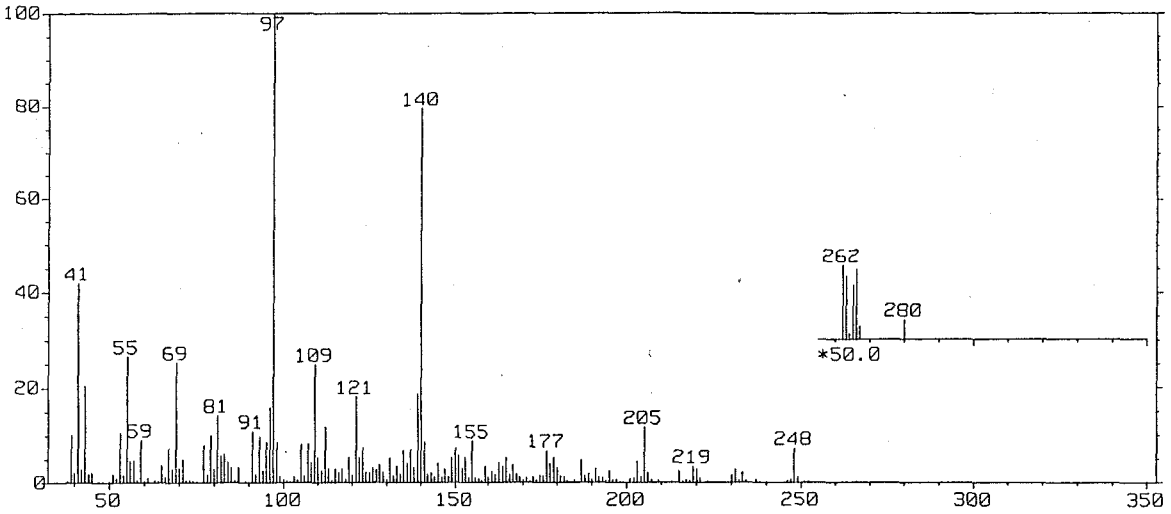

Fig. 3-127 EI-Mass Spectrum of RDA-TU-ME

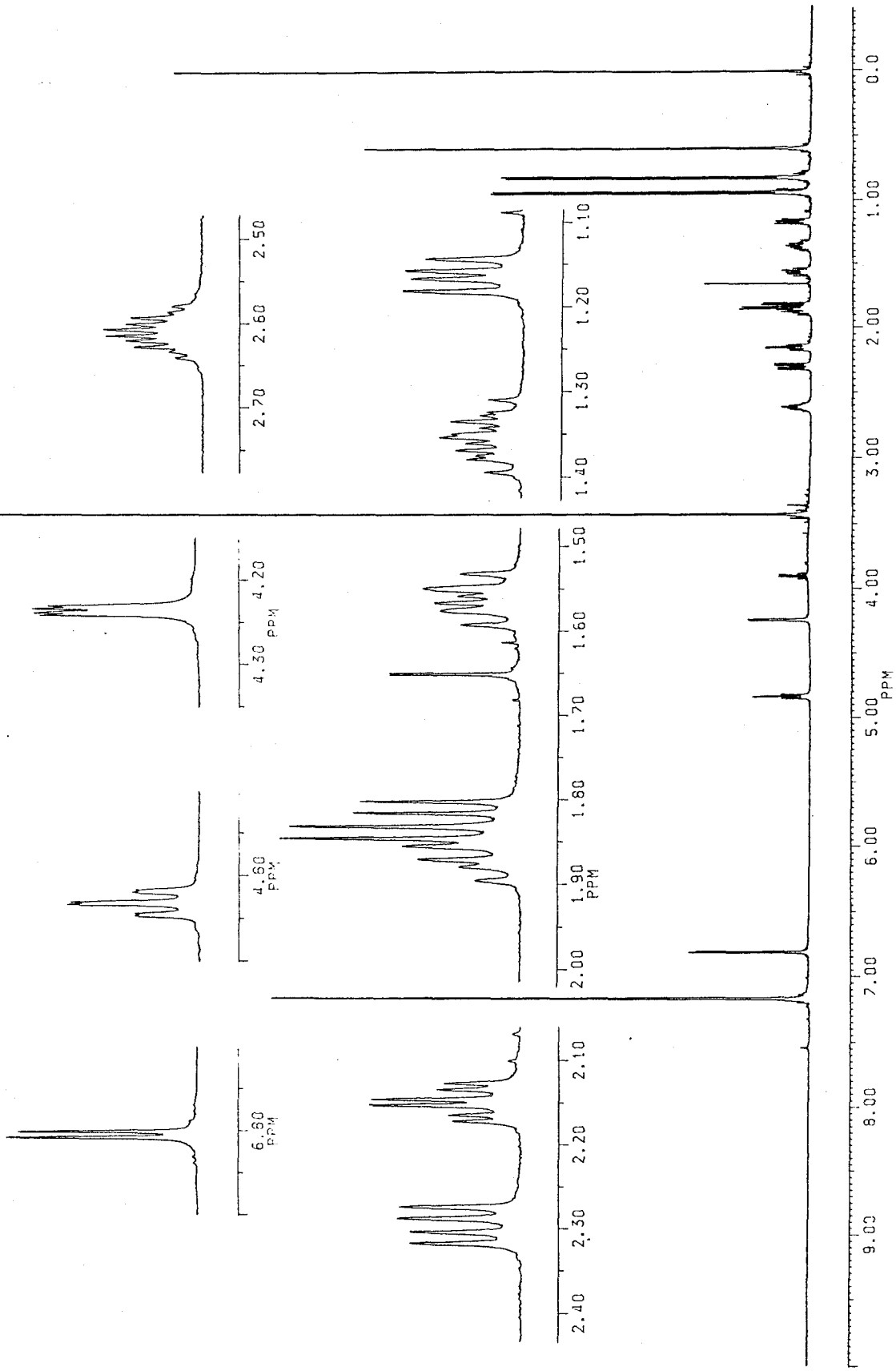

Fig. 3-128 ^{1}H-NMR Spectrum of RDA-TU-ME (500 MHz, in C_6D_6)

Table 3-49 Physicochemical properties of RDA-TU-ME (2b)

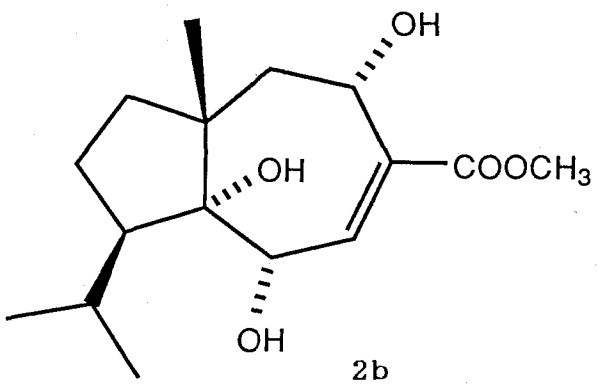

2b

A fine plate from benzene, mp. 58-61°C

Rf: 0.28 (H-EA 1:1, *cf.* **2a**; 0~0.02)

Vanillin-H_2SO_4 color: grayish purple

EI-MS *m/z* (%): 280 (M^+-H_2O, trace), 262 (M^+-H_2O, trace), 248 (7.4), 219 (3.6), 205 (12), 187 (4.9), 177 (7.0), 155 (8.9), 140 (80), 139 (19), 121 (18), 109 (25), 97 (100), 96 (16), 91 (11), 81 (14), 79 (10), 69 (25), 55 (27), 53 (11), 43 (21), 41 (42).

^{1}H-NMR $\delta_{TMS}^{C_6D_6}$ (500 MHz): 4.233 (1H, dd, *J*= 3.7 and 1.4 Hz, C-2-H), 6.808 (1H, d, *J*= 3.7 Hz, C-3-H), 4.831 (1H, ddd, *J*= 6.9, 6.8 and 1.2 Hz, C-5-H), 2.296 (1H, dd, *J*= 15.0 and 6.8 Hz, C-6-Ha), 1.824 (1H, dd, *J*= 15.0 and 6.9 Hz, C-6-Hb), 1.863 (1H, ddd, *J*= 12.1, 11.9 and 7.9 Hz, C-8-Ha), 1.630 (1H, dd, *J*= 11.9 and 7.2 Hz, C-8-Hb), 1.562 (1H, ddd, *J*= 13.0, 9.4 and 7.9 Hz, C-9-Ha), 1.352 (1H, dddd, *J*= 13.0, 12.1, 9.4 and 7.2 Hz, C-9-Hb), 2.149 (1H, ddd, *J*= 9.4, 9.4 and 3.7 Hz, C-10-H), 2.614 (1H, double-sept., *J*= 6.8 and 3.7 Hz, C-11-H), 0.932 (3H, d, *J*= 6.8 Hz, C-12-H_3), 0.816 (3H, d, *J*= 6.8 Hz, C-13-H_3), 0.588 (3H, s, C-15-H_3), 3.423 (3H, s, C-14'-H_3).

3-4 Endoperoxide Conversion in Rugosal-type Carotane Peroxides

3-4-1 Introduction to Peroxide Conversion

Rugosal A (1) and rugosic acid A (2) are revealed to possess a unique endoperoxy bridge linked between C-1 and C-5 of the carotane skeleton and intramolecularly hydrogen-bonded with an allylic hydroxyl group at C-2. In addition, an olefinic bond involved in the 1,2-dioxa-4-cycloheptene ring is conjugated with a carbonyl group (C-14) substituted on C-4, and two of the allylic carbons are both oxygenated. Thus, the peroxy bridge in these carotane peroxides was suggestive of showing a uniqe behavior in chemical reactions.

In a cyclo-1,2-dioxa or R-O-O-R′ type of peroxides, some chemical rearrangements have been reported. As an acid-catalyzed endoperoxide cleavage under an anhydrous condition, a series of rearrangement into acetal derivatives known as Hock cleavage has been well studied [113,114]. Hock cleavage has been examined on various hydroperoxides and 1,4-endoperoxides (Scheme 3-8). In the typical reaction, the compound is temporarily converted into a carbocation at one of the α-carbon, as a result of protonation, followed by O-O bond cleavage. The intermediate was then stabilized to yield a ketal derivative through the Cα-Cβ bond cleavage.

One exception is the case of prostaglandin H_2 (PGH_2, **82**) and its analogs, having 1,3-peroxide linkage [115,116]. Since PHG_2 (**82**) is convertible into thromboxane A_2 (TXA_2, **83**) as the result of a peroxide rearrangement (Scheme 3-9), some model reactions using its analogs (**84**, **85**) have been carried out [117,118]. In this series of reactions, these analogs are converted into a ketal derivative *via* an intermediate of a carbonyl extrusion biradical, according to their scheme (Scheme 3-10). However, these reactions are possible to be regarded as a kind of Hock cleavage. The C,C-

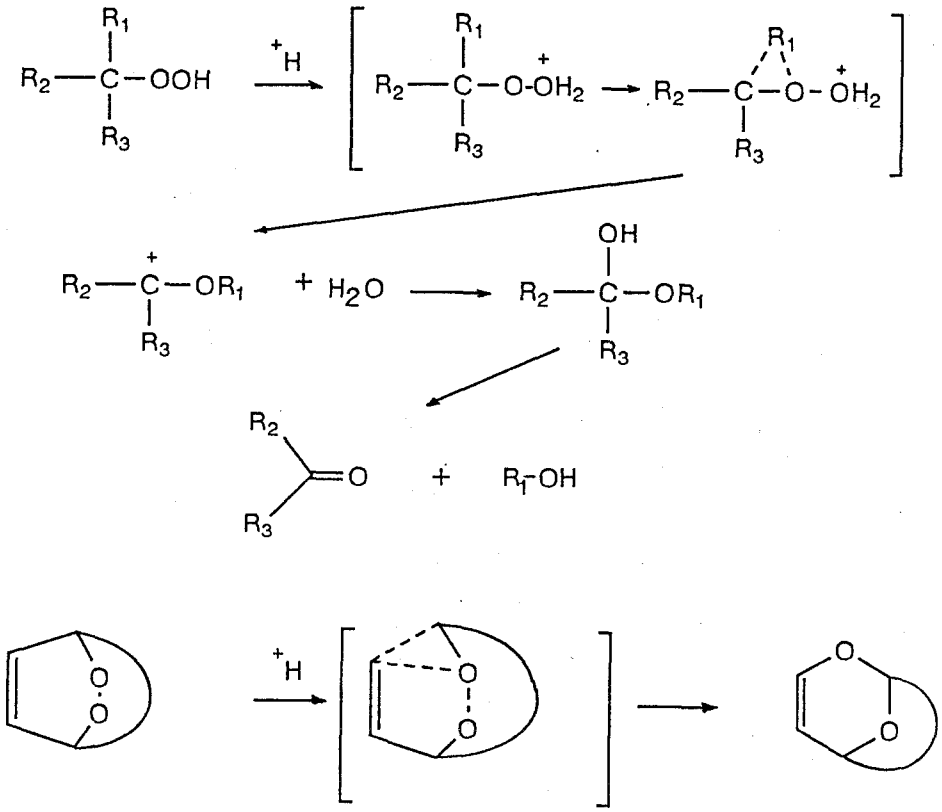

Scheme 3-8 Hock Cleavage Reaction of *Exo*- and *Endo*-Peroxides

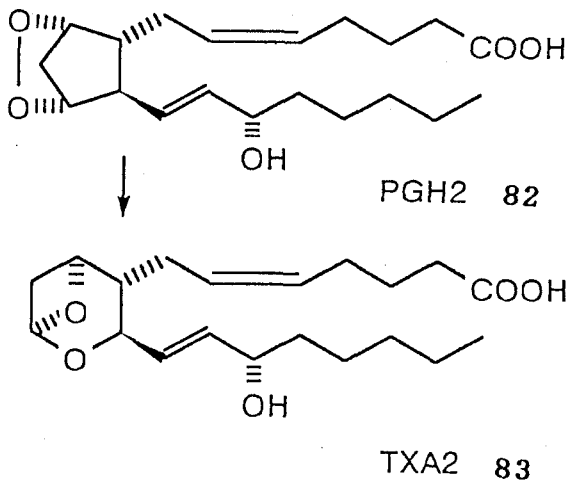

Scheme 3-9 Endoperoxide rearrangement of PGH_2 to yield TXA_2

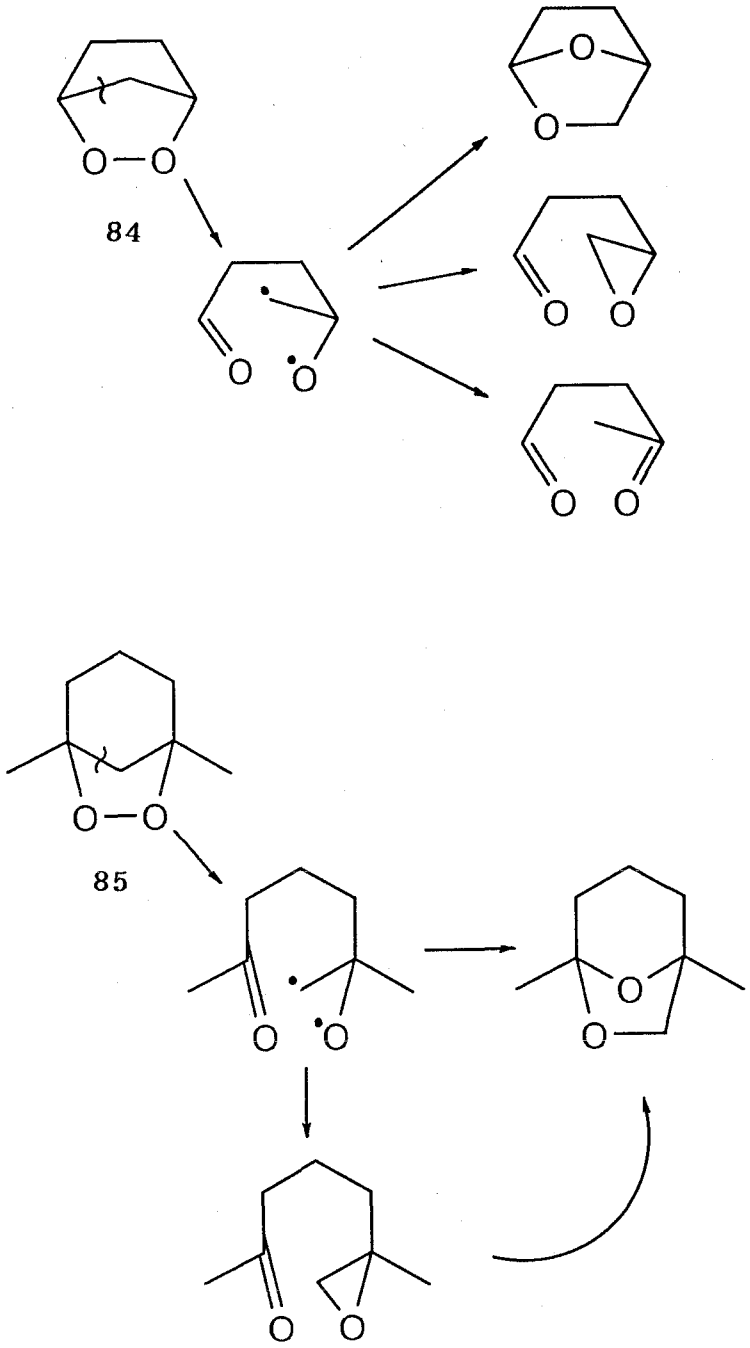

Scheme 3-10 Endoperoxide Rearrangement of PGH_2 Analogues

bond cleavage was believed to be subjected by the dihedral angle between the C(1)-O(1)-O(2) bond and the O(1)-C(1)-C(2) taking the smallest value among three of the C,C-bond on the endoperoxy oxygen-bearing carbon (30 ° in **85**, Fig. 3-129) [118]. The appropriate angle provides a measure of the overlap between the peroxide bond orbitals and the bridgehead carbon orbitals. This better overlap with the carbon bond leads to its more facile rupture in a concerted carbonyl extrusion.

Another example is an acidic rearrangement of hanalpinol (**80**), a guaian type endoperoxide possessing the same 1,5-peroxide system as that of **1**. In **80**, C,C-cleavage occurs on C(9)/C(10) possibly as the result of Hock cleavage. Since the hemiacetal intermediate is further protonated, successive dehydration occurs to yield furopelargone B (**81**) (See Scheme 3-3, pp **141**). In this rearrangement, the C,C-cleavage seems to be subjected to stability of carbocation in the intermediate, or dihedral angle of the reactive bonds as described above.

While acid-catalyzed endoperoxide cleavage of rugosal A (**1**) was examined, this carotane peroxide exhibited a unique reaction different from known types of Hock cleavage referred in Section 3-2 (pp. 148). In this peroxide conversion under an anhydrous acidic condition, the C,C-cleavage occurred between C-1 and C-10, concerted with the oxygen migration to form a ketal derivative, RSA-TSA (**1i**).

It has also been revealed that **1** easily cleaves to a hemiacetal compound RSA-PY (**1g**) under an alkalin condition. This reaction was, like the acid-catalyzed reaction, quite different from other typical base-catalyzed endoperoxide cleavages [118,119]. Since rugosal A-type carotane peroxides seemed to exhibit unique peroxide conversions, peroxide rearrangements of rugosic acid A (**2**) and RSA-NBH-1 (**1c**) are also carried out. Based on these results, the reaction mechanisms are discussed in this section, in comparison with some other types of endoperoxide conversion.

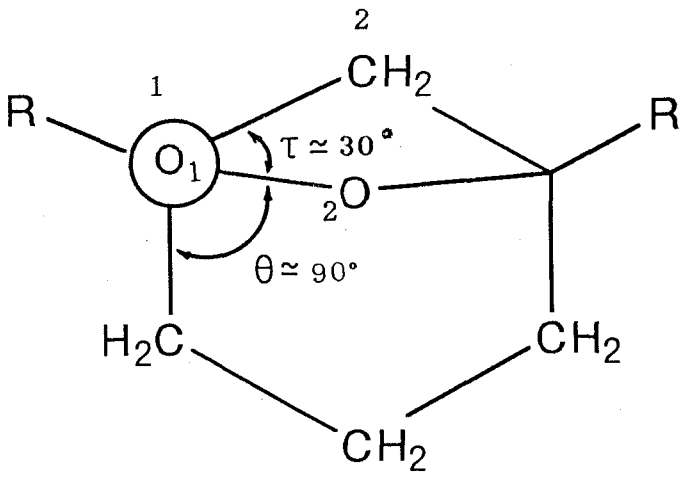

Fig. 3-129 Dihedral Angle between C1-O1-O2 and O1-C1-C2 in the Molecules of PGH_2 Analogs

3-4-2 Acid-Catalyzed Conversion of an Endoperoxide into a Ketal

1) Conversion of Rugosic Acid A

Rugosal A (1) was converted into a ketal derivative (1i), when the compound was treated with *p*-TSA under the anhydrous and thermal conditions. If rugosic acid A (2) is also convertible to the corresponding ketal, it will be proved that the aldehyde group of 1 does not contribute to the acid-catalyzed reaction. Although rugosic acid A (2) was not converted by the treatment with *p*-TSA or conc. H_2SO_4 at room temperature, when 2 was heated at 80 °C, 2 was easily converted into the desired derivative.

By the treatment of 2 with formic acid (Scheme 3-11), two major products negative to the peroxide reagent (RDA-FA-1 and RDA-FA-2, shown in Fig. 3-130) were obtained each as a colorless syrup (RDA-FA-1, 8.4 mg, *Rf* 0.35 and RDA-FA-2, 7.8 mg, *Rf* 0.32; in 37 and 35 % yields, respectively). On the other hand, a mixture of 2 (43.0 mg) and *p*-TSA (21.6 mg) in 2 ml of benzene was also kept at 80 °C to give a single product indistinguishable from RDA-FA-2 in TLC and ^{1}H-NMR (27.1 mg, in a yield of 63 %).

Rugosic Acid A (2, 20.7 mg)
↓ dissolved in 1 ml of HCOOH
↓ kept at 80 °C for 1.5 hr in ampoule
↓ dilute with 20 ml of distilled water
↓ extracted with 15 ml of EtOAc
Organic Layer
↓ washed with 20 ml of saturated NaCl solution
↓ dried over Na_2SO_4
PTLC (in C-M-F 100:5:2)
↓
Two Major Products

Scheme 3-11 Preparation of acid-catalyzed conversion product from rugosic acid A

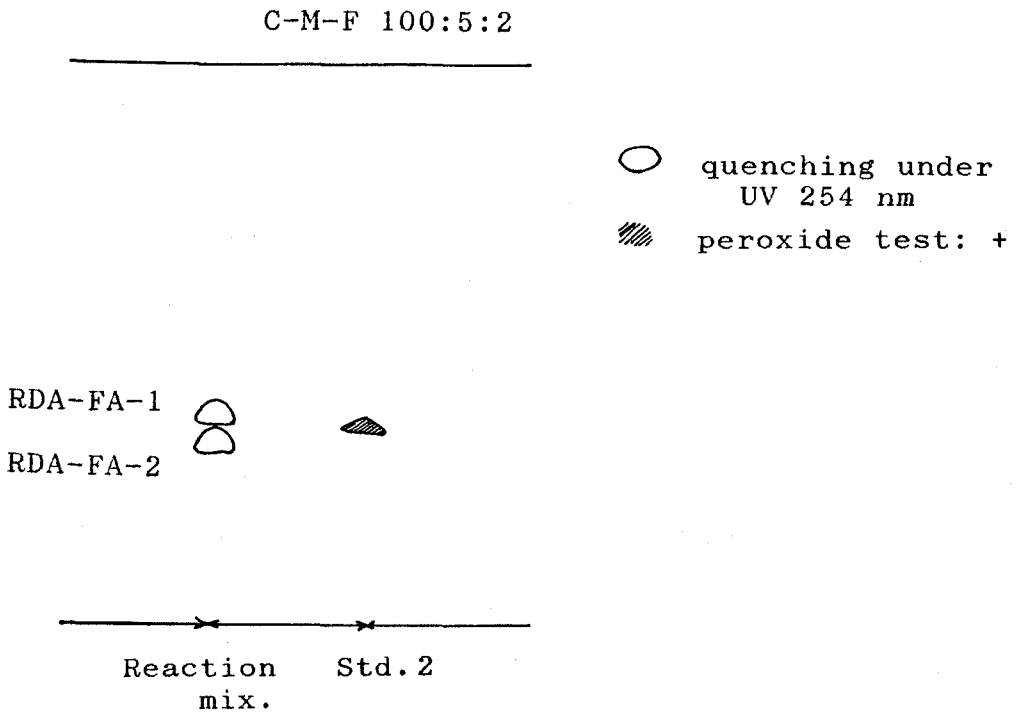

Fig. 3-130 TL Chromatograms of Reaction Products Obtained by Acid-catalyzed Peroxide Conversion of Rugosic Acid A

RDA-FA-2 showed its molecular ion 282 in FD-MS [*m/z* 283 (M^++1, 100 %)] (Fig. 3-131). In EI-MS, however, the molecular ion was undetectable and the dehydration peak (*m/z* 264, 2.9 %) was observed as the largest fragment (Fig. 3-132). As shown in Fig. 3-133 and Table 3-50, ^{1}H-NMR spectrum of RDA-FA-2 revealed two spin-spin coupling system, similar to RSA-TSA (**1f**). For example, a double-double doublet signal of a methine proton at $_H$ 3.642 assignable to C-10-H was well corresponded to that of **1f**. Furthermore, ^{13}C-NMR spectrum of RDA-FA-2 showing a good correspondence with that of **1f** gave a structure **2c** for the derivative. The C-1 ketal carbon at δ_C 105.5 and oxygenated methine carbons at δ_C 70.1 (C-2), 65.4 (C-5) and 76.2 (C-10) were well compatible with the structure (Fig. 3-134 and Table 3-50).

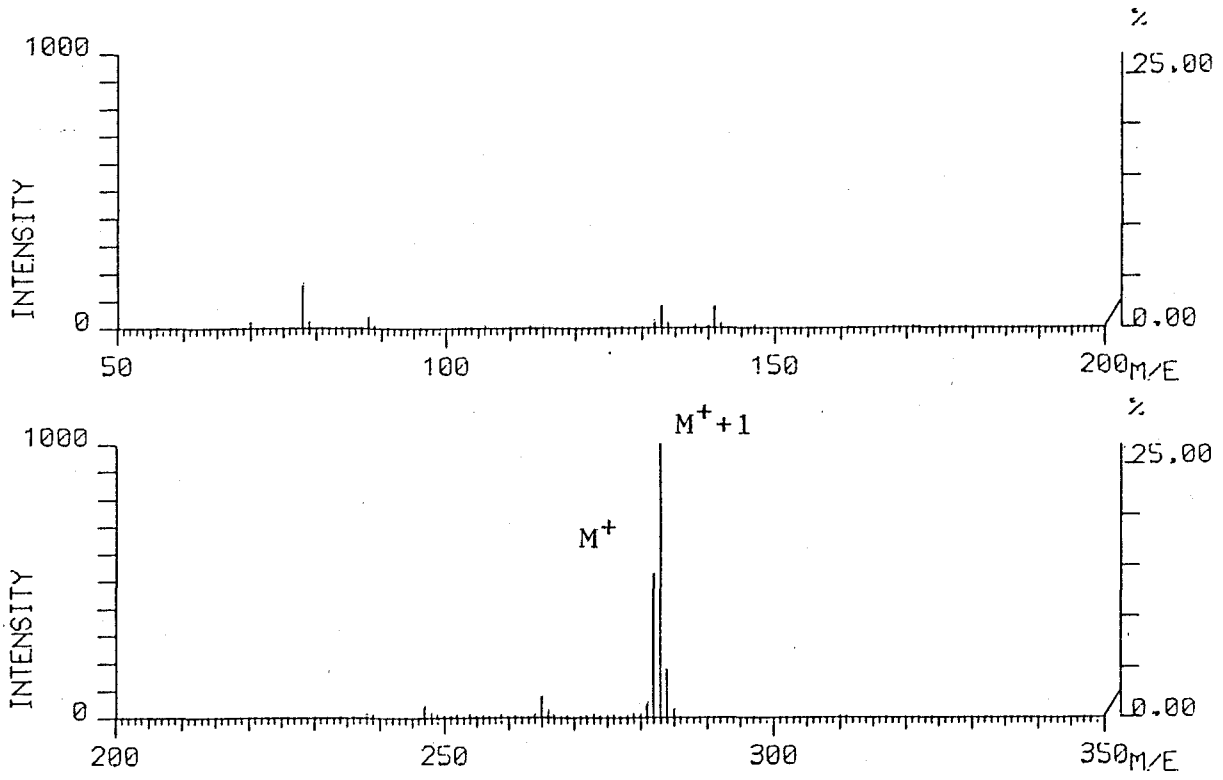

Fig. 3-131 FI-Mass Spectrum of RDA-FA-2

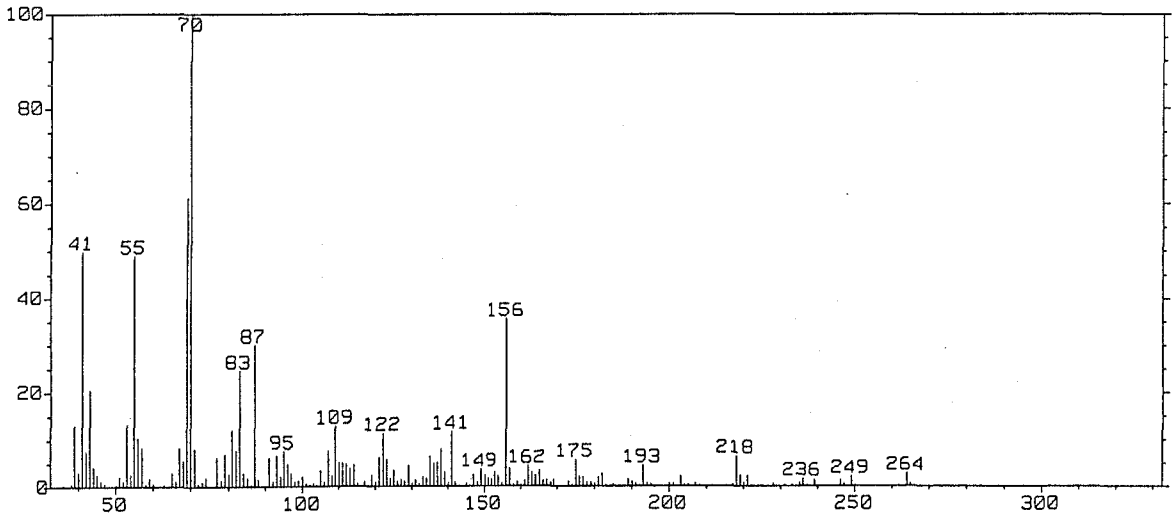

Fig. 3-132 EI-Mass Spectrum of RDA-FA-2

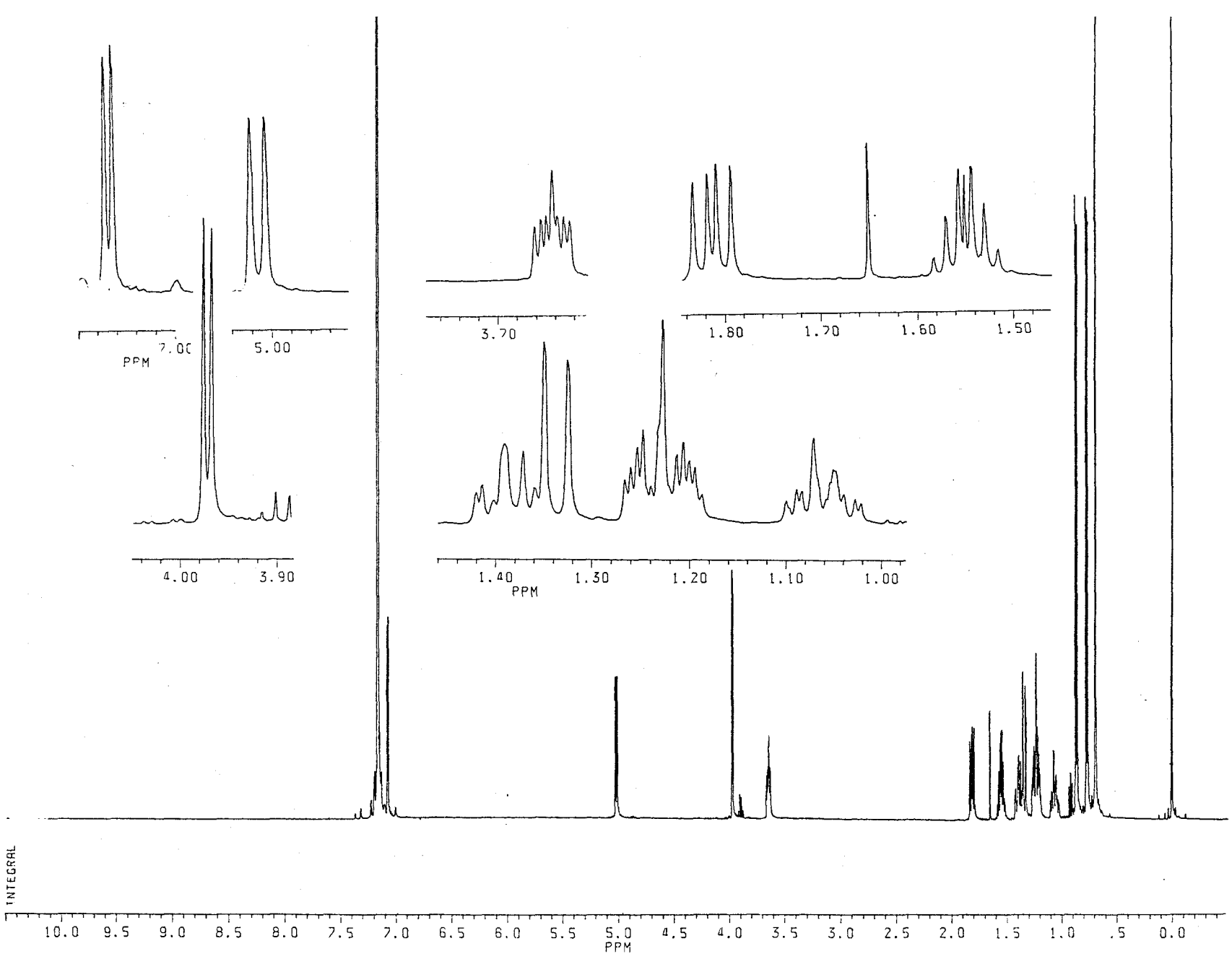

Fig. 3-133 ^{1}H-NMR Spectrum of RDA-FA-2 (500 MHz, in C_6D_6)

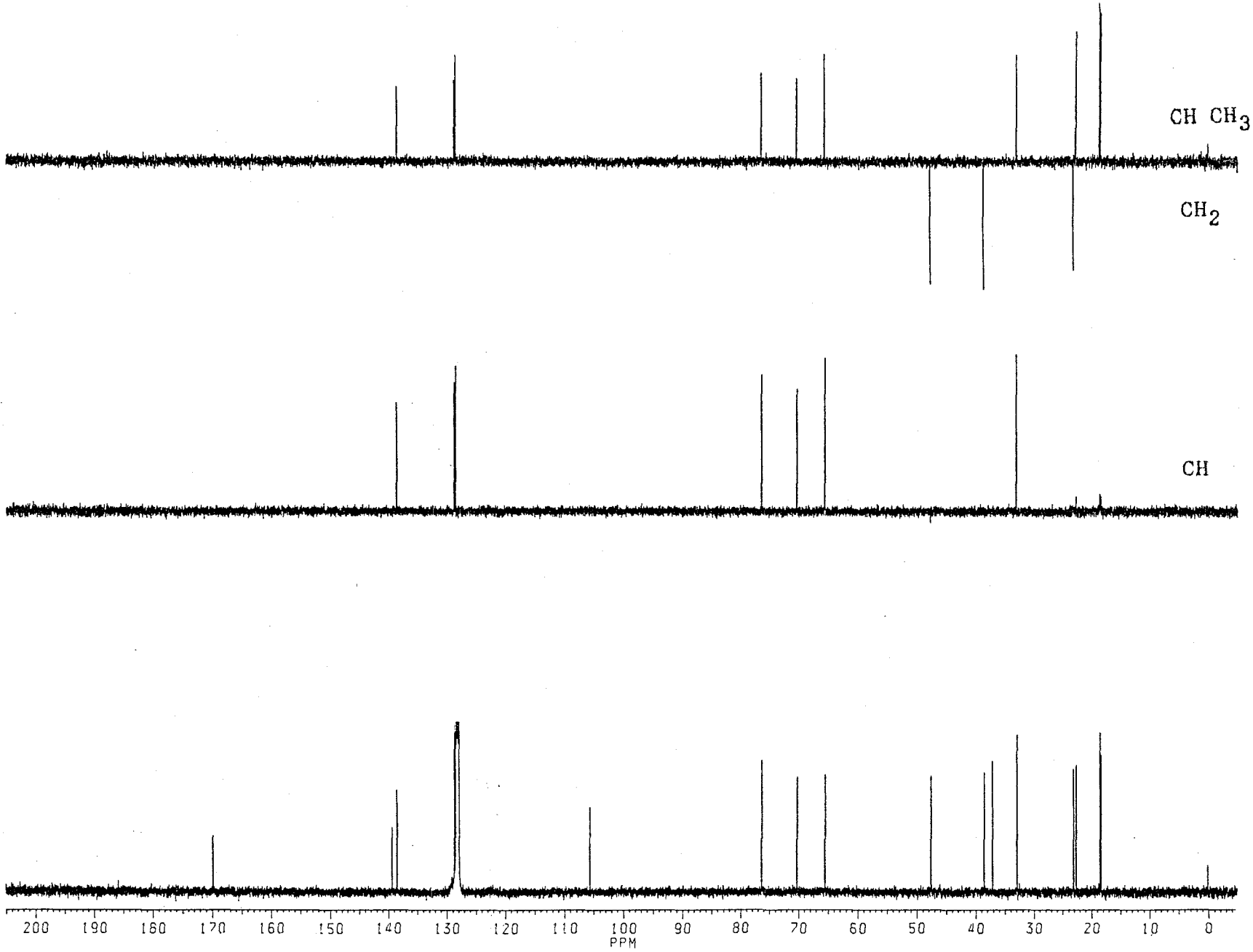

Fig. 3-134 ^{13}C-NMR Spectra of RDA-FA-2 (125 MHz, in C_6D_6)

Stereostructure of RDA-FA-2 was revealed by the NOE experiment to be C-10*S* as with RSA-TSA (**1i**), due to the same NOEs among five membered ring protons and C-15-H_3 (Fig. 3-135) as previously found in **1i**. This stereo-selectivity was also observed in acid-catalyzed endoperoxide rearrangement of **2**, suggesting the same reaction process on rugosal A-type of endoperoxides.

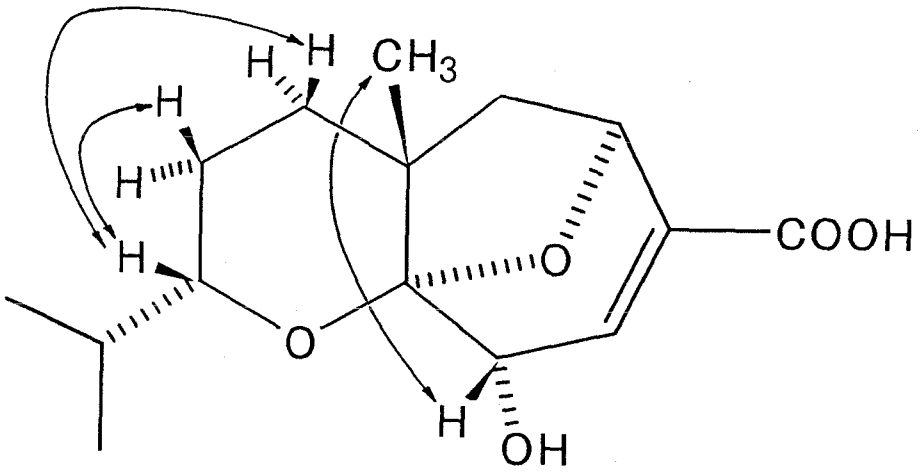

Fig. 3-135 NOEs Observed in RDA-FA-2

Table 3-50 Physicochemical properties of RDA-FA-2 (2c)

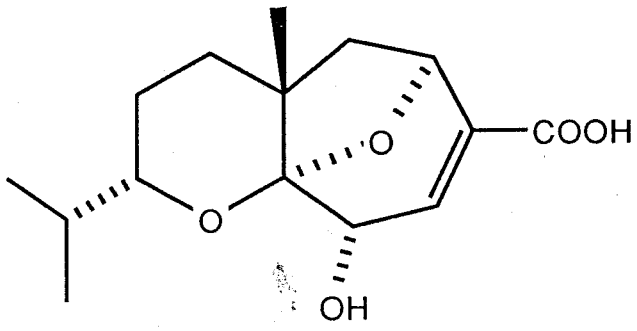

2c

Colorless column from Et_2O/benzene, mp. 131-132°C

Rf: 0.32 (C-M-F 50:5:1)

Vanillin-H_2SO_4 color: grayish yellow → grayish pink

N,*N*-dimethyl-*p*-phenylenediamine sulfate test: negative

FD-MS *m/z* (%): 283 (M^++1, 100), 282 (M^+, 53)

EI-MS *m/z* (%): 264 (M^+-H_2O, 2.9), 249 (2.3), 246 (1.4), 239 (1.6), 236 (1.8), 218 (6.6), 193 (4.6), 175 (5.8), 162 (4.5), 156 (36), 141 (12), 138 (8.1), 122 (11), 109 (13), 87 (30), 83 (25), 81 (12), 70 (100), 69 (61), 56 (11), 55 (49), 53 (13), 43 (21), 41 (50).

^{1}H-NMR $\delta_{TMS}^{C_6D_6}$ (500 MHz): 3.971 (1H, d, *J*= 4.2 Hz, C-2-H), 7.067 (1H, d, *J*= 4.2 Hz, C-3-H), 5.013 (1H, br. d, *J*= 7.6 Hz, C-5-H), 1.812 (1H, dd, *J*= 12.3 and 7.6 Hz, C-6-Ha), 1.337 (1H, br. d, *J*= 12.3 Hz, C-6-Hb), 1.390 (1H, m, C- 8-Ha), *ca* 1.25 (1H, m, C-8-Hb), *ca* 1.21 (1H, m, C-9-Ha), 1.060 (1H, m, C-9-Hb), 3.642 (1H, ddd, *J*= 9.3, 6.3 and 3.2 Hz, C-10-H), 1.548 (1H, double-sept., *J*= 6.7 and 6.3 Hz, C-11-H), 0.863 (3H, d, *J*= 6.8 Hz, C-12-H_3), 0.767 (3H, d, *J*= 6.8 Hz, C-13-H_3), 0.688 (3H, s, C-15-H_3).

^{13}C-NMR $\delta_{TMS}^{C_6D_6}$ (125 MHz): 105.5 (C, C-1), 70.1 (CH, C-2), 138.4 (CH, C-3), 139.3 (C, C-4), 65.4 (CH, C-5), 47.5 (CH_2, C-6), 37.0 (C, C-7), 38.4 (CH_2, C-8), 23.0 (CH_2, C-9), 76.2 (CH, C-10), 32.6 (CH, C-11), 18.4 (CH_3, C-12), 18.2 (CH_3, C-13), 169.8 (C, C-14), 22.5 (C, C-15).

On the other hand, RDA-FA-1 gave the molecular ion *m/z* 310 (2 + 28 mass units) in FD- and EI-MS (Fig. 3-136 and 137). As shown in Fig. 3-138 and Table 3-51, the ^{1}H-NMR spectrum of RDA-FA-1 was also similar to **2c**. As a unique signal, a proton attributable to a formyl group (δ_H 7.800, 1H, d, *J*= 1.0 Hz, coupling with C-2-H) was observed. It was therefore concluded that RDA-FA-1 is a formate of **2c**. The position of formyl group was deduced to be C-2, since the C-2 methine proton in RDA-FA-1 was offerd a marked deshielding effect (δ_H 5.577 in RDA-FA-1, by 1.6 ppm from **2b**). RDA-FA-1 was accordingly elucidated as **2c**.

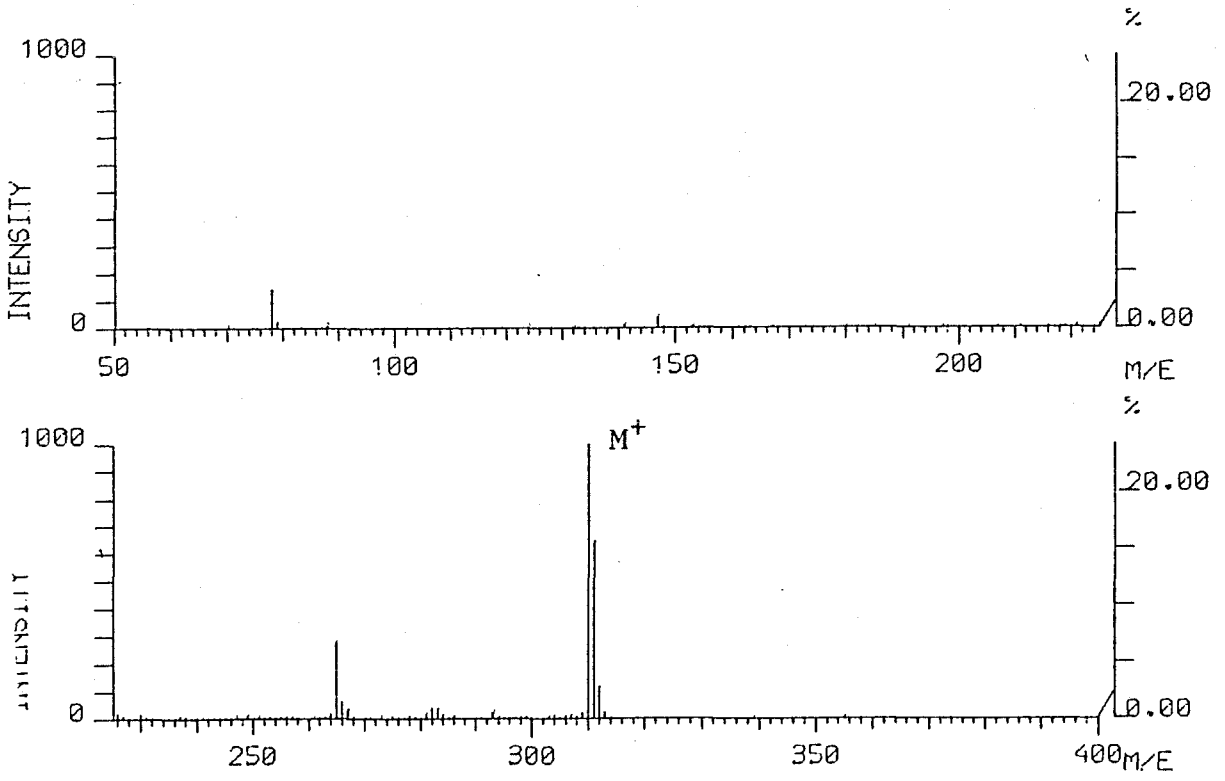

Fig. 3-136 FI-Mass Spectrum of RDA-FA-1

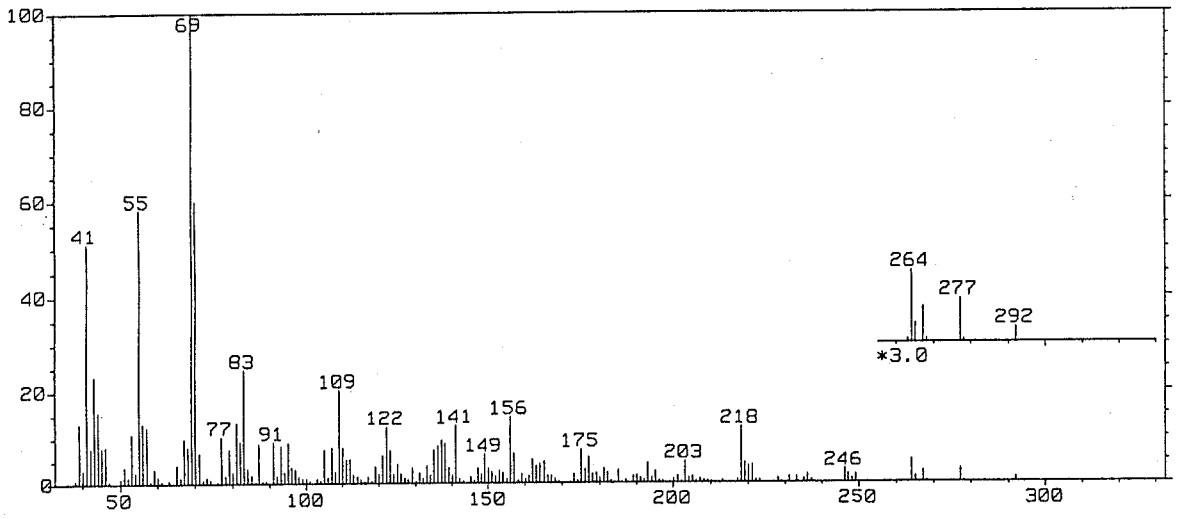

Fig. 3-137 EI-Mass Spectrum of RDA-FA-1

Accordingly, it was confirmed that **2** is also convertible into a ketal derivative through Hock cleavage under heating and acidic conditions, and that this rearrangement is characteristic of the rugosal A-type carotane endoperoxides.

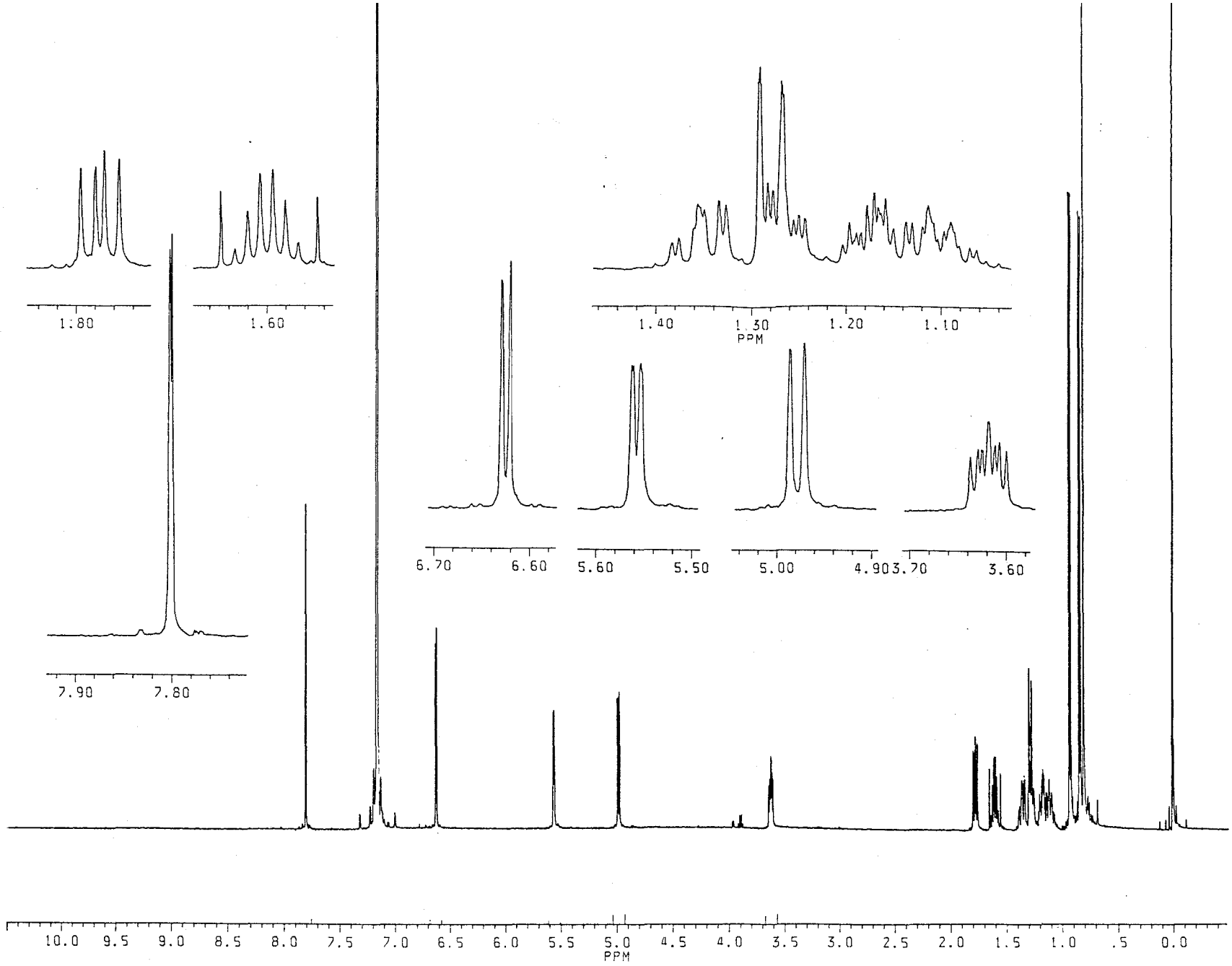

Fig. 3-138 ^{1}H-NMR Spectrum of RDA-FA-2 (500 MHz, in C_6D_6)

Table 3-51 *^{1}H-NMR chemical shift values of RDA-FA-1*

(500 MHz, in C_6D_6, TMS as an int. std.)

δ_H	Coupling	Assignment
5.577	dd *J*= 4.3, 1.0 Hz	C-2-H
6.625	d *J*= 4.3 Hz	C-3-H
4.978	dd *J*= 7.7, 0.7 Hz	C-5-H
1.774	dd *J*= 12.4, 7.7 Hz	C-6-Ha
1.278	dd *J*= 12.4, 0.7 Hz	C-6-Hb
1.356	m	C-8-Ha
1.263	m	C-8-Hb
1.181	m	C-9-Ha
1.101	m	C-9-Hb
3.619	ddd *J*= 9.3, 6.0, 3.8 Hz	C-10-H
1.601	double sept *J*= 6.8, 6.0 Hz	C-11-H
0.923	d *J*= 6.8 Hz	C-12-H_3
0.835	d *J*= 6.8 Hz	C-13-H_3
0.801	s	C-15-H_3
7.800	d *J*= 1.0 Hz	C-2-C<u>H</u>O

Table 3-52 Physicochemical properties of RDA-FA-1 (2d)

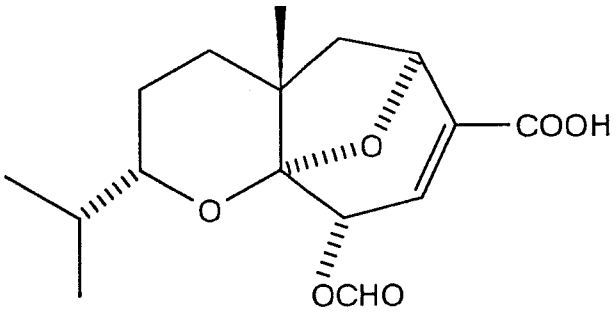

2d

A colorless syrup

Rf: 0.51 (H-EA-F 25:25:1), 0.36 (C-M-F 100:5:2)

Vanillin-H_2SO_4 color: grayish brown

N,*N*-dimethyl-*p*-phenylenediamine sulfate test: negative

FI-MS *m/z* (%): 311 (M^++1, 65), 310 (M^+, 100), 265 (24)

EI-MS *m/z* (%): 292 (M^+-H_2O, 1.1), 277 (3.1), 267 (M^+-COOH, 2.6), 264 (5.1), 246 (M^+-$2H_2O$-CO, 3.1), 218 (12), 203 (4.8), 195 (4.6), 175 (7.5), 156 (15), 141 (13), 122 (12), 109 (20), 83 (25), 81 (13), 77 (10), 70 (60), 69 (100), 67 (10), 57 (12), 56 (13), 55 (58), 53 (11), 44 (16), 43 (23), 41 (51)

^{1}H-NMR data are shown in Table 3-51.

2) Conversion of an Alcohol Derivative RSA-NBH-1

In biochemical conversion of PGH_2 (**82**) into TXA_2 (**83**), a Hock cleavage-like endoperoxide rearrangement occurs. This reaction mechanism was examined using analogs of **85** (See Scheme 3-10, pp. 230) [117]. During the reaction, a C,C single bond cleavage occurred at C(11)-C(12) of the 1,2-dioxacyclopentane ring. Selectivity of the C,C-cleavage is dependent on dihedral angle between the C(11)-O(4)-O(3) and the O(4)-C(11)-C(11α). Between two C,C-bonds which afford the latter plane, the bond taking the smaller dihedral angle actually tends to cleave in **85**. In that case, the distance between two reactive bonds makes its proximity increase, according to Willson and Rucker's model reaction [117].

However, in the reaction of **1** and **2** this speculation is not acceptable, since the dihedral angle among O(1)-O(3) and C(1)-C(10) takes almost 180 ° on the molecular model (Fig. 3-139). The dihedral angle of the carotane peroxides was calculated to be 178.3 ° by MM2 program [120] for RSA-NBH-1 (**1c**), since the calculatio was not applicable to **1** or **2** due to the conjugation system in them. This fact provide a scope for reexamination whether mechanism of the peroxy oxygen migration is a kind of Hock cleavage.

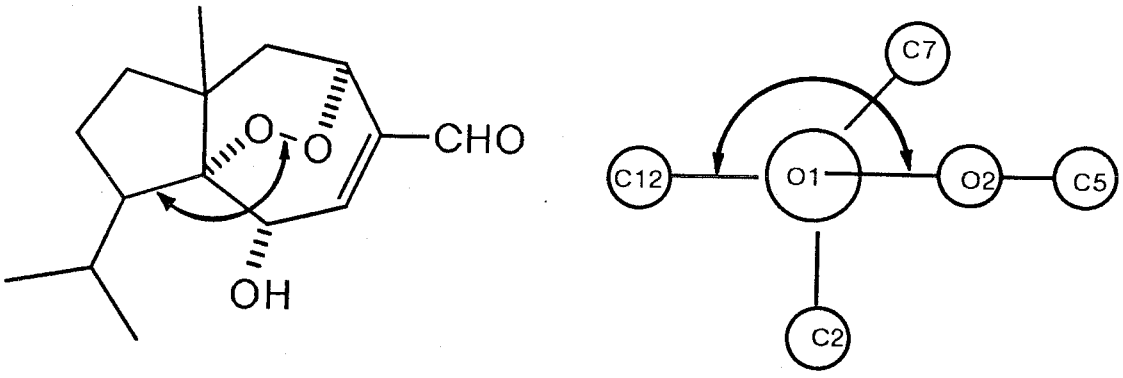

Fig. 3-139 Dihedral Angle between C1-O1-O3 and O1-C1-C10 in the Molecule of RSA-NBH-1 (**1c**): The value was calculated with MM2 program.

Accordingly, derivative **1c** was firstly examined if it was convertible to the corresponding ketal derivative. By the reaction, it was also expected to reveal contribution of the conjugated carbonyl group at C-14 in the conversions of 1 and 2 into the ketal derivatives.

When the Hock cleavage was attempted under several thermal conditions (with equivalent of *p*-TSA, in benzene at 80 °C and 60 °C for 0.5~3 hr), RSA-NBH-1 (**1c**) was completely decomposed to hundreds of compounds. Next, the reaction was carried out at room temperature. When a mixture of **1c** (10.5 mg) and *p*-TSA (8.5 mg) was stirred in 2.5 ml of benzene for 3 hr at room temperature, only one product was detected at *Rf* 0.07 in *n*-hexane-EtOAc 1:1 (Fig. 3-140). Partitionated with 5 % aq. $NaHCO_3$ and EtOAc, from the latter 2.9 mg of the product RSA-NBH-TSA was consequently obtained as colorless needles in a yield of 28 %, together with 6.2 mg of unreacted material (59 %).

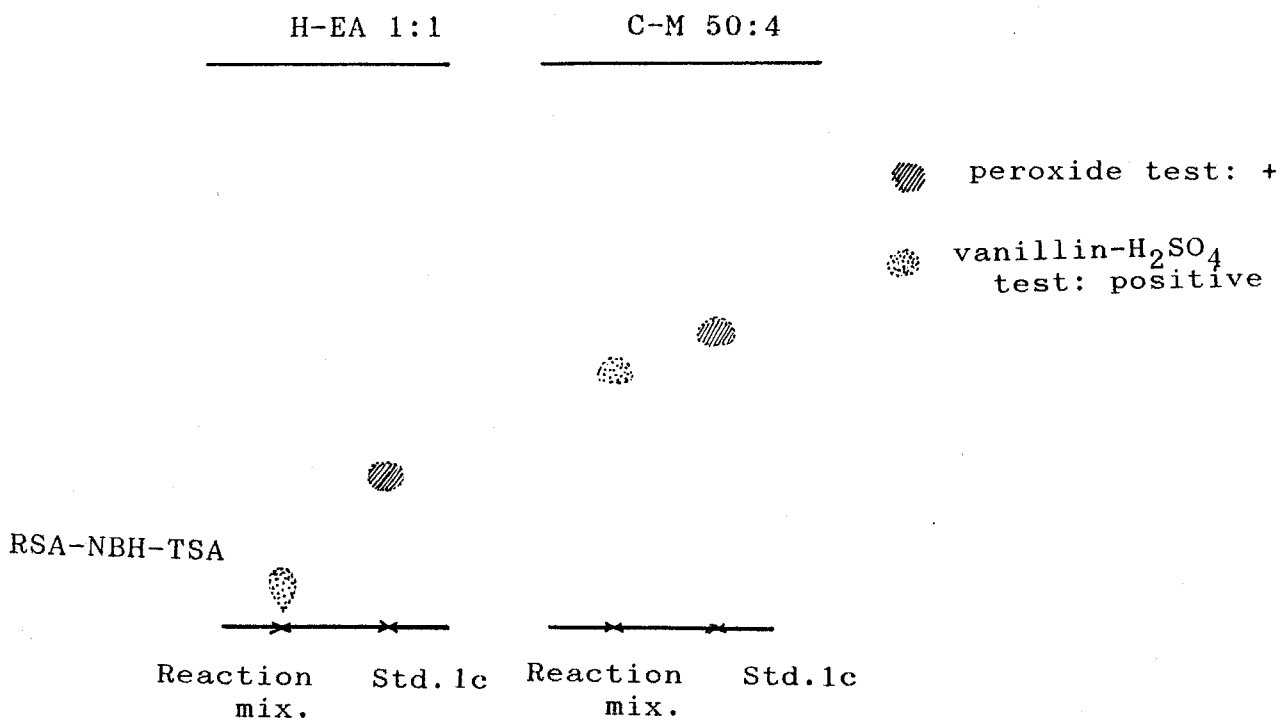

Fig. 3-140 TL Chromatograms of Reaction Product Obtained by Acid-catalyzed Endoperoxide Conversion of Alcohol Derivative, RSA-NBH-1 (**1c**)

RSA-NBH-TSA showing M^+ 268 (100%) in FD-MS (Fig. 3-141, *cf.* EI-MS in Fig. 3-142) gave its ^{1}H-NMR spectrum characteristic of the ketal derivatives (Fig. 3-143 and Table 3-53). A double-double doublet methine signal at δ_H 3.709 was well indicative of the structure **1n**. ^{13}C-NMR spectrum of RSA-NBH-TSA also showed a good correspondence with RSA-TSA (**1i**) or RDA-FA-2 (**2c**), except the C-14 carbon (Fig. 3-144 and Table 3-54). Furthermore, chemical conversion of **1i** into **1n** was successufully carried out (Scheme 3-12). When 3.2 mg of **1i** was reduced with excess amounts of $NaBH_4$ in EtOH/benzene (16.7 mg in 1.5 ml/0.5 ml), 1.0 mg of colorless column (RSA-TSA-NBH, in a 33 % yield*) indistinguishable from **1n** in TLC and ^{1}H-NMR (Fig. 3-145, 146 and Table 3-56) was obtained. Accordingly, the structure of RSA-NBH-TSA was proved as **1n**. ^{1}H- and ^{13}C-NMR spectra of **1n** certainly indicated that the derivative was a stereo-chemically pure compound. Compound **1n** is, like **2c**, also considered to have the same configuration as that of **1i**.

---

* The reaction mixture was diluted with EtOAc/H_2O, and the organic layer was dried and then concentrated. The concentrate was stored in a refrigerator, gave some colorless columns, and the crystallines were washed with *n*-hexane/EtOAc to give 1.0 mg of pure compound.

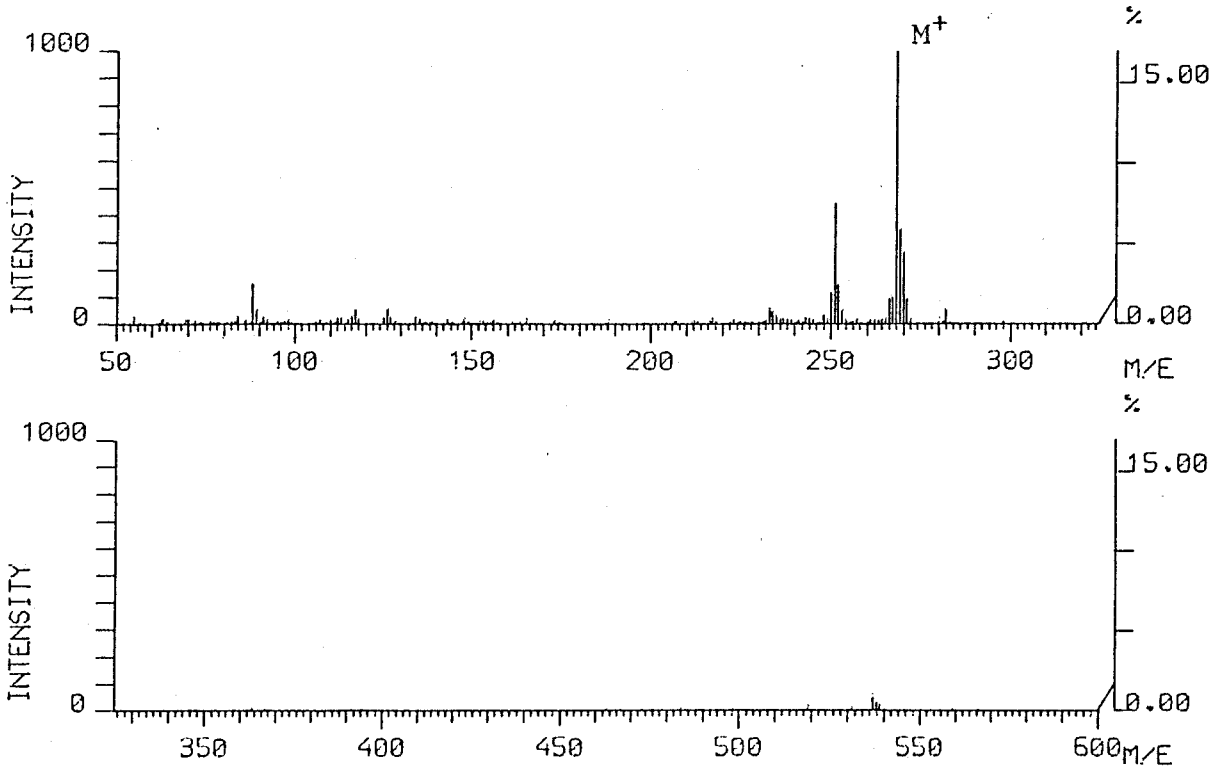

Fig. 3-141 FD-Mass Spectrum of RSA-NBH-TSA

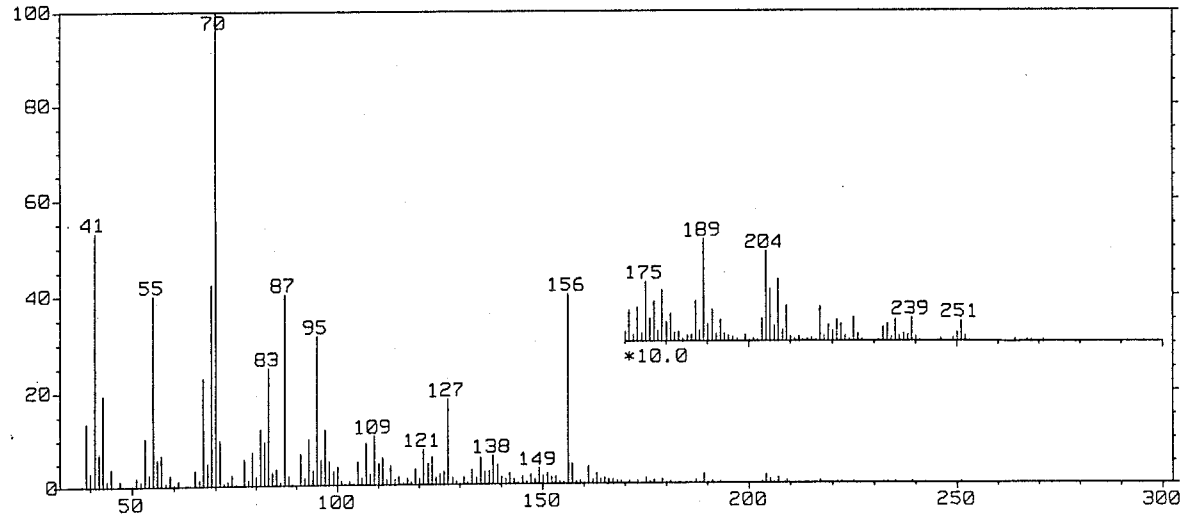

Fig. 3-142 EI-Mass Spectrum of RSA-NBH-TSA

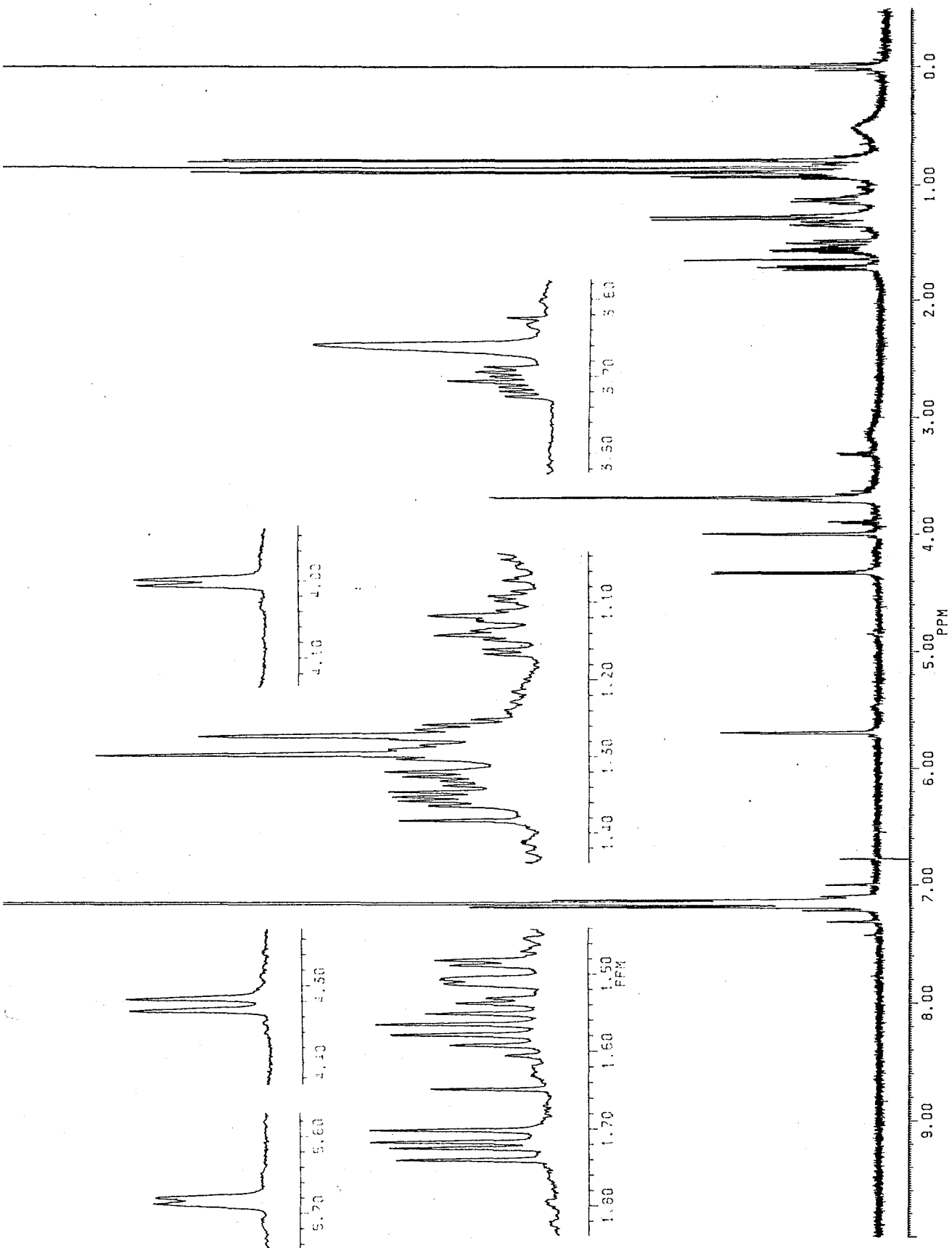

Fig. 3-143 ^{1}H-NMR Spectrum of RSA-NBH-TSA (500 MHz, in C_6D_6)

Table 3-53 ^{1}*H-NMR chemical shift values of RSA-NBH-TSA*

(270 MHz, in C_6D_6*, TMS as an int. std.)

δ_H	*J*(Hz)	Assignment
3.996	br. d (4.4)	C-2-H
5.689	br. d (4.4)	C-3-H
4.324	br. d (7.7)	C-5-H
1.718	dd (11.8, 7.5)	C-6-Ha
1.285	dd (11.8, 0.8)	C-6-Hb
1.504	ddd (13.2, 11.9, 3.3)	C-8-Ha
1.341	ddd (13.2, 5.9, 3.3)	C-8-Hb
1.280	m	C-9-Ha
1.080	m	C-9-Hb
3.705	ddd (9.3, 6.3, 3.4)	C-10-H
1.569	double sept (6.8, 6.7)	C-11-H
0.885	d (6.8)	C-12-H_3
0.786	d (6.8)	C-13-H_3
3.680	br. s	C-14-H_2
0.850	s	C-15-H_3

* C-2-OH was undetectable.

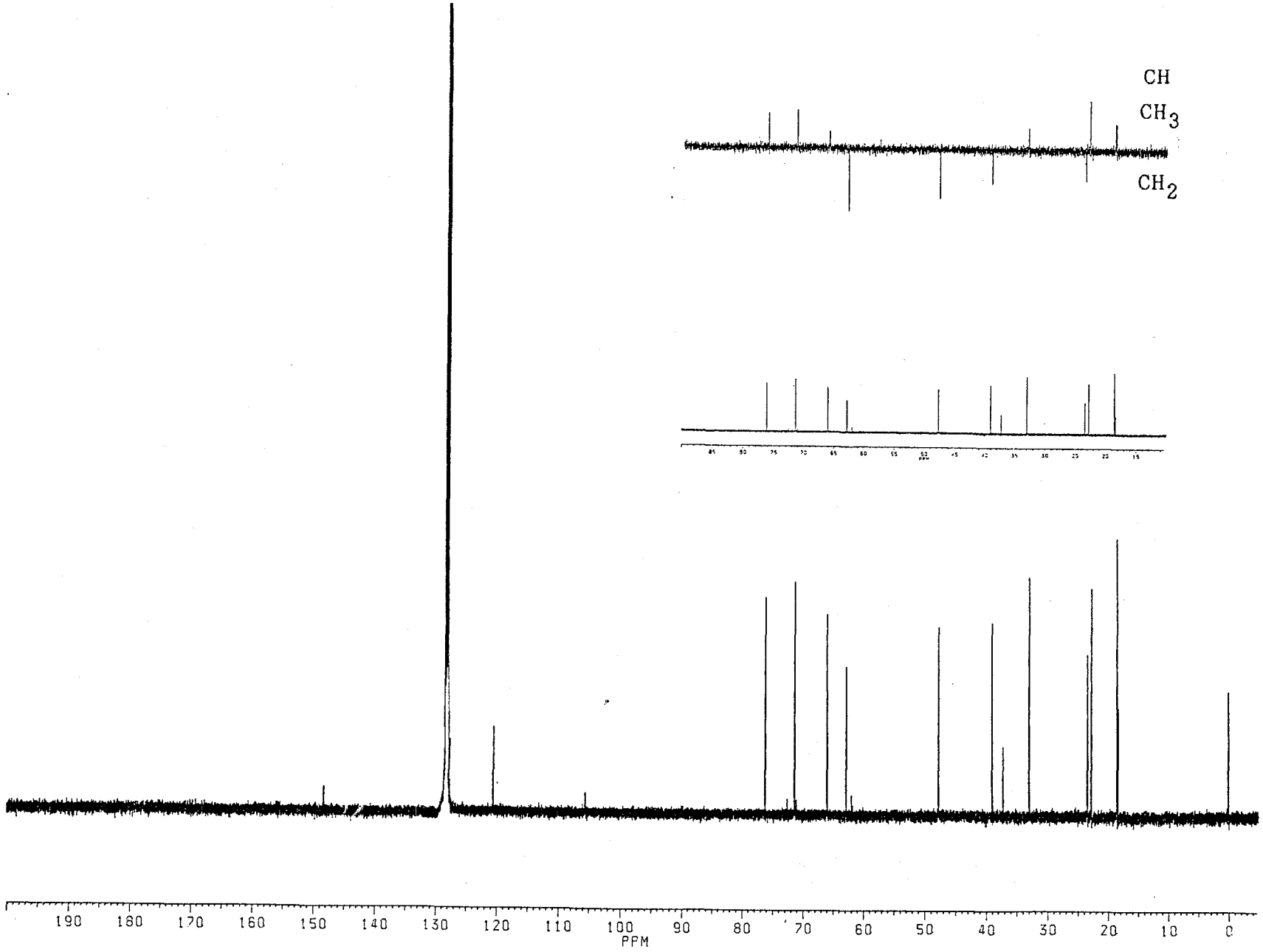

Fig. 3-144 ^{13}C-NMR Spectrum of RSA-NBH-TSA (125 MHz, in C_6D_6, COM and DEPT)

Table 3-54 *^{13}C-NMR chemical shift values of RSA-NBH-TSA*

(125 MHz, in C_6D_6, TMS as an int. std.)

δ_C	δ_H	Assignment
105.6	C	C-1
71.3	CH	C-2
120.5	CH	C-4
148.3	C	C-5
65.9	CH	C-5
47.6	CH_2	C-6
37.2	C	C-7
39.0	CH_2	C-8
23.3	CH_2	C-9
76.1	CH	C-10
32.9	CH	C-11
18.5	CH_3	C-12
18.3	CH_3	C-13
62.8	CH_2	C-14
22.7	CH_3	C-15

Table 3-55 Physicochemical properties of RSA-NBH-TSA (1n)

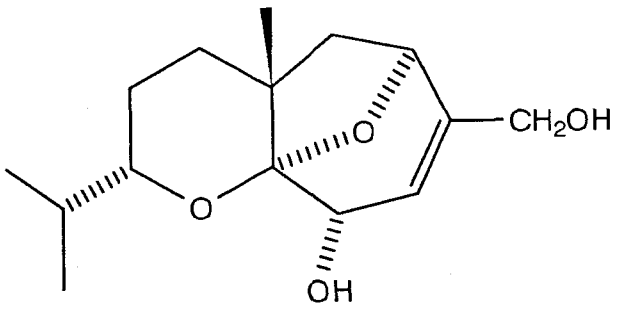

1n

Colorless column, mp 131-132 °C

Rf: 0.45 (C-M 50:4, *cf.* **1c**; 0.52), 0.07 (H-EA 1:1, *cf.* **1c**; 0.27)

Vanillin-H_2SO_4 color: dark yellow

FD-MS *m/z* (%): 268 (M^+, 100), 251 (45).

EI-MS *m/z* (%): 251 (0.4), 239 (0.5), 235 (0.5), 225 (0.5), 217 (0.7), 209 (0.7), 207 (1.3), 204 (1.9), 189 (2.2), 156 (40), 138 (6.4), 127 (18), 109 (11), 95 (32), 87 (40), 83 (25), 70 (100), 69 (42), 67 (23), 55 (40), 43 (19), 41 (53).

^1H- and ^{13}C-NMR data are shown in Tables 3-53 and 3-54, respectively.

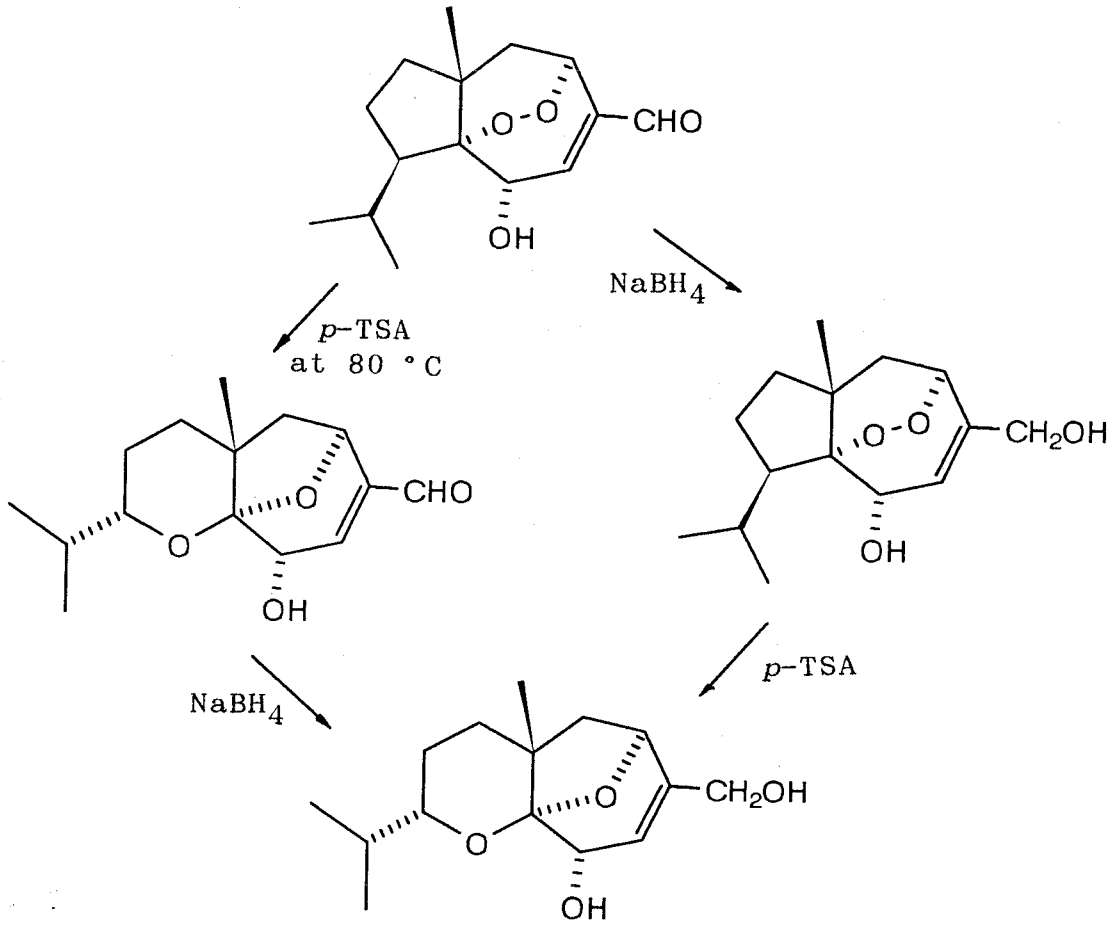

Scheme 3-12 Conversion pathway to compound 1n, and structure relation between RSA-NBH-TSA (1i) and RSA-TSA (1e)

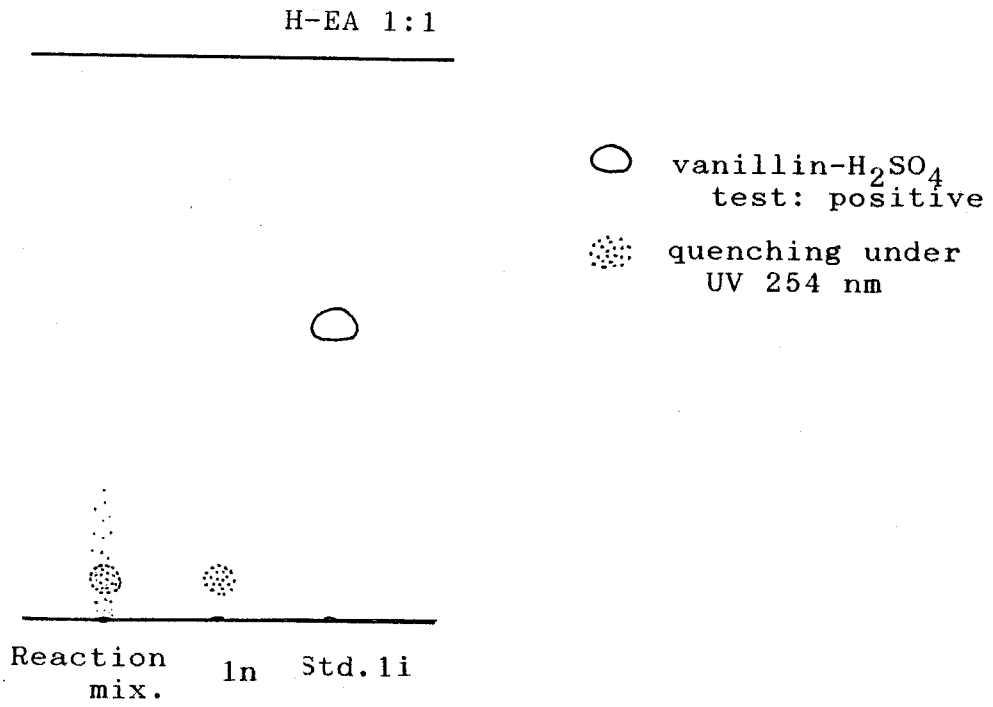

Fig. 3-145 TL Chromatogram of RSA-TSA (1i) Reduction Product Obtained by Treatment with $NaBH_4$

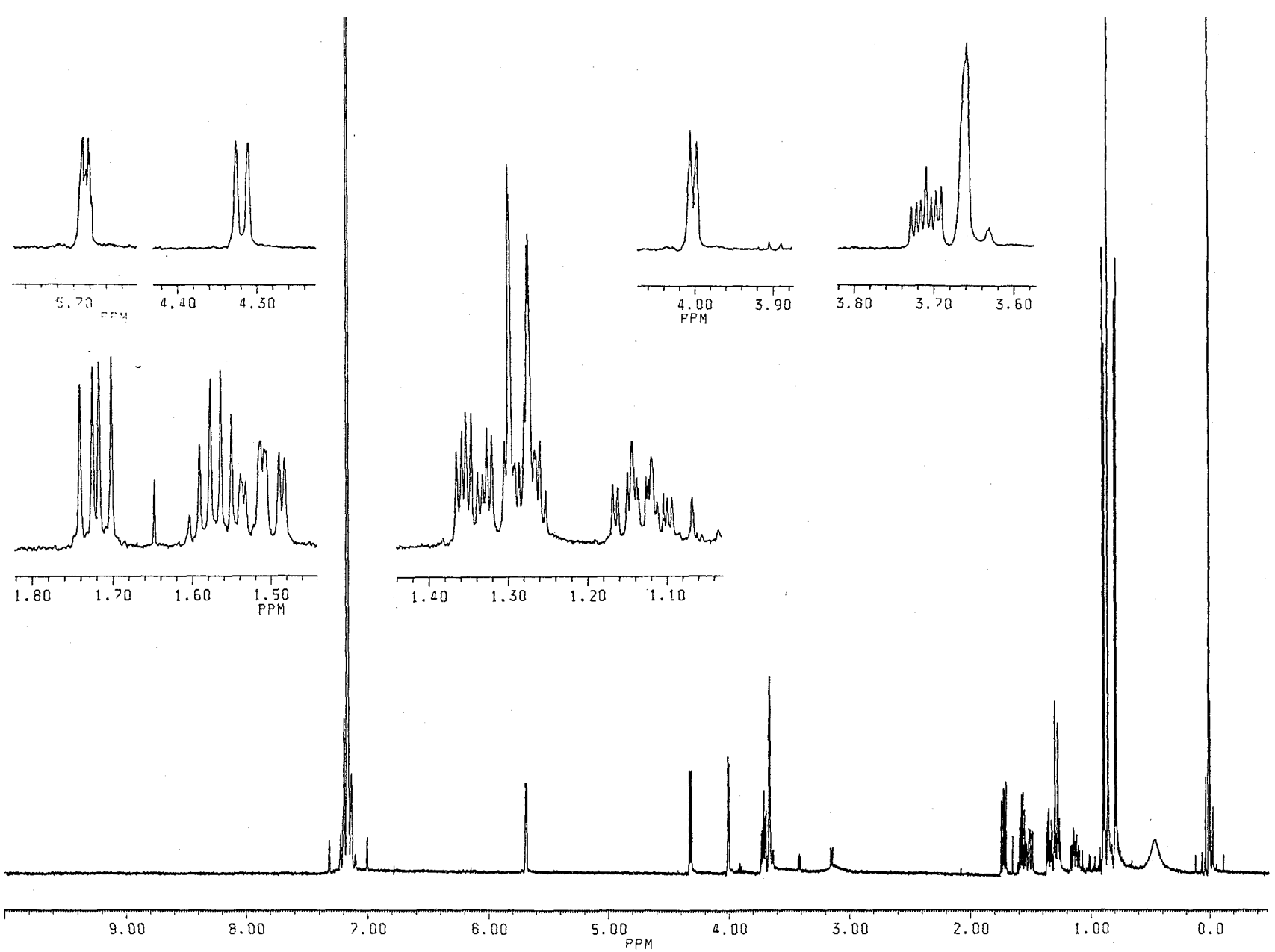

Fig. 3-146 ^{1}H-NMR Spectrum of RSA-NBH-TSA (500 MHz, in C_6D_6)

Table 3-56 ^{1}H-NMR chemical shift values of RSA-TSA-NBH

(270 MHz, in C_6D_6*, TMS as an int. std.)

δ_H	*J*(Hz)	Assignment
4.001	br. d (4.3)	C-2-H
5.683	br. d (4.3)	C-3-H
4.317	br. d (7.6)	C-5-H
1.720	dd (11.8, 7.6)	C-6-Ha
1.285	dd (11.8, 0.8)	C-6-Hb
1.509	ddd (13.2, 11.9, 3.4)	C-8-Ha
1.341	ddd (13.2, 5.9, 3.3)	C-8-Hb
1.280	m	C-9-Ha
1.080	m	C-9-Hb
3.709	ddd (9.3, 6.3, 3.4)	C-10-H
1.569	double sept (6.8, 6.3)	C-11-H
0.885	d (6.8)	C-12-H_3
0.786	d (6.8)	C-13-H_3
3.659	br. s	C-14-H_2
0.850	s	C-15-H_3

* C-2-OH was undetectable.

*Table 3-57 Physicochemical properties of RSA-TSA-NBH (**1n**= RSA-NBH-TSA)*

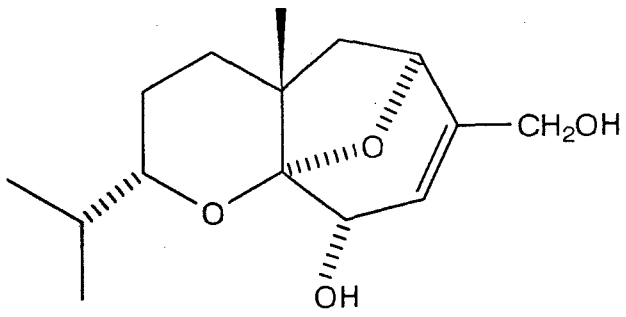

1n

Colorless column, mp 132-133 °C

Rf: 0.08 (H-EA 1:1, *cf.* 0.52 of **1i**)

Vanillin-H_2SO_4 color: dark yellow

^{1}H-NMR data are shown in Table 3-56.

3) Reaction Mechanism and Chemical Aspects

The dihedral angle 178.3 ° showed that C-1, C-10, O-1 and O-3 atoms exist almost on the same plane to take antiperiplanar conformation between O(1)-O(3) and C(1)-C(10). As well known in dehydration reactions, antiperiplanar conformation takes an advantage for electron transfer, due to the electron uniformity and excitation on the planar bonds. In **1c**, and possibly in 1 and 2 also, the activated bonds takes an antiperiplanar form (Fig. 3-147). Consequently, it was considered that stereostructure of the carotane peroxides causes the cleavage of C,C-bond between the C-1 and the C-10 during the Hock cleavage reaction.

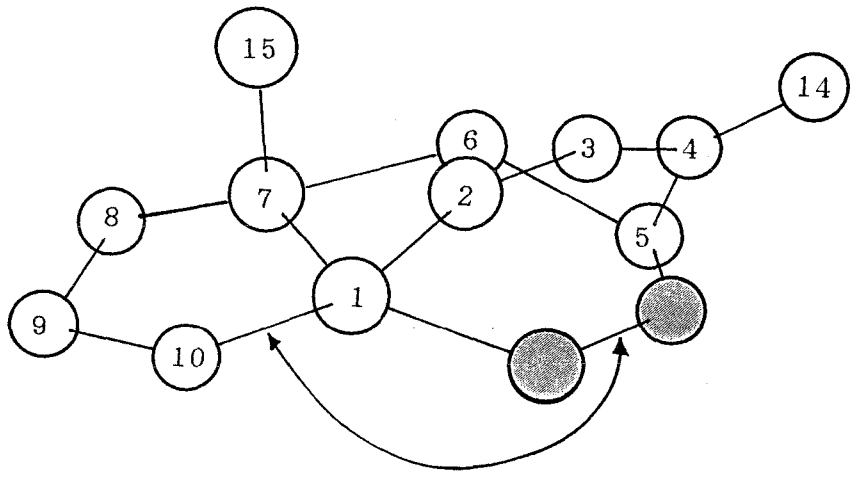

Fig. 3-147 Antiperiplanar Conformation of Two Active Bond

On the other hand, it was also suggested that the conjugation system of 1 or 2 does not contribute to the endoperoxide cleavage but rather makes them more inactive under mild reaction conditions. The result of the acid-catalyzed reaction in **1c** certainly indicates some effect of the conjugation system on the stability of 1 and 2.

In the Hock cleavage of the carotane peroxides, stereochemical inversion at reformed C-10 chiral carbon was also observed. Stereo-selectivity in a product of Hock cleavage is sometimes observed in ketal derivatives. The most examined case is probably

conversion of PGH_2 (**82**) into TXA_2 (**83**). In this case, the reformed chiral carbon at C-12 is, on the contrary, preserved its stereochemistry (See Scheme 3-16, pp. 281).

However, regarding the chemical conversions of those carotane peroxides as a similar reaction with that of **82** never gives any resolution about the C-10 stereo-inversion, since formation of **83** is catalyzed by the enzyme (thromboxane synthetase). Any stereoselectivity in an enzymatic reaction products is usually acceptable to organic chemists without any doubt even though a theoretically enough explanation was not afforded. Since the rearrangement of those carotane peroxides was pure chemical reaction, stereoselectivity at C-10 of the rearranged ketal derivatives should be explained only by transient state on a basis of reaction mechanism.

The intermediary state was therefore considered to be the key point. As an intermediary state during the reaction have already been proposed in some Hock cleavages of endoperoxides (See Scheme 3-8) [121], an intermediate from the carotane peroxide to the ketal was also depicted as shown in Scheme 3-13 and -14 in the light of the proposal by Ruchardt *et al.* [111] and C-10 chirality inversion. According to these two possible pathways, each intermediate was proposed (A and B). In the case of the pathway of **A**, the intermediate should take less hindered stereo-structure at C-10 carbocation. On the other hand, in the other pathway for B, chirality inversion of the reformed C-10 carbon should occur by attack of the oxide radical (on C-1) to the C-10 chiral carbon from the side of C-10-H. Accordingly, it was presumed that the theoretical intermediary state either A or B provide the stereoinversion of chirality at C-10 carbon during the Hock cleavage of carotane peroxides.

Although **83** is produced by an enzymatic reaction, it may be possible to consider that the stereochemical selectivity of **65** is not for a conformation of reactive site on the enzyme but only due to its intermediary form in the reaction.

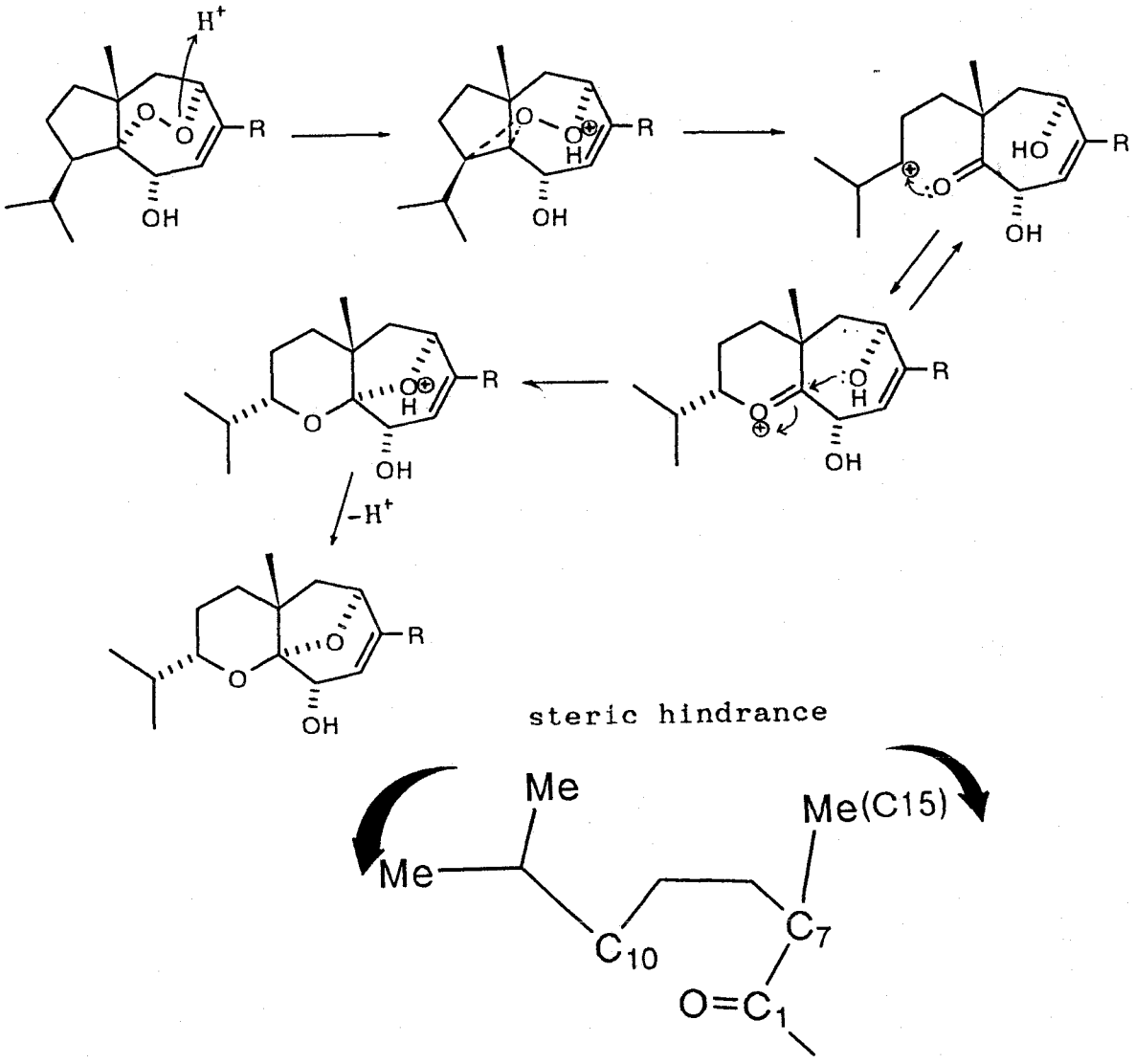

Scheme 3-13 **Possible conversion pathway of acid-catalyzed endoperoxide rearrangement on carotane peroxides:** Carbocation on C-10 results in C-O bond formation with carbonyl group on C-1, in which reaction stereoselectivity at C-10 is considered to be due to a steric hindrance between the isopropyl group and C-15 methyl group.

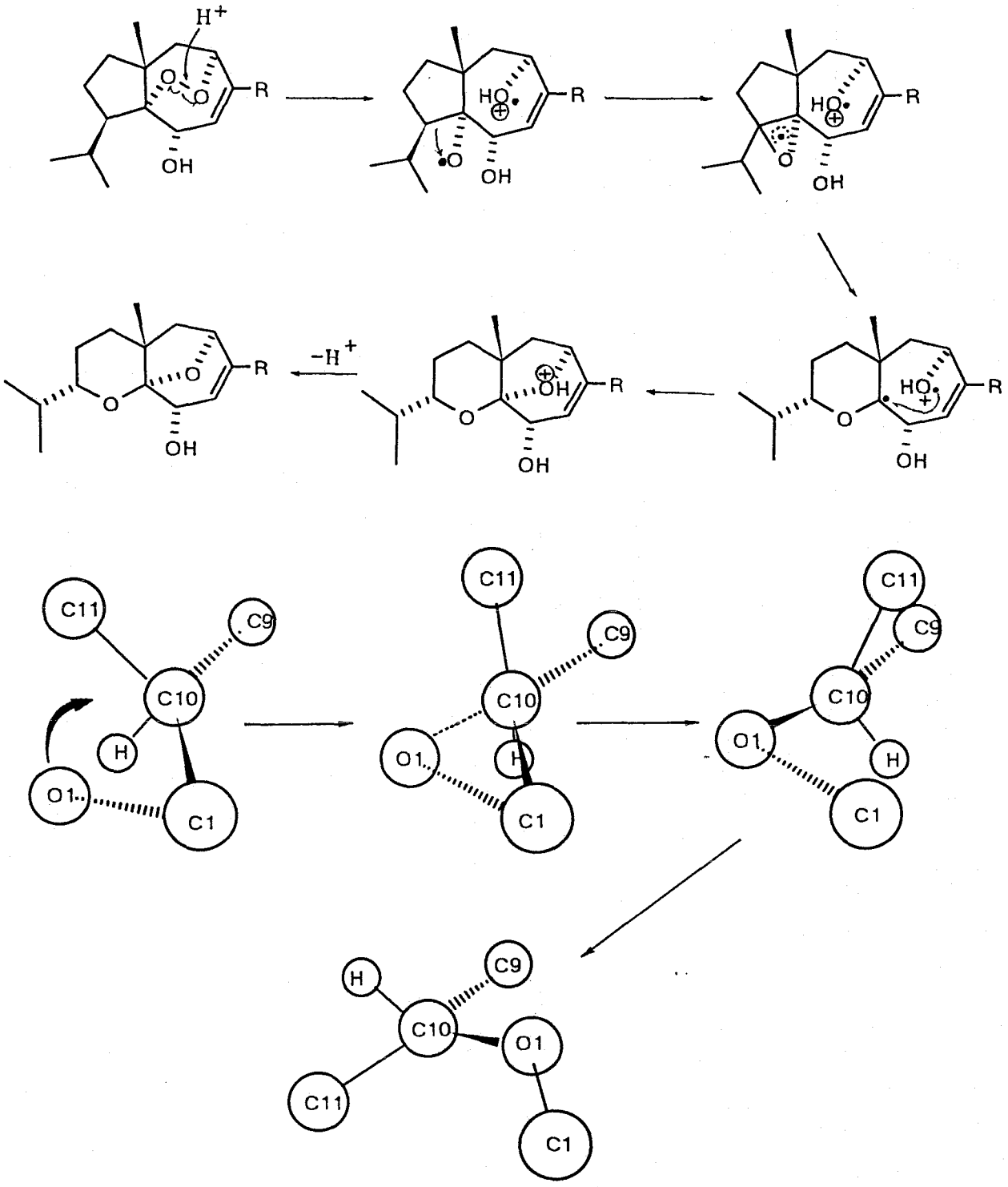

Scheme 3-14 Another possible conversion pathway of acid-catalyzed endoperoxide rearrangement on carotane peroxides: An oxide radical attacks C-10 from the proton side to result in chiral inversion of C-10.

3-4-3 Base-catalyzed Conversion of an Endoperoxide into a Hemiacetal

1) Conversion of Rugosic Acid A

In this reaction, base-catalyzed proton abstraction occurs on a hydrogen bearing carbon attached to the peroxide linkage [118, 119]. As the result of the proton abstraction, more stable carbonyl group and oxide anion ($-O^{\ominus}$) are concertedly formed *via* peroxy-bond cleavage (β-elimination). On the other hand, when rugosal A (**1**) was treated with a base, the carotane peroxide was uniquely converted into a hemiacetal derivative (**1g**) as described above.

Since the carboxyl group of **2** is more stable than the aldehyde group of **1**, base-catalyzed rearrangement of the endoperoxide is able to examine with a strong base. As shown in Scheme 3-19, **2** was treated with KOH dissolved in MeOH. By this reaction, 77.7 mg of colorless needles negative to the endoperoxide reagent was obtained from 101.8 mg of **2** in a 76 % yield (*Rf* 0.18 in C-M-F 50:2.5:1, Fig. 3-148). This derivative, RDA-KOH showed its molecular weight 282 in FD-MS [*m/z* 283 (M^++1, 100 %)] (Fig. 3-149). In EI-MS, the dehydration fragment was observed at *m/z* 264 (1.5 %) (Fig. 3-150). When ^{1}H-NMR spectrum of RDA-KOH was taken in acetone-d_6, a pair of isolated methylene protons characteristic of the hemiacetal derivative was observed at δ_H 2.164 and 1.970 (each 1H, d, *J*= 11.9 Hz) associated with disappearance of C-5 methine proton (Fig. 3-151). Including these signals, the signal patterns showed a good accordance with those of a hemiacetal derivative of **1** (**1f**) (Table 3-58). Accordingly, the structure **2e** was proposed for RDA-KOH.

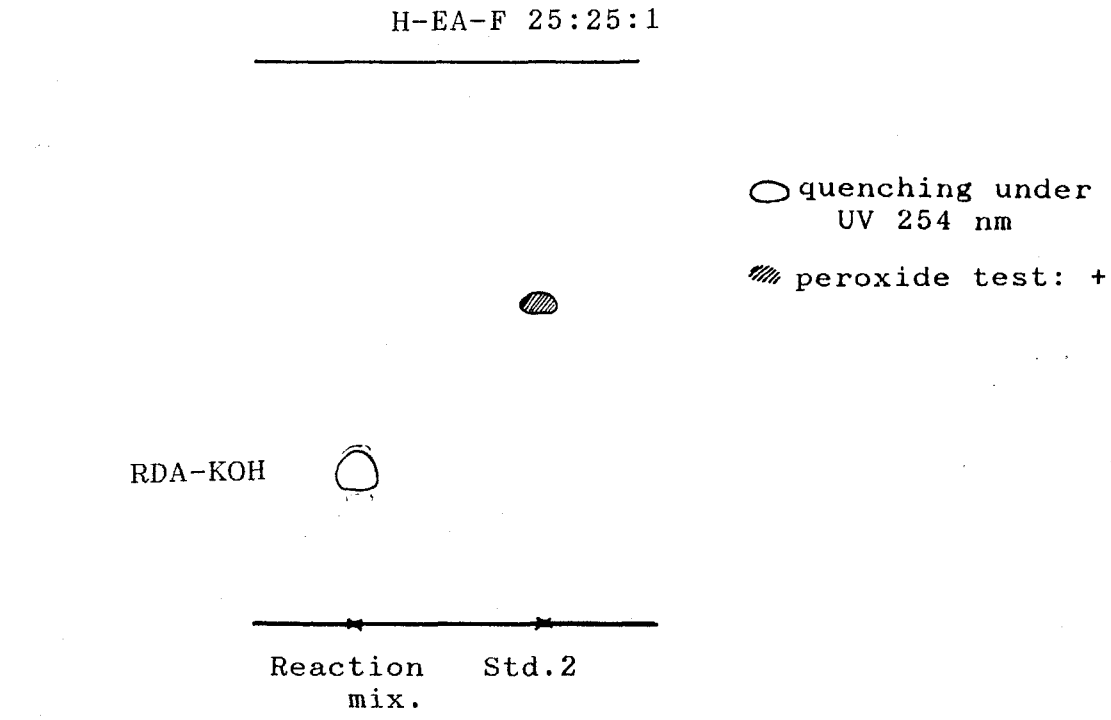

Fig. 3-148 TL Chromatogram of Reaction Product Obtained by Base-catalyzed Conversion of Rugosic Acid A

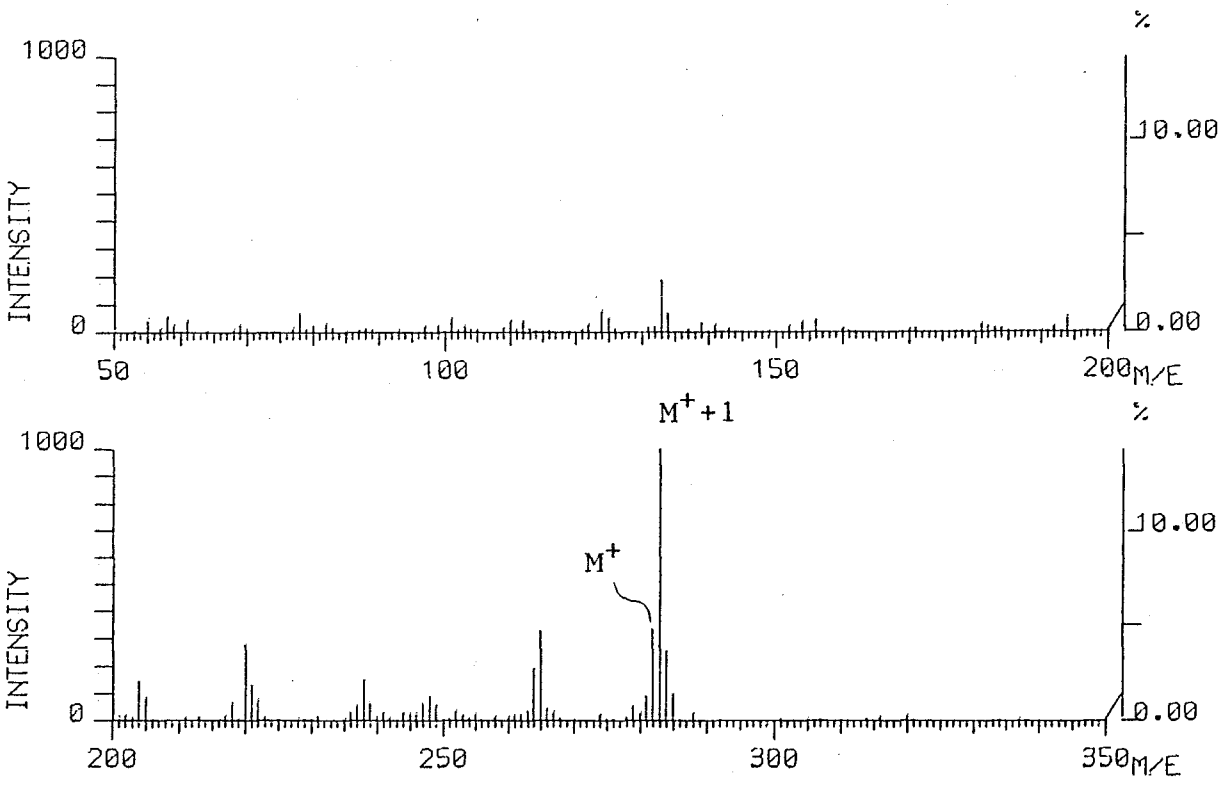

Fig. 3-149 FD-Mass Spectrum of RDA-KOH

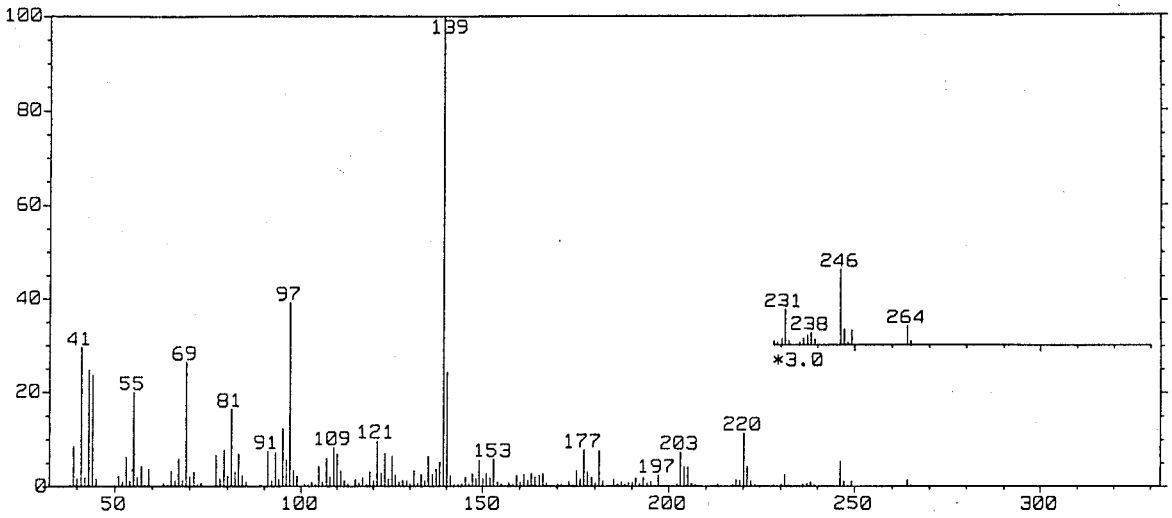

Fig. 3-150 EI-Mass Spectrum of RDA-KOH

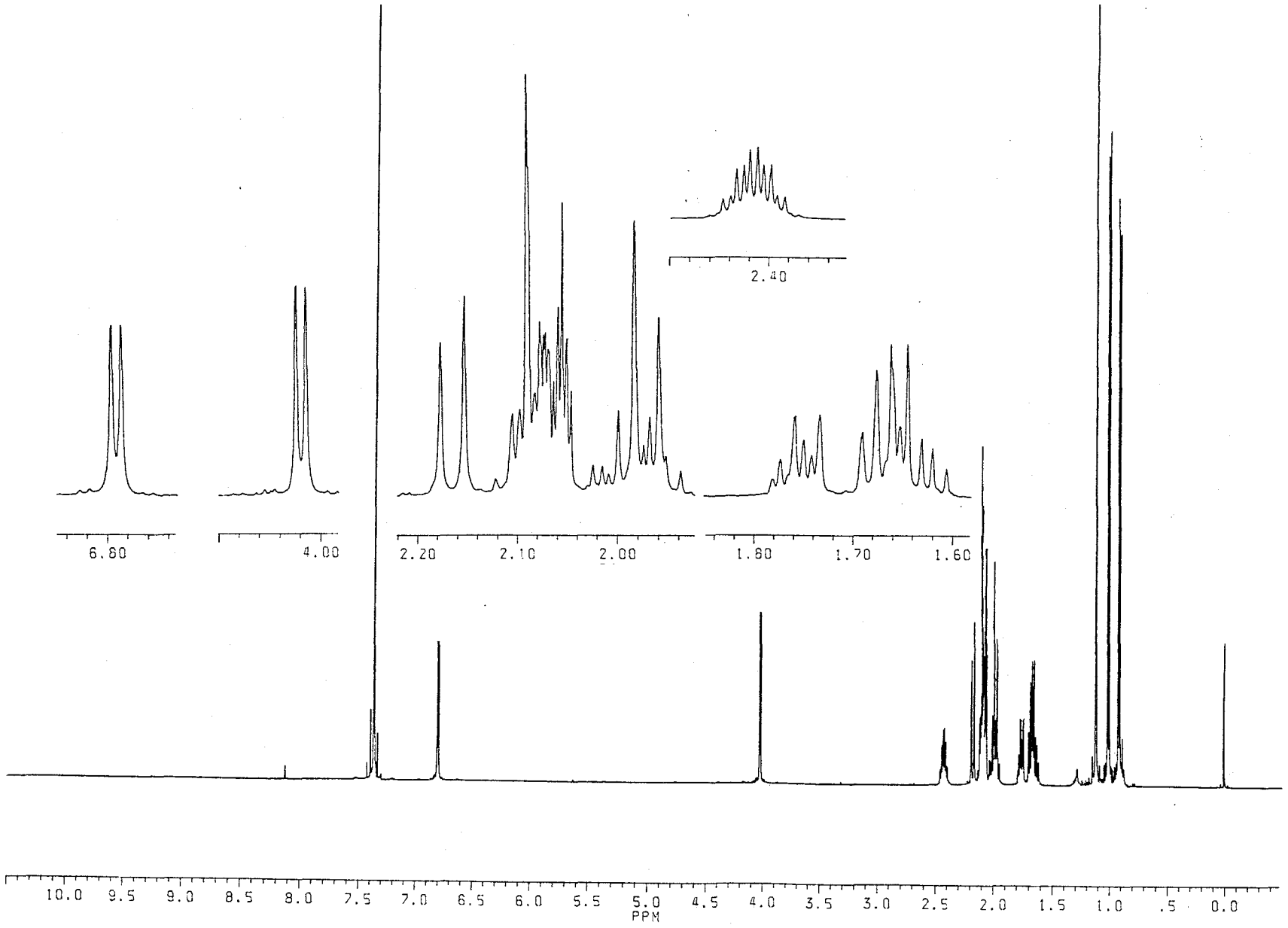

Fig. 3-151 ^{1}H-NMR Spectrum of RDA-KOH (500 MHz, in acetone-d_6)

Table 3-58 ^{1}H*-NMR chemical shift values of RDA-KOH*

(500 MHz, in acetone-d_6, TMS as an int. std.)

δ_H		Coupling	Assignment
4.018	1H	d *J*= 3.9 Hz	C-2-H
6.790	1H	d *J*= 3.9 Hz	C-3-H
2.164	1H	d *J*= 11.9 Hz	C-6-Ha
1.970	1H	d *J*= 11.9 Hz	C-6-Hb
1.754	1H	m	C-8-Ha
1.668	1H	dd *J*= 15.7 and 8.4 Hz	C-8-Hb
1.97 (approx.)	1H	m	C-9-Ha
1.636	1H	ddd *J*= 12.6, 11.0 and 7.2 Hz	C-9-Hb
2.10 (approx.)	1H	overlapped *J*= 3.9 Hz	C-10-H
2.414	1H	double sept *J*= 6.9 and 3.9 Hz	C-11-H
1.002	3H	d *J*= 6.9 Hz	C-12-H_3
0.910	3H	d *J*= 6.9 Hz	C-13-H_3
1.110	3H	s	C-15-H_3

Exchangeable protons were all undetectable.

To measure ^{1}H-NMR in C_6C_6, RDA-KOH was methylated by CH_2N_2, and the methylation product (RDA-KOH-ME, **2f**, quantitatively, the TLC and EI-MS are shown in Fig. 3-152 and 153, respectively) showed a good resolution of the signals in the ^{1}H-NMR spectrum (Fig. 3-154). As shown in Table 3-59 all of the protons were assigned by decoupling experiments (Fig. 3-155) to prove the structure **2f**. A singlet methyl signal attributable to -COOC$\underline{H}_3$ was reasonably detected at δ_H 3.341.

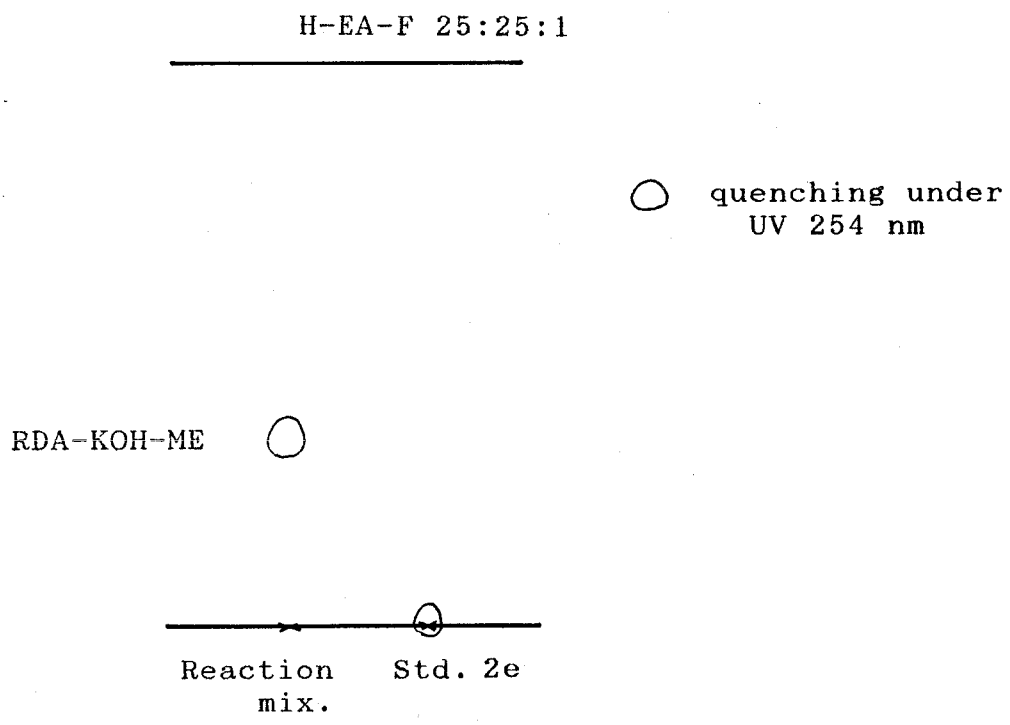

Fig. 3-152 TL Chromatogram of Methylated RDA-KOH Obtained by Treatment of RDA-KOH (**2e**) with CH_2N_2

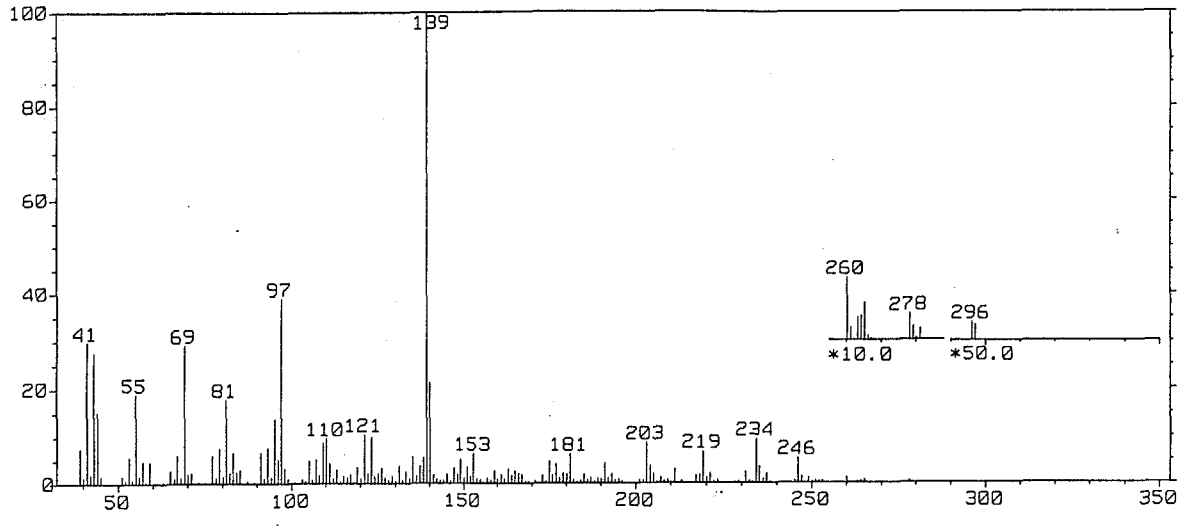

Fig. 3-153 EI-Mass Spectrum of RDA-KOH-ME

Accordingly, the proposed structure **2e** for RDA-KOH was further confirmed. As expected, conversion of the carotane peroxide with a strong base was successfully undergone. This fact proved that conversion of rugosal A (1) into RSA-AC-2 (**1b**) or RSA-PY (**1f**) occurred as the result of base-catalyzed endoperoxide rearrangement. While RDA-KOH (**2e**) was elucidated its structure, a derivative yielded from rugosic acid A (2) during $LiAlH_4$ reduction in MeOH was identified as **2e**. This fact indicated that **2** was transformed into **2e** by catalytic action of $MeO^{\ominus}$ ($LiAlH_3$/MeOH).

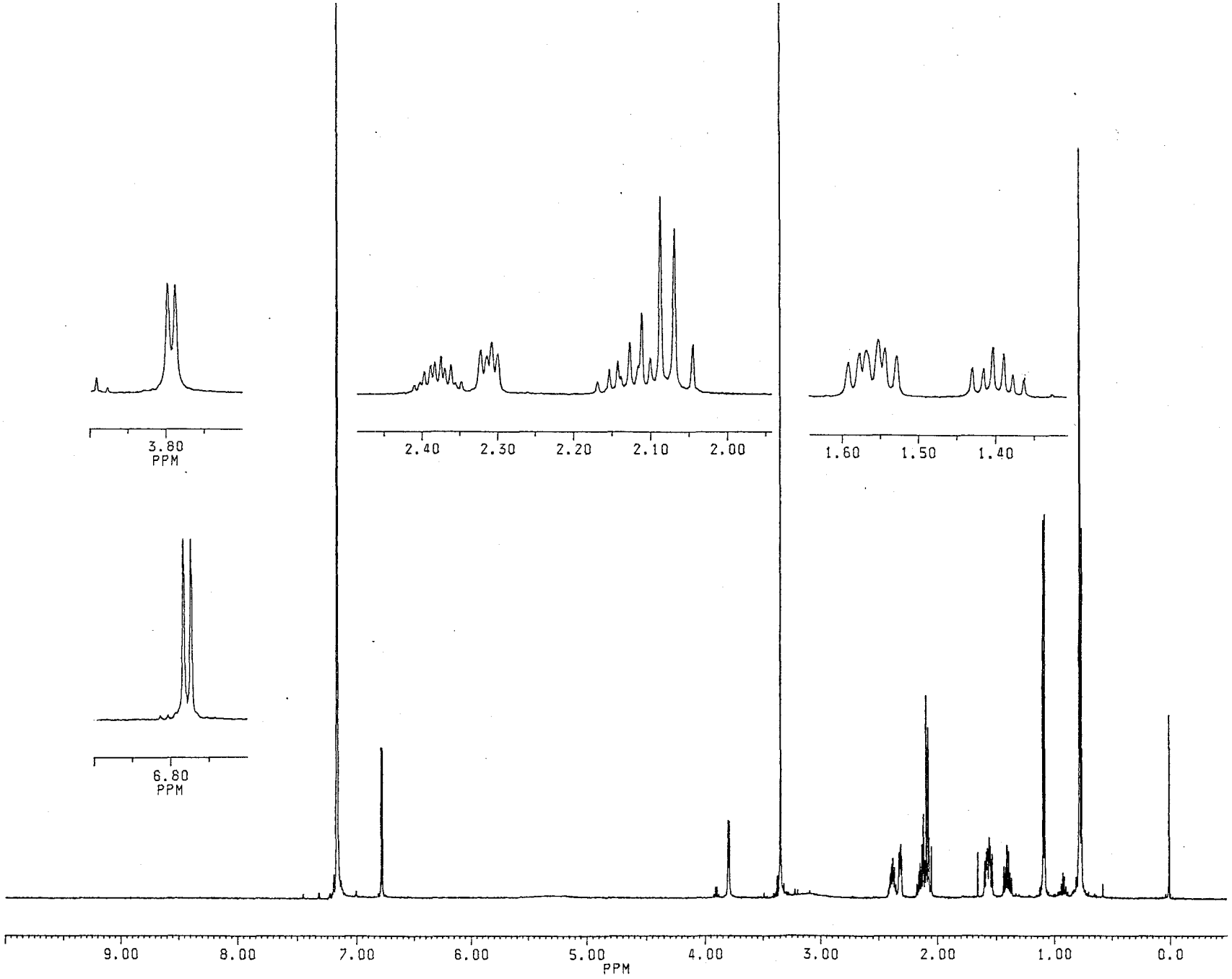

Fig. 3-154 ^{1}H-NMR Spectrum of RDA-KOH-ME (500 MHz, in C_6D_6)

Table 3-59 *^{1}H-NMR chemical shift values of RDA-KOH-ME*

(500 MHz, in C_6D_6, TMS as an int. std.)

δ_H	Coupling	Assignment
3.792	d *J*= 4.9 Hz	C-2-H
6.777	d *J*= 4.9 Hz	C-3-H
2.099	d *J*= 12.1 Hz	C-6-Ha
2.057	d *J*= 12.1 Hz	C-6-Hb
1.573	br. dd *J*= 11.7, 7.2 Hz	C-8-Ha
1.548	br. dd *J*= 11.7, 7.3 Hz	C-8-Hb
2.110	m	C-9-Ha
1.378	ddd *J*= 13.1, 13,1, 7.2, 7.2 Hz	C-9-Hb
2.311	dd *J*= 7.3, 4.0 Hz	C-10-H
2.378	double sept *J*= 6.9, 4.0 Hz	C-11-H
1.083	d *J*= 6.9 Hz	C-12-H_3
0.762	d *J*= 6.9 Hz	C-13-H_3
0.722	s	C-15-H_3
3.341	s	C-14'-H_3

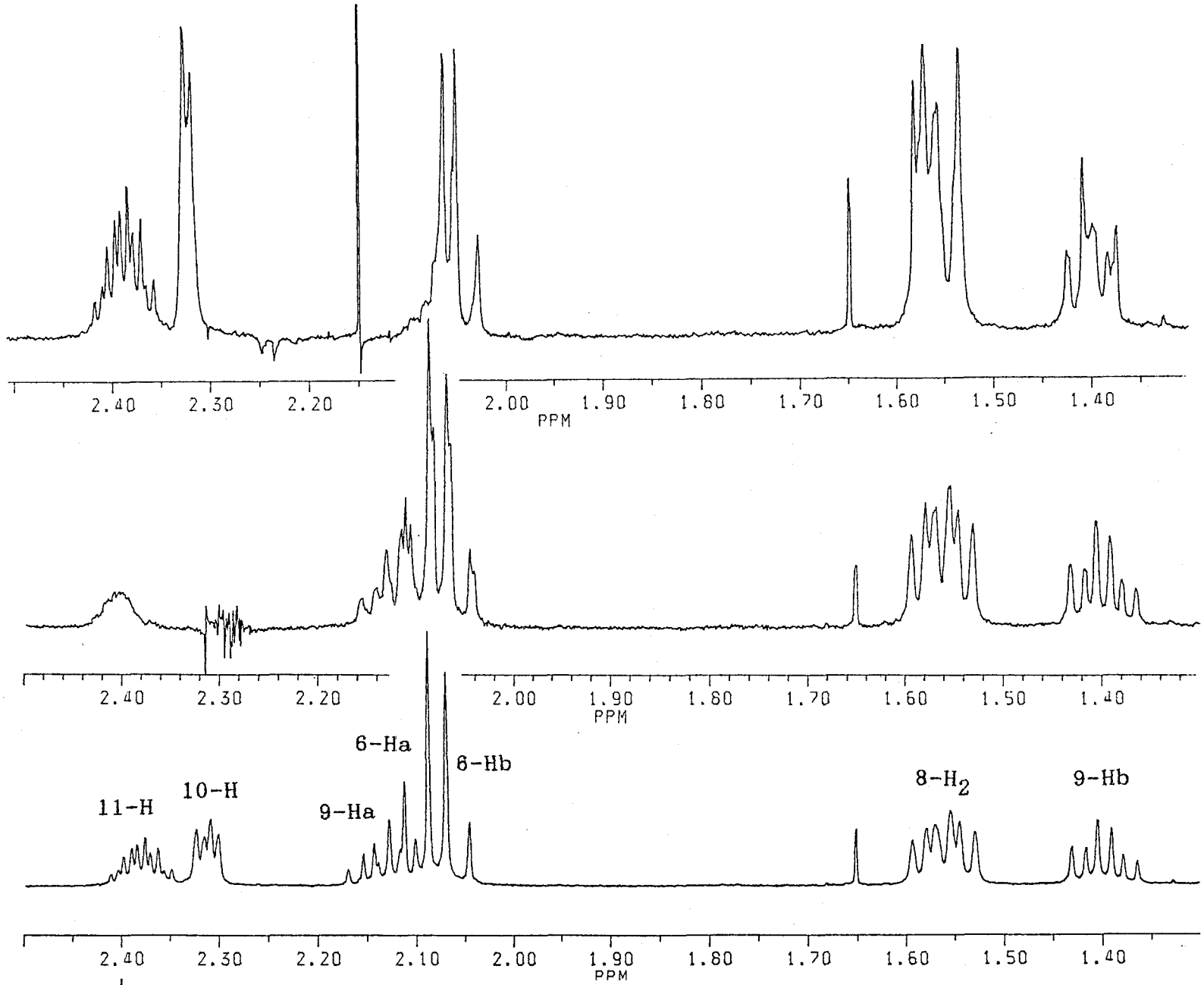

Fig. 3-155 ^{1}H-NMR Spectrum of Decoupling Experiment on RDA-KOH-ME: Proton sequences of the product were unambiguously confirmed.

Table 3-60 Physicochemical properties of RDA-KOH (2e)

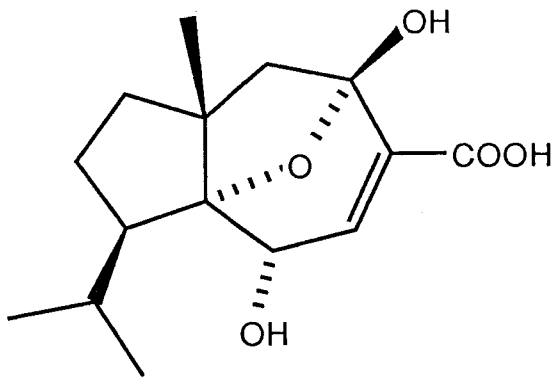

2e

Colorless needles from acetone, mp. 138-140°C (melted and crysterized at 73-74°C)

Rf: 0.27 (H-EA-F 25:25:1), 0.18 (C-M-F 50:5:1)

Vanillin-H_2SO_4 color: yellow

N,*N*-dimethyl-*p*-phenylenediamine sulfate test: negative

FD-MS *m/z* (%): 283 (M^++1, 100), 282 (M^+, 34), 265 (33).

EI-MS *m/z* (%): 264 (M^+-H_2O, 1.5), 246 (M^+-$2H_2O$, 5.5), 238 (0.9), 231 (2.6), 220 (11), 203 (7.4), 181 (7.7), 177 (7.9), 140 (24), 139 (100), 128 (10), 97 (39), 95 (12), 81 (17), 69 (26), 55 (20), 44 (24), 43 (25), 41 (30).

^{1}H-NMR data are shown in Table 3-58.

Table 3-61 Physicochemical properties of RDA-KOH-ME (2f)

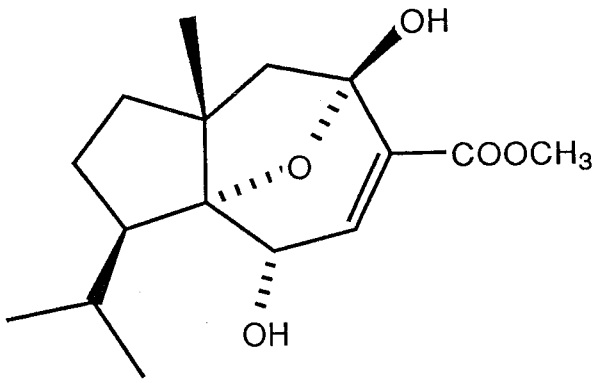

2f

Colorless column from benzene, mp. 133-136°C

Rf: 0.35 (H-EA-F 25:25:1, *cf.* **2e**; 0~0.03)

Vanillin-H_2SO_4 test: yellow

EI-MS *m/z* (%): 296 (M^+, 0.1), 278 (M^+-H_2O, 0.6), 265 (0.8), 260 (M^+-2H_2O, 1.4), 246 (5.5), 234 (9.6), 219 (6.9), 203 (8.9) 181 (6.4), 140 (22), 139 (100), 123 (10), 121 (11), 110 (10), 97 (39), 95 (14), 81 (18), 69 (29), 55 (19), 44 (15) 43 (28), 41 (30).

^{1}H-NMR data are shown in Table 3-59.

2) Conversion of an Alcohol Derivative RSA-NBH-1

Like the acid-catalyzed endoperoxide conversion, a simple question whether the conjugation system contributes to the rearrangement or not, was also raised in the base-catalyzed reaction. RSA-NBH-1 (**1c**) was therefore treated in a NaOH/MeOH solution. If the reaction successfully occurs, the product will be agreeable with RSA-NBH-2 (**1d**, tentatively proposed previously) provided as a byproduct during $NaBH_4$ reduction of rugosal A (**1**). As shown in Scheme 3-15 the major product RSA-NBH-NAOH was obtained as a colorless columns (3.7 mg from 6.6 mg of **1c**, *Rf* 0.24 in $CHCl_3$-MeOH 50:4, Fig. 3-156).

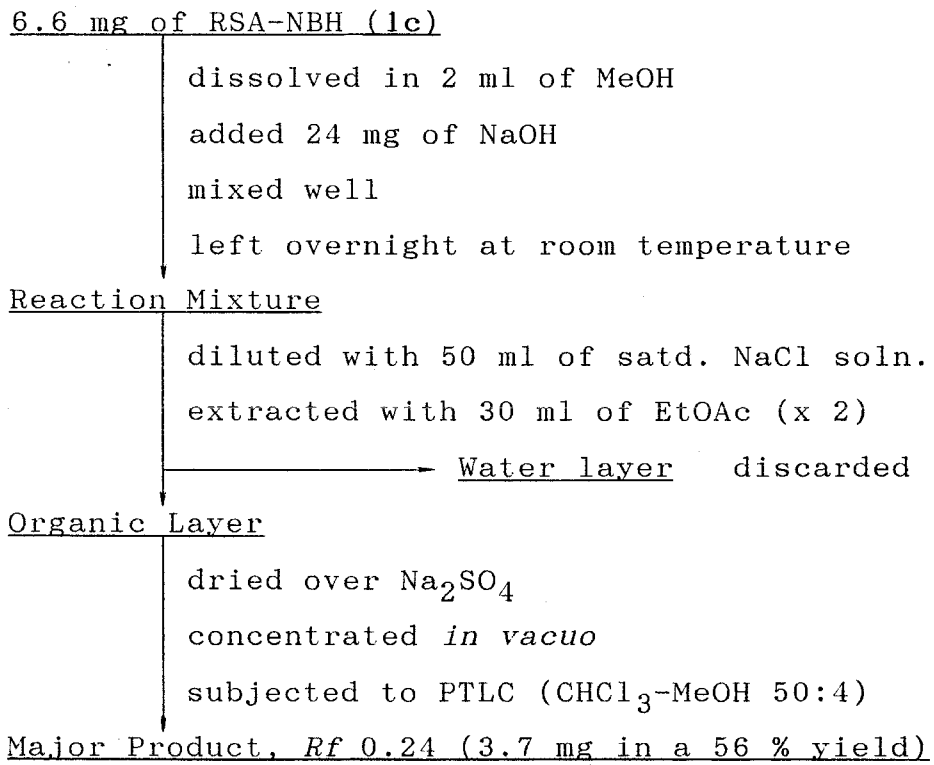

Scheme 3-15 Reaction and isolation procedures for RSA-NBH-NAOH

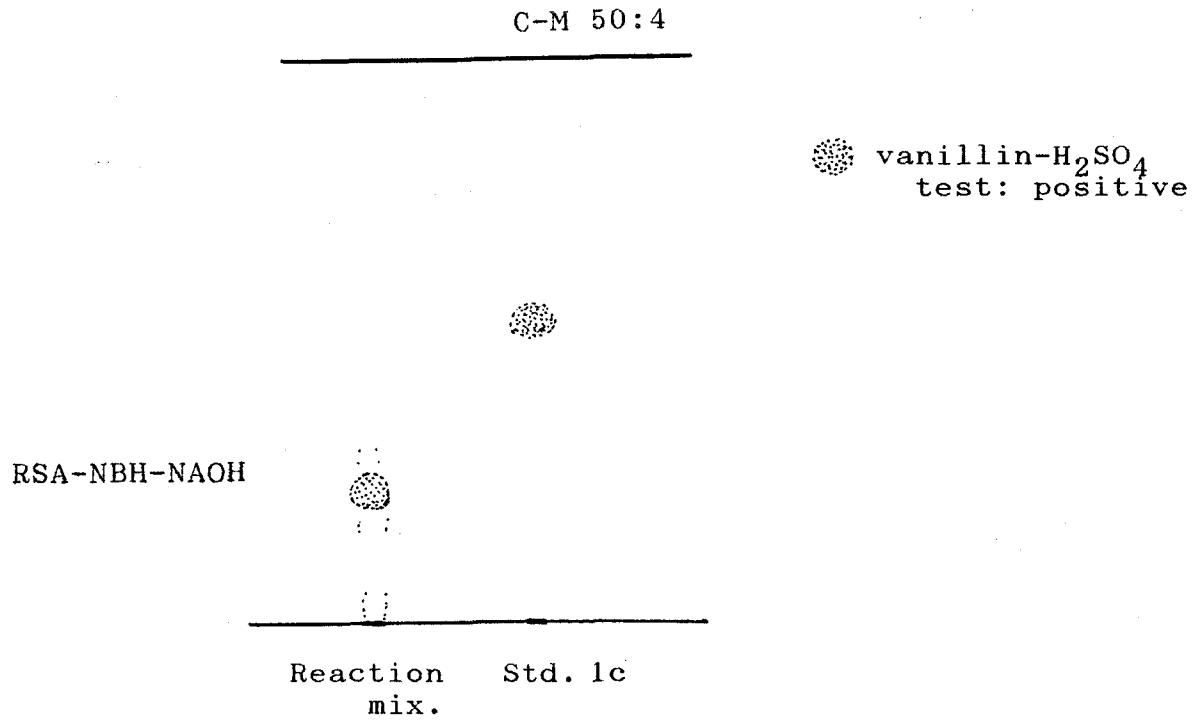

Fig. 3-156 TL Chromatogram of Reaction Product Obtained by Base-catalyzed Conversion of RSA-NBH-1 (**1c**)

RSA-NBH-NAOH showing its molecular weight 268 in FD-MS (Fig. 3-157) was identical with **1d** in EI-MS comparisons (Fig. 3-158). ^{1}H- and ^{13}C-NMR spectra of the product were completely compatible with the proposed structure (Fig. 3-159 and 160). Although a pair of methylene protons of C-14-H_2 was detected at δ_H 4.243 and 4.047 (both d, *J*= 13.0 Hz), chemical shifts and coupling constants of other proton signals showed a good correspondence with those of **1g**, including a pair of isolated methylene protons (δ_H 1.968 and 1.894, both *J*= 12.1 Hz). Furthermore, the olefinic proton (δ_H 5.851) and the C-5-OH proton (δ_H *ca* 4.54) both showing upfield shifts were indicative of structure **1d**, corresponding to an alcohol derivative of RSA-PY (**1g**) (Table 3-62). The ^{13}C-NMR spectrum also indicated in accordance with that of **1g**, except signal for C-14 carbon (Table 3-62). Thus, structure of RSA-NBH-NAOH was elucidated as **1d**, and accordingly the RSA-NBH-2 was proved to be derived by the base catalyst during the $NaBH_4$ reduction, like RDA-KOH (**2e**) accidentally yielded during rugosic acid A (**2**) reduction with $LiAlH_4$.

By this reaction, the conjugated carbonyl groups of 1 and 2 were proved not to be particularly concerned in the base-catalyzed peroxide rearrangement.

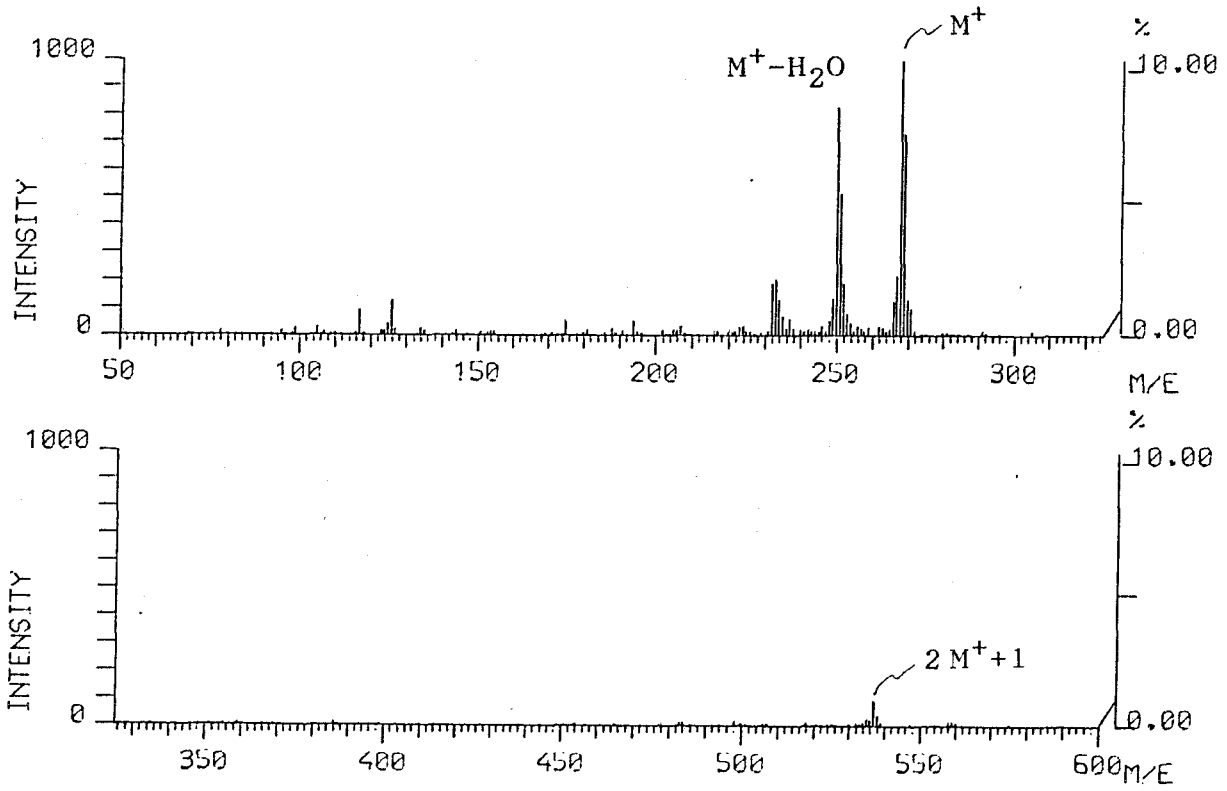

Fig. 3-157 FD-Mass Spectrum of RSA-NBH-NAOH

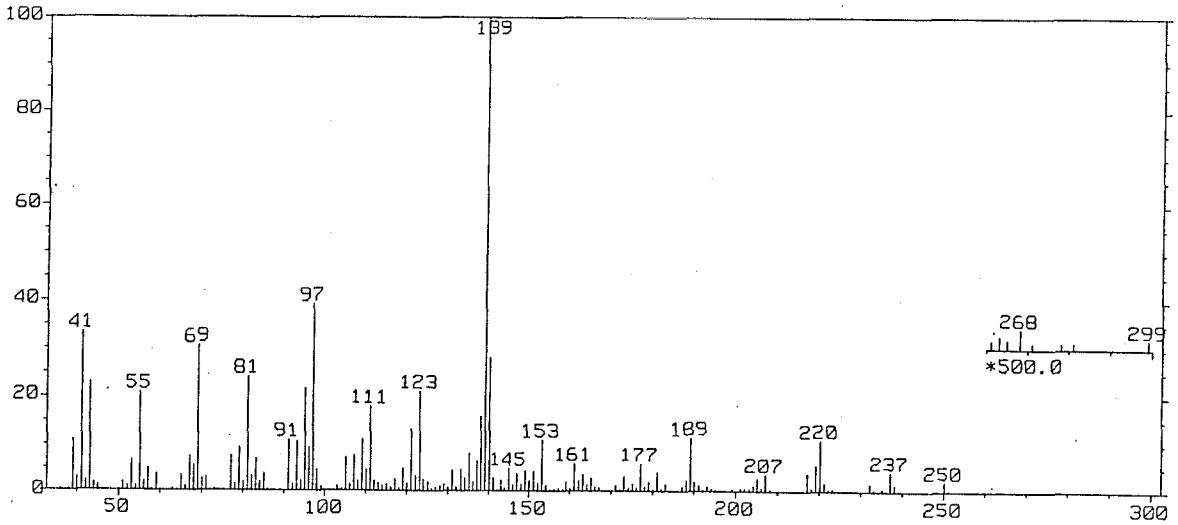

Fig. 3-158 EI-Mass Spectrum of RSA-NBH-NAOH

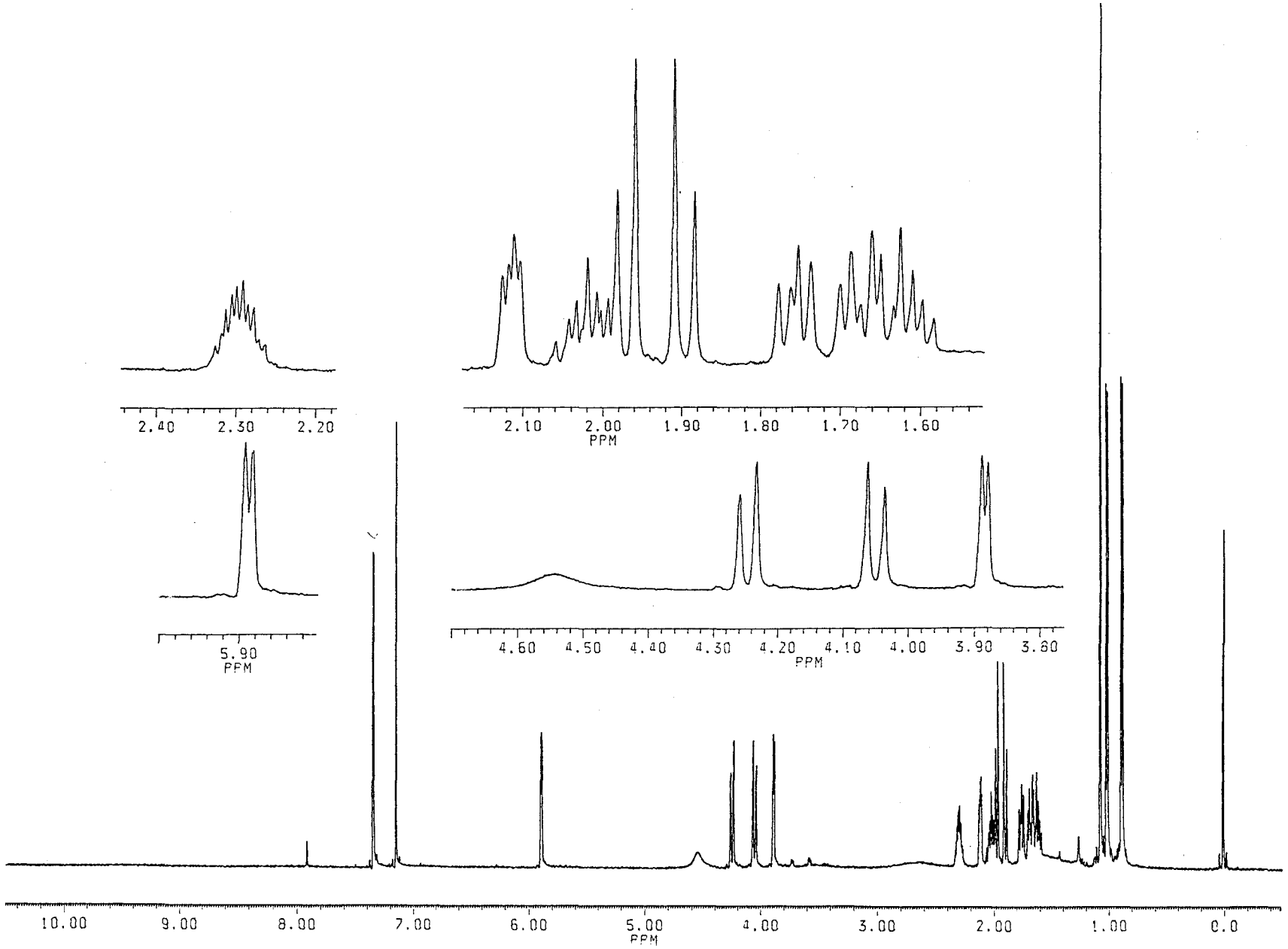

Fig. 3-159 ^{1}H-NMR Spectrum of RSA-NBH-NAOH (500 MHz, in $CDCl_3$): A small amount of benzene was contaminated to show a signal at δ_H 7.35.

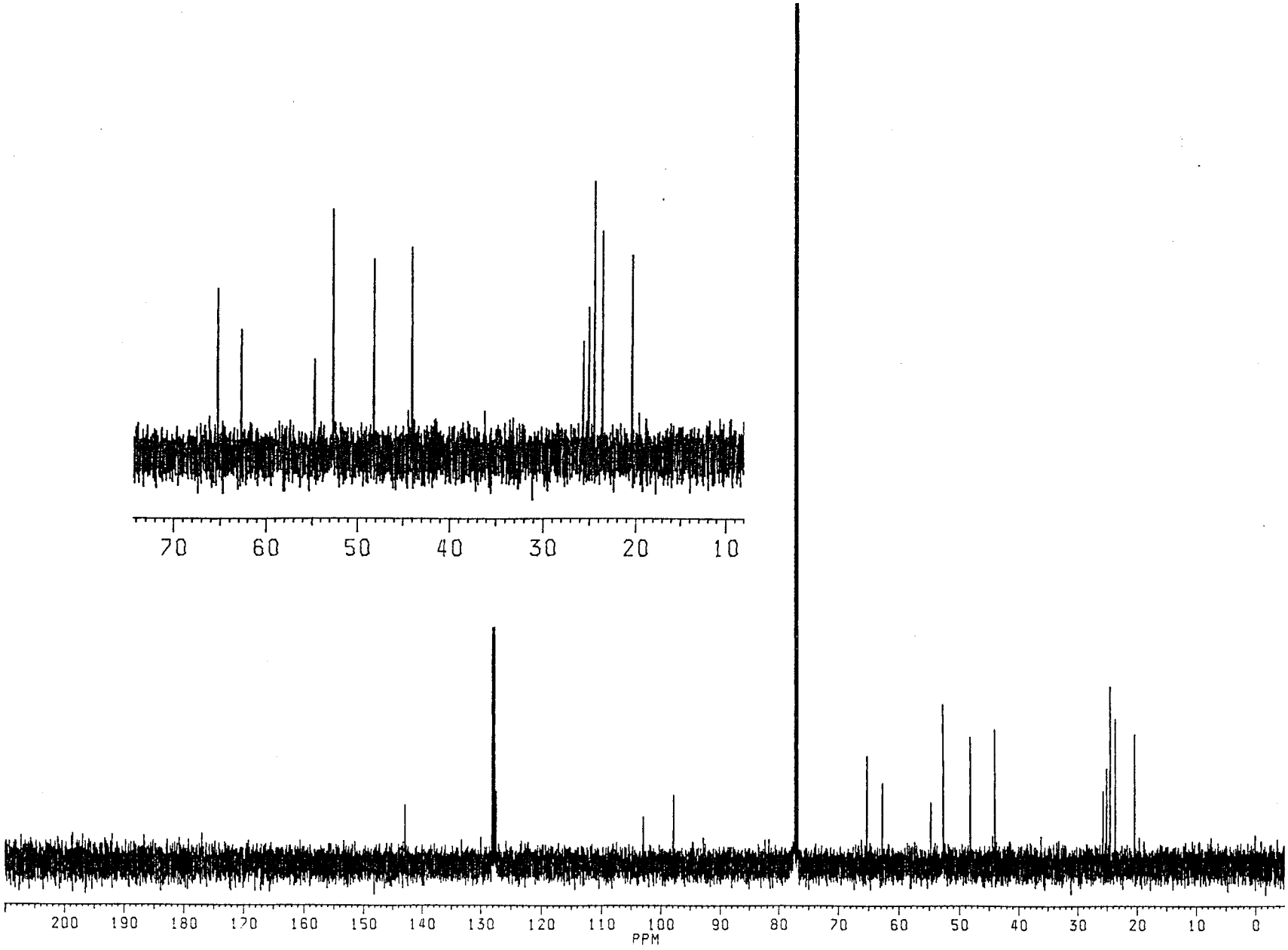

Fig. 3-160 ^{13}C-NMR Spectrum of RSA-NBH-NAOH (125 MHz, in $CDCl_3$): A small amount of benzene was contaminated to show signals at δ_C *ca* 128.

Table 3-62 Physicochemical properties of RSA-NBH-NAOH (1d)

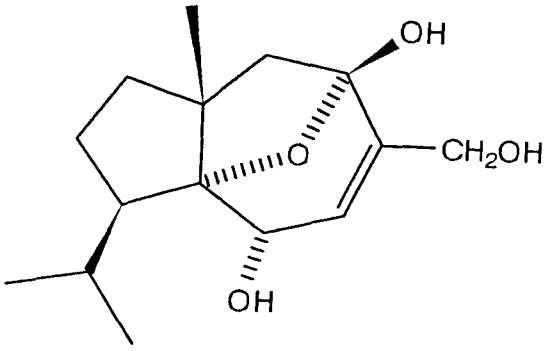

1d

Colorless column from $CHCl_3$, mp. 107-110°C

Rf: 0.24 (C-M 50:4)

Vanillin-H_2SO_4 color: yellowish orange

FD-MS *m/z* (%): 269 (M^++1, 74), 268 (M^+, 100), 251 (52), 250 (M^+-H_2O, 83), 233 (21), 232 (M^+-2H_2O, 19).

EI-MS *m/z* (%): 268 (trace), 250 (M^+-H_2O, 2.2), 237 (4.3), 220 (11), 219 (5.7), 217 (4.0), 207 (3.7), 189 (12), 177 (6.0), 161 (6.1), 153 (11), 140 (28), 139 (100), 138 (16), 123 (21), 121 (13), 111 (18), 109 (11), 97 (39), 95 (22), 81 (24), 69 (31), 55 (21), 43 (23), 41 (33).

^{1}H-NMR $\delta^{C_6D_6}_{TMS}$ (500 MHz): 3.882 (1H, d, *J*= 4.6 Hz, C-2-H), 5.851 (1H, d, *J*= 4.6 Hz, C-3-H), *ca* 4.54 (1H, br. s, C-5-OH), 1.968 (1H, d, *J*= 12.1 Hz, C-6-Ha), 1.894 (1H, d, *J*= 12.1 Hz, C-6-Hb), 1.756 (1H, br. dd, *J*= 12.7 and 7.6 Hz, C-8-Ha), 1.602 (1H, dd, *J*= 12.7 and 7.2 Hz, C-8-Hb), 2.012 (1H, m, C-9-Ha), 1.666 (1H, m, C-9-Hb), 2.112 (1H, dd, *J*= 7.2 and 3.8 Hz, C-11-H), 2.294 (1H, double-sept., *J*= 6.8 and 3.8 Hz, C-11-H), 1.006 (3H, d, *J*= 6.8 Hz, C-12-H_3), 0.877 (3H, d, *J*= 6.8 Hz, C-13-H_3), 4.243 (1H, d, *J*= 13.0 Hz, C-14-Ha), 4.047 (1H, d, *J*= 13.0 Hz, C-14-Hb), 1.065 (3H, s, C-15-H_3).

^{13}C-NMR $\delta^{C_6D_6}_{TMS}$ (125 MHz): 97.7 (C-1), 65.1 (C-2), 127.4 (C-3), 142.8 (C-4), 102.8 (C-5), 48.0 (C-6), 52.6 (C-7), 43.9 (C-8), 24.3 (C-9), 54.6 (C-10), 25.6 (C-11), 23.5 (C-12), 20.2 (C-13), 62.6 (C-14), 24.9 (C-15).

3) Reaction Mechanism and Chemical Aspects

It is also known that endoperoxide bridges are easily cleaved in the presence of a catalytic amount of a base, in which reaction, a base-catalyzed proton abstraction initially occurs on a hydrogen bearing carbon attached to the peroxide linkage [119]. As the result of the proton abstraction, a β-elimination on O-O cleavage occurs to result in concerted formation of a stable carbonyl and an oxide anion groups (Scheme 3-16). The reaction in those carotane peroxides is also expected to take a similar process. The reaction is considered to take a process as follows. Firstly, the base triggers proton abstraction of a proton attached to the C-5 carbon of the endoperoxy group, to result in a β-elimination on the peroxy bridge. Secondly, a keto oxide anion intermediate, bearing a carbonyl group at C-5 and an oxide anion originated in O-1 on C-1, is transiently formed according to the β-elimination reaction. Thirdly, the oxide anion ($-O^{\ominus}$) attacks the carbonyl group at C-5 to form a hemiacetal group (Scheme 3-17).

The formation of a hemiacetal carbon would be affected by α.β-unsaturated carbonyl group at C-14 (even single olefinic bond between C-3 and C-4), causing decrease of the electron density at the reactive carbonyl of C-5. By the effect, the hydrogen attached to C-5 is more easily abstructed by a base. Furthermore, it may make the oxide anion easy to give an electron to the carbonyl oxygen, to form a tetrahydrofuran ring. In addition, this re-cyclization step is probably controlled by the three dimensional conformation of the active sites of the carotane peroxides as well. Since the distance of C-1 and C-5 becomes close by the hydrogen bond of C-2-OH and the conformation due to its *trans*-bicyclic form, the oxide anion can attack the C-5 carbonyl selectively. On the other hand, the C-1-$O^{\ominus}$ cannot attack C-14 carbonyl group intramolecularly, due to the presence of olefinic bond between them. With the same reason, C-2-OH, if possible to be an oxide anion group after giving its proton to C-1-$O^{\ominus}$, cannot come close

anion group after giving its proton to C-1-$O^{\ominus}$, cannot come close enough to the C-5 carbonyl group to attack it (Scheme 3-23).

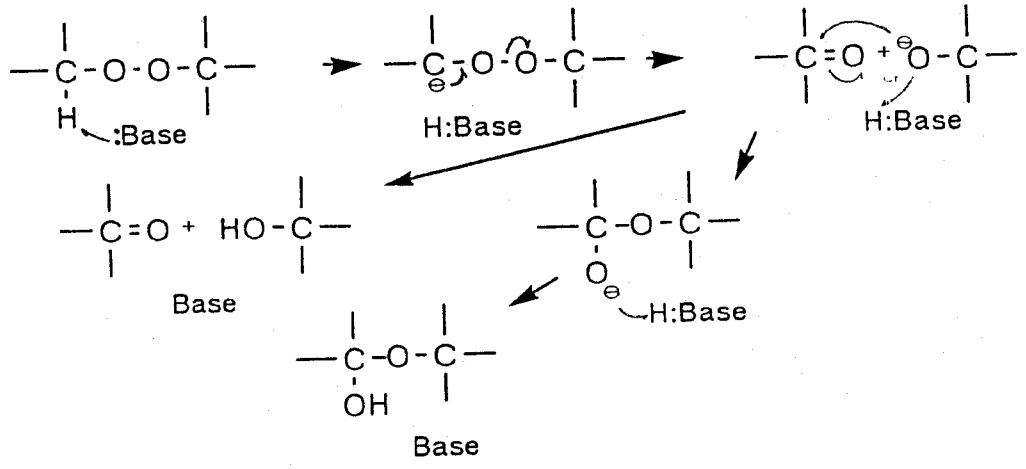

Scheme 3-16 A typical base-catalyzed endoperoxide conversion

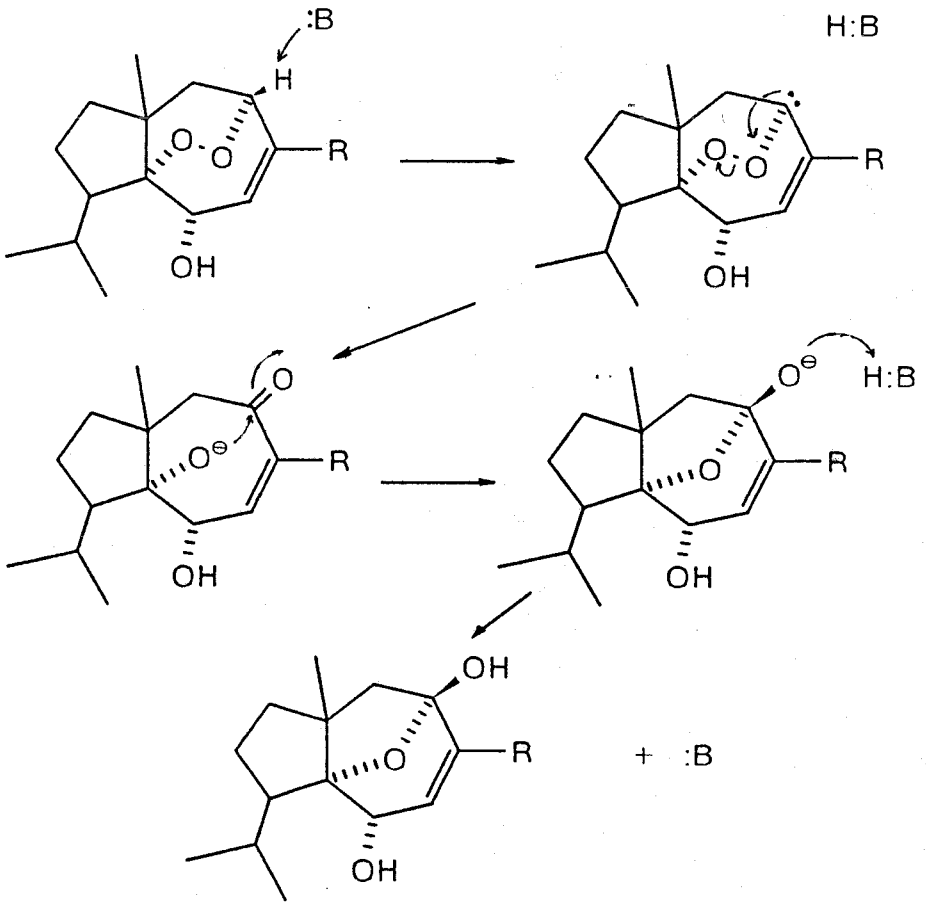

Scheme 3-17 Possible pathway of base-catalyzed conversion of the carotane peroxides

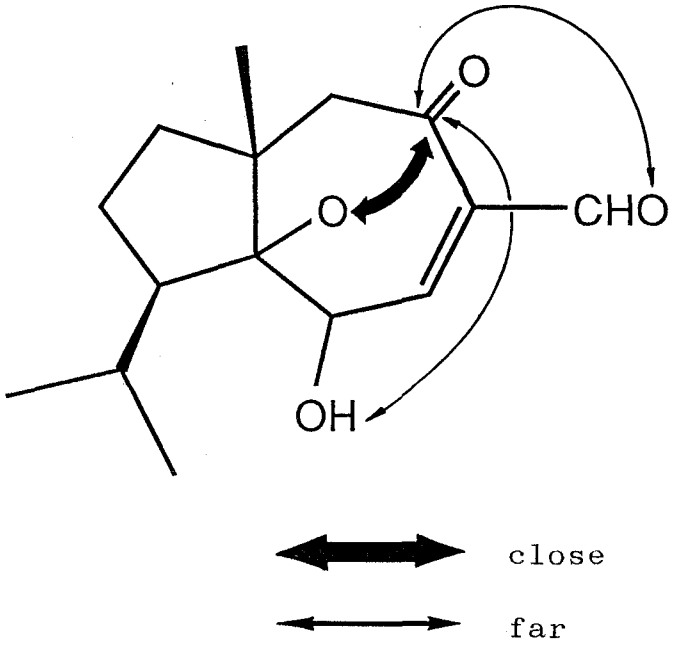

Fig. 3-161 Distance of Two Active Sites on the 5-Ketol-oxide Anion Intermediate of the Rearranged Carotane Peroxides: C-1-$O^{\ominus}$ and C-5 carbon can take the closest distance among C-5/C-2-OH, C-5/C-14-O and C-5/C-1-$O^{\ominus}$ due to the presence of C3/C4 olefinic bond.

3-5 A Precursor of Rugosal A, Carota-1,4-Dienaldehyde and Its Autoxidation to Rugosal A

3-5-1 Introduction to Endoperoxide Formation

As previously described, *Rosa rugosa* leaves contain a carotane aldehyde, rugosal A (**1**) which possesses a unique endo-peroxy bridge in the molecule. Since **1** is highly oxygenated, it was anticipated that a less oxygenated carotane aldehyde is contained in the leaf constituents as a precursor for **1**.

In naturally occurring endoperoxides, the endoperoxide bridge is usually formed through Diels-Alder reaction between singlet oxygen and a 1,3-diene part in the corresponding precursor. For example, ascaridol (**86**) [122] and a guaiane endoperoxide (**79**) [99] are typical 1,4-endoperoxides falling under this category. Those kind of *endo*-peroxidation are depicted as Scheme 3-18. However, this type of endoperoxide formation is not applicable to **1**, because any 1,3-diene precursor for **1** cannot exist due to the presence a quarternary carbon at C-7.

On the other hand, another endoperoxide formation system is known, in which an exoperoxy radical is formed as an intermediate. Some model reactions regarding this type of peroxidation have been demonstrated [123,124]. As an example of the peroxidation to yield a naturally occurring peroxide, autoxidation of unsaturated fatty acids having *cis*, *cis*-1,4-diene partial structure can be picked up. Although endoperoxides derived from these unsaturated fatty acids, such as prostaglandin H_2 (PHG_2, **82**), are ordinarily unstable, some of them were successfully isolated and revealed their physicochemical properties. In this type of endoperoxide formation, firstly occurs abstraction of a hydrogen radical at the active methylene site by singlet oxygen to result homolitic re-distribution of the π-electrons followed by successive translocation of the olefine bond as the initial step [125]. In

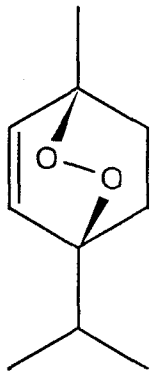

ascaridol (86)

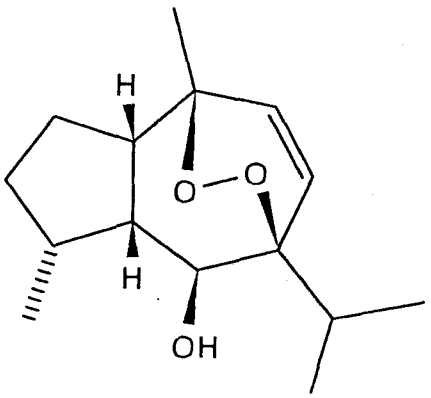

guaia-6,9-diene (79)

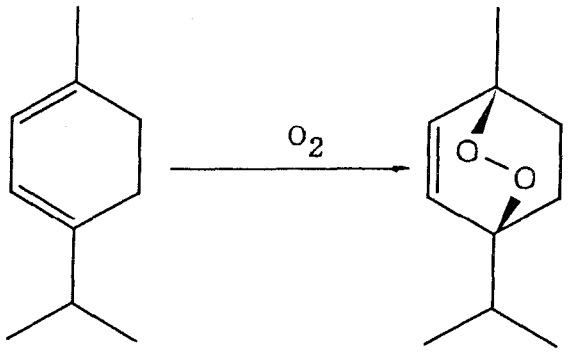

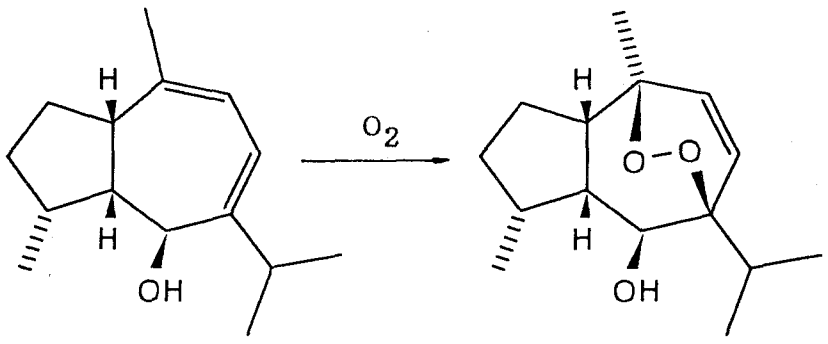

Scheme 3-18 Some typical peroxylations on 1,3-diene precursors to yield the corresponding 1,4-dndoperoxides

this step, *cis*, *trans*-1,3-diene is newly formed in a association with new carboradical formation at the allyl carbon. To the radical, triplet oxygen attacks to form the *exo*-peroxy radical (Scheme 3-19). Even in monoenes, *exo*-peroxidation concerted to olefine transferation is known to occur (Scheme 3-20) [126]. In case this reaction scheme is applicable to sesquiterpenes with 1,4-diene part structure, the endoperoxide formation of 1 is also expectable according to the systems shown in Scheme 3-19, expectable in two possible ways (Scheme 3-21).

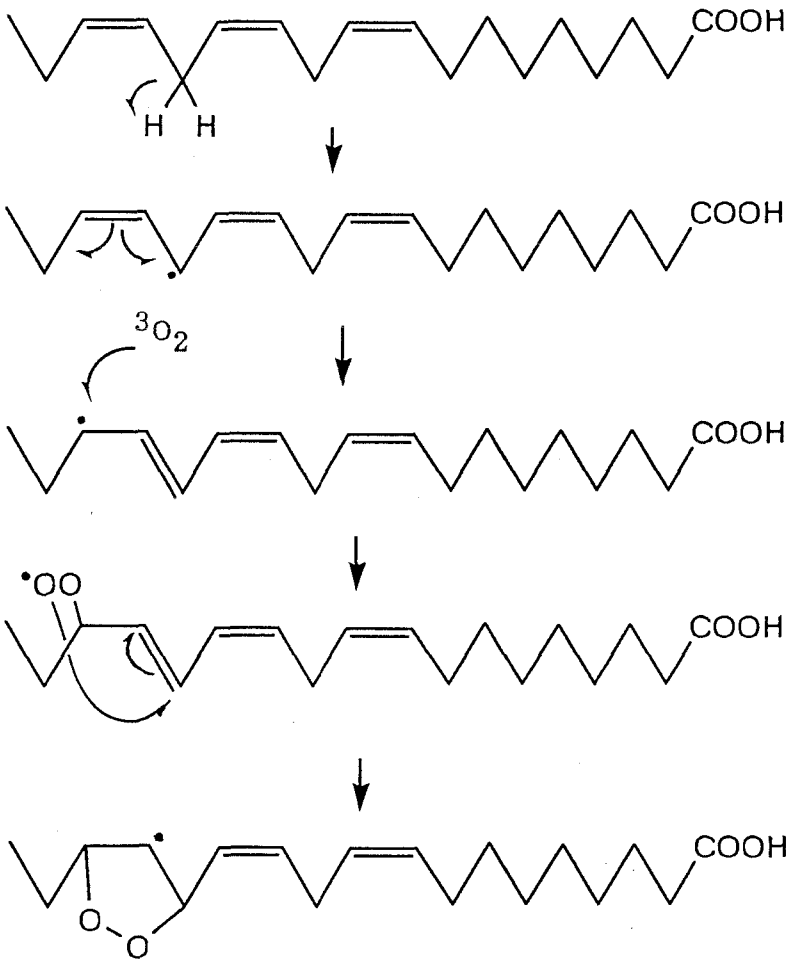

Scheme 3-19 Autoxidation process for γ-linolenic acid

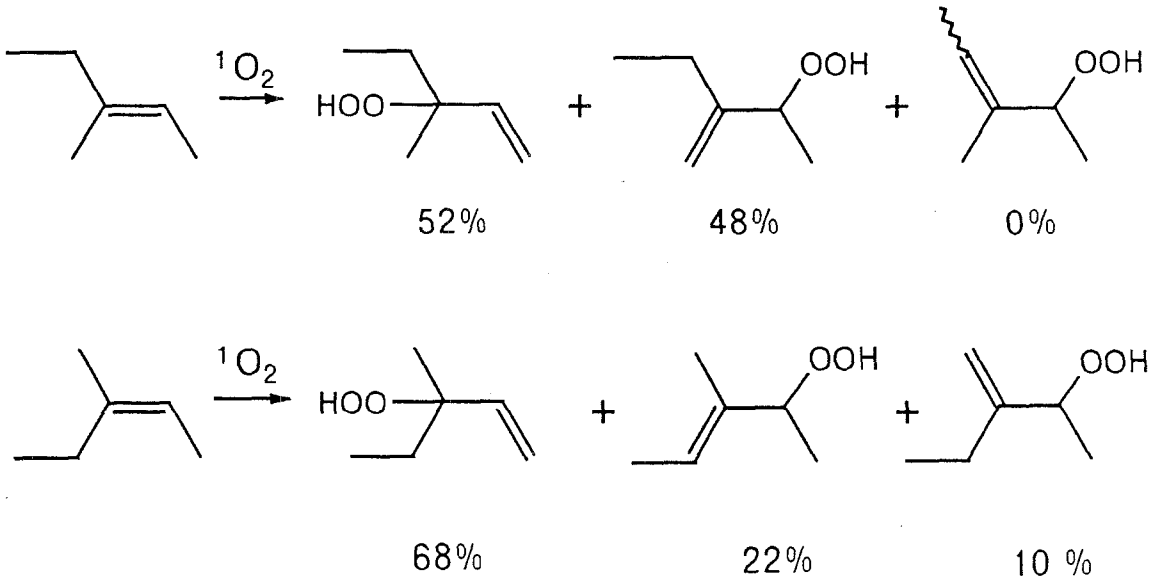

Scheme 3-20 Peroxylation of monoene with singlet oxygen

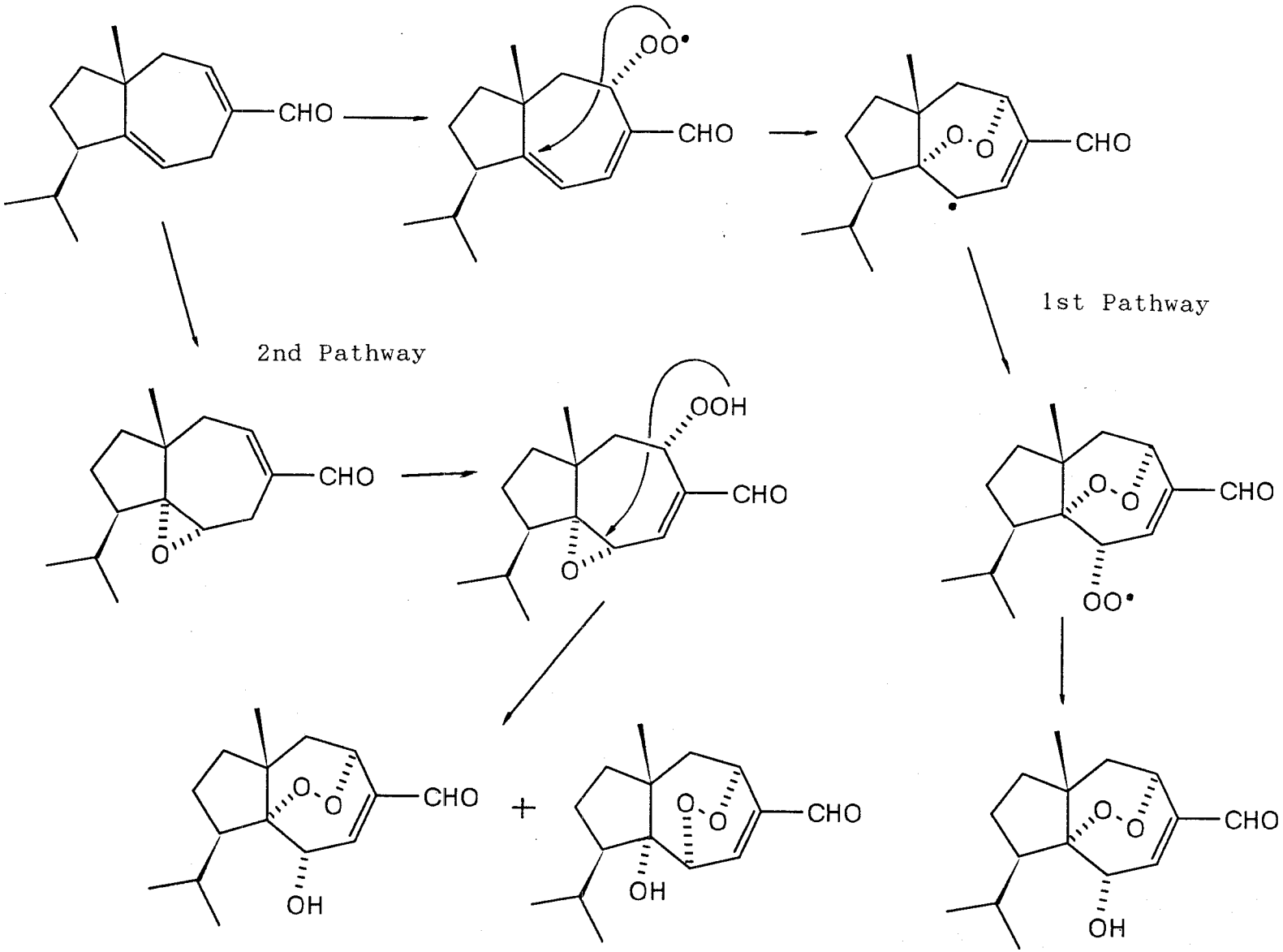

Scheme 3-21 Two Ppssible conversion pathway to yield rugosal A from a presume precursor: Tf these carotanoids were found in *Rosa rugosa* leaves, the 2nd pathway would also be possible.

On the other hand, photochemical formation of hanalpinol (**80**) from guaia-6,9-diene (**87**) is currently reported by Morita *et al.* (Scheme 3-22) [127]. During the photooxidation of **87**, some intermediates, **88**, **89** and **90** were isolated or confirmed (Fig. 3-162). These results suggested that **80** formation passes by way of a hydroperoxy radical intermediate in the initial step. This scheme indicated that rugosal A (**1**) is also convertible from the corresponding 1,4-diene precursor through the first pathway shown in Scheme 3-21 (See pp. 287). More importantly, C-9-OH of **80** derived from C-9-OOH suggested that the allylic OH group of **1** is also originated in a hydroperoy group or a exoperoxy radical formed on C-2. Through this speculation the second pathway in Scheme 3-21 was tentatively excluded, and a precursor of **1** was presumed to have a 1,4-diene structure on the carotane skeleton oxygenated at C-14 to α,β-unsaturated aldehyde group (Scheme 3-23). First of all, the hypothetical 1,4-diene precursor (possible structure **3**) was therefore surveyed in MeOH extract of *Rosa rugosa* leaves.

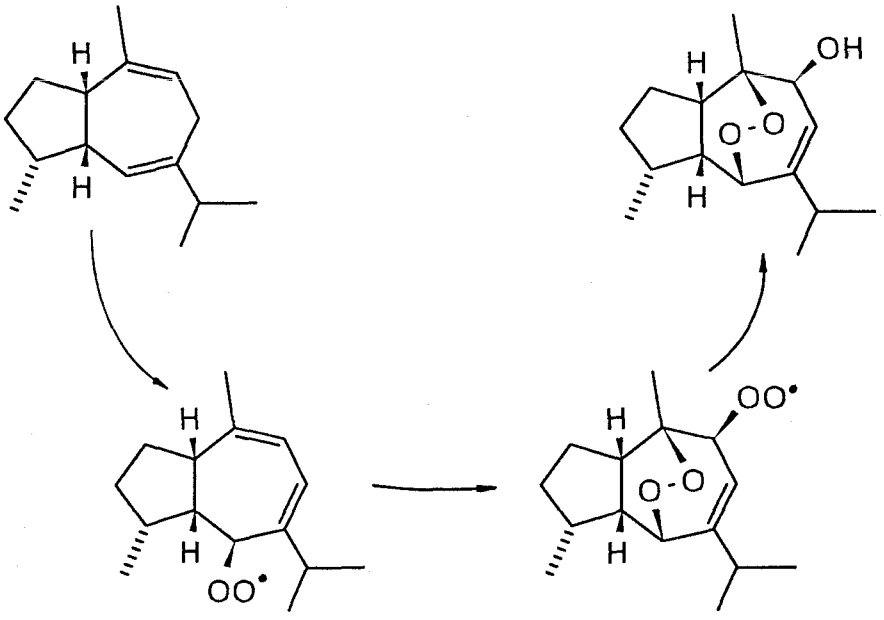

Scheme 3-22 Autoxidation of guaia-6,9-diene (87) to form hanalpinol (80) [127]

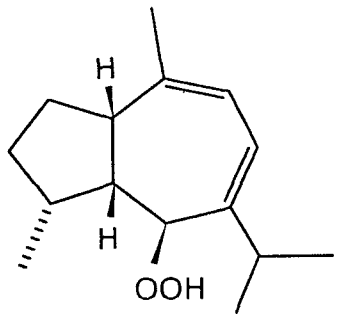

hydroperoxide intermediate (88)

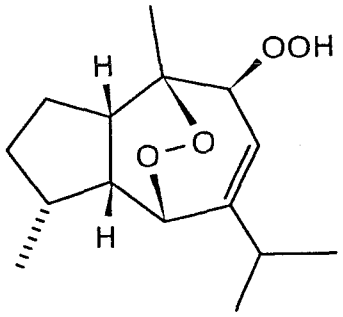

hanalpinone (89)

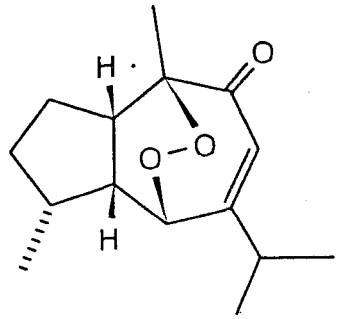

hydroperoxyhanalpinol (90)

Fig. 3-162 Some Intermediates and By-products as the Result of Autoxidation of Guaia-6,9-diene

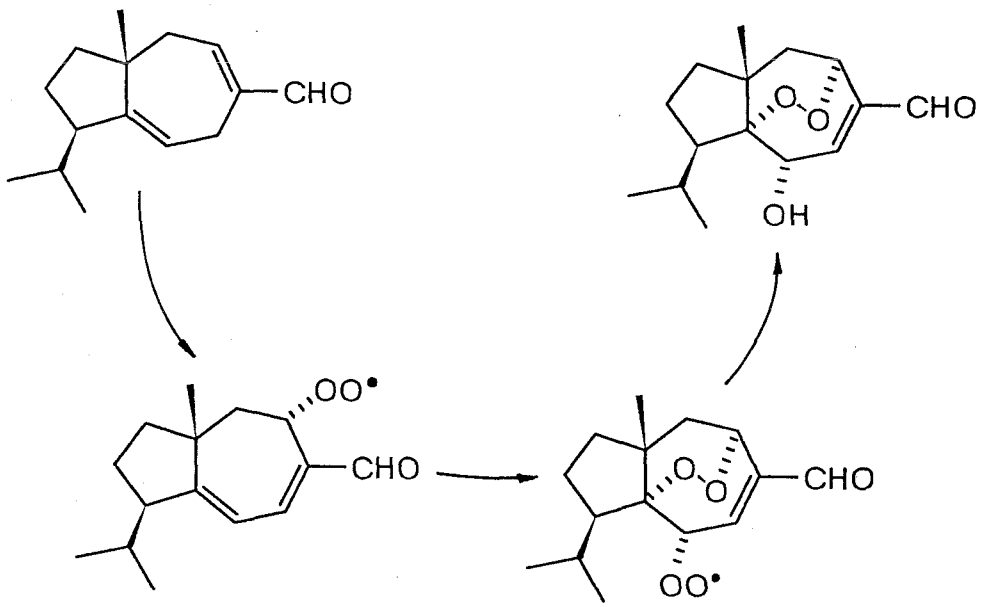

Scheme 3-23 Possible steps to rugosal A

3-5-2 Isolation of a Precursor, Carota-1,4-dienaldehyde

The precursor of rugosal A (1) was carefully surveyed in the *n*-hexane-soluble fraction directly extracted from the MeOH extract of *Rosa rugosa* leaves (Sample VII), collected when the level of 1 was notably high in the tissues [128]. Fresh *Rosa rugosa* leaves were soaked in 95 % MeOH (*ca* 50 liters) for two months, then the MeOH extract was collected and extracted twice with *n*-hexane (MeOH:*n*-hexane= 3:1, v/v). The combined *n*-hexane extracts were concentrated to *ca* 1000 ml, and washed once an equal volume of 5 % aq. $NaHCO_3$. The neutral substances (*ca* 12 g) dissolved in small amounts of *n*-hexane were successively chromatographed on silica gel column. The $NaHCO_3$ washings contained only small amounts (less than 1 g) of acidic constituents.

The *n*-hexane solubles (8 g) were charged onto silica gel column (500 ml silica gel in *n*-hexane; column, 8 cm i.d.) and then chromatographed. After washing the column with Fr-H-1 (1500 ml of 2 % EtOAc/ hexane), the successive fractions Fr-H-2 and -3 (250 ml each) eluted with 2 % EtOAc/hexane containing some low polar and quenching (on F_{254} plates) substances were obtained (Fig. 3-163).

To recover the aimed compound, the residual MeOH layer was concentrated to obtain *ca* 1 liter of water suspension. The suspension was mixed with acetone (total 2.5 liters), and to the acetone/water mixture was added excess NaCl and stirred overnight. The partitioned acetone layer was further concentrated. The residue dissolved in EtOAc (1.5 liter) and washed with saturated NaCl solution was concentrated once more and re-dissolved in benzene (800 ml). The benzene layer washed with 5 % $NaHCO_3$ solution (700 ml)was concentrated after dehydration over Na_2SO_4 to give *ca* 48 g of a dark oil. The content of the focused substances in this fraction seemed to be rather high than that of the *n*-hexane extract.

To the focused spots, 2,4-DNPH reagent was used to detect

aldehyde derivatives. The third spot showing a clear orange color was isolated by PTLC (hexane-EtOAc 20:1) from a small part of Fr-H-2 (Fig. 3-164). This isolated fraction (RL fraction) was subjected to gas chromatography (GC; 5 % PEG-20M on Celite 545 AW, 1 m) to give five major peaks (tentatively named RL-A: relative intensisty 10 %, retention time 17 min, B: 8 %, 19 min, C: 61 %, 21 min, D: 2 %, 22 min, E: 20 %, 24 min) (Fig. 3-165). By the GC-MS analysis of the fraction, each constituent showed its molecular ion at *m/z* 218, except RL-D with M^+ 216. Since M^+ 218 was requested for the hypothetical precursor, the main component RL-C (relative intensity, 61 %) was firstly focused.

After separation of the major part by PTLC in *n*-hexane-EtOAc 20:1 (*Rf ca* 0.20), final purification of RL-C was carried out using preparative HPLC (Unisil Q 100-5, solvent; 2.5 % EtOAc/*n*-hexane, detector; UV 230 nm, flowing rate; 2 ml/min). The most abundant substance on the UV monitor (Fig. 3-166) was obtained as a colorless syrup. The major constituent was further purified (2.5 % EtOAc/*n*-hexane) to give a single peak on HPLC, and eventually *ca* 40 mg of a colorless oil of which EI-mass spectrum showed a good correspondence with the GC-mass spectrum of RL-C (Fig. 3-167). Furthermore, its molecular formula (M^+ 218.165, $C_{15}H_{22}O$ in EI-HR-MS, requires 218.167) was agreeable with that required for the presumable precursor depicted in Scheme 3-23 (structure A, pp. 289).

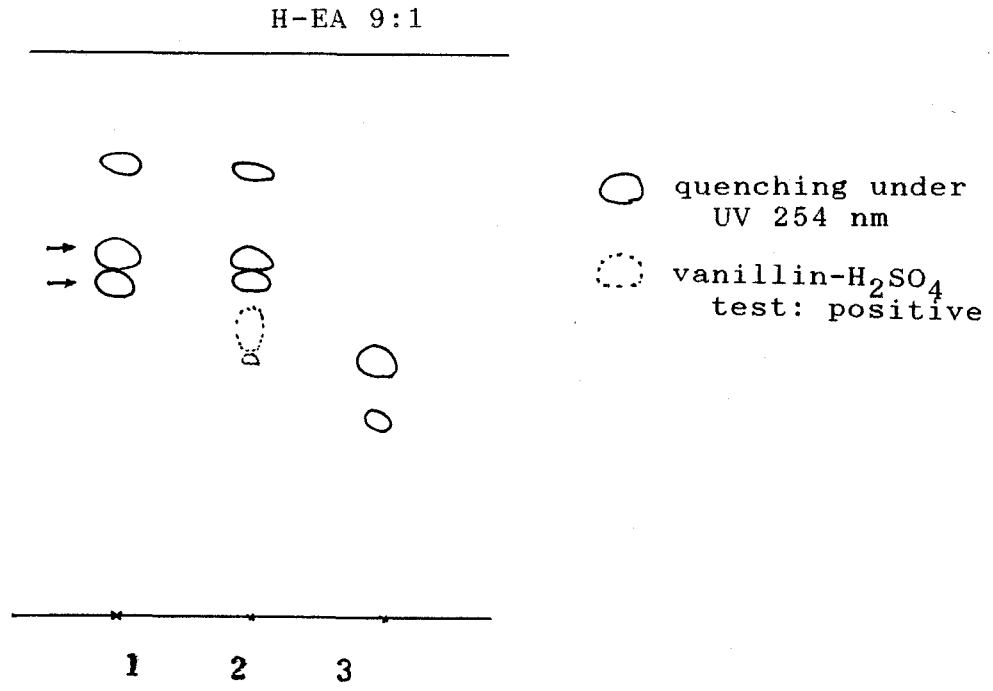

Fig. 3-163 TL Chromatogram of Fractions Eluted from the Silica Gel Column Charged with Low Polar Constituent of *Rosa rugosa* Leaves (Sample V)

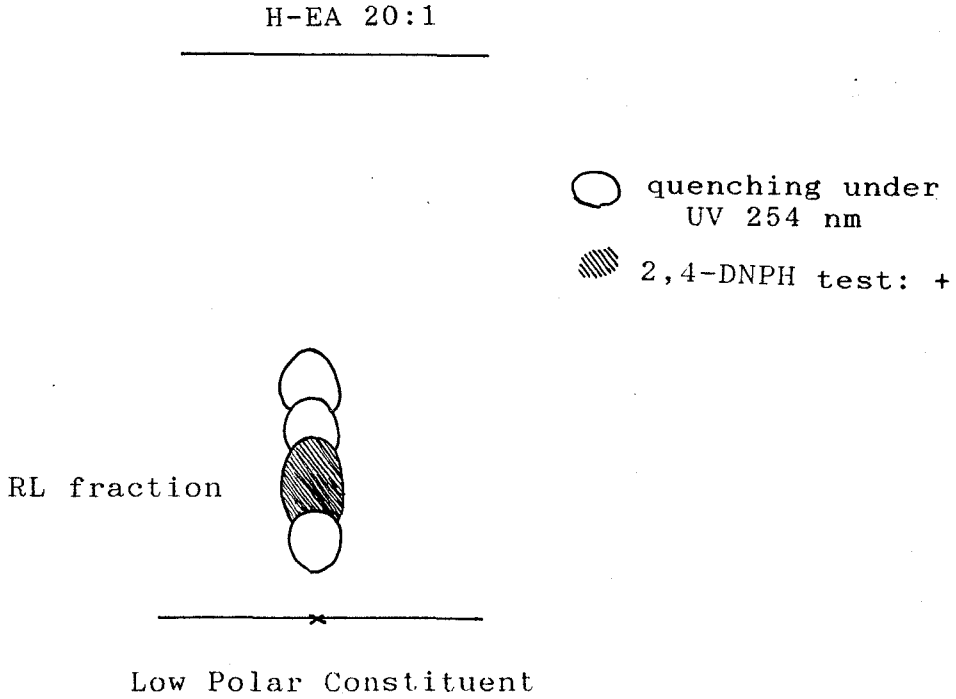

Fig. 3-164 TL Chromatogram of Fr-V-1 and -2 Mixture

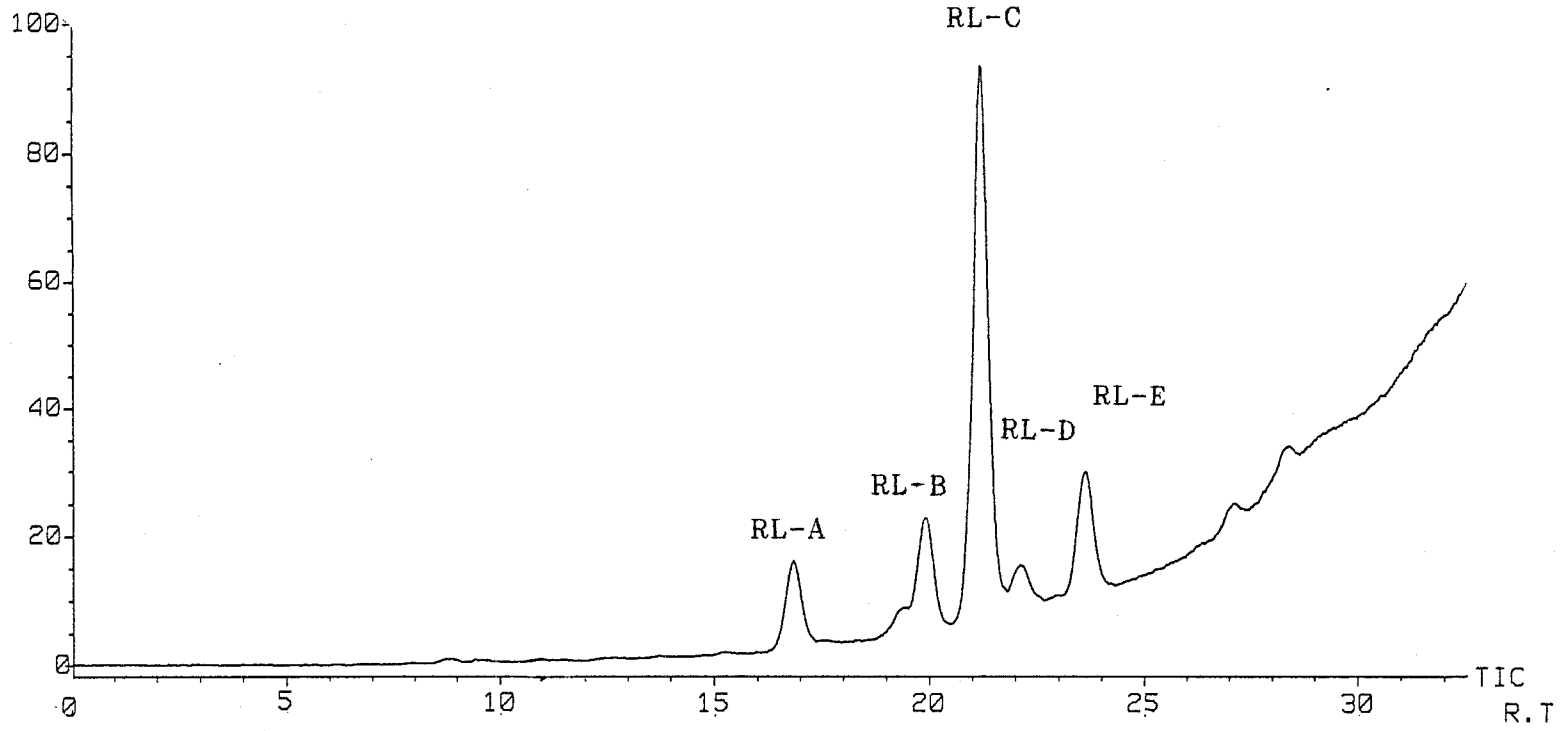

Fig. 3-165 Gas Chromatogram of RL Fraction (pp. 290) (5 % PEG-20M on Celite 545 AW, 1 m; Detector, TIC)

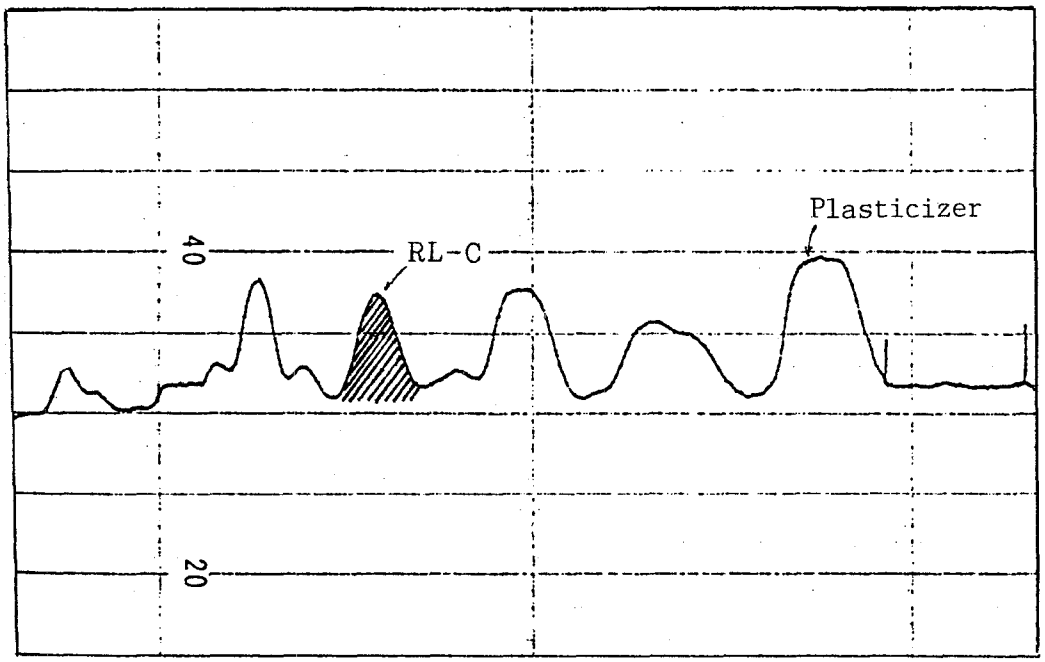

Fig. 3-166 HPLC Pattern of RL Fraction Recorded on UV Detector at 230 nm (Unisil Q 100-5, 12 mm x 220 mm, 2.5 % EtOAc/*n*-hexane)

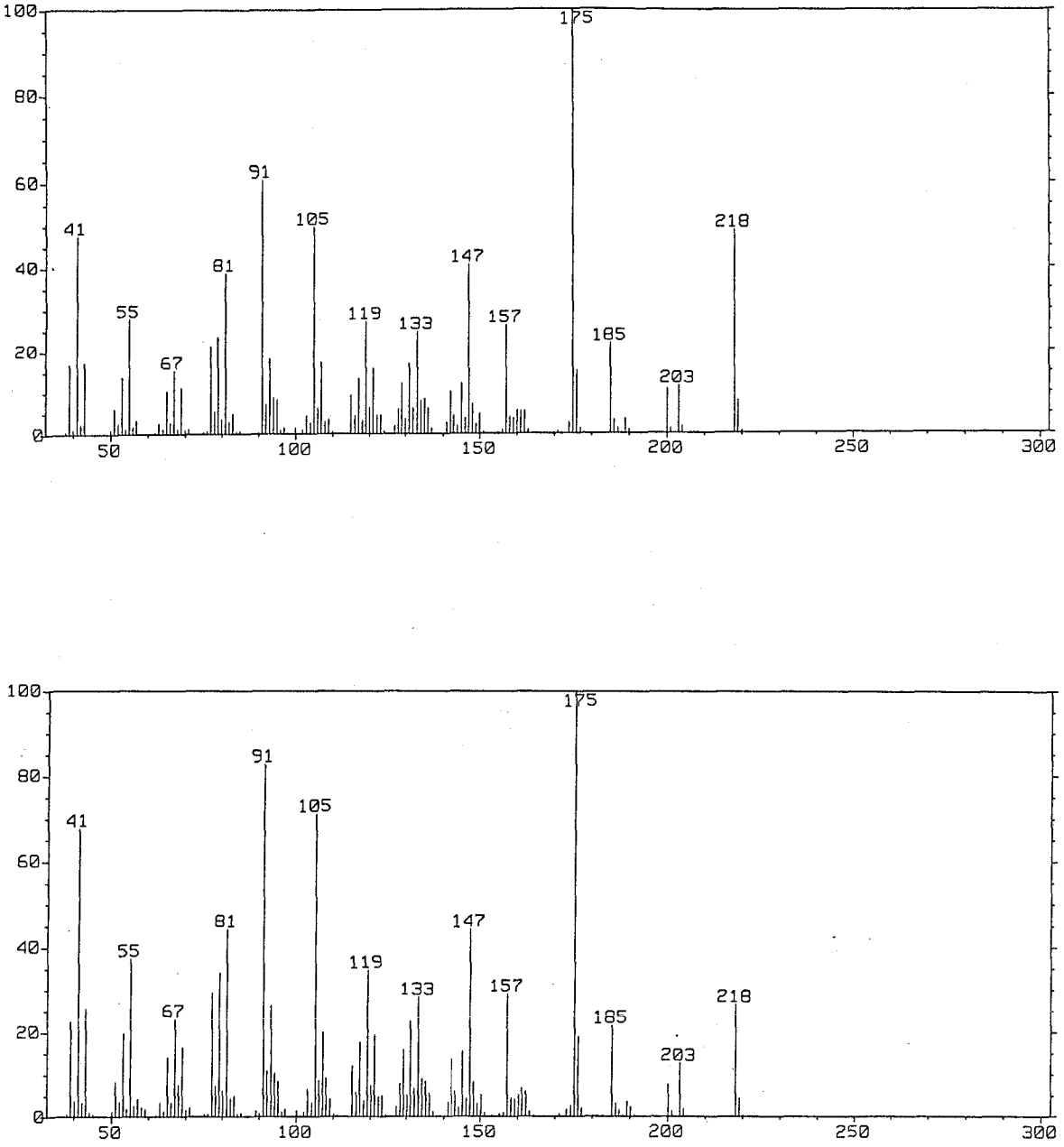

Fig. 3-167 GC-Mass Spectrum of the Interested Compound (RL-C) in RL Fraction and EI-Mass Spectrum of the Isolated RL-C

3-5-3 Structure Elucidation of Carota-1,4-dienaldehyde

In UV spectrum of RL-C, its methanolic UV absorption maximum at 230.5 nm rapidly disappeared with a small amount of HCl, of which properties were similar to those of rugosal A (1) possessing an α,β-unsaturated aldehyde group. Accordingly, IR spectrum of RL-C, showing absorption bands assignable to the aldehyde group (2800 and 2740 for CHO, and 1680 for C=C-C=O), proved the presence of an α,β-unsaturated aldehyde partial structure in the molecule (Fig. 3-168).

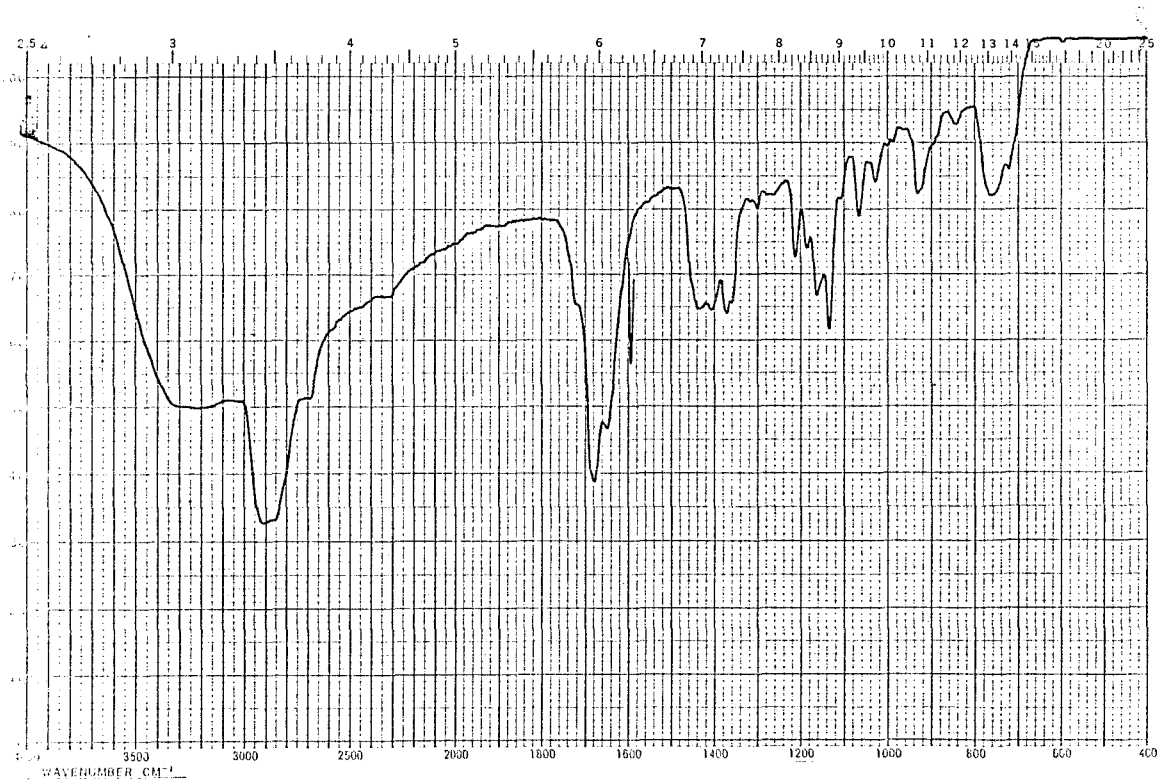

Fig. 3-168 IR Spectrum of RL-C (liquid film)

^{1}H-NMR spectrum of RL-C (500 MHz in C_6D_6) showed the presence of a singlet formyl proton (δ_H 9.126, 1H, s) and an isopropyl group [δ_H 0.888 (1H, d, *J*= 6.8 Hz), 0.742 (3H, d, *J*= 6.8 Hz) and 1.704 (1H, octet-like signal, *J*= *ca* 6.8 Hz)] in addtion to a bridge-head methyl group (δ_H 0.847, 3H, s), all of which were required of a carotane-14-aldehyde skeleton. The octet-like methine proton of the isopropyl group suggested that the isopropyl group is allocated on a methine carbon whose proton showed a vicinal coupling *J*= *ca* 6.8 Hz (Fig. 3-169 and Table 3-63).

The ^{13}C-NMR (DEPT and CH-COSY) spectra proved the presence of four sp^2 carbons at δ_C 152.0 (=C<), 150.9 (=CH-), 141.1 (=C<) and 116.0 (=CH-) attributable to two C,C-double bonds. Two olefinic protons detected at δ_H 5.122 (1H, ddd, *J*= 6.6, 3.4, and 2.8 Hz) and 6.065 (1H, dddd, *J*= 7.9, 3.3, 1.7 and 0.8 Hz) on C-2 (δ_C 116.0) and on C-4 (δ_C 150.9), respectively, did not show any vicinal coupling between them. The coupling constants of the olefinic protons suggested that each be vicinally coupled with a pair of different methylene protons (Fig. 3-170, 171 and Table 3-64, 65).

Proton spin-spin decoupling experiments deduced the proton-proton sequence shown in Fig. 3-172. By the irradiation on the δ_H 5.122 olefinic proton (C-2-H), a pair of methylene protons resonating at δ_H 3.218 (1H, multiply divided broad doublet, *J*= 22.2 Hz) and 3.113 (1H, multiply divided double-doublets, *J*= 22.2 and 6.6 Hz) geminally coupled with each other was simplified into two broad doublets (C-3-Ha and C-3-Hb, each *J*= 22.2 Hz). On the other hand, when the δ_H 6.065 olefinic proton at C-5 was irradiated, clear collapse of signals at δ_H 2.175 (1H, *J*= 17.7 and 3.3 Hz) and 1.983 (1H, *J*= 17.7 and 7.9 Hz) of C-6-H_2 was observed (two broad double-doublets → two broad-doublets). In addition, the C-3 methylene signals were slightly sharpened by the latter irradiation. This result was indicative of an allyl coupling between the C-5 and the C-3 methylene protons, and consequently a partial structure around those olefinic bonds appeared.

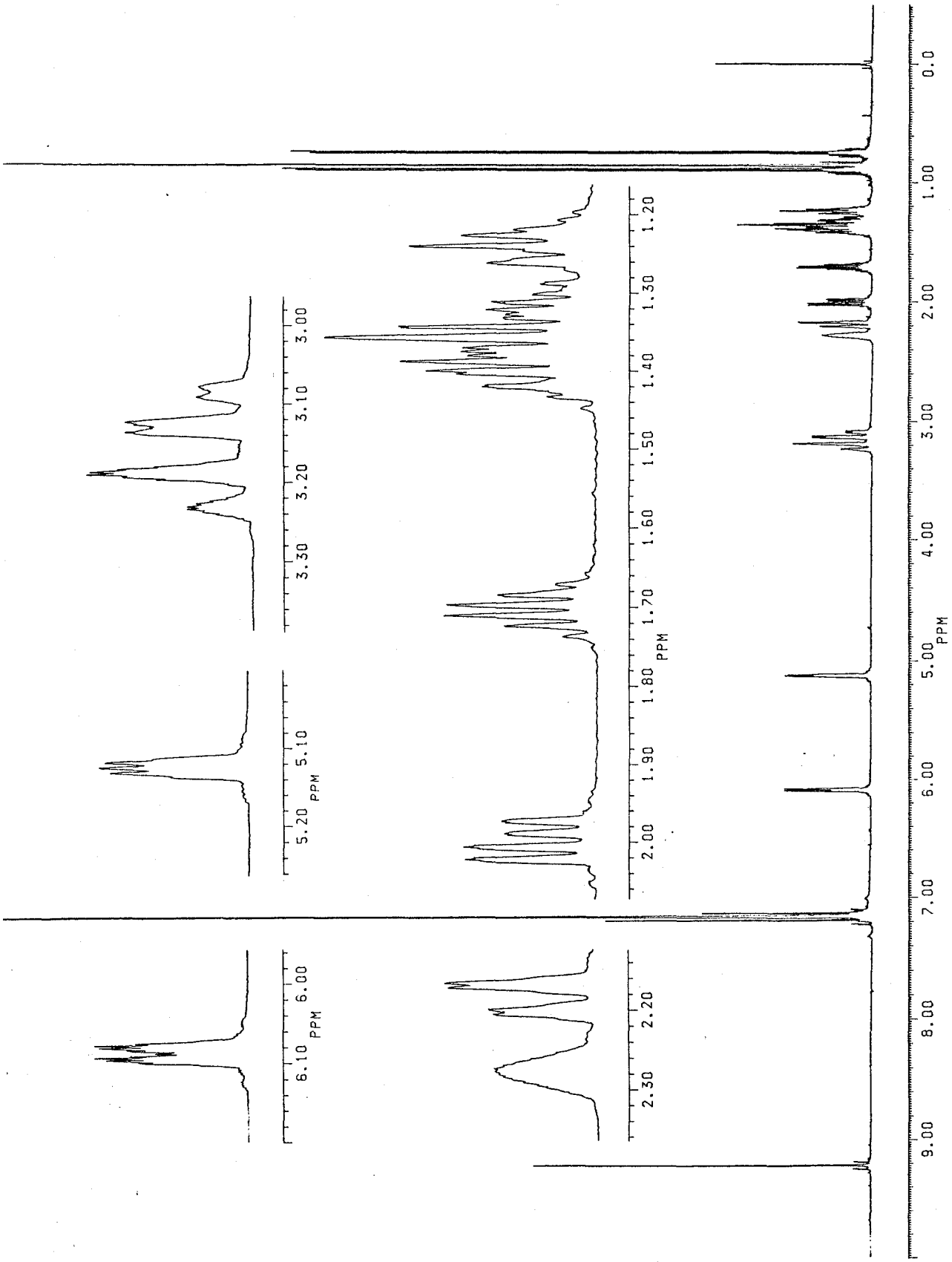

Fig. 3-169 ^{1}H-NMR Spectrum of RL-C (500 MHz, in C_6D_6)

Table 3-63 ^{1}*H-NMR chemical shift values of carota-1,4-dienaldehyde (3)*

(500 MHz, in C_6D_6, TMS as an int. std.)

carbon No	δ_H		J(Hz)
1	-		
2	5.122	ddd	(6.5, 3.4, 2.8)
3	3.218	br. d	(22.2)
	3.113	br. d	(22.2, 6.5)
4	-		
5	6.065	dddd	(7.9, 3.3, 2.9, 0.8)
6	2.175	br. dd	(17.7, 7.9)
	1.983	br. dd	(17.7, 3.3)
7	-		
8	1.40 (approx.)	m	
	1.327	m	
9	1.374	m	
	1.230	m	
10	2.274	br. m	
11	1.704	br. double sept	(6.8, *ca* 6.8)
12	0.888	d	(6.8)
13	0.742	d	(6.8)
14	9.216	s	
15	0.847	s	

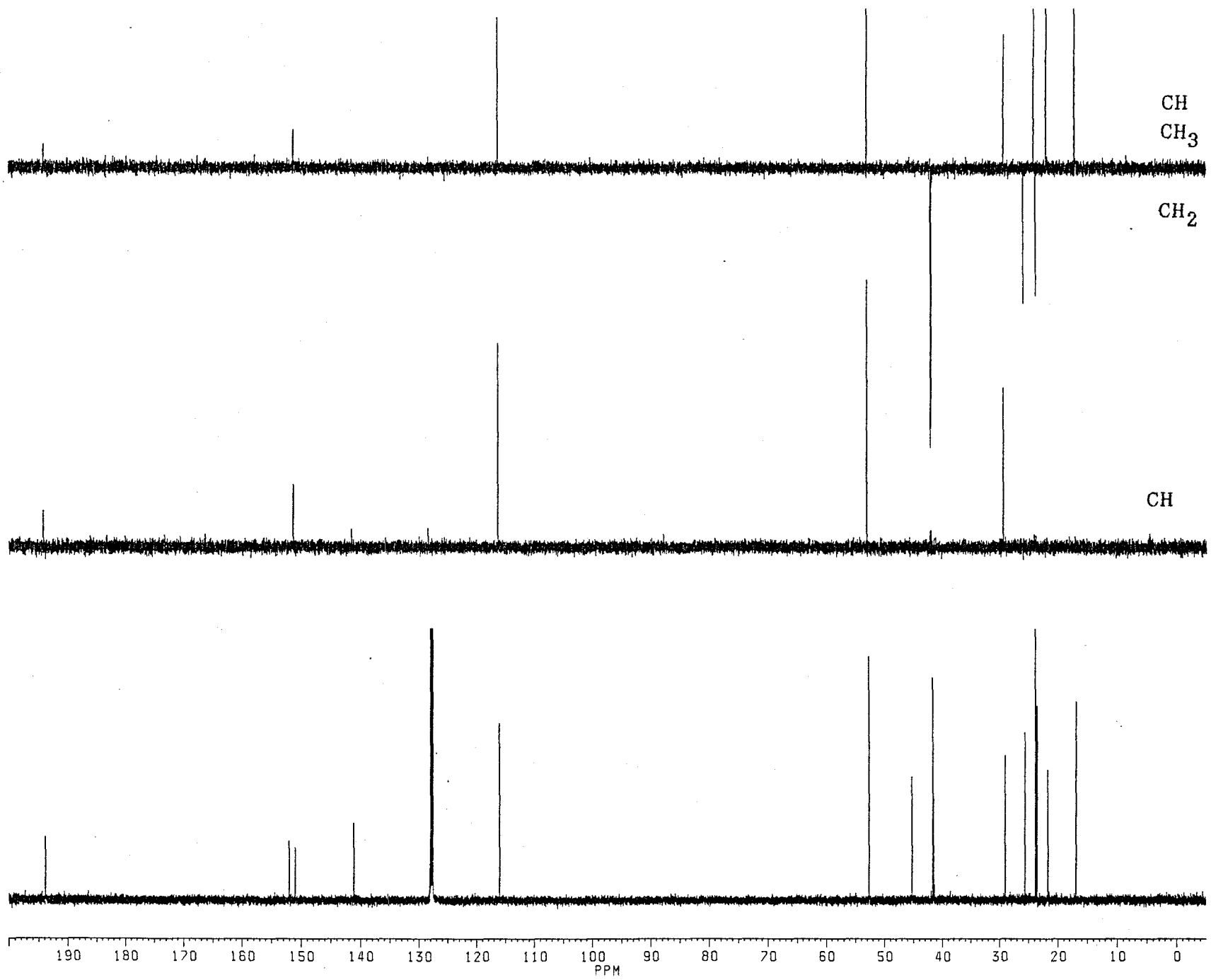

Fig. 3-170 ^{13}C-NMR Spectra of RL-C (125 MHz, in C_6D_6, COM and DEPT)

Table 3-64 ^{13}C-NMR chemical shift values of carota-1,4-dienaldehyde (3)

(125 MHz, in C_6D_6, TMS as an int. std.)

carbon No	δ_C	Property
1	152.0	=C
2	116.0	=CH
3	25.5	CH_2
4	141.1	=C
5	150.9	=CH
6	41.6	CH_2
7	45.2	-C-
8	41.5	CH_2
9	23.4	CH_2
10	52.6	CH
11	28.9	CH
12	21.6	CH_3
13	16.8	CH_3
14	193.8	-CHO
15	23.7	CH_3

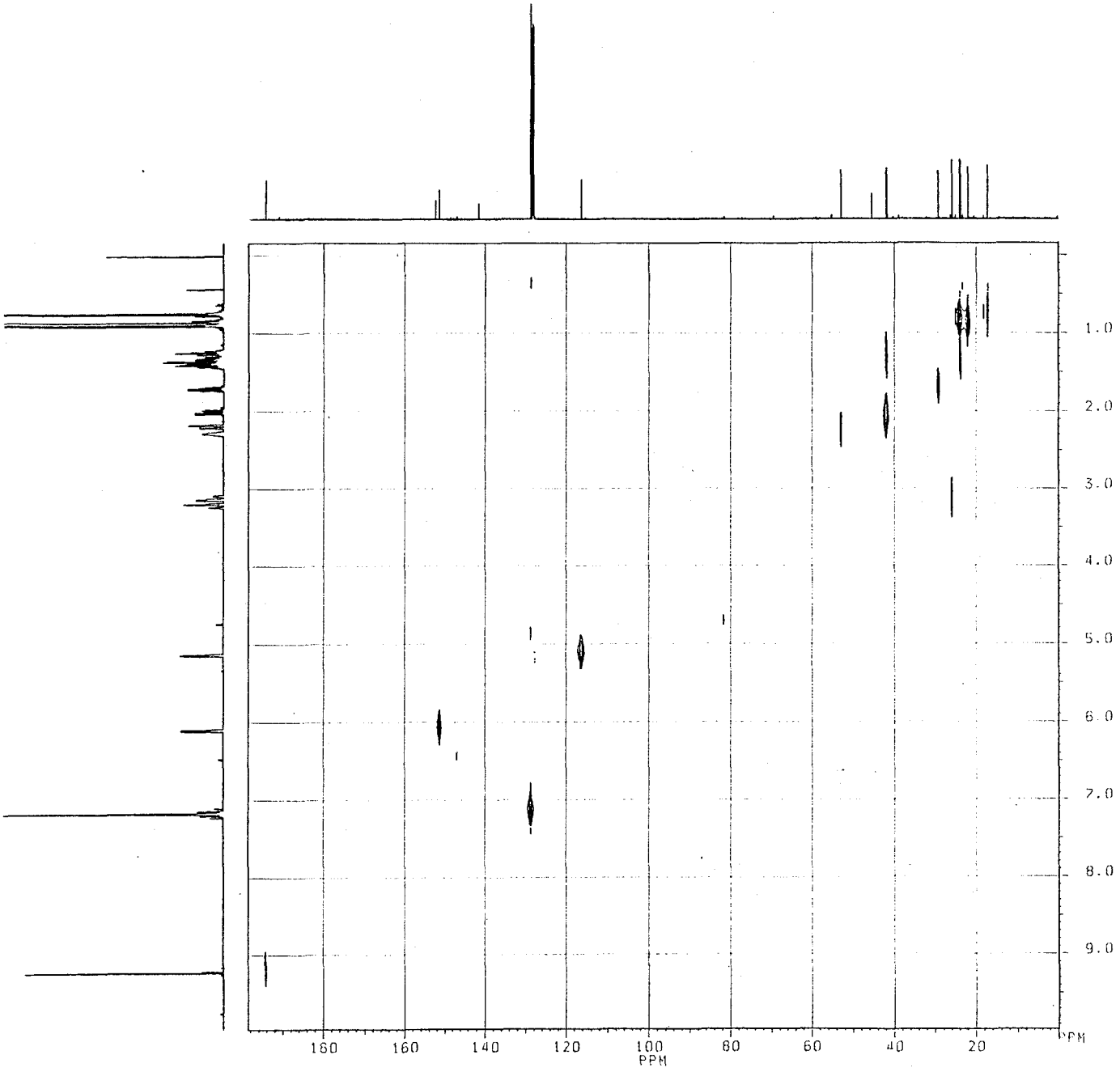

Fig. 3-171 CH-COSY Spectrum of RL-C (500 and 125 MHz, in C_6D_6)

Table 3-65 Proton-carbon correlation elucidated by CH-COSY of carota-1,4-dienaldehyde (3)

(500 and 125 MHz, in C_6D_6, TMS as an int. std.)

No	Carbon	Proton
1	152.0	-
2	116.0	5.112
3	25.5	3.218, 3.113
4	141.1	-
5	150.9	6.065
6	41.6	2.175, 1.983
7	45.2	-
8	41.5	1.40 (approx.), 1.327
9	23.4	1.374, 1.230
10	52.6	2.274
11	28.9	1.704
12	21.6	0.880
13	16.8	0.742
14	193.8	9.216
15	23.7	0.847

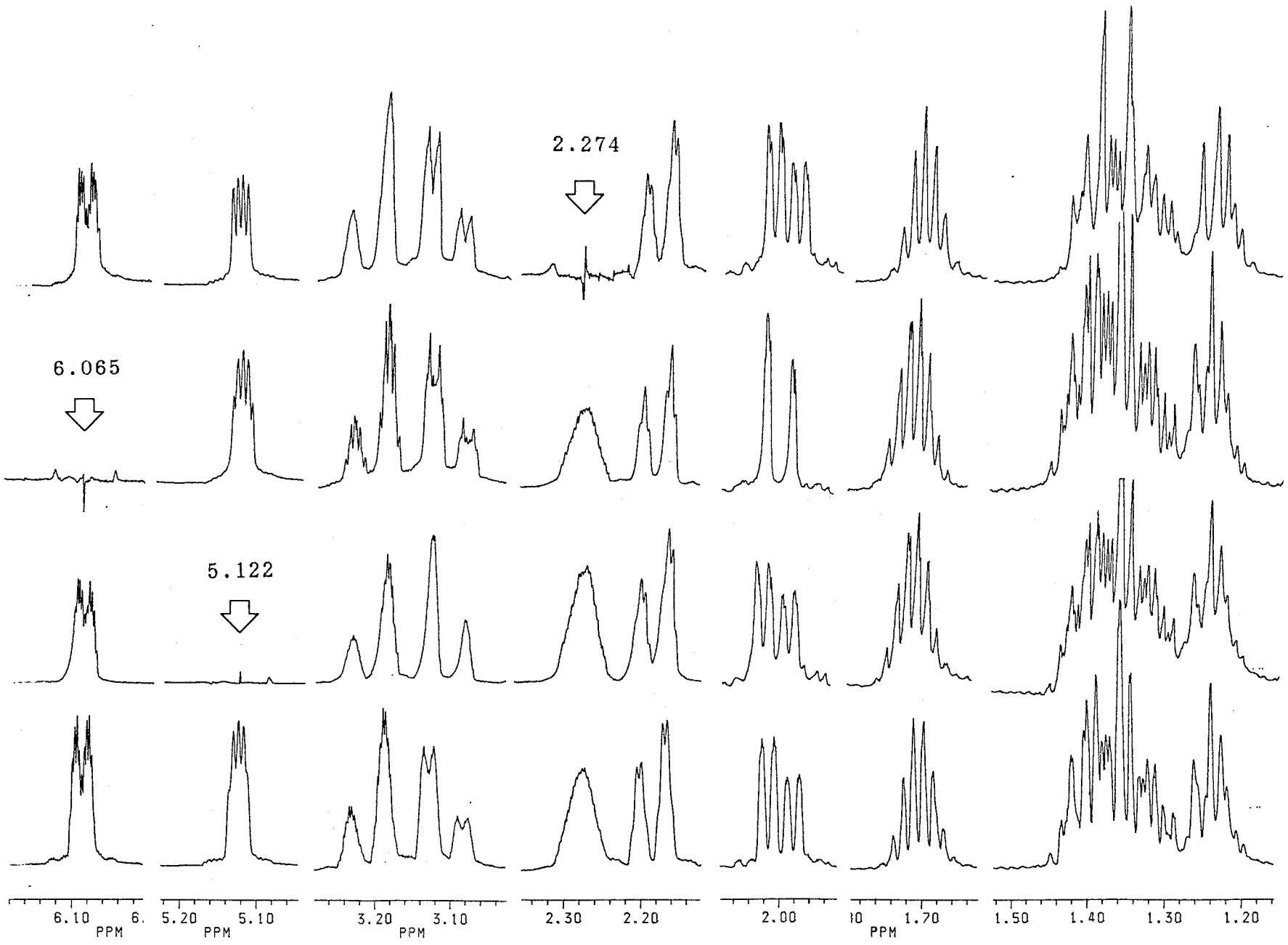

Fig. 3-172 Decoupling Experiments on RL-C (500 MHz, in C_6D_6)

Since a clear deshielding effect is observed on the olefinic proton at δ_H 6.065 and the pair of methylene protons at δ_H 3.218 and 3.113, the conjugated aldehyde group should be allocated to a position complying with both of the deshielding effects. The aldehyde group was therefore substituted on C-4, the β-position from those deshielded protons. Furthermore, the double bond between C-3 and C-4 is revealed to be *cis* regarding the formyl group and the olefinic proton on C-3 as with rugosal A (pp. 68). Accordingly, a partial structure shown in Fig. 3-173 became feasible.

When unassignable δ_H 1.704 signal (1H, a broad multiplet) was irradiated, C-11 methine proton originally divided into eight peaks became a clear septet (*J*= 6.8 Hz). This result indicated that the proton of 1.704 ppm should be assigned to a C-10 methine proton vicinally coupled with the C-11 methine proton by *ca J*= 6.8 Hz. By this irradiation, the C-2 olefinic proton (ddd) at δ_H 5.122 further collapsed into a double-doublet (*J*= 6.6 and 3.4 Hz), and the C-3 methylene protons at δ_H 3.218 and 3.113 also into a broad doublet (*J*= 22.2 Hz) and a broad double-doublet (*J*= 22.2 and 6.6 Hz), respectively. The latter result allowed a speculation that an allylic and a homoallylic couplings exist between the C-10 methine proton and those C-2 and C-3 protons. Accordingly, the non-conjugated olefinic bond (-C=CH-) between C-10 and C-3 became feasible, and those proton sequence deduced a partial structure for RL-C

Moreover, a pair of multiple signals at δ_H 1.230 (1H) and 1.374 (1H), both showing a cross peak with δ_C 23.4 of methylene carbon in the CH-COSY spectrum, were markedly changed its signal patterns by the irradiation at δ_H 1.704 (See Fig. 3-170). This fact further indicated that the irradiated C-10 methine proton was vicinally coupled with another pair of methylene protons assignable to C-9-H_2. The remaining methylene carbon (δ_C 41.5) showing cross peaks with two multiplets at δ_H 1.327 and *ca* 1.40 (each 1H) was

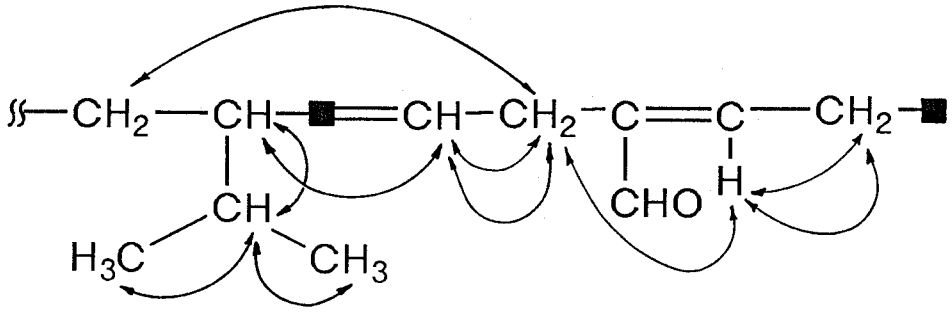

Fig. 3-173 Proton Coupling Sequence around the Olefinic Protons of RL-C

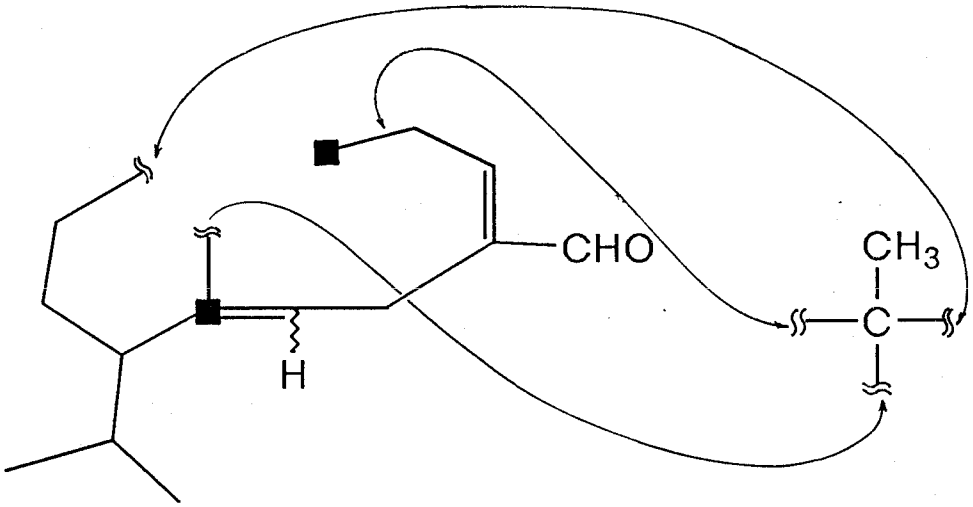

Fig. 3-174 Elucidated Partial Structure of RL-C Consisting of α, β-Unsaturated Aldehyde and Isopropyl Groups

presumed to connect with the C-9 methylene, since no other position can accept the methylene group showing a vicinal proton coupling. Thus, 11 carbons out of total 15 in the compound was eventually assigned to form the partial structure consisting of the α,β-unsaturated aldehyde and the isopropyl groups as shown in Fig. 3-174.

Among four of the unassigned carbons, the sp^3 quarternary carbon (δ_C 52.6) only afforded to connect with the bridgehead methyl (δ_H 0.847, δ_C 23.7), the C-9 methylene (δ_C 41.5) and the C-1 olefinic (δ_C 152.0) carbons all possessing an unassigned C,C-single bond. Consequently, all protons and carbons in RL-C were assigned to give a planar structure **3** having a carotane skeleton with a 1,4-diene partial structure, completely acceptable as a precursor of **1** (Fig. 3-175). RL-C found as a novel sesquiterpene was named carota-1,4-dienaldehyde.

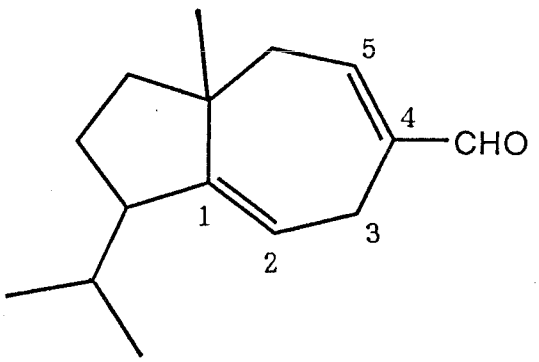

Fig. 3-175 Structure of RL-C Having 1,4-Diene Moiety to Be a Possible Precursor of Rugosal A

Table 3-66 Physicochemical properties of carota-1,4-dienaldehyde (3)

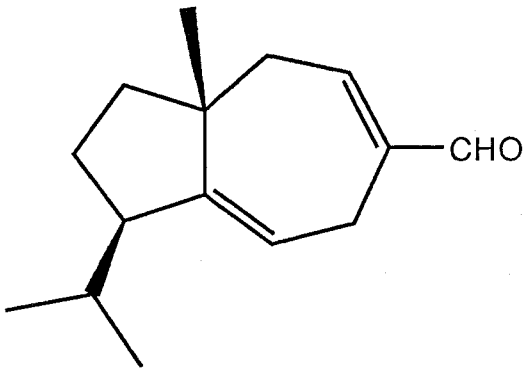

3

A colorless oil

Vanillin-H_2SO_4 color: grayish brown

UVλ_{max}^{MeOH}: 230.5 nm (disappeared with minute 1N HCl)

EI-HR-MS: 218.165 ($C_{15}H_{22}O$ requires 218.167)

GC-MS *m/z* (%): 218 (M^+, 49), 203 (M^+-CH_3, 12), 200 (11), 185 (22), 176 (19), 175 ($M^+-C_3H_7$, 100), 157 (27), 147 (41), 133 (25), 131 (17), 119 (27), 117 (14), 107 (17), 105 (50), 91 (61), 81 (39), 79 (24), 77 (21), 67 (16), 55 (28), 43 (17), 41 (54).

EI-MS *m/z* (%): 218 (M^+, 27), 203 (M^+-CH_3, 13), 200 (7.8), 185 (22), 176 (19), 175 ($M^+-C_3H_7$, 100), 157 (29), 147 (44), 133 (28), 131 (23), 119 (35), 117 (18), 107 (20), 105 (71), 93 (27), 91 (83), 81 (44), 79 (34), 77 (29), 67 (23), 55 (37), 43 (25), 41 (68). (54).

IR $\nu_{max}^{thin\ film}$ cm^{-1}: 2940 br., 2860 (CHO), 2700 (CHO), 1685 (C=O), 1655 (C=C), 1445, 1420, 1380, 1170, 1140.

^1H- and ^{13}C-NMR data are shown in Tables 3-63, 3-64 and 3-65, respectively.

5-4 Chemical Conversion of Carota-1,4-dienaldehyde

1) Conversion into Methoxycarbonyl Derivative

To obtain some line of coevidence for an elucidated planar structure, some chemical conversions of carota-1,4-dienaldehyde (**3**) were carried out. Firstly, **3** was converted into the methoxycarbonyl derivative according to Corey's method [101,102]. Active MnO_2 (120 mg), NaCN (*ca* 22 mg) and AcOH (22 mg) were added to 1 ml of MeOH containing 5.2 mg of **3**, and the mixture was stirred overnight at room temperature. The reaction mixture was then diluted with 50 ml of distilled water and extracted with 20 ml of EtOAc. After washing twice with 30 ml of distilled water, the organic layer was dried over Na_2SO_4, concentrated and subjected to PTLC in *n*-hexane-EtOAc 20:1. The main product (RL-C-ME, *Rf* 0.63, 1.5 mg, in a 20 % yield) were obtained as a colorless syrup, in addition to unreacted **3** (4.0 mg, *Rf* 0.37, 58 %) (Fig. 3-176).

In EI-MS, RL-C-ME showed the molecular ion at *m/z* 248 (**3** + 30 mass units, 8.6 %), and other fragments at *m/z* 217 (M^+-OCH_3, 2.4 %) and 189 (M^+-$COOCH_3$, 5.1 %) which were indicative of the presence of the methoxy carbonyl group in the derivative (Fig. 3-177). Concerted disappearance of the formyl proton, the methoxy proton signal was observed at δ_H 3.430 in the ^{1}H-NMR spectrum (Fig. 3-178). In addition, all other protons showed a good correspondence with those of **3**, except C-5 olefinic proton at δ_H 7.211 deshielded by the methoxycarbonyl group (Table 3-67). In C_6D_6, C-5 olefinic proton of **3a** is markedly deshielded from the starting material ($\Delta\delta$ 1.15 ppm by **3**). This characteristic deshielding effect is due to the C-14 methoxycarbonyl group, as observed in RDA-TU-ME (**2b**) on C-3-H, [δ_H 6.808, deshielded by 0.97 ppm from that of the corresponding proton of RSA-TU (**1e**, δ_H 5.841)]. Unlike **3**, resolution of C-8 and C-9 protons was enhanced in this product enough to prove all the proton sequence. Thus, structure of RL-C-ME was proved to be **3a**.

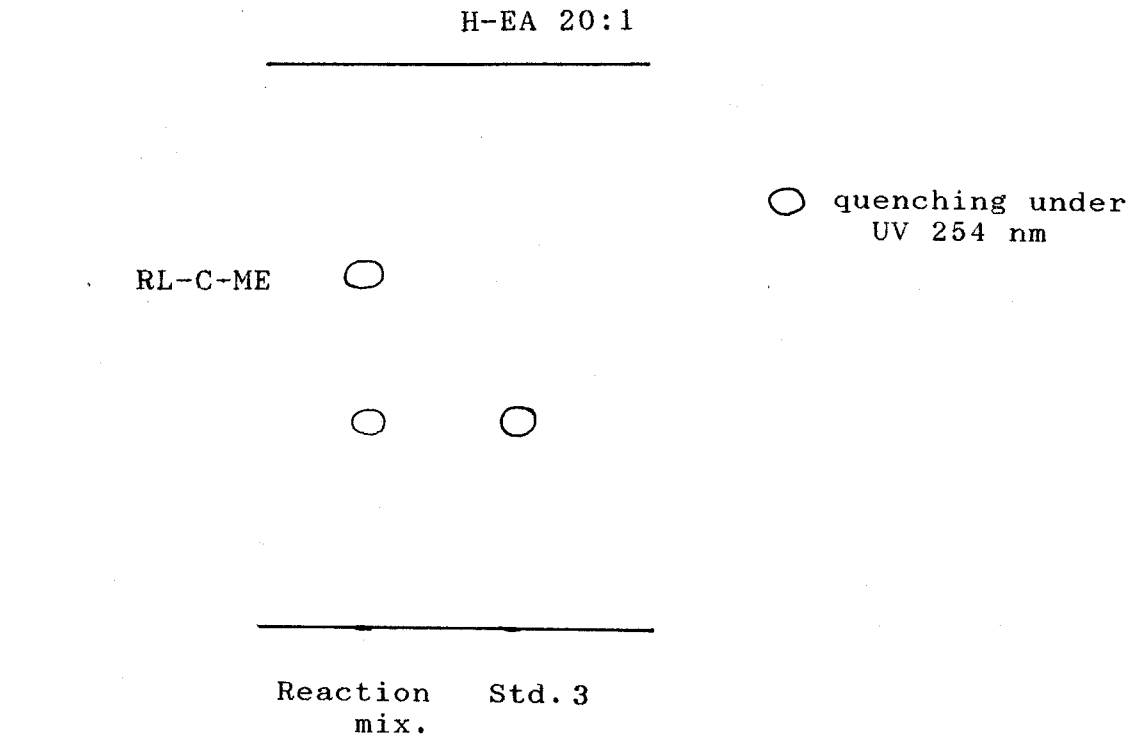

Fig. 3-176 TL Chromatogram of RL-C-ME Converted from Carota-1,4-Dienaldehyde (3) by Treatment with Active Manganese Dioxide and Sodium Cyanide

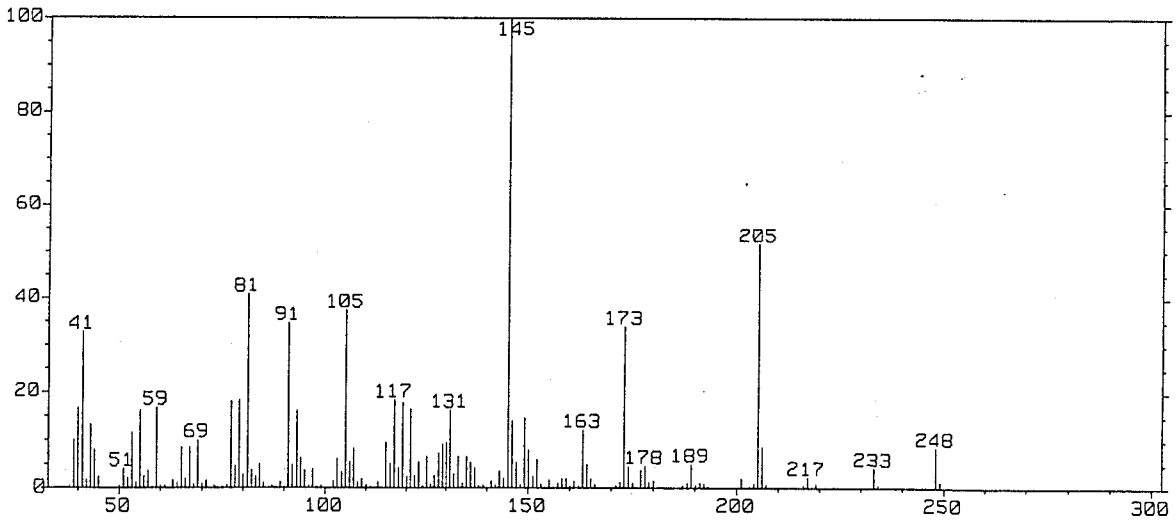

Fig. 3-177 EI-Mass Spectrum of RL-C-ME

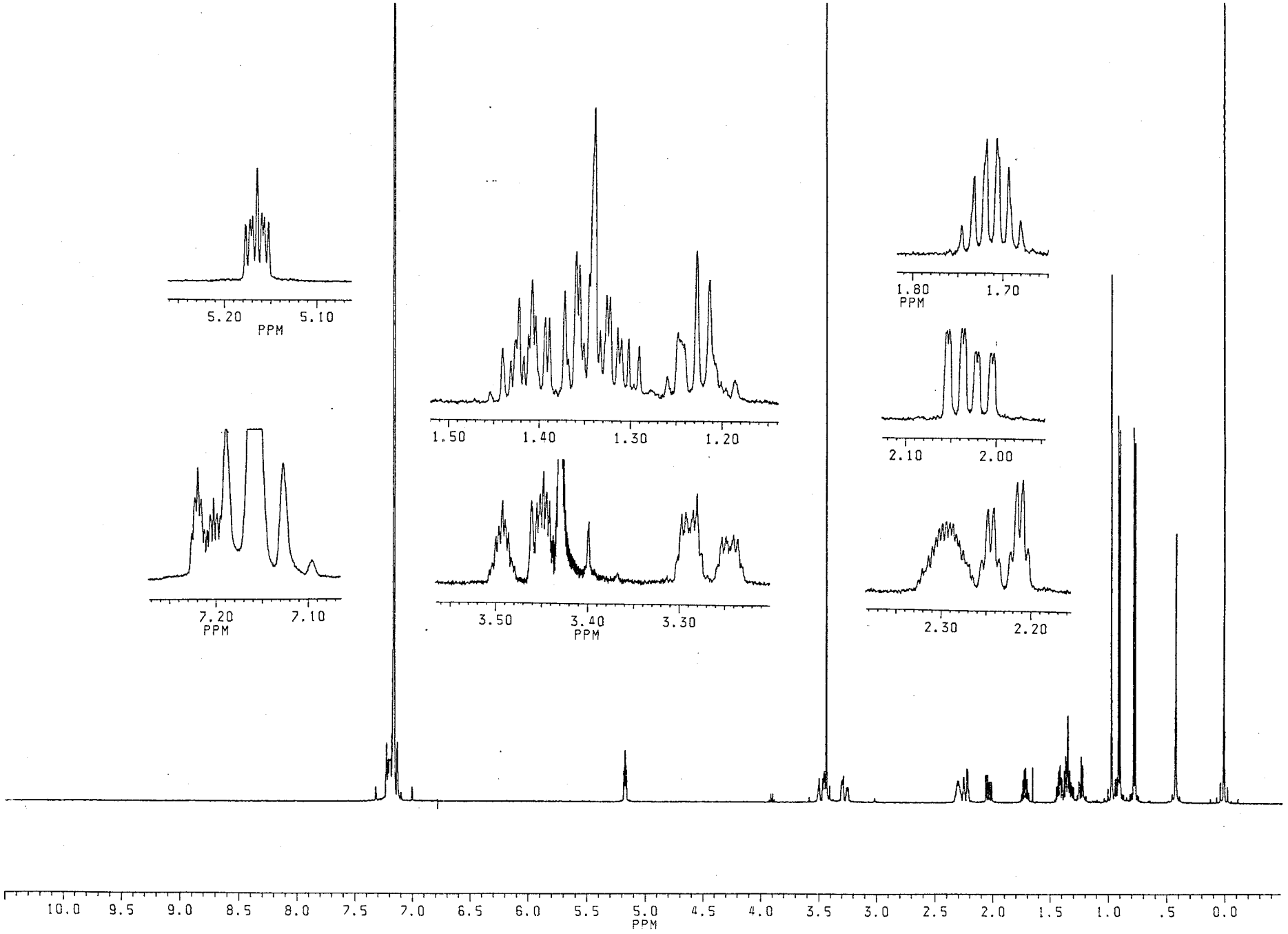

Fig. 3-178 ^{1}H-NMR Spectrum of RL-C-ME (500 MHz, in C_6D_6)

Table 3-67 *^{1}H-NMR chemical shift values of RL-C-ME*

(500 MHz, in C_6D_6, TMS as an int. std.)

δ_H		Coupling	Assignment
5.164	ddd	*J*= 6.2, 3.7 and 2.3 Hz	C-2-H
3.470	br. d	*J*= 22.2 Hz	C-3-Ha
3.266	ddd	*J*= 22.2, 6.2 and 2.1 Hz	C-3-Hb
7.211	br. dd	*J*= 8.4 and 3.5 Hz	C-5-H
2.230	br. dd	*J*= 16.2 and 3.5 Hz	C-6-Ha
2.029	br. dd	*J*= 16.2 and 8.4 Hz	C-6-Hb
1.35 (approx.)	m		C-8-Ha
1.227	ddd	*J*= 13.8, 6.9 and 6.9 Hz	C-8-Hb
1.416	m		C-9-Ha
1.33 (approx.)	m		C-9-Hb
2.292	m		C-10-H
1.722	double sept	*J*= *ca* 6.8 and 6.8 Hz	C-10-H
0.898	d	*J*= 6.8 Hz	C-12-H_3
0.753	d	*J*= 6.8 Hz	C-13-H_3
3.430	s		C-14'-OCH_3
0.964	s		C-15-H_3

Table 3-68 Physicochemical properties of RL-C-ME (3a)

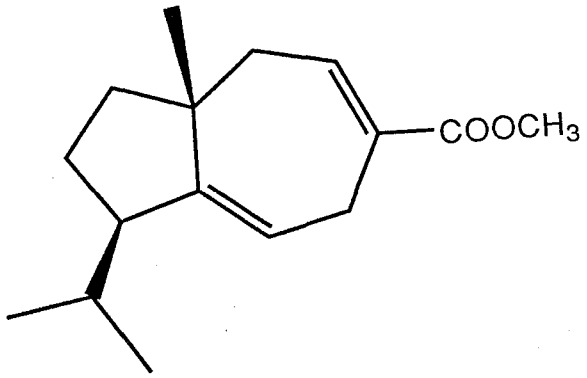

3a

A colourless syrup

Vanillin-H_2SO_4 color: pink

$[\alpha]_D$: - 125 ° (*c* 0.02 in EtOH)

EI-MS *m/z* (%): 248 (M^+, 8.6), 233 (M^+-CH_3, 4.2), 217 (M^+-OCH_3, 2.4), 206 (8.6), 205 (M^+-C_3H_7, 52), 189 (M^+-$COOCH_3$, 5.1), 178 (4.7), 173 (34), 163 (12), 149 (15), 146 (14), 145 (100), 131 (16), 121 (17), 119 (18), 117 (19), 105 (38), 93 (16), 91 (35), 81 (41), 79 (18), 77 (18), 59 (17), 55 (16), 43 (13), 41 (33), 40 (17).

^{1}H-NMR data are shown in Table 3-67.

2) Conversion into Epoxy Derivative

m-CPBA (*metha*-chlorperbenzoic acid) is known as an epoxidation reagent which can convert selectively a non-conjugated olefine into an epoxide [129]. When carota-1,4-dienaldehyde (3) is treated with *m*-CPBA, 3 will give a monoxygenated derivative possessing an epoxy group on C-1 and C-2, if the proposed structure is correct. Carota-1,4-dienaldehyde (3, 2.1 mg) dissolved in 0.5 ml of acetone was stirred with 8.2 mg of *m*-CPBA overnight at room temperature. The reaction mixture was concentrated *in vacuo* and subjected to PTLC (*n*-hexane-EtOAc 9:1). Together with *ca* 0.8 mg of the starting material (*Rf* 0.55, 38 % recovery), the main product (RL-C-CPBA, *Rf* 0.21, 1.2 mg, in a 54 % yield) was obtained as a colorless syrup (Fig. 3-179).

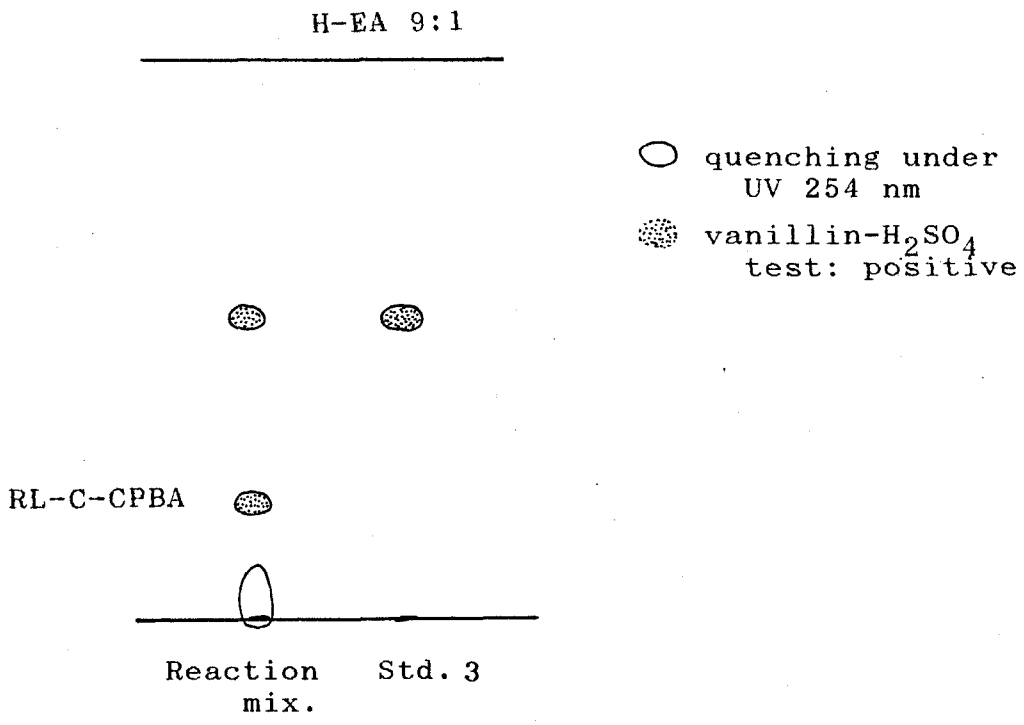

Fig. 3-179 TL Chromatogram of RL-C-CPBA Converted from Carota-1,4-Dienaldehyde (3) by Treatment with *m*-CPBA

The product with molecular weight of 234 (M^+, 2.4 % in EI-MS, Fig. 3-180) showed the C-2 methine proton (δ_H 3.005, br. d, J= 5.1 Hz), locating on the epoxy ring and coupled with one of the C-3 methine proton (δ_H 3.341, br. dd, J= 19.8 and 5.1 Hz), in the ^{1}H-NMR spectrum (Fig. 3-181). Since the 1,4-diene system which had caused the allylic or homoallylic coupling in **3** was blocked, completely separated two coupling sequences of the epoxy derivative became feasible as shown in Fig. 3-182. The C-8, C-9 and C-10 protons showed a good resolution in the higher magnetic field, and were all unambiguously assigned by the decoupling experiments. Consequently, these proton sequences proved the structure of RL-C-CPBA as **3b**, a derivative monoxyganated at the non-conjugated olefinic bond in **3**.

In the ^{13}C-NMR, the C-2 methine carbon was detected at δ_C 51.9 which is a typical chemical shift value to a methine carbon of epoxy ring, while another epoxy carbon, C-1 was reasonably observed at δ_C 71.5 (Fig. 3-183 and Table 3-70).

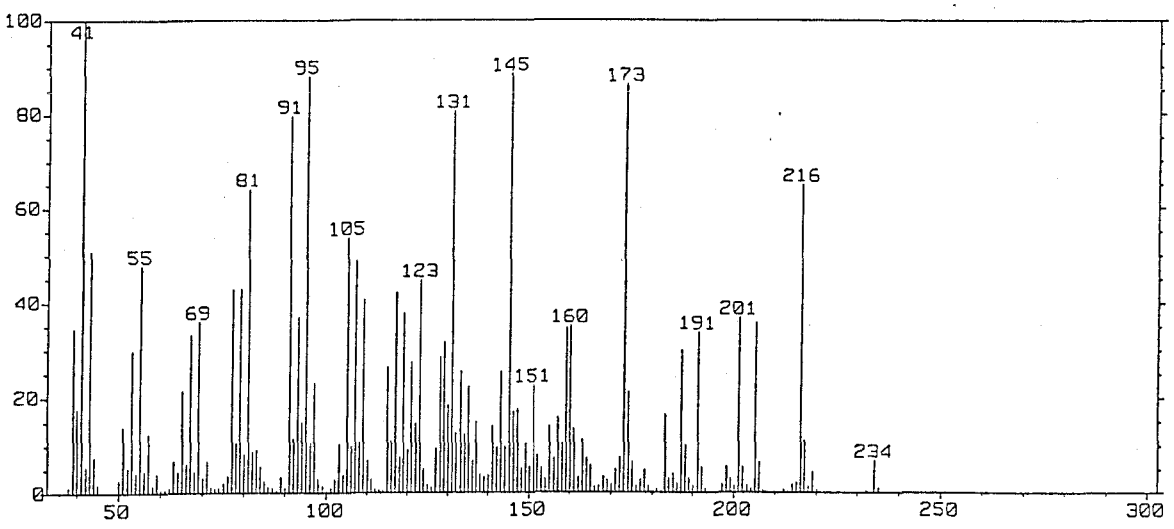

Fig. 3-180 EI-Mass Spectrum of RL-C-CPBA

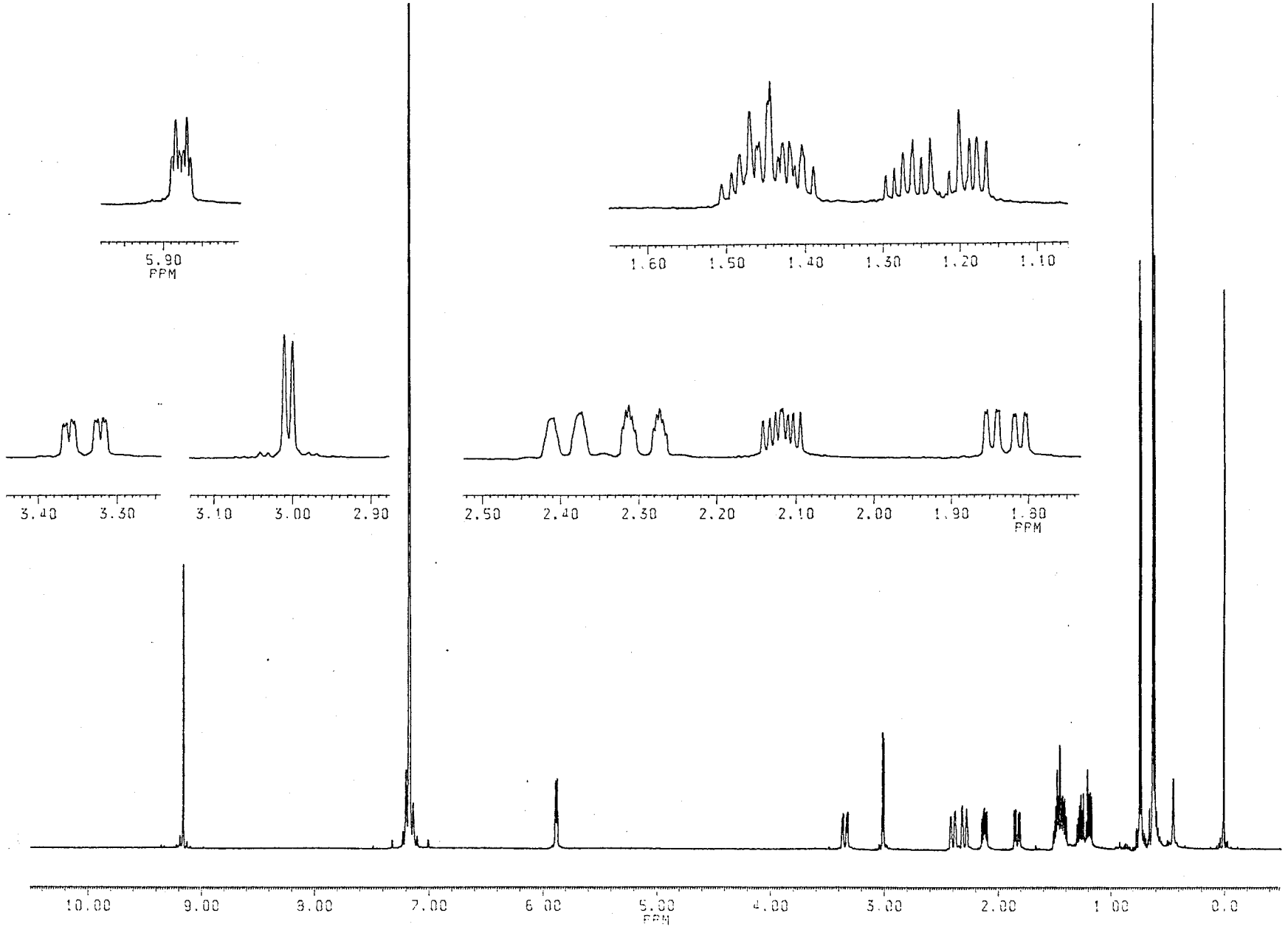

Fig. 3-181 ^{1}H-NMR Spectrum of RL-C-CPBA (500 MHz, in C_6D_6)

Table 3-69 ^{1}*H-NMR chemical shift values of RL-C-CPBA*

(500 MHz, in C_6D_6, TMS as an int. std.)

δ_H	Coupling		Assignment
3.005	d	*J*= 5.1 Hz	C-2-H
3.341	br. dd	*J*= 19.8 and 5.1 Hz	C-3-Ha
2.294	br. d	*J*= 19.8 Hz	C-3-Hb
5.873	ddd	*J*= 7.1, 2.3 and 2.3 Hz	C-5-H
2.391	br. d	*J*= 18.7 Hz	C-6-Ha
1.827	br. dd	*J*= 18.7 Hz	C-6-Hb
1.487	dd	*J*= 11.4 and 6.4 Hz	C-8-Ha
1.193	dd	*J*= 11.4 and 6.4 Hz	C-8-Hb
1.416	m		C-9-Ha
1.266	ddd	*J*= 11.7, 11.5 and 6.4 Hz	C-9-Hb
2.118	ddd	*J*= 11.7, 8.0 and 4.5 Hz	C-10-H
1.475	m		C-11-H
0.729	d	*J*= 6.9 Hz	C-12-H_3
0.612	d	*J*= 6.9 Hz	C-13-H_3
9.152	s		C-14-H_3
0.620	s		C-15-H_3

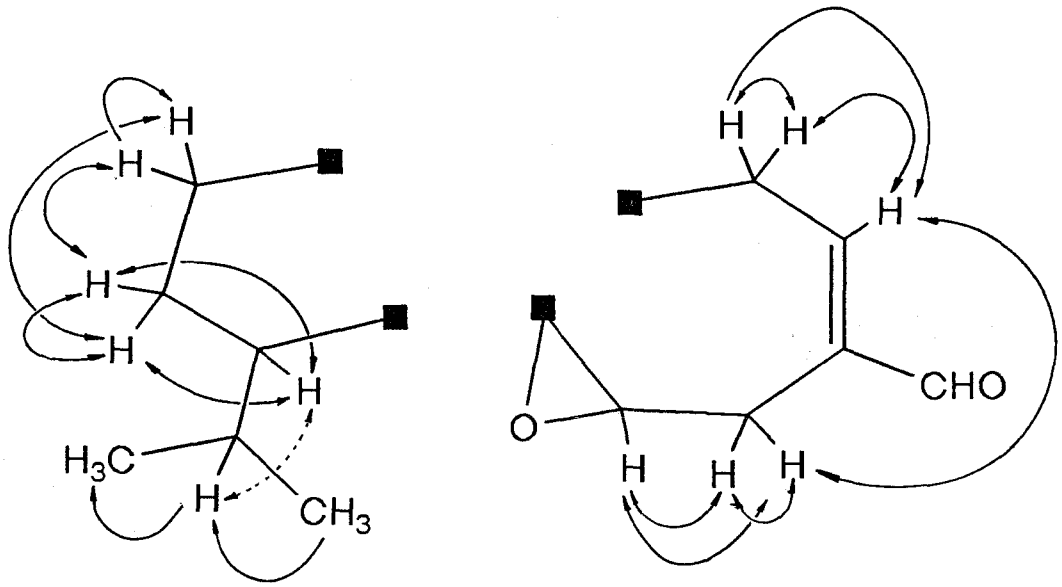

Fig. 3-182 Two Proton Coupling Sequence of RL-C-CPBA

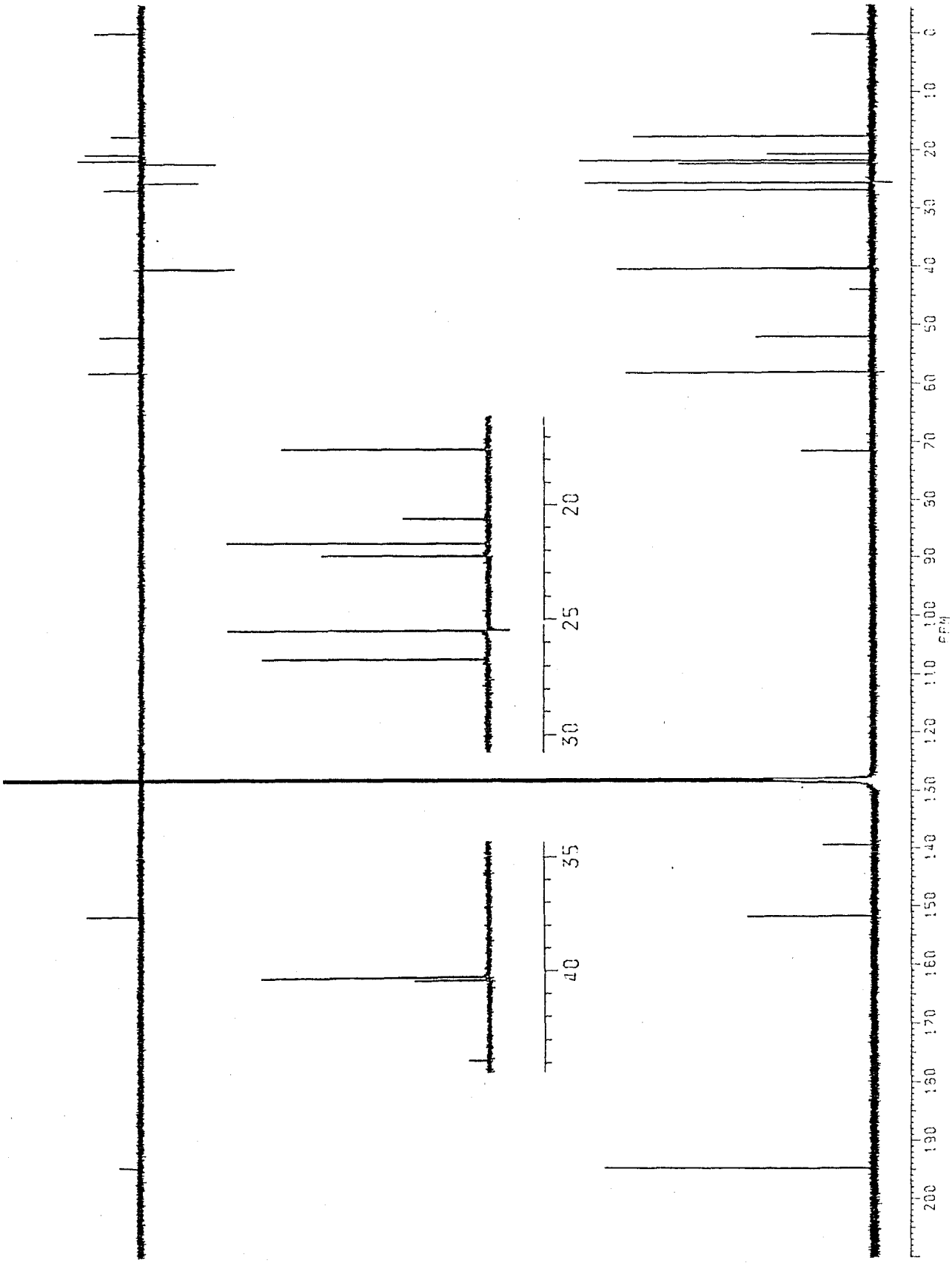

Fig. 3-183 ^{13}C-NMR Spectra of RL-C-CPBA (125 MHz, in C_6D_6, COM and DEPT)

Table 3-70 *^{13}C-NMR chemical shift values of RL-C-CPBA*

(125 MHz, COM and DEPT, in C_6D_6, TMS as an int. std.)

δ_C	Hydrogenation	Possible assignment
194.5	CH	14-CH
151.5	CH	5-CH
139.3	C	4-C
71.5	C	1-C
57.9	CH	2-CH
51.9	CH	10-CH
43.8	C	7-C
40.3	CH_2	8-CH_2 (or 6-H_2)
40.2	CH_2	6-CH_2 (or 8-H_2)
26.7	CH	11-CH
25.4	CH_2	3-CH_2
22.2	CH_2	9-CH_2
21.6	CH_3	15-CH_3
20.5	CH_3	12-CH_3
17.5	CH_3	13-CH_3

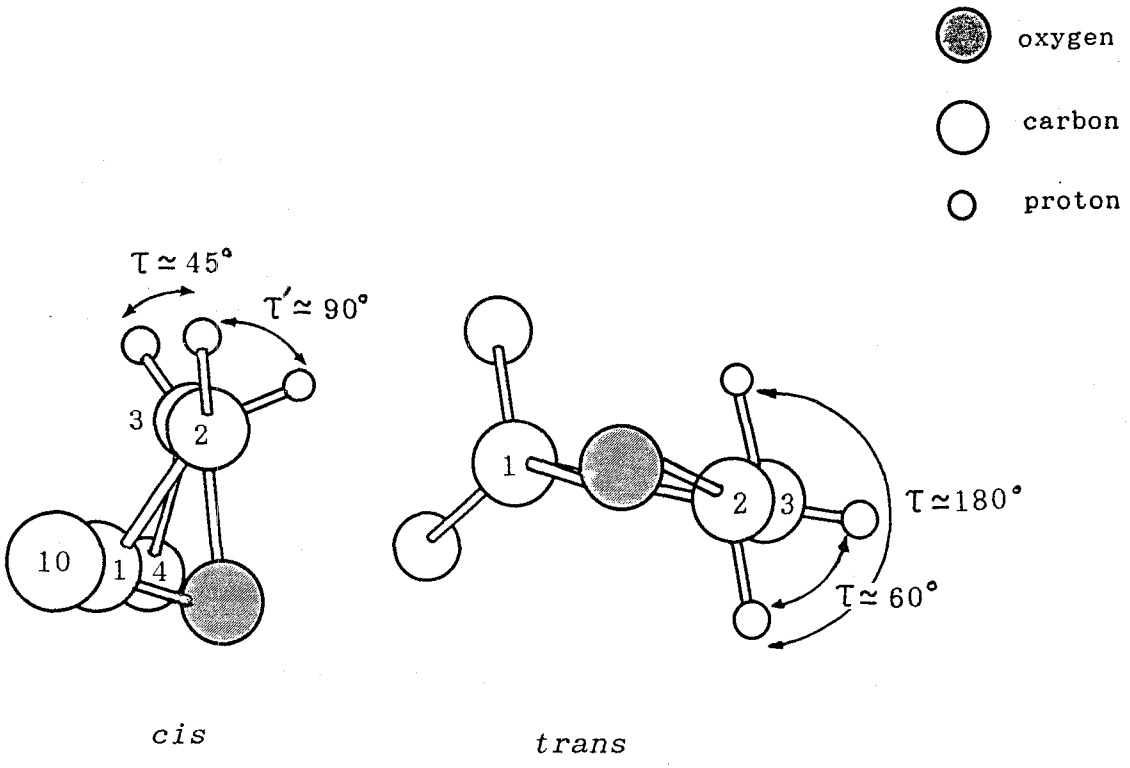

Fig. 3-184 Angle between C-2 Methine Proton and C-3 Methylene Protons on a Molecular Model of RL-C-CPBA

From the ^{1}H-NMR spectrum of **3b**, stereo-selective epoxidation in **3** was obvious. Since the coupling constants of the C-2 proton are comparatively small (J= 5.1 and less than 1 Hz), the epoxy ring is presumed to be *cis* in the light of Stenger-Jackmann function (Fig. 3-184) [92]. Indeed, a *trans*-epoxy ring seems hardly to be formed on the trisubstituted olefinic bond in such a bicyclic system involving a bridgehead carbon. To elucidate the relative configuration of the epoxy-ring, NOEs were measured on **3b**. Consequently, some NOEs were observed as shown in Fig. 3-185. Among them, a small NOE between C-15-H_3 and C-2-H was certainly indicative of the absolute configuration of epoxy ring (1***R***, 2***S***). This selectivity is presumably caused by steric effects of the isopropyl and C-15 bridgehead methyl groups. In addition, stereostructure at C-10 was also revealed as ***R*** due to the NOE between C-15-H_3 and C-12-H_3 (***R*** at C-7 are shown in pp. 333).

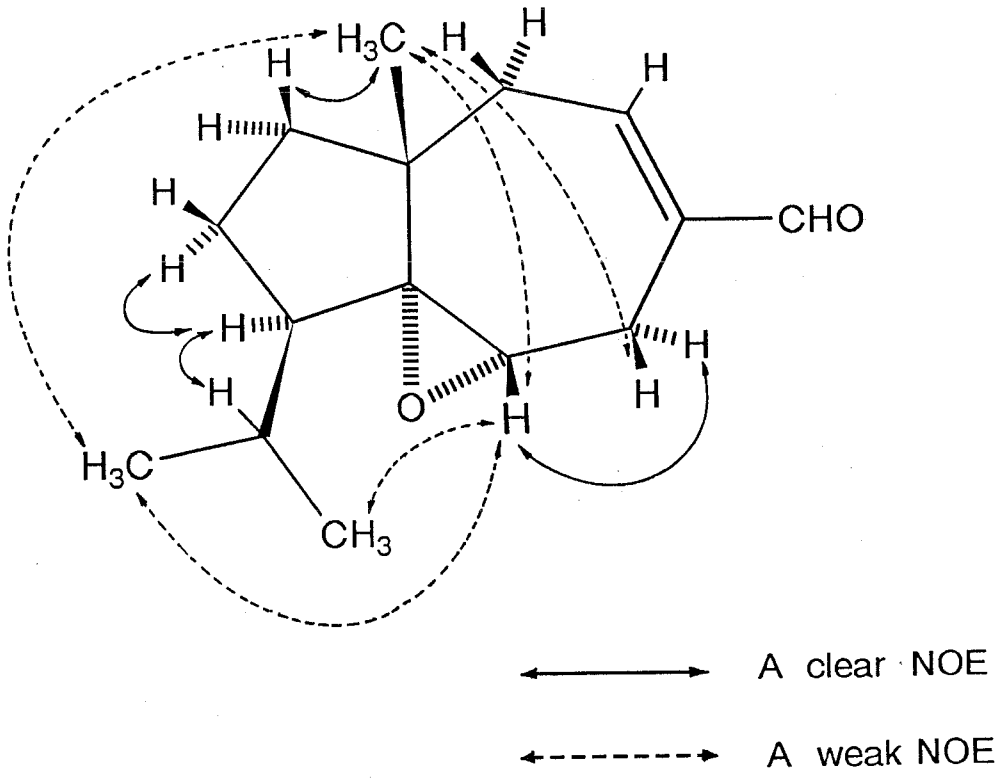

Fig. 3-185 NOEs Observed on RL-C-CPBA

*Table 3-71 Physicochemical properties of RL-C-CPBA (**3b**)*

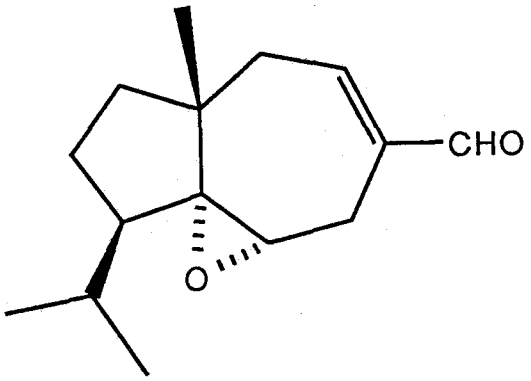

3b

A colourless syrup

Vanillin-H_2SO_4 color: brownish orange

EI-MS *m/z* (%): 234 (M^+, 7.0), 216 (M^+-H_2O, 65), 205 (36), 201 (37), 191 (34), 187 (30), 173 (87), 160 (35), 159 (35), 145 (89), 131 (81), 123 (45), 119 (38), 117 (42), 109 (41), 107 (49), 105 (54), 95 (88), 91 (80), 81 (64), 69 (36), 55 (48), 43 (51), 41 (100).

^1H- and ^{13}C-NMR data are shown in Tables 3-69 and 3-70, respectively.

3-5-5 Related Sesquiterpene Acid, Carota-1,4-dienoic Acid

The benzene solubles (See pp. 290) dissolved in 10 % EtOAc/hexane were subjected to silica gel column chromatography (Wako gel C-200, 750 ml in hexane; column, 4 cm i.d.) to give six fractions (Table 3-72 and Fig. 3-186).

Table 3-72 Fractions obtained by silica gel column chromatography of the benzene solbles from Sample VI

Fraction	Eluting solvent	Volume (ml)	Eluant (g)
Fr-B-1	10 % EtOAc/*n*-hexane	400	0
Fr-B-2	10 % EtOAc/*n*-hexane	400	2.4
Fr-B-3	10 % EtOAc/*n*-hexane	400	2.5
Fr-B-4	20 % EtOAc/*n*-hexane	400	2.1
Fr-B-5	20 % EtOAc/*n*-hexane	400	5.8
Fr-B-6	35 % EtOAc/*n*-hexane	400	3.6

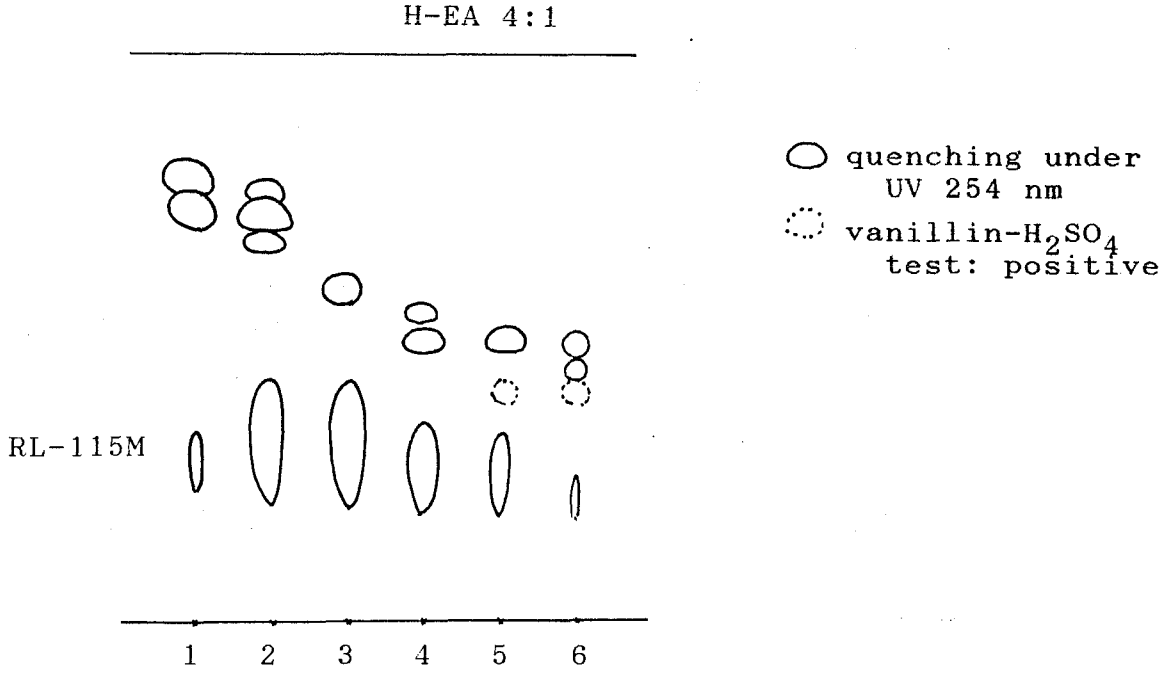

Fig. 3-186 TL Chromatogram of Fractions Eluted from Silica Gel Column Applied Benzene Soluble of Sample VI

In Fr-B-2 to -5, an unknown component was detected at *Rf* 0.31 in *n*-hexane/EtOAc 4:1 as a major constituent (RL-115M, *ca* 200 mg/kg leaves), showing a pinkish color with vanillin-H_2SO_4 reagent. By a small scale of PTLC developed in the same solvent system, *ca* 10 mg of a colorless syrup was obtained from Fr-B-3, and FI-MS and ^{1}H-NMR analyses revealed the isolate to be a mixture of M^+ 234 compounds (Fig. 3-187 and 188). On the basis of its severe tailing on the TLC, this mixture was expected to be consisting of carboxylic acids. Since it was hard to purify each compound by PTLC, its ^{1}H-NMR spectrum was preliminarily taken in the state of mixture.

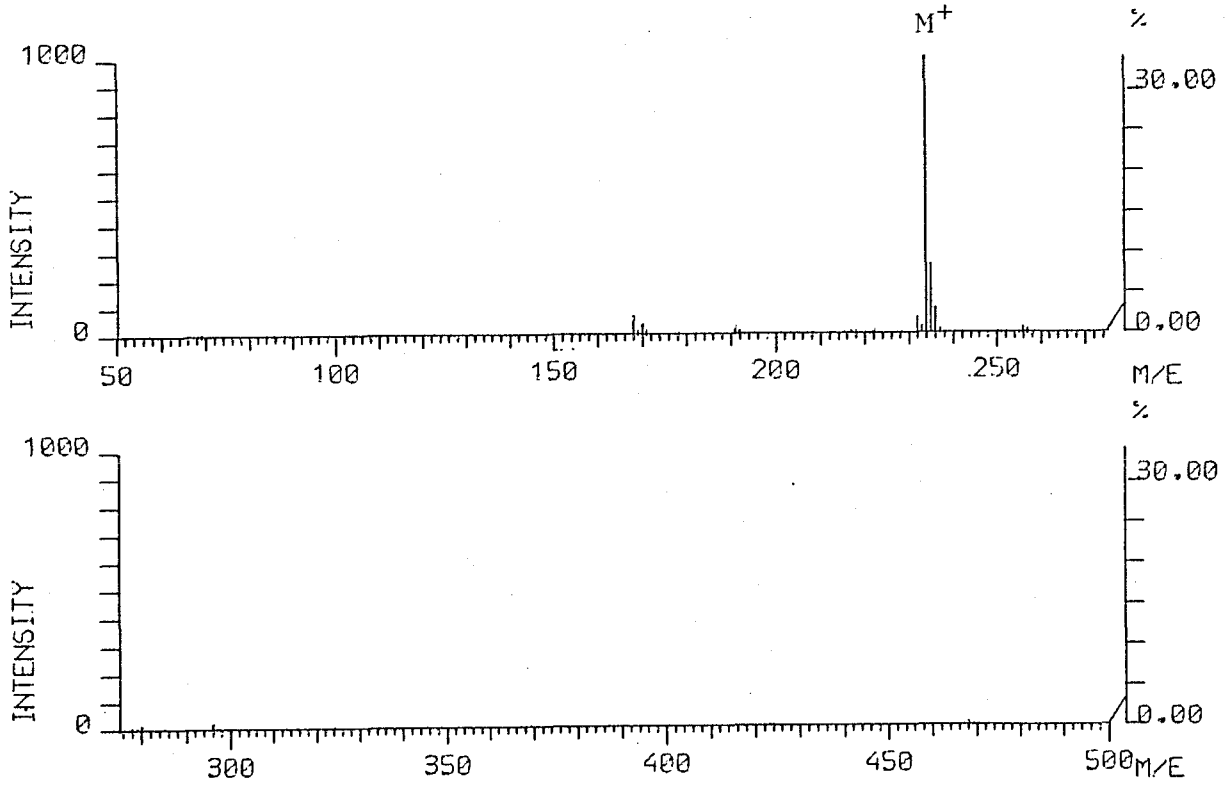

Fig. 3-187 FI-Mass Spectrum of RL-115M

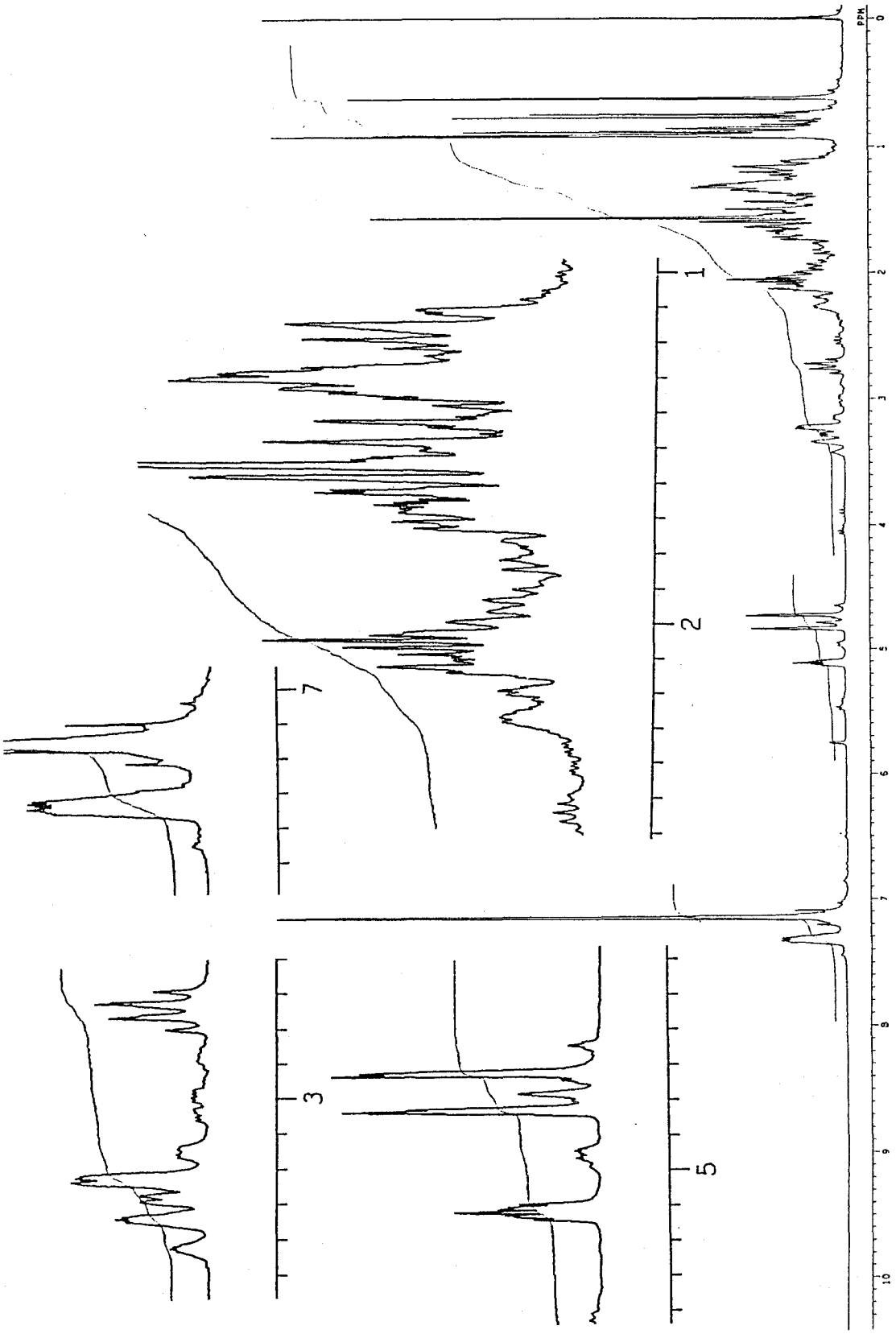

Fig. 3-188 ^{1}H-NMR Spectrum of RL-115M (270 MHz, in C_6D_6)
Mainly two constituents are involved.

In the ^{1}H-NMR spectrum, the major substance RL-115M-A showing some features of carotane skeleton having the 1,4-diene structure corresponding to 3 [*e.g.* C-15 methyl group at δ_H 0.915 (3H, s), isopropyl group at δ_H 0.895 (3H, d, *J*= 6.8 Hz) and 0.759 (3H, d, *J*= 6.8 Hz)], and some similar proton signals to those of 3 [*e.g.* δ_H 3.385 (1H, br. d, *J*= 23.7 Hz), 3.192 (br. d, *J*= 23.7 Hz) both possibly assignable to C-3-H_2 and 2.270 (1H, br. m) to C-10-H] (Fig. 3-188). Furthermore, lack of a C-14 formyl proton and deshielding of C-5 olefinic proton at δ_H 7.331 in C_6D_6 were well indicative of properties as a carboxylic acid, although *ca* 8 mg of acidic constituents, recovered from aq. $NaHCO_3$ solution of the benzene solubles, contained only a trace amount of the focused compounds.

Unexpectedly, it was quite hard to isolate each compounds under an acid free condition. Esterification of RL-115M-A with CH_2N_2 was therefore carried out. To 51 mg of the mixture containing RL-115M-A was added excess amounts of diluted CH_2N_2 trapped in CH_2Cl_2, and left overnight at room temperature. The reaction mixture was once chromatographed (PTLC in *n*-hexane-EtOAc 10:1) to give *ca* 30 mg of the methylation products (*Rf ca* 0.8). Accordingly, the presence of a carboxyl group in the constituents was proved. Successively, the methylated constituents were separated by HPLC (Unisil-Q 100-5, solvent; 5 % EtOAc/hexane, detector; UV 220 nm) to obtain *ca* 10 mg of the main product, RL-115M-A-ME (Fig. 3-189).

The methyl ester RL-115M-A-ME, showing its molecular ion at *m/z* 248 (25 %, in EI-MS), was identical with **3a** derived from **3** in TLC (*n*-hexane-EtOAc 20:1, *Rf* 0.63), EI-mass spectrum, ^{1}H-NMR spectrum (Fig. 3-190, 191 and 192) and optical rotation (both laevorotatory). Consequently, structure of RL-115M-A-ME was elucidated as **3a**. Therefore, carotane acid (carota-1,4-dienoic acid, 4) corresponding to 3 was also confirmed as a constituent of *Rosa rugosa* leaves.

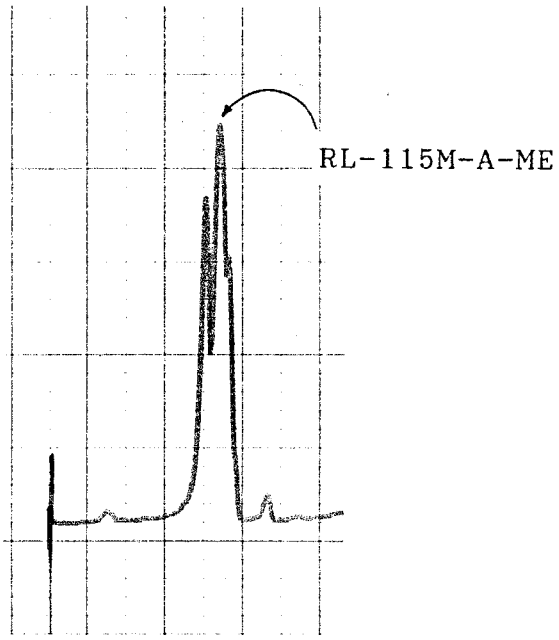

Fig. 3-189 HPLC Pattern of Methylated RL-115M Mixture Recorded on UV Detector at 230 nm (Unisil Q 100-5, 12 mm x 220 mm, 5 % EtOAc/*n*-hexane)

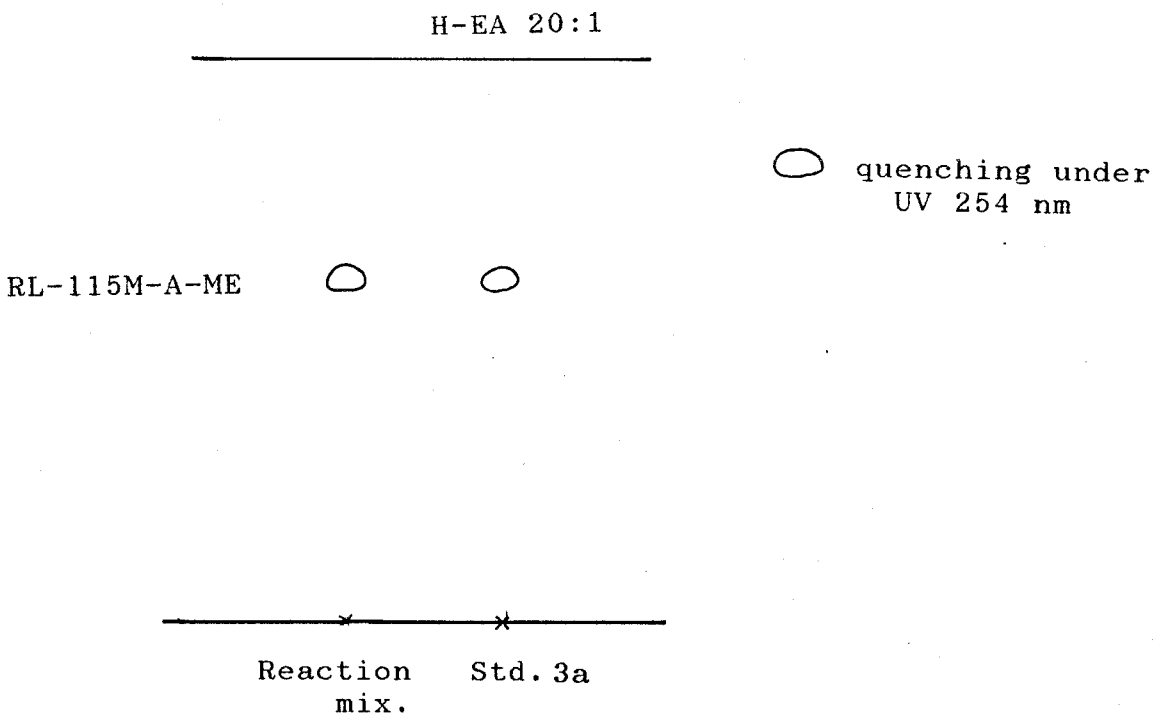

Fig. 3-190 TL Chromatogram of 115-M-A-ME: The isolate was completely agreeable in *Rf* value and response to vanillin-H_2SO_4 reagent with those of RL-C-ME (3a)

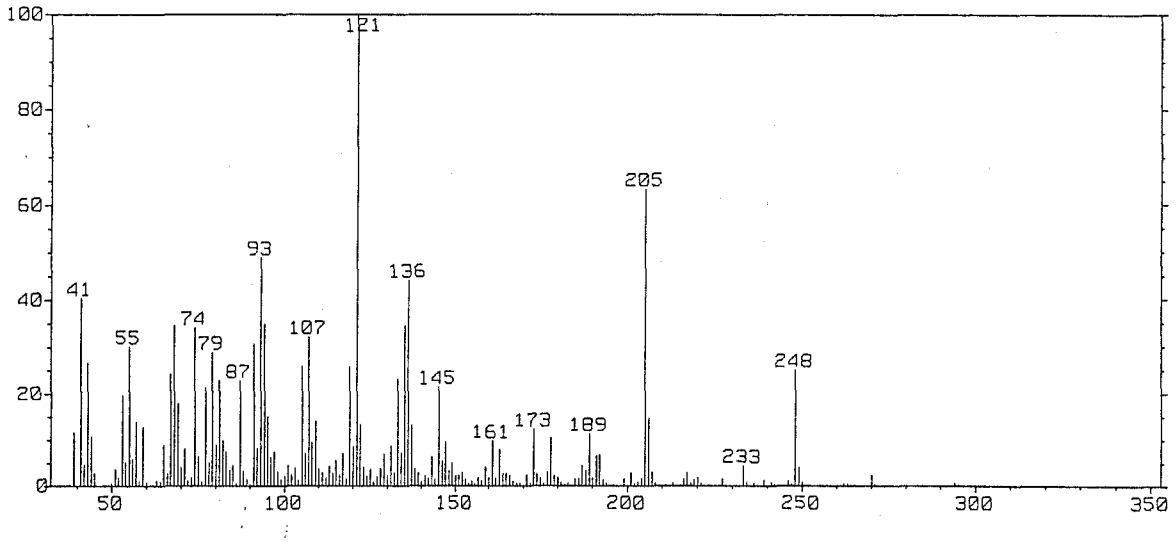

Fig. 3-190 EI-Mass Spectrum of 115M-A-ME

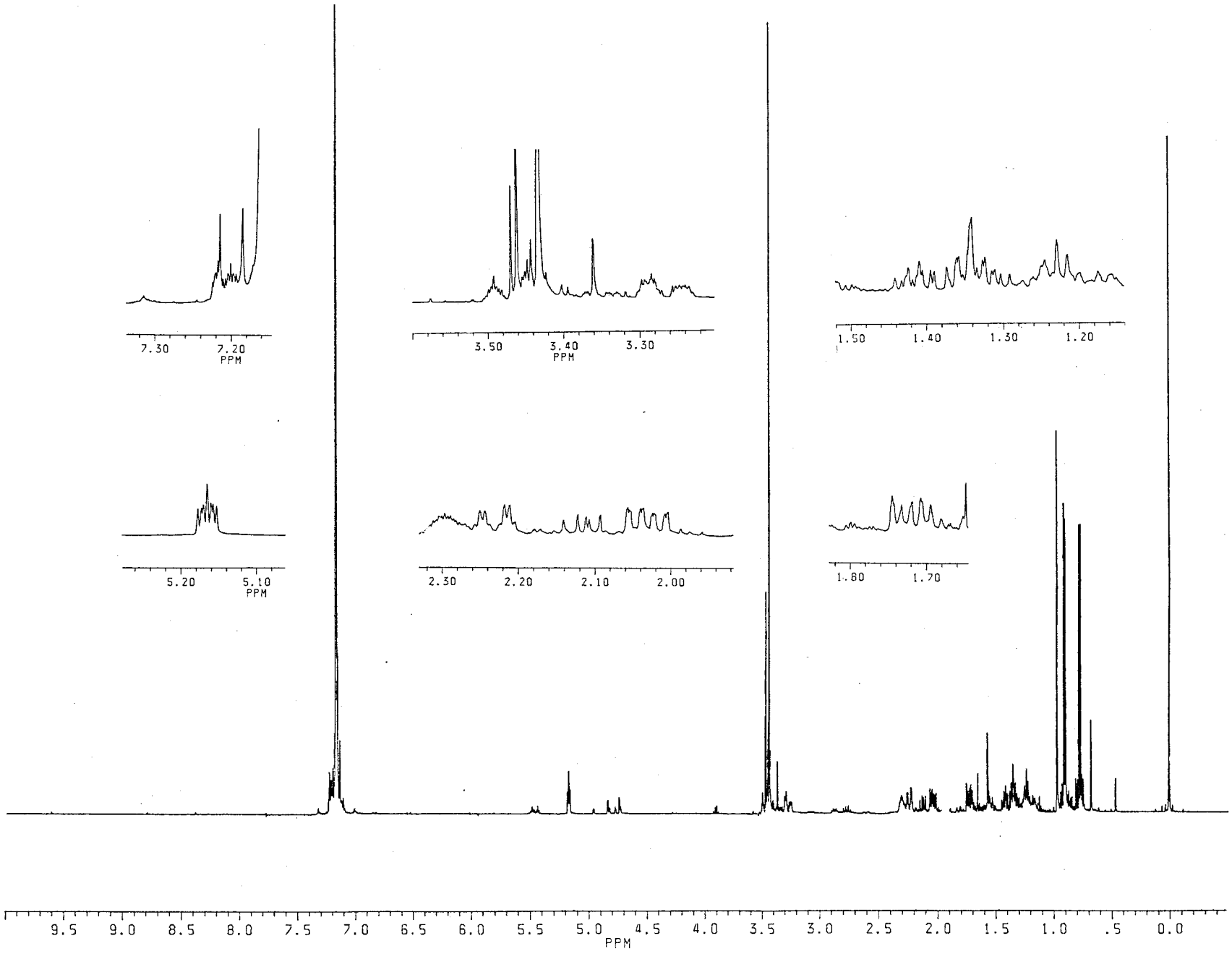

Fig. 3-192 ^{1}H-NMR Spectrum of 115-M-A-ME (500 MHz, in C_6D_6)

Table 3-73 Physicochemcal properties of carota-1,4-dienoic acid (4)

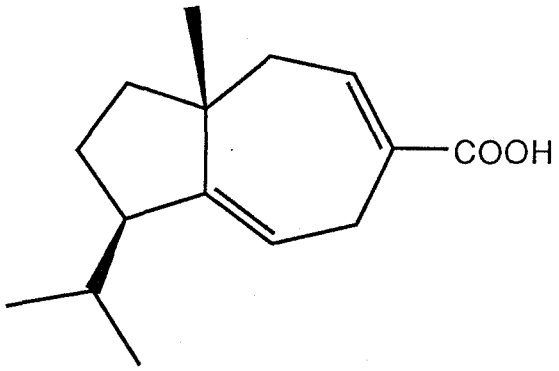

4

A colorless syrup (as a crude mixture with its isomers)

Vanillin-H_2SO_4 test: pinkish red (as the mixture)

FI-MS *m/z* (%): 234 (M^+, 100) (as the mixture)

^{1}H-NMR $\delta_{TMS}^{C_6D_6}$ (270 MHz): 5.124 (1H, ddd, *J*= 6.3, 3.7 and 2.3 Hz, 2-H), 3.385 (1H, br. dd, *J*= 23.7 Hz, 3-Ha), 3.192 (1H, br. d, *J*= 23.7 Hz, 3-Hb), 7.331 (1H, br. m, 5-H), 2.270 (1H, br. m, 10-H), 0.895 (3H, d, *J*= 6.6 Hz, 12-H_3), 0.759 (3H, d, *J*= 7.0 Hz, 13-H_3), 0.915 (3H, s, 15-H_3). These signals were picked up from the ^{1}H-NMR spectrum of the mixture. Other protons were hardly assignable.

*Table 3-74 Physicochemical properties of RL-115M-A-ME (**3a**)*

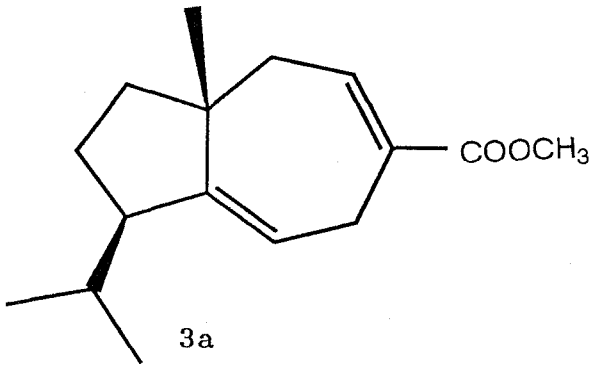

3a

A colorless syrup

Rf: 0.63 (H-EA 20:1)

$[\alpha]_D$: - 65 ° (*c* 0.1 in EtOH)*

EI-MS *m/z* (%): 248 (M^+, 25), 233 (4.7), 206 (15), 205 (64), 189 (12), 178 (11), 173 (12), 161 (10), 145 (22), 136 (44), 135 (35), 133 (23), 121 (100), 119 (26), 107 (32), 105 (26), 94 (35), 93 (49), 91 (31), 79 (29), 74 (34), 68 (35), 55 (30), 43 (27), 41 (40).

^{1}H-NMR $\delta_{TMS}^{C_6D_6}$ (500 MHz): 7.209 (1H, m, C-5-H), 5.165 (1H, ddd, *J*= 6.2, 3.7 and 2.4 Hz, C-2-H), *ca* 3.47 (1H, d-like m, C-3-Ha), 3.431 (3H, s, C-7'-H_3), *ca* 3.26 (1H, d-like m, C-3-Hb), *ca* 2.29 (1H, br. m, C-10-H); 2.232 (1H, br. dd-like signal, C-6-Ha), 2.032 (1H, br. ddd-like signal, C-6-Hb), 1.713 (1H, octet-like signal, C-11-H), *ca* 1.42 (1H, m, C-9-Ha), *ca* 1.35 (1H, m, C-8-Ha), *ca* 1.32 (1H, m, C-9-Hb), 1.228 (1H, m, C-8-Hb), 0.964 (3H, s, C-15-H_3), 0.904 (3H, d, *J*= 6.9 Hz, C-12-H_3), 0.768 (3H, d, *J*= 6.9 Hz, C-13-H_3)

* The purity of this sample is around 80 %.

3-5-6 Air Oxidation of Carota-1,4-dienaldehyde

1) Rugosal A and Rugosic Acid A as Stable Oxidation Products

Purified carota-1,4-dienaldehyde (**3**) showed a markedly unstable property under air exposure, and gave some high polar compounds positive to peroxide reagent (*N,N*-dimethyl-*p*-phenylenediamine sulfate). During exposure to air for one day at room temperature in the dark, **3** was converted into some high polar and unstable compounds positive to the peroxide reagent. When the mixture had further been left in a refrigerator for more than 2 weeks, some stable products were yielded (Fig. 3-193). From 51.7 mg of the autoxidation products, two constituents (RL-C-OX1 and RL-C-OX2) were successfully isolated by PTLC. In comparisons of EI-MS and ^{1}H-NMR, RL-C-OX1 (3.7 mg, *Rf* 0.41 in *n*-hexane-EtOAc 3:1) and RL-C-OX2 (1.9 mg, *Rf* 0.59 in *n*-hexane-EtOAc-HCOOH 50:50:2) were indistinguishable from rugosal A (**1**) and rugosic acid A (**2**), respectively (Fig. 3-194, 195, 196, 197, and Table 3-75, 76). In addition, those derivatives from **3** were respectively agreeable with the authentic and naturally occurring **1** and **2** in their optical rotations (RL-C-OX1 $[\alpha]_D$ + 125 °, *c* 0.1 in MeOH; **1**, $[\alpha]_D$ + 183 ° and RL-C-OX2 $[\alpha]_D$ + 130 °, *c* 0.1 in MeOH; **2**, $[\alpha]_D$ + 159 °, respectively). Furthermore, CD spectrum of RL-C-OX1 was completely the same as that of **1** (Fig. 3-198).

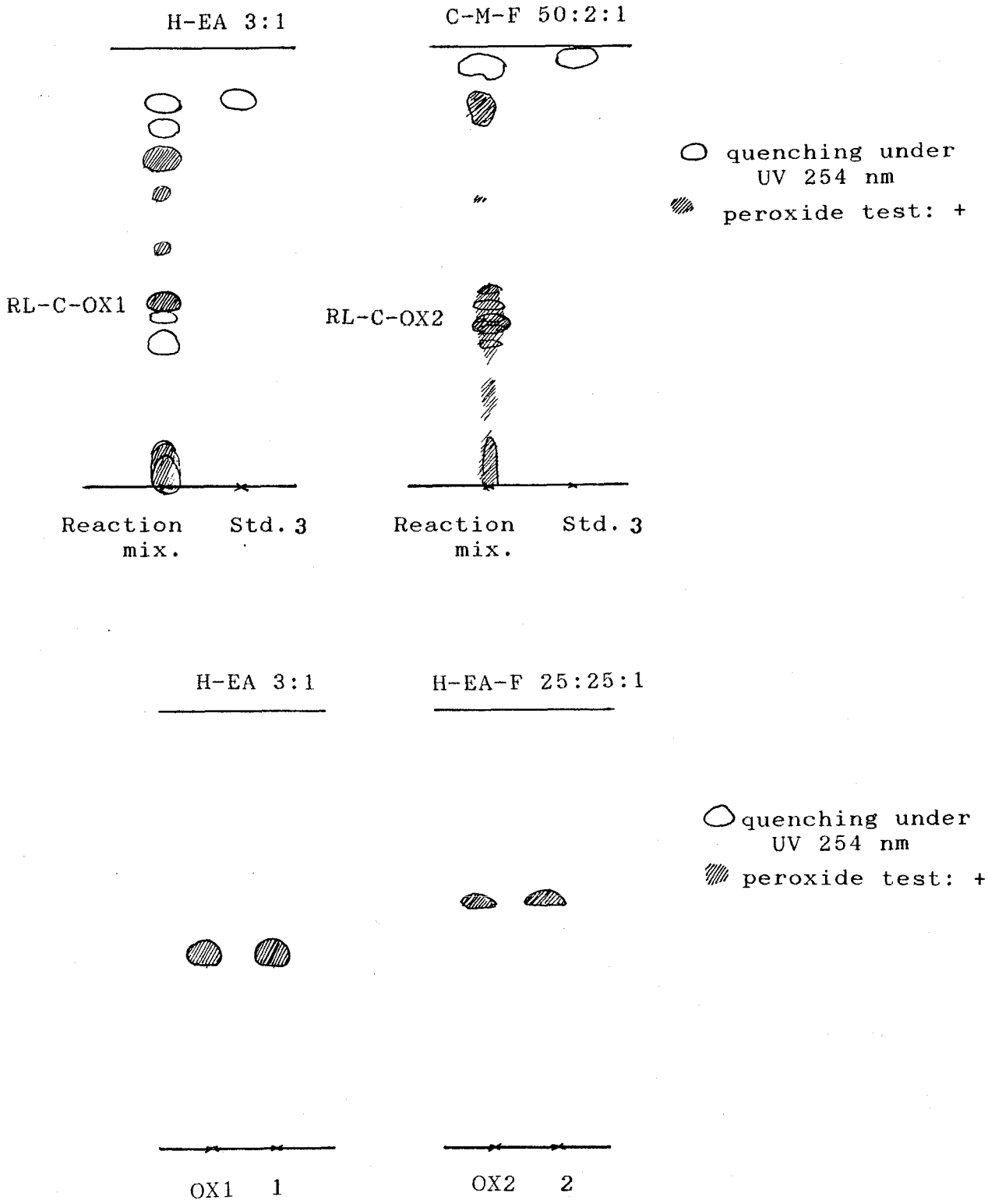

Fig. 3-193 TL Chromatograms of Autoxidation Products from Carota-1,4-dienaldehyde (3): Most of the products showed a positive response to peroxide test; however, those were quite unstable except two denoted as RL-C-OX1 and RL-C-OX2 in the chromatogram.

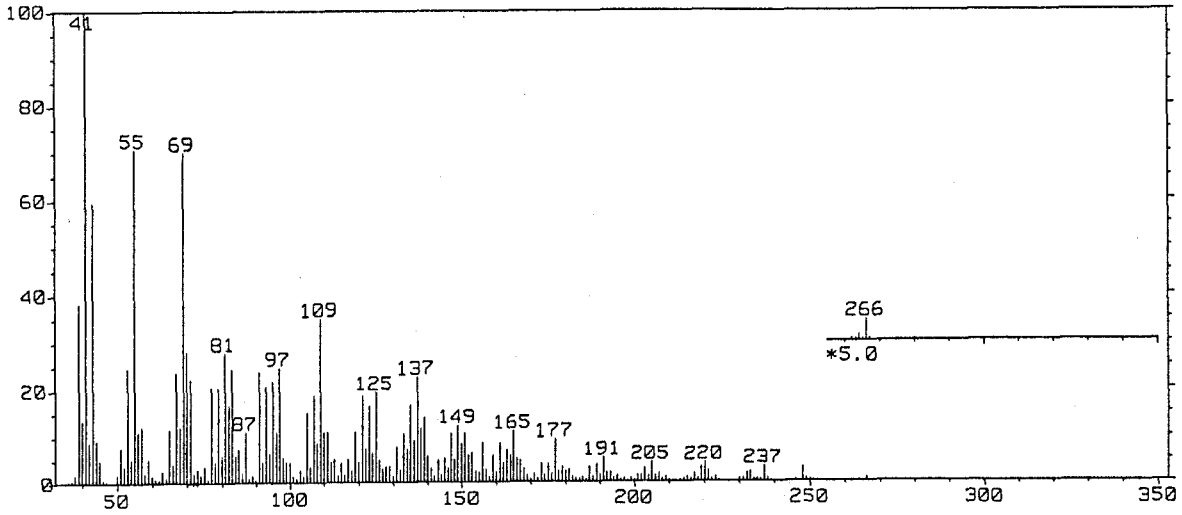

Fig. 3-194 EI-Mass Spectrum of RL-C-OX1

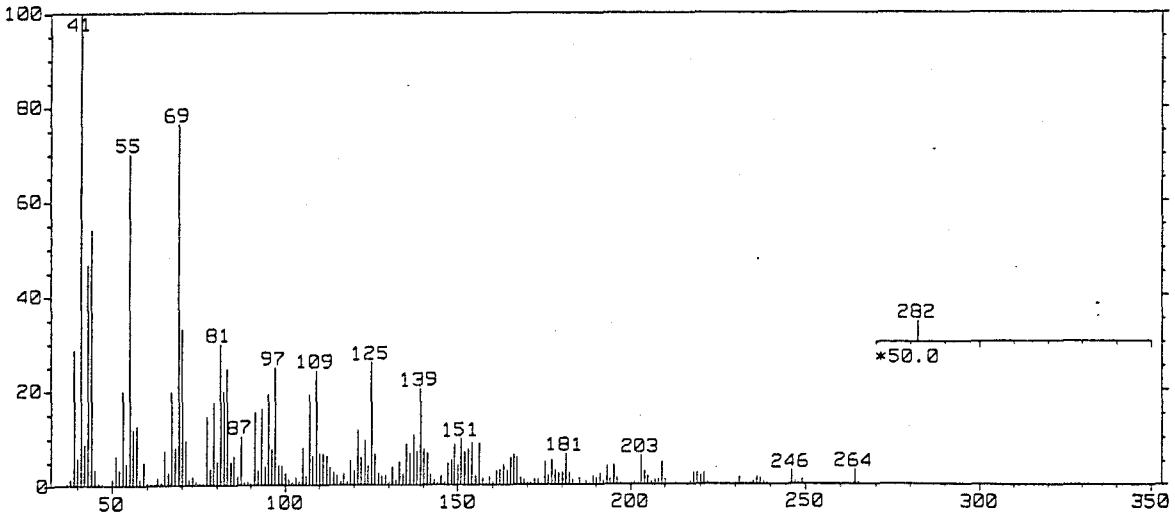

Fig. 3-195 EI-Mass Spectrum of RL-C-OX2

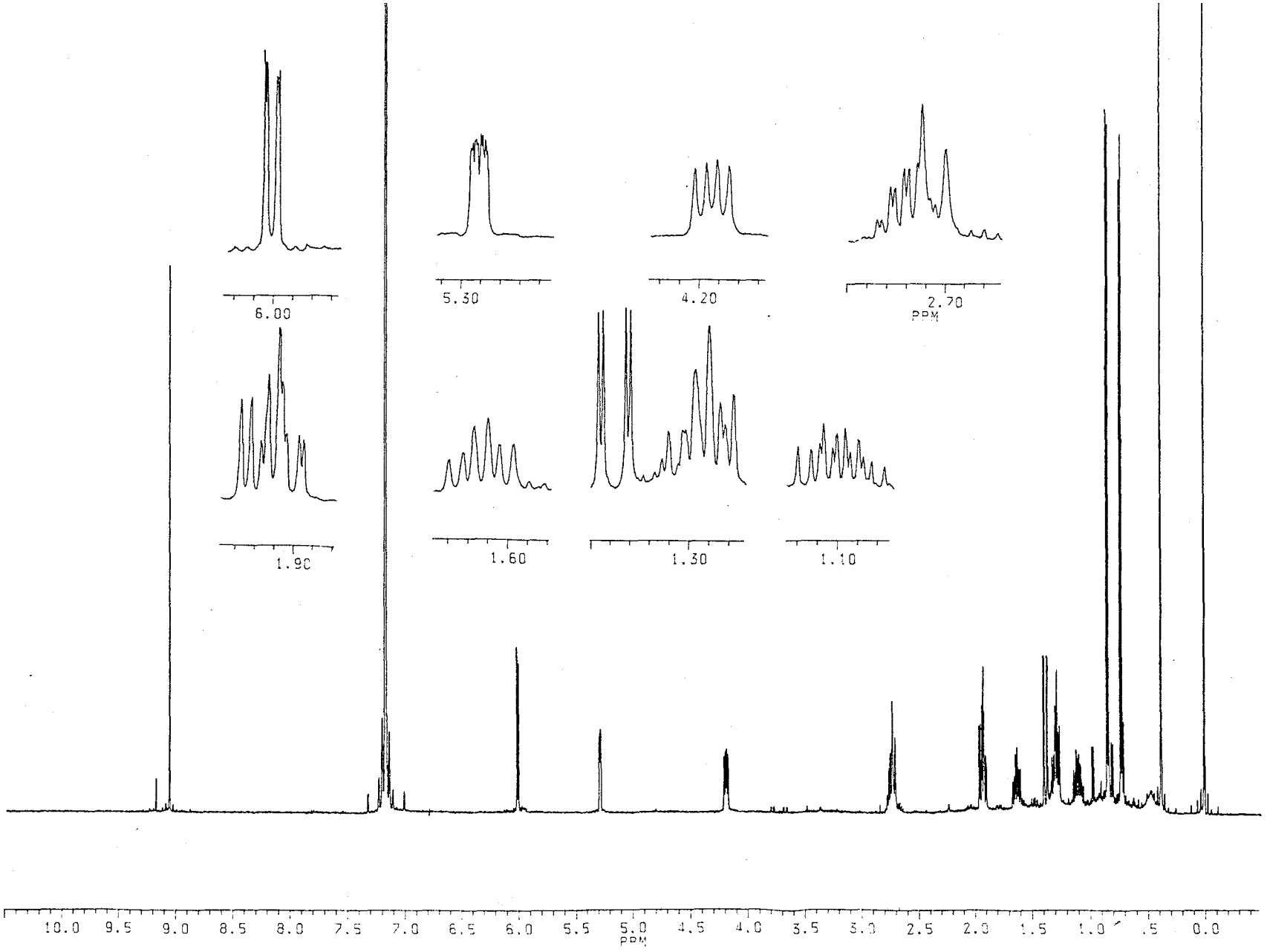

Fig. 3-196 ^{1}H-NMR Spectrum of RL-C-OX1 (500 MHz, in C_6D_6)

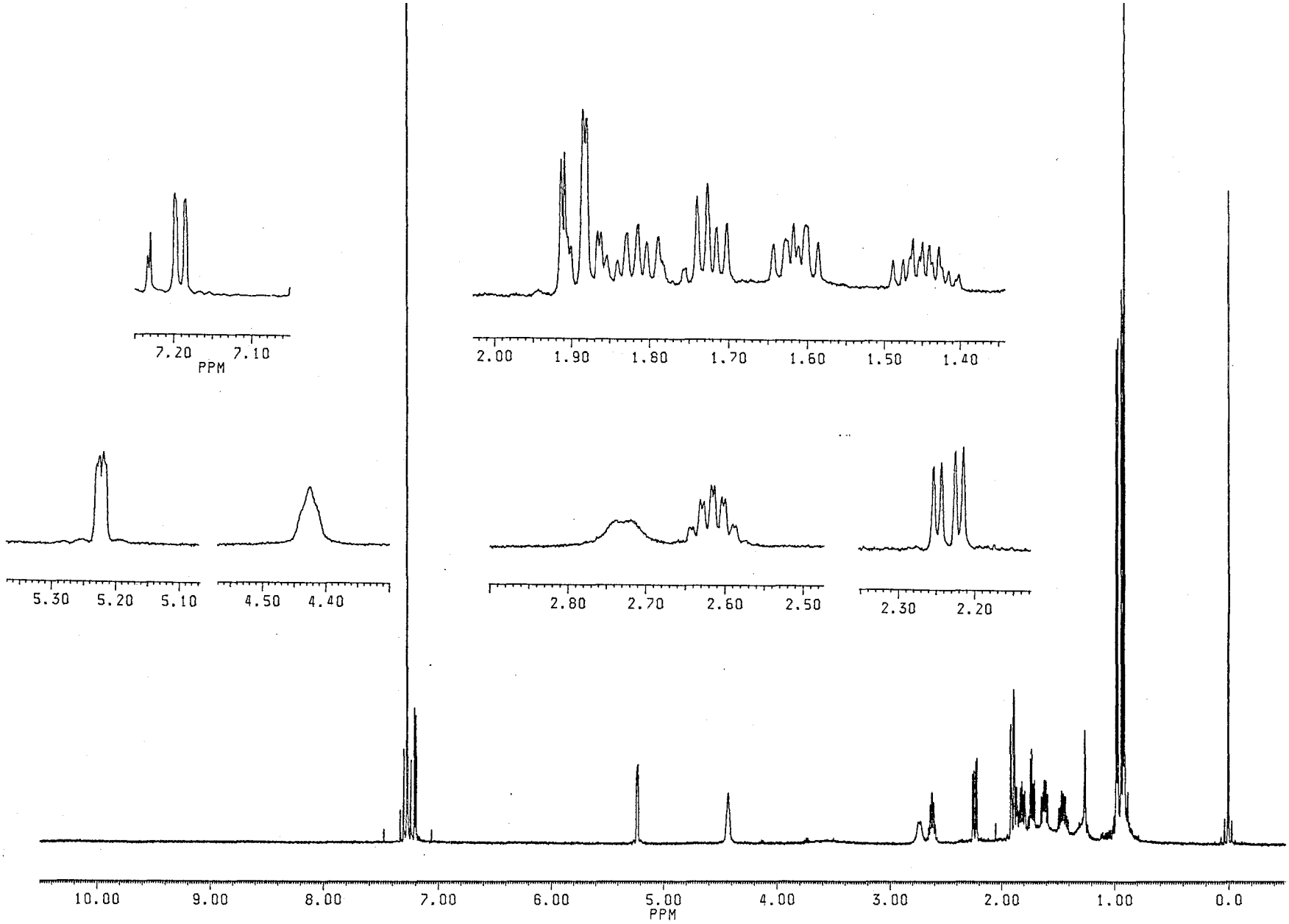

Fig. 3-197 ^{1}H-NMR Spectrum of RL-C-OX2 (500 MHz, in C_6D_6)

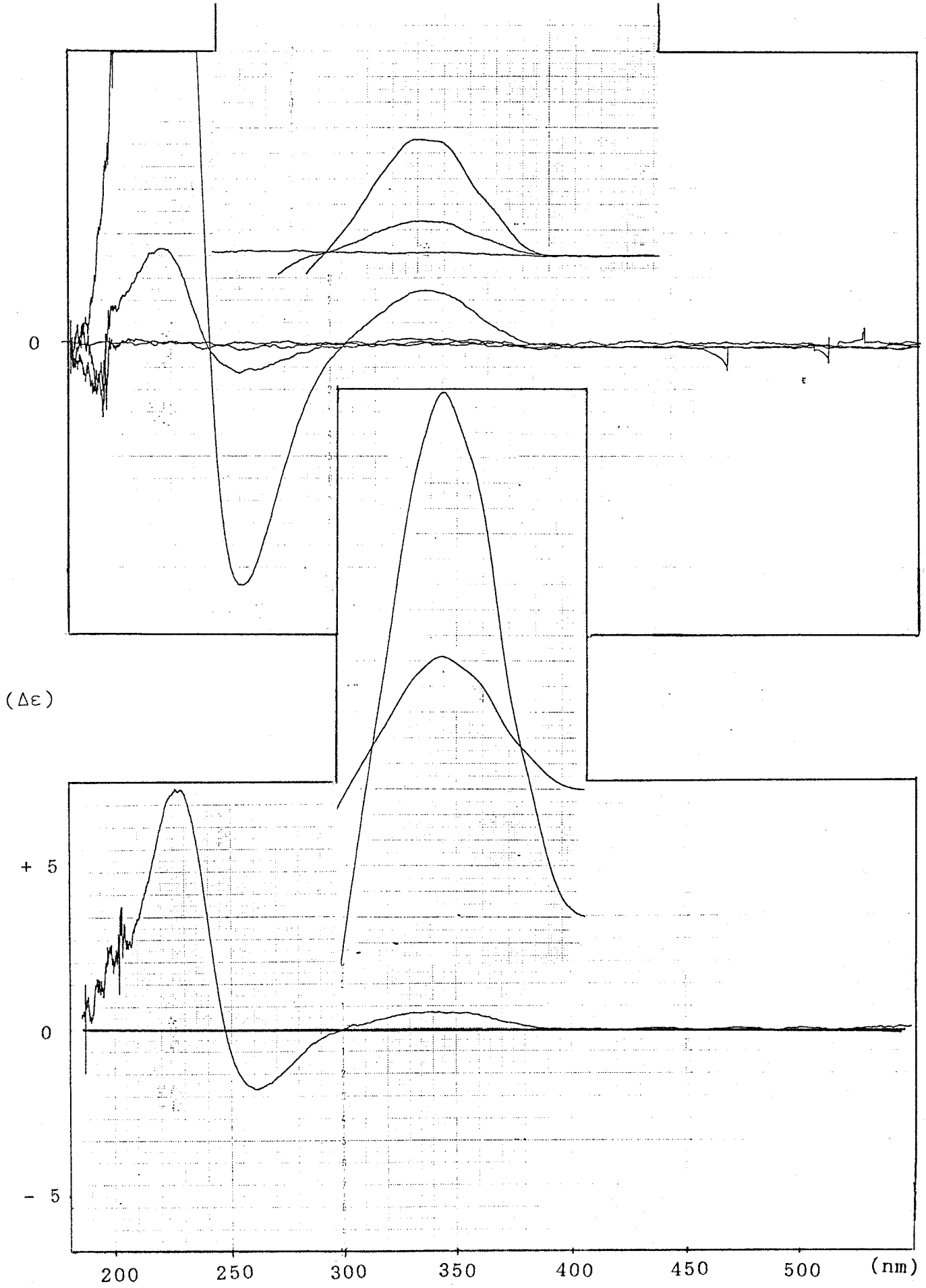

Fig. 3-198 CD Spectra of Rugosal A (1, top) and RL-C-OX1 (bottom): As the CD pattern are superimposable, the stereochemistry of RL-C-OX1 and 1 are the same.

Table 3-83 Physicochemical properties of RL-C-OX1 (=rugosal A, 1)

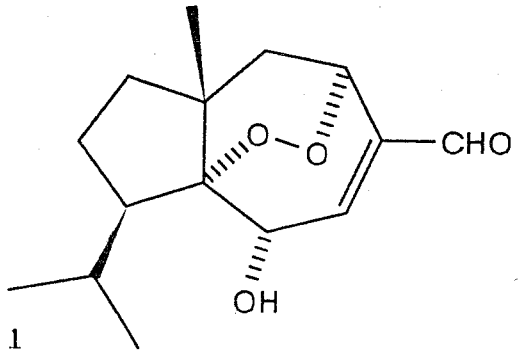

1

Colorless needles, mp.

Rf: 0.41 (H-EA 3:1)

$[\alpha]_D$: + 125 ° (*c* 0.1 in EtOH)

CD [θ] (nm): 343 (+,Δε 6.8), 261 (-,Δε 1.8), 230 (+,Δε 0.4)

N,N-dimethyl-*p*-phenylenediamine sulfate test: positive (orange/pink)

EI-MS *m/z* (%): 266 (M^+, 0.9), 248 (M^+-H_2O, 3.2), 237 (3.5), 220 (4.4), 205 (4.4), 191 (5.4), 177 (9.5), 165 (11), 137 (23), 125 (19), 109 (35), 97 (25), 81 (28), 70 (28), 69 (70), 55 (71), 43 (60), 41 (100).

^{1}H-NMR $\delta^{C_6D_6}_{TMS}$ (500 MHz): 4.186 (1H, dd, *J*= 11.4 and 5.0 Hz, C-2-H), 6.001 (1H, dd, *J*= 6.2 and 0.9 Hz, C-3-H), 5.281 (1H, ddd, *J*= 5.0, 2.4 and 0.9 Hz, C-5-H), 1.935 (1H, dd, *J*= 14.2 and 5.0 Hz, C-6-Ha), 1.375 (1H, dd, *J*= 14.2 and 2.4 Hz, C-6-Hb), 1.626 (1H, ddd, *J*= 12.9, 12.5 and 7.1 Hz, C-8-Ha), 1.273 (1H, dd, *J*= 12.5 and 6.6 Hz, C-8-Hb), 1.291 (1H, m, C-9-Ha), 1.095 (1H, dddd, *J*= 12.9, 12.9 10.9 and 6.6 Hz, C-9-Hb), 1.912 (1H, ddd, *J*= 10.9, 8.9 and 2.3 Hz, C-10-H), 2.739 (1H, double sept., *J*= 6.8 and 2.3 Hz, C-11-H), 0.840 (3H, d, *J*= 6.8 Hz, C-12-H_3), 0.725 (3H, d, *J*= 6.8 Hz, C-13-H_3), 9.047 (1H, s, C-14-H), 0.378 (3H, s, C-15-H_3).

Table 3-84 Physicochemical properties of RL-C-OX2 (=rugosic acid A, 2)

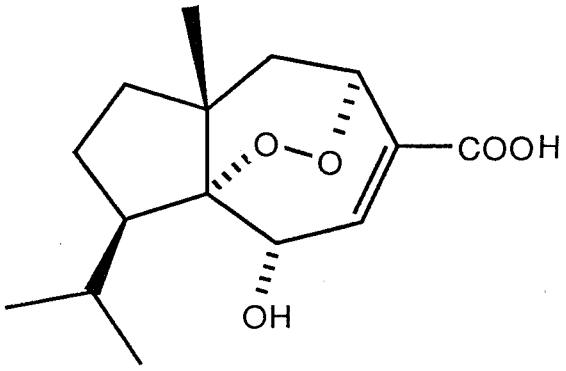

2

Colorless needles, mp.

Rf: 0.59 (H-EA-F 50:50:2)

$[\alpha]_D$: + 130 ° (*c* 0.1 in EtOH)

N,N-dimethyl-*p*-phenylenediamine sulfate test: positive (clear pinkish red)

EI-MS *m/z* (%): 282 (M^+, 0.1), 264 (M^+-H_2O, 3.4), 246 (3.2), 209 (5.0), 203 (6.4), 181 (6.9), 151 (10), 139 (21), 125 (26), 109 (24), 107 (19), 97 (25), 83 (25), 81 (30), 70 (33), 69 (76), 55 (70), 44 (54), 43 (47), 41 (100)..

^{1}H-NMR $\delta^{CDCl_3}_{TMS}$(500 MHz): 4.426 (1H, br. m, C-2-H), *ca* 2.73 (1H, d-like br, C-2-OH), 7.191 (1H, d, *J*= 6.6 Hz, C-3-H), 5.223 (1H, br. m, C-5-H), 2.234 (1H, dd, *J*= 14.3 and 5.1 Hz, C-6-Ha), 1.896 (1H, dd, *J*= 14.3 and 2.4 Hz, C-6-Hb), 1.821 (1H, ddd, *J*= 13.0, 12.1 and 7.1 Hz, C-8-Ha), 1.720 (1H, dd, *J*= 12.1 and 6.5 Hz, C-8-Hb), 1.614 (1H, ddd, *J*= 12.8, 8.5 and 7.1 Hz, C-9-Ha), 1.445 (1H, dddd, *J*= 13.0, 12.8, 10.8 and 6.5 Hz, C-9-Hb), 1.882 (1H, ddd, *J*= 10.8, 8.0 and 2.1 Hz, C-10-H), 2.615 (1H, double sept., *J*= 6.8 and 2.1 Hz, C-11-H), 0.973 (3H, d, *J*= 6.8 Hz, C-12-H_3), 0.929 (3H, d, *J*= 6.8 Hz, C-13-H_3), 0.912 (1H, s, C-15-H_3). The C-2-OH proton probably became feasible due to a diluted condition.

Accordingly, it was proved that 3 is the precursor of rugosal A (1) in the autoxidation reaction. Furthermore, the stereochemistry of 3 was elucidated as C-7*S*, C-10*R* in the light of the stereochemistry of 1. In spite of their low yields, the possibility that 1 and 2 came from imprity was eliminated because of high purity of the starting material examined by ^{1}H-NMR. In *Rosa rugosa* leaf tissues, conversion of 3 into 1 is expected to be catalyzed by a lipoxygenase-like enzyme. The low yield of 1 from 3 in the autoxidation is therefore not an essential problem. As an unlightened point, mechanism of the autoxidation including the conversion pathway from 3 into 1 remained unsolved.

In hanalpinol (**80**), photochemical derivatization from guaia-6,9-diene (**87**) was reported, and its chemical conversion scheme was proposed as shown in Scheme 3-22 (pp. 288) [127]. Since 1 possesses the same endoperoxide system as that of **80** including the olefinic bond and the allylic hydroxyl group, a peroxidation pathway for 1 can be illustrated after that for **80** (See Scheme 3-23, pp. 289). To prove this hypothetical scheme, detection or isolation of some intermediates was focused on.

2) Survey of Intermediates in the Autoxidation Reaction

To prove the hypothetical scheme for rugosal A formation, some intermediates must be isolated or identified. Therefore, a reproducible condition was requested to demonstrate the autooxidative conversion, and consequently pure carota-1,4-dienaldehyde (3) was exposed to air under two different conditions: **a**; standing overnight at - 4 °C in the dark, and **b**; keeping at + 40 °C for 3 hr also in the dark. To make the compoun expose well to air, the substrate was dissolved in 2 ml of *n*-hexane in a helzflask, and then removed the solvent by using a rotary evaporation to give a thine layer of of **3** on a surface of glass wear. As shown in Fig. 3-199, both treatment (**a** and **b**) resulted in almost the same TLC pattern, in which some quenching compounds obviously different from rugosal A (1) were visible. Including the starting material, 1 and rugosic acid A (2), two major (RL-C-OX-A1 and RL-C-OX-A2) and five minor products (RL-C-OX-B1~B5) were detected each as a quenching band during PTLC (in *n*-hexane-EtOAc 3:1). RL-C-OX-A1 was identical to the starting material (3) in direct comparison with authentic 3 in TLC, and the recovery rate of 3 in these reactions indicated that oxidation of 3 occurs comparatively slowly. Furthermore, it was suggestive that heat may be an important factor in the oxidation reaction, since 3 disappeared more rapidly under the condition **b** than the condition **a** (Table 3-77).

Table 3-77 Yield of the autooxidation products from carota-1,4-dienaldehyde (3): mg (yield %)

		RL-C-OX						
Product		A1	B1	B2	B3	B4	A2	B5
Condition								
a	5.1*	2.9 (57)	0.1<	0.1<	0.1<	0.1<	0.7 (13)	0.1<
b	8.5*	2.2 (26)	0.1	0.1	0.1<	0.1	3.9 (43)	0.1

* Starting material

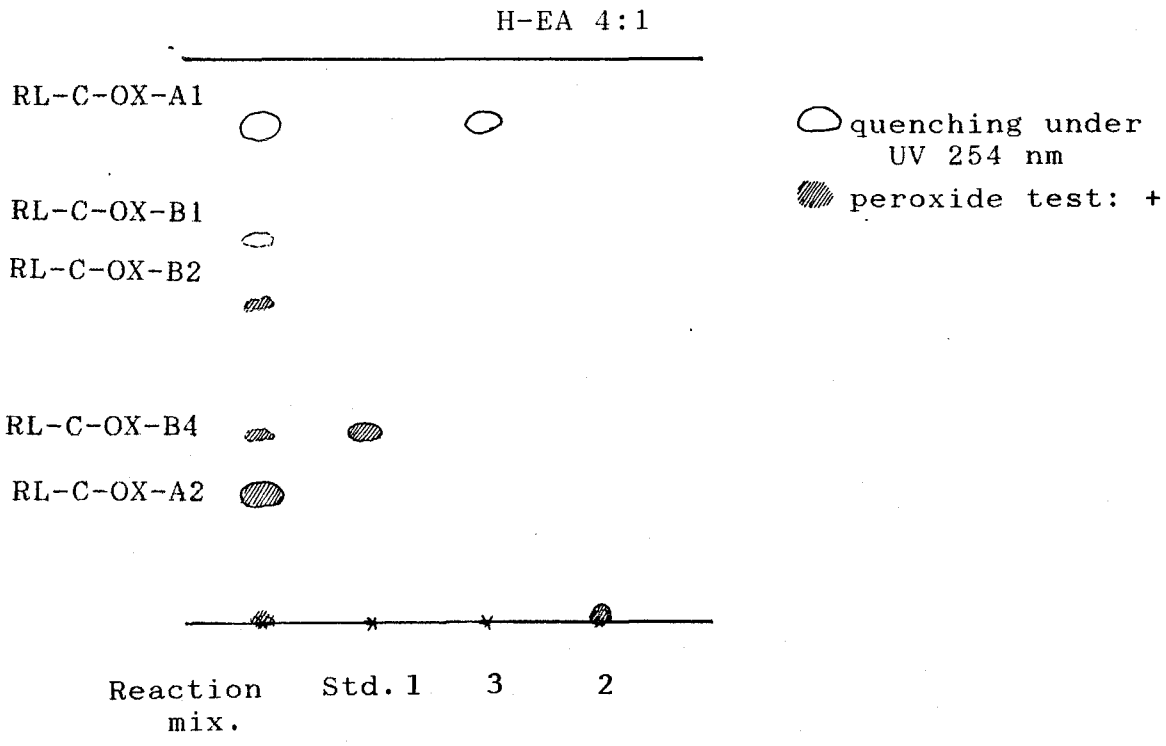

Fig. 3-199 TL Chromatogram of Autoxidation Products from Carota-1,4-Dienaldehyde (3)

The second major product, RL-C-OX-A2 was isolated by PTLC to give a colorless syrup. The relatively good yield of RL-C-OX-A2 indicated that this product was on a major flow of the oxidation reaction and one of relatively stable intermediates (Table 3-77). In FI-MS, its molecular ion was detected at *m/z* 282 (100 %, 1 + 16 mass units), and EI-MS fragmentation was quite similar to that of 1 (Fig. 3-200 and 201). The ^{1}H-NMR spectrum of the isolate was also showed a good accordance with that of 1 both in chemical shifts and coupling constants; however, some protons (*e.g.* at δ_H 2.032 assignable to C-10 methine proton and 4.634 to C-2 methine proton) were clearly shifted to a down field. As another difference between them in the ^{1}H-NMR, C-2-OH proton was invisible in the spectrum of RL-C-OX-A2, even though a formyl proton was detected at δ_H 9.153. Instead of the C-2-OH proton, an exchangeable proton was detected at δ_H 8.94 (1H) as a broad singlet, which was strongly deshielded probably by the C-14 aldehyde group (-OO<u>H</u> is usually detectable around 8 ~ 8.5 ppm in $CDCl_3$ [130,131]) (Fig. 3-202, 203 and Table 3-78).

In ^{13}C-NMR spectra, a further resemblance of chemical shift values of these two compound was recognizable. Only an oxygenated methine carbon assignable to C-2 showed a marked shift to a lower field (δ_C 81.5, shifted by 11.6 ppm) (Fig. 3-204 and Table 3-78). Together with a clear response to *N,N*-dimethyl-*p*-phenylenediamine reagent (clear pinkish red without heating, *cf.* orange/pink with a slow response), those physicochemical properties suggested that RL-C-OX-A2 should have not only an endoperoxide bridge between C-1 and C-5 but also a hydroperoxy group at C-2 instead of C-2-OH in 1. Thus, RL-C-OX-A2 was provided with structure **3c**.

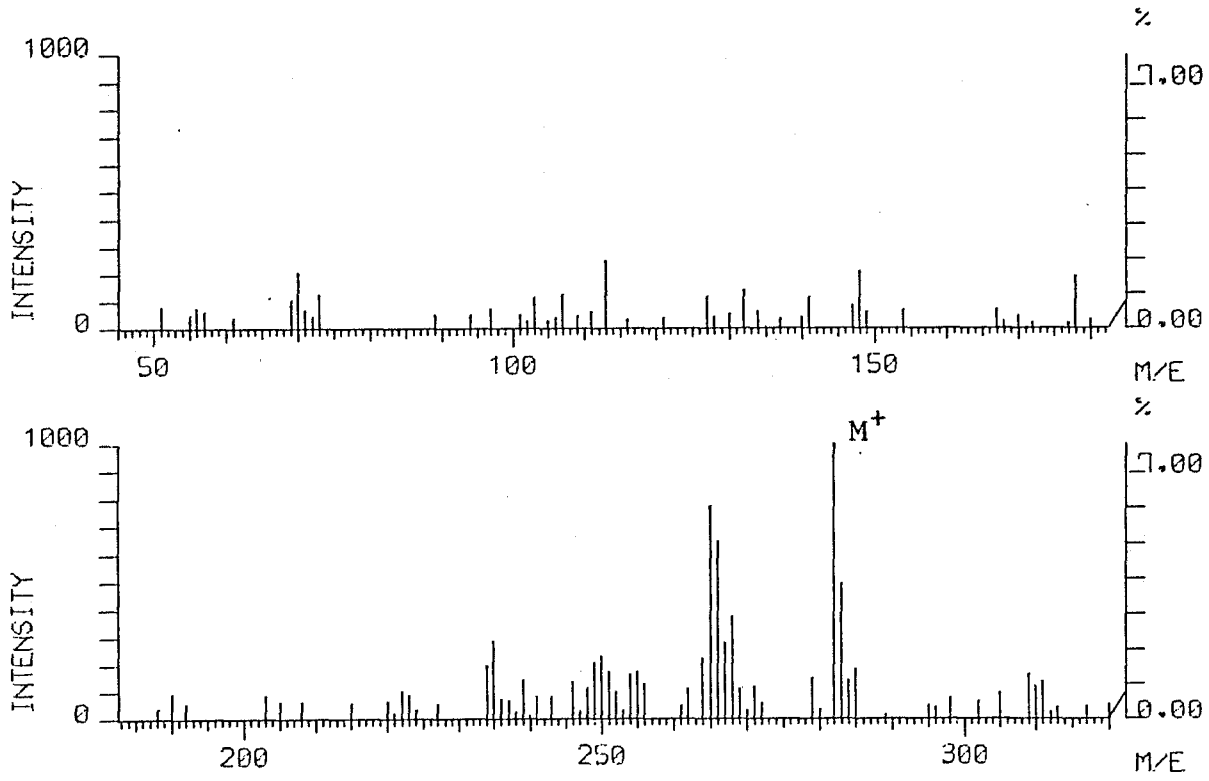

Fig. 3-200 FI-Mass Spectrum of RL-C-OX-A2

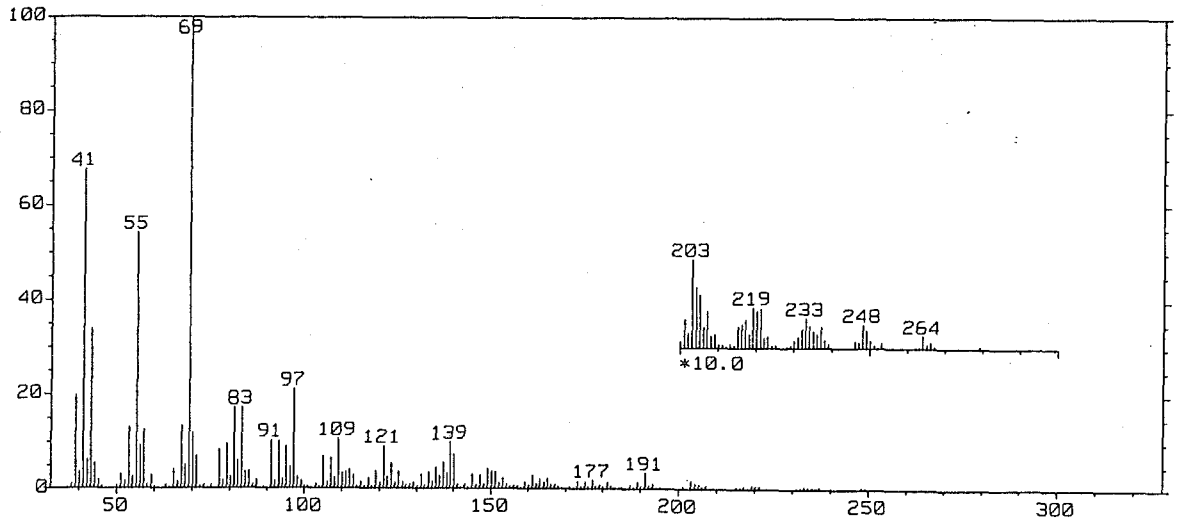

Fig. 3-201 EI-Mass Spectrum of RL-C-OX-A2

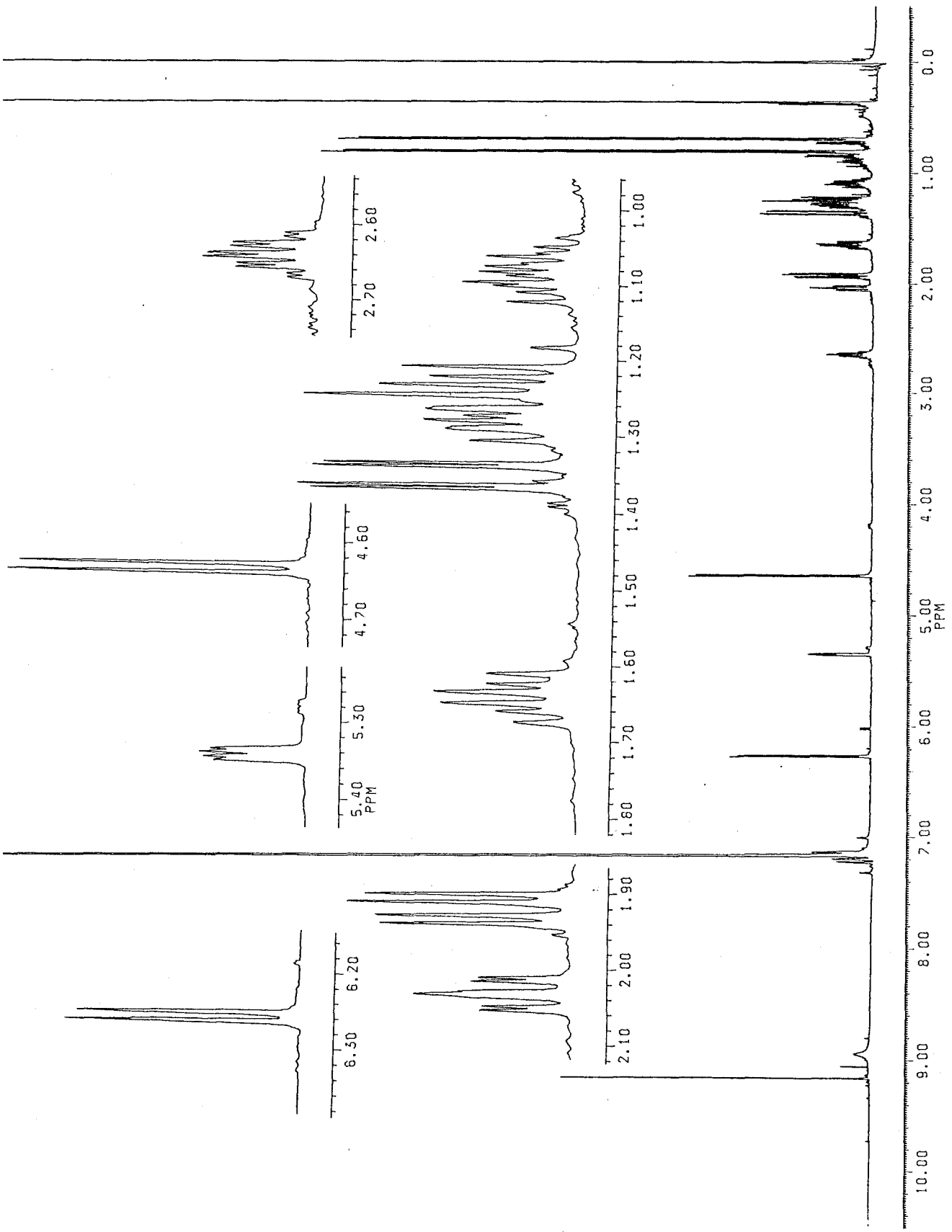

Fig. 3-202 ^{1}H-NMR Spectrum of RL-C-OX-A2 (500 MHz, in C_6D_6)

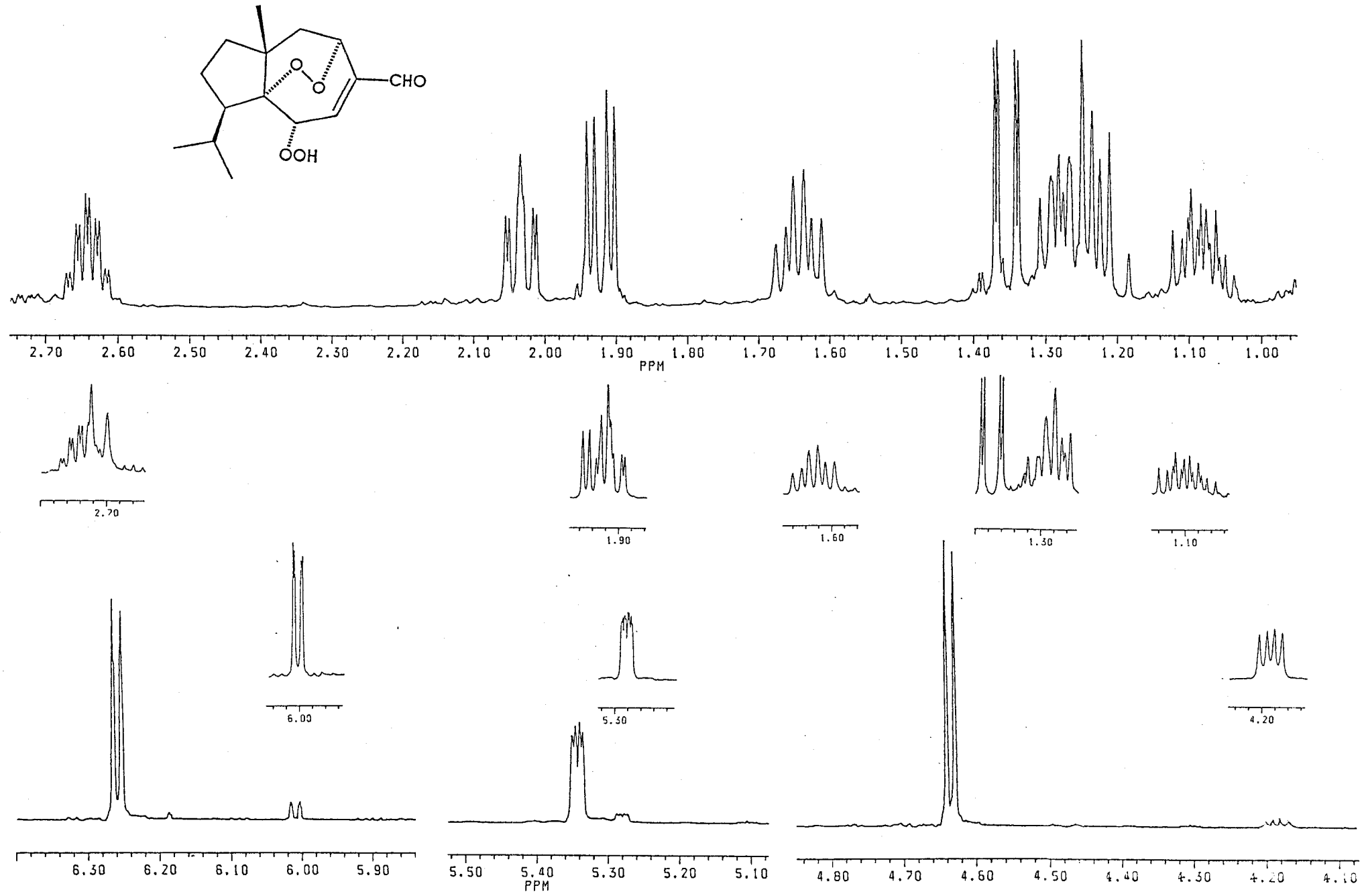

Fig. 3-203 Proton Signals of RL-C-OX-A2 and the Corresponding Protons of Rugosal A (1): In the spectrum of the oxidation product, some small signals attributable to rugosal A appeared during the measurement as a result of further decomposition of the product.

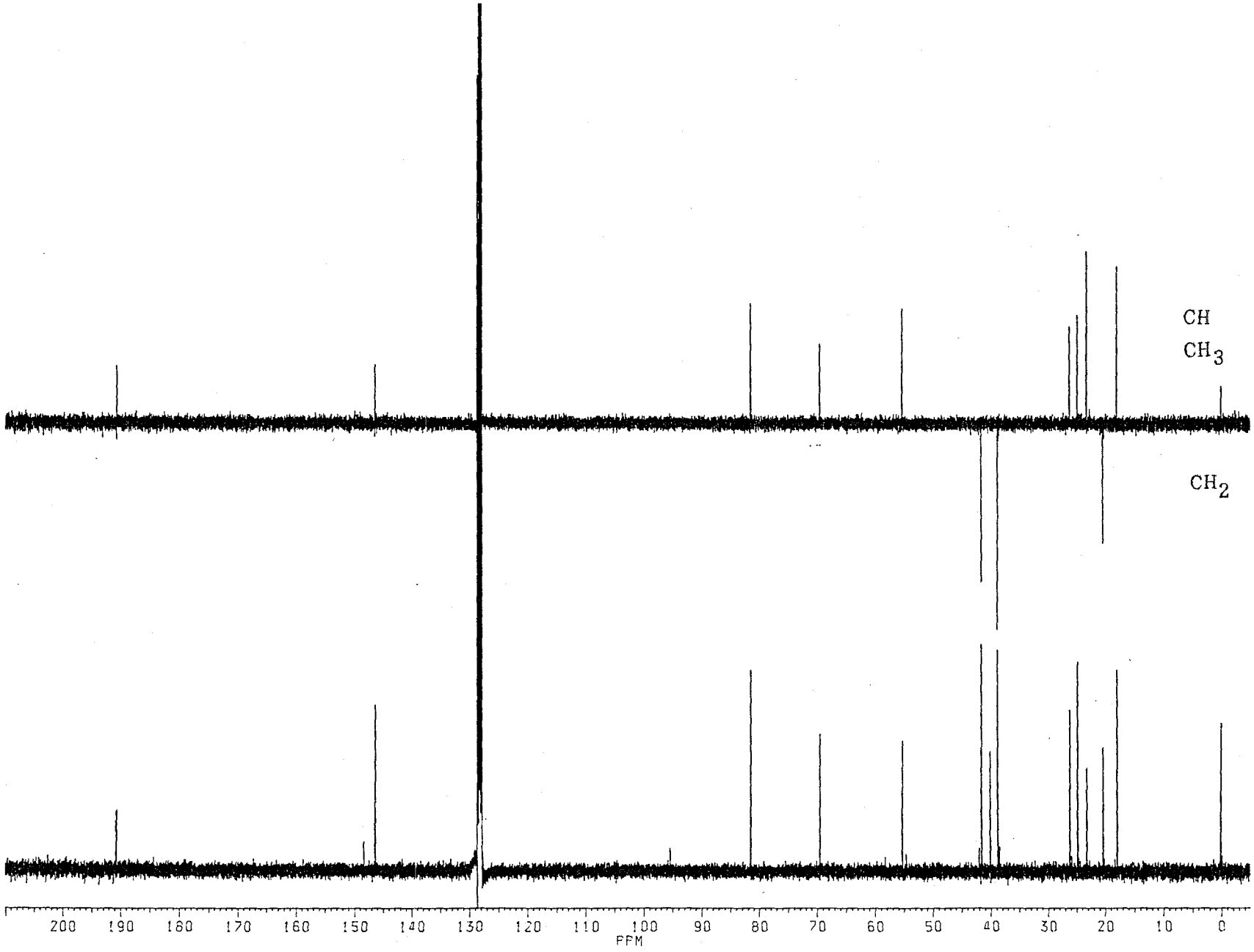

Fig. 3-204 ^{13}C-NMR Spectra of RL-C-OX-A2 (125 MHz, in C_6D_6, COM and DEPT)

Table 3-78 Proton and carbon chemical shift values of RL-C-OX-A2 and its comparison with those of rugosal A (1)

(500 and 125 MHz, in C_6D_6, TMS as an int. std.)

RL-C-OX-A2 Proton (JHz)	Carbon	Carobon-No	Rugosal A (1) Proton (JHz)	Carbon*
-	95.4	C-1	-	94.8
4.634 d (5.7)	81.5	C-2	4.198 dd (11.7, 6.4)	69.1
6.257 d (5.7)	146.3	C-3-H	6.031 dd (6.4, 1.1)	149.4
-	148.3	C-4	-	146.5
5.342 dd (5.2, 2.4)	69.5	C-5-H	5.277 ddd (5.1, 2.6, 1.1)	70.1
1.920 dd (14.1, 5.2)	41.5	C-6-H_2	1.942 dd (13.9, 5.1)	42.0
1.352 dd (14.1, 2.4)			1.384 dd (13.9, 2.6)	
-	40.0	C-7	-	39.6
1.642 ddd (12.5, 11.5, 7.4)	38.7	C-8-H_2	1.630 ddd (12.8, 12.5, 7.3)	38.5
1.227 br. dd (12.5, 7.1)			1.275 br. dd (12.5, 6.6)	
1.277 br. ddd (12.9, 9.0, 7.4)	20.4	C-9-H_2	1.295 m	20.2
1.078 dddd (12.9, 11.5, 10.6, 7.1)			1.105 dddd (12.8, 10.6, 10.3, 6.6)	
2.032 ddd (10.6, 9.0, 2.6)	55.1	C-10-H	1.912 ddd (10.6, 9.7, 2.6)	54.6
2.641 d sept (6.8, 2.6)	26.2	C-11-H	2.739 d sept (6.8, 2.6)	24.8
0.801 d (6.8)	23.2	C-12-H_3	0.845 d (6.8)	22.8
0.689 d (6.8)	17.9	C-13-H_3	0.732 d (6.8)	18.2
9.153 s	190.7	C-14-H	9.046 s	190.7
0.359 s	24.8	C-15-H_3	0.393 s	25.9
8.94 (approx.) br. s	-	exchangeble proton	2.758d (11.7)	-

This structure was eventually proved by hydroperoxide oxidation of the compound under a mild condition to yield 1. To 2.1 mg of RL-C-OX-A2 dissolved in 2 ml of MeOH was added 1.2 mg of thiourea and the mixture was stirred for 1 hr at room temperature. As shown in Fig. 3-205, the starting material completely disappeared, and two products were detected on TLC. Major product, OX-A2-TU1 (*Rf* 0.43 in hexane-EtOAc 3:1, 1.2 mg, in a 50 % yield) was identical with 1 in TLC, EI-MS, ^{1}H-NMR and CD (Fig. 3-206, 207, 208 and Table 3-80). This fact was certainly indicative of the validity of structure **3c** for RL-C-OX-A2, which can give 1 by reduction of a C-2 hydroperxy group into an OH group. On the other hand, the minor product C-OX-A2-TU2 (*Rf* 0.12, 0.5 mg, 25 %) was indistinguishable from RSA-TU (**1d**), a reduction derivative of 1 in TLC, EI-MS and ^{1}H-NMR (Fig. 3-209, 210 and Table 3-81). This formation of this minor product is explicable with successive reduction of the C-2 exoperoxy and the endoperoxy groups of **3c**.

RL-C-OX-A2 was comparatively unstable, and gradually converted into 1 even in benzene. Like conversion of PGG_2 (**91**) into PGH_2 (**82**) automatically progressed (Scheme 3-24) [132], this *endo*-exoperoxide probably stabilizes itself through the exoperoxide cleavage to a hydroxyl compound. The proposed scheme for the conversion pathway was therefore partly proved (step 3 in Scheme 3-27). More importantly, the fact that this intermediate was yielded in the dark and even under ice point, meaningfully shows that this oxygenation reaction requires only small energy.

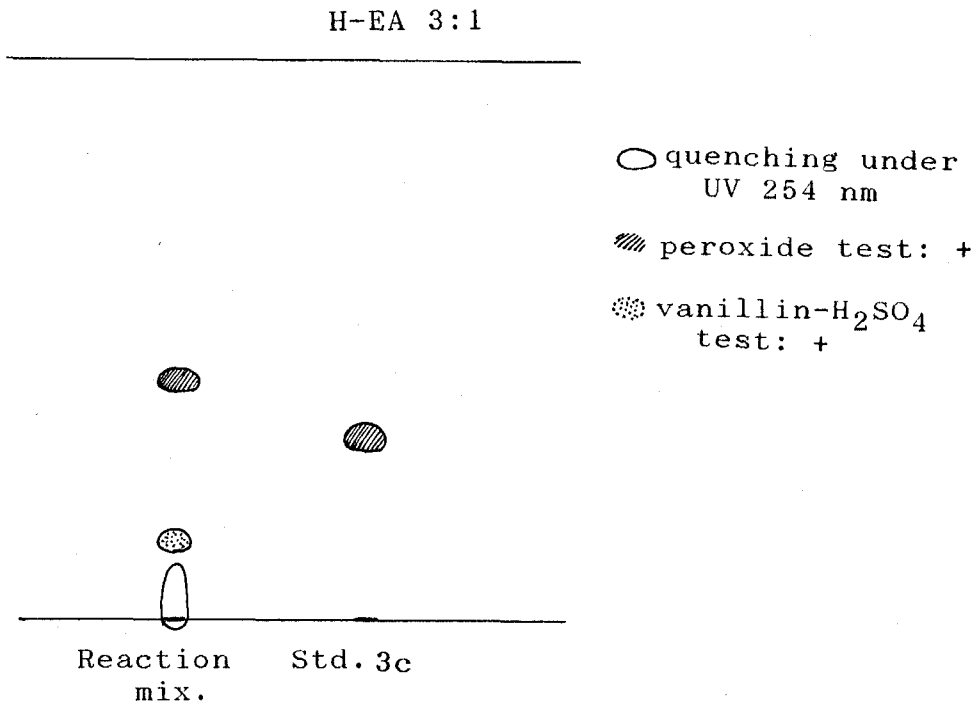

Fig. 3-205 TL Chromatogram of RL-C-OX-A2 Reduction Products Obtained by Treatment with Thiourea

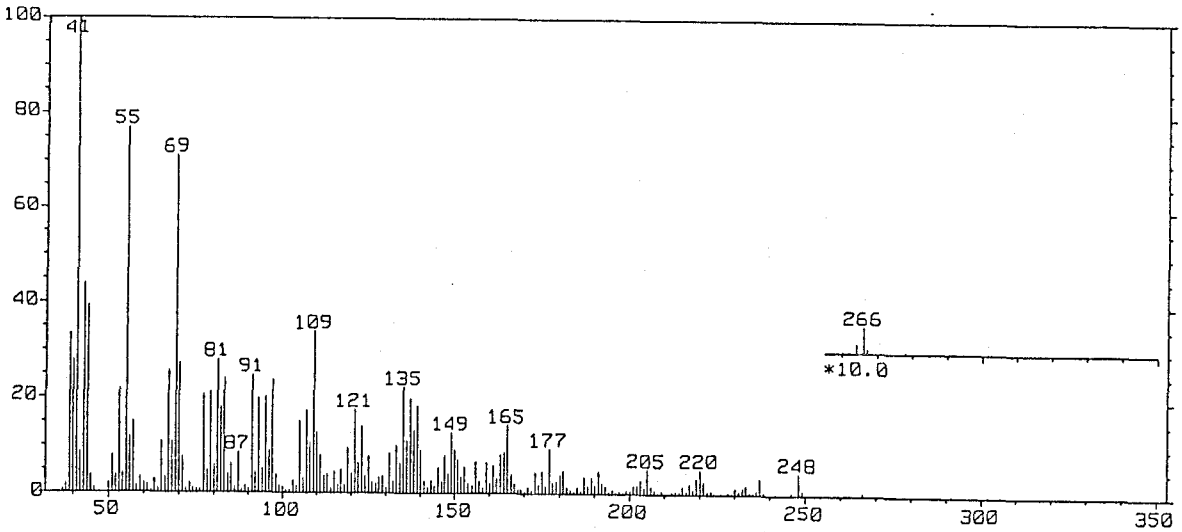

Fig. 3-206 EI-Mass Spectrum of C-OX-A2-TU1

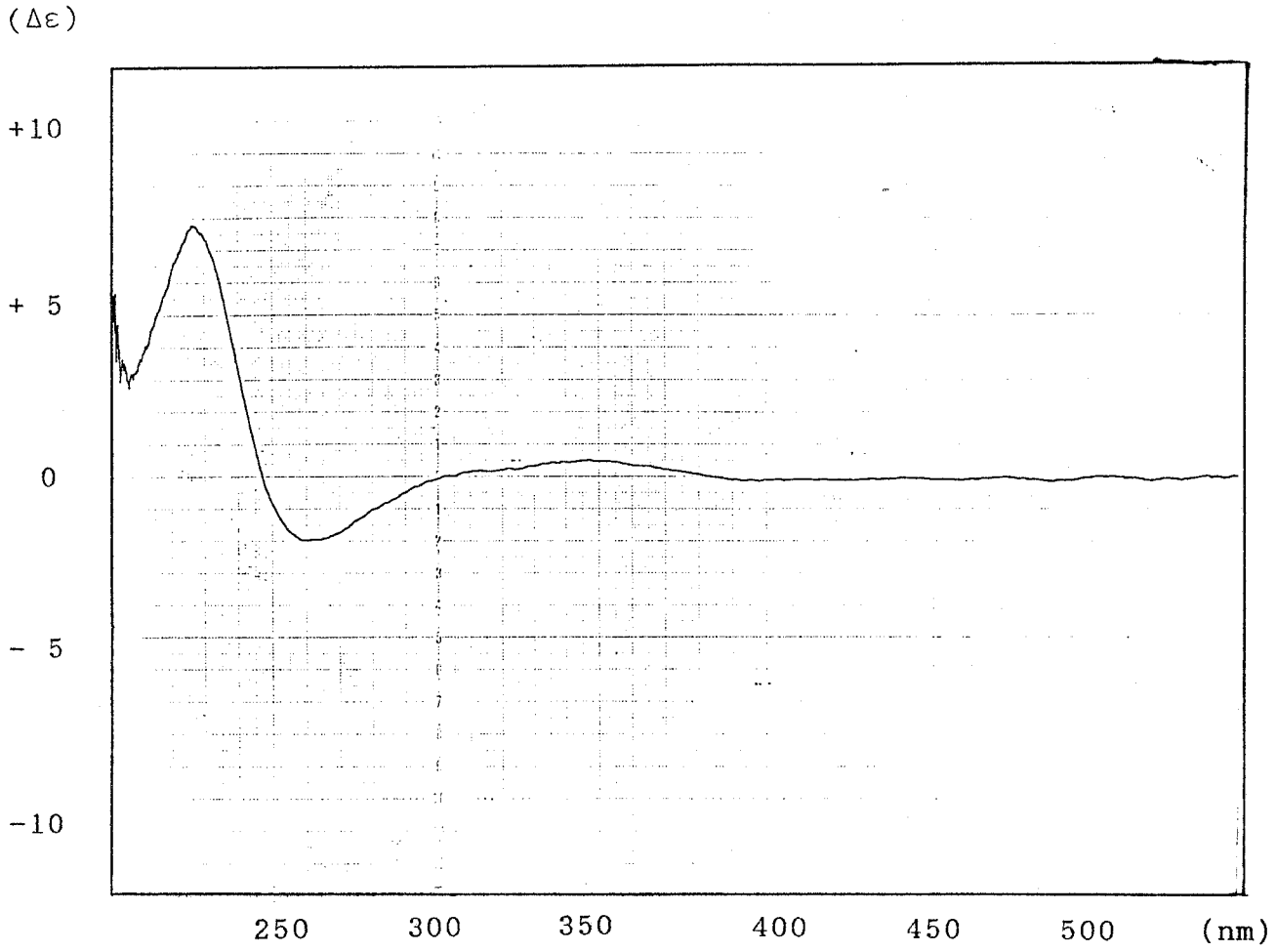

Fig. 3-207 CD Spectrum of C-OX-A2-TU1: The Cotton effects were completely agreeable with those of rugosal A (1). The result indicated that the stereostructure of RL-C-OX-A2 was the same as that of 1 (See Fig. 3-197).

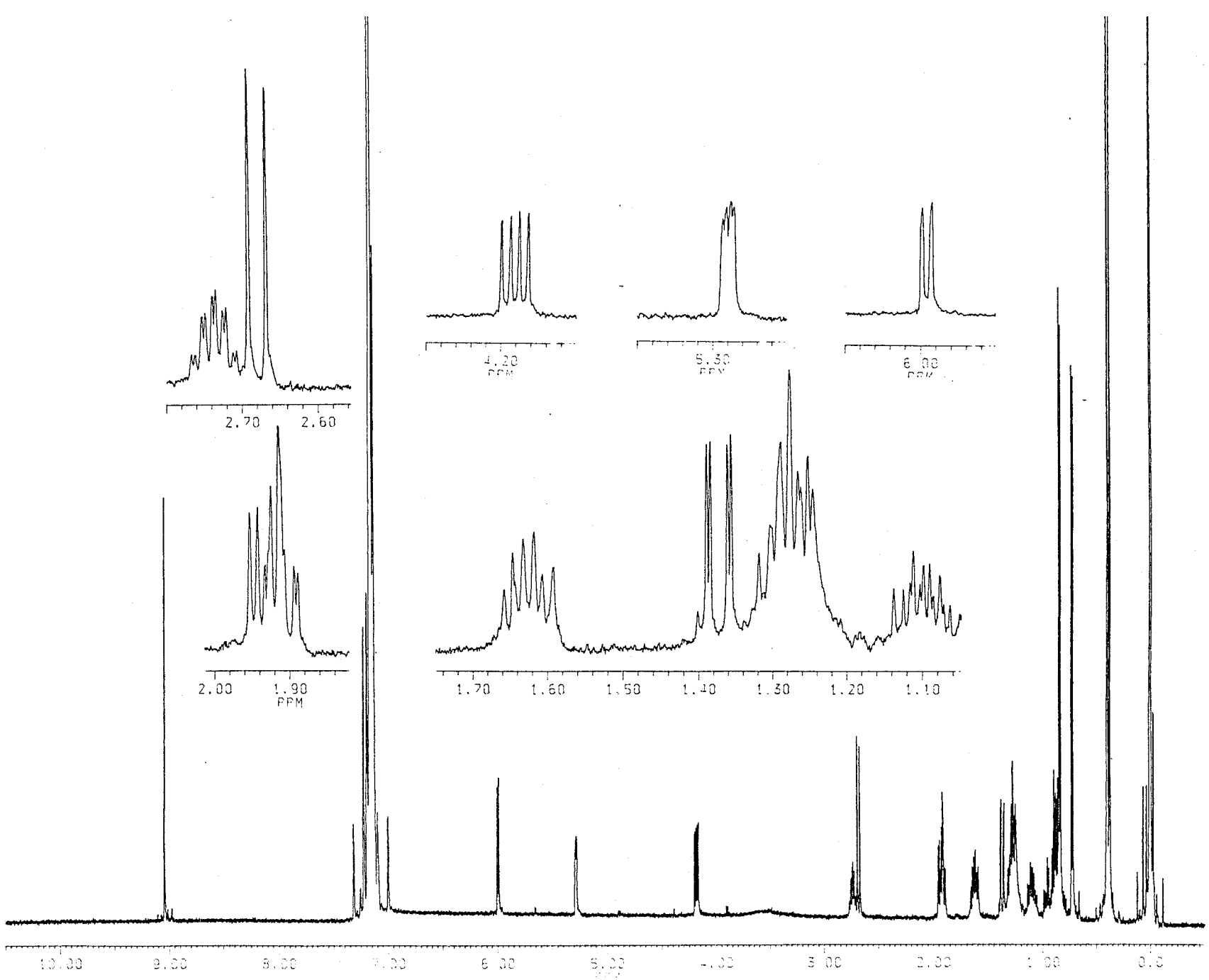

Fig. 3-208 ^{1}H-NMR Spectrum of C-OX-A2-TU1 (500 MHz, in C_6D_6): The spectrum was complete agreeable with that of rugosal A (1, See Fig. 3-10, pp. 59).

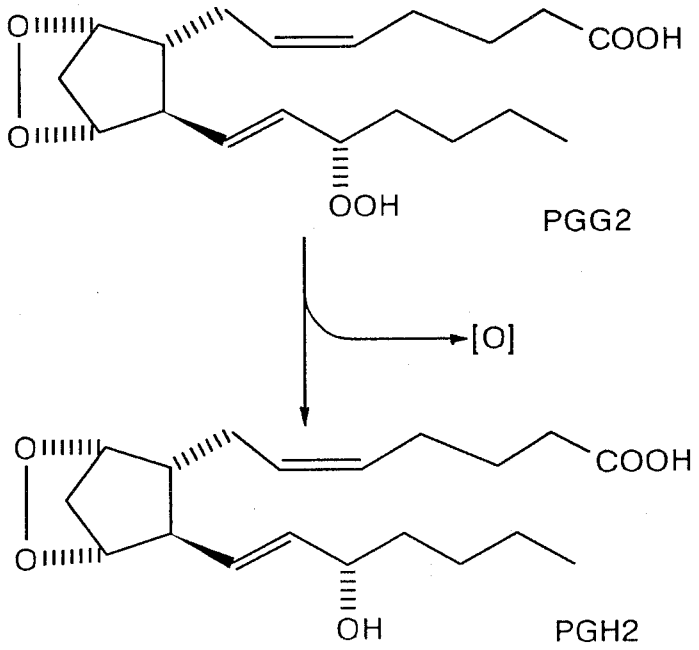

Scheme 3-24 Conversion of PGG_2 into PGH_2

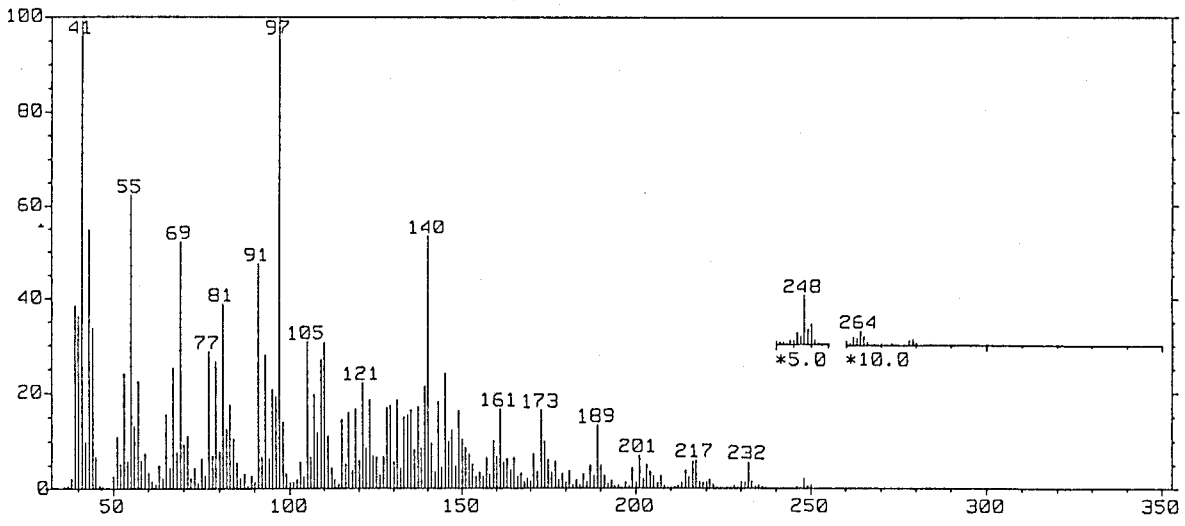

Fig. 3-209 EI-Mass Spectrum of C-OX-A2-TU2: The spectrum was agreeable with that of RSA-TU (1e, See Fig. 3-47, pp. 112).

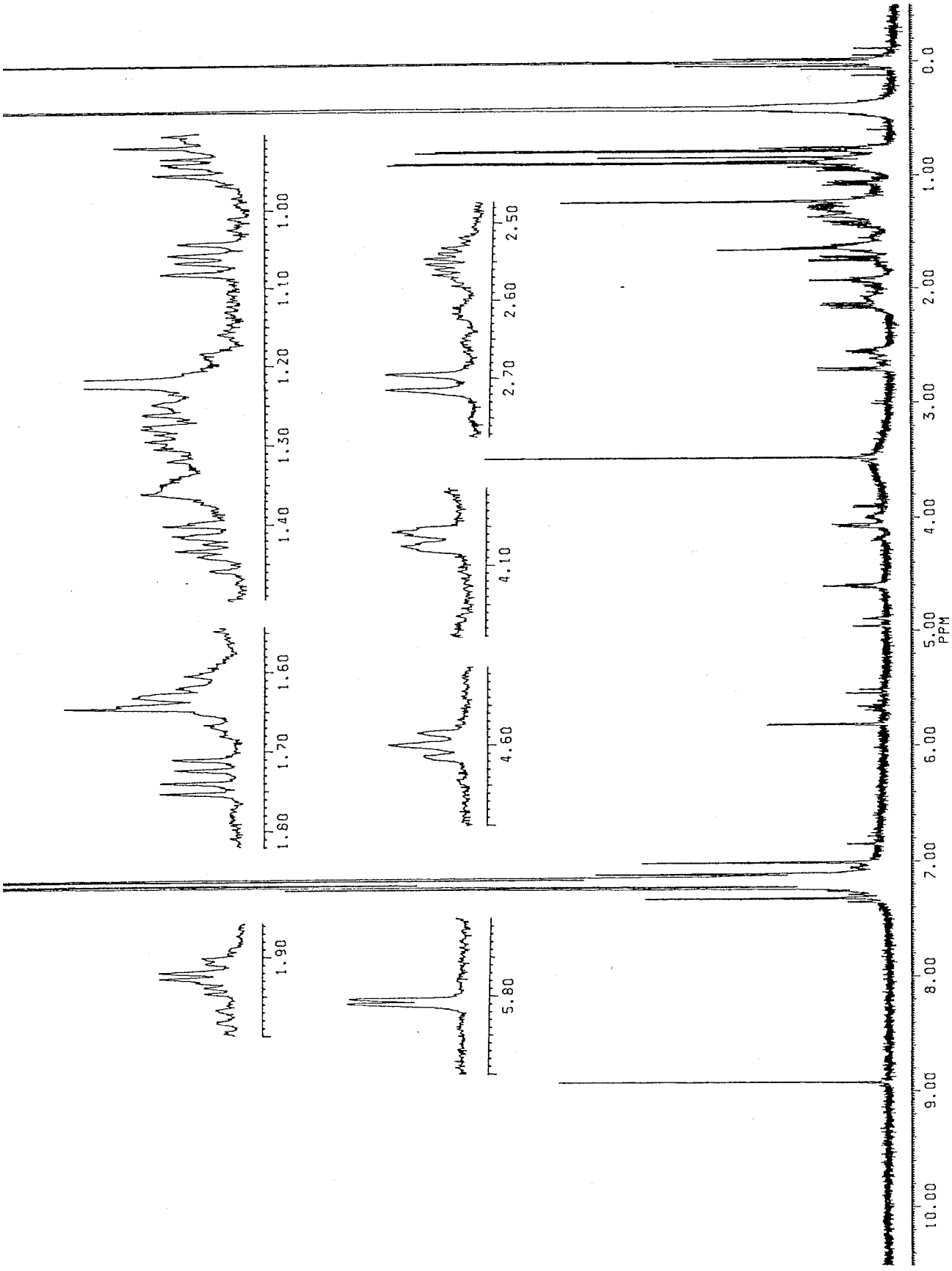

Fig. 3-210 ^{1}H-NMR Spectrum of C-OX-A2-TU2 (500 MHz, in C_6D_6)

Table 3-79 Physicochemical properties of RL-C-OX-A2 (3e)

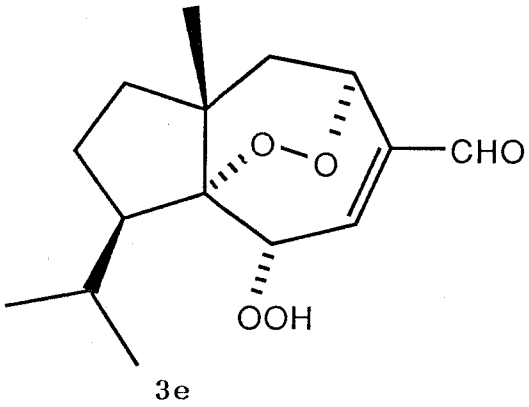

3e

A colorless syrup

Rf: 0.33 (H-EA 3:1)

N,N-dimethyl-*p*-phenylenediamine sulfate test: positive (clear pink)

FD-MS *m/z* (%): 283 (M^++1, 50), 282 (M^+, 100), 268 (38), 266 (65) 265 (78).

EI-MS *m/z* (%): 266 (0.4), 264 (0.3), 248 (0.6), 237 (0.7), 233 (1.2), 220 (1.4), 219 (1.3), 205 (1.7), 203 (1.9), 191 (3.8), 1.77 (2.1), 165 (2.5), 139 (10), 137 (5.9), 121 (9.2), 109 (11), 97 (21), 83 (17), 81 (17), 70 (12), 69 (100), 55 (54), 43 (34), 41 (68).

^{1}H- and ^{13}C-NMR data are shown in Table 3-78,

Table 3-80 Physicochemical properties of OX-A2-TU-1 (rugosal A, 1)

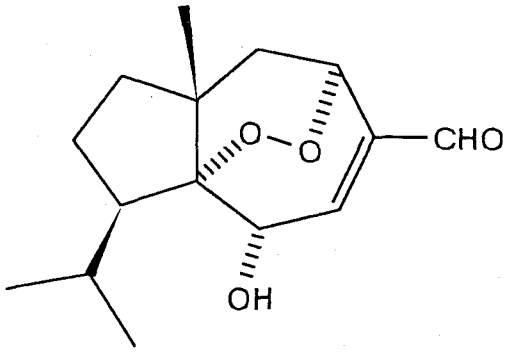

1

Colorless needles

Rf: 0.41 (H-EA 3:1)

CD (nm): 343 (+), 261 (-), 230 (+)

N,N-dimethyl-*p*-phenylenediamine sulfate test: positive (orange/pink)

Vanillin-H_2SO_4 test: dark brown

EI-MS *m/z* (%): 266 (M^+, 0.6), 248 (4.7), 237 (3.4), 220 (5.2), 205 (5.2), 191 (4.8), 177 (9.5), 165 (14), 149 (13), 135 (22), 121 (17), 109 (34), 91 (25), 81 (28), 69 (71), 67 (26), 55 (77), 44 (39), 43 (44), 41 (100).

^{1}H-NMR $\delta^{C_6D_6}_{TMS}$ (500 MHz): 4.186 (1H, dd, *J*= 11.4 and 5.0 Hz, C-2-H), 6.001 (1H, dd, *J*= 6.2 and 0.9 Hz, C-3-H), 5.281 (1H, ddd, *J*= 5.0, 2.4 and 0.9 Hz, C-5-H), 1.935 (1H, dd, *J*= 14.2 and 5.0 Hz, C-6-Ha), 1.375 (1H, dd, *J*= 14.2 and 2.4 Hz, C-6-Hb), 1.626 (1H, ddd, *J*= 12.9, 12.5 and 7.1 Hz, C-8-Ha), 1.273 (1H, dd, *J*= 12.5 and 6.6 Hz, C-8-Hb), 1.291 (1H, m, C-9-Ha), 1.095 (1H, dddd, *J*= 12.9, 12.9 10.9 and 6.6 Hz, C-9-Hb), 1.912 (1H, ddd, *J*= 10.9, 8.9 and 2.3 Hz, C-10-H), 2.739 (1H, double sept., *J*= 6.8 and 2.3 Hz, C-11-H), 0.840 (3H, d, *J*= 6.8 Hz, C-12-H_3), 0.725 (3H, d, *J*= 6.8 Hz, C-13-H_3), 9.047 (1H, s, C-14-H), 0.378 (3H, s, C-15-H_3).

Table 3-81 Physicochemical properties of OX-A2-TU-2 (= RSA-TU, 1d)

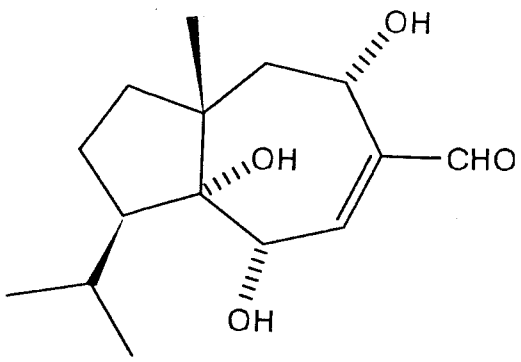

1d

A colorless syrup

Rf: 0.12 (H-EA 3:1)

N,*N*-dimethyl-*p*-phenylenediamine sulfate test: negative

EI-MS *m/z* (%): 250 (0.9), 248 (2.2), 232 (M^+-$2H_2O$, 5.7), 217 (6.1), 216 (5.9), 201 (7.1), 189 (13), 173 (16), 161 (17), 140 (54), 121 (22), 105 (31), 97 (100), 91 (48), 81 (39), 77 (29), 69 (52), 55 (62), 41 (99).

^{1}H-NMR $\delta^{C_6D_6}_{TMS}$ (500 MHz): 4.186 (1H, dd, *J*= 11.4 and 5.0 Hz, C-2-H), 6.001 (1H, dd, *J*= 6.2 and 0.9 Hz, C-3-H), 5.281 (1H, ddd, *J*= 5.0, 2.4 and 0.9 Hz, C-5-H), 1.935 (1H, dd, *J*= 14.2 and 5.0 Hz, C-6-Ha), 1.375 (1H, dd, *J*= 14.2 and 2.4 Hz, C-6-Hb), 1.626 (1H, ddd, *J*= 12.9, 12.5 and 7.1 Hz, C-8-Ha), 1.273 (1H, dd, *J*= 12.5 and 6.6 Hz, C-8-Hb), 1.291 (1H, m, C-9-Ha), 1.095 (1H, dddd, *J*= 12.9, 12.9 10.9 and 6.6 Hz, C-9-Hb), 1.912 (1H, ddd, *J*= 10.9, 8.9 and 2.3 Hz, C-10-H), 2.739 (1H, double sept., *J*= 6.8 and 2.3 Hz, C-11-H), 0.840 (3H, d, *J*= 6.8 Hz, C-12-H_3), 0.725 (3H, d, *J*= 6.8 Hz, C-13-H_3), 9.047 (1H, s, C-14-H), 0.378 (3H, s, C-15-H_3).

Two minor products RL-C-OX-B4 and RL-C-OX-B5 were easily identified as 1 and 2, respectively. Those compounds, especially 2, were more effectively yielded from 3 at lower temperature. However, those were almost in trace amount, contrary to the large amount of 1 and 2 in the *Rosa rugosa* tissues [128].
This fact may suggest that 1 and 2 are converted from 3 by an enzyme reaction in the tissues.

Contrary to the other minor products, RL-C-OX-B1 was the only substance negative to the peroxide reagent. In EI-MS, ^{1}H- and ^{13}C-NMR analyses, the product was indistinguishable from the epoxy derivative of 3, RL-C-CPBA (**3b**) (Fig. 3-211, 212 and 213). The presence of RL-C-OX-B1 was suggestive that RL-C-OX-A2 (**3c**) gives active oxygen to 3 to result in the formation of **3b** while **3c** is stabilized into 1 in the reaction system. Accordingly, the isolated olefinic bond of 3 is oxygenated to form an epoxide group at **3c**. Rugosic acid A (2) may also have been yielded from 1 as the result of scavenging active oxygen (Scheme 3-25).

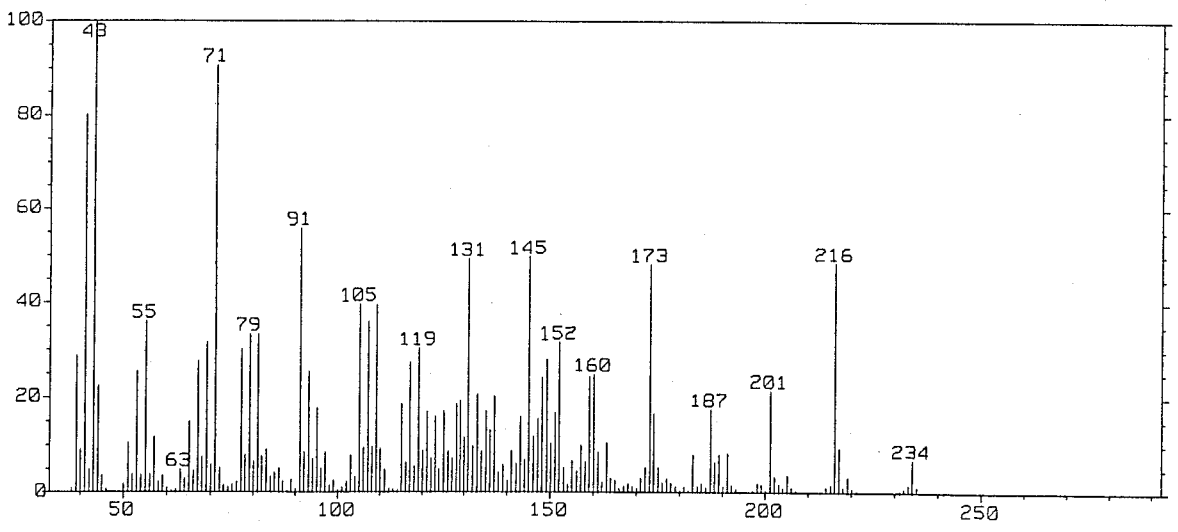

Fig. 3-211 EI-Mass Spectrum of RL-C-OX-B1

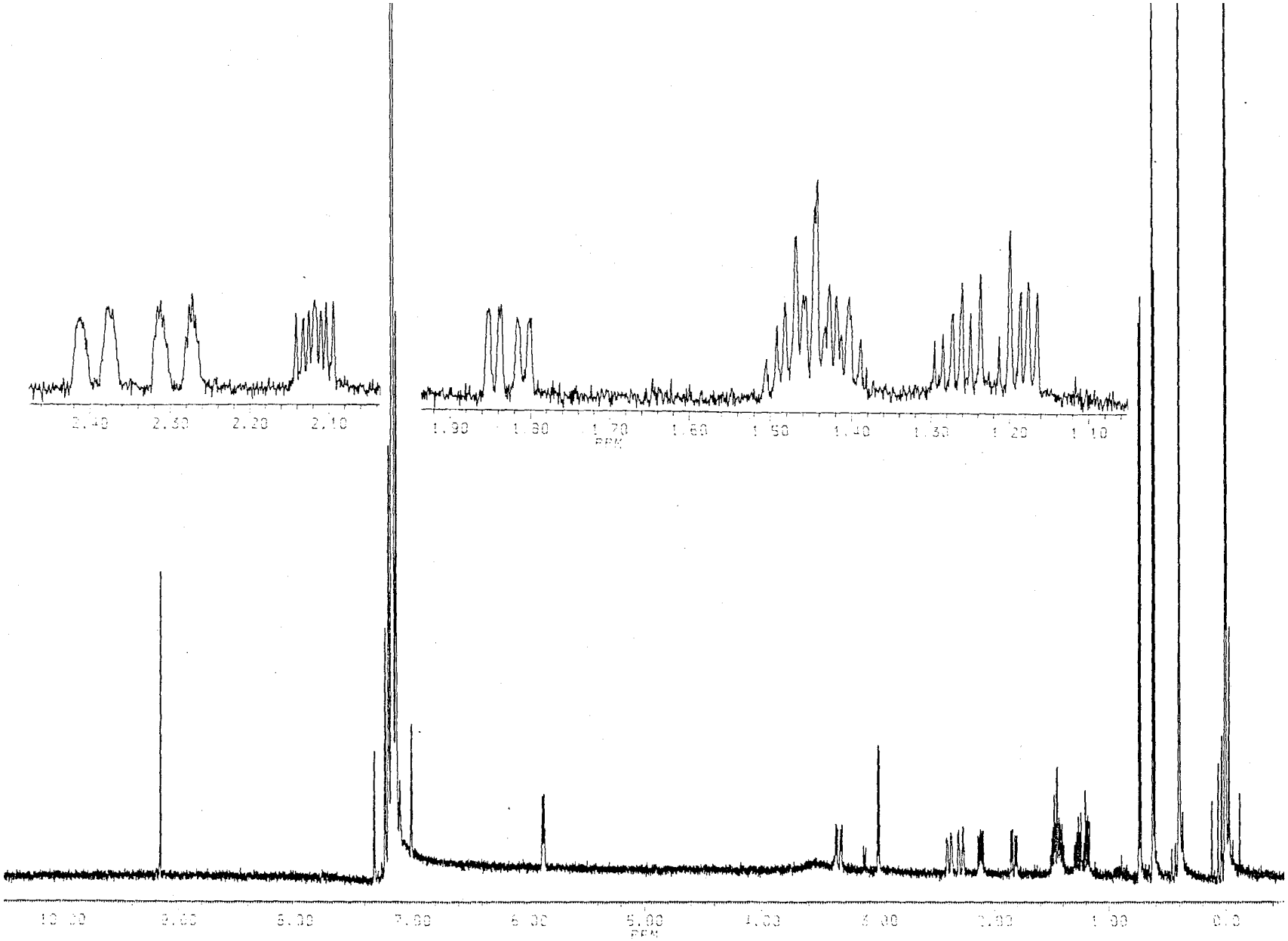

Fig. 3-212 ^{1}H-NMR Spectrum of RL-C-OX-B1 (500 MHz, in C_6D_6): The signal are well agreeable with those of RL-C-CPBA (**36**, See Fig. 3-180, pp. 316).

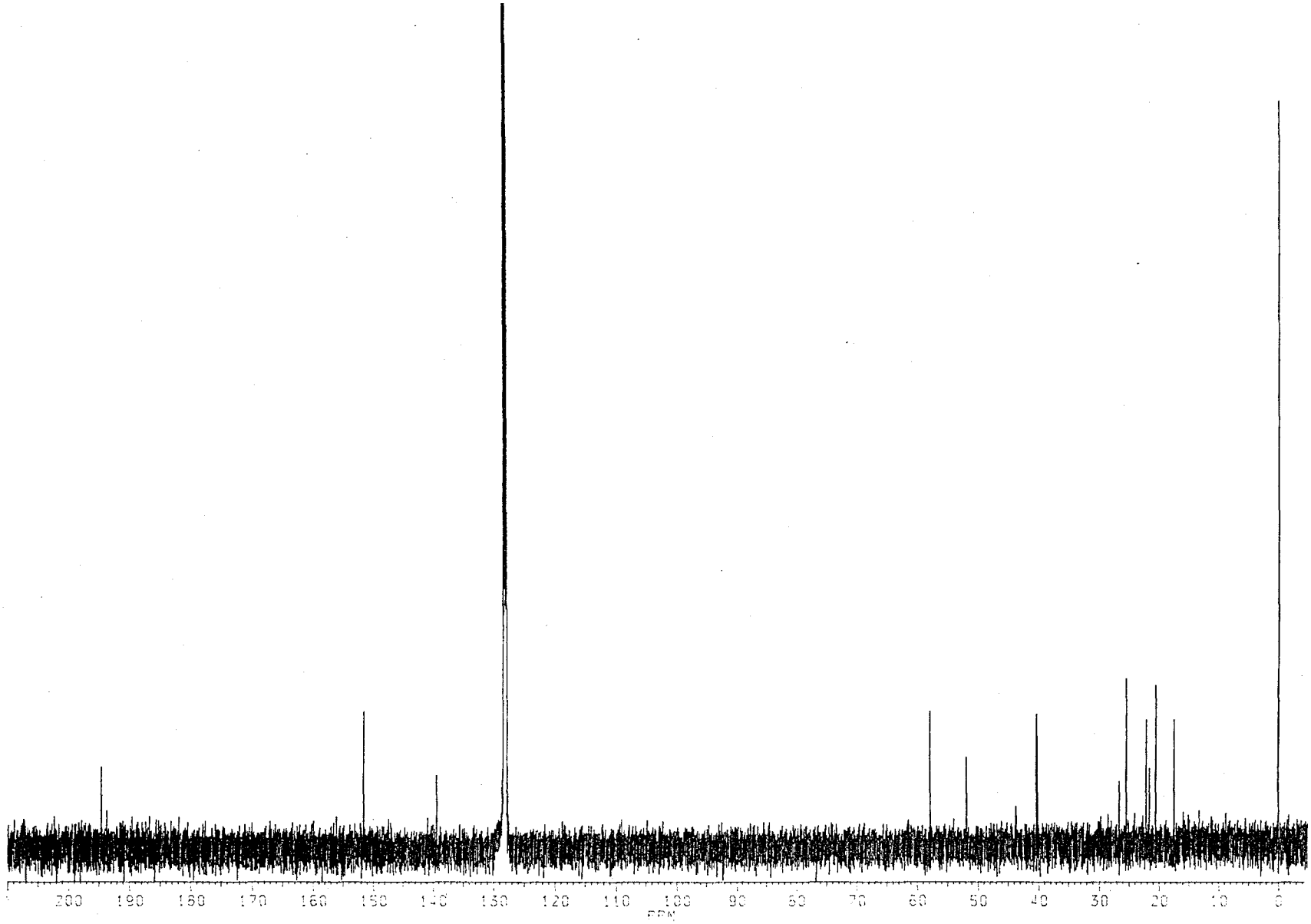

Fig. 3-213 ^{13}C-NMR Spectrum of RL-C-OX-B1 (125 MHz, in C_6D_6): The sample was further obtained from a oxgenated mixture of crude carota-1,4-dienaldehyde (3).

Table 3-83 Physicochemical properties of RL-C-OX-B1 (= RL-C-CPBA, 3b)

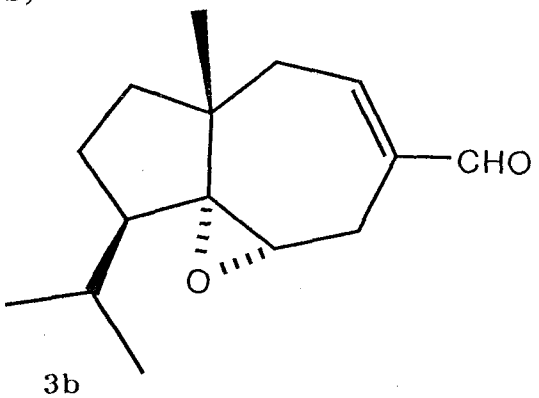

3b

A colorless syrup

Rf: 0.41 (H-EA 3:1)

N,N-dimethyl-*p*-phenylenediamine sulfate test: negative (pale yellow)

EI-MS *m/z* (%): 234 (M^+, 7.0), 216 (49), 201 (21), 187 (18), 173 (48), 160 (25), 159 (24), 152 (32), 149 (28), 145 (50), 131 (49), 119 (30), 109 (40), 107 (36), 105 (40), 91 (56), 81 (33), 79 (33), 71 (91), 69 (32), 55 (36), 43 (100), 41 (80).

^{1}H-NMR $\delta^{C_6D_6}_{TMS}$ (500 MHz): 4.186 (1H, dd, *J*= 11.4 and 5.0 Hz, C-2-H), 6.001 (1H, dd, *J*= 6.2 and 0.9 Hz, C-3-H), 5.281 (1H, ddd, *J*= 5.0, 2.4 and 0.9 Hz, C-5-H), 1.935 (1H, dd, *J*= 14.2 and 5.0 Hz, C-6-Ha), 1.375 (1H, dd, *J*= 14.2 and 2.4 Hz, C-6-Hb), 1.626 (1H, ddd, *J*= 12.9, 12.5 and 7.1 Hz, C-8-Ha), 1.273 (1H, dd, *J*= 12.5 and 6.6 Hz, C-8-Hb), 1.291 (1H, m, C-9-Ha), 1.095 (1H, dddd, *J*= 12.9, 12.9 10.9 and 6.6 Hz, C-9-Hb), 1.912 (1H, ddd, *J*= 10.9, 8.9 and 2.3 Hz, C-10-H), 2.739 (1H, double sept., *J*= 6.8 and 2.3 Hz, C-11-H), 0.840 (3H, d, *J*= 6.8 Hz, C-12-H_3), 0.725 (3H, d, *J*= 6.8 Hz, C-13-H_3), 9.047 (1H, s, C-14-H), 0.378 (3H, s, C-15-H_3).

^{13}C-NMR $\delta^{C_6D_6}_{TMS}$ (125 MHz, COM): 51.9 (C-2), 25.4 (C-3), 139.3 (C-4), 151.5 (C-5), 40.2 (C-6), 43.8 (C-7), 40.3 (C-8), 22.2 (C-9), 57.9 (C-10), 26.7 (C-11), 20.6 (C-12), 17.5 (C-13), 194.5 (C-14), 21.6 (C-15). C-1 carbon was invisible. The compound for the ^{13}C-NMR was prepared from oxidized mixture of RL fraction (*ca* 100 mg of **3** was contained) using HPLC (Unisil Q 100-5, 2.5 % *iso*PrOH-*n*-hexane).

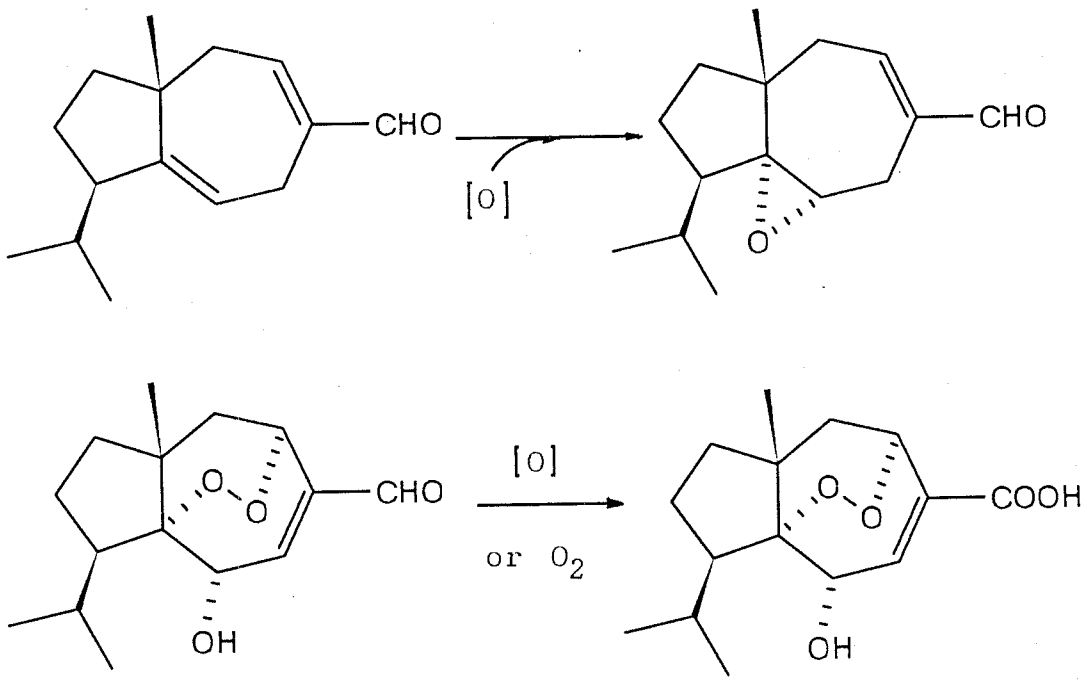

Scheme 3-25 Scavenge of active oxygen from RL-C-OX-A2 (3c)

In addition to those previously obtained compounds, a small amount of RL-C-OX-B2 positive to the peroxide reagent was isolated as colorless semisolid. In FI-MS, the isolate indicated M^+ 250 (100 %, **3** + O_2 as a peroxide group) (Fig. 3-214). Based on its presumable molecular formula ($C_{15}H_{22}O_3$), the compound should possess a hydroperoxy group. The presence of a hydroperoxy group was also suggested from EI-MS fragmentation (Fig. 3-215). These facts indicated a possibility of RL-C-OX-B2 as an intermediate in the step 1 in Scheme 3-23 (pp. 289). Although it was quite small amount, ^{1}H-NMR spectrum of RL-C-OX-B2 was taken, and as the result, some characteristic proton signals were observed (Fig. 3-216). A singlet resonated at δ_H 9.126 (1H) disappeared on D_2O addition. This exchangable signal which is strongly deshielded and sharpened probably due to hydrogen-bonding with the C-14 carbonyl group was considered to be attributable to the hydroperoxy proton.

Since the starting material has two olefinic bonds, hydroperoxidation may occur at C-1, C-2, C-4 or C-5 (**A**, **B**, **C** and **D**, respectively, in Fig. 3-217), concerted translocation of the olefinic bond. Firstly, peroxidation at C-4 (**C**) in this compound was ruled out because the resulting product (**C**) lacking a conjugation system was contradictory to RL-C-OX-B2 in a quenching property. The peroxidation at C-5 position was also eliminated by its ^{1}H-NMR and UV analyses. If C-5 was oxygenated to yield **D**, the olefinic bond would be translocated to C-3, C-4 to extend the conjugation system as step 1 in Scheme 3-27 (pp. 371). However, UV λ_{max}^{MeOH} of the compound was observed at 229 nm, which was indicative of not an $\alpha,\beta;\alpha',\beta'$-unsaturated carbonyl system but an α,β-unsaturated one. In fact, a singlet formyl proton and a deshielded olefinic proton (δ_H 9.268 and 6.205, respectively) involved in the conjugation system were detected in the ^{1}H-NMR spectrum. Furthermore, the olefinic proton (1H, br. dd, *J*= 8.2 and 6.3 Hz) was vicinally coupled with a pair of methylene protons at δ_H 2.049 (1H, dd, *J*= 13.4 and 6.3 Hz) and 1.905 (1H, dd, *J*= 13.4 and 8.2

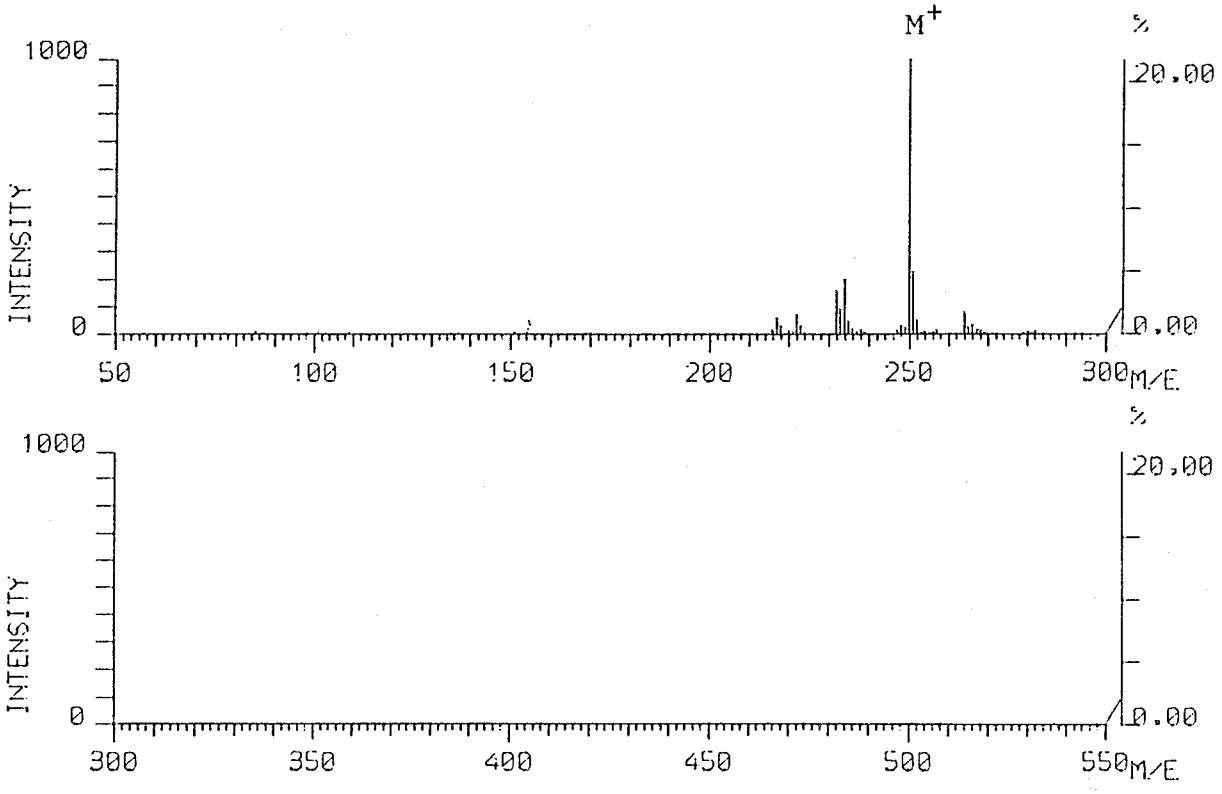

Fig. 3-214 FI-Mass Spectrum of RL-C-OX-B2

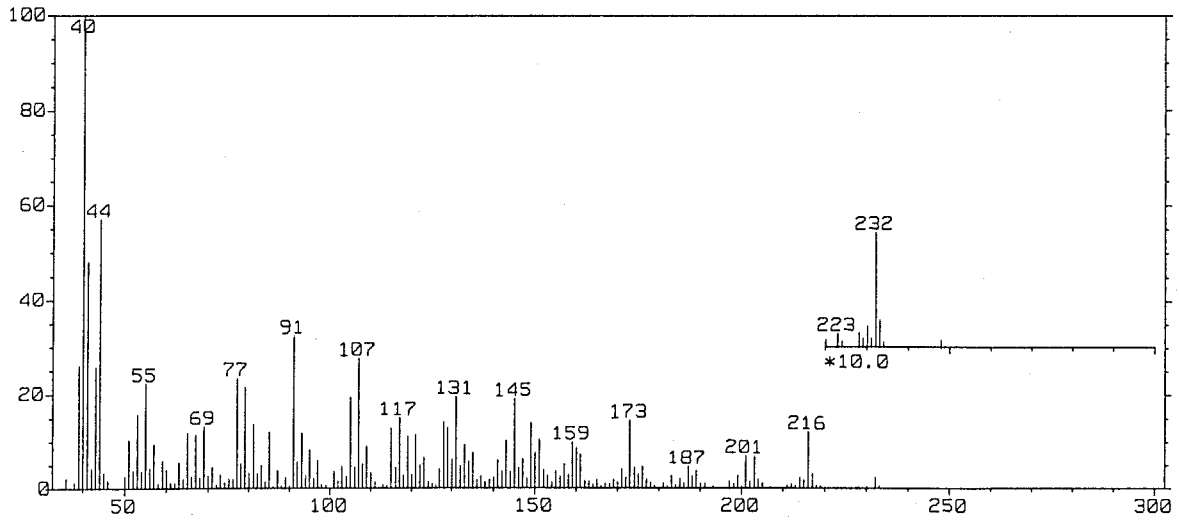

Fig. 3-215 EI-Mass Spectrum of RL-C-OX-B2

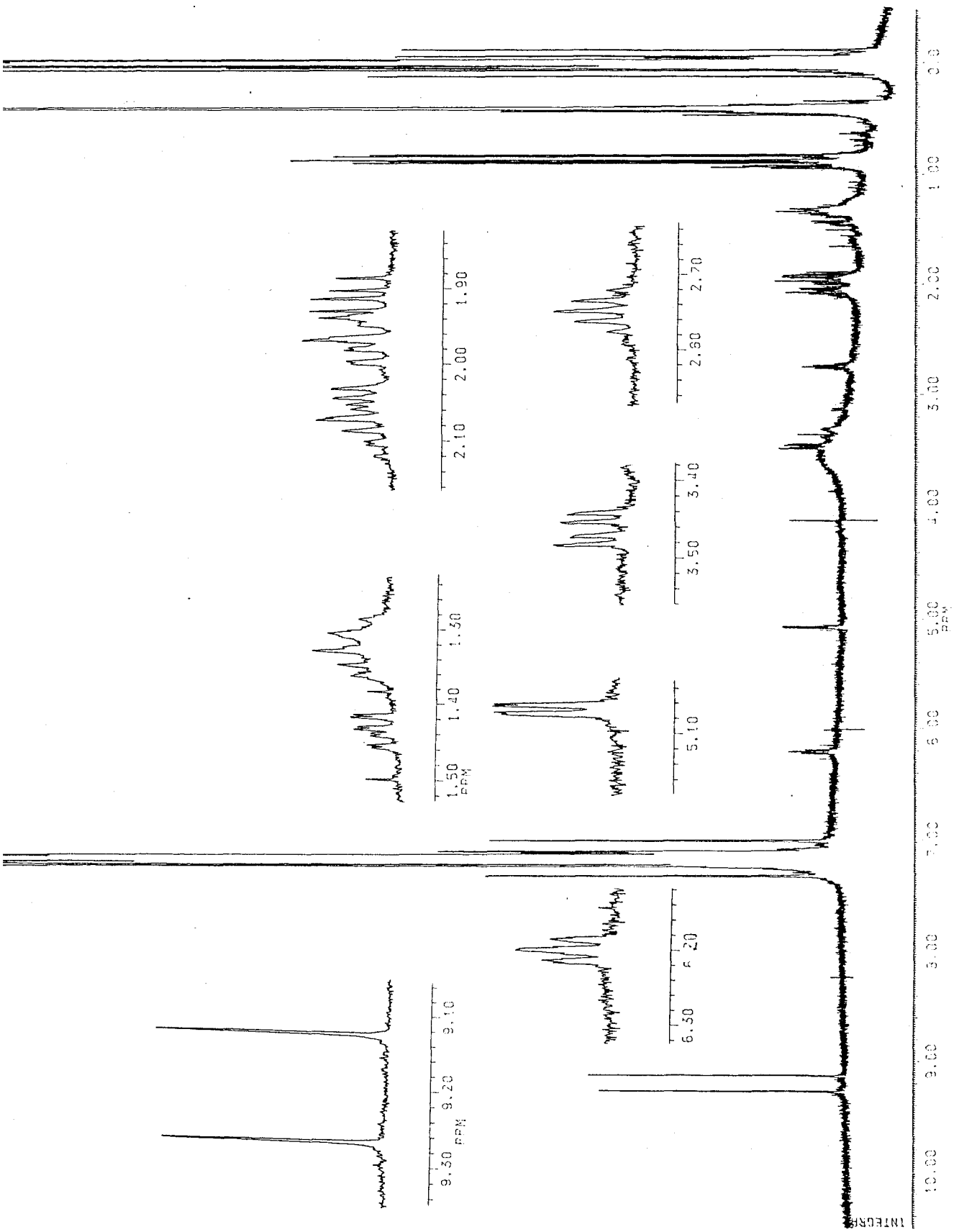

Fig. 3-216 ^{1}H-NMR Spectrum of RL-C-Ox-B2 (500 MHz, in C_6D_6)

Table ***3-83*** *^{1}H-NMR chemical shift values of RL-C-OX-B2* ***(3d)***

(500 MHz, in C_6D_6, TMS as an int. std.)

δ_H	Coupling *J*(Hz)	Assignment
5.027	br. dd (5.6, 1.3)	C-2-H
3.452	br. dd (14.5, 5.6)	C-3-Ha
1.949	br. d (14.5)	C-3-Hb
6.205	br. dd (8.2, 6.3)	C-5-H
2.049	dd (13.4, 6.3)	C-6-Ha
1.905	br. dd (13.4, 8.2)	C-6-Hb
1.436	ddd (11.8, 7.6, 1.6)	C-8-Ha
1.316	ddd (11.8, 9.4, 9.1)	C-8-Hb
2.083	ddd (16.8, 9.4, 7.6)	C-9-Ha
1.970	ddd (16.8, 9.1, 1.6)	C-9-Hb
2.747	sept (6.9)	C-11-H
0.885	d (6.9)	C-12-H_3
0.824	d (6.9)	C-13-H_3
9.268	s	C-14-H
0.865	s	C-15-H
9.126	s exchangeable	C-2-OOH

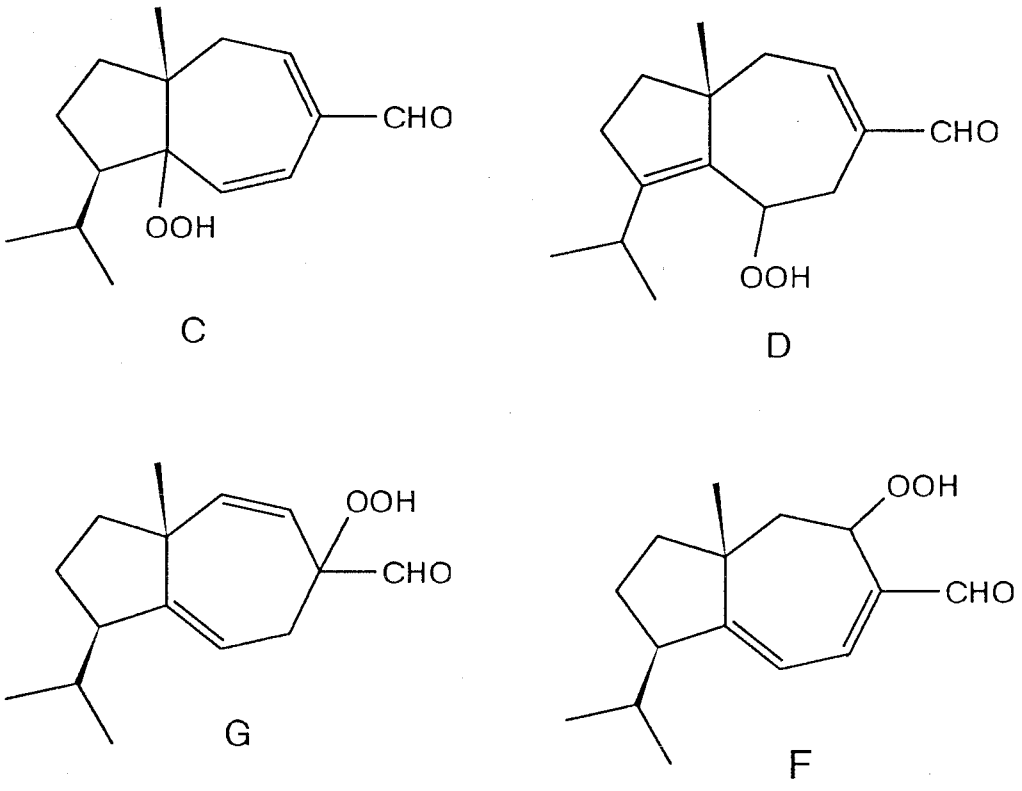

Fig. 3-217 Four Possible Structures for RL-C-OX-B2

Hz). The structure D, A and C were therefore rejected, and B was thus remained as a possible and collect structure for RL-C-OX-B2.

On the other hand, the proton signal at δ_H 5.027 (1H, br. dd, *J*= 5.6 and 1.3 Hz) assignable either an olefinic proton or an oxygenated-methine proton was vicinally coupled with another pair of methylene protons (δ_H 3.452 and 1.949, geminally coupled with *J*= 14.5 Hz). Since one of the protons was markedly deshielded, the methylene carbon should be located to C-3. Accordingly, the proton at δ_H 5.027 was deduced to be a methine proton allocated on the oxygenated (namely hydroperoxylated) C-2 carbon.

The structure B was also supported by ^{1}H-NMR detection of the C-11 methine proton signal observed as a clear septet (δ_H 2.747, *J*= 6.9 Hz). This splitting was explicable only with a part structure of the isopropyl group on the non-hydrogen bearing C-10 carbon like B. Accordingly, RL-C-OX-B2 was elucidated as **3d**. Including C-8-H_2 and C-9-H_2 part, all the proton signals were assigned as shown in Fig. 3-218. The hydroperoxyl group seems to be able to form a stable eight-membered ring through intramolecular hydrogen bonding with the aldehyde group, as some known examples of intramolecular hydrogen bonding between a hydroperoxy group and a carbonyl group [133]. Stereochemistry at C-2 was considered as ***S*** due to the steric effect of the bridgehead methyl group.

This compound showed the evidence that a proton radical can be abstracted not only from C-3 but also C-10 in **3** to result in homolytic re-distribution of two π-electrons on 1-olefinic bond. Accordingly, a new redical is formed on C-2 on which triplet O_2 attacks, as shown in Scheme 3-26. However, the exoperoxy radical cannot cyclize due to its position (Scheme 3-27) and just form a hydroperoxyl group stabilized by the hydrogen bonding between -OO<u>H</u> and C-14 carbonyl oxygen (Fig. 3-219).

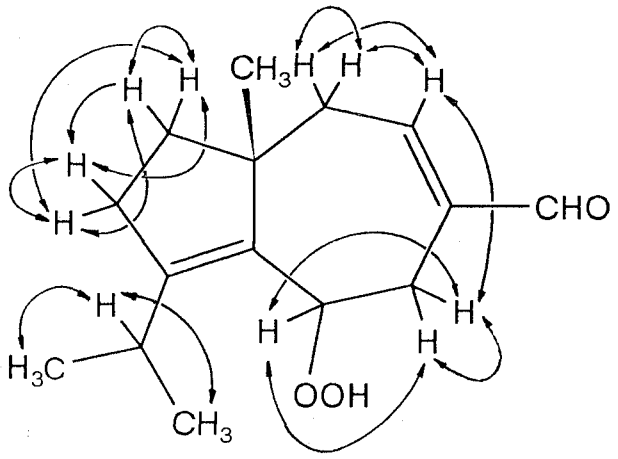

Fig. 3-218 Proton Sequences of RL-C-OX-B2 (**3d**) Observed by decoupling Experiments

⟷ Observed H-H Coupling Sequence

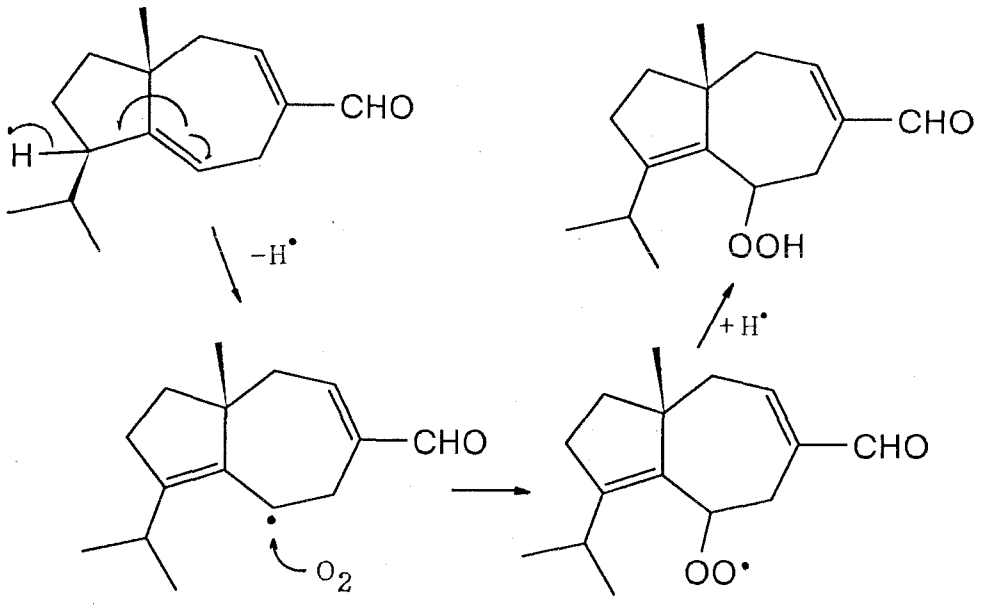

Scheme 3-26 Peroxylation Process to Yield RL-C-OX-B2 (3d)

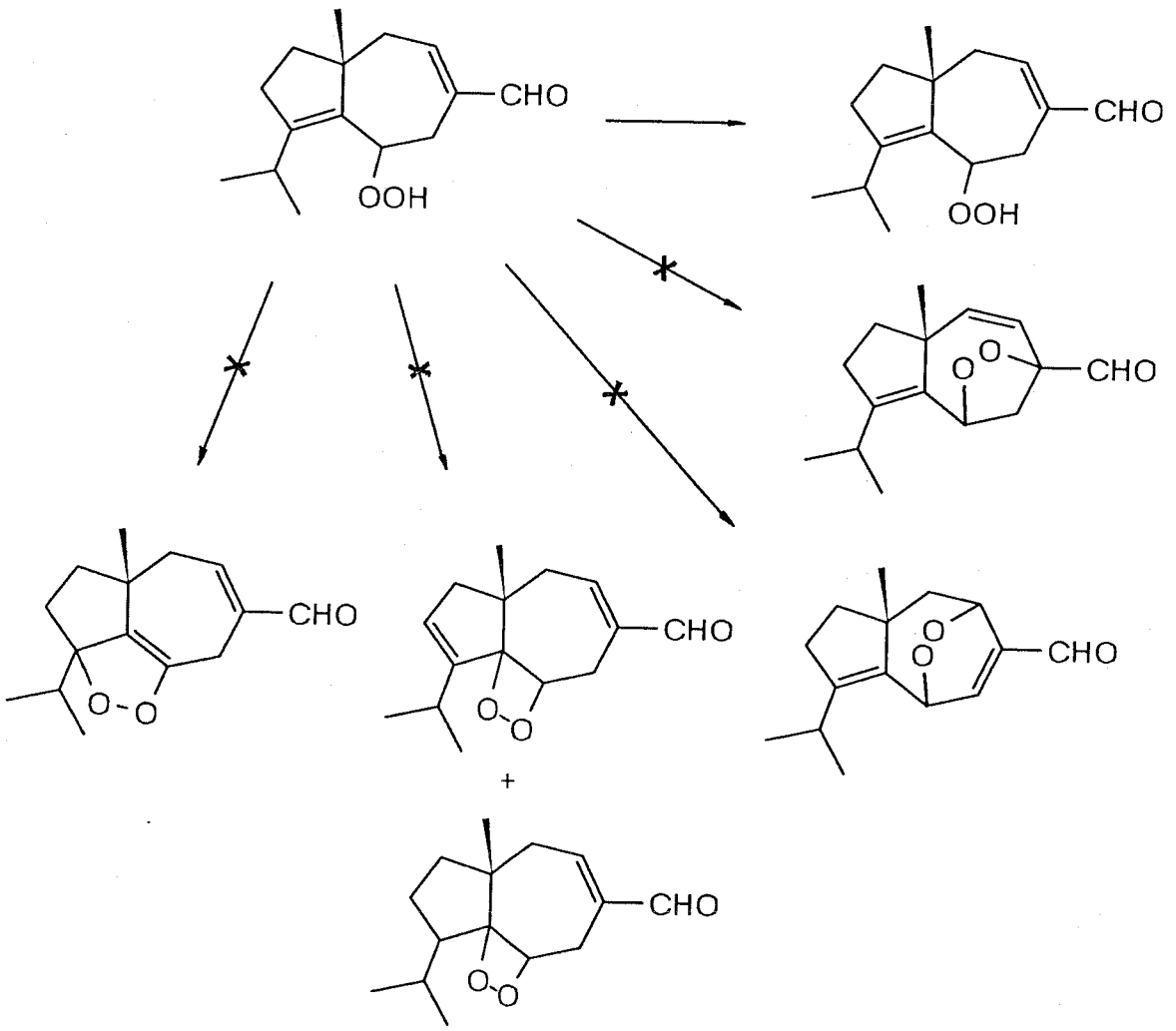

Scheme 3-27 Several obstacles to cyclization of endopeoxy radical of RL-C-OX-B2 intermediate: Any type of cyclization of exoperoxy radical takes a disadvantage. For example, cyclization of the radical to C-10 results in formation of an enolic carbon at C-2, and if it cyclized to C-1, the endoperoxy linkage must take a dioxethane structure. On the other hand, π-electrons on the C-4/C-5 is localized to C-4 due to the presence of conjugation system with C-14 carbonyl group, and this polarization prevents homolysis of the π-electrons. In addition, cyclization at C-4 is probably impossible because the conjugation system would be broken down during the re-formation. On the contrary, the peroxide is unexpectedly stable due to a intramolecular hydrogen-bond between the hydroperoxide and aldehyde groups.

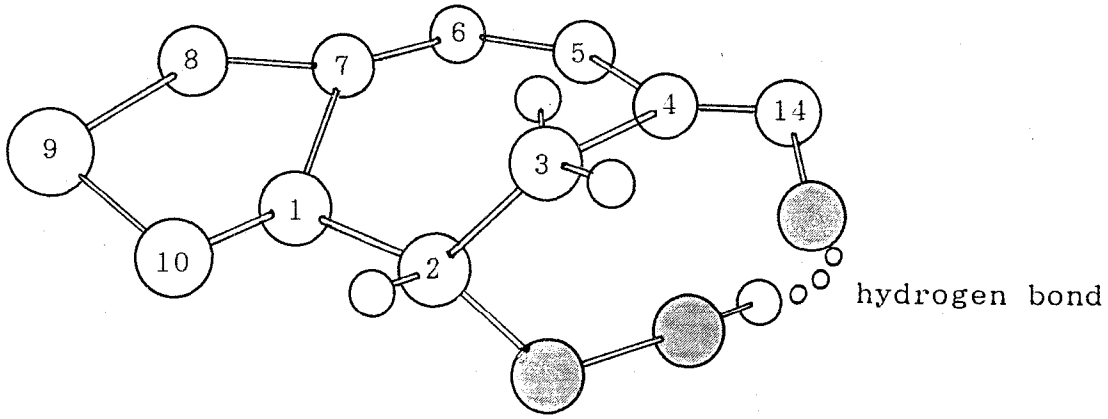

Fig. 3-219 Hydrogen Bond between C-2-OOH and C-14-CHO Groups

Table 3-84 Physicochemical properties of RL-C-OX-B2 (3d)

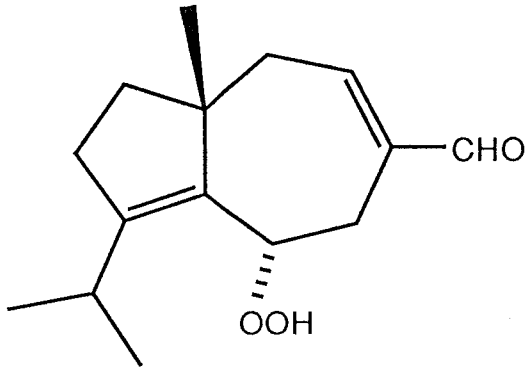

3d

A colorless semisolid

N,N-dimethyl-*p*-phenylenediamine sulfate test: positive (pinkish red)

UV λ_{max}^{MeOH}: 229 nm

FI-MS *m/z* (%): 251 (M^++1, 22), 250 (M^+, 100), 234 (15), 232 (21).

EI-MS *m/z* (%): 232 (M^+-H_2O, 2.4), 216 (12), 203 (6.9), 201 (7.0), 187 (4.7), 173 (15), 160 (8.8), 159 (9.9), 149 (14), 145 (19), 131 (20), 117 (15), 107 (28), 105 (19), 91 (36), 79 (22), 77 (23), 55 (22), 44 (57), 41 (48), 40 (100).

^{1}H-NMR data are listed in Table 3-83.

3) Autoxidation Product under a Low Concentration of Dissolved O_2

During a survey of oxidation products in a stored carota-1,4-dienaldehyde (3) solution, an unknown substance positive to the peroxide test was detected (Fig. 3-220). The peroxide (RL-C-OX3) produced in the dilute EtOAc solution of **3** (*ca* 50 mg/200 ml solvent), was isolated by PTLC (*Rf* 0.67 in H-EA 4:1) as a colorless syrup. The isolate showed the molecular ion at *m/z* 236 in FD-MS (Fig. 3-221). The methanolic UV absorption maximum at 230 nm suggested the presence of an α,β-unsaturated aldehyde group. However, only a decarboxylated ion (*m/z* 192, M^+-44, 7.4 %) was observed as the largest peak in EI-MS (Fig. 3-222). Furthermore, a formyl proton was undetectable in ^{1}H-NMR spectrum of RL-C-OX3, and a pair of isolated olefinic protons indicating *cis* coupling (δ_H 6.372 and δ_H 6.310, each 1H, d, *J*= 11.3 Hz) was observed (Fig. 3-223 and Table 3-85). Its ^{13}C-NMR spectrum was indicative only 14 carbons (Fig. 3-224 and Table 3-85), in which a non-hydrogen bearing carbonyl carbon attributable to the conjugation system was detected at δ_C 203.3. In addition, two olefinic methine carbons assignable to a single olefinic bond in the molecule were detected. By the spin-spin decoupling, $-CH_2-CH_2-$ and $-CH_2-CH_2-CH-(CH_3)_2$ sequences were revealed to provide a structure **3e** to RL-C-OX3 (Fig. 3-225).

A conversion scheme from **3** to **3e** was proposed as Scheme 3-28. The fact that **3e** was only recognizable in a solution (less aerobic) was suggestive of thw presence of an allyl radical intermediate in the reaction. As it was presumed that **3** in solution was oxygenated comparatively slowly by dissolved O_2, the second oxidation at C-4 may occur under the low concentration of O_2. Due to the electron delocalization (allyl radical) and/or the tertiary radical at C-4, the reaction intermediate seems to be stabilized.

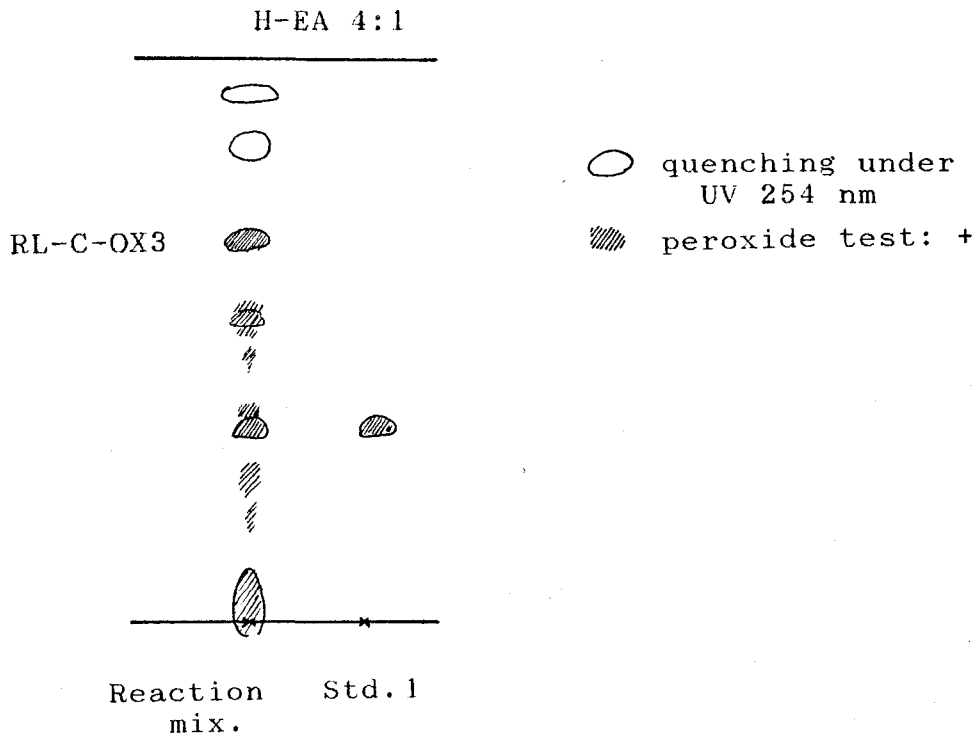

Fig. 3-220 TL Chromatogram of Oxidation Products Obtained from EtOAc-diluted Carota-1,4-dienaldehyde (3)

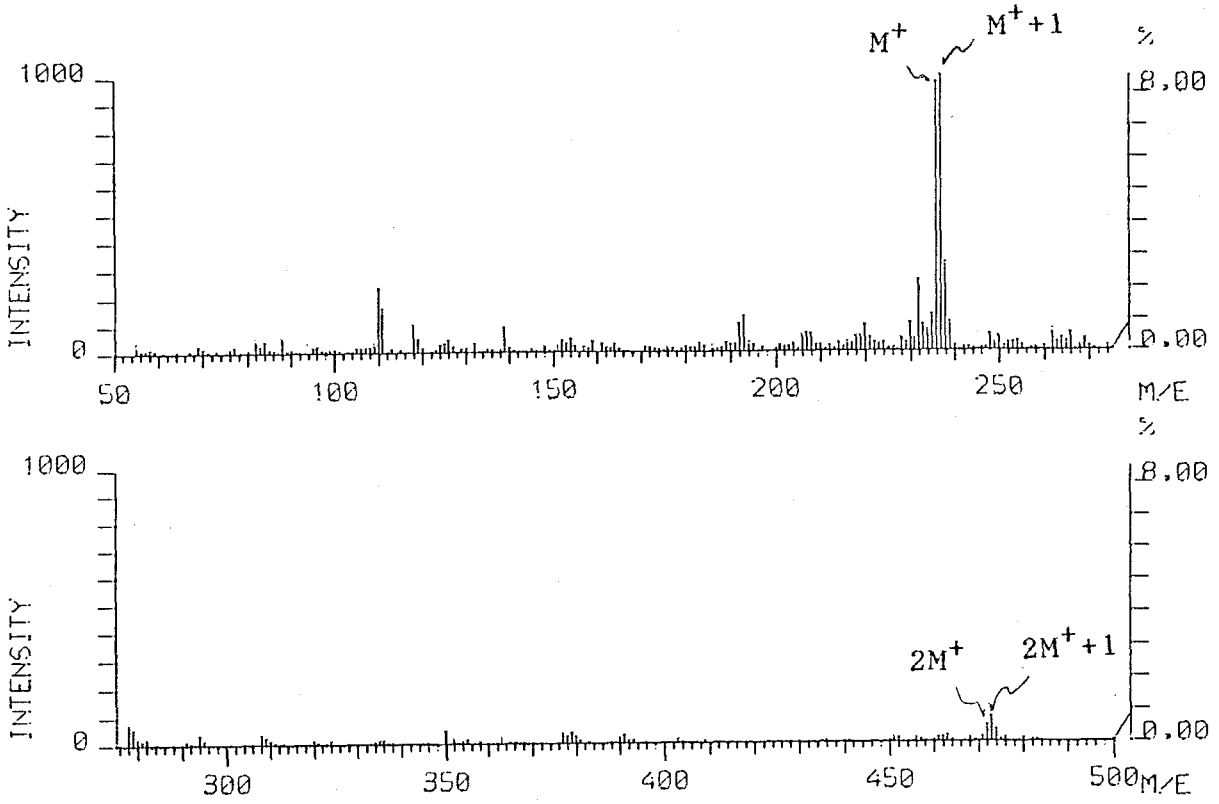

Fig. 3-221 FD-Mass Spectrum of RL-C-OX3

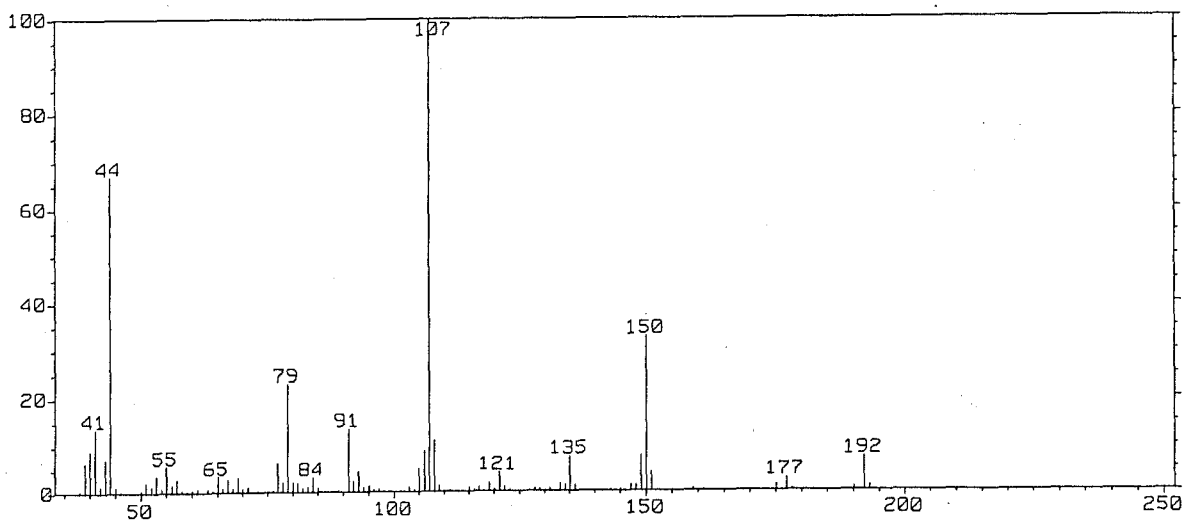

Fig. 3-222 EI-Mass Spectrum of RL-C-OX3

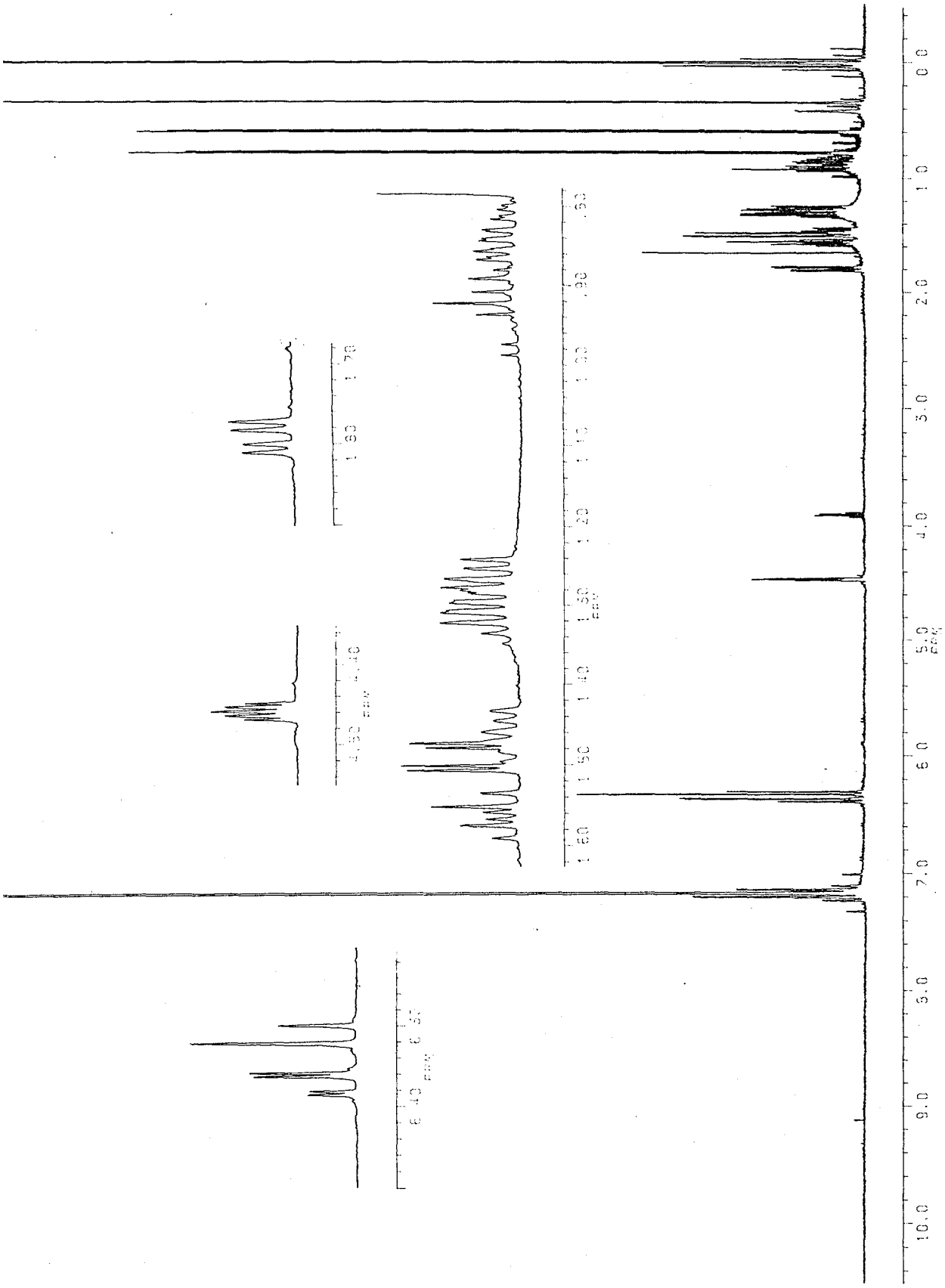

Fig. 3-223 ^{1}H-NMR Spectrum of RL-C-OX3 (500 MHz, in C_6D_6)

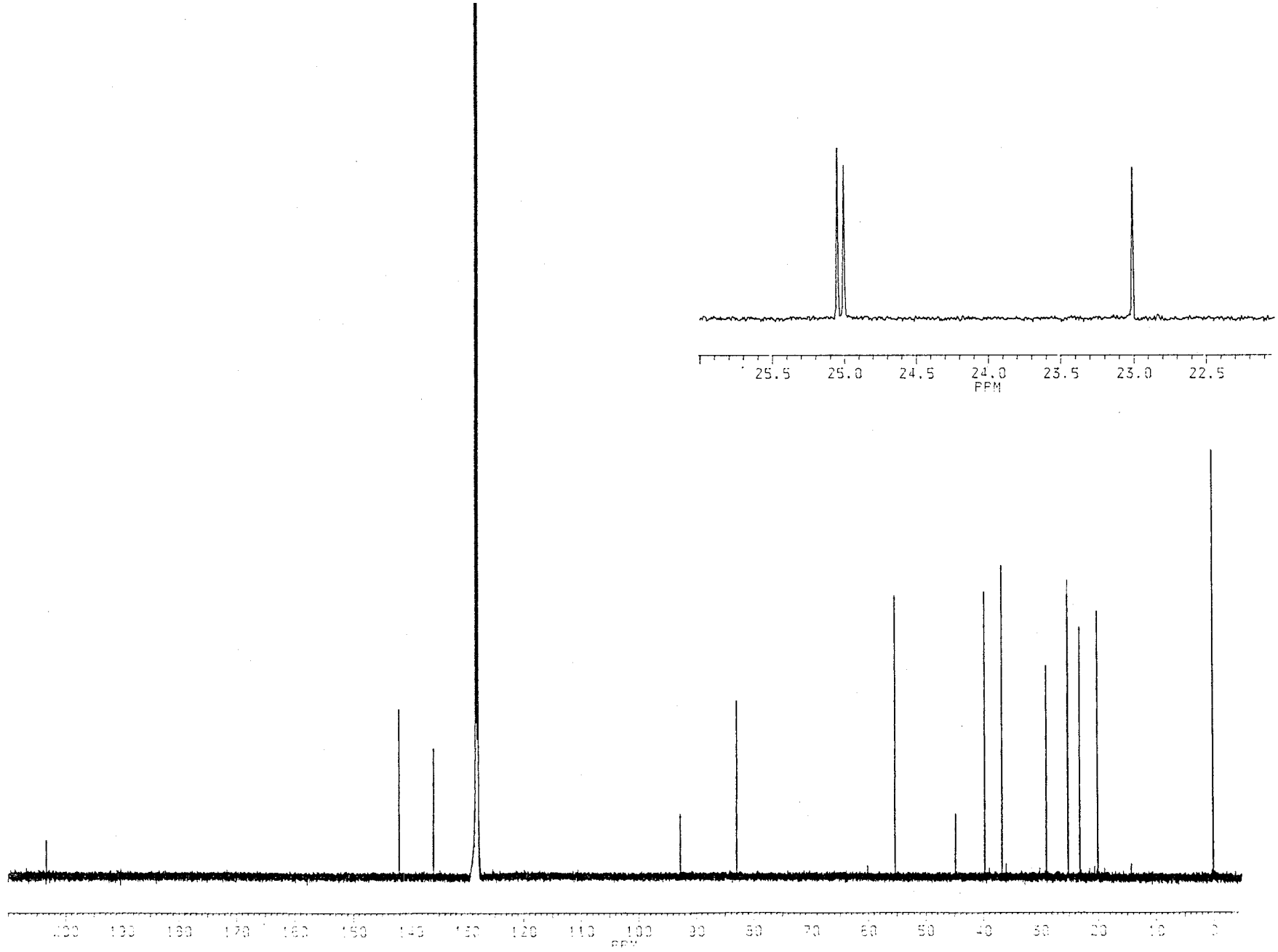

Fig. 3-224 ^{13}C-NMR Spectra of RL-C-OX3 (125 MHz, in C_6D_6, COM and DEPT)

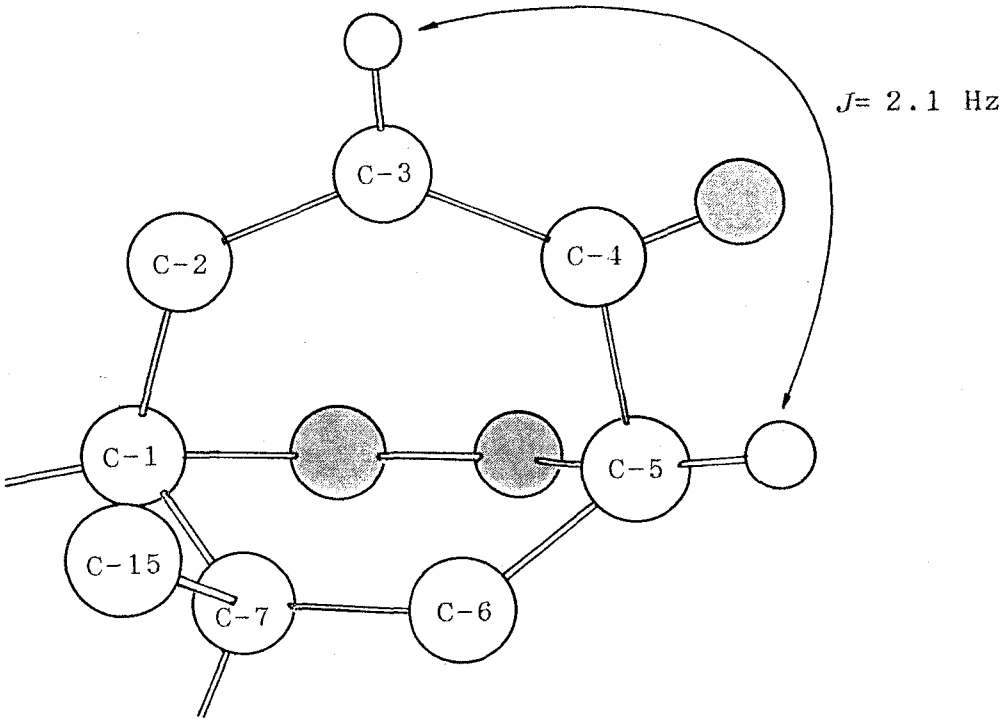

Fig. 3-225 Conformation of RL-C-OX3 around the α,β-Unsaturated Carbonyl Group: The C-3 olefinic proton and C-5 methine proton indicate a W-shaped conformation to show a typical long range coupling.

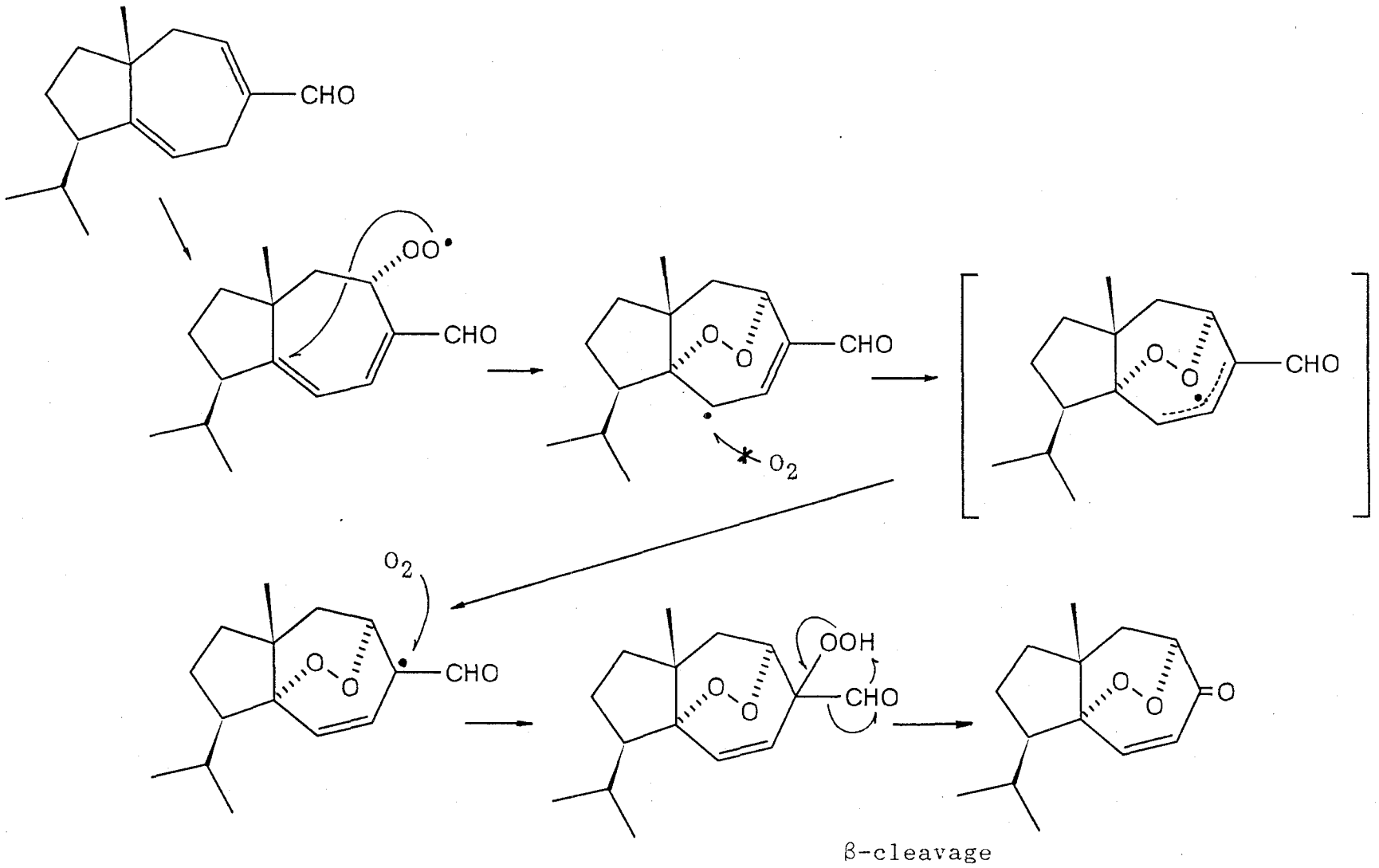

Scheme 3-28 Conversion processes to yield RL-C-OX3 from carota-1,4-dienaldehyde (3): With a samll partial pressure of O_2, the C-2 radical intermediate is convertible into the C-4 radical intermediate to cause β-cleavage of C-14 aldehyde group after peroxylation at C-4.

Table 3-85 Physicochemical properties of RL-C-OX3 (3e)

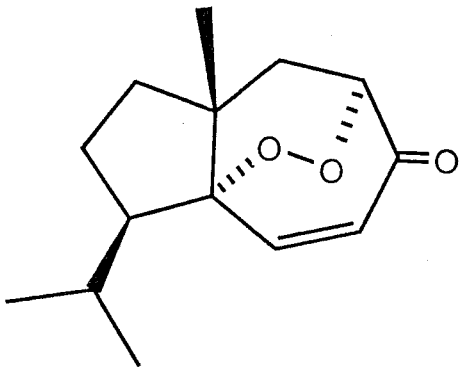

3e

A colorless syrup

Rf: 0.67 (H-EA 4:1)

Vanillin-H_2SO_4 test:

N,N-dimethyl-*p*-phenylenediamine sulfate test: positive (clear pink)

FD-MS *m/z* (%): 473 ($2M^+$+1, 10), 472 ($2M^+$, 7), 237 (M^++1, 100), 236 (M^+, 98), 110 (24).

EI-MS *m/z* (%): 192 (7.4), 177 (2.8), 150 (33), 149 (7.6), 135 (7.5), 121 (4.1), 108 (11), 107 (100), 91 (14), 79 (23), 44 (67), 41 (14).

^{1}H-NMR $\delta_{TMS}^{C_6D_6}$ (500 MHz): 6.310 (1H, d, *J*= 11.2 Hz, C-2-H), 6.372 (1H, dd, *J*= 11.3 and 2.1 Hz, C-3-H), 4.458 (1H, ddd, *J*= 5.4, 2.8 and 2.1 Hz, C-5-H), 1.790 (1H, dd, *J*= 14.0, 5.4 Hz, C-6-Ha), 1.489 (1H, dd, *J*= 14.0 and 2.8 Hz, C-6-Hb), 1.463 (1H, ddd, *J*= 12.9, 12.0 and 6.1 Hz, C-8-Ha), 1.258 (1H, dd, *J*= 12.0 and 5.7 Hz, C-8-Hb), 1.292 (1H, m, C-9-Ha), 0.847 (1H, dddd, *J*= 12.9, 12.4, 11.7 and 5.7 Hz, C-9-Hb), 1.562 (1H, 11.7, 8.1 and 8.0 Hz, C-10-H), 1.314 (1H, double sept., *J*= *ca* 8 and 6.5 Hz, C-11-H), 0.773 (3H, d, *J*= 6.5 Hz, C-12-H_3), 0.591 (3H, d, *J*= 6.5 Hz, C-13-H_3), 0.341 (3H, s, C-14-H_3).

^{13}C-NMR $\delta_{TMS}^{C_6D_6}$ (125 MHz): 92.7 (1-C), 141.9 (2-CH), 135.7 (3-CH), 203.3 (4-C), 82.9 (5-CH), 39.6 (6-CH_2), 44.7 (7-C), 36.6 (8-CH_2), 25.0 (9-CH_2), 55.2 (10-CH), 28.8 (11-CH), 23.0 (12-CH_3), 20.0 (13-CH_3), 25.0 (14-CH_3).

3-5-7 Autoxidation of Carota-1,4-dienoic Acid

During storage in refrigerator, carota-1,4-dienoic acid (4) was also converted into a high polar compound positive to the peroxide reagent. This more polar product RL-115M-A-OX was isolated by PTLC (H-EA-F 20:20:1), 5 mg as a colorless syrup from *ca* 20 mg of RL-115M mixture (Fig. 3-226). Its molecular ion M^+ 298 (100 %) detected in FD-MS was indicative of introduction of four oxygen atoms into the molecule of 4 (Fig. 3-227, *cf.* EI-MS of RL-115M-A-OX in Fig. 3-228). In the ^{1}H-NMR spectrum, this acidic substance showed a similar pattern to that of RL-C-OX-A2 (**3c**) (Fig. 3-229 and Table 3-86 , and the results suggested the product to be *endo*- and *exo*-peroxy derivative as with **3c**.

This speculation was supported by its ^{13}C-NMR spectrum (Fig. 3-230 and Table 3-87). In comparison of carbon chemical shifts of **3c** with those of rugosal A (1), rugosic acid A (2) and RL-115M-A-OX, δ_C between 1 and **3c** showed a good correspondence with those between 2 and RL-115M-A-OX, as listed in Table 3-88. Accordingly, the structure of RL-115M-A-OX was revealed to be **4b**.

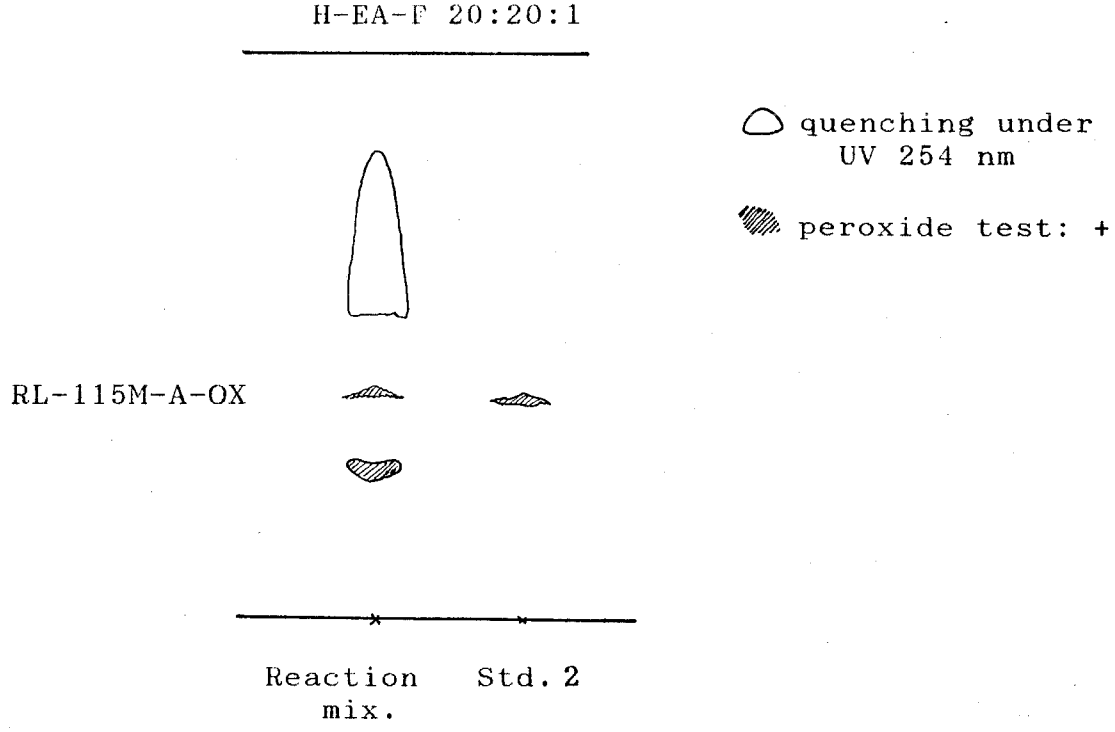

Fig. 3-226 TL Chromatogram of RL-115M Oxidation Products: Other constituents of RL-115M mixture were comparatively stable and practically unchanged.

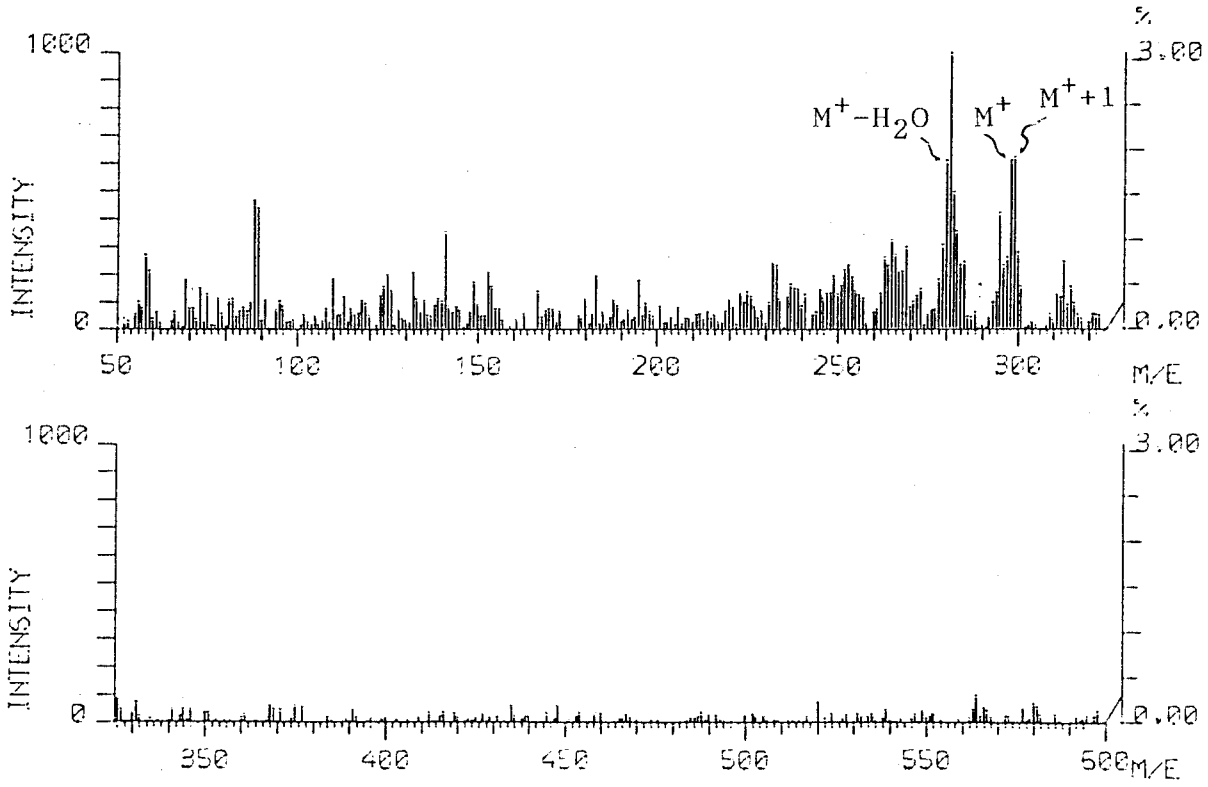

Fig. 3-227 FD-Mass Spectrum of RL-115M-A-OX

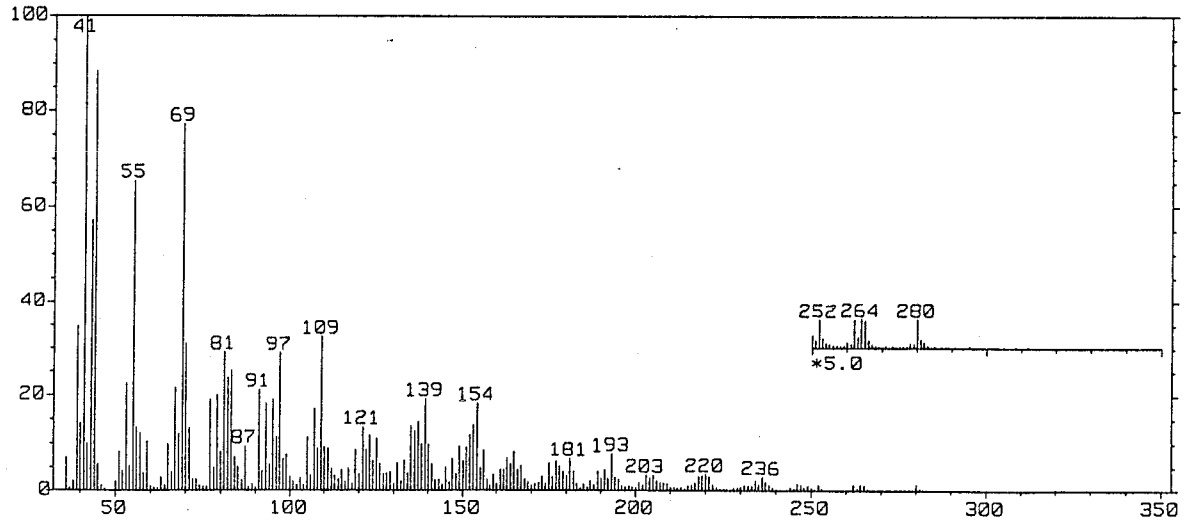

Fig. 3-228 EI-Mass Spectrum of RL-115M-A-OX

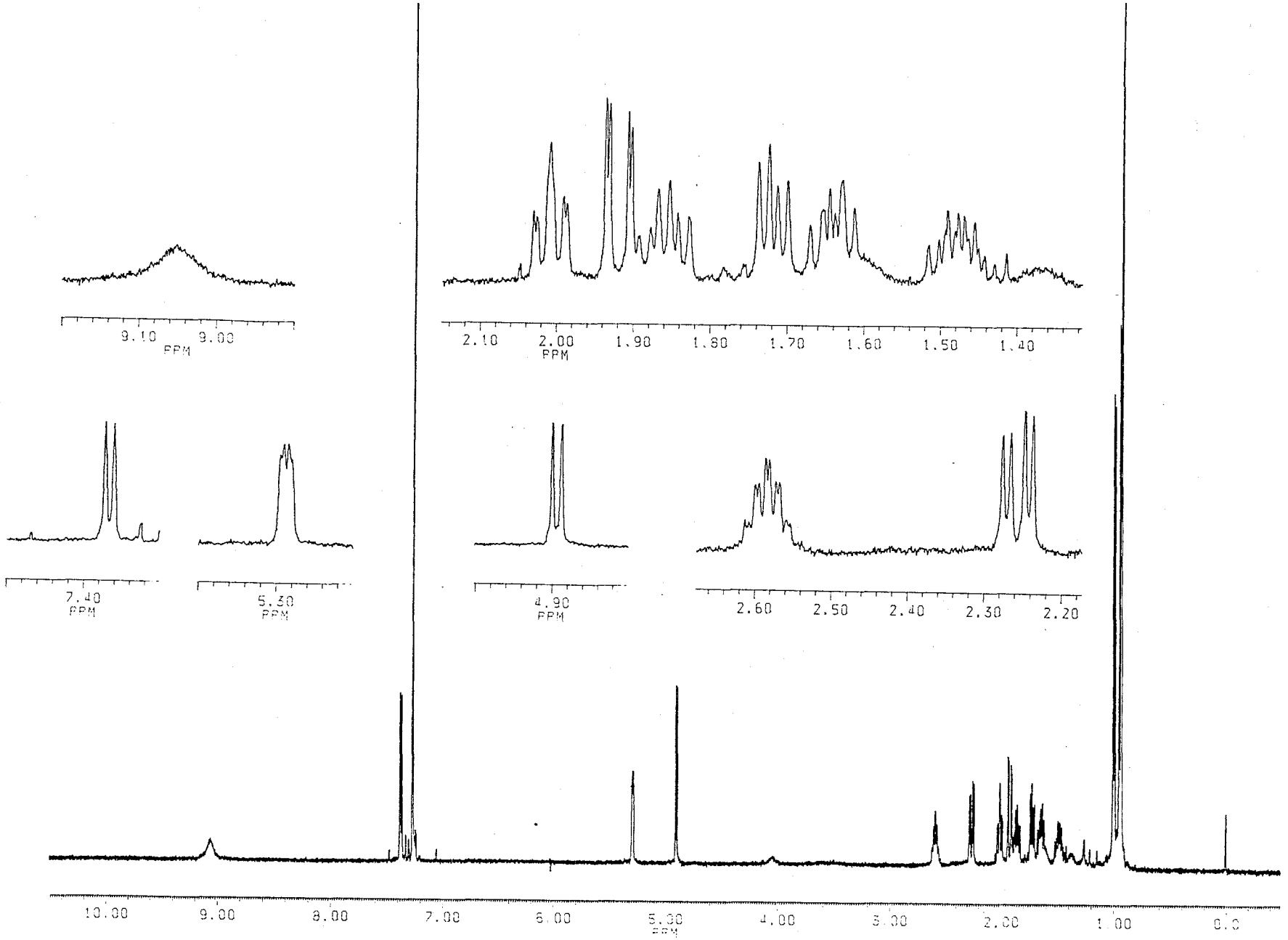

Fig. 3-229 ^{1}H-NMR Spectrum of RL-115M-A-OX (500 MHz, in $CDCl_3$)

Table ***3-86*** *^{1}H-NMR chemical shift values of RL-115M-A-OX*

(500 MHz, in $CDCl_3$, TMS as an int. std.)

δ_H	Coupling	Assignment
9.05	(approx.) br. s	C-2-OOH
7.366	d *J*= 5.9 Hz	C-3-H
5.287	br. d *J*= 5.2 Hz	C-5-H
4.894	d *J*= 5.9 Hz	C-2-H
2.584	d sept *J*= 6.9, 2.4 Hz	C-11-H
2.256	dd *J*= 14.2, 5.2 Hz	C-6-Ha
2.008	ddd *J*= *ca* 10.6, 8.8, 2.4 Hz	C-10-H
1.918	dd *J*= 14.2, 2.3 Hz	C-6-Hb
1.860	ddd *J*= 13.2, 12.3, 7.3 Hz	C-8-Ha
1.718	dd *J*= 12.3, 6.6 Hz	C-8-Hb
1.641	ddd *J*= 12.8, 8.8, 7.3 Hz	C-9-Ha
1.472	dddd *J*= 13.2, 12.8, 10.6, 6.6 Hz	C-9-Hb

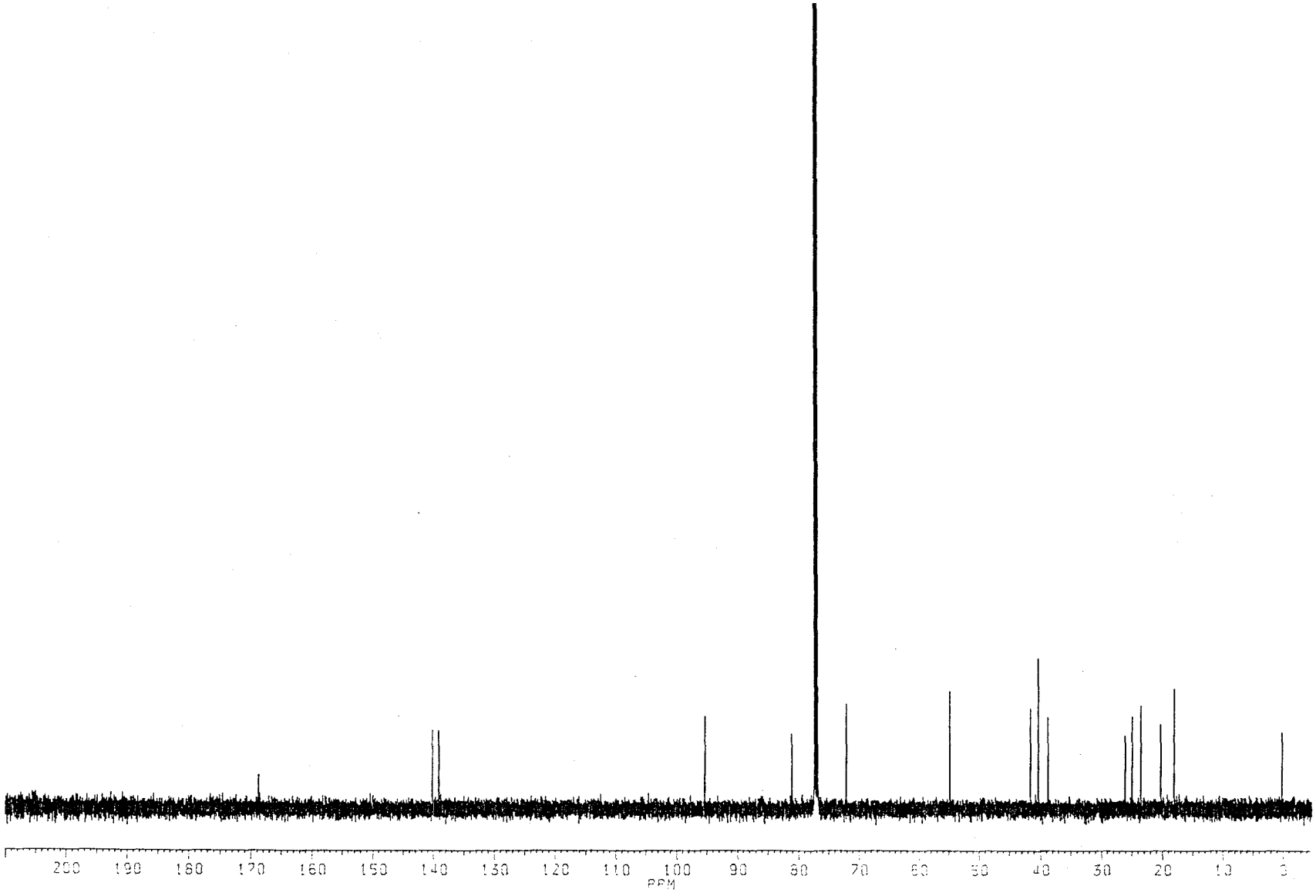

Fig. 3-230 ^{13}C-NMR Spectrum of RL-115M-A-OX (125 MHz, in $CDCl_3$, COM and DEPT)

Table 3-87 ^{13}C-NMR chemical shift values of RL-115M-A-OX

(125 MHz, in $CDCl_3$, TMS as an int. std.)

δ_C	Hydrogenation	Possible assignment
168.5	C	14-CH
140.0	CH	3-CH
139.0	C	4-C
95.2	C	1-C
81.0	CH	2-CH
72.0	CH	5-CH
54.7	C	10-C
41.4	CH_2	8-CH_2
40.1	C	7-C
38.6	CH_2	6-CH_2
26.0	CH	11-CH
24.8	CH_3	15-CH_2
23.4	CH_3	12-CH_3
20.1	CH_2	9-CH_2
18.0	CH_3	13-CH_3

Table 3-88 Comparison of carbon chemical shift values between the C-2-OOH derivatives and C-2-OH carotanoids in rugosal A and rugosic acid A

C-No	3e	1	$\Delta\delta_C$ (ppm)	2	Calcd ($2-\Delta\delta_C$)	Found (4b)
1	95.4	94.8	+ 0.6	94.9	95.5	95.2
2	81.5	69.1	+12.4	68.6	80.1	81.0
3	146.3	149.4	- 3.1	143.5	140.4	140.0
4	148.3	146.5	+ 1.8	136.8	138.6	139.0
5	69.5	70.1	- 0.6	72.4	71.8	72.0
6	41.5	42.0	- 0.5	41.9	41.4	41.4
7	40.0	39.6	+ 0.4	39.6	40.0	40.1
8	38.7	38.5	+ 0.2	38.4	38.6	38.6
9	20.4	20.2	+ 0.2	20.0	20.2	20.1
10	55.1	54.6	+ 0.5	54.1	54.6	54.7
11	26.2	24.8	+ 1.4	24.7	26.1	26.0
12	23.2	22.8	+ 0.4	23.0	23.4	23.4
13	17.9	18.2	- 0.3	18.3	18.0	18.0
14	190.7	190.7	$\pm$ 0	169.7	169.7	168.5
15	24.8	25.9	- 1.1	25.7	24.6	24.8

Table 3-89 Physicochemical properties of RL-115M-A-OX (4b)

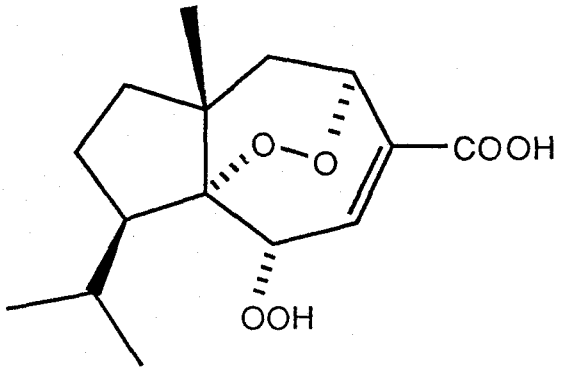

4b

A colorless syrup

Vanillin-H_2SO_4 color:

N,N-dimethyl-*p*-phenylenediamine test: positive (pinkish red)

FI-MS *m/z* (%): 296 (M^+, 100)

EI-MS *m/z* (%): 280 (M^+-H_2O, 1.30), 265 (1.2), 264 (1.3), 246 (1.5), 237 (1.9), 236 (3.0), 220 (3.6), 203 (3.4), 193 (7.7), 181 (6.7), 154 (18), 139 (19), 121 (13), 109 (33), 97 (29), 91 (21), 83 (25), 81 (29), 70 (31), 69 (77), 55 (66), 44 (88), 57 (43), 41 (100).

^1H- and ^{13}C-NMR data are shown in Tables 3-87 and 88, respectively.

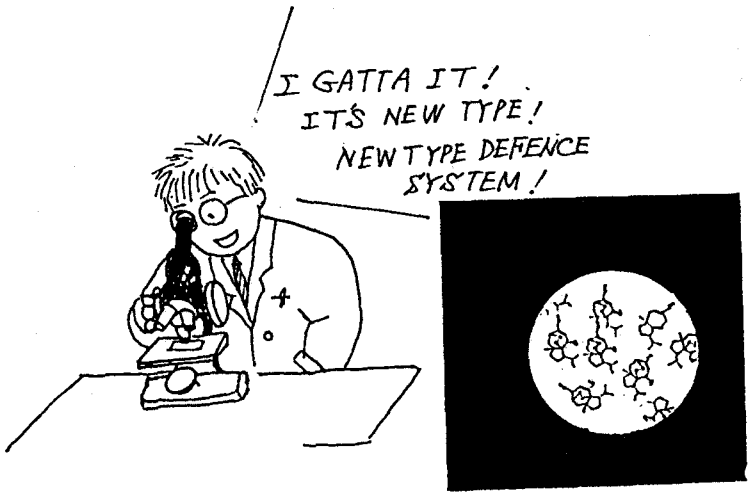

Although the yield of RL-115M-A-OX (**4b**) was not calculated because the starting material was impure, this product certainly indicated that **4** is also convertible into rugosic acid A (**2**). In the synthetic pathway of carotanoids originated in *Rosa rugosa*, it is natural to consider that **2** is yielded from rugosal A (**1**) through oxidation of the aldehyde group. Nontheless, the fact that **2** is also derived from **4** by autoxidation is an interesting aspect (Scheme 3-29). A high content of **2** in the *Rosa rugosa* tissues may be explicable with the nature of **2** as a highly oxydized but relatively stable metabolite in the metabolism of carotanoids mentioned above.

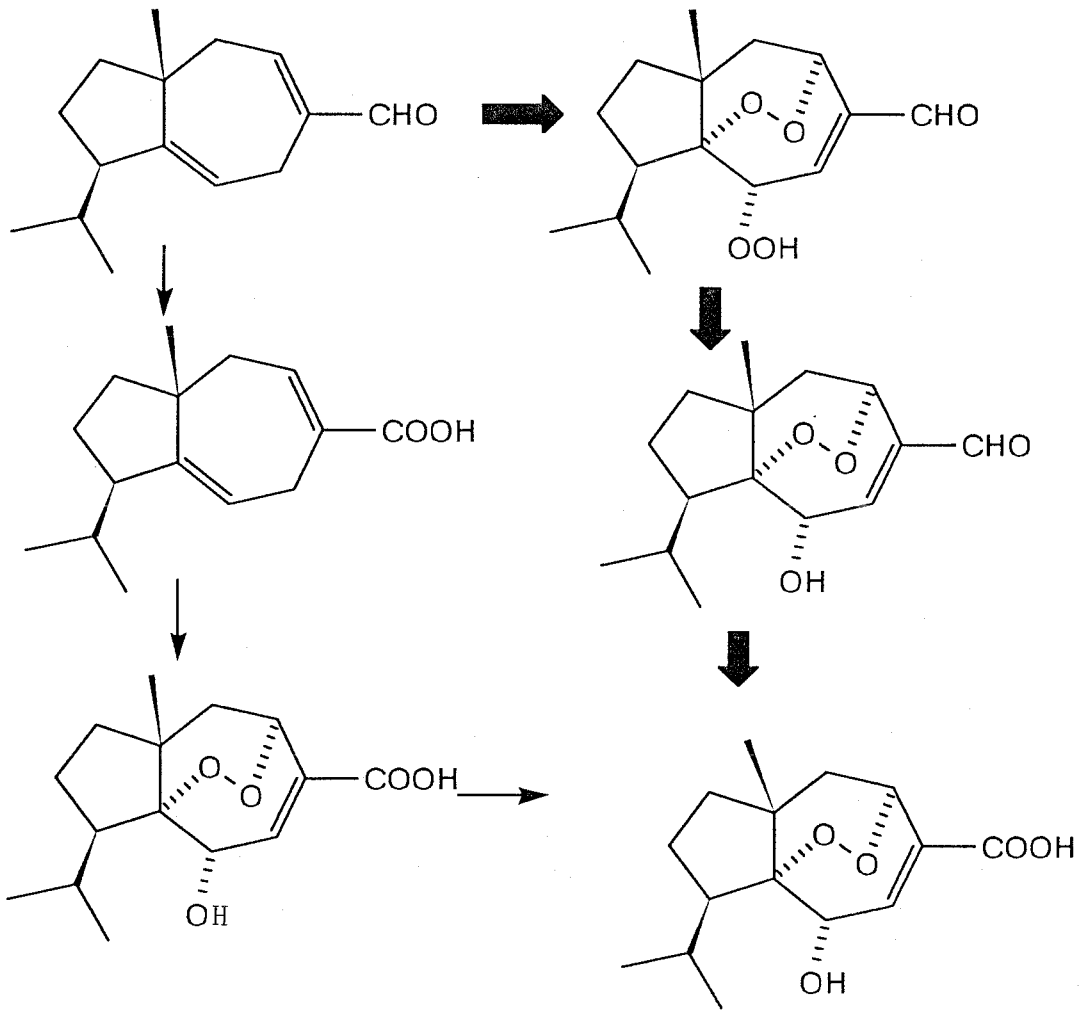

Scheme 3-29 Conversion pathways to yield rugosic acid A (2) from carota-1,4-dienaldehyde (3): It is possible take two pathway; however, it is natural to consider that rugosic acid A (**2**) is formed *via* rugosal A (**1**) is the tissues.

3-5-8 Conclusion

Through the structural analyses of autoxidation products obtained from carota-1,4-dienaldehyde (**3**), the production route for rugosal A (**1**) was nearly elucidated. Especially, products RL-C-OX-A2 (**3c**) and RL-C-OX3 (**3d**) were quite informative. Compound **3c** certainly indicated that **3** was converted into **1** by introduction of two oxygen molecules, while **3d** was suggestive that the relevant 1,5-endoperoxy-2-carboradical is temporarily present during the conversion. The intermediated radical is considered to be attacked immediately by triplet oxygen when O_2 concentration was comparatively high.

As known in several *cis*-1,4-diene compounds, such as linolenic acid (**92**) and arachidonic acid (**93**), autoxidation on the 1,4-diene part is initiated by abstraction of a hydrogen radical from the C-3 methylene called an active methylene (Scheme 3-30) [124]. As a result, homolitic re-distribution of π-electrons on -C(4)=C(5)- occurs to form a *cis-trans*-conjugated diene with an odd electron at C-5 (See also Scheme 3-19, pp. 285). These reaction steps are applicable to formation of **1** from **3**.

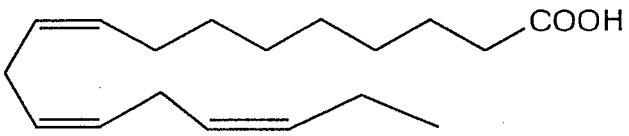

linolenic acid (92)

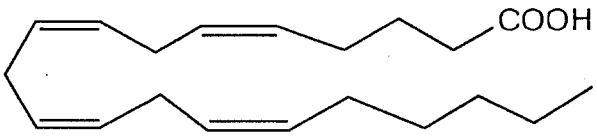

arachidonic acid (93)

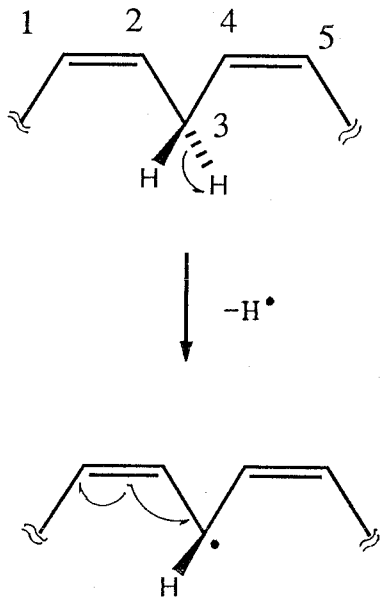

Scheme 3-30 The Initial Step of Peroxidation on a 1,4-Diene

According to Scheme 3-31, the C-3 proton of **3** is initially abstracted as a hydrogen radical to result in the corresponding carboradical at C-3 (intermediate **E**). Subsequently, not the C-1/C-2 but the C-4/C-5 π-electron bond homolitically cleaves to translocate the olefinic bond to C-3/C-4, and a new radical carbon appears at C-5 (**F**, Step 1). The priority of C-4/C-5 bond to C-1/C-2 in the homolytic re-distribution of π-electrons is due to a low electron density on the conjugated olefinic bond.

To the radical, triplet oxygen attacks to form an exoperoxy radical (**G**, Step 2). The stereoselectivity (back-side attack) during the peroxidation is expricable with steric hindrance of the C-15 bridgehead methyl group. Successively, the cyclization immediately occurs (Step 3). The exoperoxy radical only attacks not C-2 but C-1. Usually, selectivity of radical addition depends on the stability of the resulting radical, as follows: primary radical < secondary radical < tertiary radical (Fig. 3-231) [134]. Nonetheless, this cyclization occurs to yield not tertiary but secondary radical intermediate (**H**) (Fig. 3-232). This serectivity may be explicable with stability of the latter intermediate as an allyl radical. Nonetheless, any derivatives on the production route for **3d** were not found as an autoxidation reaction product under aerobic conditions. If the resulting intermediate in Step 3 were stabilized, some C-4 peroxylated products including **3d** would be detectable with a marked amount.

The distance of those olefinic carbons from the radical is also considerable as an important factor for the selectivity in the cyclization. However, the distances of C-1 and C-2 from the radical oxygen is almost the same in a molecular model of the intermediate, and was therefore negligible as the factor.

On the other hand, electron density and charge on the reactive carbon can be considered as another factor. To the radical addition reaction, lower electron density of the reactive carbon may contribute. However, simply polarized π-electrons on olefines,

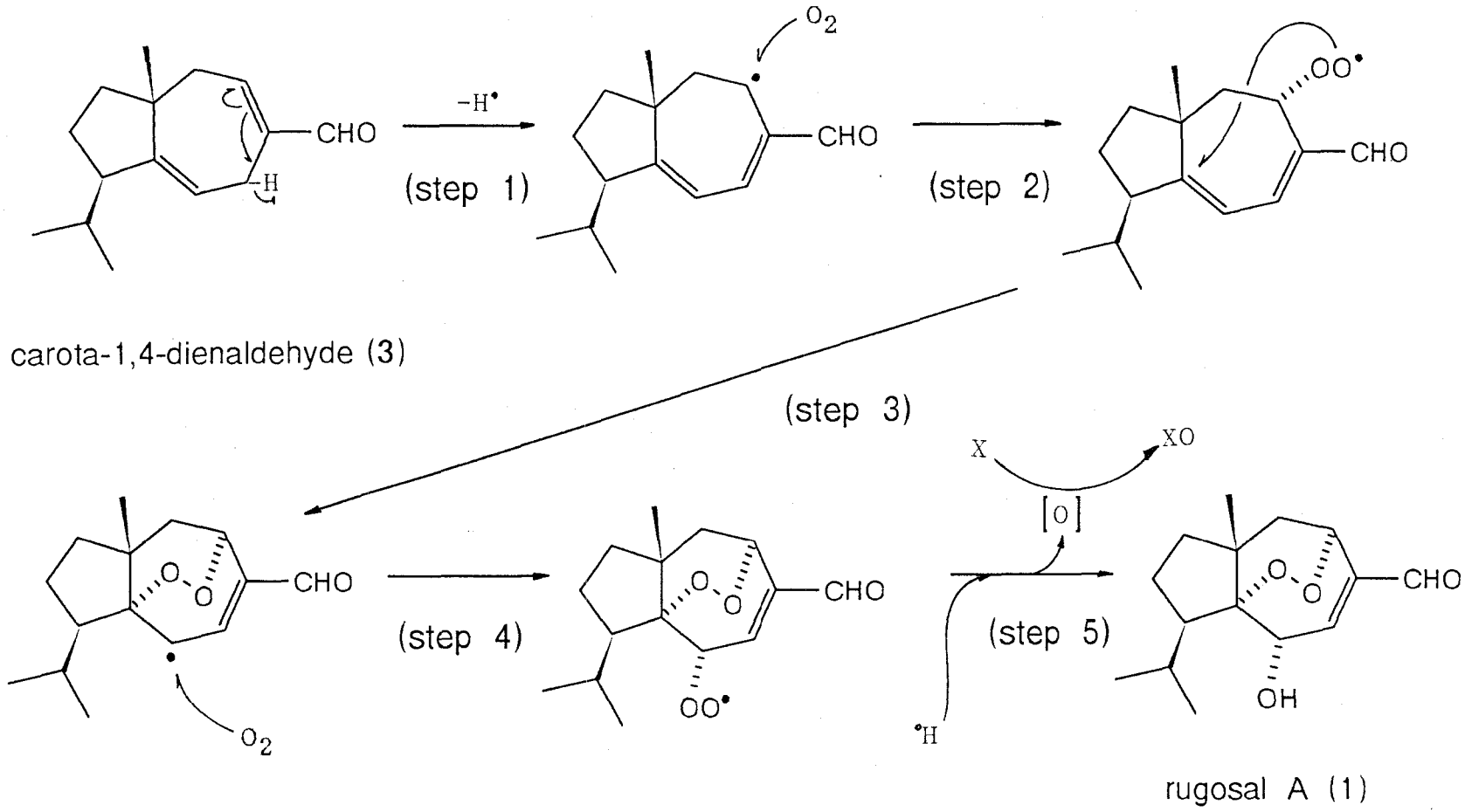

Scheme 3-31 Conversion pathway of carota-1,4-dienaldehyde (3) into rugosal A (1)

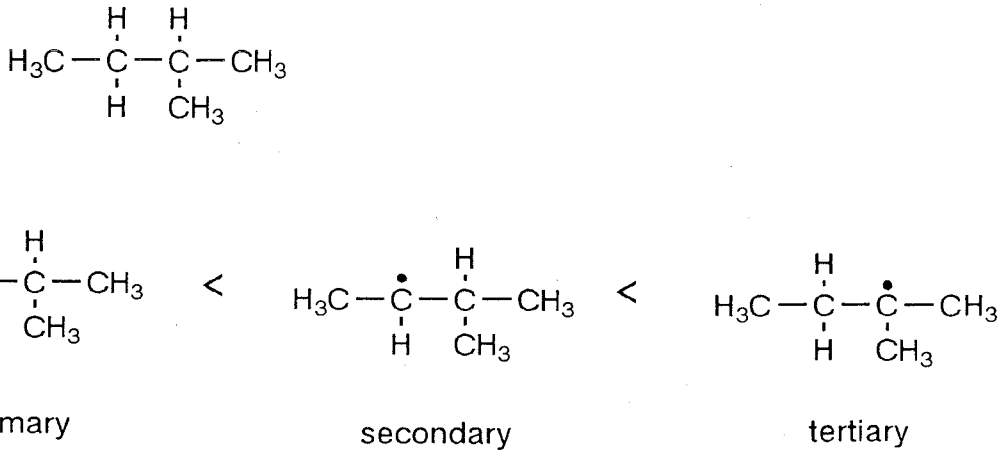

Fig. 3-231 Stability of Carboradicals: Tertiary carboradical is most stable among these three.

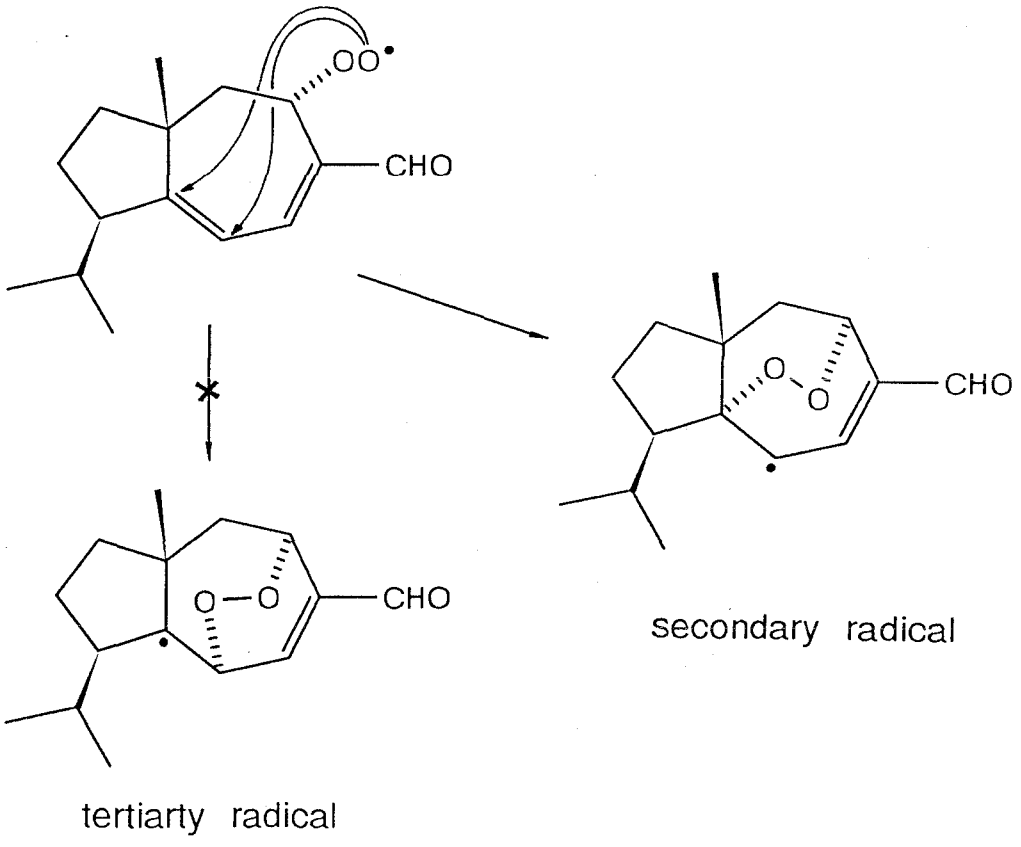

Fig. 3-232 Cyclization of Exoperoxy Radical in the Formation of Rugosal A

like an α,β-unsaturated ketone group whose π-electrons are mostly localized on the α-carbon, makes the target carbon rather inactive, as the reaction has to result in homolysis of π-electron bond.

In cyclization of the peroxy radical intermediate g, the reactive olefinic carbon (C-1) is expected to exhibit the lowest electron density among the carbons (C-1~C-4) forming the conjugation system. Nonetheless, π-electron still remains on the disubstituted reactive carbon (>C=CH-) due to steric effect. In disubstituted olefinic carbons, electron density tends to be higher than in monosubstituted olefinic bond. Consequently, the homolysis easily occur in the C-1/C-2 bond. For that reason, the C-5 exoperoxy radical probably allowed to attack the C-1 carbon selectively (Fig. 3-233).

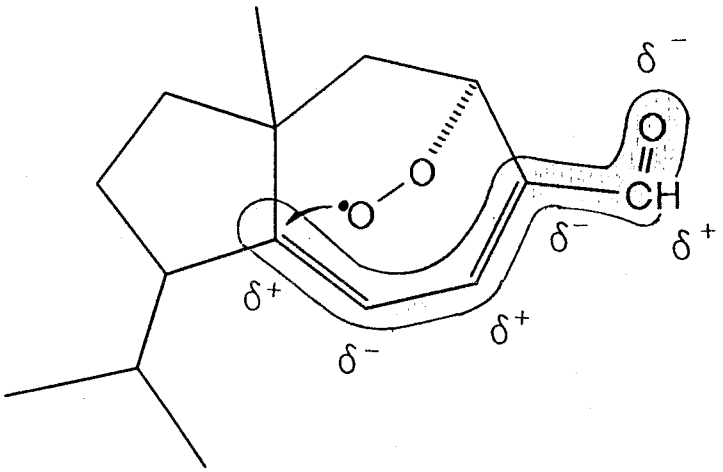

Fig. 3-233 Model of Electron Density in the Peroxy Radical

Furthermore, direction of bonding orbital concerned with the newly formed C-O bond during the cyclization may also be an important factor. Direction of the orbitals on C-1 and C-2 are definitely different. Contrary to C-2 carbon whose bonding orbital is nearly coplanar with C-3/C-4 due to the conjugation, C-1 is independent and possesses an orbital almost perpendicular to the five-membered ring. The latter orbital can sufficiently overlap with the binding orbital of the exoperoxy radical (Fig. 3-234). By such complex factors, the selectivity seems to appear during the cyclization.

To the C-2 radical carbon, another triplet oxygen further attacks (Step 4). In this process, stereoselection is also observed at C-2 carbon of the intermediate (I). The stereo-selectivity is due to steric hindrance mainly caused by the isopropyl group on the C-10. This step is considered to occur almost simultaneously, with the cyclization in the peroxy radical G.

On the other hand, if the allyl radical intermediate H was yielded under less aerobic conditions, a C-4 carboradical would be accordingly formed. RL-C-OX3 (**3d**), which was only detected in the autoxidation product mixture obtained under less aerobic condition, indicates this route, even though it can hardly be regarded as major route in *Rosa rugosa* leaf tissues.

The isolated hydroperoxide intermediate (RL-C-OX-A2, **3c**) is stabilized by abstraction of hydrogen radical. This peroxide is further transformed through elimination of active oxygen [O] into rugosal A (**1**) that is more stable than **3c** (Step 5). During this final step, [O] is possibly scavenged with **3** or **1** as described above. This proposed pathway (Scheme 3-35) is for the autoxidation reaction of **3**; however, in the tissues of *Rosa rugosa*, in principle the reaction shown in the scheme must take place.

Morita *et al.* have provided a discussion concerning the formation of hanalpinol (**80**) in the rhizomes of *Alpina japonica*,

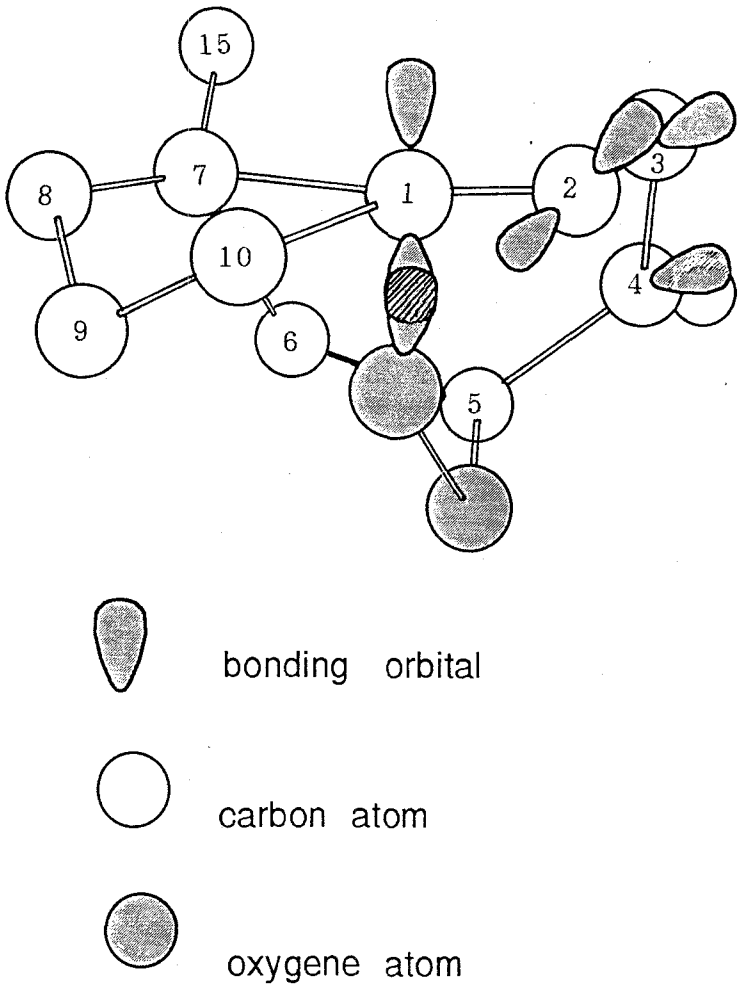

Fig. 3-234 Model of Direction of Bonding Orbitals on the Exo-peroxy Radical: The orbital of C-1 can sufficiently overlap with that of radical.

in which they speculated that **80** was formed by catalytic autoxidation of its precursor, guaia-6,9-diene (**87**). They referred to the fact that the rhizome of the plant is remarkably rich in ferric ion, and suggested the hypothesis that the ferric ion catalyze the autoxidation [127].

Rosa rugosa has also been known as a plant who has ability to accumulate in the leaves heavy metals (as pollutants) from the air [135]. In the author's opinion, however, the idea that production of carotane peroxides depends on autoxidation seems unacceptable, at least in the case of *Rosa rugosa*. In leaves, photosynthesis takes place. As the result in Hill reaction, inner thylacoid declines to an oxidative condition to membrane lipids. Such a peroxylation condition on thylacoid or cell membrane road to lethal damage in the cells. Therefore, the cells involving thylacoids are equipped with several reduction tools, such as ascorbic acid reductase and superoxide dismutase (SOD). If **3** was easily oxygenated by autoxidation in the tissues, the cell functioning would be surely disrupted by peroxylation and degradation of the membrane lipids, because radical reactions like autoxidation of **3** are progressed as a chain reaction. By the reason, oxydation of **3** must be well controlled in the tissues.

If **3** was, by autoxidation, converted into **1** in a ratio of 100 mg/kg fresh leaf, polyunsaturated fatty acid forming thylacoids or cell membrane might be peroxylated very easily. It is therefore reasonable to consider that peroxylation of carotanoids is rationally controlled by a lipoxygenase-like enzyme and the oxygenation product is utilized as defense agent of *Rosa rugosa* . Or more systematically, **3** might function as an radical scavenger in the leaf-tissues.